ANALYSIS OF THE STRESS-INDUCED MODIFICATIONS OF NUCLEOCYTOPLASMIC TRAFFICKING IN STRESSED MAMMALIAN CELLS

By

Mohamed Kodiha

Department of Physiology

McGill University

Montreal, Qc, Canada

August, 2009

A thesis submitted to McGill University in partial fulfilment of the requirements of the degree of Doctor of Philosophy

Table of Contents

Dedication

This thesis is dedicated to my parents Amal Fahmy El-Sayed and Farouk F. Kodiha, who taught me everything in this life, as well as Dr. Hanan Ghozlan who put my feet on the right track and supported my first steps in the scientific carrier. I also would like to dedicate this thesis to my first science teacher, Mrs. Madiha Gommaa, the soul of my mother in law Mrs. Azza El-Nakhal, and finaly my wife Rehab Hassan and my little angles Loai, Zeina.

Abstract

Environmental stress is a fundamental factor that negatively impacts different cellular components and impinges on numerous aspects of cellular function. In fact, the ability of a cell to cope with different stressors determines its fate. One of the essential cellular systems which are targeted by stress is the nucleocytoplasmic transport apparatus. As such, the classical import pathway is inhibited by different forms of stress. The research presented in this thesis analyzed the effects of stress on nucleocytoplasmic transport with particular focus on how stress impinges on individual components of the transport apparatus. Furthermore, nuclear trafficking of the chaperone hsc70 and AMP-activated protein kinase (AMPK), which are implicated in numerous physiological processes have been analyzed under normal and stress conditions.

To gain further insight into how stress regulates nucleocytoplasmic trafficking in eukaryotes HeLa cells were used as model system to analyze the effect of mild oxidative stress on the localization of soluble transport factors. My research revealed that oxidative stress mislocalizes transport receptors importin-α, and CAS as well as nucleoporins Nup153, and Nup88 all of which accumulate in nuclei upon oxidant treatment. In addition, I have shown that these soluble transport factors became immobile in the nuclei of stressed cells where they were retained in large insoluble complexes.

A crucial component of the cell signaling machinery which is regulated by modulation of nuclear trafficking is AMPK. My research provided new insights into how different stressors affect the activation and subcellular localization of

AMPK. As such, my results demonstrated that several forms of stress including heat, energy depletion and oxidants concentrate AMPK in nuclei. Furthermore, I showed that under normal growth conditions AMPK shuttles between the nucleus and cytoplasm, a process that depends on the nuclear exporter Crm1. Moreover, my results demonstrated that signaling through the MEK→ERK1/2 cascade plays a crucial role in controlling the localization of AMPK.

In addition to AMPK, I focused on the effect of stress on heat shock protein 70 (hsc70), an essential component of the chaperoning machinery which plays a crucial role in the repair of stress-induced damage. Following stress exposure, hsc70 accumulates in nuclei, but relocates to the nucleoli and subsequently the cytoplasm when cells recover from stress. I have defined at the molecular level the mechanisms that control hsc70 transport in and out of the nucleus upon stress. Specifically, retention in nuclei and nucleoli of stressed cells was identified as the main cause that delays hsc70 exit from the nucleus. My research has identified the nucleolar components fibrillarin and the rpS6 ribosomal protein as interacting components of hsc70 which possibly anchor the chaperone in nucleoli upon stress. In addition, I have shown that libration of hsc70 from these anchors is a prerequisite to exit the nucleus.

As part of my research objectives, my work was directed towards improving the technical approaches that are used to detect the subcellular distribution of proteins. To this end, I have developed a new quantitative immunofluorescence approach to analyze in a quantitative fashion the distribution of proteins in different subcellular compartments, including the nucleus, cytoplasm and nuclear

envelope NE. The protocols described in this thesis were successfully employed to analyze the distribution of transport receptors and signaling molecules under normal and stress conditions. Developing new tools to quantify the levels of proteins in the different subcellular location opens the door to understand the dynamic organization of different cellular components and how such dynamic state regulates their function.

Résumé

Le stress environnemental est un facteur fondamental qui a des effets négatifs sur diverses composantes cellulaires et qui empiète sur de nombreux aspects du fonctionnement cellulaire. En fait, la capacité d'une cellule à faire face à différents éléments stressants va déterminer son sort. Un des systèmes cellulaires essentiel qui est ciblé par le stress est l'appareil du transport nucléocytoplasmique. Par exemple, le système classique d'importation au noyau est inhibé par différentes formes de stress. Les recherches présentées dans cette thèse analysent les effets du stress sur le transport nucléocytoplasmique en se concentrant plus précisément sur la façon dont le stress empiète sur les composantes individuelles de l'appareil de transport. De plus, le transport nucléaire de la chaperone hsc70 et de la protéine kinase activée par l'AMP (AMPK), qui sont impliquées dans de nombreux processus physiologiques, ont été analysées sous des conditions normales et de stress.

Afin d'obtenir un meilleur aperçu de la capacité du stress à réguler le transport nucléocytoplasmique chez les eucaryotes, les cellules HeLa furent utilisées comme système model pour analyser les effets d'un stress oxydatif léger sur la localisation des facteurs de transport solubles. Mes recherches révèlent que le stress oxydatif modifie la localisation des récepteurs de transport importine-α et CAS, ainsi que les nucléoporines Nup153 et Nup88 qui s'accumulent toutes dans les noyaux suite à un traitement oxydatif. De plus, je démontre que ces facteurs solubles de transport deviennent immobiles dans les noyaux de cellules stressées où elles sont retenues dans de grands complexes insolubles.

Une composante cruciale de la machinerie de la signalisation cellulaire qui est régulée par la modulation du transport nucléaire est l'AMPK. Mes recherches fournissent de nouveaux aperçus sur la façon dont les différents éléments stressants affectent l'activation et la localisation subcellulaire de l'AMPK. Par exemple, mes résultats démontrent que plusieurs formes de stress incluant la chaleur, la réduction d'énergie et les agents oxydants concentrent l'AMPK dans les noyaux. De plus, je démontre que sous des conditions normales de croissance cellulaire, l'AMPK voyage entre le noyau et le cytoplasme, un processus qui dépend sur l'exportateur nucléaire Crm1. Par ailleurs, mes résultats ont démontrés que la signalisation par la cascade MEK-ERK1/2 joue un rôle crucial dans le contrôle de la localisation de l'AMPK.

En plus de l'AMPK, je me suis concentré sur l'effet du stress sur la protéine de stress à la chaleur hsc70 (heat shock protein 70), une composante essentielle de la machinerie des chaperones qui joue un rôle crucial dans la réparation des dommages induits par le stress. Suite à une exposition à un stress, hsc70 s'accumule dans les noyaux, mais est ensuite relocalisée dans les nucléoles et subséquemment dans le cytoplasme pendant le rétablissement des cellules. J'ai défini, au niveau moléculaire, les mécanismes qui contrôlent le transport de hsc70 vers et hors du noyau lors d'un stress. Spécifiquement, la rétention dans les noyaux et les nucléoles des cellules stressées fut identifié comme cause majeure qui retarde la sortie de hsc70 du noyau. Mes recherches ont identifié la fibrillarine, composantes nucléolaire, ainsi que la protéine ribosomale rpS6 comme composantes qui interagissent avec hsc70 en ancrant possiblement la

chaperone dans les nucléoles lors d'un stress. De plus, j'ai démontré que la libération de hsc70 de ces ancres est un pré-requis pour quitter le noyau.

Faisant partie de mes objectifs de recherche, mon travail fut dirigé vers l'amélioration des approches techniques employées pour la détection de la distribution subcellulaire des protéines. Pour cette fin, j'ai développé une nouvelle approche quantitative de la fluorescence afin d'analyser de manière quantitative la distribution des protéines dans différents compartiments subcellulaires, incluant le noyau, le cytoplasme et l'enveloppe nucléaire (NE). Les protocoles décrits dans cette thèse furent employés avec succès afin d'analyser la distribution des récepteurs de transport et molécules de signalisation sous des conditions normales et de stress. Le développement de nouveaux outils afin de quantifier les niveaux de protéines dans divers endroits subcellulaires ouvre la voie vers la compréhension de l'organisation dynamique des différentes composantes cellulaires, ainsi que de la manière dont leur état dynamique régule leur fonction.

Acknowledgment

I would like to acknowledge the following persons for their help and support during my PhD program. First of all, I am eternally grateful to my supervisor Dr. Ursula Stochaj for her unlimited support during my graduate studies. Her exceptional supervision and guidance were the corner stone to my success in the scientific field. I have learned a lot from her practical advices which helped me to accomplish my experiments in a reasonable fashion. Her constructive intervention has greatly helped me to improve my skills and devote myself into the research career. I am also grateful to her for giving me the opportunity to participate in several international conferences and get involved in the training of many undergraduate students. I am privileged to have such a great mentorship during my PhD program. I am also thankful for Dr. Stochaj for her generous financial support along the program without which I would not even be able to start my studies.

I am also obliged to my committee members Dr. John White, Dr. Mark Featherstone, and Dr. Prem Ponka for their guidance and advices throughout my program. Their feedback and suggestions gave me new ideas which helped me to complete my research.

I also would like to extend my appreciation to my former and present colleagues in the laboratory, Xin xin Quan and Piotr Bański whom I enjoyed working with over many years. Their nice equanimity and calmness created an exceptional working environment which I will miss. Their support and honest advices helped me during my studies. In particular I am grateful to Piotr for his

efforts in generating the French version of my thesis abstract. I also would like to extend my deep gratitude to Neola Matusiewicz for her technical support and tips which helped me to organize my working environment and avoid pitfalls while performing my experiments. I am also thankful to the wonderful group of the undergraduate students whom worked with me, Dennis Ho-Wo-Cheong, Andrea Morogan, Cynthia Qian and Dan Tran.

I would also like to acknowledge the following funding agencies for their financial support to my research, McGill University Faculty of medicine, FRSQ and Heart and Stroke Foundation of Canada.

I would like to take this opportunity to extend my appreciation for all the members of the Department of Physiology at McGill University for providing an exceptional working environment and unlimited support. In particular I would like to thank Christine Pamplin for her tremendous help throughout my studies.

List of Figures

Chapter 1

Chapter 2

Chapter 3

Chapter 4

Chapter 5

List of Tables

Chapter 2

Chapter 3

Chapter 4

Chapter 5

List of Abbreviations

ARM repeats	Armadillo repeats
ACC	Acetyl-CoA carboxylase
AMPK	5´-AMP-activated protein kinase
BAG-1	Bcl-2-associated athanogene
BSA	Bovine serum albumin
CaMKKα	Ca^{2+}/calmodulin-dependent protein kinase kinase α
CaMKK β	Ca^{2+}/calmodulin-dependent protein kinase kinase β
CAS	Cellular apoptosis susceptibility factor
CHIP	Carboxy terminus of Hsc70 interacting protein
CHX	Cycloheximide
cNLS	Classical nuclear localization signals
CBS	Cystathionine β-synthase
Crm1	Exportin-1, nuclear carrier involved in export of proteins with hydrophobic nuclear export sequences
Cyt B	Cytochalasin B
DAPI	4',6-diamidino-2-phenylindole
DEM	Diethyl maleate
DFC	Dense fibrillar components
EDMD	Emery-Dreifuss Muscular Dystrophy
EGFP	Enhanced GFP
ER	Endoplasmic reticulum
ERK	Extracellular signal-regulated kinase

FAS	Fatty acid synthase
FG	Phenylalanine-Glycine
FxFG	Phenylalanine-x-Phenylalanine-Glycine
GFP	Green fluorescent protein
GFP-β-gal	GFP-β-galactosidase
GLFG	Glycine-Leucine-Phenylalanine-Glycine
GR	Glucocorticoid receptor
GRE	Glucocorticoid response element
HGPS	Hutchinson-Gilford Progeria Syndrome
Hip	Hsc70 interacting protein
Hsc70	Heat shock protein cognate
Hsps	Heat shock proteins
Hop	Hsp70-hsp90-organizing protein
IBB	Importin-ß binding domain
INM	Inner nuclear membrane
Lat B	Latrunculin B
LDH	Lactate dehydrogenase
LMB	Leptomycin B
MAPK	Mitogen-activated protein kinase
MEK	Mitogen-activated protein kinase kinase
mRNA	Messenger RNA
NE	Nuclear envelope
NES	Nuclear export signal
NLS	Nuclear localization signals
NPCs	Nuclear pore complexes

NP40	Nonidet P-40
Nrf2	Nuclear factor E2-related factor 2
NTF2	Nuclear transport factor 2
Nuc/cyt	Nuclear/cytoplasmic ratio
Nups	Nucleoporins
ONM	Outer nuclear membrane
p-AMPK-α1/2	AMPK-α1/2 phosphorylated on Thr172
p-ERK	Dually phosphorylated ERK
PI3K	Phosphatidylinositol 3-kinase
PKA	Protein kinase A
PKI	Inhibitor of cAMP-dependent protein kinase
PKIα	Protein kinase inhibitor α
PP2Cα	Protein phosphatase 2α
PTHrP	Parathyroid hormone-related proteins
RanBP1	Ran-binding protein
RanGAP1	RanGTPase activating protein
RanGEF	Guanine nucleotide exchange factor
RCC1	Regulator of chromosome condensation
ROS	Reactive oxygen species
snRNPs	Small nuclear ribonucleoproteins
SV40T-ag-NLS	Simian virus 40 large T-antigen-NLS
SREBP-2	Sterol regulatory element-binding protein 2
t-AMPK	Total AMPK.
Thr172	Threonine residue 172
t-ERK	Total ERK

TPR	Tetratricopeptide repeat
tRNA	Transfer RNA

Contributions of Authors

This thesis is based on four published papers for which I am the first author.

All the experiments presented in this thesis were done under the supervision of Dr. Ursula Stochaj. I did most of the experiments presented in these papers and I also contributed to the design of experiments as well as optimizing the experimental approaches used to perform the research work. My research work has greatly benefited from the continuous guidance and constructive feedback from Dr Stochaj. My co-authors have contributed to some of the experiments (see below).

Chapter 2

This chapter is based on the paper entitled "Oxidative stress mislocalizes and retains transport factor importin-α and nucleoporins Nup153 and Nup88 in nuclei where they generate high molecular mass complexes" by ***Mohamed Kodiha***, *Dan Tran, Cynthia Qian, Andreea Morogan, John F. Presley, Claire M. Brown and Ursula Stochaj.* This paper has been published in *Biochemica et Biophysica Acta (BBA) - Molecular Cell Research* 1783: 405-418, 2008.

Dr. John F. Presley gave me advice on how to acquire images using confocal microscopy. Dr. Claire M. Brown has contributed to the fluorescent signal quantification using high throughput screening technology. Andrea Morogan and Cynthia Qian performed, under my supervision, some of the experiments that study the effect of oxidative stress on importin-α and CAS distribution. Dan Tran

performed the experiments that addressed the effect of oxidative stress on the nuclear retention of Nup88. Dr. Ursula Stochaj performed the experiments that generated the Figures 2.6 and 2.8. I carried out all other experiments presented in this chapter.

Chapter 3

This chapter is based on the paper entitled "The localization of AMP kinase is regulated by stress, cell density and signaling through the MEK→ERK1/2 pathway". By ***Mohamed Kodiha***, *James G. Rassi, Claire M. Brown, and Ursula Stochaj*. This paper has been published in *Am. J. Physiol. Cell Physiol.* 293: C1427-1436, 2007. Cell fractionation, western blotting and quantification of ECL signals were done by Dr. Ursula Stochaj. James G. Rassi contributed (under my supervision) to the experiments that analyze the effect of oxidative stress on AMPK localization. Dr. Claire M. Brown gave me advice on the quantification of fluorescence signals. I performed the rest of the experiments presented in this chapter.

Chapter 4

I published this chapter as ***Kodiha M***, Chu A, Lazrak O, and Stochaj U. Stress inhibits nucleocytoplasmic shuttling of heat shock protein hsc70. *Am. J. Physiol. Cell Physiol.* 289: C1034-1041, 2005. Dr. Ursula Stochaj performed the immunoprecipitation experiments in Figure 4.7B. Angel Chu performed the

experiments in Figure 4.3. Omar Lazrak did the cloning for the reporter EGFP-hsc70. I performed the rest of the experiments in this paper.

Chapter 5

This chapter was published in Science Signaling as ***Kodiha M,*** Brown CM, and Stochaj U**.** Analysis of signaling events by combining high-throughput screening technology with computer-based image analysis. *Sci. Signal.* 1: pl2-, 2008.

I have written most of the protocols and contributed to the writing of the introduction as well as the notes and remarks section. I carried out all the experiments that were used to generate images which were analyzed by the different protocols described in this paper. I have also contributed to the development and optimization of these protocols. Dr. Ursula Stochaj contributed to the writing of the introduction and note and remarks section as well as the development and optimization of the different protocol. She also contributed to the editing of the whole manuscript. Dr. Claire M. Brown has helped in the editing of the manuscript and optimizing the multi wavelength cell scoring module.

CHAPTER 1

Introduction and Review of the Literature

1. Organization of eukaryotic cells

Eukaryotic cells are distinguished from prokaryotes by the presence of a membrane-bounded nucleus (1). The nuclear envelope (NE) demarcates the nucleus and separates the nuclear genomic material from the rest of the cell (2). The spatial separation between DNA replication, RNA synthesis in the nucleus from protein synthesis in the cytoplasm is a unique strategy to confer tight control on the essential cellular activities such as gene expression and signal transduction (3). This feature allows eukaryotic cells to maintain cellular homeostasis and rapidly respond to environmental changes such as stress. Furthermore, it enables a better control of the large amount of genetic information stored in the eukaryotic genome via segregation of the transcription and translation processes, which ultimately led to the development of higher organisms (4). Concomitantly, from the separation of nuclei and cytoplasm arises the need for bi-directional exchange of thousands of molecules between the two compartments. As such, nuclear proteins like histones, transcription factors have to reach their final destination in the nucleus. Conversely, the synthesis of transfer RNA (tRNA), messenger RNA (mRNA), and other RNAs occurs in the nucleus while their destination compartment is the cytoplasm (reviewed in 5).

Communication between the nucleus and cytoplasm occurs via nuclear pore complexes (NPCs), which are large protein assemblies embedded in the NE. NPCs are the only gates that mediate exchange of molecules between the nucleus and cytoplasm (6). Different mechanisms control the movement of molecules across the NE. Ions, small metabolites and proteins less than 20-30 KD can

diffuse freely through the aqueous channel of the NPCs, while macromolecules larger than 40 KD need an active transport system for translocation across the nuclear pore (reviewed in 5).

1.1 Nuclear envelope (NE)

The NE provides a physical barrier that isolates the nucleus from the cytoplasm thereby generating two distinct compartments. It is responsible for keeping the defined biochemical characteristics of each compartment (reviewed in 7).

Electron microscopy studies revealed the structural features of the NE. The key components of the NE are two nuclear membranes, the inner nuclear membrane (INM) and the outer nuclear membrane (ONM). The INM and ONM are fused together at the sites where NPCs span the NE. The two membranes of the NE are separated by the perinuclear space which forms the NE lumen (reviewed in 4). Extended from the ER lumen, the NE lumen is aqueous in nature and provides a milieu for the luminal domains of the integral membrane proteins that are anchored to the INM and nuclear pore membrane (Fig.1.1A) (reviewed in 8). The integral membrane proteins of the INM and nuclear pore membrane are implicated in maintaining the structural and functional organization of the chromatin and NPCs, respectively (reviewed in 9).

The ONM is characterized by the presence of many ribosomes and is joined with the membranes of the endoplasmic reticulum (ER). By contrast, the INM is ribosome free and supported from its inner face by a fibrous layer of proteins which constitutes the nuclear lamina (Fig. 1.1B) (reviewed in 4, 7-9). The nuclear

Figure 1.1

(A)

Structure of the nuclear envelope (NE)

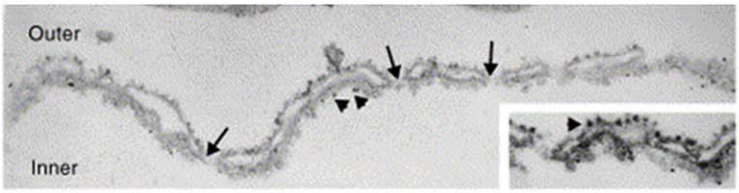

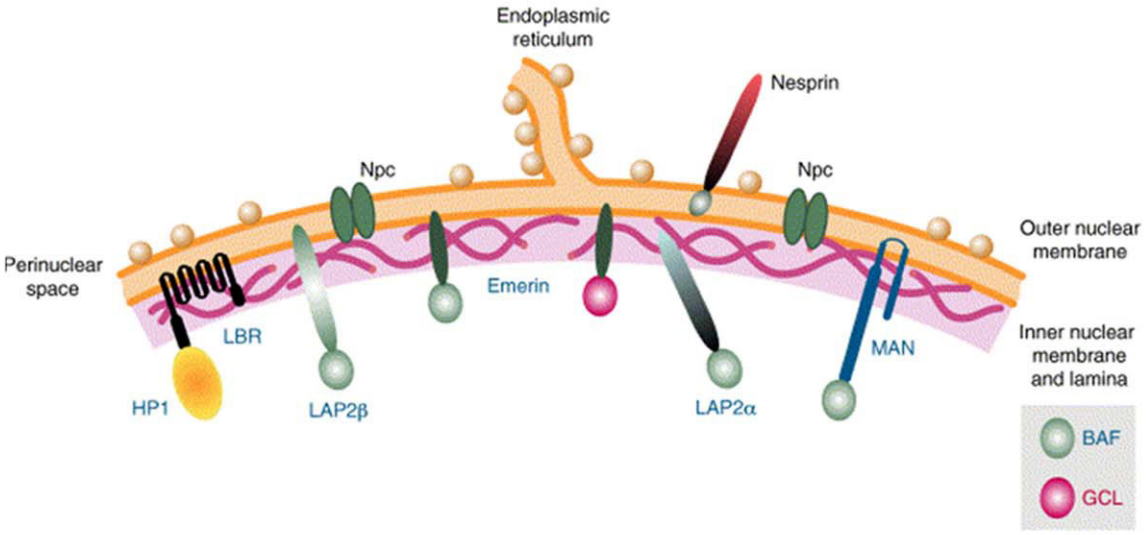

(B)

Nuclear lamins

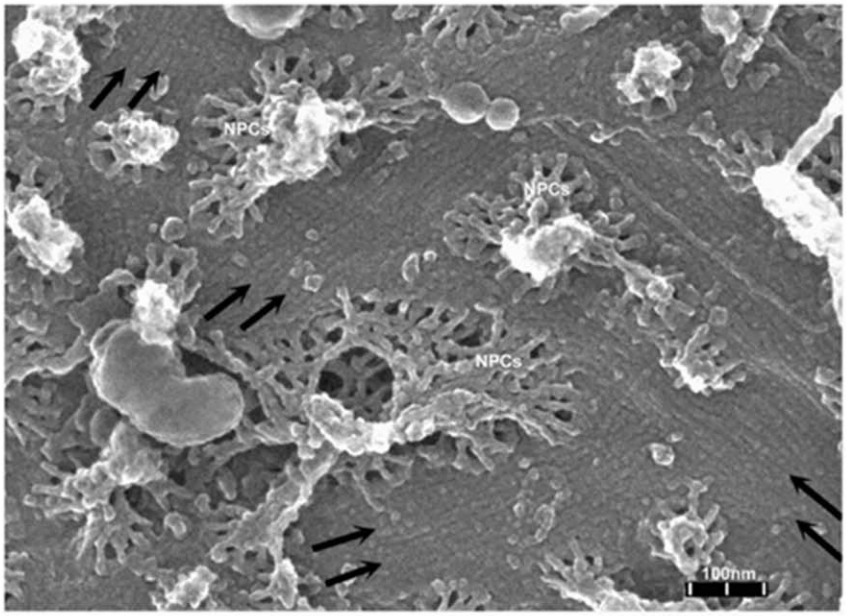

Figure 1.1 Organization of the nuclear envelope (NE)

(A) NEs of rat liver nuclei as they appear in the electron microscope image. The NE consists of two membranes; the inner nuclear membrane (INM) and the outer nuclear membrane (ONM) which are spanned by NPCs (indicated by black arrows). The nuclear lamina which associates with inner face of INM is stained by gold particles and indicated by arrowheads. The cartoon shows the structural organization of the NE, note that the ONM contains many ribosomes and is continuous with the membranes of the ER while the INM is ribosome free and supported from its inner face by the lamina. The INE and ONM are associated with a whole set of membrane proteins that mediate their interaction with actin cytoskeleton. **(B)** Electron micrograph of the nuclear side of NEs in *Xenopus* oocyte showing lamin filaments (building blocks of lamina) pointed by black arrows.

This Figure is modified from

1- **Mounkes L**, **Kozlov S**, **Burke B**, **Stewart CL**. The laminopathies: nuclear structure meets disease. *Curr. Opin. Genet. Dev.* 13(3):223-30*,* 2003.

2- **Goldberg MW**, **Fiserova J**, **Huttenlauch I**, **Stick R**. A new model for nuclear lamina organization. *Biochem. Soc. Trans.* 36(Pt 6):1339-43, 2008.

Figure 1.2

(A)

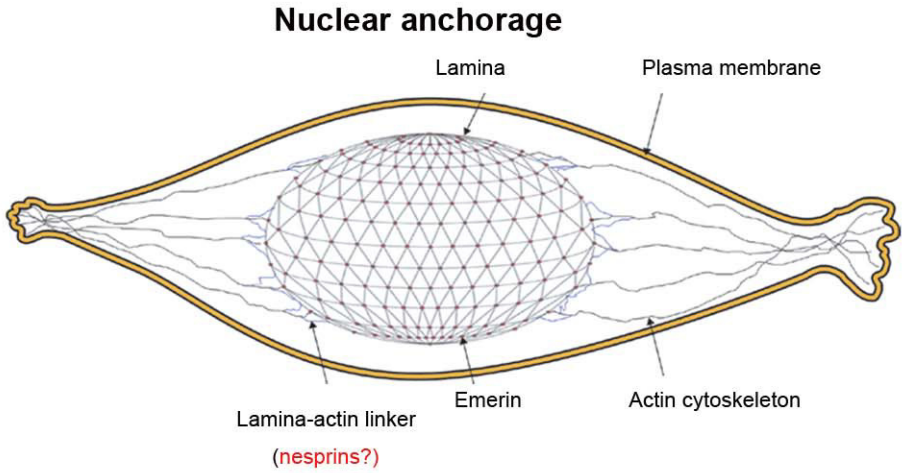

(B) KASH-domain proteins (nesprins) anchor the nucleus to F-actin

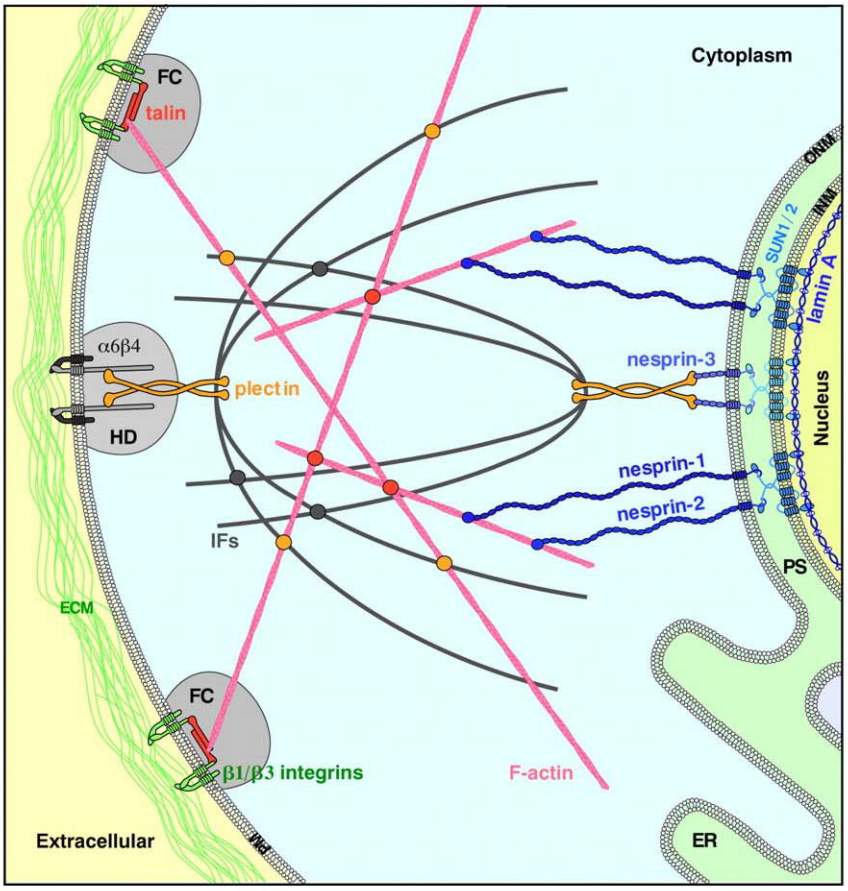

Figure 1.2 The NE mediates the nuclear anchorage

(A) The NE plays a key role in maintaining the correct spatial position of the cell nucleus by association with the actin cytoskeleton via distinct sets of NE proteins. **(B)** Two groups of membrane proteins mediate the association of the NE with F-actin, SUN- and KASH- domain proteins. The KASH-domain proteins like nesprins bind the NE through one end while they associate with actin cytoskeleton through the other end thereby providing nuclear anchors. KASH-domain proteins associate with the NE via binding to SUN-domain proteins, which are attached to the nuclear lamina.

This Figure is modified from

1- Wilhelmsen K, Ketema M, Truong H, and Sonnenberg A. KASH-domain proteins in nuclear migration, anchorage and other processes. *J Cell Sci* 119: 5021-5029, 2006.

2- Hutchison CJ, and Worman HJ. A-type lamins: guardians of the soma? *Nat Cell Biol*. 11: 1062-7, 2004.

lamina is composed of intermediate filament proteins called lamins. It provides attachment sites for chromatin at the nuclear margin and is considered to be the main framework for the NE structure (reviewed in 2, 4, 10 and 11).

Nuclear lamins are involved in different aspects of cellular functions. This includes, transcription, DNA replication and DNA repair as well as cell proliferation. Furthermore, there is a growing body of evidence that suggest a role for lamin A-binding proteins in viral infectivity. As such, phosphorylation-mediated lamin disassembly is a prerequisite step for the packing of viral nucleocapsids with INM; this association precedes the nucleocapsids fusion with ONM which is required for their exit out of the nucleus (11). Thus, the NE is of fundamental importance in maintaining the structural and functional organization of the eukaryotic nucleus. Not only does it provide the exclusive gates for nucleocytoplasmic transport; the NPCs, but it also helps to maintain the nuclear shape and integrity.

Another aspect of NE function is that it plays an essential role in nuclear anchorage and movement and therefore is responsible for maintaining the correct spatial position of the nucleus (Fig. 1.2A). This is mediated by a two families of membrane proteins that span the INM and ONM and known as SUN- and KASH-domain proteins, respectively. The KASH-domain proteins (for instance, nesprins) bind to the NE from one side (by association with INM-SUN domain proteins) while interact with different components of the cytoskeleton such as F-actin with the other end thereby providing nuclear anchors (Fig. 1.2B) (12).

Many human diseases have been attributed to mutations in one of the NE proteins. As such, mutations in the genes which encode lamin-A/C proteins or emerin may cause cardiac and skeletal myopathies such as Emery-Dreifuss Muscular Dystrophy (EDMD), as well as the premature aging disease know as Hutchinson-Gilford Progeria Syndrome (HGPS) (reviewed in 7, 11, and 13).

1.2 Nuclear pore complexes (NPCs)

NPCs are massive protein assemblies that penetrate the NE and provide aqueous channels that mediate the exchange of molecules between the nucleus and cytoplasm. They are the exclusive passageways through which proteins, RNAs and other substances may translocate across the NE (Fig. 1.3A) (14, 15). The average molecular mass of the NPC varies between different organisms and ranges from ~55-66 MDa in yeast to ~125 MDa in mammalian cells (16, 17). Several factors such as the cell size and proliferative activities determine the requirements for nuclear transport to be mediated by NPCs. Therefore the number of NPCs varies greatly with the complexity and the developmental stage of the organism. This is exemplified by the diverse numbers of NPCs found in yeast cell (~190 NPCs/nucleus) as compared to mammalian cell (~3000-5000 NPCs/nucleus), and mature *Xenopus* oocyte (5 x10^7 NPCs/nucleus) (5, 18, 19). Recent advances in proteomics have led to the characterization, at the molecular level, of the basic constituents of the NPCs. As such, proteomic analysis has defined the molecular components of the mammalian NPC as ~30 different proteins that are referred to collectively as nucleoporins or Nups (20).

Figure 1.3

(A) **Nuclear Pore Complexes (NPCs)**

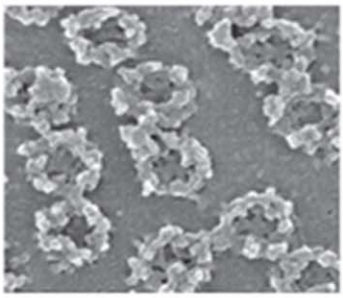

Cytoplasmic side

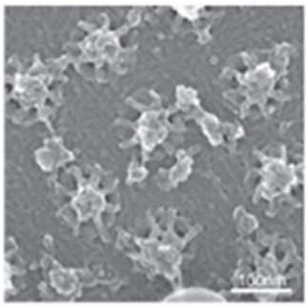

Nuclear side

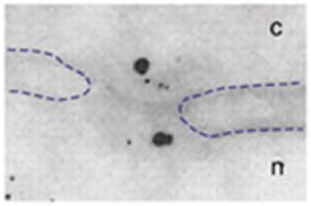

Bi-directional transport

(B) **Structure of the NPC**

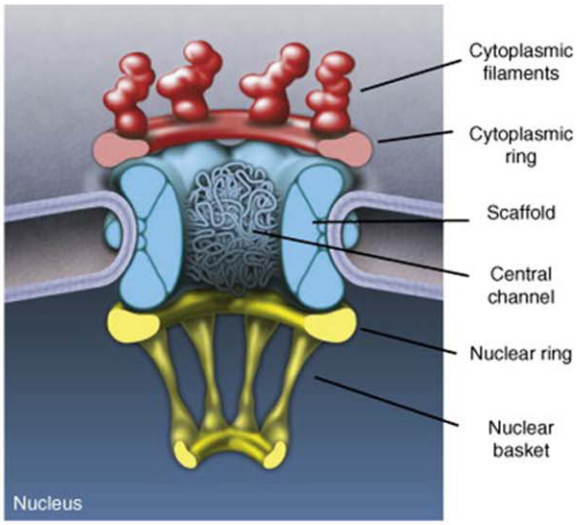

(C) **Nucleoporins; the building blocks of the NPC**

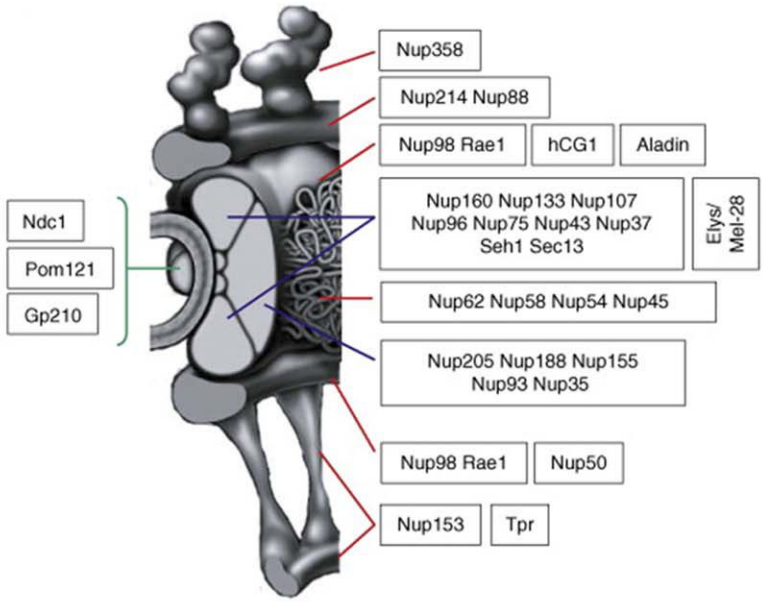

Figure 1.3 Nuclear Pore Complexes (NPCs)

(A) Cytoplasmic and nuclear views of the nuclear pore complexes (NPCs) of *Xenopus laevis* oocyte as shown by electron microscopy. Note that the nuclear side of the pore is characterized by the presence of the nuclear baskets. The ability of NPC to mediate bi-directional transport of protein and RNAs is demonstrated by monitoring the translocation of gold-labeled nucleoplasmin and tRNA using immune-electron microscopy. The nucleoplasmin-gold (large particle *nuclear*) and tRNA (small particle *cytoplasmic*) were initially injected into the cytoplasm and the nucleus of *Xenopus laevis* oocyte respectively. The translocation of both substrates occurs through the NPC. **(B)** Simplified model of the NPC. The central transport channel is surrounded by nuclear and cytoplasmic rings which contain the nuclear basket and cytoplasmic filaments respectively. **(C)** Nucleoporins (Nups) are the building blocks of the NPC. The different Nups organize into modules with distinct functions.

This Figure is modified from

1- **D'Angelo MA and Hetzer MW.** Structure, dynamics and function of nuclear pore complexes. *Trends in Cell Biology* 18: 456-466, 2008.

2- **Terry LJ, Shows EB, and Wente SR.** Crossing the nuclear envelope: hierarchical regulation of nucleocytoplasmic transport. *Science* 318: 1412-1416, 2007.

A proposed structural model depicts the NPC as a scaffold structure with eight-fold symmetry embedded in the NE perpendicularly to its plane. This structure comprises a central plug which is thought to contain the transport channel. The central plug is surrounded by eight spokes that are sandwiched by four coaxial rings, the inner spoke ring, the outer spoke ring, the cytoplasmic ring, and the nuclear ring. The cytoplasmic side of the NPC is characterized by the presence of eight cytoplasmic filaments attached to the cytoplasmic ring, whereas the nuclear side of the pore has filaments that extend from the nucleoplasmic ring and fuse together at their distal ends by a ring to form the nuclear basket (Fig. 1.3B) (21, reviewed in 22). This architecture is achieved and maintained by certain groups of nucleoporins that are organized to form subcomplexes which function as building blocks for the different structural components of the NPC. A combination of mass spectrometry and immunoelectron microscopy has generated a map of these subcomplexes and assigned them to the different subunits of the NPC as seen in cryo-EM studies. This revealed that Nup107-160 and Nup214-88 complexes are located at the central spoke ring and cytoplasmic ring respectively, whereas the nucleoporin Tpr is a main component of the nuclear basket filaments (Fig. 1.3C) (reviewed in 23).

A large group of nucleoporins is characterized by the presence of domains that contain multiple repeats of the amino acid sequence Phenylalanine-Glycine (FG), Glycine-Leucine-Phenylalanine-Glycine (GLFG) or Phenylalanine-X-Phenylalanine-Glycine (FxFG) (where x represents a spacer amino acid), which are referred to collectively as FG repeats. Several studies have demonstrated a key

role for these repeats in nuclear transport. As such, nuclear import pathways are sensitive to antibodies against FxFG repeats such as; the monoclonal antibody 414 (reviewed in 24). Inhibiting the RNA export by antibodies against Nup98 (a GLFG- containing nucleoporin) revealed that Nup98 is a key player in RNA export pathways (25). This indicates that the FG-containing nucleoporins have different functions in different transport pathways (reviewed in 24). Several FG-containing nucleoporins have asymmetric distribution to both sides of the pore. For instance, Nup358, and Nup214 are located at the cytoplasmic fibrils, whereas Tpr localization is restricted to the nuclear basket (26, 27, and reviewed in 28). Furthermore, a large number of FG-rich nucleoporins are residing mostly at the central transport channel of the NPC where the hydrophobic repeats constitute a selective permeability barrier that sieves out the macromolecules and prevents their translocation through the NPC. At the same time, the FG repeats mediate the interaction between soluble transport receptors and NPCs thereby facilitating the receptor-mediated transport of selected cargoes (reviewed in 29).

Despite the NPC being initially thought to be a static structure of defined composition, a new picture is now emerging that reveals the dynamic nature of the NPC. The dynamic organization of the NPC is manifested by changing its conformation or altering the nucleoporin position or association with the NPC. A prominent example is the conformational change of the NPC in response to nuclear transport activities (reviewed in 30). As such, structural analysis of NPCs in nuclei that are competent for nuclear import using cryoelectron tomography has revealed that NPCs which are actively transporting cargo adopt a different

conformation in which the positions of the central plug/transporter as well as the cytoplasmic filaments change as compared to cargo-free NPCs (31). For instance, the cytoplasmic fibrils of the NPCs which are extended in the absence of transport substrates but bend to approach the central gate of the nuclear pore when they are involved in cargo transport (reviewed in 30, 31).

Another factor that regulates the dynamic nature of the NPC is the transient association of mobile nucleoporins with the pore (reviewed in 30). Although the nucleoporins which function as *bona fide* structural components of the NPC, for instance, the Nup107-160 complex, are stably associated with the pore, other FG containing Nups that are involved in transport activities such as Nup153 and Nup50 are mobile and transiently associate with the NPC (32). The ability of certain nucleoporins to move across the pore seems to be necessary to perform the different tasks of nucleocytoplasmic transport such as delivering the cargo to the NPC and/or dissociation of the transport complex (33). Several observations substantiate this hypothesis, for instance, the FG repeat domains of Nup153 and Nup214 relocate according to the transport status of the NPC and their distribution appears to correlate with the substrate movement across the central channel of the pore. This is exemplified by the redistribution of the C-terminal FG domain of Nup214 to the nuclear side of the pore in response to microinjection of poly (A+) RNA into *Xenopus* oocyte nuclei (34, 35). Furthermore, Nup153 has been shown to shuttle between the nuclear and cytoplasmic sides of the NE and is believed to mediate the translocation of export complexes to the cytoplasm (36). Mobile nucleoporins may have roles in other cellular activities as well. A

prominent example is Nup98 which localizes to multiple subcellular compartments. The mobility of Nup98 depends on transcription and may help to direct newly transcribed RNAs to the pore (37).

Thus, as a vital component of the transport machinery, the nucleoporins play a crucial role in maintaining the cellular homeostasis under normal conditions, and mediating the cellular responses upon stress. Chapter 2 in my thesis will focus on analyzing the effect of oxidative stress on the localization as well as the functional integrity of nucleoporins that are involved in nuclear transport.

2. Transport between the nucleus and cytoplasm: passive diffusion versus facilitated (signal-mediated) transport

The aqueous channel of the NPC has an approximate diameter of ~ 9 nm and length of 40-50 nm (38, 39). It mediates transport of different molecules between the nucleus and cytoplasm via two different mechanisms; passive diffusion and facilitated transport (reviewed in 40). The transport mode depends on the size of the cargo and its ability to interact with the FG motifs of the nucleoporins that line the transport channel. As such, water, ions and small molecules which are less than ~ 5 nm radius, that do not interact with the FG repeats (i.e. inert molecules) can diffuse through the central channel of the pore (38, 41).

The passive diffusion does not rely on interactions between the cargo and FG-containing nucleoporins nor does it require metabolic energy (reviewed in 5, 38, and 41). The efficiency of this pathway decreases as the size of the molecule approaches the diameter of the central channel. Analyzing the size limits of the

diffusion channel using fluorescently labeled dextrans showed that molecules ≥ 40 KDa cannot pass through the channel (39). Thus, macromolecules that exceed the diameter of the central channel depend on other transport routes to translocate across the pore, the facilitated or carrier-mediated transport (42, 43).

In contrast to passive diffusion, carrier-mediated transport is an active process that needs energy and relies on the interaction between transport cargoes and nucleoporins. This interaction assists the translocation through the pore and is mediated by a large group of transport receptors known as karyopherins. The transport factors may act like "a boat that carry transport cargoes and slide over a surface of dense FG repeats" (44).

Members of the importin-ß family (also known as karyopherins) are the best characterized nuclear transporters. According to the direction of transport, they can be classified into two groups, importins and exportins. Importins mediate translocation of molecules from the cytoplasm to the nucleus, whereas exportins function in export from the nucleus to the cytoplasm. The directionality of the transport reaction is determined by different sets of signals that exist on the cargo to be translocated. For instance, nuclear proteins carry a nuclear localization signal (NLS); alternatively, proteins destined for export to the cytoplasm contain a nuclear export signal (NES). Importins and exportins recognize and bind the signal-containing cargoes either directly or via adapter molecules, then facilitate their translocation across the pore by their ability to interact with FG repeats that line the transport channel (reviewed in 45). This interaction can increase the functional diameter of the transport channel up to ~40 nm, thereby allowing for

translocation of large molecules (46). The carrier-mediated transport requires energy which is supplied at least in part, via GTP- hydrolysis by a small GTPase called Ran (reviewed in 47). Ran plays a key role in the formation of import and export complexes between the transport receptors and translocating molecules (Fig. 1.4) (reviewed in 48).

To mediate different rounds of import and export, the transport receptors need to be recycled between the nucleus and cytoplasm, different mechanisms ensure the fast movement and availability of transport receptors at both sides of the envelope (49) (see below). Recent data support a model with a single translocation channel that occupies the middle of the NPC and mediates passive diffusion as well as the signal-mediated transport (50). The facilitated transport mechanism explains the high translocation capacity of the NPC which is capable to afford a mass flow of 100 MDa/sec and a transport rate of 10^3 translocation reactions/sec (41). The different components of signal-mediated transport such as transport signals, soluble transport receptors are discussed in the following sections.

2.1 Nuclear localization signals (NLSs)

Nuclear localization signals (NLSs) are permanent signals that can be present anywhere in the protein, and target it to the nucleus. In contrast to many other targeting signals for example secretory proteins signals (51), the NLS is not cleaved after the termination of the import reaction. The nuclear localization sequence for the nuclear protein nucleoplasmin was first described by *Dingwall et al.* (43). Their work revealed that a polypeptide domain in the tail structure of

Figure 1.4

Carrier-mediated transport

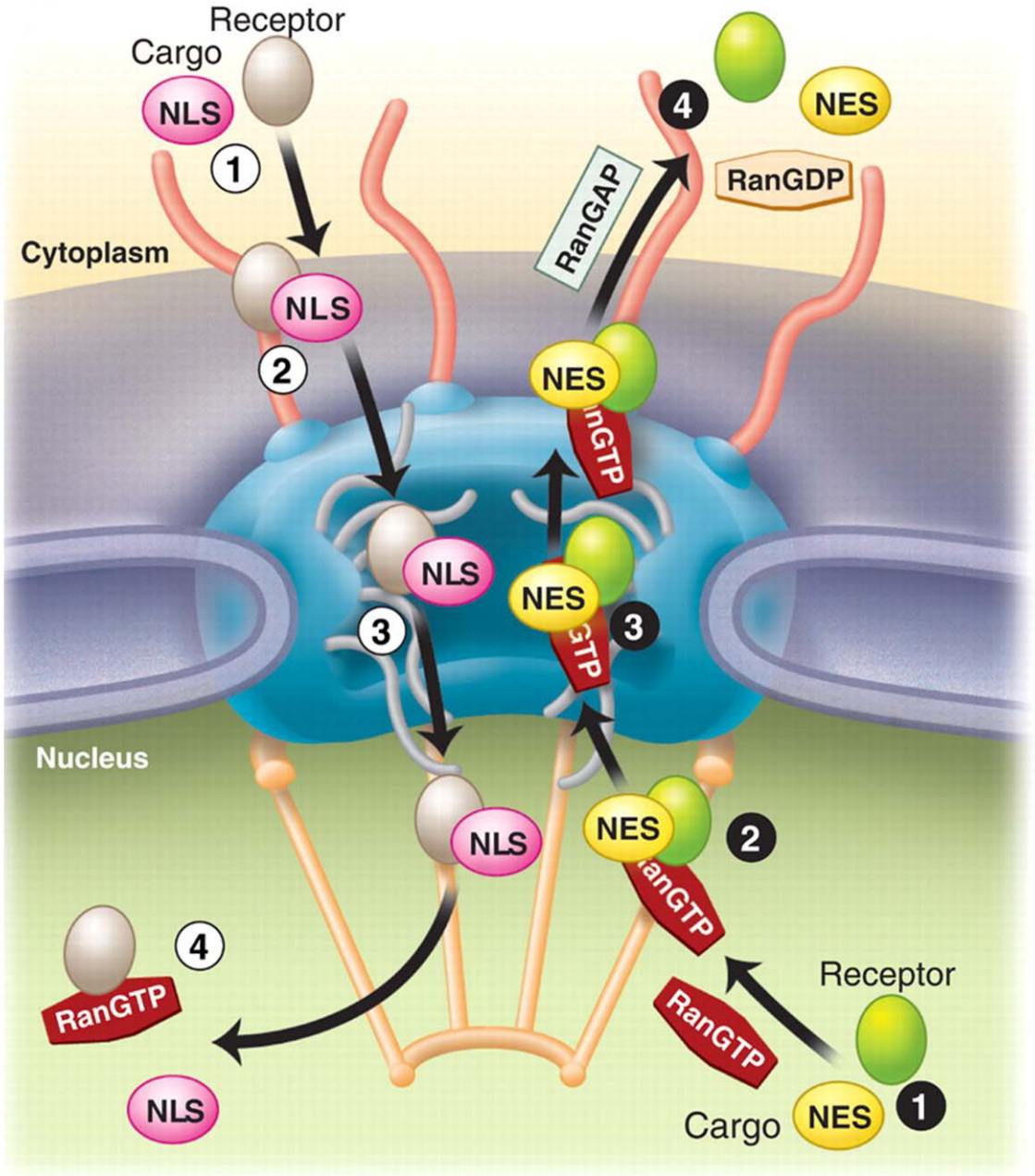

Figure 1.4 Carrier-mediated nucleocytoplasmic transport

Carrier-mediated transport is a multistep process that depends on soluble transport receptors and requires energy. For import, the transport receptor binds to the NLS-bearing cargo in the cytoplasm to form an import complex which then docks at the cytoplasmic fibril of the NPC. Translocation through the NPC occurs by interaction of the transport receptor with the nucleoporins of the central gated channel of the NPC. Export occurs by the same mechanism, yet in the opposite direction. Note that the energy required for the transport reaction is supplied by RanGTP which plays a key role in formation and disassembly of transport complexes.

This Figure is modified from

1- Terry LJ, Shows EB, and Wente SR. Crossing the nuclear envelope: hierarchical regulation of nucleocytoplasmic transport. *Science* 318: 1412-1416, 2007.

nucleoplasmin is necessary for its targeting to the nucleus (43). Another type of NLS that mediates nuclear localization is present in the simian virus 40 large T-antigen (SV40 T-ag). SV40T-ag-NLS represents the simplest form of nuclear localization signals and consists of a single cluster of basic amino acids (P**KKKRK**V[132]) (52, 53). The SV40-NLS is classified as a monopartite signal.

Unlike monopartite signals the nucleoplasmin NLS contains two clusters of basic amino acids that are separated by a 10-amino acid linker region and therefore classified as bipartite signal (**KR**PAATKKAGQA**KKKK**[171)] (54). The mono- and bipartite classes of positively charged NLS are referred to collectively as classical NLS (cNLS). Some NLSs are recognized and bound directly by importin-ß, while other NLSs bind to importin-ß via the adapter molecule importin-α, which forms a heterodimeric import receptor with importin-ß (reviewed in 55). The prevalence of lysines or arginines in the NLS is the limiting factor that determines the mode of interaction with importin-ß. As such, arginine–rich NLSs bind directly to importin-ß (56, 57). A prominent example, Rex protein of human T-cell leukemia virus type 1 contains an arginine-rich NLS that binds directly to importin-ß. Conversely, a lysine-rich NLS favors the importin-α mediated interaction with importin-ß (55-57). The ability of arginine-rich NLSs to directly interact with importin-ß can be explained by its structural similarity to the arginine-rich importin-ß binding (IBB) domain of the adapter molecule importin-α (reviewed in 55).

2.1.1 Different classes of NLS

Although cNLSs mediate nuclear import of a large number of nuclear proteins, the presence of a sequence that fits the consensus for a cNLS does not necessarily indicate a function in nuclear import. As such, many plasma membrane proteins contain motifs that resemble a cNLS (58). Furthermore, in many nuclear proteins a potential cNLS is non-functional, and the nuclear import of these proteins relies on other types of NLS that are structurally different (reviewed in 55). This is exemplified by the hnRNP A1 NLS which consists of 38 amino acids and known as M9 sequence. The import of hnRNP A1 occurs via a distinct transport pathway that relies on transportin-1 (an importin-ß like receptor) to recognize and bind the M9 sequence (59). Another example for a non-classical NLS is the nuclear targeting sequence identified in the homeodomain of the yeast repressor α2 (Matα2) (60). This NLS contains polar or charged residues that are separated by non-polar linkers (60, reviewed in 61). A different class of NLS is represented by the one identified for c-myc protein. The c-myc NLS is characterized by a central basic amino acids cluster which has upstream residues of proline and aspartic acid (PAA) and followed by a dipeptide residue (LD) (PAAKRVKLD). The position of proline and aspartic acid residue has shown to be critical for the nuclear targeting function of c-myc NLS (62, 63).

2.1.2 Regulation of importin-α/cNLS recognition modulates nuclea transport

The recognition and binding of the nuclear targeting sequence by transport receptors is the first step in the transport reaction. This step is of fundamental importance as it impinges on the fate of the transport process and thus can be

targeted by different cellular strategies that aim to modulate nuclear transport. Different transport pathways are regulated *in vivo* by modulating the transport receptor-signal interaction. This regulation occurs by several mechanisms (reviewed in 61). For instance, changing the composition of the cellular pool of importins by differential expression of certain importin gene, may favor the import of certain proteins over the others. This depends primarily on which NLSs are recognized by the pool (reviewed in 61, and 64).

Another level of regulation is realized by competition between several proteins with NLSs for binding to the same transport receptor. In this situation, the affinity between the transport receptor and the targeting signal will be the limiting factor that determines which protein to be imported. A prominent example is the intense demand for importin-β1 to mediate the import of NLS-containing proteins either directely or through importin-α. The same principle applies if the same NLS can be recognized and bound by several transport receptors (Reviewed in 61).

Furthermore, the interaction between targeting signals and transport receptors can be regulated by phosphorylation. This is exemplified by the import of NLS-containing *Drosophila morphogen* Dorsal which is mediated by heterodimeric importin-α/ß receptor. Phosphorylation of Dorsal by cAMP-dependent protein kinase facilitates its import by augmenting the interaction affinity between the receptor and NLS up to seven-fold (65). Modifying the target sequence by phosphorylation does not always enhance its recognition by transport factors. As such, Crm1-dependent export of cyclin B1 is sensitive to phosphorylation by cdk/MAPK which interferes with Crm1-NES association (reviewed in 61, 66).

Another strategy that controls the recognition of a transport signal relies on masking of the targeting sequence by binding to another molecule (reviewed in 61). As such, binding of I-κBα protein to the NLS of the NF-κB p65 subunit masks the NLS and thereby inhibits the nuclear import of the protein. Sequential events of phosphorylation and proteolytic degradation remove the masking components, thus putting a tight control on NF-κB nuclear import (67).

Regulating the transport receptor-signal interaction via different ways indicates that multiple mechanisms are likely to control the cNLS dependent import.

2.2 Nuclear Export Signal (NES)

The nuclear export signal (NES) is a short sequence (~9-14 amino acids) which contains hydrophobic residues. The NES targets a cargo to be exported from the nucleus to the cytoplasm (68). This signal can be found in HIV-Rev protein and the protein kinase A (PKA) inhibitor (68, 69). HIV-Rev NES consists of a cluster of hydrophobic leucine-rich sequence and identified as (**LPPLERLTL**) (69). The export of NES-containing cargoes is dependent on Crm1, the best characterized member of a group of importin-ß transport receptors referred to collectively as exportins (5, 70). To date, up to 80 proteins have been reported to contain an NES that is recognized by Crm1 (71).

2.3 Nuclear carriers

Nuclear carriers, represent a large group of soluble transport receptors that are involved in import (referred as importins) and export (referred as exportins) of macromolecules in and out of the nucleus (reviewed in 72). Some transport

receptors such as mammalian importin 13 and yeast Msn5 have a dual role and can function as both importins and exportins (reviewed in 73). The majority of transport receptors belong to the evolutionary conserved importin-ß family which comprises ~ 22 members in higher eukaryotes and 14 in yeast (74 and reviewed in 75). The importin-ß family members have molecular mass of ~ 90-130 KDa (74 and references therein). Their function as transport factors is based on their ability to interact with different components of the transport machinery such as RanGTP, nucleoporins, and different cargoes (reviewed in 5, 75).

2.4 Importins

Importins bind their substrate in the cytoplasm, translocate across the NE, and then release their cargoes in the nuclear compartment. Importin-ß1, also known as karyopherin-ß1 in higher eukaryotes or Kap95 in yeast, is the best characterized member of the importins subfamily (reviewed in 5). At the molecular level, the structural components of importin-ß1 are tandem arrays of 19 helical motifs, known as HEAT repeats (76). Each of these repeats is made of approximately 40 residues and consists of two ß helices A and B that are spaced by a turn to form a hairpin-like helical structure. The 19 repeats are connected to each other by linker regions and spatially organize into an S-shaped superhelix that represents the full length importin-ß1. The S-shaped conformation of importin-β switches to a snail-shaped conformation upon binding to importin-α (Fig. 1.5A, B) (reviewed in 75, 76, and 77). Crystal structure analysis of HEAT repeats allocated different functions to different repeat groups. As such, interaction with RanGTP depends on HEAT repeats 1-8, whereas the repeat groups 4-8 and 7-19 play a key role in

mediating binding of importin-ß1 to the importin-ß1-binding (IBB) domain of importin-α and FxFG motifs at the NPC, respectively (reviewed in 75, 76, 78, 79 and 80). Another group of HEAT repeats located at the N-terminal part (1-485) is required to interact with parathyroid hormone-related proteins PTHrP (81). Crystallography studies on importin-ß1 alone or in complex with other binding partners such as RanGTP, importin-α, or import cargoes revealed that it undergoes conformational changes upon interaction with other molecules (Fig. 1.5C) (76-78). For instance, import of dimeric molecules such as sterol regulatory element-binding protein 2 (SREBP-2), needs a more open conformation that gives importin-ß1 a pseudo-two fold symmetry to enable cargo binding (82). Other conformational changes are thought to facilitate the formation or disassembly of import complexes as well as the interaction with different nucleoporins.

Mapping the functional domains in importin-ß1 revealed the presence of a RanGTP binding domain at the N-terminus, and a cargo binding domain at the C-terminus. Another nucleoporin binding domain has been located at the amino-terminal/central region at residues 152-352 (Fig. 1.5D) (75, 78 and 79). The ability to undergo different conformational changes together with the presence of multiple binding sites for the different cargoes as well as components of the transport machinery, are the key features that underlie the structural flexibility of the molecule and allow importin-ß1 to transport a large diversity of import substrates (reviewed in 73).

Importin-ß1 can bind to its import substrate either directly or through adaptor molecules. Importin-α is the best characterized adaptor molecule for importin-ß1,

Figure 1.5

(A)

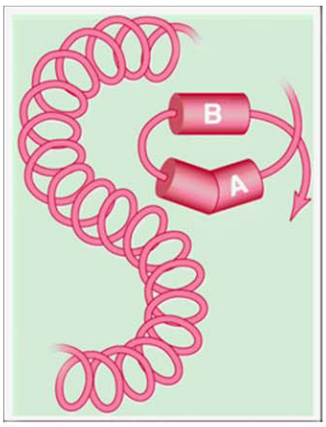

S-shaped superhelix

(B)

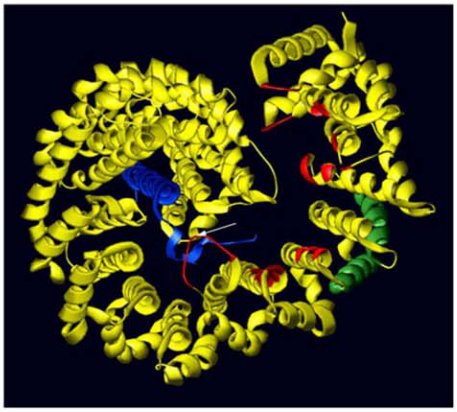

Snail-shaped importin-β

(C) Importin-β adopts different conformation upon binding to various cargoes

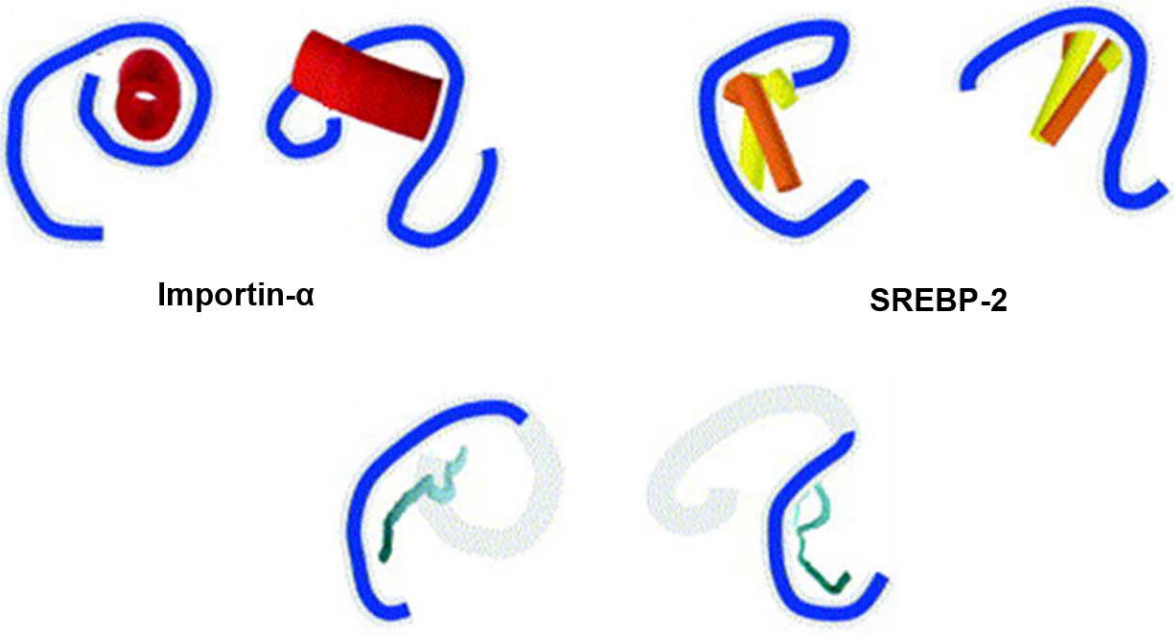

Importin-α

SREBP-2

PTHrP NLS

(D) The functional domains of importin-β

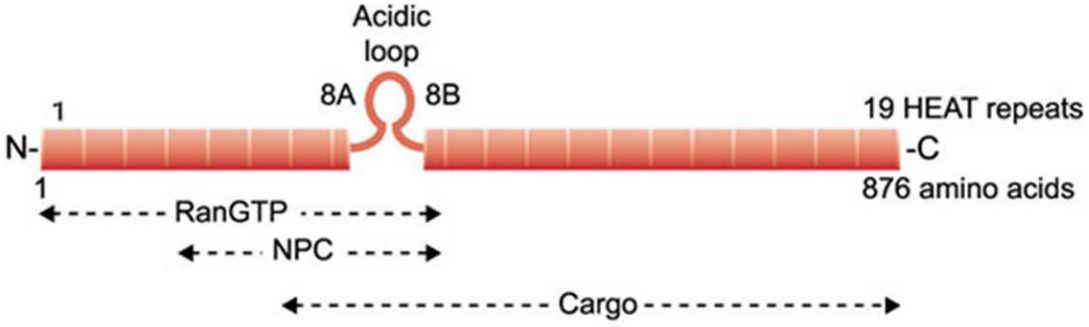

Figure 1.5 Structure of importin-β

(A) The cartoon shows the structure of importin-β as S-shaped superhelics made of 19-tandem HEAT repeats, the inset reveals that each repeat contains 2 α-helices (A, B) that are spaced by a turn. **(B)** The S-shaped conformation of importin-β switches to a snail-shaped conformation upon binding to importin-α. **(C)** Importin-β adopts different conformations upon binding to different cargoes. The structure of importin-β in complex with importin-α, PTHrP and SREBP-2 is depicted. Note that in contrast to its closed snail shaped conformation upon binding to importin-α, importin-β has a more open conformation when it binds to (SREBP-2). See text for details. **(D)** The functional domains of importin-β. The RanGTP binding domain is located at the N-terminal end, whereas the cargo binding domain is at the C-terminal end.

This Figure is modified from

1- **Strom AC and Weis K.** Importin-β-like nuclear transport receptors. *Genome Biology* 2: 3008.1 - 3008.9, 2001.

2- **Mosammaparast N and Pemberton LF.** Karyopherins: from nuclear-transport mediators to nuclear-function regulators. *Trends in Cell Biology* 14: 547-556, 2004.

3- **Conti E, Müller CW, and Stewart M.** Karyopherin flexibility in nucleocytoplasmic transport. *Current Opinion in Structural Biology* 16: 237-244, 2006.

it interacts with cNLS containing cargoes (83) (see below). Other proteins such as Snurportein1 and XRIPα can function as adaptors for importin-ß1 as well (reviewed in 75, 84, and 85). Snurportein1 has an importin-ß1 binding domain in its N-terminal portion and an m_3G-cap binding domain in the C-terminal domain. It mediates the importin-ß1 dependent import of m_3G-capped small nuclear ribonucleoproteins snRNPs (84). XRIPα is another adaptor protein that links importin-ß1 to its import substrate replication protein A (RPA) in *Xenopus* eggs (85). In addition to adaptor-dependent transport, many cargoes are imported via direct binding to importin-ß1. Examples for such cargoes include PTHrP, T-cell protein tyrosine phosphatase, HIV TAT and Rev proteins, ribosomal proteins L23a, S7 and cyclin B1 (reviewed in 75, 86).

The intracellular distribution of importin-ß1 is crucial for its function. Under normal growth conditions, importin-ß1 associates with nuclei where it accumulates at the NE. In addition, a considerable amount can also be detected in the cytoplasm. Several forms of stress have been shown to relocate importin-ß1. As such severe oxidative stress confines the transport receptor to the nuclear compartment and diminishes its association with the NE (87).

Importin-ß like receptors associate with multiple components of transport machinery, these interactions can be either simultaneous or mutually exclusive. As such, importin-ß1 binds the nucleoporins and cargo at the same time to facilitate its passage through the NPC. By contrast, binding of RanGTP and substrate to importin-ß1 is mutually exclusive, which provides the key mechanism for the dissociation of import complexes (88).

2.5 Exportins

Like importins exportins mediate the translocation of many molecules across the NE although in the opposite direction, i.e. from the nucleus to cytoplasm. Exportins bind their cargoes in the nucleoplasm where they form export complexes which are translocated across the NE, then dissociate on the cytoplasmic side of the NPC (89). They play a fundamental role in the export of numerous molecules; this includes shuttling proteins, signalling proteins, transcription factors, tRNA as well as the transport receptor importin-α which relies on the exporter CAS to be recycled back to the cytoplasm (89, and reviewed in 90). Furthermore, proteins which are confined to the cytoplasm like translation initiation and elongation factors rely on nuclear exporters such as Crm1 and Exp5 to be excluded from the nucleus (91). In addition to protein export, some exportins function in the export of specific classes of RNA. This is exemplified by exportin-t which is the nuclear exporter of t-RNA (92).

Crm1 also known as Exportin1 or Xpo1p in yeast is the best characterized importin-ß-like export receptor. It recognizes and binds leucine-rich NESs and translocates its cargoes from the nucleus to the cytoplasm (93). Among the Crm1 dependent export substrates are protein kinase inhibitor α (PKIα), cyclin B1, and the transcription factor NF-AT4 (reviewed in 75). Furthermore, the export of 40S and 60S ribosomal subunits is mediated via Crm1 dependent route (reviewed in 94). In addition the yeast homolog Xpo1p plays a key role in the export of yeast heat shock protein Ssb1p (reviewed in 75).

The interaction between Crm1 and its export substrate is modulated by different factors. As such, RanGTP and RanBP3 promote the association between Crm1 and its export cargoes (93, 95), whereas RanGTP hydrolysis stimulates the dissociation of export complexes (70, 93). Crm1 dependent export of NES-containing proteins can be inhibited by the cytotoxin leptomycin-B (LMB) which covalently modifies Crm1, thereby preventing the formation of export complex (93). The affinity between Crm1 and an NES is weaker as compared to the binding of other exportins like, CAS, Exp-t and Exp-4, to their export cargoes. This is thought to facilitate the efficient release of Crm1-export complex from the NPC (90). Another important export receptor that belongs to importin-ß family is the cellular apoptosis susceptibility factor (CAS) or Cse1p in yeast. The essential function of CAS is to export the adaptor importin-α to the cytoplasm once import complexes have been dissociated in the nucleus. Thus, CAS plays a crucial role in nuclear transport as it ensures the efficient recycling of importin-α to cytoplasm thus enabling it to mediate multiple rounds of import (96).

2.6 Importin-α

Importin-α is a soluble import receptor that recognizes and binds cNLS bearing cargoes and mediates their interaction with importin-ß. Thus, it works as an adaptor molecule that bridges importin-ß to its import substrate (reviewed in 5). The crystal structure of importin-α revealed two characteristic domains, importin-ß binding (IBB) domain and a cNLS binding domain in the shape of a groove (reviewed in 97). The cNLS binding domain of importin-α consists of ten tandem armadillo (ARM) repeats that are arranged into a superhelical structure

with a groove that serves as cNLS binding pocket (reviewed in 97, 98) (Fig. 1.6A). Two cNLS interacting sites were mapped on the importin-α molecule. These sites are located at the residues (121-247) and (331-417) which correspond to the ARM repeats 2-4 and 7-9 respectively (Fig. 1.6B) (99). Crystallographic analysis revealed that importin-α binds to a wide range of cNLS types for instance the monopartite and bipartite classical NLSs albeit with distinctive manners (rev in 98, 100). As such, the monopartite NLS occupies only one binding site, whereas the bipartite signal binds to the two binding sites of the NLS binding domain (100, 101).

Different factors determine the recognition of a cNLS by importin-α, these include hydrogen bonding, electrostatic and hydrophobic interactions between the positively charged basic motif of the cNLS and ARM repeats of importin-α (98, 100).

The IBB is a flexible domain located in the N-terminal region of importin-α; the main function of this domain is to mediate the interaction with importin-ß (Fig. 1.6D). The IBB domain contains a specific sequence that mimics the cNLS and overlaps with the importin-ß binding motif (102). Crystallographic analysis of the mouse importin-α revealed that this internal NLS motif binds to the NLS binding domain of importin-α and thereby inhibits its binding to an external cNLS. This finding suggested an autoinhibitory model, where IBB modulates the interaction of importin-α with its import substrates (103, 104). According to this model, when importin-α is free, i.e. not bound to importin-ß, the intramolecular binding between the internal cNLS-like signal and NLS binding sites reduces the

Figure 1.6

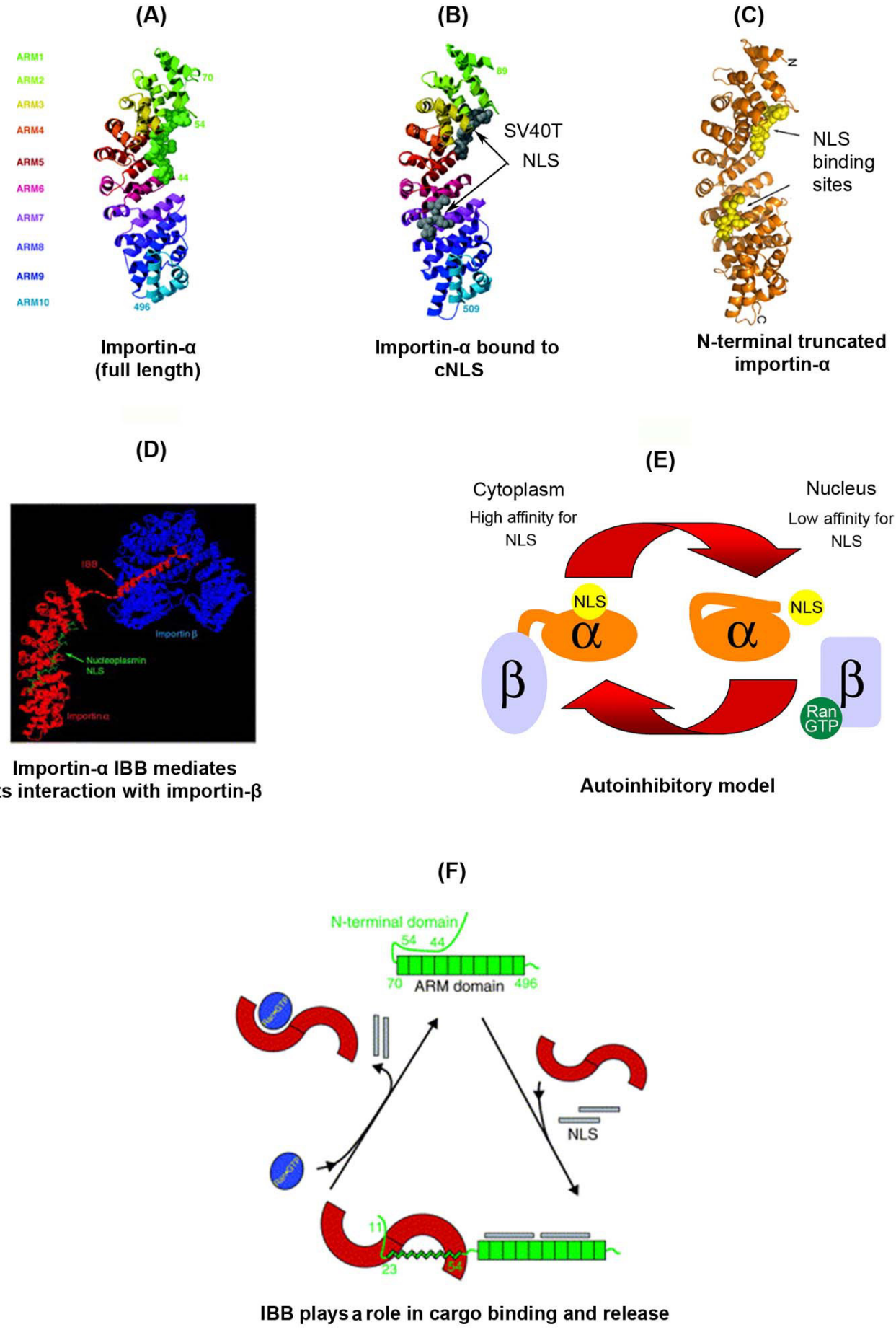
(A)
ARM1
ARM2
ARM3
ARM4
ARM5
ARM6
ARM7
ARM8
ARM9
ARM10
70
54
44
496
Importin-α
(full length)
(B)
89
SV40T
NLS
509
Importin-α bound to
cNLS
(C)
N
NLS
binding
sites
C
N-terminal truncated
importin-α
(D)
IBB
Importin β
Nucleoplasmin
NLS
Importin α
Importin-α IBB mediates
its interaction with importin-β
(E)
Cytoplasm
High affinity for
NLS
Nucleus
Low affinity for
NLS
NLS
α
NLS
α
β
β
Ran
GTP
Autoinhibitory model
(F)
N-terminal domain
54
44
70
ARM domain
496
NLS
11
23
54
IBB plays a role in cargo binding and release

Figure 1.6 Structural and functional organization of importin-α

(A) Schematic diagram shows Mouse full-length importin-α with the autoinhibitory domain (green) occupies the NLS binding site. Note that the ten tandem armadillo (ARM) repeats which constitute the building blocks of importin-α are depicted. **(B)** NLS binding sites in N-terminally truncated importin-α molecule. **(C)** N-terminally truncated yeast importin-α bound to SV40 NLS. **(D)** Importin-α interacts with importin-β via the importin-β binding domain IBB, which is located at the N-terminal region. **(E)** The autoinhibitory model explains how IBB modulates the interaction of importin-α with its substrates. **(F)** The autoinhibitory function of the IBB is required for cargo binding and release.

This Figure is modified from

1- **Chook Y and Blobel G.** Karyopherins and nuclear import. *Current Opinion in Structural Biology* 11: 703-715, 2001.

2- **Goldfarb DS, Corbett AH, Mason DA, Harreman MT, and Adam SA.** Importin alpha: a multipurpose nuclear-transport receptor. *Trends in Cell Biology* 14: 505-514, 2004.

3- **Lange A, Mills RE, Lange CJ, Stewart M, Devine SE, Corbett AH.** Classical nuclear localization signals: definition, function, and interaction with importin alpha. *J Biol Chem.* 282(8):5101-5, 2007.

affinity of importin-α to import substrates. However, upon interaction with importin-β, the IBB dissociates from the NLS binding domain in order to bind importin-β. This frees the NLS binding site of importin-α and restores its ability to bind an external cNLS (Fig. 1.6E) (reviewed in 97, 98, 103, and 104). The model is supported by measuring the binding of full length as well as N-terminally truncated importin-α (Fig. 1.6C) to cNLS substrates. This work revealed that deleting the autoinhibitory domain of importin-α leads to a remarkable increase in its affinity to NLS-containing cargoes. Whereas, binding of the wild type importin-α (which contain the autoinhibitory domain) to its import substrate is strictly dependent on the presence of importin-β (104). The autoinhibitory function of IBB appears to be necessary for cargo release in the nucleus. As such, the liberation of importin-β from the import complex (stimulated by high RanGTP in the nucleus) renders the IBB free, which then retains its autoinhibitory effect and subsequently competes with the import cargo for binding to importin-α. Consequently, the nuclear cargo dissociates from the carrier and is released into the nucleoplasm (Fig. 1.6 E, F) (reviewed in 98).

The dissociation of import substrate from importin-α is further facilitated by interaction with Nup50 (also known as Nup2p in yeast). Nup50 resides in the nuclear interior and interacts with importin-α at sites that overlap with NLS binding sites. This interaction occurs after the dissociation of importin-ß from the import complex as it requires a free IBB. It was proposed that the interaction with Nup50 may accelerate the termination of the import reaction by enhancing cargo release in the nucleus (105). Upon completion of the import process, the transport

receptors have to be recycled to the cytoplasm. The export of importin-α is mediated by CAS and requires RanGTP (96).

Higher eukaryotes contain six different importin-α isoforms that are grouped into three categories (reviewed in 97). Beside their vital role in nucleocytoplasmic transport, importin-α isoforms have other distinct functions. For instance; importin-α2 and 3 are of fundamental importance for the reproduction and development of *Drosophila melanogaster.* As such, a mutation in *Drosophila* gene that encodes importin-α2 interferes with essential reproductive processes such as gametogenesis, and oogenesis which ultimately leads to the development of sterile females (reviewed in 97). The overlap in transport functions between the different importin-α isoforms adds to the complexity of nucleocytoplasmic transport.

2.7 Ran, Ran regulators and RanGTPase cycle

With predominant nuclear localization, the small GTPase Ran is a 25 kDa protein that shares sequence homology with members of the Ras superfamily. Despite its preferential localization in the nucleus, a considerable portion of Ran is also found in the cytoplasm (106). According to the nucleotide bound state, cellular Ran exists in two forms, RanGDP and RanGTP. Alternating between these two nucleotide-bound states requires GTP hydrolysis and guanine nucleotide exchange (reviewed in 5).

Initially, several data proposed that Ran is implicated in nuclear transport. As such, *in vitro* analysis of nuclear import using digitonin-permeabilized cells

Figure 1.7

(A) **Ran regulates the formation and disassembly of transport complex**

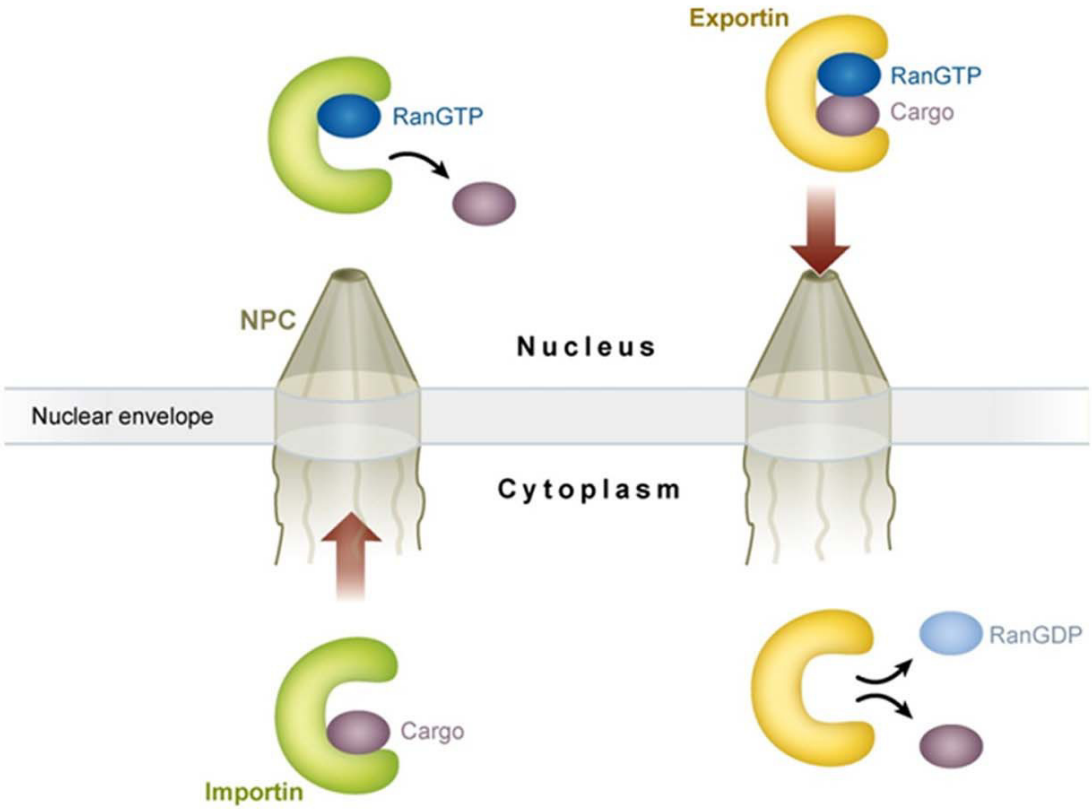

(B)

The Ran GTPase cycle

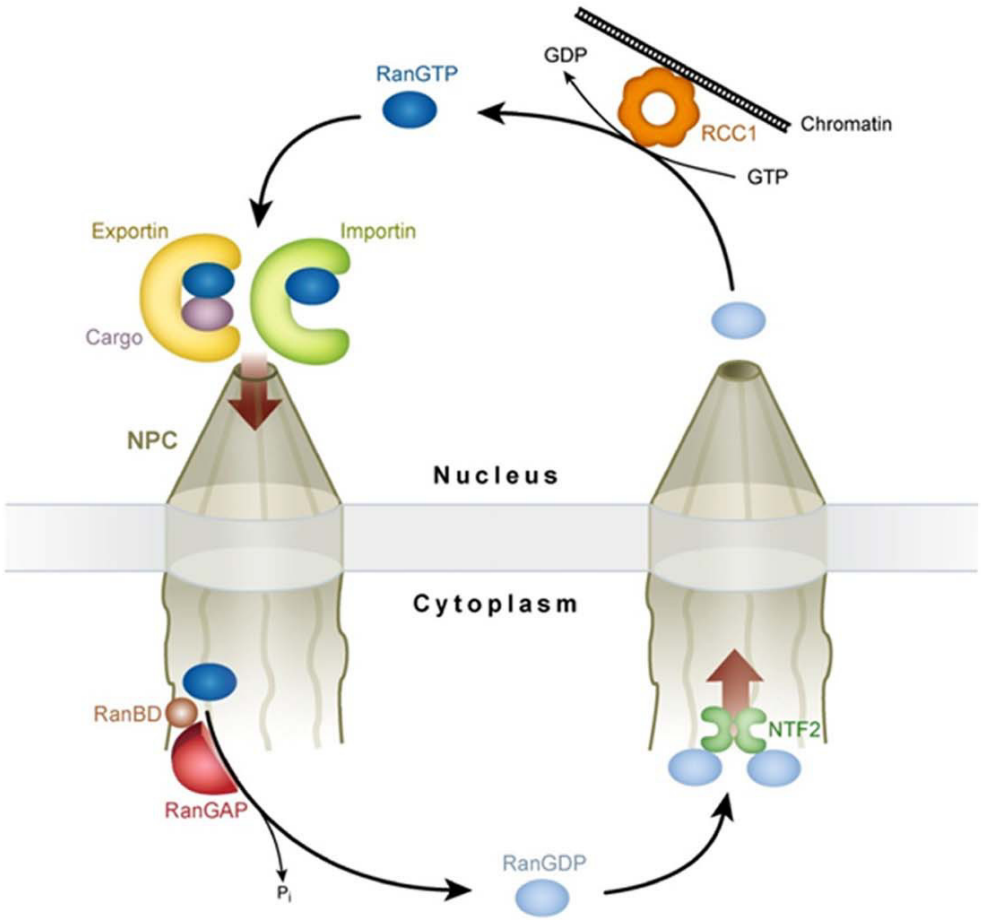

Figure 1.7 Ran function and Ran GTPase cycle

(A) Ran regulates the formation and disassembly of transport complex. The absence of RanGTP from the cytoplasm allows the formation of import complexes, while the high concentration of RanGTP in the nucleus favours the dissociation of transport receptors from import complexes and cargo release in the nucleus. The opposite scenario occurs for export. **(B)** RanGTPase cycle. Ran alternates between GTP and GDP bound states with the assistance of a set of Ran regulators. RanGAP generates RanGDP in the cytoplasm by stimulating GTP hydrolysis, while RanGEF (RCC1) converts RanGDP to RanGTP by stimulating nucleotide exchange in the nucleus. The import of RanGDP into the nucleus is mediated by NTF2.

This Figure is modified from

1- **Cook A, Bono F, Jinek M, Conti E.** Structural biology of nucleocytoplasmic transport. *Annu Rev Biochem.* 76:647-71, 2007

revealed that it requires Ran-dependent GTP hydrolysis (107, 108). Currently, the pivotal role of Ran and its regulators in nuclear transport is well established.

Ran orchestrates the nucleocytoplasmic transport by regulating substrate binding and release from the transport carrier in the origin and destination compartments, respectively. This is achieved by generating a RanGTP gradient across the NE with RanGTP localized mostly in the nucleus, while RanGDP is confined to the cytoplasm (reviewed in 5, 45, and 109). The Ran gradient model explains how Ran confers the directionality of the transport reaction. As such, the transport receptors do not bind RanGDP while they bind RanGTP with high affinity (110). Therefore, in the absence of RanGTP in the cytoplasm, the formation of import complexes (the first step in nuclear import) can take place. Conversely, binding of RanGTP to the transport receptor in the nucleus, initiates a sequence of events which ultimately lead to the dissociation of the import complex and cargo release in the nucleoplasm (111). The opposite scenario emerges for the export reaction, as the RanGTP-enriched milieu in the nuclear compartment permits the assembly of ternary export complex between the transport receptor, cargo, and RanGTP which then translocate together to the cytoplasm (Fig. 1.7A). Furthermore, the empty carriers are recycled back to the cytoplasm in complex with RanGTP after termination of the import reaction (112).

Given the low intrinsic GTPase activity as well as nucleotide exchange rate of Ran (reviewed in 106), the RanGTP gradient is expected to collapse after several rounds of transport reactions due to the continuous export of RanGTP. However,

this is not the case as the Ran cellular gradient is maintained by the action of a whole set of Ran regulatory proteins that function to stimulate the GTPase activity, guanine nucleotide exchange rate as well as Ran import (reviewed in 109, 113). These regulatory factors are distributed asymmetrically on both sides of the NE according to the required Ran nucleotide-bound state for each compartment (114). As such, the RanGTPase activating protein (RanGAP1) and Ran-binding protein (RanBP1), which stimulate GTP-hydrolysis by Ran are localized exclusively in the cytoplasm, thereby ensuring constant depletion of cytoplasmic RanGTP and maintaining high levels of RanGDP in the cytoplasm (reviewed in 5, 45, 109). RanGAP1 accelerates GTP- hydrolysis by Ran up to $\sim 10^5$ fold (5, 45, 115, and 116). RanGAP1 associates with Nup358 (also known as RanBP2) at the cytoplasmic filament of the NPC, and this interaction is necessary for nuclear import (117). Sumoylation of RanGAP1 by SUMO-1 protein is a prerequisite for its association with Nup358.

The Ran intrinsic rate of GTP-hydrolysis is further increased by RanBP1 to reach ~100,000 fold of its original intrinsic hydrolysis rate. RanBP1 also acts as antagonist of the guanine nucleotide exchange factor (RanGEF) in the absence of RanGAP1, thereby interfering with the nucleotide exchange and holding Ran in the GDP-bound state. (118). Studies on RanBP1 and its yeast homologue Yrb1p have shown that it is a shuttling protein that uses Crm1 to exit the nucleus. Despite the shuttling behavior of RanBP1, its steady state distribution is mainly cytoplasmic (119, 120).

On the contrary, (RanGEF) also known as RCC1 (regulator of chromosome condensation) or Prp20 in yeast and its stimulating factor RanBP3 are predominantly nuclear and excluded from the cytoplasm (121-123 and reviewed in 45). The Ran-guanine nucleotide exchange rate is amplified by RanGEF up to 10,000 times as compared to its nucleotide exchange rate in the absence of RanGEF, this magnitude is further augmented 10-fold in the presence of RanBP3. RanBP3 is a 55 KDa protein that associates with RCC1 and increases its catalytic activity (124). Furthermore, association with other nuclear proteins such as histones H2A and H2B enhances the catalytic activity of RCC1 as well (125). Collectively, this leads to the concentration of RanGTP in the nucleoplasm.

Several pieces of evidence further substantiated the crucial role of Ran binding proteins in nuclear transport. As such, mutant forms of the yeast RanGTPase activating protein (Rna1p) and its activator, yeast Ran binding protein (Yrb1p) were demonstrated to inhibit classical nuclear import *in vitro* and *in vivo* respectively (126, 127).

As the export of at least one molecule of RanGTP per transport round will eventually diminish its concentration in the nucleus, the nuclear pool of Ran is replenished by import of RanGDP followed by RanGEF-enhanced nucleotide exchange. Nuclear transport factor 2 (NTF2) is the transport receptor that mediates Ran import; it binds preferentially to RanGDP at the cytoplasmic side of the NPC, and releases it in the nucleoplasm upon nucleotide exchange (128).

Thus far a simple outline for the Ran cycle can be depicted. As such, RanGTP in the nucleus dissociates the import complex by interacting with the transport

receptor. Then it translocates to the cytoplasm together with the empty carrier or as a component of export complexes. Once in the cytoplasm, GTP hydrolysis takes place by means of RanGAP1 and RanBP1, 2. The resulting RanGDP molecule is reimported to the nucleus by NTF2. In the nucleus, RanGEF converts RanGDP to RanGTP which then dissociates from NTF2 and starts another round of transport (Fig. 1.7B).

2.8 Classical nuclear import pathway

So far, the classical import is the best characterized nuclear transport pathway. The key components as well as the underlying mechanisms of this transport route are defined at the molecular level. A typical classical import reaction is initiated by the formation of the heterodimeric importin-α/importin-ß receptor in the cytosol. Upon binding to importin-ß, the affinity of importin-α to NLS-bearing cargoes increases due to the relief of its autoinhibitory effect. Subsequently, importin-α as part of the dimeric receptor binds the NLS and forms a trimeric import complex which is stable in the cytoplasm due to the low concentration of RanGTP. The next step of the nuclear import involves docking of the import complex at the cytoplasmic filaments of the NPC. Docking occurs through the interaction of importin-ß with Nup358 which resides at the tips of cytoplasmic fibrils. After docking, the import complex moves along the NPC via interactions of importin-ß with FG-containing nucleoporins located in the transport channel such as Nup62. Several models were proposed to explain the translocation through NPCs (see below). Once in the nucleus, the import complex dissociates by means of high RanGTP and with the help of nucleoporins such as Nup50 and

Figure 1.8

Classical nuclear import pathway

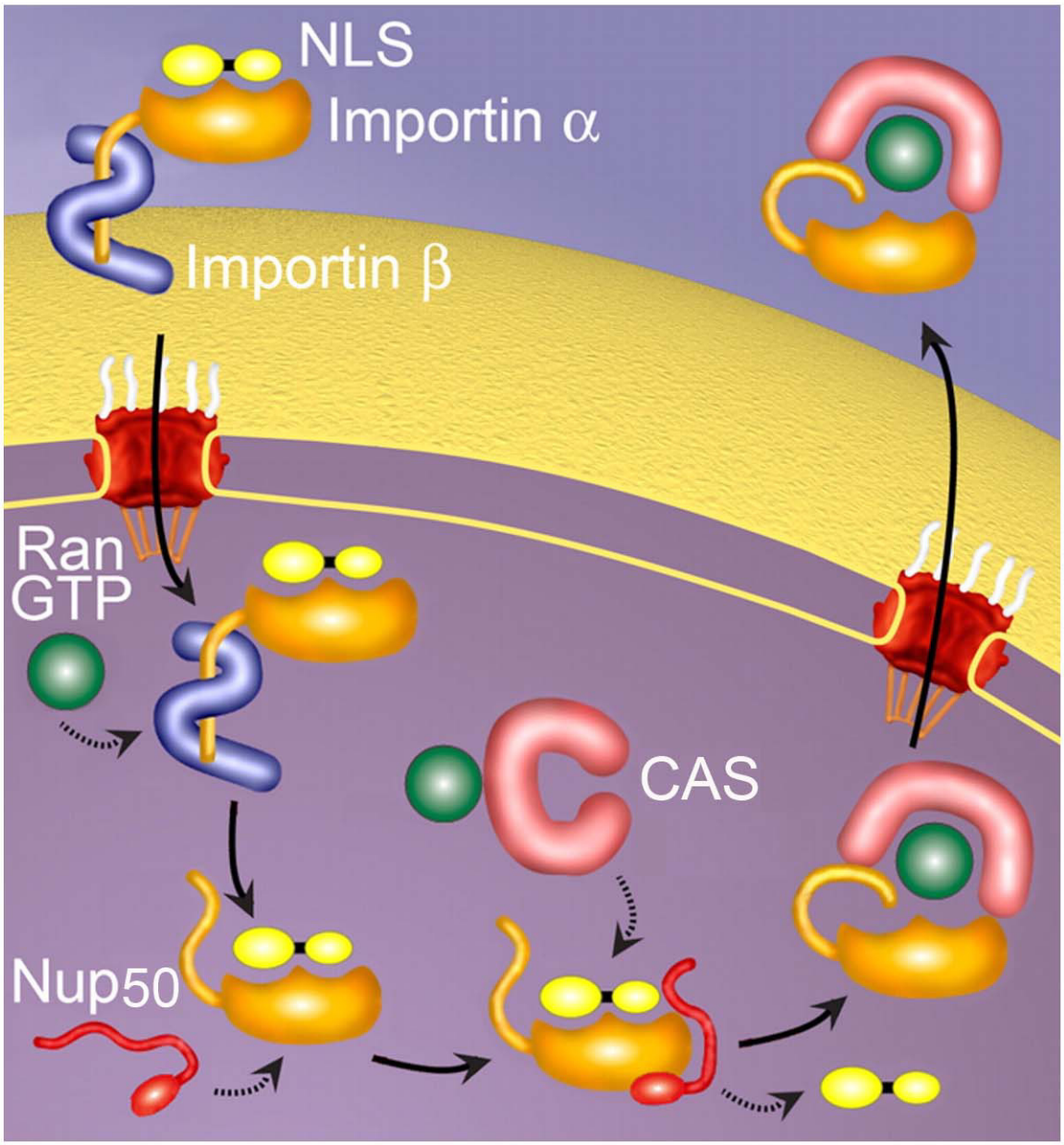

Figure 1.8 Classical nuclear import pathway

The dimeric receptor importin-α/importinβ1 recognizes and binds proteins with classical nuclear localization signals (NLSs) in the cytoplasm resulting in the formation of import complexes. The transport receptors facilitate the translocation of the import complex through the NPC by their ability to interact with FG containing nucleoporins. Upon completion of the import reaction, importin-β1 dissociates from the import complex by interaction with RanGTP, then Nup50 dissociates importin-α from its import substrate. Importin-α is exported to the cytoplasm by its exporter CAS to mediate other rounds of import cycle.

This Figure is modified from

1- **Terry LJ, Shows EB, and Wente SR.** Crossing the nuclear envelope: hierarchical regulation of nucleocytoplasmic transport. *Science* 318: 1412-1416, 2007.

Figure 1.9

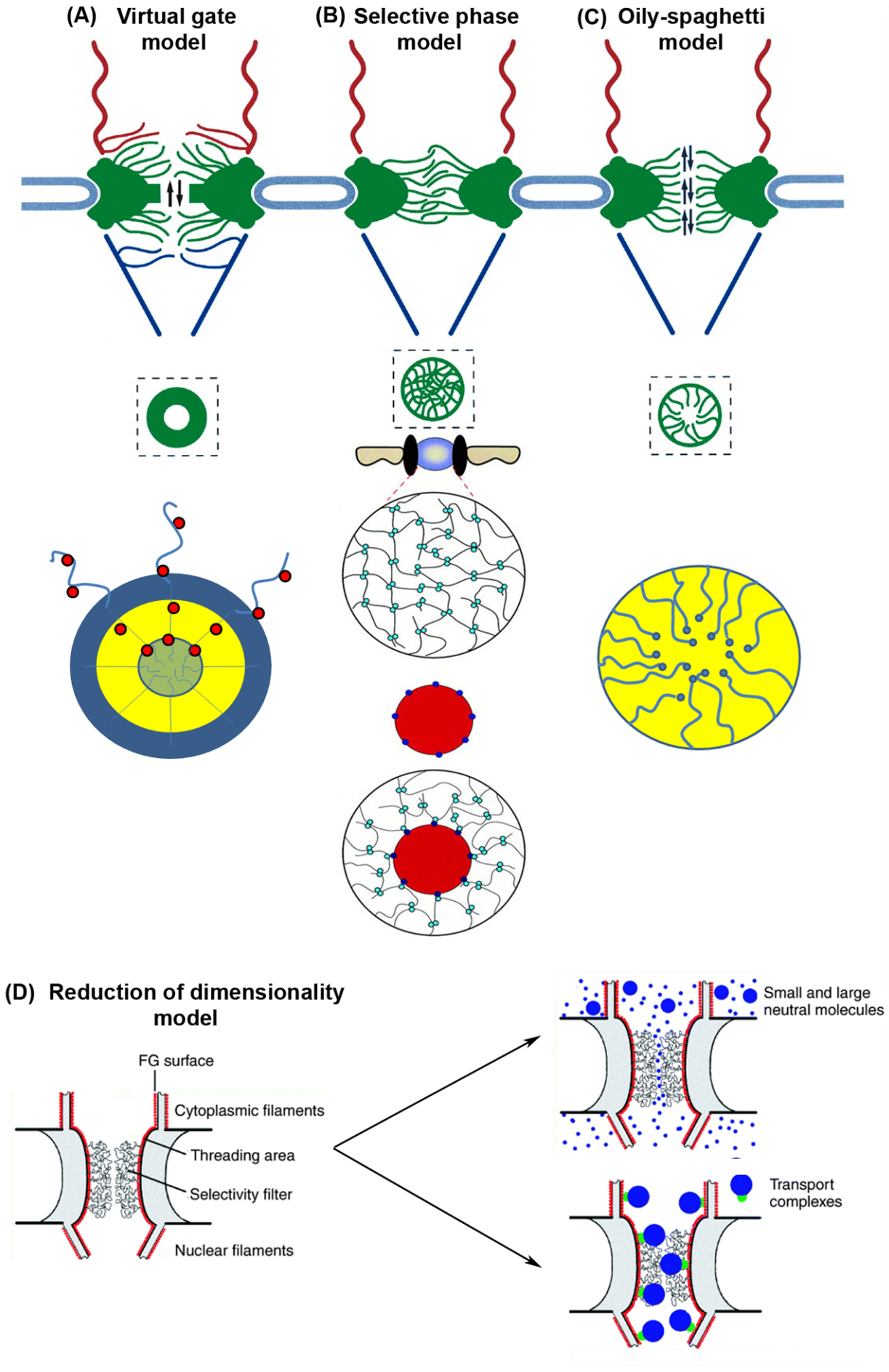
(A) Virtual gate model
(B) Selective phase model
(C) Oily-spaghetti model
(D) Reduction of dimensionality model
FG surface
Cytoplasmic filaments
Threading area
Selectivity filter
Nuclear filaments
Small and large neutral molecules
Transport complexes

Figure 1.9 Models for the translocation across the NPC

The cartoon depicts the different mechanisms that have been proposed to explain the translocation of macromolecules through the narrow central channel of the NPC. Certain models rely on the presence of physical barriers, for instance selective phase, Oily-Spaghetti, and reduction of dimensionality models, while others adopt the energy barrier theory such as the virtual gate model. In all models described, interaction between soluble transport factors and FG containing nucleoporins is the key factor that facilitates the translocation of macromolecules through the NPC. See text for details.

This Figure is modified from

1- **Ribbeck K and Görlich D.** Kinetic analysis of translocation through nuclear pore complexes. *EMBO J* 20: 1320–1330, 2001.

2- **Peters R.** Translocation through the nuclear pore complex: selectivity and speed by reduction of dimensionality. *Traffic* 6: 421-427, 2005.

3- **Mosammaparast N and Pemberton LF.** Karyopherins: from nuclear-transport mediators to nuclear-function regulators. *Trends in Cell Biology* 14: 547-556, 2004.

4- **Weis K.** Regulating access to the genome: nucleocytoplasmic transport throughout the cell cycle. *Cell* 112: 441-451, 2003.

Tpr. Upon termination of the import reaction, both subunits of the classical transport receptor are recycled back to the cytoplasm, albeit by different mechanisms. As such, importin-ß returns to the cytoplasm in complex with RanGTP, whereas importin-α relies on its exporter CAS to exit the nucleus (Fig. 1.8) (reviewed in 5, 45, and 109).

2.9 Models of entry into and translocation across the NPC

2.9.1 Virtual gate model

According to the virtual gate model the presence of an energetic barrier rather than physical obstruction is the key determinant of the selective permeability of the NPCs. It is proposed that, the restricted movement of macromolecules in the narrow central gate channel of the NPC (as compared to their free movement in the cytoplasm) constitutes an energetic barrier that hinders their entry and crossing of the transport channel. The energetic barrier increases with the size of the macromolecule. The movement restriction is caused mainly by the FG repeats that line the central channel of the nuclear pore. The interaction of transport factors with the FG repeats of the NPC facilitates the entry of macromolecules into the NPC, thereby lowering the energetic barrier (129 and reviewed in 29) (Fig. 1.9A).

2.9.2 Selective phase model

This model proposes that the NPC contains a net-like structure that is created by hydrophobic interactions between the FG repeats. The passage of inert molecules (that do not interact with the FG repeats) is limited by the size of the openings of

the net. Thus, the different molecules will be sieved; those which are smaller than the mesh size will pass while the larger ones will be excluded. According to the selective phase model, binding of transport carriers to FG repeats disturbs the weak hydrophobic interaction in the vicinity and allows for the partitioning of macromolecules in the semi-liquid phase. This mechanism facilitates the entry of macromolecules that possess transport signals and exceed the porous size of the sieve-like meshwork (41) (Fig. 1.9B).

2.9.3 Oily-Spaghetti model

In this model the FG repeats are predicted to extend and move inside the pore like wobbly "oily spaghetti", where they constitute an obstacle against the diffusion of macromolecules. The transient association of transport carriers with repeats is accompanied by random movement that occurs between consecutive binding and release rounds, thereby facilitating the translocation of the carriers with their accompanying macromolecules through the nuclear pore channel by simple diffusion (reviewed in 29, 109) (Fig. 1.9C).

2.9.4 Reduction of dimensionality model

This model assumes that there is a narrow channel at the center of the NPC which permits the diffusion of small inert molecules but restricts the passage of large ones. The selective passage of macromolecules occurs through an extensive surface of FG repeats that surrounds the transport channel and spreads from the cytoplasmic to the nuclear side of the NPC. This sheet of FG repeats functions as a selective filter that only allows the passage of molecules which are associated with transport receptors. In this process, the transport receptor's trip through the

NPC must start by binding the FG repeats at one side of the pore and then continues via two-dimension random crawling to the other side. Movement of transport receptors across the NPC is mediated by repeated interactions with the FG motifs (44) (Fig. 1.9D).

3. 5´-AMP-activated protein kinase (AMPK)

5´-AMP-activated protein kinase (AMPK) plays a key role in regulating different metabolic pathways, thereby maintaining cellular energy homeostasis. AMPK senses the drop in cellular energy which is induced by exposure to different metabolic stresses, for instance glucose deficiency, hypoxia or ischemia. The increase in AMP/ATP ratio activates the enzyme in order to rescue the balance of cellular energy by switching cellular metabolism toward catabolic rather than anabolic processes. AMPK is at the center of control for major metabolic pathways that are involved in the consumption or generation of cellular energy. Its pivotal role in regulating lipid metabolism and glucose homeostasis is well established (reviewed in 130-133). Activated AMPK inhibits fatty acid synthesis by targeting the key players in fatty acid synthesis pathways. These include acetyl-CoA carboxylase (ACC), fatty acid synthase (FAS) as well as malonyl-CoA decarboxylase. At the same time, activation of AMPK stimulates fatty acid oxidation in mitochondria (reviewed in 134). Furthermore, AMPK is a master regulator of glucose metabolism; it controls both glucose uptake in skeletal muscles as well as liver glucose production via hepatic glycogenesis (reviewed in 135). Upon AMPK activation, glucose transporter GLUT4 synthesis is induced

and its translocation to the plasma membrane is stimulated. This is the underlying mechanism that enhances glucose entry to fast-twitch (glycolytic) muscles during exercise practicing (136). While the prominent role for AMPK in regulating glycogen synthesis is mediated at least in part by its ability to associate with glycogen via the β subunit central-carbohydrate binding domain (reviewed in 131). The fundamental importance of AMPK in maintaining glucose homeostasis and lipid metabolism makes AMPK a potential drug target for treatment of type 2 diabetes and obesity (137).

Analysis of AMPK structure reveales a heterotrimeric complex that contains three different subunits. In mammalian cells, the catalytic α subunit has two isoforms α1, α2 and is characterized by the presence of a conserved threonine residue (Thr172) which needs to be phosphorylated by upstream kinases in order to activate AMPK. The two other subunits, β and γ, are encoded by two and three genes, respectively; they are known to have regulatory functions (138). The β subunit provides a platform for AMPK assembly as it links α and γ subunits. Three different γ isoforms are present in mammalian cells and known as γ1, γ2 and γ3. The γ subunit associates with the β subunit through a β-binding motif which is present near the N-terminal region. Downstream to that motif are found Bateman domains which consist of pairs of cystathionine β-synthase (CBS) motifs that comprise the ATP/AMP binding sites (139).

Recently, the N-terminal Bateman domain has been shown to play a major role in the alllosteric activation of the AMPK. As such, CBS2 motif in the Bateman domain contains a pseudo substrate sequence that binds to the kinase

domain and prevents the interaction between AMPK and its substrate. Concomitantly, this pseudo substrate sequence mediates the interaction with AMP. Thus, binding to AMP releases the autoinhibitory effect of the pseudo sequence and allows the interaction between AMPK and its substrates. In addition to allosteric activation, AMP promotes the activation of AMPK by preventing protein phosphatase 2α (PP2Cα)-mediated dephosphorylation, thereby maintaining the phosphorylated state of Thr172 (138-140). Different upstream kinases are involved in the activation of the AMPK. These include the tumor suppressor LKB1 as well as Ca^{2+}/calmodulin-dependent protein kinase kinase α (CaMKKα) and β (CaMKK β). The fundamental importance of AMPK as key regulator in cellular metabolism requires tight control of the enzyme activity. This is achieved by different mechanisms that mediate the AMPK activation (141).

AMPK is found in the nucleus and cytoplasm which reflects functions for the enzyme in both compartments (139). However, this distribution is dynamic and subject to change in response to different environmental stimuli. For example, the AMPK α2 subunit translocates to the nuclei of muscle cells upon exercise (142) indicating that the adaptation of skeletal muscle to metabolic-stress during exercise is mediated at least in part via the relocation of AMPK. Moreover, AMPK may be involved in modulating the gene expression in skeletal muscle to enhance glucose uptake and increase sensitivity to insulin. These findings point to the importance of AMPK intracellular distribution for its function. In chapter 3 I have undertaken a systematic analysis to dissect the effects of various stressors on the subcellular distribution of AMPK α and β subunits.

4. Heat shock proteins (HSPs)

Heat shock proteins (HSPs) represent a diverse group of proteins that are induced upon exposure to environmental stress. The term heat shock stems from their initial discovery in *Drosophila* where their synthesis was induced in response to heat stress, however, other forms of stress such as oxidative stress and anoxia lead to the induction of heat shock proteins as well (143). HSPs function mainly as molecular chaperones. They protect the cellular proteins from damage induced by different environmental insults. Furthermore, different members of heat shock protein families are implicated in essential cellular processes such as folding of newly synthesized proteins and protein translocation. According to their molecular mass, members of heat shock proteins are classified into 5 different families among which Hsp70s and Hsp90s are the best characterized (reviewed in 144). The following section will focus on the heat shock protein 70 family, which is directly relevant to my research.

4.1 Heat shock protein 70 family (Hsp70s)

As the name implies, heat shock protein 70 family members (Hsp70s) have molecular mass of ~ 70 KDa (reviewed in 145). In humans, ~13 genes are found that encode different hsp70 isoforms, this reflects the large functional diversity among hsp70s members (reviewed in 146). In addition to stress-induced expression of hsp70 genes, certain members of the Hsp70 family, for instance heat shock protein cognate (hsc70), are constitutively expressed (reviewed in 147). Hsp70s are ubiquitously present in all subcellular compartments and organelles and become more abundant upon stress. Their importance for living

cells is substantiated by their universal expression in all organisms from bacteria to higher eukaryotes (reviewed in 148).

4.2 Diverse functions of Hsp70s

As molecular chaperones, Hsp70s have numerous tasks under normal and stress conditions. They are implicated in a wide range of cellular activities such as protein folding and translocation, refolding or degradation of damaged proteins, regulation of transcription and signal transduction (reviewed in 149, 150). Here, I will focus on the chaperoning function of hsp70s.

Under normal growth conditions, the main function of hsp70s is to facilitate folding of newly synthesized polypeptides to reach their final functional conformation. Folding of newly synthesized proteins *in vivo* is challenged by different factors. For instance, the protein folding occurs simultaneously with translation. As the folding information which are determined by the amino acid sequence of the full length protein become available only upon the completion of translation, beginning the protein folding process while possibly missing some of the necessary folding instructions, could render the folding process less efficient and may result in functionally inactive, partially folded protein. Although the co-translational folding of individual domains in multidomain proteins may reduce the risk of misfolding, the lack of intramolecular interactions may leave the folded domain unstable. Another problem which encounters the proper protein folding is the crowdedness of the cellular environment with high concentration of proteins. All these conditions raise the probability of protein misfolding and shift the balance toward aggregate formation. The proper folding of newly synthesized

proteins strictly depends on the action of hsp70s and their co-factors (see below). Hsp70s assist the *de novo* protein folding by binding to the nascent polypeptide chains thereby preventing them from improper association with other molecules. At the same time, hsp70s help to correctly fold these polypeptides to reach their native conformation through multiple rounds of binding and release (reviewed in 151). Under normal and stress conditions hsp70s have a surveillance function, they monitor the different proteins in the cell, refold those which are not correctly folded or denatured to regain their functional conformation, and target those which are severely damaged to the proteasome for degradation. By doing so, hsp70s prevent the aggregation of damaged proteins into large inclusion bodies inside the cell which may cause irreversible cellular damage and ultimately leads to cell death. Thus hsp70s are of fundamental importance as central component of the protein quality control system which assures the structural and functional integrity of cellular proteins thereby protects the cells from stress-induced proteotoxicity and maintain the cellular protein homeostasis (reviewed in 152).

The role of hsp70s becomes even more important upon stress due to the high incidence of protein damage in response to the cellular insult. This is substantiated by the induction of certain hsp70s members, like hsp70, upon exposure to different forms of stress. Damaged proteins are characterized by the exposure of highly interactive hydrophobic motifs which are normally hidden intramolecularly in the native state. Due to their adhesive nature, the hydrophobic polypeptides of the damaged proteins tend to interact with each other as well as with other proteins in the vicinity. This condition, if left without proper

intervention, leads to the formation of large aggregates which could interfere with essential cellular activities and cause severe cellular injury. Thus, stress raises the demand for the chaperoning intervention of hsp70s (reviewed in 148).

Beside their role in protein folding, hsp70s are involved in intracellular trafficking. For example, the endoplasmic hsp70, Bip assists the translocation of proteins across the ER membrane in an ATP-dependent manner via two different mechanisms, trapping and pulling. Furthermore, the mitochondrial matrix hsp70 (mt-hsp70) mediates the import of mitochondrial precursor proteins by pulling the protein across the translocation pore then refolding them in the other side of the membrane (reviewed in 153).

4.3 Structure and molecular basis for hsp70 function

Structural analysis of DnaK (the bacterial hsp70) revealed the presence of two conserved functional domains, an ATP binding domain (~44 KDa) which is located at the N-terminal region, and a peptide binding domain at the C-terminus (~18 KDa). The peptide binding domain is further distinguished into a β-sandwich subdomain which confers the peptide binding site and an α-helical segment which functions as a latch that fastens the substrate to the chaperone molecule (154, 155). A third domain of approximately 10 KDa is found at the C-terminus and thought to mediate the binding of hsp70s with their DnaJ co-chaperones (see below) (reviewed in152).

The function of hsp70s as molecular chaperones is realized by their ability to recognize and bind the hydrophobic stretches which characterize the unfolded or damaged proteins. The protein folding function of hsp70s requires successive

binding and release of the chaperone substrate. Such repetitive rounds of interaction rely on the ATP cycle, and hsp70 is switching between two nucleotide-bound states; ATP and ADP. The nucleotide- bound state of hsp70 determines its affinity for substrate. Whereas ATP hydrolysis stabilizes the chaperone-substrate complex, replacing the ADP by ATP lowers the binding affinity and stimulates substrate release. A proposed model for the mechanism of substrate binding and release relies on the intramolecular rearrangement of the substrate binding cleft and the α-helical lid of hsp70 upon ATP binding. According to this model, in the ATP-bound state the chaperone molecule adopts an open conformation which allows for rapid substrate binding and release. Conversely, in the ADP-bound state, the α-helical lid closes the peptide binding cavity and locks in the chaperone substrate, thereby stabilizing binding. It is noteworthy that in both nucleotide-bound states there is equilibrium between the open and closed conformation, however the substrate exchange is much faster in the open conformation and becomes significantly slower upon ATP hydrolysis (156).

4.4 Hsp70s co-chaperones

Stable association of hsp70 with its substrates is a prerequisite for hsp70 activity and requires ATP hydrolysis. The extremely low intrinsic ATPase activity of hsp70 decreases the efficiency of this step. On the other hand, the release of folded substrate is facilitated by nucleotide exchange. The productive chaperone cycle of hsp70 relies on the action of a whole set of interacting partners that are referred to collectively as co-chaperones. The interaction of these co-chaperones

with hsp70 modulates the chaperone function by stimulating the ATP hydrolysis and accelerating nucleotide exchange, thereby regulating substrate binding and release, respectively.

Prominent examples of the co-chaperones which stimulate the ATPase activity of hsp70 are members of the Hsp40s family, the eukaryotic homologs of the bacterial DnaJ. Hsp40s are structurally characterized by the presence of a specific domain of ~ 70 amino acid residues, called J domain. This domain contains a characteristic tripeptide sequence of histidine-proline-aspartate (HPD) and mediates the interaction of hsp40 with hsp70 (reviewed in 157). Hsp40s exert their co-chaperoning function by simultaneous interaction with the polypeptide substrate and the ATPase domain of hsp70s. Thereby, they enhance the ATP hydrolysis by hsp70s and at the same time facilitate uploading of the peptide substrate into the chaperone molecule (reviewed in 158). Hsp40-promoted ATP hydrolysis is the rate limiting factor that determines the activity of hsp70 and the overall efficiency of the chaperone cycle (reviewed in 159). The number of hsp40 isoforms varies widely among the different organisms and ranges from six homologs as in E. coli to more than 20 in mammalian cells. Besides their role as co-chaperoning partners of hsp70, hsp40s have other cellular functions. As such, members of the hsp40s/DnaJ family have been shown to play a role in protein translocation (ERdj1/Mtj1 and ERdj2/hSec63) and degradation (HSJ1 and Ydj1). Furthermore, in addition to hsp70, hsp40 cooperates with other chaperones such as Hsp90 in protein folding processes (reviewed in 158).

Another co-chaperone which cooperates with hsp40s is the hsc70 interacting protein (Hip). Although Hip does not stimulate the ATPase activity of hsc70, its binding to the ATPase domain of the hsc70 renders the ADP state of the chaperone more stable. The preceding ATP hydrolysis by assistance of hsp40 promotes the interaction of Hip with hsc70. This interaction permits longer association of hsc70s with their substrates, thereby enhancing the chaperoning function (reviewed in 159).

A different class of important regulatory proteins that control the hsp70s chaperone cycle are the nucleotide exchange factors. Although ATP hydrolysis is the rate limiting factor that drives the chaperone cycle, nucleotide exchange plays an important role in the termination of the chaperone reaction and subsequent substrate release. BAG-1 (Bcl-2-associated athanogene) is the best characterized nucleotide exchange factor that modulates the function of hsc70. The interaction of BAG-1 with hsc70 results in ADP dissociation and ATP rebinding. The nucleotide exchange by assistance of BAG-1 switches hsc70 to the open conformation with minimal binding affinity and stimulates substrate release. Thus the interaction of BAG-1 with hsc70 antagonizes the effect of Hip which stabilizes the chaperone-substrate binding. Concomitantly, Hsp40-stimulated hydrolysis of ATP is a prerequisite for BAG-1 to exert its nucleotide exchange function (reviewed in 160).

CHIP (carboxy terminus of hsc70 interacting protein) is a co-chaperone which upon association with hsc70 inhibits the ATP hydrolysis (reviewed in 161). Structural analysis of CHIP revealed 3 characteristic domains, an N-terminal

tetratricopeptide repeat (TPR), a central charged domain, and C-terminal U-box domain. It is the TPR domain that mediates the binding of CHIP to the carboxy terminus of Hsc70. Interaction of CHIP with hsc70 stabilizes the chaperone in the ATP-bound state and promotes the fast substrate exchange, thereby negatively regulating the protein folding process (161, reviewed in 162). Furthermore, CHIP participates in protein degradation by promoting substrate ubiquitylation which is a prerequisite for targeting proteins to the proteasome. CHIP's role in protein degradation is mediated by the E3 ubiquitin ligase activity of the U-box domain. It appears that CHIP transfers the damaged proteins that cannot be refolded from the chaperone machinery to the proteasome degradation pathway (reviewed in 162, 163).

An important co-chaperone that interacts with hsp70 as well as hsp90 is the Hsp70-hsp90-Organizing Protein (Hop). The gene encoding Hop was first discovered in the yeast *Saccharomyces cerevisiae* as a stress inducible gene and hence was referred to as STI1. The product of STI1 gene was identified as ~ 66 KDa protein which contains 589 amino acids. Analysis of mutants of this gene indicated that it encodes a protein that plays an important role in stress tolerance as STI1 mutant strains failed to grow at temperatures that are lower or higher than the optimal growth temperature (164, reviewed in 165). Mammalian Hop was identified later as a 60 KDa protein that co-purified from different mammalian tissue extracts, where it is present in complexes that contain the chaperones hsp70 and hsp90 (166).

Hop is structurally characterized by the presence of two TPR domains; TPR1 is located at the N-terminal region while TPR2 occupies the central and C-terminal end of the protein. These TPR domains mediate the association of Hop with the chaperones hsp70 and hsp90. Analysis of hsp70-Hop-hsp90 chaperone complex revealed that Hop TPR1 domain at the N-terminal end binds to the C-terminal region of hsp70 whereas the association of Hop with hsp90 occurs via the C-terminal Hop TPR2 domain (167, 168). Although Hop and hsp40 both bind to the C-terminal region of hsp70, structural analysis studies revealed that the binding sites for Hop and hsp40 at the carboxy-terminal domain of hsp70 are distinct and do not overlap with each other. This feature allows simultaneous binding of both co-chaperones to hsp70 which may provide additional control of the hsp70 chaperoning function (169). Unlike other hsp70 co-chaperones, the role of Hop in modulating the chaperone function as well as ATPase activity of hsp70 remains controversial (170). As such, in luciferase refolding assay the effect of Hop on reactivation of the denatured enzyme was dependent on the presence of Hap-46, a co-chaperone that interferes with the refolding process. Although the addition of Hop in combination with Hap-46 to the refolding system reduced the inhibitory effect seen by Hap-46 by about 50%, Hop by itself hindered the refolding reaction (171). By contrast, other reports demonstrate that Hop enhances protein folding by hsp70 (172).

Hop is known to inhibit the ATPase activity of hsp90 (173) whereas previous work revealed that Hop stimulates nucleotide exchange on hsp70 there by

accelerating its chaperone cycle (reviewed in 174). However, studies from other groups failed to support this finding (172)

Despite the controversial interpretations regarding the ability of Hop to directly modulate the interaction between hsp70 and its client substrates, it is well established that Hop is an important component of the hsp70-hsp90 multichaperone complex. This chaperone machinery is responsible for the assembly and maturation of steroid receptors, for instance progesterone and glucocorticoide receptors. It has been hypothesized that Hop works as an adaptor molecule that bridges hsp70 and hsp90 thereby promoting the assembly of hsp70-hsp90 chaperone complex (167, 170, 175, and reviewed in 176). According to this model, hsp70 binds the steroid receptor to form hsp70-receptor complex which is then delivered to hsp90 with the assistance of Hop. This model is substantiated by a study in which mutant Hop that cannot bind hsp70 or hsp90 interfered with the integration of hsp90 into the hsp70-receptor complex, whereas the formation of an hsp70-receptor complex was not affected, even when Hop was completely omitted from the assay (170).

Taken together, Hop plays a key role in regulating hsp70-hsp90 mediated protein folding. This is of fundamental importance to the cell as many signalling molecules depend on this chaperone machinery to reach their functional conformation. Future experiments will have to address the effect of Hop on the function of hsp70. In particular how interaction with Hop will affect the nucleotide exchange rate as well as the ATPase activity of the chaperone. Impinges of Hop/hsp70 interactions on the chaperone cycle of hsp70 might as

well affect the intracellular trafficking of the chaperone. As modulating the affinity of hsp70 to its substrates may either lead to the retention of the chaperone in certain locations where it is being anchored by its client substrates or facilitate its movement by librating it from the potential anchors.

Understanding the mechanisms by which Hop modulates hsp70-substrate interactions and thus the hsp70 trafficking will highlight the physiological relevance of Hop intervention and may help to enhance the overall chaperoning function of hsp70 in the cell.

5. Objective

The main objective of the research presented in this thesis is to analyze the effect of different forms of stress on the defined aspects of eukaryotic cell physiology with particular focus on nucleocytoplasmic trafficking.

The specific objectives are:

1- Analyzing the effect of oxidative stress on the subcellular distribution of individual components of the nuclear transport apparatus, such as transport receptors and nucleoporins.

2- Studying how stress (in particular heat stress) modulates the nucleocytoplasmic transport of the molecular chaperone hsc70.

3- Analyzing the effect of different forms of stress on the subcellular distribution of the signaling molecule 5′-AMP-activated protein kinase (AMPK).

4- Developing new quantitative approaches that can be used to precisely measure the fluorescence signals in the different subcellular locations.

CHAPTER 2

Oxidative Stress Mislocalizes and Retains Transport Factor Importin-α and Nucleoporins Nup153 and Nup88 in Nuclei Where They Generate High Molecular Mass Complexes

Mohamed Kodiha, Dan Tran, Cynthia Qian, Andreea Morogan, John F. Presley[#], Claire M. Brown[§] and Ursula Stochaj.

Department of Physiology, [#]Anatomy and Cell Biology, [§]Biochemistry and Life Sciences Imaging Facility, McGill University, Montreal, PQ, H3G 1Y6, Canada

2.1 Specific introduction to chapter 2

Oxidative stress is the prevalent insult that contributes to various heart and neurodegenerative diseases. In fact, oxidants are the key components that induce the damage caused by heart attack, ischemia/reperfusion injury, stroke as well as Alzheimer's disease. The damage caused by oxidants can lead to contractile dysfunction, arrhythmias, as well as cell death in the myocardium and central nervous system. Prevention of and recovery from oxidative injury is therefore of fundamental importance to improve the survival and restore cellular functions in the diseased heart and brain.

Oxidative stress affects different cellular processes, but not all of them are characterized at a molecular level. The complex impact of oxidative stress on different aspects of cell physiology makes it necessary to define the cellular reactions that are sensitive to oxidants. Nucleocytoplasmic transport is one of the essential cellular processes that are sensitive to stress. I have initially demonstrated that transport of macromolecules between nucleus and cytoplasm is inhibited upon exposure to severe oxidative stress. Furthermore, my preliminary data revealed that multiple mechanisms are implicated in classical import inhibition induced by exposure to hydrogen peroxide which creates severe oxidative stress. Yet, the oxidative stress associated with different diseases and pathophysiologies is usually milder than oxidative stress generated by the conditions used in my experiments. Therefore, I wanted to explore the effect of mild oxidative stress, which is more relevant to many human diseases, on

classical nuclear transport with particular focus on how oxidants affect the components of the nucleus/cytoplasm transport apparatus.

The main objective of this study is to identify and characterize new targets that are damaged by oxidants. This will help to develop therapeutics that aim at several cellular components to cope with the stress-induced damage and rescue cellular homeostasis. The specific objectives are to define the effects of oxidative stress on the localization of transport factors importin-α, CAS and several nucleoporins which are implicated in nucleocytoplasmic transport. To achieve this, I have analyzed nuclear transport in human cells that are treated with the oxidant diethyl maleate (DEM). The data from this study have generated the paper entitled: Oxidative stress mislocalizes and retains transport factor importin-α and nucleoporins Nup153 and Nup88 in nuclei where they generate high molecular mass complexes. ***Mohamed Kodiha****, Dan Tran, Cynthia Qian, Andreea Morogan, John F. Presley, Claire M. Brown and Ursula Stochaj.* This paper has been published in the journal Biochemica Biophysica Acta (BBA) in 2008. Chapter 2 is based on this paper.

2.2 Abstract

Nuclear trafficking of proteins requires the cooperation between soluble transport components and nucleoporins. As such, classical nuclear import depends on the dimeric carrier importin-α/β1, and CAS, a member of the importin-β family, which exports importin-α to the cytoplasm. Here we analyzed the effect of oxidative stress elicited by diethyl maleate (DEM) on classical nuclear transport. Under conditions that do not induce death in the majority of cells, DEM has little effect on the nucleocytoplasmic concentration gradient of Ran, but interferes with the nuclear accumulation of several reporter proteins. Moreover, DEM treatment alters the distribution of soluble transport factors and several nucleoporins in growing cells. We identified nuclear retention of importin-α, CAS as well as nucleoporins Nup153 and Nup88 as a mechanism that contributes to the nuclear concentration of these proteins. Both nucleoporins, but not CAS, associate with importin-α in the nuclei of growing cells and *in vitro*. Importin-α generates high molecular mass complexes in the nucleus that contain Nup153 and Nup88, whereas CAS was not detected. The formation of high molecular mass complexes containing importin-α, Nup153 and Nup88 is increased upon oxidant treatment, suggesting that complex formation contributes to the anchoring of importin-α in nuclei. Taken together, our studies link oxidative stress to the proper localization of soluble transport factors and nucleoporins and to changes in the interactions between these proteins.

Key words: Stress, oxidants, nucleus, nuclear transport.

Words: 208

2.3 Introduction

The appropriate response to stress is fundamental to cell survival and the recovery from different insults, such as oxidant exposure (177-180). Oxidative stress generated by the increase in reactive oxygen species (ROS) is the most prominent insult that causes ischemia/reperfusion injury, which can lead to apoptotic or necrotic cell death (181-184). ROS-mediated stress contributes to cell death not only in cardiovascular diseases and stroke, but also in Alzheimer's disease and many other neurodegenerative disorders and syndromes (183-185). The glutathione/glutathione disulfide (GSH/GSSG) system is one of the major contributors to redox homeostasis and of particular importance to the intracellular redox state (181-184, 186). Changes in the GSH/GSSG ratio have been observed for several human diseases, pathologies and during aging (reviewed in 187). Oxidative stress affects many intracellular processes, and DEM treatment may affect protein modification, cell biochemistry, physiology and even behavior of an organism (188-191). At present, not all of the consequences of oxidative stress are understood at the molecular level. In particular, the impact on nuclear transport is only beginning to emerge.

Many of the proteins transported in or out of the nucleus require a specialized transport apparatus which includes members of the importin-β family (3, 192). For instance, classical nuclear import relies on importin-β1 and the adaptor importin-α. Together, importin-α/β1 generate a dimeric nuclear import receptor that recognizes classical nuclear localization sequences (cNLS) in the cytoplasm, transports cNLS-containing cargo across the nuclear pore complex (NPC) and

delivers this cargo to the nuclear side of the NPC. Once in the nucleus, binding of RanGTP to importin-β1 dissociates the importin-α/β1/cargo complex. Upon delivery of the cargo to the nucleus, importin-α and importin-β1 return independently to the cytoplasm. Importin-α is exported to the cytoplasm by CAS (cellular apoptosis susceptibility protein), a carrier of the importin-β family, and RanGTP is necessary to generate trimeric export complexes (193). Importin-α and CAS are not only involved in nuclear transport, but also in other cellular processes (reviewed in 97, 194, 195).

Like nuclear carriers, nucleoporins play a key role in moving cargo across the NPC, as they provide sites for the translocation of import and export complexes. Nucleoporins are organized into modules that generate defined components of the NPC (23); they may be involved in nuclear import and/or export of macromolecules. Some nucleoporins are stably bound to NPCs, whereas others play a more dynamic role and reversibly interact with the nuclear pore (30). Nup153 and Nup50 are dynamic nucleoporins predominantly located on the nuclear side of the NPC, where they participate in nuclear trafficking. As such, Nup153 is implicated in nuclear import and export of protein and RNA (196), whereas Nup50 plays a role in the final step of classical nuclear import by interacting with the adaptor importin-α (reviewed in 197). Nup50 may increase the efficiency of classical protein import by promoting the disassembly of transport complexes at the nuclear side of the NPC (198). On the cytoplasmic side, nucleoporins Nup214 and Nup88 contribute to CRM1-mediated nuclear export of proteins, ribosomal and other types of RNA (reviewed in 199). Together

with Nup214, the nucleoporin Nup88 is a structural component of cytoplasmic NPC filaments, but also present on the nuclear side of the NE, suggesting functions inside the nucleus (200).

Classical nuclear import in higher eukaryotes and yeast is sensitive to various forms of stress (87, 201, 202, 203). Ultimately, severe stress conditions inhibit nuclear transport and may also lead to cell death (87). The molecular mechanisms that link oxidative stress to changes in nuclear trafficking are presently not understood, and little is known about the impact of stress and oxidants in particular on nucleoporin localization. This prompted us to analyze how non-lethal oxidative stress, conditions that are likely to mimic the oxidant-induced physiological changes observed upon ischemia/reperfusion injury and other pathologies, affects the classical nuclear import apparatus. To gain further insight into these questions, we exposed human culture cells to the oxidant diethyl maleate (DEM). DEM is a weak electrophile that can deplete GSH pools by alkylation of its SH-group (204, 205) and has been used widely to generate oxidative stress. Our studies now demonstrate that the exposure to DEM interferes with classical nuclear import, redistributes transport components, induces the formation of high molecular mass complexes in nuclei and the nuclear retention of several soluble transport components and nucleoporins that participate in nuclear protein import and export.

2.4 Materials and methods

2.4.1 Growth and stress exposure of HeLa cells

HeLa cells were grown in multiwell chambers to 50 to 70% confluency (206) and subjected to incubation with DEM or the solvent ethanol as indicated. All of the results were obtained for at least three independent experiments.

2.4.2 Flow cytometry

Cell death was analyzed by staining with annexin-V-fluorescein combined with propidium iodide. In brief, two 100 mm dishes were incubated with ethanol or 2 mM DEM for 4 hours at 37°C. Attached cells and cells in the medium were washed with PBS and together incubated overnight in fresh medium. The next day, cells attached to the dish were collected by trypsination and combined with cells in the medium. After washing in PBS, cells were incubated with annexin-V-fluorescein and propidium iodide according to the manufacturer (Roche, Germany). Binding of annexin-V-fluorescein and propidium iodide was quantified by flow cytometry.

2.4.3 Analysis of nuclear protein import in growing cells

Nuclear protein import was analyzed with NLS-GFP as previously described (87) and with GFP-tagged glucocorticoid receptor essentially as in reference 207. Endogenous import cargos HuR and galectin-3 were located as described in section **2.4.4**

2.4.4 Immunofluorescent staining

All steps were carried out essentially as described (208). Antibodies against the following proteins were used: Ran (sc-1156, Santa Cruz Biotechnology, CA),

HuR, importin-α1, CAS and α-tubulin (sc-5261, sc-6917, sc-1708, sc-5286), galectin-3 (Thermo Fisher, Fremont, CA), 7A8 is specific for Nup153 (209) (gift of Dr. Franke, Heidelberg). Primary antibodies were used as suggested by the suppliers; supernatant 7A8 was diluted 1:100. Anti-Nup50 was a gift of Dr. Gerace, La Jolla. Bound primary antibodies were detected with Cy3-conjugated secondary antibodies (1:500, Jackson ImmunoResearch, West Grove, PA). DNA was visualized with 4',6-diamidino-2-phenylindole (DAPI) and samples were mounted in Vectashield (Vector Laboratories, Burlingame, CA). Cells were analyzed with a Zeiss 510 LSM or a Nikon Optiphot and photographed with Kodak T-MAX 400 films. Images were processed with Photoshop 5.5 and 8.0.

2.4.5 Data analysis

Images were collected using the ImageXpress Micro automated imaging system from Molecular Devices (Sunnyvale, CA) using excitation from a 300 W Xenon light source and a CoolSnapHQ CCD camera (Photometrics, Tucson, AZ). Images were collected using 2x2 camera binning with a Nikon x40 PlanFluor ELWD (0.60 NA) objective using the automated focusing option in the MetaXpress software to find the cover slip-mounting media interface and then offset by a fixed amount to image the nuclear DAPI staining (Chroma Technologies Corp, Rockingham, VT, #49000) with 20 ms exposure times. Images were than taken in the same image plane for either NLS-GFP or GR-GFP using the FITC cube with 3182 ms exposure times (Chroma Technologies Corp, Rockingham, VT, #49002) or endogenous HuR and galectin-3 using the Cy3 cube with 3182 exposure times (Chroma Technologies Corp, Rockingham, VT,

#49005). Between 55 and 100 cells were analyzed for each condition. Image analysis was performed using the MetaXpress software and the Multiwavelength Cell Scoring module as described (210) or the Translocation Enhanced Module. For the Translocation Enhanced Module nuclei were identified as 100-350 μm^2 area with a width of ~10 μm and an intensity of DAPI staining over local background of > 5 intensity units. The segmentation regions identified by DAPI staining were then used to measure intensities of the GFP or Cy3 images. An inner region corresponding to the nuclear intensity was identified as the area 0.9 μm from the edge of the segmentation identified by DAPI staining. The outer region was identified as a ring 0.5 μm from the edge of the segmentation identified by DAPI staining with a width of 0.8 μm, corresponding to the cytosolic intensity. All images were corrected for contributions from background intensity using regions of the images that did not contain cells. Ratios of the average intensities of nuclear/cytosolic regions were calculated for individual cells. All segmentation data sets were inspected manually to ensure accuracy of the data and cells with inaccurate segmentation were removed from the analysis.

2.4.6 Purification of proteins synthesized in E. coli and labeling with tetramethylrhodamine

Tagged proteins were synthesized in *E. coli* and purified under native conditions following standard procedures. Purified importin-α or CAS was labeled with tetramethylrhodamine-maleimide (TMR, Molecular Probes) overnight on ice as recommended by the supplier. Non-incorporated dye was removed by gel exclusion chromatography with Sephadex G-25.

2.4.7 In vitro nuclear import of importin-α and CAS

Import of TMR-labeled importin-α or CAS was analyzed in semi-intact HeLa cells at a final concentration of 400 nM in transport buffer (211). Import assays were supplemented with 3 mg/ml cytosol prepared from control or DEM-treated HeLa cells (4 hours, 2mM DEM) as indicated. After 5 min at 30°C, samples were fixed and stained with DAPI. Transport factors were localized by fluorescence microscopy and intranuclear fluorescence was quantified.

2.4.8 Measurement of mean intranuclear fluorescence for in vitro import assays

To quantify intranuclear fluorescence of TMR-labeled importin-α or CAS, cells were optically sectioned using a Zeiss 510 LSM laser scanning confocal microscope with a x63 objective (NA 1.4, full width half maximum of 0.65 μm for the optical slice at the pinhole setting used). A single optical slice through the center of the nucleus was chosen for quantitation. The effective nuclear thickness is much greater than the optical slice thickness under our imaging conditions, therefore cytosolic fluorescence should not contribute to the measured intensity. Average pixel intensities over the nuclei were quantified using Metamorph software (Universal Imaging). Fluorescent signals for 53 to 59 individual cells and background intensities were determined for each of the conditions. All images to be directly compared were taken under identical microscope settings using appropriate rhodamine optics.

2.4.9 Statistics

To measure fluorescence signals in nuclei and cytoplasm, data for at least 50 cells were acquired for each of the different conditions. Data were obtained for at least three independent experiments. Results are shown as means ± STDEV and Student's *t* test (two-tailed) for unpaired samples was carried out to identify significant differences.

2.4.10 Western blot analysis

HeLa cells were grown on dishes to 50 to 70% confluency. Cells were stressed as described above, washed with PBS and stored at -70°C until use. Crude extracts were prepared by solubilizing proteins in gel sample buffer, pH 8.0, containing protease inhibitors (aprotinin, leupeptin, pepstatin, each at 1 μg/ml; 1 mM PMSF), 20 mM β-glycerophosphate, 1 mM NaN_3, 2.5 mM NaF. Samples were incubated for 10 min at 95°C and vortexed with glass beads to shear DNA. After centrifugation (5 min, 13,000 rpm, microfuge) equal amounts of protein were separated by SDS-PAGE. Proteins were blotted to nitrocellulose and blots processed as described (87). Antibodies were used at the following dilutions: Nup153, (1:200); mab414 (1:5,000; BabCo, Richmond, CA), Nup88 (1:100; Novocastra, Newcastle, UK, or 1:1,000; BD Biosciences; Mississauga, ON); hsc70 (1:2,000; SPA-815 and SPA-816, Stressgen); actin (1:1,000, Chemicon, Temecula, CA). All other antibodies were purchased from Santa Cruz Biotechn.: importin-α1 (1:500, sc-6917), importin-β1 (1:400, sc-11367), CAS (1:200, sc-1708), Ran (1:500, sc-1156), tubulin (1:2,000, sc-5286).

2.4.11 Indirect immunoprecipitation

For immunoprecipitations under native conditions control and stressed cells were extracted with 40 μg/ml digitonin in PBS for 5 min on ice. All subsequent steps were carried out at 4°C. Cells were washed with cold PBS and proteins were solubilized in PBS, 1% NP40, 2.5 mM NaF, 20 mM β-glycerophosphate, 1 mM NaN_3, and a mixture of protease inhibitors (aprotinin, leupeptin, pepstatin, each at 1μg/ml, 1 mM PMSF). After 10 min incubation samples were vortexed several times with glass beads, cleared by centrifugation (5 min, 15,000 rpm, microfuge) and pre-treated with protein G-Sepharose (Pharmacia Biotech, Baie d'Urfé) for 30 min with gentle agitation. Supernatants obtained after 5 min centrifugation at 13,000 rpm were incubated with antibodies against importin-α1, Nup153 or Nup88 for 1 h, followed by addition of protein-G-Sepharose and overnight incubation. Beads were collected by centrifugation (3 min, 13,000 rpm) and washed three times with PBS/1 mM NaN_3. Bound material was released by incubation in gel sample buffer for 10 min at 95°C and supernatants (5 min, 13,000 rpm, room temperature) were subjected to Western blot analysis.

2.4.12 Affinity purification with immobilized importin-α

His6-tagged importin-α was purified from bacteria and dialyzed against 20 mM MOPS, 100 mM sodium acetate, 5 mM magnesium acetate, 5 mM imidazole, 2.5 mM NaF, pH 7.1 (binding buffer). Ni-TA resin (Qiagen) was preloaded with importin-α in binding buffer for 1 h at 4°C and washed three times with binding buffer. Crude extracts were generated from digitonin-treated control or stressed cells in binding buffer containing 0.5 mM DTT, 0.5 % SDS and protease

inhibitors (aprotinin, leupeptin, pepstatin, each at 1 μg/ml; 1 mM PMSF). Samples were diluted into binding buffer containing protease inhibitors and Triton X-100 to give a final concentration of 1% Triton X-100, 0.1 % SDS and 0.1 mM DTT. Samples were vortexed with glass beads, centrifuged (3 min, 13,000 rpm) and incubated with immobilized importin-α for 1 h at 4°C. Beads were washed three times with binding buffer containing 1% Triton X-100 and bound material was analyzed by Western blotting.

2.4.13 Protein crosslinking and gel chromatography

Control and DEM-treated cells were extracted with 40 μg/ml digitonin in PBS for 5 min on ice, washed with ice-cold PBS and incubated with 0.2 mM 3.3'-Dithiobis [sulfosuccinimidylproprionate] (DTSSP, Pierce, Rockford, IL) in PBS for 1 h on ice. Plates were washed with ice-cold PBS and stored at -70°C. Proteins were solubilized in 10 mM Tris HCl pH 7.4, 1% SDS, 2.5 mM NaF, 1 mM NaN_3, containing protease inhibitors (aprotinin, leupeptin, pepstatin, each at 1 μg/ml; 1 mM PMSF). Samples were vortexed with glass beads and cleared by centrifugation (3 min, 13,000 rpm, microfuge). Supernatants were separated on a Superose-12 column (Pharmacia) and eluted in 10 mM Tris HCl pH 7.4, 0.1% SDS. A total of 25 fractions (1 ml) were collected and aliquots of each fraction were analyzed by Western blotting. For indirect immunoprecipitation, peak fractions were pooled and concentrated with Amicon centrifugal filters (Molecular weight cut off 10 KD). Samples containing 10 mM Tris HCl pH 7.4, 150 mM NaCl, 0.1% SDS, 1% NP40, 2.5 mM NaF, 20 mM β-glycerophosphate, 1 mM NaN_3, and a mixture of protease inhibitors (aprotinin, leupeptin, pepstatin,

each at 1μg/ml; 1 mM PMSF) were pre-treated with protein G-Sepharose and incubated with anti-Nup153 or anti-Nup88 antibodies as in section **2.4.11**.

2.4.14 Extraction of unfixed HeLa cells

Samples were treated buffer, detergent, DNase, NaCl, DNase + RNase essentially as described in ref. 212. After each step samples were processed for indirect immunofluorescence. Confocal imaging for each antigen was carried out at identical settings for all extraction steps.

2.5 Results

2.5.1 The effect of diethyl maleate (DEM) on nuclear envelope integrity

To determine whether DEM-treatment alters the permeability barrier of nuclear envelopes (NEs), we incubated HeLa cells with 1, 2 and 5 mM DEM or the solvent ethanol for 4 hours at 37°C (Fig. 2.1). Changes in nuclear membrane integrity were monitored with two independent assays (213). First, HeLa cells were transiently transfected with a plasmid encoding GFP-β-galactosidase, a fusion protein that is excluded from the nucleus. The absence of GFP-β-galactosidase from the nucleus indicates that the NE is intact (Fig. 2.1). Second, we tested whether antibodies against lamin B have access to the nuclear lamina when cells were fixed and treated with the detergent digitonin (213). Digitonin permeabilizes the plasma membrane, but leaves the NE intact, and staining with anti-lamin B antibodies is only observed when NEs have been disrupted. Both the localization of GFP-β-galactosidase and binding of antibodies against lamin B revealed that after 2 mM DEM treatment nuclear membranes remained intact, but

became permeable upon incubation with 5 mM DEM (Fig. 2.1 and reference 213).

2.5.2 Recovery of cells from DEM-induced oxidative stress

To test the effect on cell viability, we treated cells for 4 h with 2 mM DEM, allowed them to recover overnight and quantified the percentage of apoptotic and necrotic cells. In ethanol treated controls, approximately 4% of the cells were apoptotic or necrotic, which increased to approximately 20% upon incubation with DEM (Fig. 2.2). However, about 70% of the DEM-treated cells were neither necrotic nor apoptotic, suggesting that the majority of cells recovered from DEM-induced stress.

2.5.3 DEM treatment interferes with nuclear protein import

To determine whether DEM affects nuclear import, different substrates were analyzed, including transiently synthesized reporter proteins tagged with GFP or endogenous substrates HuR and galectin-3. The nuclear/cytoplasmic (nuc/cyt) distribution was quantified for each cargo for non-stress or stress conditions, and the nuc/cyt ratio in unstressed cells was defined as 1. A reduction of the nuc/cyt ratio in stressed cells would be consistent with impaired nuclear import.

In HeLa cells transiently transfected with a plasmid encoding NLS-GFP, which carries the SV40-NLS, the fluorescent reporter accumulates in nuclei only when classical nuclear import is constantly active (87). Upon treatment with 2 mM DEM the amount of NLS-GFP in the cytoplasm was increased, indicating that classical import was less efficient (Fig. 2.3A). The fluorescent tag GFP did

not change its localization in the presence of DEM; GFP was nuclear and cytoplasmic under all conditions tested (not shown).

A different reporter protein, GFP-tagged glucocorticoid receptor [GFP-GR (207)] is imported into the nucleus by importin-α1/β1 and importin-β7 (214). In the absence of hormone, GFP-GR was nuclear as well as cytoplasmic (Fig. 2.3B). Addition of dexamethasone resulted in the rapid nuclear accumulation of GFP-GR in unstressed cells (Fig. 2.3B), whereas most of the DEM-treated cells failed to concentrate GFP-GR in nuclei.

Using nontransfected cells, the effect of oxidative stress on endogenous substrates HuR and galectin-3 was analyzed. Both proteins are involved in RNA transport or processing and transported into nuclei via the classical importin-α dependent pathway (215, 216). HuR is nuclear under normal conditions, whereas a significant amount is cytoplasmic in stressed cells. Galectin-3, nuclear and cytoplasmic in unstressed cells, becomes less abundant in the nuclei following DEM exposure. Taken together, DEM treatment reduces the nuc/cyt ratio of GFP-tagged reporter proteins and endogenous cargos HuR and galectin-3 when compared with controls. These results are in line with the idea that DEM-induced oxidative stress interferes with nuclear protein import under conditions that leave the nuclear envelope intact.

2.5.4 Ran remains concentrated in nuclei upon incubation with 2 mM DEM

Stress can affect the nucleocytoplasmic Ran gradient and severe oxidative stress leads to a collapse of the gradient, ultimately causing the inhibition of nuclear transport (87). However, Ran did not relocate significantly at 2 mM DEM. By

contrast, the GTPase concentration gradient collapsed after treatment with 5 mM DEM (Fig. 2.4A), conditions that permeabilize the nuclear envelope (Fig. 2.1). This suggested that a loss of the nucleocytoplasmic Ran concentration gradient is not the key factor that interferes with nuclear transport upon treatment with 2 mM DEM and prompted us to analyze the effect of DEM on other nuclear transport components.

2.5.5 Importin-α, CAS, Nup153, Nup88 and Nup50 mislocalized in DEM-treated cells

Importin-α, a subunit of the dimeric classical import receptor, is exported from the nucleus by the importin-β-like carrier CAS. In HeLa cells, both importin-α and CAS concentrated in nuclei when cells were treated with 2 mM DEM, but not with the solvent ethanol (Fig. 2.4B, C). Interestingly, importin-α and CAS also accumulated in nuclei after a 5 mM DEM treatment, i.e. conditions that permeabilize the NE. This suggests that nuclear retention contributes to their nuclear concentration after oxidant exposure (see Fig. 2.7). In contrast, the localization of importin-β1 was not drastically changed at any of the DEM concentrations tested (not shown).

In addition, nucleoporins Nup153, Nup88 and Nup50 were localized in control and stressed cells. These nucleoporins were chosen because they contribute to different aspects of nuclear trafficking (see introduction); Nup153 participates in nuclear import and export, Nup88 is involved in export and Nup50 promotes importin-α-dependent nuclear import. Both Nup153 and Nup88 displayed a "ring like" staining of the nuclear periphery under non-stress conditions, and Nup88

was also detected in the cytoplasm. In control cells, Nup50 associated mostly with nuclei, but was present in the cytoplasm as well (Fig. 2.4D, E, F). After DEM treatment changes were observed for all of the nucleoporins (summarized in Table 2.1). Nup153 and Nup88 were detected in the nucleoplasm, and substantially more Nup88 was located in the cytoplasm, whereas Nup50 was no longer detected in the cytoplasm (Fig. 2.4D, E, F). Interestingly, in stressed cells the fluorescence signals for Nup153 increased, similar to the stronger signals obtained after Western blotting (see below).

2.5.6 Effect of DEM exposure on in vitro nuclear accumulation of transport factors

Different mechanisms may contribute to the nuclear accumulation of importin-α and CAS in DEM-treated cells; this may include an increase in nuclear import. We therefore measured the nuclear concentration of fluorescently labeled importin-α and CAS upon incubation with semi-intact cells. Since importin-α and CAS can be transported into nuclei *in vitro* by cytosol-dependent and independent pathways (217), nuclear accumulation was tested for six different conditions (Fig. 2.5). First, unstressed and stressed cells were semi-permeabilized and analyzed in the absence of exogenously added cytosol (Fig. 2.5A, B). Second, unstressed and stressed semi-intact cells were combined with cytosol prepared from control or DEM-treated cells (Fig. 2.5B). To detect minor differences in nuclear accumulation, the intranuclear fluorescence was measured for all of the conditions. There was little effect on importin-α nuclear accumulation for any of the conditions tested, although a small increase was seen when unstressed cells

were supplemented with stressed cytosol (Fig. 2.5B). For CAS, nuclear import was significantly higher when cytosol and semi-intact cells or cytosol only had been treated with DEM. The strongest effect was seen with cytosol prepared from DEM-treated cells, which increased nuclear import to about 140% of control samples (Fig. 2.5B). Thus, oxidative stress upregulates nuclear import and/or reduces nuclear export of CAS, thereby increasing the steady-state concentration of the carrier in nuclei *in vitro.* Based on the quantification shown in Fig. 2.5B DEM may also stimulate the cytosol-dependent nuclear concentration of importin-α, albeit to a lesser extent when compared with CAS.

2.5.7 Effect of DEM on the stability of transport factors

Oxidative stress may trigger the degradation of transport factors and the effect of DEM on protein levels was analyzed in control and oxidant-treated cells that had been incubated in the absence or presence of cycloheximide (Fig. 2.6A). Crude extracts were prepared for whole cells and comparable amounts of protein were separated in parallel. The amounts of importin-β1 were somewhat decreased by DEM, but the concentration of other proteins was not drastically reduced. Furthermore, Western blotting did not reveal the accumulation of proteolytic degradation products after DEM treatment (not shown). Interestingly, the levels of Nup153 were slightly increased upon incubation with DEM, even in the presence of cycloheximide. Together with the data described for Nup153 immunolocalization (Fig. 2.4D) this may indicate that DEM treatment stabilizes Nup153.

In summary, Western blot analyses support the idea that the nuclear distribution of importin-α, CAS, Nup88 or Nup153 in oxidant-treated cells represents the relocation of intact proteins and not simply a mislocalization of their proteolytic products generated upon stress.

2.5.8 Importin-α stably associates with Nup153 and Nup88 in nuclei of growing cells

The nuclear localization of importin-α could be controlled by its interaction with other components in the nucleus. To address this question, we immunoprecipitated importin-α from crude nuclear extracts under native conditions and monitored the co-purification of transport factors. This approach identifies stable associations, whereas transient or unstable interactions of importin-α as well as interactions that are disrupted by the antibody will be missed. For the experiments shown in Fig. 2.6B we used the same amounts of nuclear proteins from control and DEM-treated cells as starting material. Nup153 associated with importin-α under control and stress conditions, whereas Nup88 was not detected in immunoprecipitates. The absence of Nup88 from complexes isolated with anti-importin-α antibodies may suggest that this antibody interferes with the Nup88/importin-α interaction, since both proteins co-purified when anti-Nup88 antibodies were used and in pull down experiments (see below Fig. 2.6C, D). As expected, only little importin-β1 co-purified with importin-α in nuclear extracts of unstressed cells, as import complexes are disassembled in the nucleus. This co-purification of importin-β1 was further reduced after DEM treatment. The specificity of the interaction between Nup153 and importin-α is demonstrated by

the fact that other members of the FXFG family, including Nup62 and Nup214, did not copurify with importin-α. Likewise, CAS, hsc70, actin or tubulin did not bind to importin-α under these conditions (Fig. 2.6B). Furthermore, immunoprecipitation with anti-Nup153 or anti-Nup88 under native conditions both led to the co-purification of importin-α (Fig. 2.6C), in line with the idea that nucleoporins form complexes with this transport factor in nuclei. Neither hsc70 nor actin co-purified with Nup153 or Nup88 under these conditions.

Taken together, immunoprecipitation under native conditions indicates an association of importin-α with Nup153 and Nup88; this hypothesis is further substantiated by the results described below.

2.5.9 Importin-α associates with Nup153 and Nup88 in crude extracts

Immobilized importin-α was used as bait *in vitro* to purify binding partners from nuclear extracts prepared from control or DEM-treated cells (Fig. 2.6D). With this approach, Nup153 was efficiently pulled down, when compared to the starting material (Start, 10% of the pull down). A substantial amount of Nup88 was also affinity-purified, whereas CAS, importin-β1, actin, tubulin or the FXFG nucleoporin Nup62 did not associate with immobilized importin-α. Minor amounts of hsc70s were affinity purified with immobilized importin-α as well.

2.5.10 Importin-α is present in high molecular mass complexes that contain Nup153 and Nup88

Interactions of importin-α with other proteins could be transient only, unstable under the conditions used for co-purification or promoted by *in vivo* post-translational modifications of the bait. To address this problem, we reversibly

crosslinked proteins and analyzed components present in high molecular mass complexes. Since crosslinking interfered with anti-importin-α immunoprecipitation, we solubilized complexes in SDS and separated them by gel exclusion chromatography using a Superose-12 column. Individual fractions were probed for the presence of transport factors and importin-α was detected in a high molecular mass fraction, which eluted at a position similar to the marker dextran blue (Mol. mass ~$2x10^6$). The same fraction also contained Nup153 and Nup88, whereas CAS and importin-β1 were either absent or hardly detectable (Fig. 2.6E and data not shown). Complexes containing importin-α could be prepared from control and DEM-treated cells; however, the relative amounts of Nup153, Nup88 and hsc70 were substantially increased in complexes of stressed cells.

It was possible that importin-α, Nup153 and Nup88 were components of distinct protein complexes that have a similar molecular mass. Since crosslinking interfered with anti-importin-α immunoprecipitation, we addressed this point with antibodies against Nup153 and Nup88. Using high molecular mass complexes as starting material, both antibodies co-precipitated importin-α, supporting the idea that importin-α/Nup153 and importin-α1/Nup88 complexes were generated. For complexes containing importin-α/Nup153 or importin-α/Nup88 we did not detect importin-β1, Nup214, actin or tubulin, even after prolonged exposure of the filters (Fig. 2.6F, summarized in Table 2.2). Importantly, Nup153 and Nup88 co-purified under these conditions, indicating a Nup153/Nup88 association. These results established complexes that contained importin-α/Nup153, importin-

α/Nup88 or Nup153/Nup88. However, the experiments did not determine whether complexes are generated that harbor all three components (see model, Fig. 2.8). To begin to address this question, we used identical samples to quantify the input (defined as 100%) and the amounts of importin-α1 that co-purified with anti-Nup153 or anti-Nup88 (Fig. 2.6G). In these experiments, 81% of importin-α was precipitated with anti-Nup153 and 68% with anti-Nup88 antibodies, suggesting that at least some of complexes contained importin-α, Nup153 and Nup88 (see *Discussion* and model, Fig. 2.8).

2.5.11 Stress increases the nuclear retention of importin-α, CAS, Nup153 and Nup88

The nuclear accumulation of importin-α and CAS may be explained by increased nuclear import, increased nuclear retention, reduced nuclear export or a combination of these mechanisms. Quantitative analysis of *in vitro* nuclear trafficking of importin-α and CAS revealed that DEM treatment somewhat increased CAS and importin-α nuclear accumulation *in vitro* (Fig. 2.5). Since results described in the previous section suggested that the complex formation between importin-α and other proteins in the nucleus changes upon oxidant treatment, we tested whether these changes may correlate with stress-induced nuclear accumulation. To this end, control and DEM-treated cells were extracted with detergent, nucleases and salt. After each step, the presence of transport factors and nucleoporins was monitored by indirect immunofluorescence (Fig. 2.7, Suppl. Fig. 2.1, 2.2, 2.3). Individual proteins were solubilized at different steps of the procedure; however, in response to stress all of the components tested

became less soluble. For instance, importin-α was readily extracted in control cells, and after DNase incubation only faint signals were observed. By contrast, upon DEM-treatment a portion of importin-α remained associated with nuclei and was not extracted by any of the treatments (Fig. 2.7). Thus, the extraction of unfixed cells support the interpretation that DEM-induced oxidative stress upregulated the nuclear retention of importin-α, CAS and several nucleoporins, including Nup153 and Nup88, while the formation of high molecular mass complexes containing importin-α, Nup153 and Nup88 increased.

2.6 Discussion

We have analyzed the effects of the oxidant DEM on nuclear trafficking and demonstrated the mislocalization and nuclear retention of several nuclear transport factors. Under the stress conditions used by us most of the cells remained viable, although the number of apoptotic and necrotic cells was somewhat increased. These conditions are likely to mimic exposure to physiological stresses or the pathophysiologies seen upon ischemia/reperfusion damage (181-185).

The analyses of GFP-tagged reporter proteins or endogenous substrates HuR and galectin-3 show that the nuc/cyt ratio for all proteins is reduced by DEM treatment, consistent with an oxidant-induced inhibition of nuclear import. However, it should be kept in mind that the nucleocytoplasmic distribution of HuR and galectin-3, like most endogenous cargos, is probably subject to additional regulation, including nuclear export and interactions with nuclear or

cytoplasmic anchors. Our experiments do not address the question to which extent DEM alters these processes.

Our studies show for the first time that oxidant treatment not only relocates the soluble transport factors importin-α and CAS, but also nucleoporins Nup153 and Nup88. Interestingly, not all transport factors are affected by oxidative stress to the same extent, as we did not observe a strong effect for the localization of importin-β1. Moreover, we did not detect drastic changes in the nucleocytoplasmic Ran concentration gradient, which is sensitive to severe forms of stress that inhibit nuclear transport and may ultimately lead to cell death (87).

Results obtained for importin-α, CAS and nucleoporins are of particular interest with respect to nuclear protein trafficking. These components are required for nuclear transport of a wide variety of cargos, either as subunit of the classical NLS-receptor, to recycle importin-α to the cytoplasm or for the translocation of transport complexes across the NPC. Moreover, transport of proteins into the nucleus is an essential step of the stress response and necessary to cope with stress-induced damage, including exposure to oxidants. For instance, following oxidative stress transcription factors NF-κB, Nrf2 and members of the FoxO family translocate into the nucleus where they induce the expression of genes that encode antiapoptotic proteins or detoxifying enzymes (218-220). Changes in the steady-state distribution of importin-α and CAS may inhibit these processes or render them less efficient.

Oxidative stress not only changes the distribution of soluble transport factors and nucleoporins, but also alters their interactions in the nucleus. Specifically,

oxidant treatment leads to the formation of high molecular mass complexes which is accompanied by an increase in nuclear retention. Our experiments show for the first time that oxidant treatment relocates several nucleoporins to the nuclear interior, where they become components of high molecular mass complexes. These complexes contain importin-α, Nup153 and Nup88, but not CAS, suggesting that importin-α associates with a defined set of proteins in nuclei of stressed cells. Although importin-α containing high molecular mass complexes were isolated from control and stressed cells, the levels of Nup153 and Nup88 substantially increased after DEM treatment. Further analyses of high molecular mass complexes isolated from stressed cells demonstrated that importin-α associates with Nup153 as well as Nup88; furthermore, Nup153 binds to Nup88 (Fig. 2.8). This could be explained by the presence of different complexes containing importin-α/Nup153, importin-α/Nup88 and Nup153/Nup88, a complex harboring importin-α/Nup153/Nup88 or mixture of all four complexes. Quantitation of immunoprecipitations showed that 81% of importin-α co-purified with Nup153 and 68% with Nup88, indicating that a portion of importin-α is likely to associate with both nucleoporins to generate importin-α/Nup153/Nup88 complexes.

Several scenarios can be proposed for the biochemical mechanisms that may link oxidative stress to the changes observed by us. For instance, oxidant treatment may lead to direct damage of soluble transport factors and nucleoporins or changes in signaling events. DEM may trigger not only the oxidation of critical residues in importin-α, CAS and nucleoporins; it may also activate signaling

events that induce specific post-translational modifications of these proteins. As a consequence of oxidation or other modifications, transport across the NPC and retention within the cytoplasm or nucleus may be altered. With respect to our results one could propose that oxidative stress alters the affinity between importin-α and its binding partners in the nucleus, thereby promoting nuclear retention. The changes in affinity may result from the increased modifications of importin-α, Nup153 and Nup88, either alone or in combination. Given the molecular mass of the complexes isolated by us, they may contain additional components yet to be identified. These factors and their potential role in nuclear trafficking under normal and stress conditions will have to be defined in the future.

Little is known about stress-induced changes in the distribution and function of nucleoporins. We have shown previously that severe stress triggers the degradation of Nup153 (87). The impact of non-lethal stress on nucleoporins is only poorly understood, but could play a role in human disease. For instance, mutations in the nucleoporin ALADIN may cause Triple A syndrome, and these mutations can also induce mislocalization of ALADIN, hypersensitivity to oxidative stress and defects in nuclear transport (212, 222). Our research demonstrates that stress modulates the localization and interactions of several nucleoporins in human cells. This sets the stage to further define the role of nucleoporins in the change of nuclear functions under stress and pathophysiological conditions.

2.7 Acknowledgements

We thank Drs. L. Gerace and W. Franke for generous gifts of antibodies. We are grateful to Dr. J. Liu (HTS/HCS Facility at McGill University), K. McDonald and A. Srivastava for their help with ImageXpress Micro, FACS and confocal analyses. US was supported by grants from CIHR, NSERC and Heart and Stroke Foundation of Canada and is a chercheur national of FRSQ. MK was supported by a doctoral fellowship from FRSQ and the Heart and Stroke Foundation of Canada, CQ and AM by research bursaries from McGill University.

Table 2.1 Location of soluble transport factors and nucleoporins in control and DEM-treated cells

Protein	control conditions (ethanol)	oxidative stress (2 mM DEM)
Ran	N>>C	N>>C
Importin-α	NE, N+C	N>C
CAS	N≥C, N+C	N>C
Nup153	NE	(NE), N>C
Nup88	NE, (N<C)	(NE), N + C
Nup50	N>C	N>>C

Table 2.1 Location of soluble transport factors and nucleoporins in control and DEM-treated cells

Proteins were located by indirect immunofluorescence after 4 hours incubation under control (ethanol) conditions or treatment with DEM. N>>C, nuclear accumulation with no or little cytoplasmic staining; N>C, nuclear accumulation with cytoplasmic staining; N≥C, weak nuclear accumulation with well defined cytoplasmic staining; N+C, equal staining in nucleus and cytoplasm; NE, nuclear envelope.

Table 2.2 Analysis of high molecular mass complexes in nuclei of DEM-treated cells

Protein	anti-Nup153 IP	anti-Nup88 IP
Importin-α	+	+
Nup153	+	+
Nup88	+	+
Nup214	-	-
Importin-β1	-	-
Hsc70	(+/-)	(+/-)
Actin	-	-
Tubulin	-	-

Table 2.2 Analysis of high molecular mass complexes in nuclei of DEM-treated cells

High molecular mass complexes obtained after FPLC were subjected to immunoprecipitation with anti-Nup153 and anti-Nup88 antibodies. Immunoprecipitates were separated by SDS-PAGE and Western blots were probed with antibodies against the proteins listed. Results are shown for at least three independent experiments. Co-purification is indicated by +, variable amounts of hsc70s co-purified with anti-Nup153 and anti-Nup88 are shown as (+/-). Proteins listed as – were not detected in immunoprecipitates.

Figure 2.1

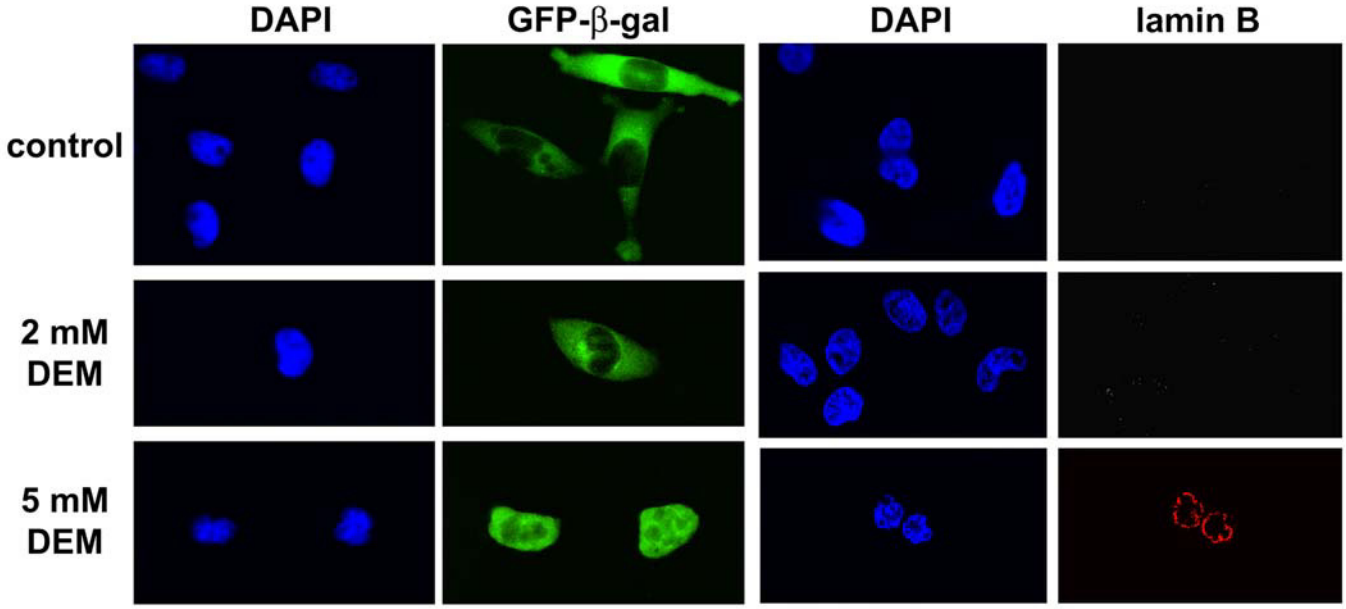

Figure 2.1 Effect of DEM on nuclear envelope integrity

HeLa cells transiently synthesizing GFP-β-galactosidase were incubated for 4 hours with ethanol (control) or DEM as indicated. Cells were fixed and the reporter protein localized by fluorescence microscopy (GFP-β-gal). Nontransfected HeLa cells were incubated with ethanol, 2 mM or 5 mM DEM. Fixed cells were semi-permeabilized with digitonin and incubated with anti-lamin B antibodies (213). Nuclei were located with DAPI. Note that GFP-β-gal appears in nuclei and lamin B is accessible to antibodies only after treatment with 5 mM, but not 2 mM DEM.

Figure 2.2

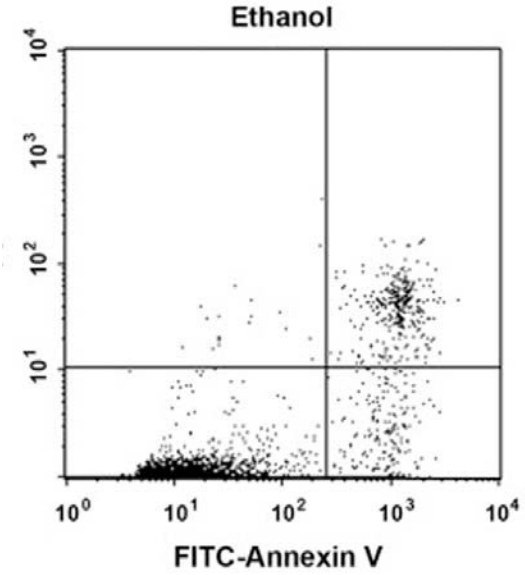

UL	132	±	156
UR	308	±	78
LL	9346	±	112
LR	215	±	190

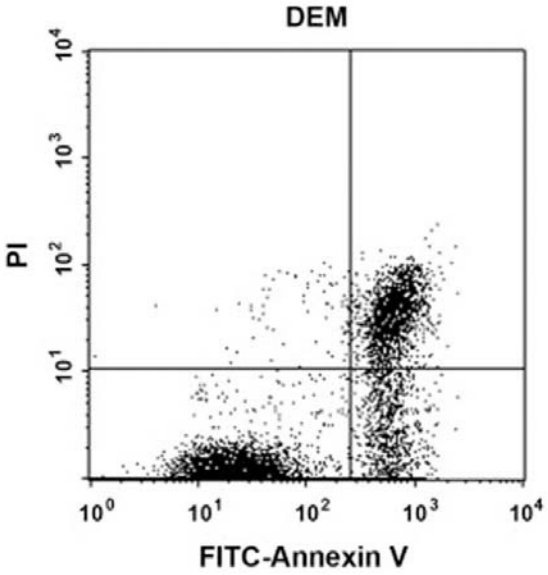

UL	76	±	6
UR	1019	±	8
LL	6648	±	137
LR	1347	±	137

Figure 2.2 Flow cytometry

HeLa cells were incubated with ethanol or 2 mM DEM for 4 hours and further treated as described in Materials and Methods. Binding of FITC-Annexin V or propidium iodide (PI) was quantified for 10,000 cells. Means and standard deviations are depicted for two separate experiments.

Figure 2.3

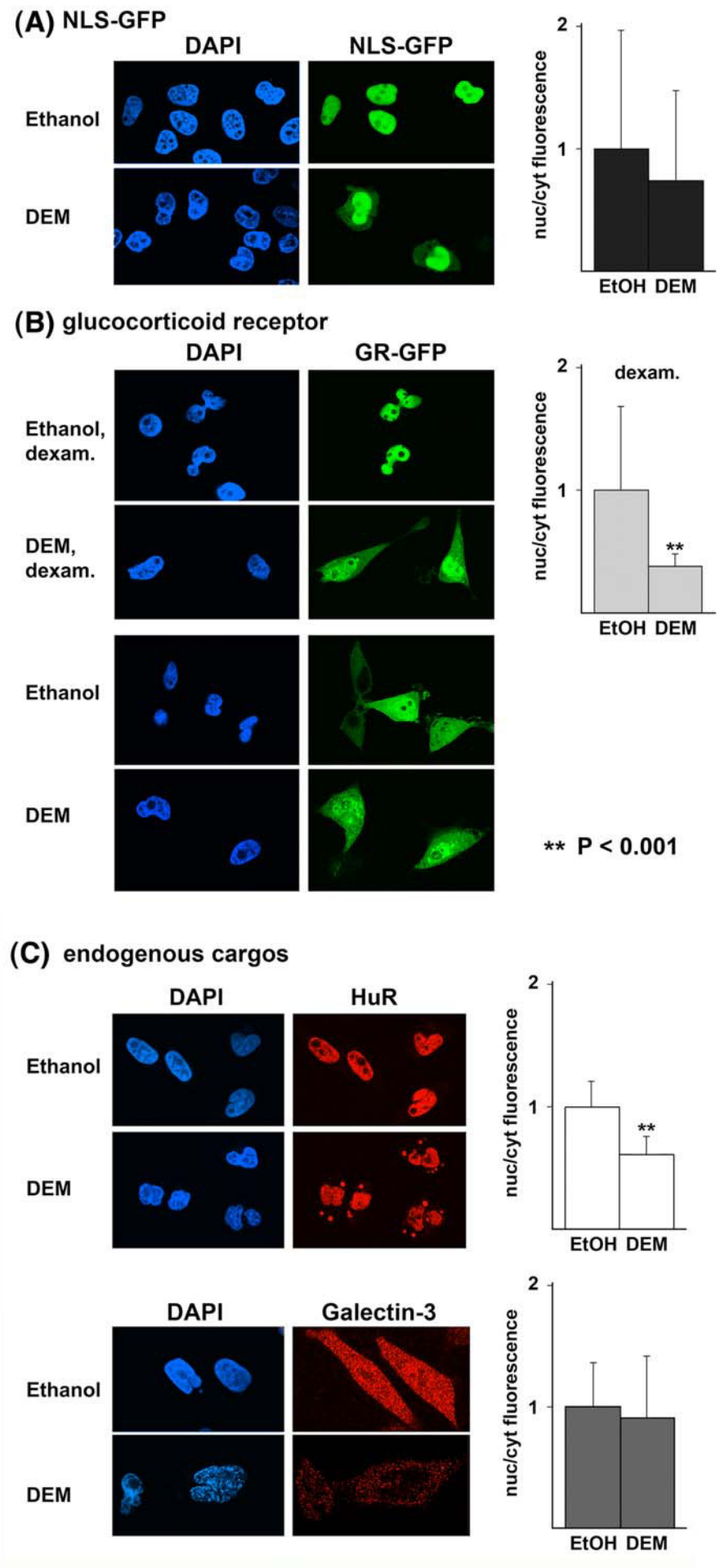
(A) NLS-GFP
DAPI
NLS-GFP
Ethanol
DEM
nuc/cyt fluorescence
2
1
EtOH DEM
(B) glucocorticoid receptor
DAPI
GR-GFP
Ethanol, dexam.
DEM, dexam.
Ethanol
DEM
dexam.
**
** P < 0.001
(C) endogenous cargos
DAPI
HuR
Ethanol
DEM
DAPI
Galectin-3
Ethanol
DEM

Figure 2.3 The oxidant DEM interferes with nuclear import in growing HeLa cells

Transiently synthesized reporter proteins **(A, B)** and endogenous cargos **(C)** were localized in HeLa cells grown for 4 hours under non-stress (ethanol) or stress conditions (DEM). NLS-GFP import is constitutively active; GR-GFP is transported into nuclei upon addition of dexamethasone (dexam.). **(C)** Endogenous proteins HuR and galectin-3 were located by indirect immunofluorescence. DAPI staining of the nuclei and signals for fluorescent signals for reporter proteins are shown. The nuclear/cytoplasmic ratio (nuc/cyt) of fluorescence was quantified for each cargo. The ratio for control cells incubated with ethanol was defined as 1. Means and STDEV are shown; ** $P < 0.01$. Note that a reduction of the nuc/cyt ratio of reporter proteins upon DEM treatment is consistent with less efficient nuclear import.

Figure 2.4

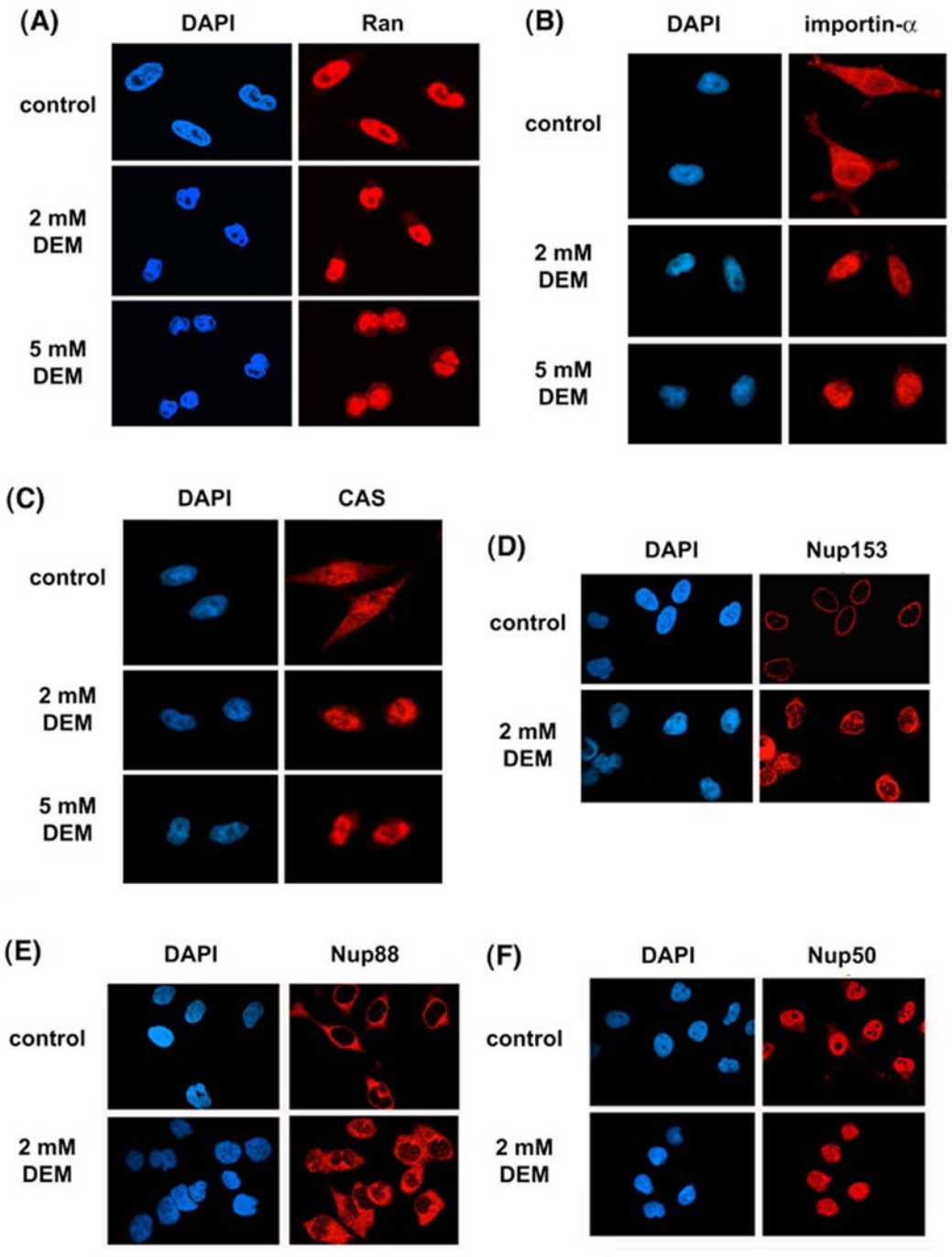
(A)
DAPI
Ran
control
2 mM DEM
5 mM DEM
(B)
DAPI
importin-α
control
2 mM DEM
5 mM DEM
(C)
DAPI
CAS
control
2 mM DEM
5 mM DEM
(D)
DAPI
Nup153
control
2 mM DEM
(E)
DAPI
Nup88
control
2 mM DEM
(F)
DAPI
Nup50
control
2 mM DEM

Figure 2.4 Effect of DEM on the location of Ran (A), importin-α (B), CAS (C), nucleoporins Nup153 (D), Nup88 (E) and Nup50 (F)

HeLa cells treated for 4 hours with ethanol (control), 2 mM or 5 mM DEM were fixed and different proteins were localized by indirect immunofluorescence followed by confocal microscopy as detailed in Materials and methods. Nuclei were visualized with DAPI.

Figure 2.5

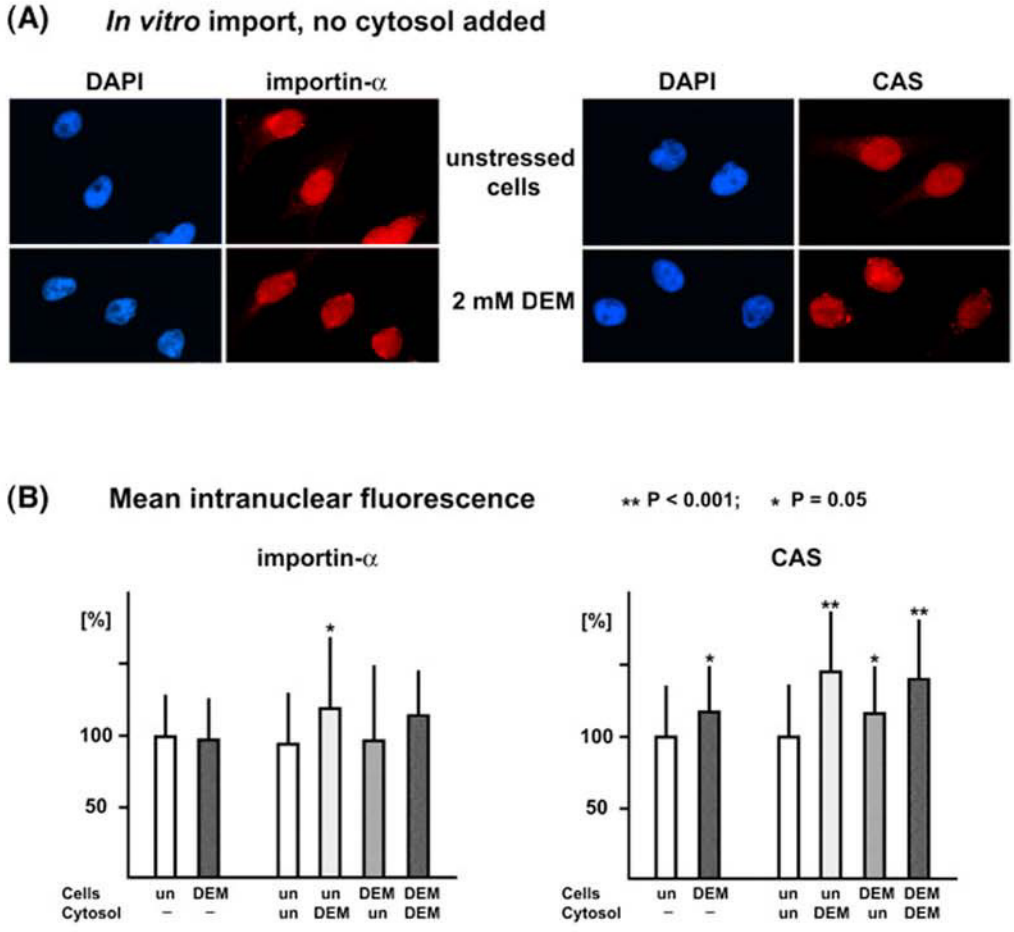
(A)
In vitro import, no cytosol added
DAPI
importin-α
DAPI
CAS
unstressed cells
2 mM DEM
(B)
Mean intranuclear fluorescence
** P < 0.001; * P = 0.05
importin-α
CAS
[%]
100
50
Cells
Cytosol
un
DEM
un
un
un
DEM
DEM
un
DEM
DEM

Figure 2.5 Stress-induced changes in nuclear accumulation of importin-α and CAS

(A) *In vitro* nuclear import of fluorescently labeled importin-α and CAS was carried out with semi-intact HeLa cells. Nuclear import was carried out *in vitro* with fluorescently labeled importin-α or CAS in the absence (-) or presence of exogenously added cytosol. Cytosol was prepared from unstressed controls (un) or DEM-treated cells (DEM). **(B)** Mean intranuclear fluorescence was quantified as described in Materials and methods. Fluorescence intensities obtained for unstressed cells were defined as 100% (white bars).

Figure 2.6

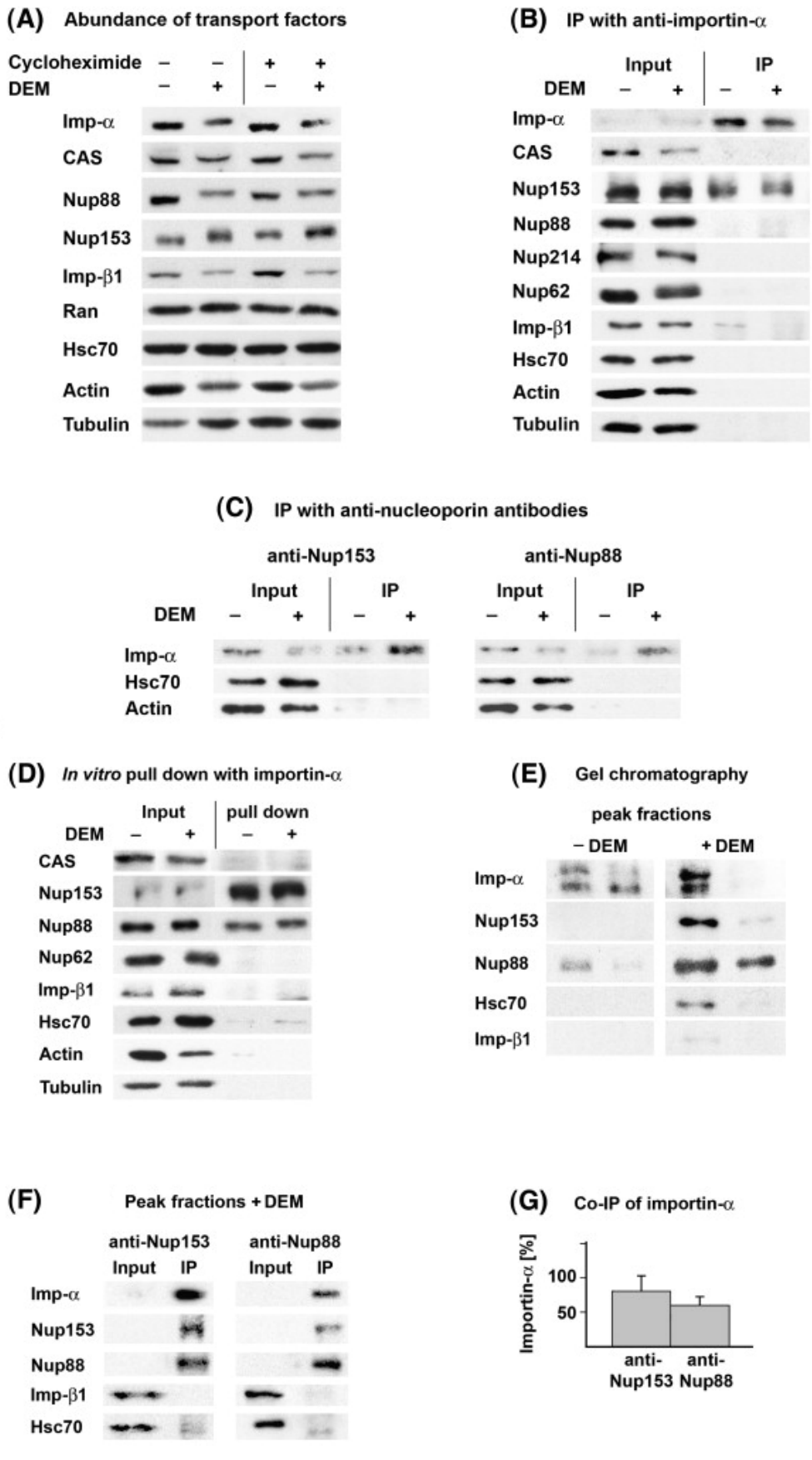
(A) Abundance of transport factors
Cycloheximide – – + +
DEM – + – +
Imp-α
CAS
Nup88
Nup153
Imp-β1
Ran
Hsc70
Actin
Tubulin
(B) IP with anti-importin-α
Input IP
DEM – + – +
Imp-α
CAS
Nup153
Nup88
Nup214
Nup62
Imp-β1
Hsc70
Actin
Tubulin
(C) IP with anti-nucleoporin antibodies
anti-Nup153
anti-Nup88
Input IP
DEM – + – +
Imp-α
Hsc70
Actin
(D) In vitro pull down with importin-α
Input pull down
DEM – + – +
CAS
Nup153
Nup88
Nup62
Imp-β1
Hsc70
Actin
Tubulin
(E) Gel chromatography
peak fractions
– DEM + DEM
Imp-α
Nup153
Nup88
Hsc70
Imp-β1
(F) Peak fractions + DEM
anti-Nup153 anti-Nup88
Input IP Input IP
Imp-α
Nup153
Nup88
Imp-β1
Hsc70
(G) Co-IP of importin-α
Importin-α [%]
100
50
anti-Nup153
anti-Nup88

Figure 2.6

(A) Effect of DEM on protein abundance. HeLa cells were incubated with the solvent ethanol (-DEM) or 2 mM DEM for 4 hours. Cycloheximide was present at 100 μg/ml as indicated. Equal amounts of protein from whole cell extracts were analyzed side-by-side. **(B)** Interaction of importin-α with other nuclear transport factors in growing cells. Nuclear extracts from control and stressed cells were used to immunoprecipitate importin-α under native conditions. Co-purified proteins were detected by Western blotting of the immunoprecipitates. Aliquots of the starting material (Input) represent 8% of the immunoprecipitates (IP). **(C)** Interaction of Nup153 and Nup88 with importin-α. Immunoprecipitations with anti-Nup153 and anti-Nup88 were carried out as described for part **(B)**. Immunopurified material was analyzed for the presence of importin-α, hsc70 and actin. **(D)** Binding of nuclear transport factors to purified importin-α *in vitro*. His6-tagged importin-α was purified from bacteria and immobilized on Ni-NTA beads. Equal amounts of protein from nuclear extracts were added to immobilized importin-α and material bound was analyzed by Western blotting. Input shows 10% of the starting material used for affinity purification. Note that Nup153 and Nup88 were efficiently pulled down under these conditions. **(E)** Importin-α forms high molecular weight complexes with Nup153 and Nup88 in nuclei. Control and DEM-treated cells were extracted with digitonin and proteins were reversibly crosslinked. Equal amounts of crosslinked protein were separated by gel exclusion chromatography (FPLC) and peak fractions containing high molecular mass complexes (molecular mass of > 1MD) were analyzed by Western blotting. ECL-signals for control and DEM-treated samples were obtained under identical conditions. **(F)** High molecular mass complexes obtained after

FPLC were analyzed by immunoprecipitation with anti-Nup153 and anti-Nup88 antibodies. Input represents 8% of the starting material. Note that prolonged exposure times were required to visualize importin-β1. **(G)** To quantify the co-purification of importin-α with Nup153 and Nup88 peak fractions were split into three identical samples to measure the input or co-purification with Nup153 or Nup88 by quantitative Western blotting (210). Importin-α present in the input was defined as 100%. The graph shows means and STDEV of four independent experiments.

Figure 2.7

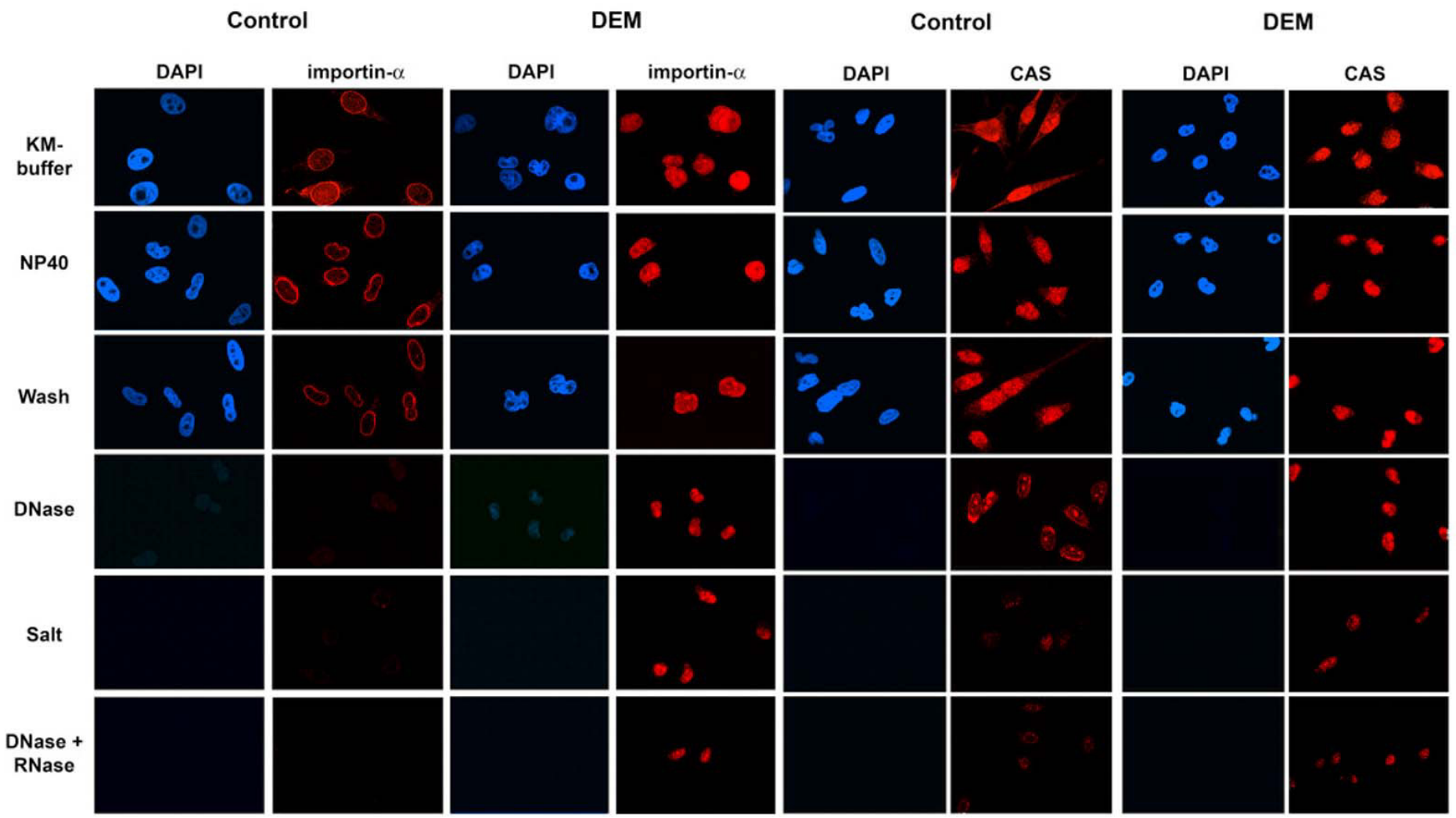
Control
DEM
Control
DEM
DAPI
importin-α
DAPI
importin-α
DAPI
CAS
DAPI
CAS
KM-buffer
NP40
Wash
DNase
Salt
DNase + RNase

Figure 2.7 Oxidative stress increases the nuclear retention of importin-α and CAS

Control and DEM-stressed cells were incubated with KM buffer followed by treatment with NP40, washing with buffer and treatment with DNase, salt as well as DNase + RNase (212). Samples were fixed after each step and proteins were located by indirect immunofluorescence. For each protein, all samples were visualized with identical settings of the confocal microscope.

Figure 2.8

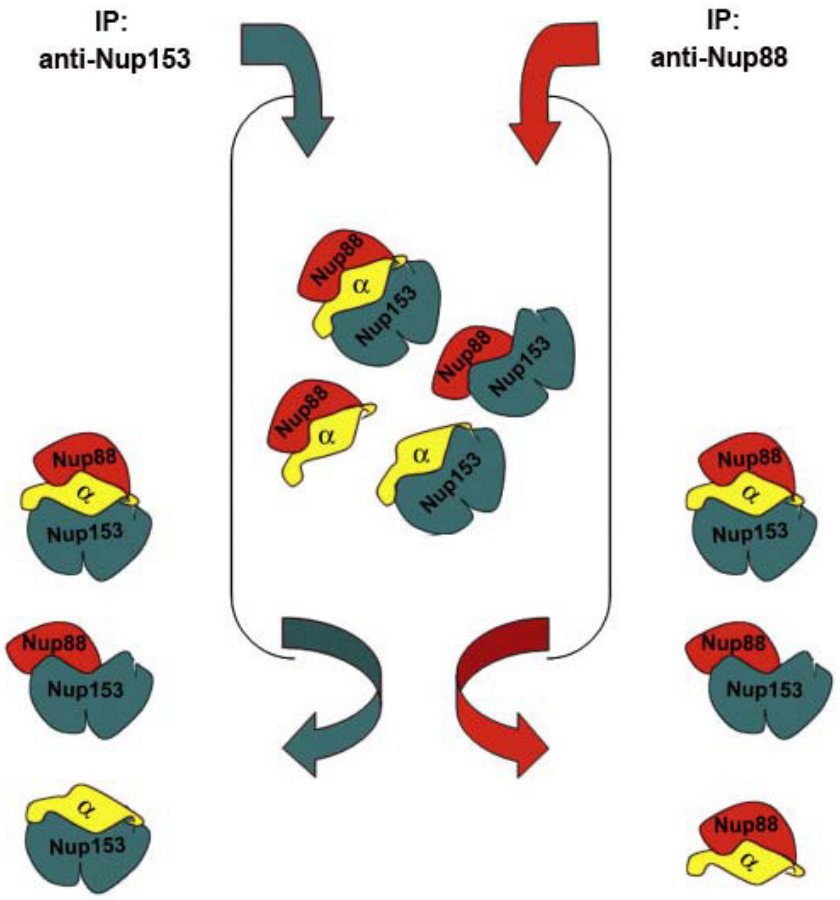

Figure 2.8 Simplified model for the isolation of high molecular mass complexes containing Nup153 or Nup88

High molecular mass complexes analyzed in Fig. 2.6E and F may contain Nup153, Nup88 and/or importin-α as depicted. For simplicity, other subunits of the complexes which have yet to be identified were omitted. See text for details.

Suppl. Figure 1

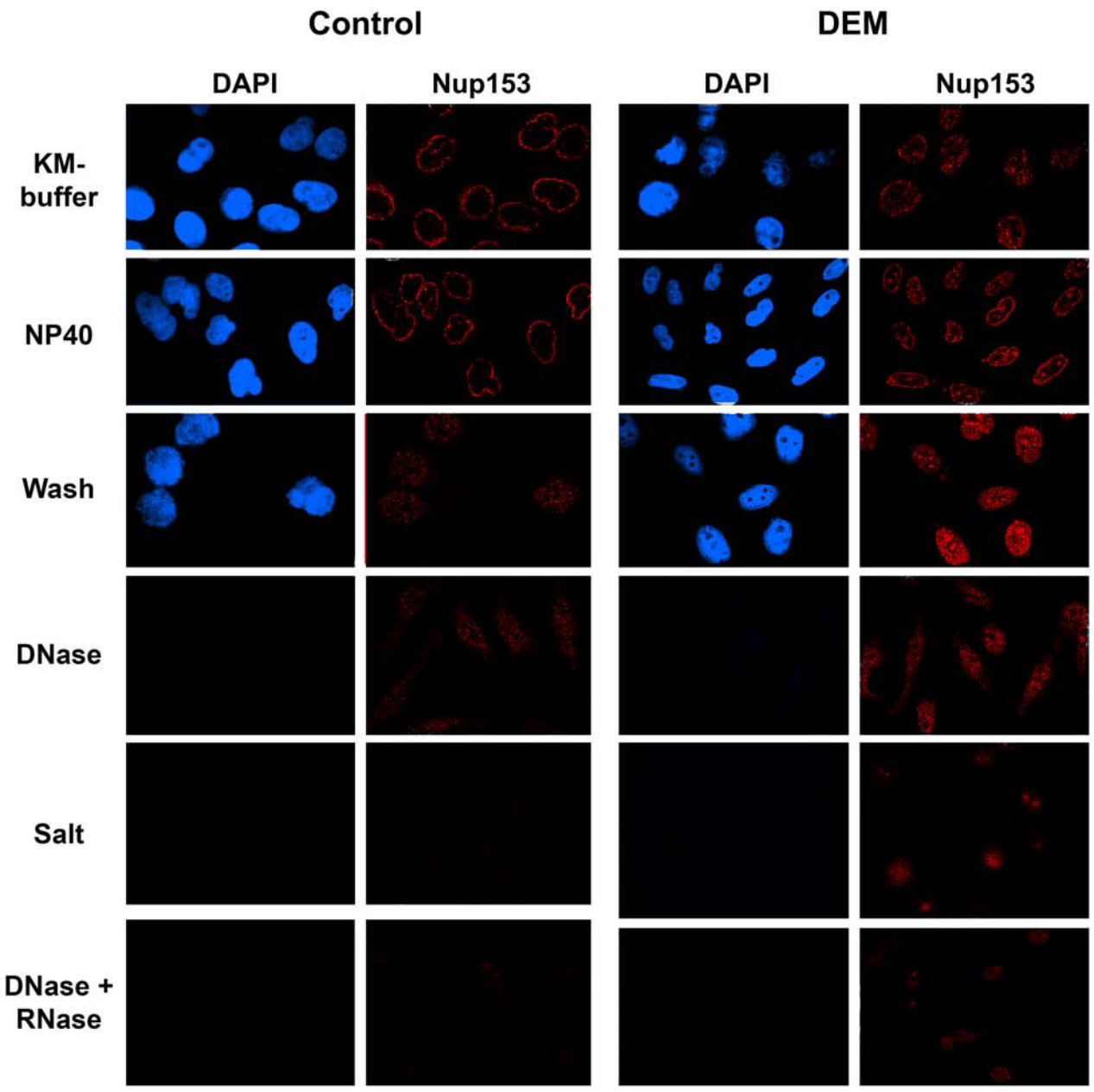

Suppl. Fig. 2.1

Nuclear retention of Nup153 was analyzed as described for Fig. 2.7

Suppl. Figure 2

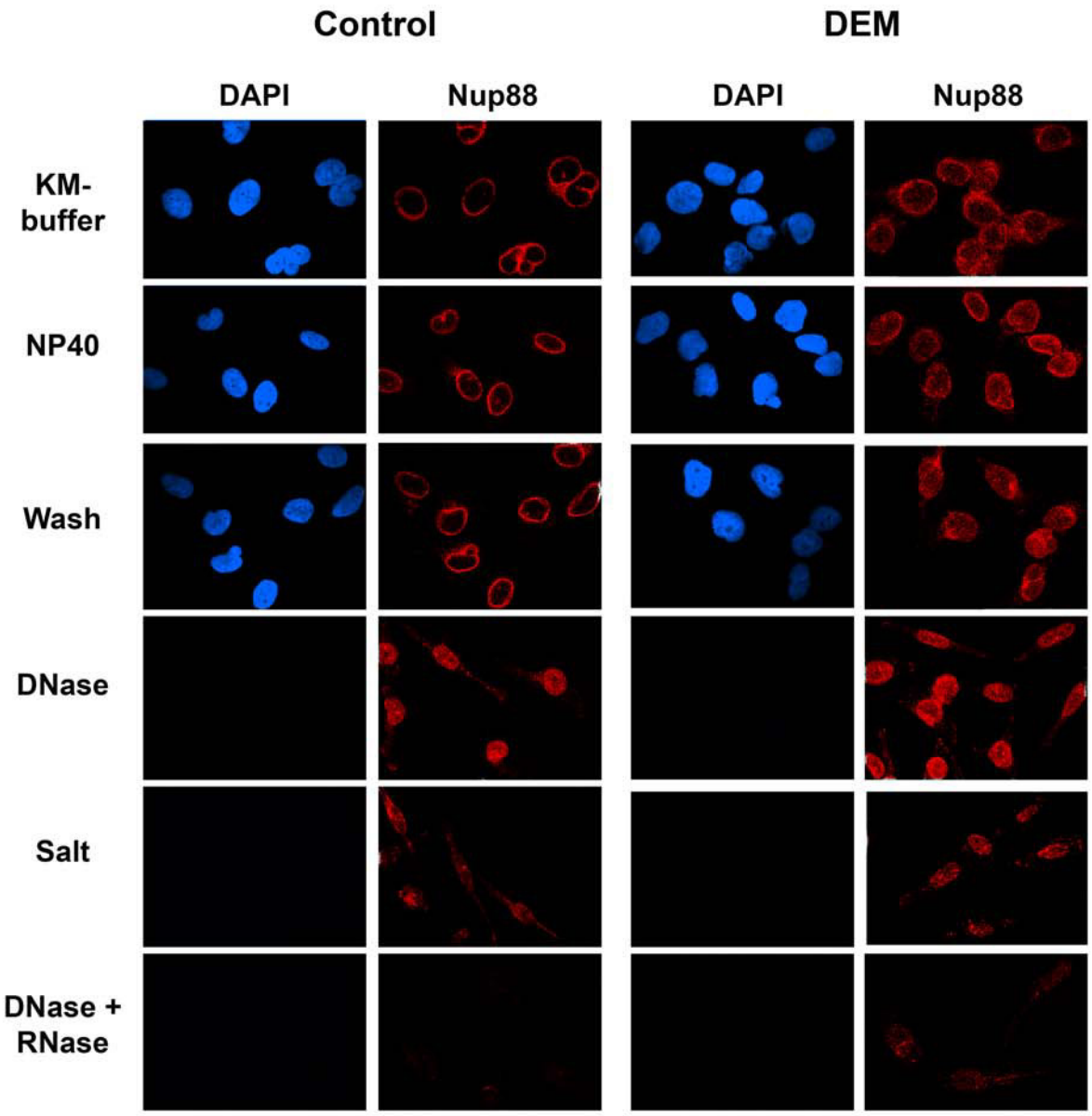

Suppl. Fig. 2.2

Retention of Nup88 in nuclei was determined as in Fig. 2.7

Suppl. Figure 3

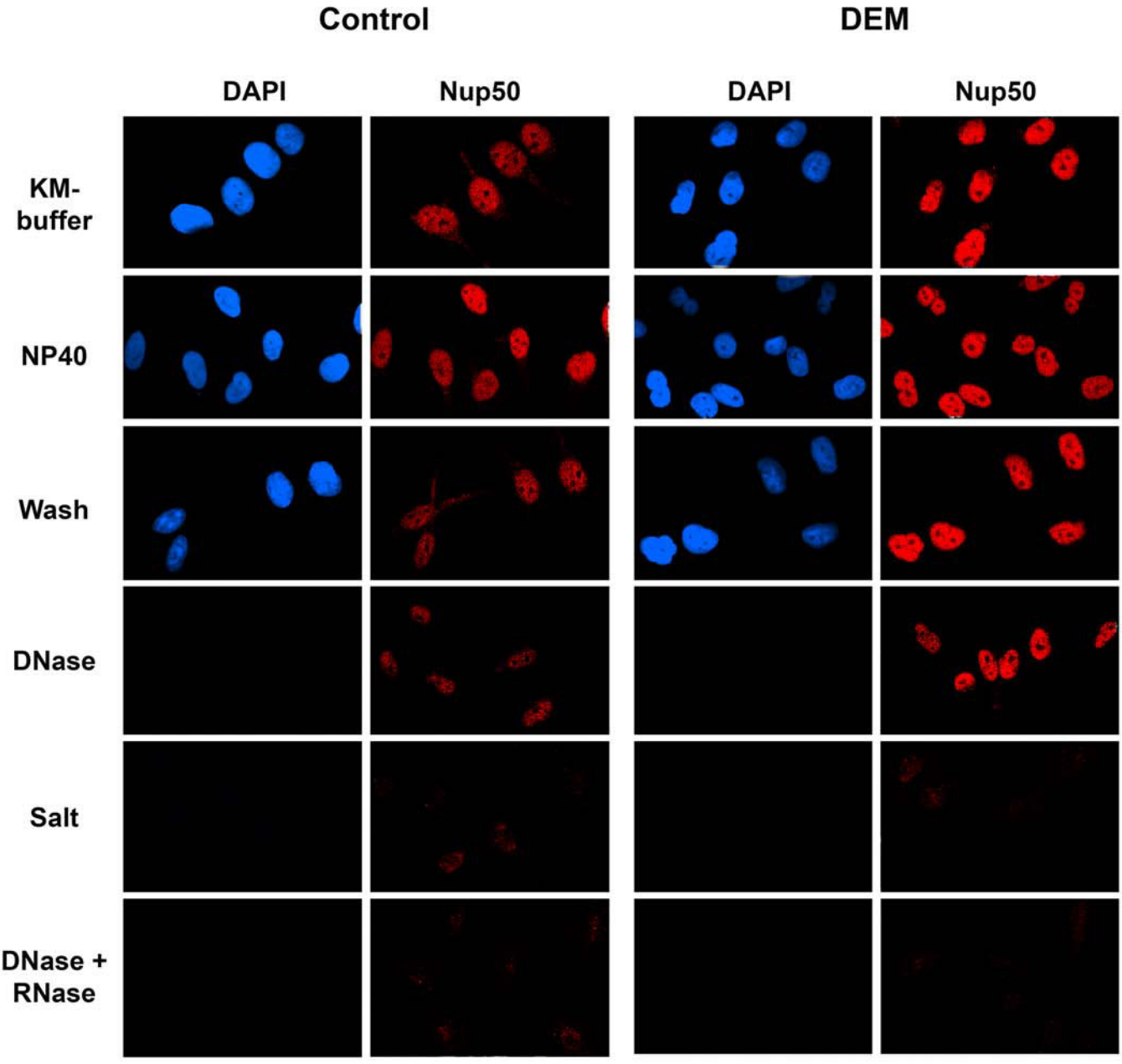

Suppl. Fig. 2.3

Nuclear retention of Nup50 was monitored as in Fig. 2.7

CHAPTER 3

Localization of AMP Kinase Is Regulated By Stress, Cell Density and Signaling Through the MEK→ERK1/2 Pathway

Mohamed Kodiha, James G. Rassi, *Claire M. Brown, and Ursula Stochaj

Department of Physiology, *Department of Biochemistry and Life Sciences
Imaging Facility, McGill University, Montreal H3G 1Y6, Canada

3.1 Connecting text to chapter 3

In the previous chapter I have analyzed the effects of oxidative stress on nucleocytoplasmic trafficking. In particular, my research defined the molecular mechanisms that control the function of soluble nuclear transport factors and nucleoporins in stressed cells. As a result of this work, I identified the stress-induced changes to transport factors importin-α, CAS as well as nucleoporins Nup153, Nup88 and Nup50. Furthermore, I demonstrated that these changes trigger the inhibition of classical nuclear import. Ultimately, classical import inhibition disrupts the proper communication between nucleus and cytoplasm. Under severe stress conditions this may lead to cell death. To obtain a broader perspective of how oxidants alter cell physiology, I have extended my research towards the characterization of cellular signaling events that are modulated by stress. Following oxidant exposure, cells respond by activating different signaling cascades, a process required for cell survival and the repair of stress-induced damage. A crucial component of the cell signaling machinery that can be regulated by modulation of nuclear trafficking is AMP-activated protein kinase (AMPK).

AMPK is a key player in many metabolic processes and central to the development of type-2 diabetes or obesity. Furthermore, activation of AMPK is required to protect heart cells against ischemia reperfusion injury.

AMPK is present in the nucleus and cytoplasm; however, little is known about the dynamic nature of this distribution. In particular, the mechanisms that regulate the intracellular localization of AMPK subunits are not characterized at the

molecular level. Such a regulated localization to different cell compartments determines the nuclear and cytoplasmic AMPK-targets that will be phosphorylated to cope with changes in the cellular environment. Despite the effect of stress on nucleocytoplasmic transport, it has not been determined previously how different forms of stress affect the intracellular distribution of AMPK.

The main objective of my research was to provide new insight into how different stressors modulate the activation and subcellular localization of AMPK. Using different human cell lines as model systems, I identified several factors, including environmental stresses such as heat, energy depletion and oxidants as well as signaling events which control the subcellular distribution of AMPK. Furthermore, I characterized the mechanisms that mediate AMPK shuttling between the nucleus and the cytoplasm, a process that depends on the nuclear exporter Crm1. Finally, my studies identified a novel links between the physiological state of the cell, the activation of MEK→ERK1/2 signaling and the nucleocytoplasmic distribution of AMPK.

These findings are important, as they will set the stage to identify specific AMPK functions in either the nuclear or cytoplasmic compartment that are dictated by changes in cell physiology. This will help to develop new strategies to regulate the intracellular distribution of AMPK and thereby the modification of its targets. Ultimately, this may lead to alternative therapeutic tools for many metabolic diseases such as diabetes and obesity. The results obtained from this study are published in the paper entitled, “The localization of AMP kinase is

regulated by stress, cell density and signaling through the MEK→ERK1/2 pathway". By ***Mohamed Kodiha****, James G. Rassi, Claire M. Brown, and Ursula Stochaj*. This paper is presented in detail in chapter 3.

3.2 Abstract

AMP kinase (AMPK) serves as an energy sensor and is at the center of control for a large number of metabolic reactions, thereby playing a crucial role in Type 2 diabetes and other human diseases. AMPK is present in the nucleus and cytoplasm; however, the mechanisms that regulate the intracellular localization of AMPK are poorly understood. We have now identified several factors that control the distribution of AMPK. Environmental stress regulates the intracellular localization of AMPK, and upon recovery from heat shock or oxidant exposure AMPK accumulates in nuclei. We show that under normal growth conditions AMPK shuttles between the nucleus and the cytoplasm, a process that depends on the nuclear exporter Crm1. However, nucleocytoplasmic shuttling does not take place in high density cell cultures, for which AMPK is confined to the cytoplasm. Furthermore, we demonstrate that signaling through the MEK→ERK1/2 cascade plays a crucial role in controlling the proper localization of AMPK. As such, pharmacological inhibitors that interfere with this pathway alter AMPK distribution under nonstress conditions. Taken together, our studies identify novel links between the physiological state of the cell, the activation of MEK→ERK1/2 signaling and the nucleocytoplasmic distribution of AMPK. This sets the stage to develop new strategies to regulate the intracellular localization of AMPK and thereby the modification of targets that are relevant to human disease.

3.3 Introduction

The presence of nutrients, such as the carbon source, regulates protein synthesis, gene expression and the activity of a large number of proteins. AMP kinase (AMPK) is a key player in these processes; the enzyme not only controls cell growth and transcription, but also the response to nutrient limitation and stress (reviewed in 223, 226, 227, 229, 239, 243, 135, and 251). AMPK is a central regulator of cellular metabolism for which it serves as an energy sensor; the enzyme is activated by a reduction of ATP/AMP levels, changes in intracellular calcium, and other forms of stress, including ischemia and hypoxia (238). Based on its central role in the control of glucose homeostasis and lipid metabolism, AMPK is an important therapeutic target in type 2 diabetes and obesity. In particular, low level activation of AMPK is likely to contribute to the global rise in obesity and diabetes (229). In addition to its regulatory function in metabolism, more recent studies demonstrate that AMPK is also crucial for cell polarity and mitosis (237).

The heterotrimeric AMPK contains a catalytic α subunit, encoded by two genes (α1 and α2). The regulatory β and γ subunits are encoded by two and three genes, respectively (reviewed in 229). Activation of AMPK includes the phosphorylation of Thr172 of the α subunit, which can be mediated by one of the two upstream regulatory kinases, LKB1 and CaMKK (224, 231 and references therein). Previous reports suggest that the α2 subunit of AMPK may be somewhat enriched in the nucleus (244), and mutations in the β1 subunit can increase its amount in nuclei (253).

The only direct means of communication between the nucleoplasm and cytoplasm is through nuclear pore complexes (NPCs, reviewed in 230, 246, 247). There are several mechanisms of macromolecular translocation along NPCs, molecules with a mass of 40 KD or less may diffuse across the NPC. By contrast, larger macromolecules rely on active transport and in most cases on specific carriers that promote transport across the NPC (230, 246, 247). Members of the importin-β family in particular play a crucial role in protein trafficking in and out of the nucleus. For instance, the nuclear exporter Crm1 recognizes hydrophobic leucine-rich signals that target a protein for export to the cytoplasm (236). Crm1-mediated nuclear export is inhibited by the drug leptomycin B (LMB) which covalently modifies the carrier (235).

To date, little is known about the nuclear and cytoplasmic pools of AMPK and how its intracellular distribution is controlled. Such a regulated localization to different cell compartments should be critical for the proper response to extra- and intracellular stimuli, leading to the phosphorylation of distinct AMPK targets. Although AMPK phosphorylates proteins in both the nucleus and the cytoplasm, it has not been determined whether its distribution is sensitive to stress or other changes in cell physiology. This knowledge is important, as it will set the stage to identify specific AMPK functions in either compartment that are dictated by physiological changes. This includes oxidative stress, a key factor that adds to the pathophysiologies in diabetic patients (242, 248, 250). To begin to answer these questions, we analyzed AMPK phosphorylation and localization in human culture cells. Since LKB1 has been associated with the activation and actions of AMPK

(reviewed in 229), we used HeLa cells, which do not synthesize LKB1 (231), as well as HEK293 cells, a human kidney cell line, which does express LKB1 (245). Our studies demonstrate that stress, cell density and signaling through the ERK1/2 mitogen-activated protein kinase (MAPK) module control the subcellular distribution of AMPK. Moreover, we show that AMPK shuttles between the nucleus and the cytoplasm and identified Crm1 as the nuclear carrier that translocates AMPK to the cytoplasm. Together, this multilayered control of intracellular localization provides a unique set of tools to rapidly adjust the distribution of AMPK to changes in cell physiology.

3.4 Materials and methods

3.4.1 Cell culture and exposure to stress

HeLa and HEK293 cells were cultured essentially as described (225, 87). In brief, cells were grown on poly-L-lysine coated cover slips in six-well dishes to ~70% confluency or high density (>100% confluency). This correlates with ~ 4 x 10^5 and > 2 x 10^6 cells/cm^2, respectively. Heat shock was for 1 hour at 45.5°C followed by recovery at 37°C for 2, 3 and 5 hours. All other treatments were at 37°C. Incubation with 2 mM diethyl maleate was for 4 hours.

3.4.2 Pharmacological tools

Energy depletion was performed with 50 mM deoxyglucose combined with 10 mM NaN_3 for 30 min. For inhibition of the ERK1/2 pathway cells were incubated with 25 μM PD98059 (Calbiochem) for 5 hours or 50 μg/ml ERK peptide inhibitor II (Calbiochem) for 1 hour. PD98059 inhibits the MAPK kinase MEK,

thereby preventing the activation of the downstream kinase ERK1/2. The ERK peptide inhibitor II contains 13 residues derived from the N-terminal portion of MEK1, binds to ERK and prevents its activation by inhibiting the binding of MEK1 (11). Leptomycin B (LMB, LC laboratories, Woburn, MA) has multiple actions, which includes inhibition of the nuclear exporter Crm1, inhibition of cell cycle progression and antitumor activity. LMB was present at 10 ng/ml for 21 hours and controls were treated with the solvent only under identical conditions. For serum starvation, cultures were grown for 18 hours without serum followed by 5 min incubation with fresh medium without or with 8% serum. After stress exposure or drug treatment cells were immediately fixed for immunofluorescence or stored at -70°C.

3.4.3 Indirect immunofluorescence and microscopy

All steps were carried out at room temperature following published procedures (208). Primary antibodies were used at the following concentrations: AMPK-α1/2 (Cell Signaling Techn. #2532), 1:200, AMPK-β1/2 (Cell Signaling Techn. #4150), 1:200, Cy3-coupled secondary antibodies (Jackson ImmunoResearch) were diluted 1:500. No signals were obtained when primary antibodies were omitted (not shown). Images were either acquired for 1 μm slices with a Zeiss LSM510 inverted microscope using a 63x oil-immersion objective with 1.4 NA, or with the Molecular Devices (Sunnyvale, CA) ImageXpress Micro equipped with a 300W Xenon light source and a CoolSnapHQ (Photometrics, Tucson, AZ). For the ImageXpress Micro images of DAPI (cube #49000) or Cy3 (#49005) were collected with cubes from Chroma Technology Inc. (Rockingham, VT). Cells

were grown on glass cover slips before labeling and mounted with Vectashield (Vector Laboratories, Burlingame, CA) following labeling. Up to 64 fields of view were imaged at 40X (PlanFluor ELWD 0.6NA) using 2x2 binning and ensuring at least 55 cells were sampled for each experimental condition. Image analysis was done with MetaXpress software. DAPI labeling was used to identify the number of cells in each field of view; protein staining with Cy3 was used to identify the entire cell. Care was taken to adjust the threshold level used to ensure that all cells were detected accurately even for lower expressing samples. The total intensity of antibody labeling in the nucleus was measured based on segmentation using DAPI staining and the intensity of the entire cell was calculated based on segmentation with the Cy3 labeling. The difference between these two intensities was taken as the total intensity of the cytosolic fraction of the protein. All images were corrected for contributions due to background intensity based on intensity measurements off of the cells for each image field. Finally, the ratio of the total intensity in the nucleus versus the total intensity of the cytosol was measured for each sample. Images were processed in Adobe Photoshop 8.0 for publication.

3.4.4 Western blotting

Cells grown on 10 cm culture dishes to ~70% confluency or at high density were exposed to stress or pharmacological inhibitors as described above. Following treatment, plates were rinsed with PBS and stored at -70°C until use. Crude extracts were prepared by solubilizing proteins in gel sample buffer, pH 8.0, containing protease inhibitors (1 mM PMSF; aprotinin, leupeptin, pepstatin, each

at 1 μg/ml), 20 mM β-glycerophosphate, 1 mM NaN_3, 2.5 mM NaF. Samples were incubated for 15 min at 95°C and vortexed with glass beads to shear DNA. After centrifugation (5 min, 13,000 rpm, microfuge) equal amounts of protein were separated in SDS-PA gels. Proteins were blotted to nitrocellulose and filters were processed as described (225). Antibodies against AMPK and dually phospho-ERK1/2 (Cell Signaling, #9106) were diluted 1:1,000; anti-ERK1/2 (StressGen, KAP-MA001C) was used at 1:2,000, anti-LDH (100-1173, Rockland, Gilbertsville, PA) at 1:2,000 and anti-lamin B (sc-6217, Santa Cruz Biotechnology, CA) at 1:2,000. ECL signals (Amersham Biosciences) were quantified by densitometry (241). Results are shown as means ± SD of at least 3 independent experiments.

3.4.5 Cell fractionation

To isolate cytoplasmic and nuclear fractions cells were incubated in lysis buffer [10 mM HEPES, pH 7.9, 10 mM KCl, 1.5 mM MgCl2, 1 mM DTT, 1 mM NaN_3 and a mixture of protease inhibitors (Roche)] for 15 min on ice. Cells were drawn through a 26 gauge needle and centrifuged 10 min at 2,000 xg. Sediments were resuspended in lysis buffer, centrifuged and washed once in lysis buffer containing 0.005% NP40. After 1 min centrifugation at 20,000 xg, nuclear proteins were obtained in the sediments. Combined supernatants contained the cytoplasmic marker protein LDH, whereas lamin B was restricted to nuclear fractions. For comparison, one equivalent of cytoplasmic proteins and two equivalents of nuclear proteins were analyzed side-by-side by Western blotting with different antibodies. ECL signals were quantified for p-AMPK-α1/2, t-

AMPK-α1/2 and AMPK-β1/2 and nuclear to cytoplasmic ratios (nuc/cyt) were calculated. Based on AMPK-α1/2 Thr172 phosphorylation and the nuc/cyt distribution of p-AMPK-α1/2 we determined the net nuclear levels of p-AMPK-α1/2. Note that the amount of t-AMPK-α1/2 was not drastically altered by the different stressors. For all conditions the net nuclear levels of controls were defined as 1.

3.4.6 Statistics

For Western blotting ECL signals were quantified as described in ref. 21. Data were acquired for at least three independent experiments. Results are shown as means ± SD. Bonferroni tests for multiple statistical comparisons (Fig. 3.1, 3.2, Suppl. Fig. 3.1) and Student's *t*-test (two-tailed) for unpaired samples were carried out to identify significant differences. For each experiment, all test results were compared with the control.

3.5 Results

3.5.1 AMPK accumulates in nuclei upon stress

Quantitative immunofluorescence and Western blotting were used to detect AMPK-α1/2 and β1/2 subunits in cultured human cells. The results are shown here for HeLa (Fig. 3.1-3.10, Suppl. Fig. 3.2, 3.3) and HEK293 cells (Suppl. Fig. 3.1). When analyzed by indirect immunofluorescence, α and β subunits of AMPK were nuclear and cytoplasmic in HeLa cells under non-stress conditions, with α subunits somewhat concentrated in nuclei. When cells were exposed to heat, energy depletion or oxidative stress, the levels of α and β subunits in nuclei

increased (Fig. 3.1A, B, 3.3A, B). In control experiments, the cytoplasmic enzyme lactate dehydrogenase (LDH) did not relocate to the nucleus for any of the stresses analyzed. Furthermore, the nuclear marker protein lamin B was confined to the nucleus under all conditions tested (Suppl. Fig. 3.2, 3.3).

Nuclear accumulation of AMPK-α1/2 and β1/2 was particularly prominent after heat stress and when cells were allowed to recover at 37°C for 2 to 3 hours; after 5 hours recovery nuclear levels of AMPK began to decrease again. The distribution of AMPK subunits under different conditions was quantified by determining nuclear and cytoplasmic fluorescence (MATERIALS AND METHODS) and calculating the nuclear/cytoplasmic ratio of fluorescence (Fig. 3.1B, nuc/cyt). Since the nucleus occupies less than 10% of the mammalian cell volume, a small increase in the nuc/cyt ratio of AMPK represents a drastic change in the nuclear concentration of the protein.

The results obtained for immunolocalization were further substantiated by cell fractionation (Fig. 3.2A, 3.4A). Cytoplasmic and nuclear fractions were analyzed by quantitative Western blotting and quantification of ECL signals (Fig. 3.2B, 3.4B). (Note that for all cell fractionations one equivalent of cytoplasmic and two equivalents of nuclear proteins were separated side-by-side.) As observed for immunolocalization, the nuc/cyt ratio of total AMPK-α1/2 and -β1/2 increased upon heat shock and started to decline upon 5 hours of recovery.

A different scenario, however, emerged for cell fractionation followed by Western blotting with antibodies that recognize phosphorylated Thr172 in α subunits (Fig. 3.2, 3.4, 3.6; p-AMPK-α1/2). In crude extracts, heat stress

significantly reduced the modification of Thr172 (Fig. 3.1C, D). By contrast, the nuc/cyt ratio of p-AMPK-α1/2 did not drastically change and slightly increased at 3 and 5 hours of recovery (Fig. 3.2B). Thus, the heat-induced changes in the nuc/cyt distribution of t-AMPK-α1/2 and p-AMPK-α1/2 were clearly different (Fig. 3.2B).

A change in the nuc/cyt ratio of p-AMPK-α1/2 does not necessarily lead to a change in the net amount of p-AMPK-α1/2 in the nucleus. To address this point, we calculated how the net amount of p-AMPK-α1/2 in nuclei changes upon exposure to heat and during recovery (MATERIALS AND METHODS). Following heat shock and after 2 or 3 hours of recovery, net nuclear levels of p-AMPK-α1/2 were reduced when compared to unstressed cells (Fig. 3.2B, net nuclear).

Like heat, energy depletion with deoxyglucose/NaN_3 (NDG) or oxidative stress triggered by diethyl maleate (DEM) induced t-AMPK nuclear accumulation as determined by quantitative immunolocalization and Western blotting (Fig. 3.3B, 3.4). Energy depletion increased the phosphorylation of AMPK-α1/2 on Thr172 as well as the nuc/cyt ratio of p-AMPK-α1/2. By contrast, DEM treatment reduced Thr172 phosphorylation and the nuc/cyt ratio of p-AMPK-α1/2 (Fig. 3.3C, D, 3.4B). Taken together, changes in the distribution of AMPK-α1/2 phosphorylated on Thr172 did not correlate with the redistribution of t-AMPK-α1/2. Table 1 summarizes the results obtained for AMPK phosphorylation and distribution and ERK1/2 activation under different experimental conditions.

3.5.2 Stress-induced dephosphorylation of AMPK-α1/2 Thr172 correlates with the activation of ERK1/2

Crosstalk between AMPK and ERK1/2 may involve positive as well as negative signaling events (248). In our experiments with HeLa cells, heat and DEM significantly activated ERK1/2, as evident from its dual phosphorylation (Fig. 3.1C, D, 3.3C, D; p-ERK1/2). At the same time, the phosphorylation of AMPK-α1/2 Thr172 (p-AMPK-α1/2) was reduced. By contrast, deoxyglucose/NaN_3 elevated Thr172 and decreased ERK1/2 phosphorylation. In HEK293 cells upon DEM treatment, we detected neither an increase in the dual phosphorylation of ERK1/2, nor significant changes in the modification of AMPKα1/2. Nevertheless, for all stress conditions analyzed there was an inverse relationship between AMPK-α1/2 Thr172 phosphorylation and the dual modification of ERK1/2 in both HeLa and HEK293 cells (Fig. 3.1, 3.3, 3.5 and Suppl. Fig. 3.1), suggesting that this effect is not restricted to a specific cell line.

3.5.3 Addition of serum to starved HeLa cells increases the amount of AMPK in nuclei.

Experiments above showed that in stressed cells the increase in ERK1/2 activation may be linked to a reduction in the net amount of p-AMPK-α1/2 in nuclei. We further addressed this point using serum-deprived cells. After 18 hours incubation in serum-free medium the addition of serum to HeLa cells rapidly induced ERK1/2 phosphorylation. Concomitantly, there was a small but significant decrease of AMPK-α1/2 Thr172 phosphorylation as well as a

reduction of the net amount of nuclear p-AMPK1/2. Unlike p-AMPK1/2, t-AMPK-α1/2 and β1/2 subunits accumulated in nuclei (Fig. 3.5, 3.6).

3.5.4 AMPK shuttles between the nucleus and the cytoplasm and is exported from nuclei by the carrier Crm1

Results for the relocation of AMPK-α and β subunits upon stress and the reversal during recovery may suggest that they shuttle between the nucleus and the cytoplasm using unknown transporters. The carrier Crm1 is involved in the export of a large number of proteins and efficiently inhibited by the drug leptomycin B (LMB). As shown for quantitative immunofluorescence (Fig. 3.7A, B) and Western blotting (Fig. 3.7C, D), incubation with LMB resulted in the nuclear accumulation of t-AMPK-α and β subunits in unstressed HeLa cells, in line with the idea that the subunits shuttle and Crm1 serves as their nuclear exporter. No significant changes were detected for the distribution of p-AMPK-α1/2 (Fig. 3.7C, D).

3.5.5 Cell density controls the distribution and shuttling of AMPK

Nuclear trafficking of proteins can be controlled by the density of the culture, and high confluency may interfere with nuclear transport of proteins (225, 232). Both α and β subunits of the kinase were nuclear and cytoplasmic at 70% confluency in unstressed HeLa cells (Fig. 3.1, 3.3, 3.5, 3.7), but were restricted to the cytoplasm in high density cultures, when analyzed by indirect immunofluorescence or cell fractionation (Fig. 3.8A, C, D). Moreover, in high density HeLa cultures treated with the inhibitor LMB, AMPK failed to accumulate in nuclei, indicating that shuttling does not take place under these conditions (Fig. 3.8A, C, D). This

density-dependent redistribution of AMPK is not simply an effect of changes in the medium of high density cultures, since AMPK was nuclear as well as cytoplasmic and able to shuttle for cells growing in less dense areas of the same cover slip (data not shown). Interestingly, in high density cells we detected little phosphorylation of AMPK-α1/2 Thr172 or activation of ERK1/2 (Fig. 3.8B). This could be in part attributed to changes in protein levels, as the total amount of AMPK-α1/2 and ERK1/2 was somewhat reduced in high density cultures. By contrast, the levels of AMPK-β1/2 were somewhat increased (Fig. 3.8B). It is not known why the nuc/cyt ratio of AMPK-β1/2 decreases in the presence of LMB (Fig. 3.8D).

3.5.6 Signaling through MAPKs ERK1/2 controls the nucleocytoplasmic distribution of AMPK

Experiments with stressed cells suggested that increasing the activity of ERK1/2 may correlate with the nuclear accumulation of p-AMPK-α1/2 (Table 3.1). Previous experiments by others indicate a complex crosstalk between AMPK activation and ERK1/2 activation, with positive as well as negative feedback between the two pathways (234). No previous studies have analyzed the possible role of MEK→ERK1/2 signaling in the intracellular localization of AMPK. In particular, it is not known whether ERK1/2 has any effect on the distribution of AMPK subunits under *nonstress* conditions. To begin to understand the events that control the nucleocytoplasmic distribution of AMPK in unstressed cells we tested a potential role of MEK→ERK1/2 signaling in this process. Two different pharmacological inhibitors, PD98059 which inhibits the upstream kinase MEK

and peptide inhibitor II, which prevents ERK binding to MEK (233), induced the nuclear accumulation of AMPK-α1/2 and β1/2 (Fig. 3.9, 3.10). Although the phosphorylation of AMPK-α1/2 Thr172 was slightly reduced, the nuc/cyt ratio of p-AMPK-α1/2 increased upon treatment with PD98059 (Fig. 3.9D, 3.10B).

3.6 Discussion

AMPK is central to the control of glucose and lipid metabolism and the rapid adaptation to changes in cell physiology. As such, the kinase modifies a variety of substrates that are involved in carbohydrate or fatty acid synthesis or degradation and protein synthesis (251). Furthermore, AMPK regulates the expression of a large number of genes, the stability of several mRNAs, cell polarity and mitosis (228, 237, 240, 254). These previous studies showed that AMPK recognizes a growing number of proteins, both in the nucleus and cytoplasm. Access to and modification of these substrates requires the proper localization of AMPK.

Our studies provide new insights into the complex regulatory processes that determine the modification and subcellular distribution of AMPK. Changes in the phosphorylation of AMPK-α 1/2 Thr172 were inversely related to changes in the activation of ERK1/2. This is not restricted to HeLa cells, which are lacking the upstream activating kinase LKB1, but was also observed with HEK293 cells, which contain LKB1.

Our results demonstrate that various forms of stress, including heat, energy depletion and oxidants, not only alter the phosphorylation state of AMPK-α1/2, but also concentrate AMPK in nuclei. The simplified model in Fig. 3.11

summarizes how different physiological conditions regulate the intracellular distribution of AMPK. In unstressed cells (Fig. 3.11A), AMPK-α and β shuttle between the nucleus and the cytoplasm, using the carrier Crm1 for export from the nucleus. Upon exposure to stress both α and β subunits accumulate in nuclei (Fig. 3.11B). This redistribution could be achieved by upregulation of AMPK nuclear import, increase in nuclear retention, reduced export, or a combination of these events. High cell density confines AMPK-α and β subunits to the cytoplasm and prevents them from shuttling (Fig. 3.11C). It is possible that contacts between neighboring cells regulate the distribution of AMPK; signaling events based on high culture density could prevent nuclear import or induce cytoplasmic anchoring of AMPK subunits. Finally, our results demonstrate a complex role for MEK→ERK1/2 signaling in the control of AMPK localization. Under nonstress conditions, inhibition of the MEK→ERK1/2 pathway triggered nuclear accumulation of AMPK α and β subunits (Fig. 3.11D).

Interestingly, the localization of p-AMPK-α1/2 and t-AMPK-α1/2 may be controlled differently. Our results indicate that there is no direct link between the phosphorylation of Thr172 of AMPK-α1/2 and the distribution of t-AMPK-α1/2. However, the changes in net nuclear p-AMPK-α1/2 are negatively correlated with ERK1/2 activation; whenever the net nuclear levels of p-AMPK-α1/2 were reduced we observed an increase in ERK1/2 activation, and vice versa (summarized in Table 3.1).

Taken together, our results support the hypothesis that p-AMPK-α1/2 localization can be linked to the activation status of ERK1/2, whereas a more

complex regulation directs the distribution of t-AMPK-α1/2 and β1/2 in stressed cells. Future experiments will have to determine whether the localization of the MAPK ERK1/2, in addition to its activation, plays a role in the nucleocytoplasmic distribution of AMPK.

At this point, we can only speculate how AMPK redistribution participates in the response to different stressors. One effect of AMPK redistribution could be changing its interactions with kinase substrates. For example, raising the nuc/cyt ratio of activated AMPK in nuclei may increase the phosphorylation of nuclear or reduce the modification of cytoplasmic targets. AMPK controls cell physiology not only by the direct phosphorylation of various metabolic enzymes, but also via transcriptional regulation (reviewed in 135). Many genes change their expression levels when a dominant-negative allele of AMPK-α2 is highly overexpressed over the endogenous wild type α subunit in skeletal muscles of transgenic mice (240). Proteins encoded by these genes participate in various functions, including energy metabolism, cell signaling, transcription and translation. Furthermore, AMPK activity contributes to the regulation of mRNA stability as the kinase controls the half-lives of p21, cyclin A, B1 and VEGF mRNAs (reviewed in 228).

A possible connection between the multiple processes that AMPK affects and the results reported here could be the transcriptional regulator p300/CBP and several transcription factors which are acetylated by p300/CBP. These include members of the FOXO family, p53 and NF-□B. AMPK phosphorylates p300/CBP on Ser89 (254) thereby modulating the interactions of p300/CBP with transcriptional regulators (reviewed in 135). Upon oxidative stress, FOXO

proteins move to the nucleus to be bound and acetylated by p300/CBP (reviewed in 249, 252). The acetylation state of FOXO proteins seems to control which genes are selected for transcription. A simplified model may propose a link between AMPK activation, p300/CBP phosphorylation and FOXO protein acetylation; and the cascade AMPK→p300/CBP→FOXO proteins could contribute to the specific gene expression following oxidative stress. Since we observed a reduction in p-AMPK-α1/2 in nuclei upon oxidant exposure, this model would predict that p300/CBP phosphorylation on Ser89 is reduced, which could modulate the subsequent interaction between p300/CBP and FOXO proteins and ultimately gene expression.

Our data show that the nucleocytoplasmic distribution of total and phosphorylated AMPK is regulated differently; AMPK subunits accumulate in nuclei upon stress independent of kinase activation. There are several possible scenarios that could explain this redistribution: (a) the redistribution of AMPK to nuclei controls its accessibility to activating upstream kinases; (b) AMPK nuclear accumulation is caused by inhibition of nuclear export in stressed cells. (c) Alternatively, AMPK subunits have additional functions that are unrelated to the kinase activity, but required in nuclei of stressed cells for other processes. Future experiments will have to explore these possibilities.

3.7 Acknowledgement

We thank P. Banski for critical reading of the manuscript and Dr. J. Liu (HTS/HCS Facility at McGill University) for help with ImageExpress Micro. This work was supported by grants from CIHR, NSERC and Heart and Stroke Foundation of Quebec to US. US is a chercheur national of FRSQ. MK was supported by doctoral fellowships from FRSQ and the Heart and Stroke Foundation of Canada.

Table 3.1 Distribution of AMPK-α1/2 phosphorylated on Thr172 and activation of ERK1/2

Treatment	p-AMPK-α1/2 nuc/cyt ratio	p-AMPK-α1/2 net nuclear content	ERK1/2 activation
heat shock	↔	↓	↑
NDG	↑	↑	↓
DEM	↓	↓	↑
serum	↓	↓	↑
PD98059	↑	↑	↓

Table 3.1 Distribution of AMPK-α1/2 phosphorylated on Thr172 and activation of ERK1/2

Results for the nuc/cyt ratio, net nuclear content of p-AMPK-α1/2 and ERK1/2 activation are summarized. The effects of stress exposure, serum starvation and incubation with the MEK inhibitor PD98059 are shown. Arrows indicate no change (↔), reduction (↓) or increase (↑).

Figure 3.1

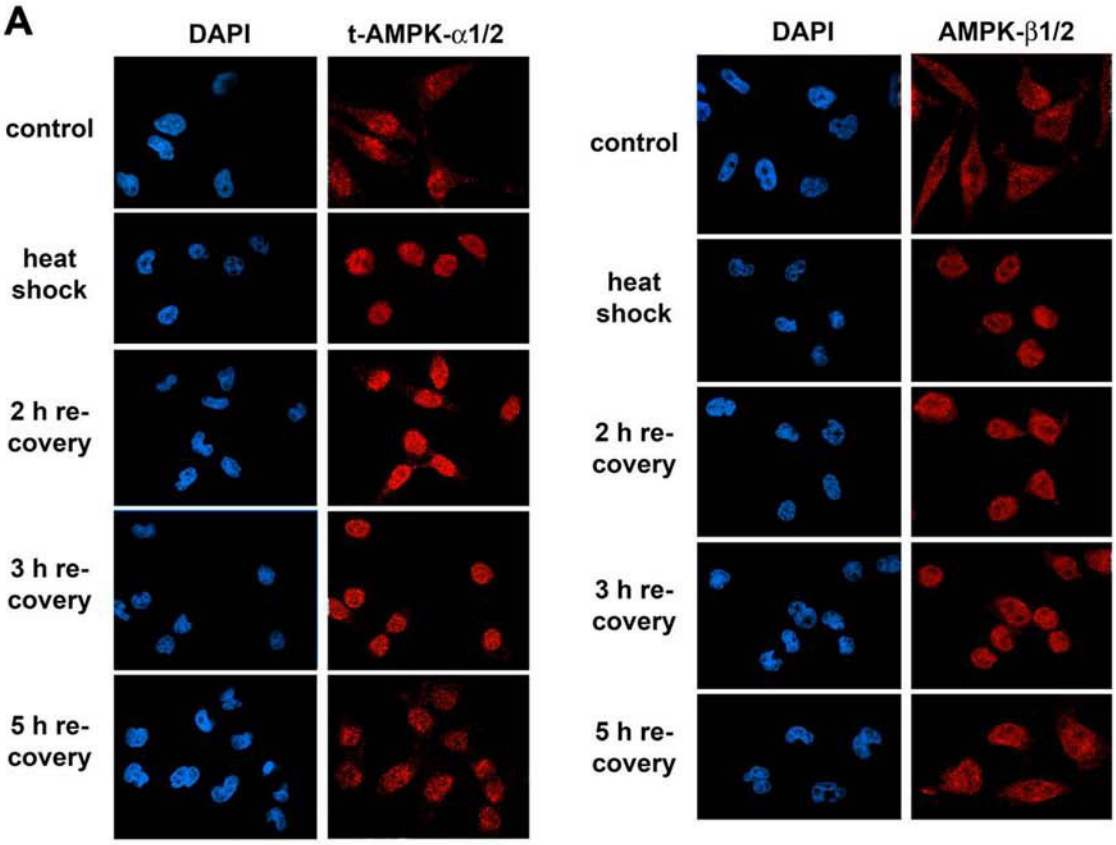
A
DAPI
t-AMPK-α1/2
DAPI
AMPK-β1/2
control
heat shock
2 h re-covery
3 h re-covery
5 h re-covery
control
heat shock
2 h re-covery
3 h re-covery
5 h re-covery

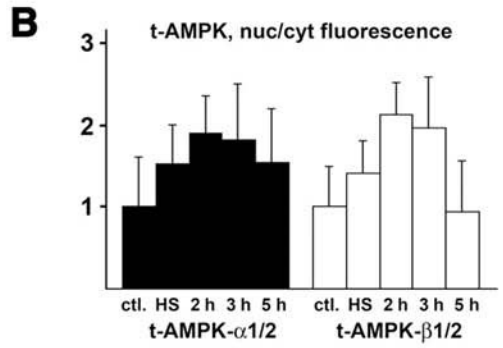
B
t-AMPK, nuc/cyt fluorescence
3
2
1
ctl. HS 2 h 3 h 5 h
ctl. HS 2 h 3 h 5 h
t-AMPK-α1/2
t-AMPK-β1/2

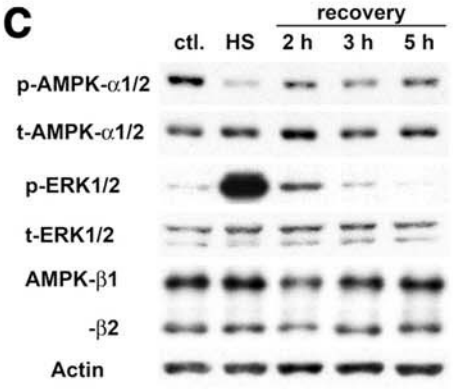
C
recovery
ctl. HS 2 h 3 h 5 h
p-AMPK-α1/2
t-AMPK-α1/2
p-ERK1/2
t-ERK1/2
AMPK-β1
-β2
Actin

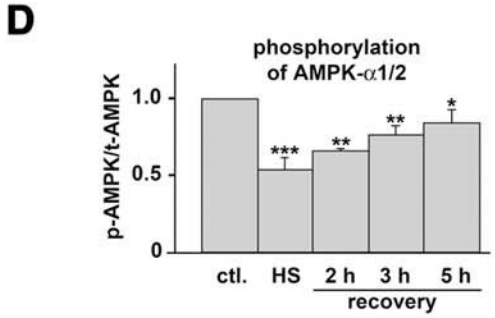
D
phosphorylation of AMPK-α1/2
p-AMPK/t-AMPK
1.0
0.5
0
***
**
**
*
ctl. HS 2 h 3 h 5 h
recovery

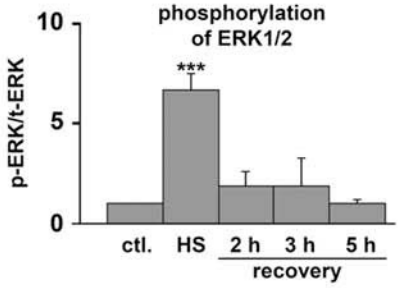
phosphorylation of ERK1/2
p-ERK/t-ERK
10
5
0
***
ctl. HS 2 h 3 h 5 h
recovery

Figure 3.1 Heat stress relocates AMPK to the nucleus of HeLa cells

Cells grown to ~70% confluency were exposed to 1 hour heat stress and allowed to recover at 37°C for the times indicated. (**A)** Total AMPK-α1/2 and AMPK-β1/2 were detected by indirect immunofluorescence. (**B)** Quantification of fluorescence signals was carried out as detailed in materials and methods. (**C)** For Western blotting equal amounts of proteins were analyzed with antibodies against AMPK-α1/2 phosphorylated on Thr172 (p-AMPK-α1/2), total-AMPK-α1/2 (t-AMPK-α1/2), dually phosphorylated ERK1/2 (p-ERK1/2), total ERK1/2 (t-ERK1/2), AMPK-β1/2 and actin. (**D)** ECL-signals were quantified for at least three independent experiments. Means and SD are shown for changes in AMPK-α1/2 Thr172 (p-AMPK/t-AMPK) and ERK1/2 phosphorylation (p-ERK/t-ERK). Untreated controls served as reference for heat-shocked and recovering cells. ***$p<0.001$; **$p<0.01$, *$p<0.05$.

Figure 3.2

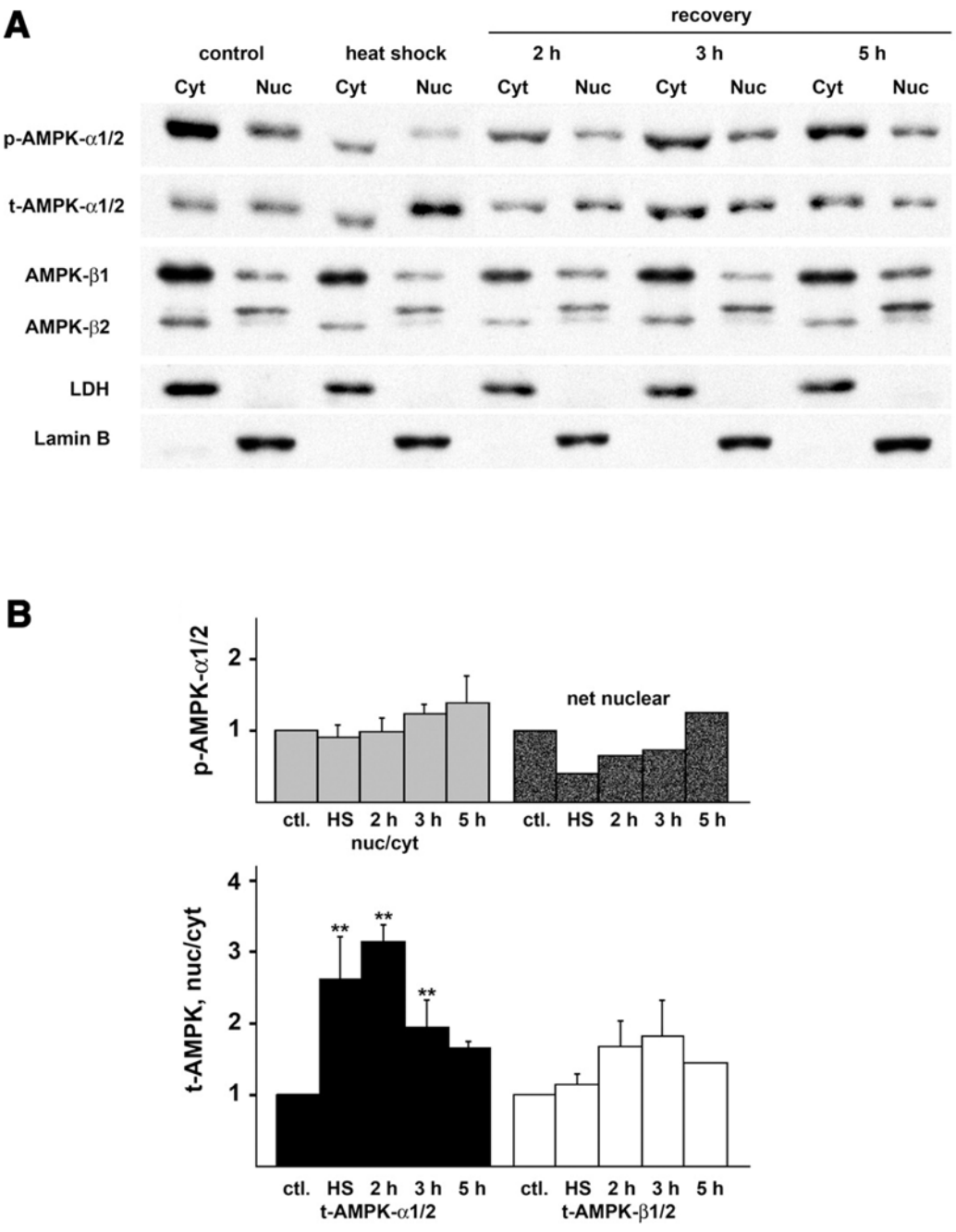
A
recovery
control
heat shock
2 h
3 h
5 h
Cyt
Nuc
Cyt
Nuc
Cyt
Nuc
Cyt
Nuc
Cyt
Nuc
p-AMPK-α1/2
t-AMPK-α1/2
AMPK-β1
AMPK-β2
LDH
Lamin B
B
p-AMPK-α1/2
net nuclear
ctl. HS 2 h 3 h 5 h
nuc/cyt
ctl. HS 2 h 3 h 5 h
t-AMPK, nuc/cyt
**
**
**
ctl. HS 2 h 3 h 5 h
t-AMPK-α1/2
ctl. HS 2 h 3 h 5 h
t-AMPK-β1/2

Figure 3.2 Analysis of AMPK distribution in heat-stressed HeLa cells by cell fractionation

(A) Control and stressed cells were fractionated followed by Western blot analysis of cytoplasmic and nuclear fractions. One equivalent of cytoplasmic and two equivalents of nuclear proteins were analyzed side-by-side. **(B)** For p-AMPK-α1/2 nuc/cyt ratios and the net nuclear content was determined (MATERIALS AND METHODS). Nuc/cyt ratios were calculated for t-AMPK-α1/2 and t-AMPK-β1/2. As controls, filters were probed for lactate dehydrogenase (LDH) and lamin B. ECL signals were quantified for AMPK as in Fig. 1. All test results were compared with the untreated control. ***$p<0.001$; **$p<0.01$, *$p<0.05$.

Figure 3.3

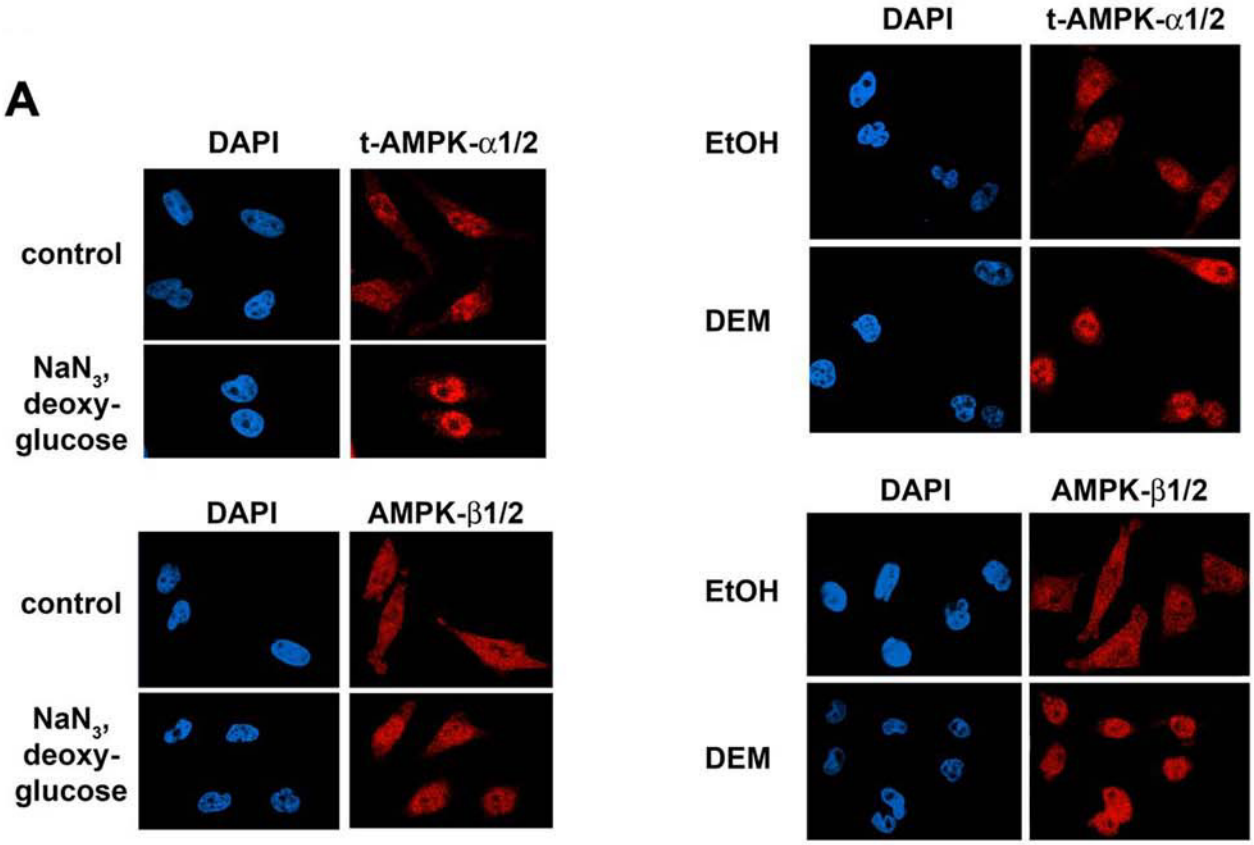
A
DAPI
t-AMPK-α1/2
control
NaN3, deoxy-glucose
EtOH
DEM
DAPI
AMPK-β1/2
control
NaN3, deoxy-glucose
EtOH
DEM

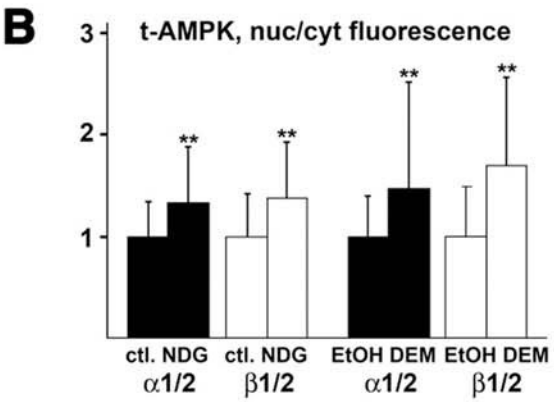
B
t-AMPK, nuc/cyt fluorescence
3
2
1
**
ctl. NDG
α1/2
ctl. NDG
β1/2
EtOH DEM
α1/2
EtOH DEM
β1/2

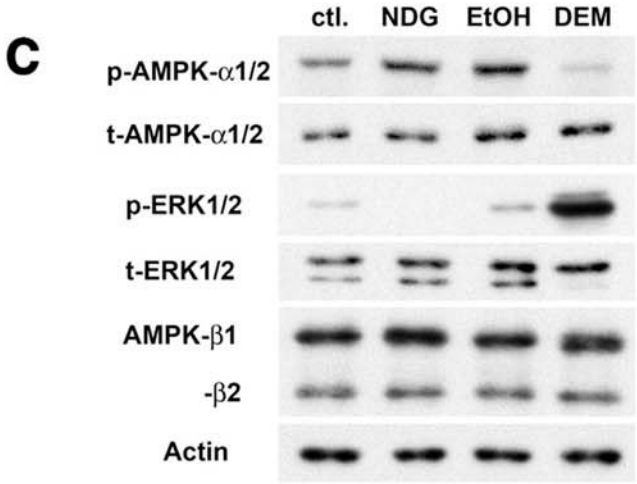
C
ctl.
NDG
EtOH
DEM
p-AMPK-α1/2
t-AMPK-α1/2
p-ERK1/2
t-ERK1/2
AMPK-β1
-β2
Actin

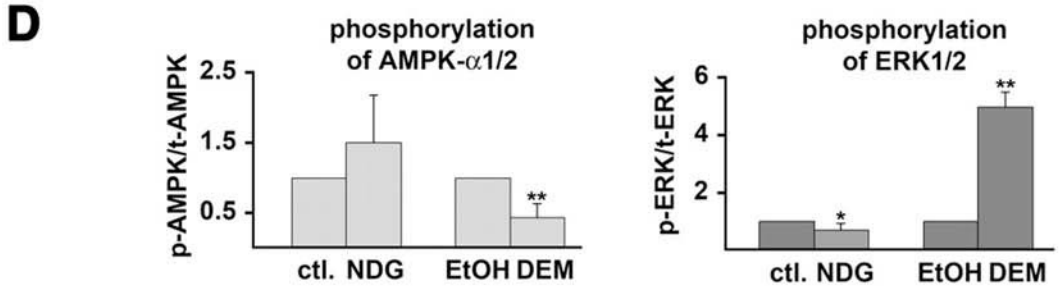
D
phosphorylation of AMPK-α1/2
p-AMPK/t-AMPK
2.5
1.5
0.5
**
ctl. NDG
EtOH DEM
phosphorylation of ERK1/2
p-ERK/t-ERK
6
4
2
*
**
ctl. NDG
EtOH DEM

Figure 3.3 Energy depletion and oxidative stress alter the distribution of AMPK in HeLa cells

Cultured cells at ~70% confluency were energy depleted with NaN_3/deoxyglucose or treated with the oxidant diethyl maleate (DEM) as described in MATERIALS AND METHODS. Controls were incubated with solvent only. **(A-D)** Localization of proteins by indirect immunofluorescence and Western blotting were carried out as described for Fig. 1A-D. Control samples served as reference for all test results. **$p<0.01$; *$p<0.05$.

Figure 3.4

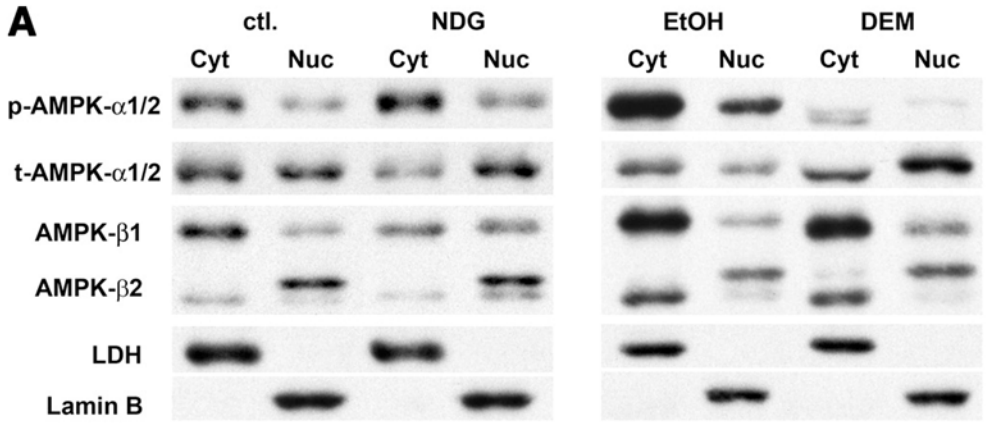
A
ctl.
NDG
EtOH
DEM
Cyt
Nuc
Cyt
Nuc
Cyt
Nuc
Cyt
Nuc
p-AMPK-α1/2
t-AMPK-α1/2
AMPK-β1
AMPK-β2
LDH
Lamin B

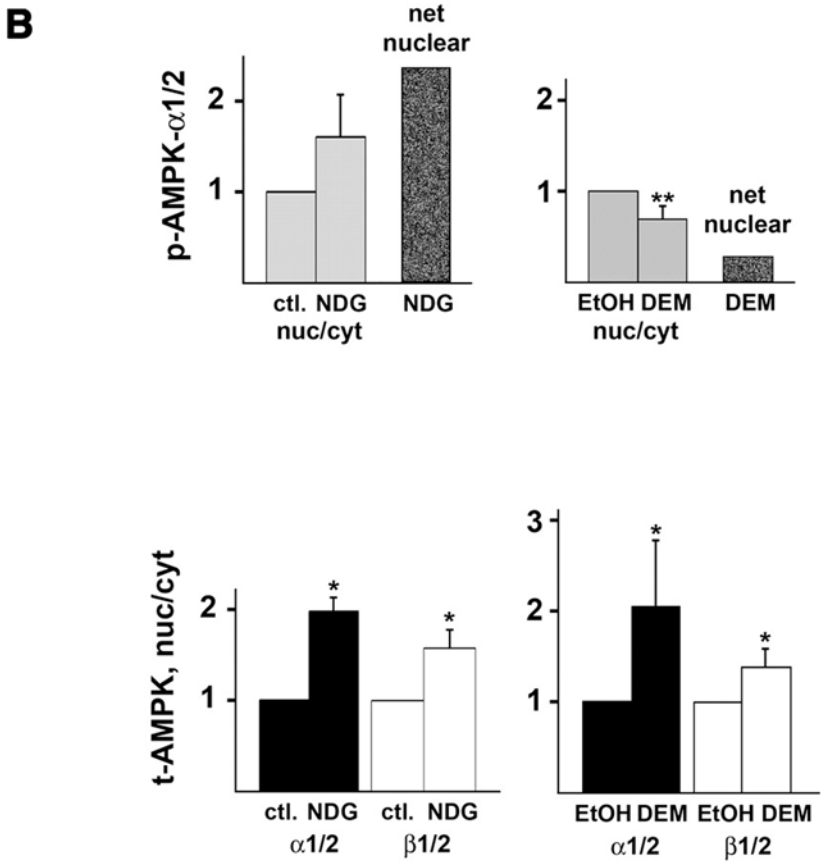
B
net
nuclear
p-AMPK-α1/2
2
1
ctl. NDG
nuc/cyt
NDG
2
1
**
net
nuclear
EtOH DEM
nuc/cyt
DEM
t-AMPK, nuc/cyt
3
2
1
*
*
*
*
ctl. NDG
α1/2
ctl. NDG
β1/2
EtOH DEM
α1/2
EtOH DEM
β1/2

Figure 3.4 (A, B) Effect of energy depletion and oxidant exposure on the distribution of AMPK in HeLa cells

Cell fractionation and quantification of ECL-signals for cytoplasmic and nuclear AMPK were as in Fig. 3.2A, B. All test results were compared with control samples. **$p<0.01$; *$p<0.05$.

Figure 3.5

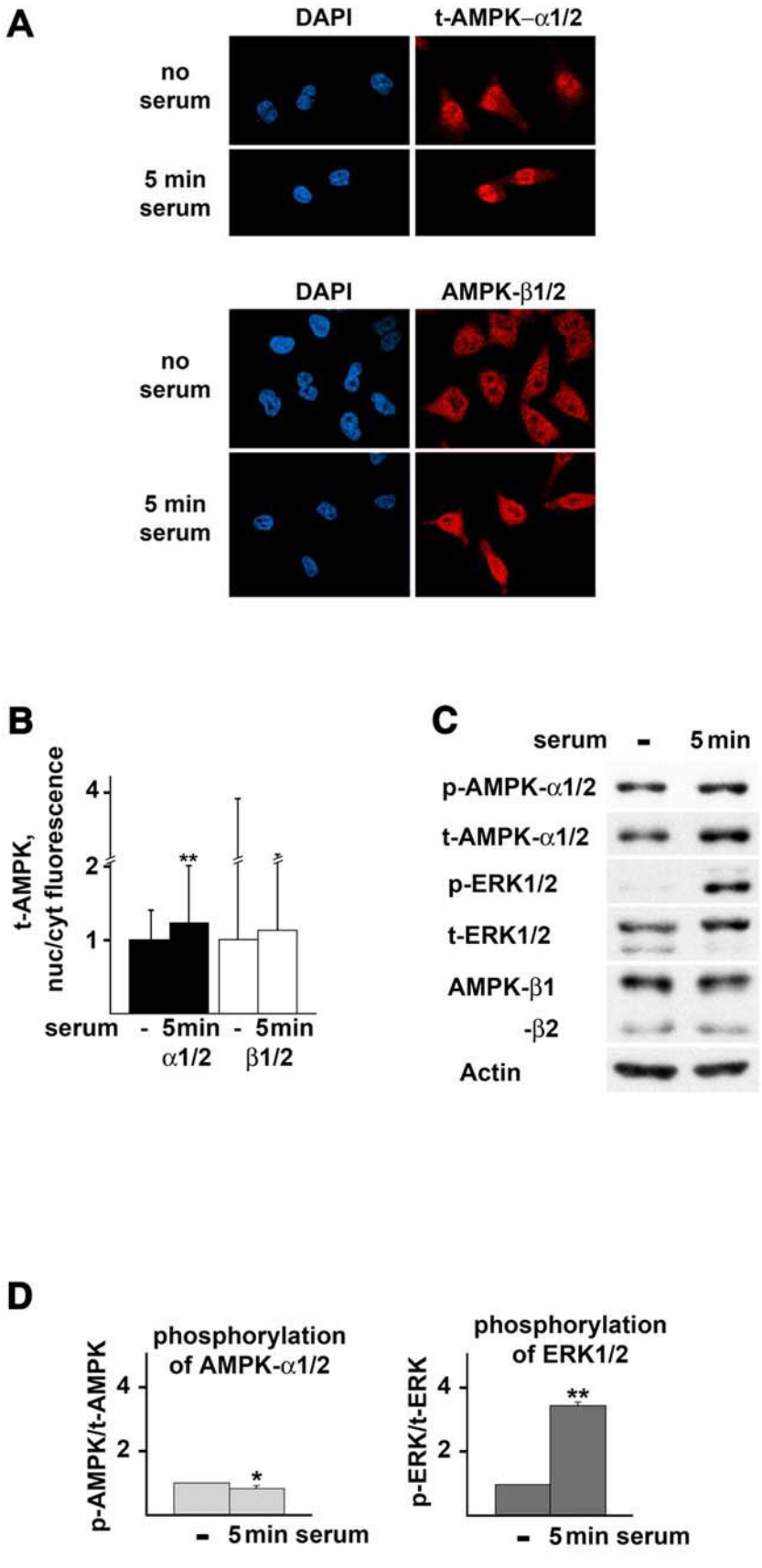
A
DAPI
t-AMPK–α1/2
no serum
5 min serum
DAPI
AMPK-β1/2
no serum
5 min serum
B
t-AMPK, nuc/cyt fluorescence
4
2
1
**
serum - 5min - 5min
α1/2 β1/2
C
serum - 5 min
p-AMPK-α1/2
t-AMPK-α1/2
p-ERK1/2
t-ERK1/2
AMPK-β1
-β2
Actin
D
phosphorylation of AMPK-α1/2
p-AMPK/t-AMPK
4
2
*
- 5 min serum
phosphorylation of ERK1/2
p-ERK/t-ERK
4
2
**
- 5 min serum

Figure 3.5 (A-D) Addition of serum to starved cells raises the nuclear levels of AMPK

HeLa cells were serum-starved for 18 hours and subsequently incubated with fresh medium without or with serum for 5 min. Indirect immunofluorescence and Western blotting were as detailed for Fig. 1A-D. All experimental results were compared with the untreated control. **$p<0.01$; *$p<0.05$.

Figure 3.6

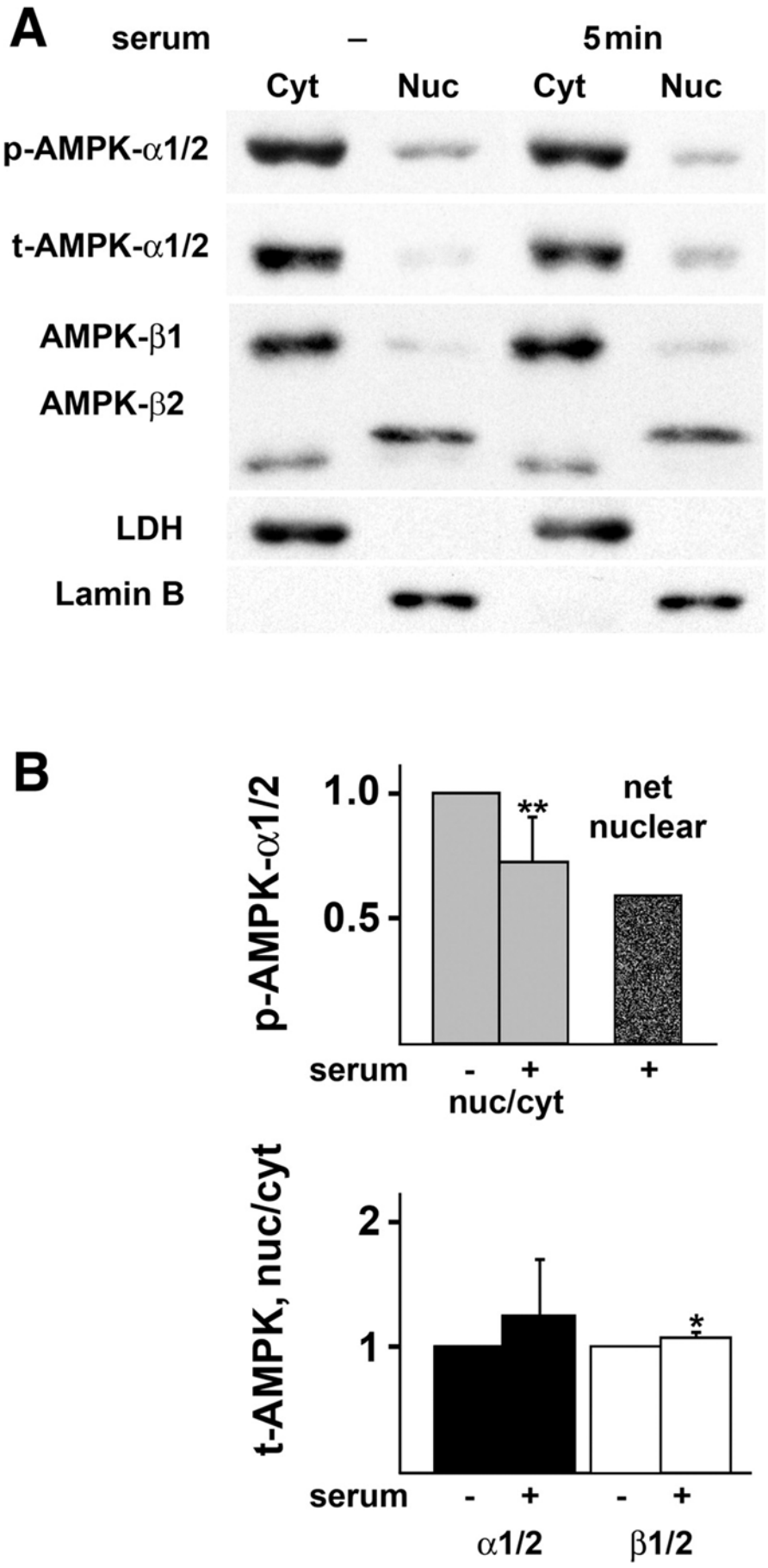
A
serum
–
5 min
Cyt
Nuc
Cyt
Nuc
p-AMPK-α1/2
t-AMPK-α1/2
AMPK-β1
AMPK-β2
LDH
Lamin B
B
p-AMPK-α1/2
1.0
0.5
**
net nuclear
serum
-
+
+
nuc/cyt
t-AMPK, nuc/cyt
2
1
*
serum
-
+
-
+
α1/2
β1/2

Figure 3.6 (A, B) Serum addition affects AMPK distribution in starved cells

HeLa cells were incubated with medium in the absence or presence of serum as described for Fig. 3.5. Cell fractionation and quantification of cytoplasmic and nuclear AMPK were as in Fig. 3.2. The untreated control was used as reference for all test results. **$p<0.01$; *$p<0.05$.

Figure 3.7

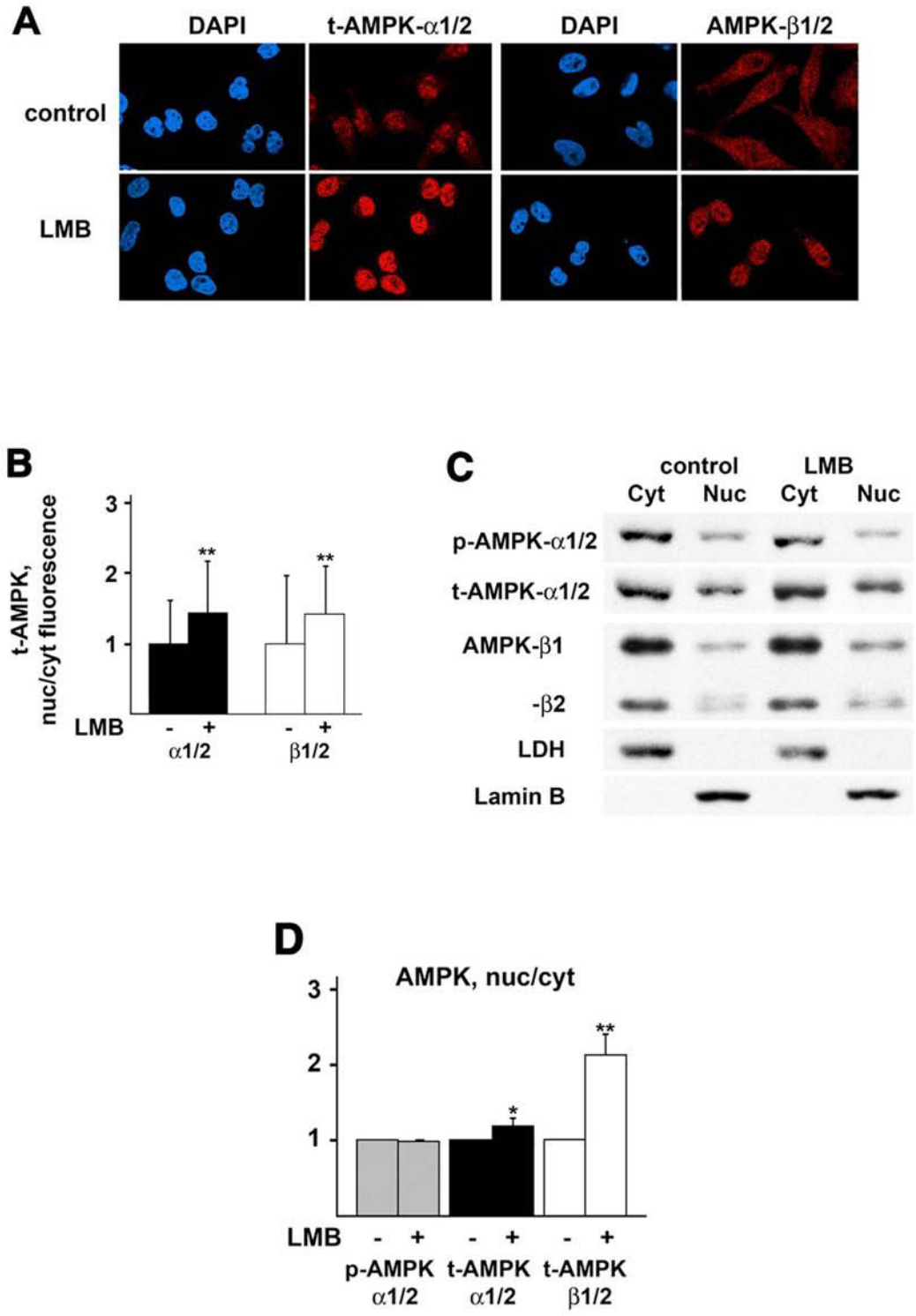
A
DAPI
t-AMPK-α1/2
DAPI
AMPK-β1/2
control
LMB
B
t-AMPK, nuc/cyt fluorescence
3
2
1
**
**
LMB
- + - +
α1/2
β1/2
C
control
LMB
Cyt
Nuc
Cyt
Nuc
p-AMPK-α1/2
t-AMPK-α1/2
AMPK-β1
-β2
LDH
Lamin B
D
AMPK, nuc/cyt
3
2
1
*
**
LMB
- + - + - +
p-AMPK α1/2
t-AMPK α1/2
t-AMPK β1/2

Figure 3.7 AMPK shuttles between the nucleus and the cytoplasm using Crm1 as the nuclear exporter

HeLa cells at 70% confluency were incubated with solvent only (control) or LMB. Indirect immunofluorescence and Western blot analysis was carried out as in Fig. 3.1 and 3.2. **(A)** AMPK-α1/2 and β1/2 were located by indirect immunofluorescence. **(B)** The ratio of nuc/fluorescence was quantified. **(C, D)** Western blotting of cytoplasmic and nuclear fraction and quantitation of ECL signals are shown. All test results were compared with the untreated control. $^{**}p<0.01$; $^{*}p<0.05$.

Figure 3.8

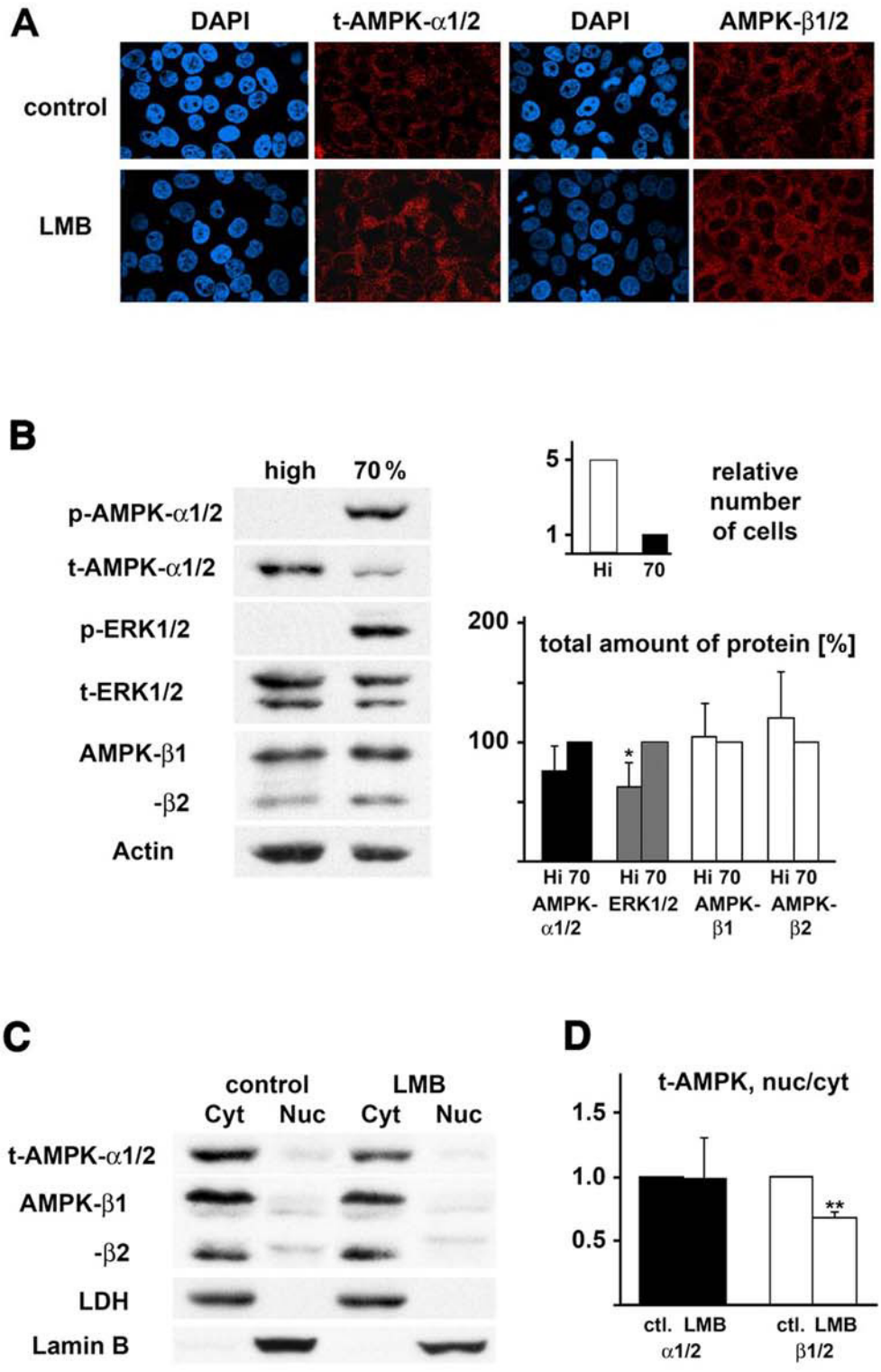
A
DAPI
t-AMPK-α1/2
DAPI
AMPK-β1/2
control
LMB
B
high
70 %
p-AMPK-α1/2
t-AMPK-α1/2
p-ERK1/2
t-ERK1/2
AMPK-β1
-β2
Actin
5
1
Hi
70
relative number of cells
200
100
total amount of protein [%]
*
Hi 70 AMPK- α1/2
Hi 70 ERK1/2
Hi 70 AMPK- β1
Hi 70 AMPK- β2
C
control
LMB
Cyt
Nuc
Cyt
Nuc
t-AMPK-α1/2
AMPK-β1
-β2
LDH
Lamin B
D
t-AMPK, nuc/cyt
1.5
1.0
0.5
**
ctl. LMB α1/2
ctl. LMB β1/2

Figure 3.8 Cell density controls the nucleocytoplasmic distribution of AMPK

High density HeLa cell cultures were treated with solvent or LMB as in Fig. 3.7. **(A)** AMPK was located by indirect immunofluorescence. **(B)** Western blot analysis showed no or little p-AMPK-α1/2 or dually phosphorylated ERK1/2 in high density cells. Note that a higher amount of total protein (140%) was loaded for high density cultures to detect weak ECL signals. Changes in the total concentrations of AMPK and ERK1/2 in high density cultures were determined with actin as a reference. Results obtained for 70% confluency (70) were used as a reference for high density cultures (Hi). **$p<0.01$; *$p<0.05$. (**C, D)** Cytoplasmic and nuclear fractions were analyzed by Western blotting and ECL signals were quantified as described for Fig. 3.2. All test results were compared with the control samples. **$p<0.01$; *$p<0.05$.

Figure 3.9

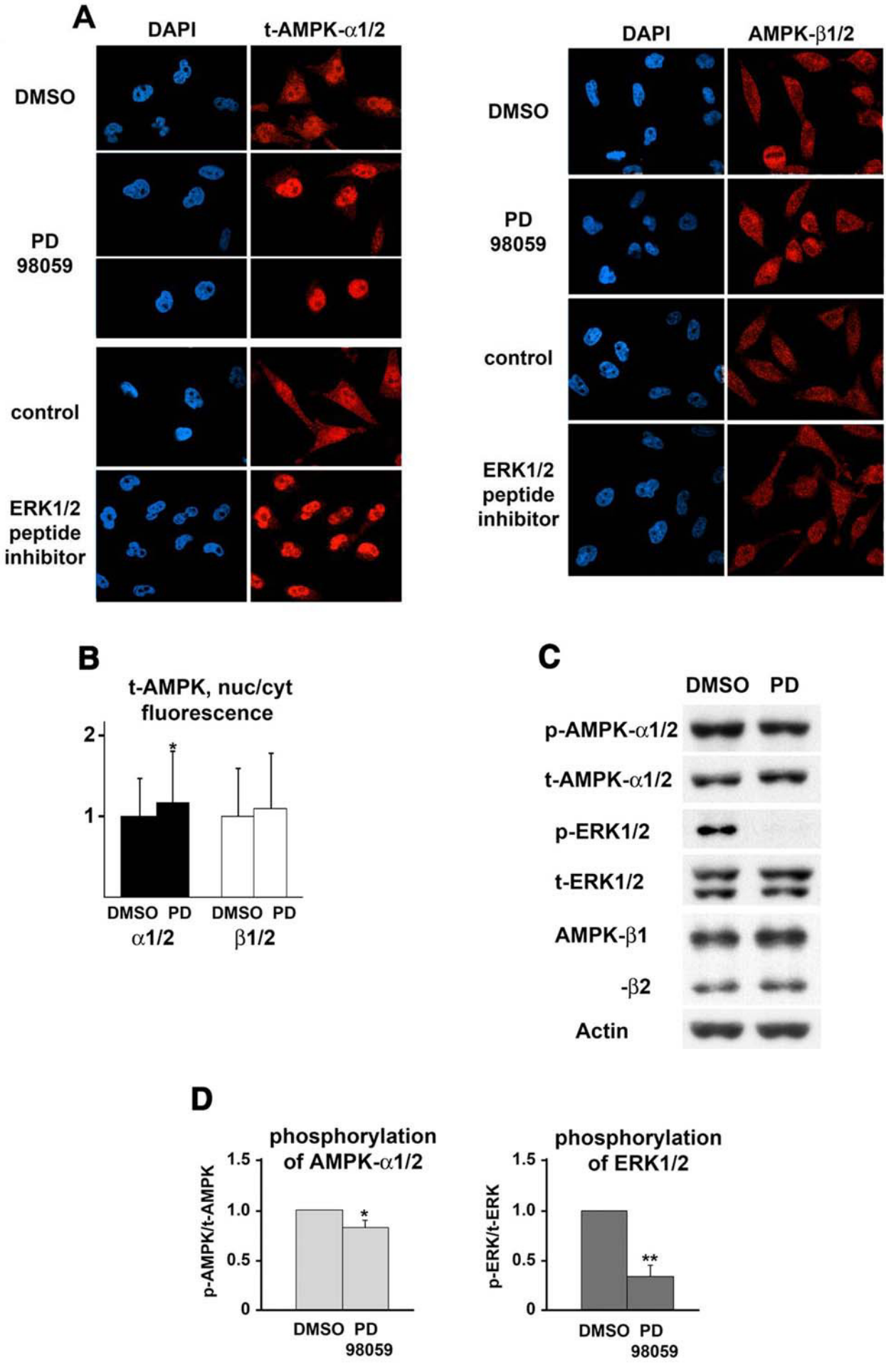
A
DAPI
t-AMPK-α1/2
DMSO
PD 98059
control
ERK1/2 peptide inhibitor
DAPI
AMPK-β1/2
DMSO
PD 98059
control
ERK1/2 peptide inhibitor
B
t-AMPK, nuc/cyt fluorescence
2
1
*
DMSO PD
α1/2
DMSO PD
β1/2
C
DMSO PD
p-AMPK-α1/2
t-AMPK-α1/2
p-ERK1/2
t-ERK1/2
AMPK-β1
-β2
Actin
D
phosphorylation of AMPK-α1/2
p-AMPK/t-AMPK
1.5
1.0
0.5
0
*
DMSO PD
98059
phosphorylation of ERK1/2
p-ERK/t-ERK
1.5
1.0
0.5
0
**
DMSO PD
98059

Figure 3.9 Signaling through MEK→ERK1/2 regulates the nucleocytoplasmic distribution of AMPK in HeLa cells

Cultures were incubated with PD98059 (PD) or ERK1/2 peptide inhibitor as described in MATERIALS AND METHODS. **(A, B)** AMPK subunits were visualized by indirect immunofluorescence and fluorescence signals were quantified. **(C, D)** Changes in the phosphorylation of AMPK-α1/2 Thr172 or ERK1/2 were determined by Western blotting and quantification of ECL signals. Indirect immunofluorescence, Western blotting and statistical analyses were carried out as described for Fig. 3.3A-D. $^{**}p<0.01$; $^{*}p<0.05$.

Figure 3.10

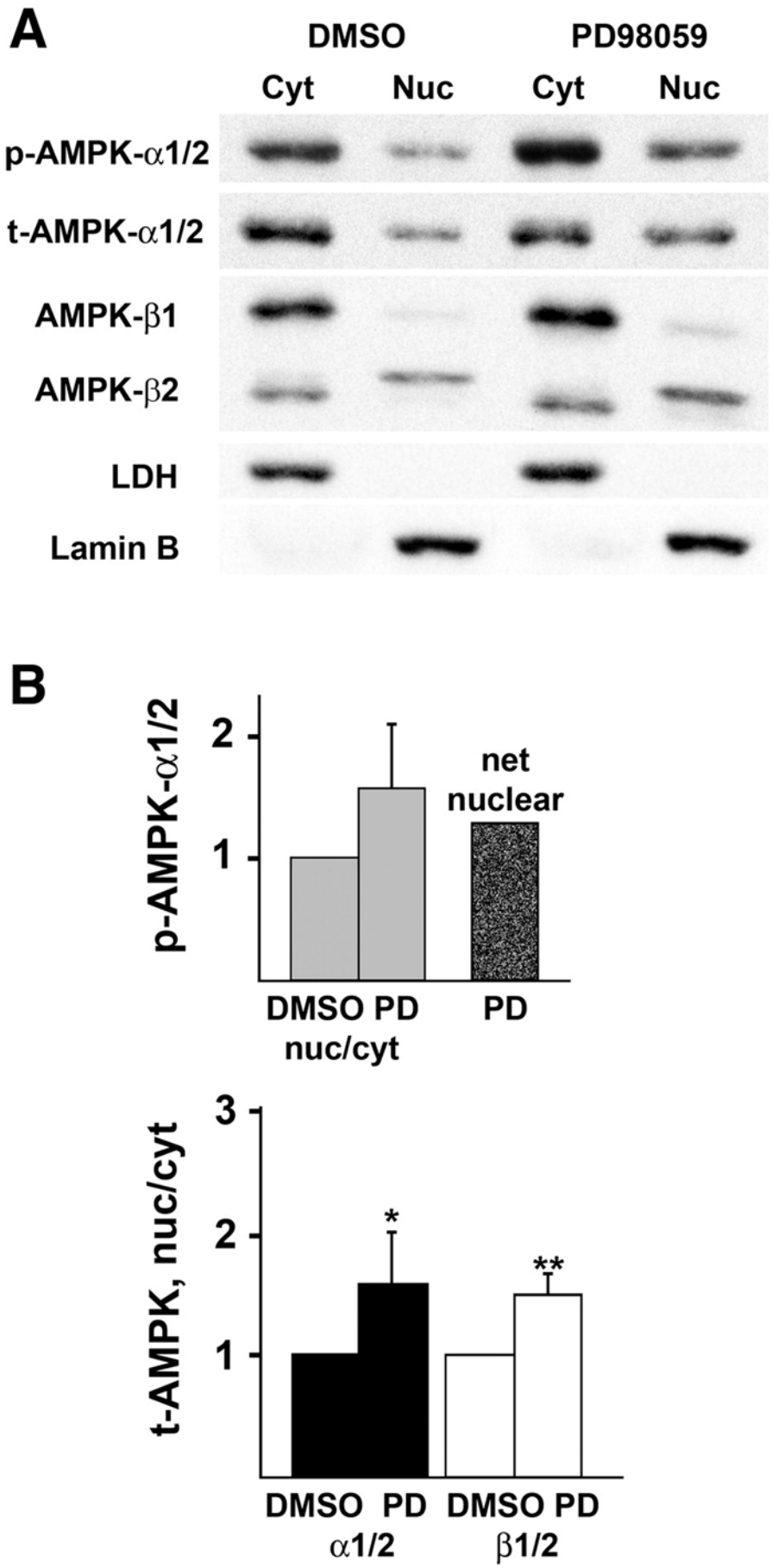
A
DMSO
PD98059
Cyt
Nuc
Cyt
Nuc
p-AMPK-α1/2
t-AMPK-α1/2
AMPK-β1
AMPK-β2
LDH
Lamin B
B
p-AMPK-α1/2
2
1
net
nuclear
DMSO PD
nuc/cyt
PD
t-AMPK, nuc/cyt
3
2
1
*
**
DMSO PD
α1/2
DMSO PD
β1/2

Figure 3.10 Inhibition of the MEK→ERK1/2 pathway alters the nuclear levels of AMPK

(A) The distribution of p-AMPK-α1/2, t-AMPK-α1/2 and AMPK-β1/2 was monitored by cell fractionation and Western blotting. **(B)** ECL signals were quantified as for Fig. 3.2. The untreated control served as reference for cells incubated with PD98059. **$p<0.01$; *$p<0.05$.

Figure 3.11

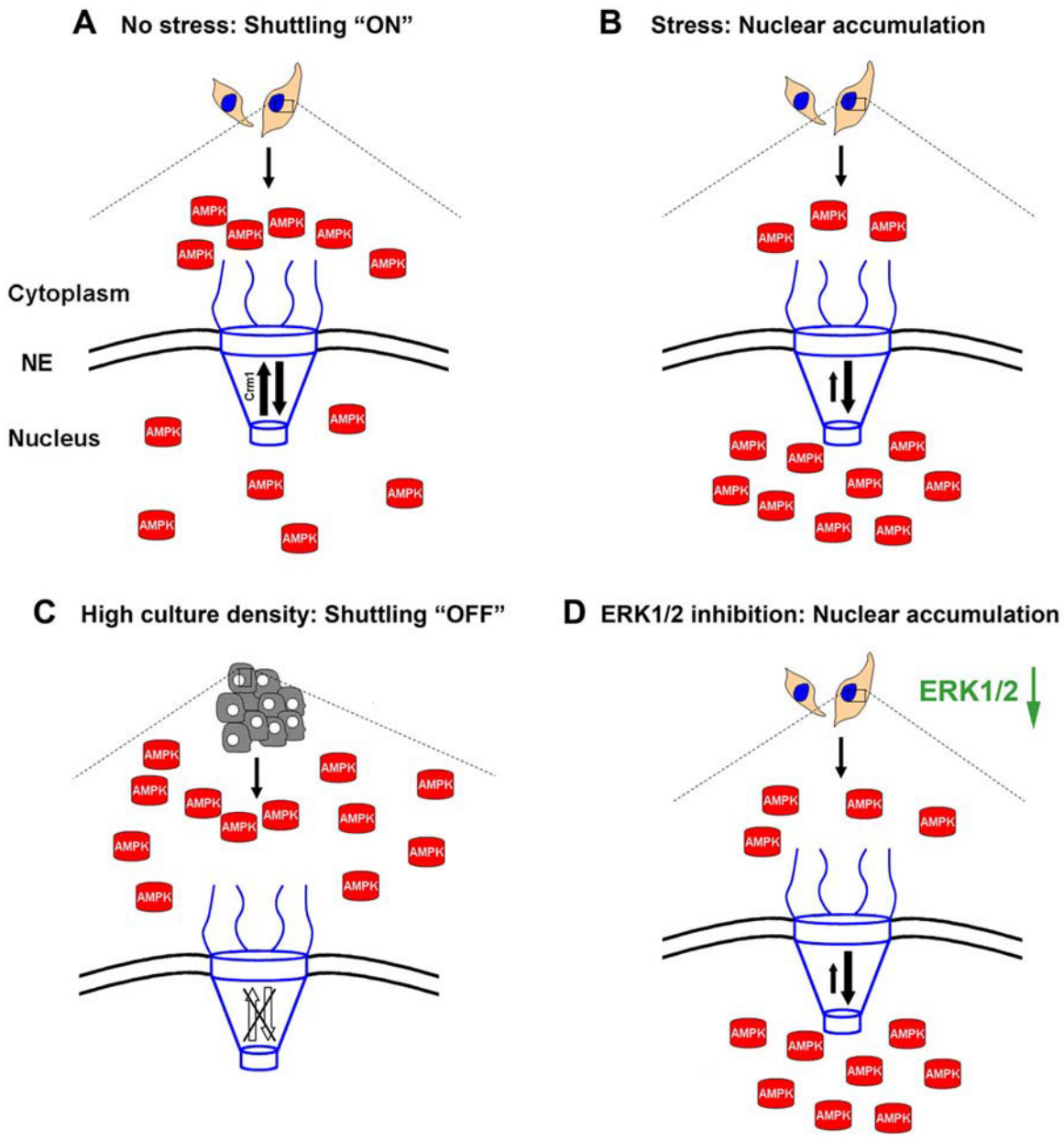
A No stress: Shuttling "ON"
B Stress: Nuclear accumulation
C High culture density: Shuttling "OFF"
D ERK1/2 inhibition: Nuclear accumulation
Cytoplasm
NE
Nucleus
Crm1
AMPK
ERK1/2

Figure 3.11 Simplified model for the control of AMPK localization under normal and stress conditions

(A) In unstressed cells AMPK shuttles between the nucleus and the cytoplasm and is present in both compartments**.** Nuclear export is mediated by the carrier Crm1. (**B)** Several forms of stress, including heat, energy depletion and oxidants, increase the levels of AMPK-α1/2 and β1/2 in nuclei. **(C)** In high density cultures, AMPK fails to shuttle and is located in the cytoplasm. (**D)** Signaling through MEK→ERK1/2 regulates the intracellular distribution of AMPK. Inhibition of the MEK→ERK1/2 pathway leads to AMPK nuclear accumulation of AMPK subunits. The redistribution of AMPK under different physiological conditions may be triggered by changes in transport across the nuclear envelope, retention in the nucleus and cytoplasm or a combination of these events.

Suppl. Figure 3.1

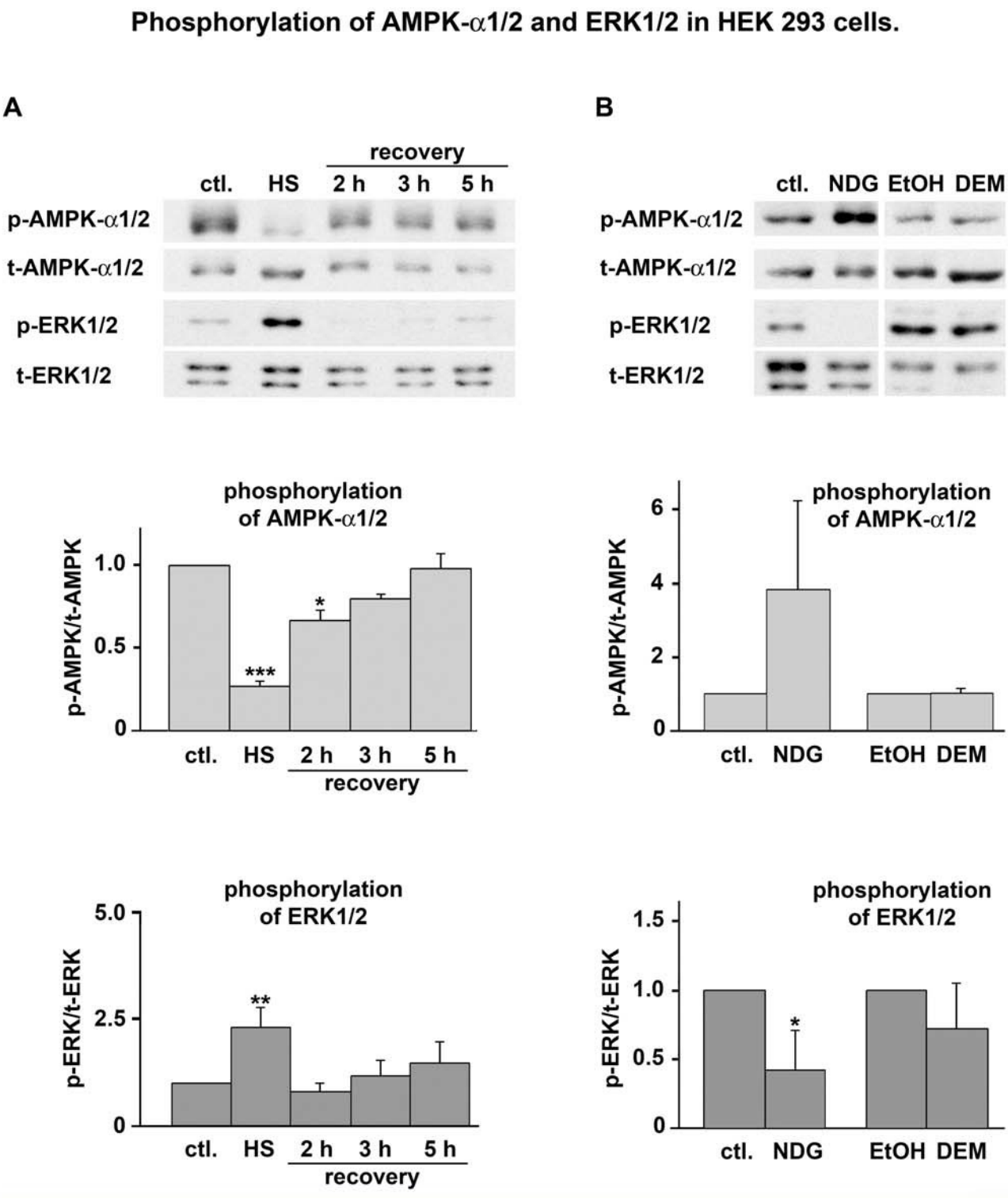

Suppl. Figure 3.1 Phosphorylation of AMPK-α1/2 and ERK1/2 in HEK293 cells upon heat shock, energy depletion or oxidant treatment

The phosphorylation of Thr172 in AMPK-α1/2 and dual modification of ERK1/2 was monitored for HEK293 cells by Western blotting as described for Fig. 3.1. Antibodies against p-AMPK-α1/2 detected the phosphorylation on Thr172 of AMPK α subunits, whereas t-AMPK-α1/2 antibodies recognize total-AMPK-α1/2. Samples were probed for dually phosphorylated ERK1/2 (p-ERK1/2), total ERK1/2 (t-ERK1/2) and total AMPK-α1/2 (t-AMPK-α1/2). Means and SD are shown for the phosphorylation of AMPK-α1/2 and dual phosphorylation of ERK1/2. Bonferroni tests for multiple statistical comparisons or Student's *t*-tests (two-tailed) for unpaired samples were carried out to identify significant differences. For each experiment, all test results were compared with the control. ***$p<0.001$; **$p<0.01$, *$p<0.05$.

Suppl. Figure 3.2

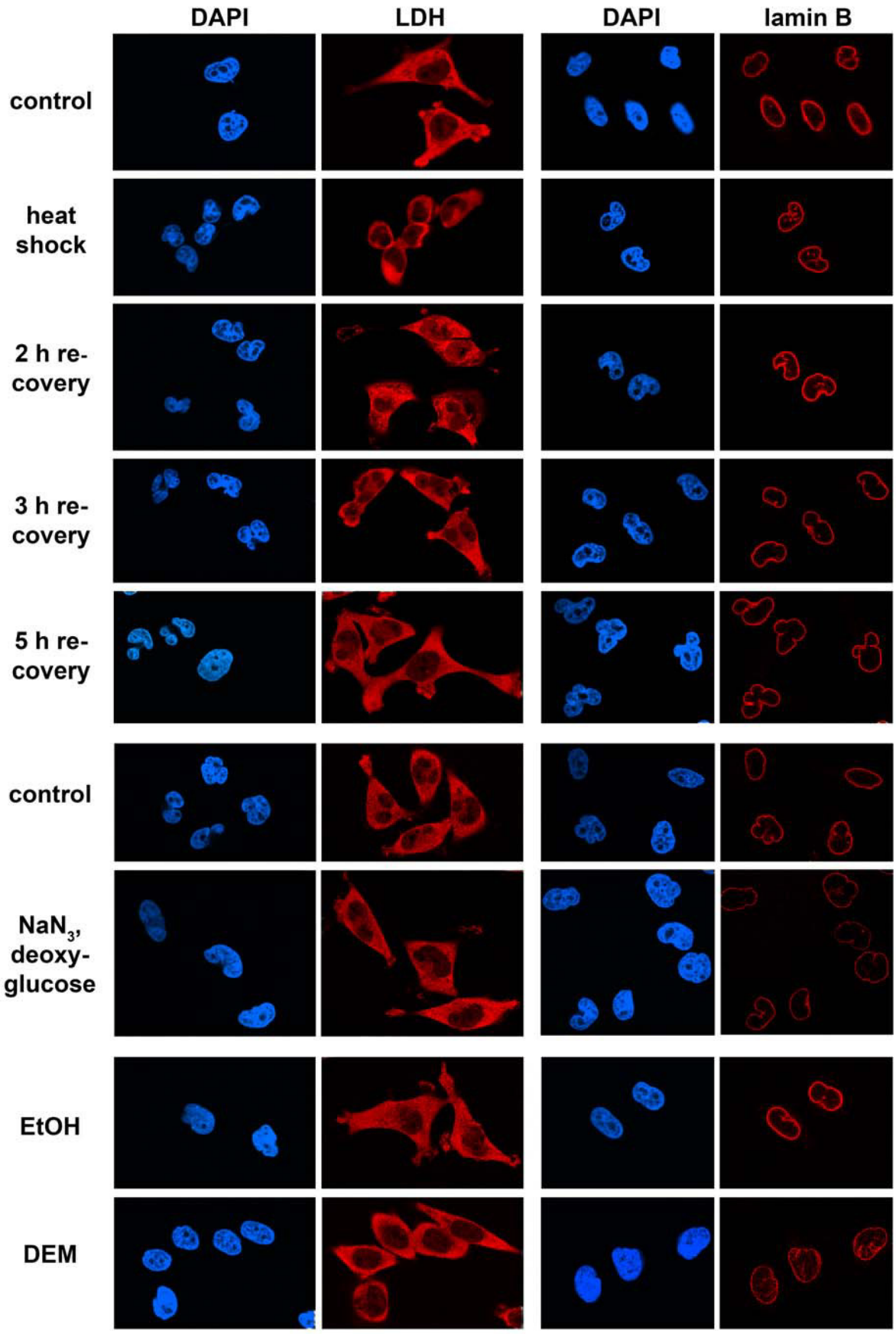

Suppl. Figure 3.2 Lactate dehydrogenase (LDH) and lamin B distribution upon heat shock, energy depletion or oxidative stress

HeLa cells were exposed to heat shock, NaN_3/deoxyglucose or DEM as described for Fig. 3.1-3.4. LDH and lamin B were localized by indirect immunofluorescence in control and stressed cells.

Suppl. Figure 3.3

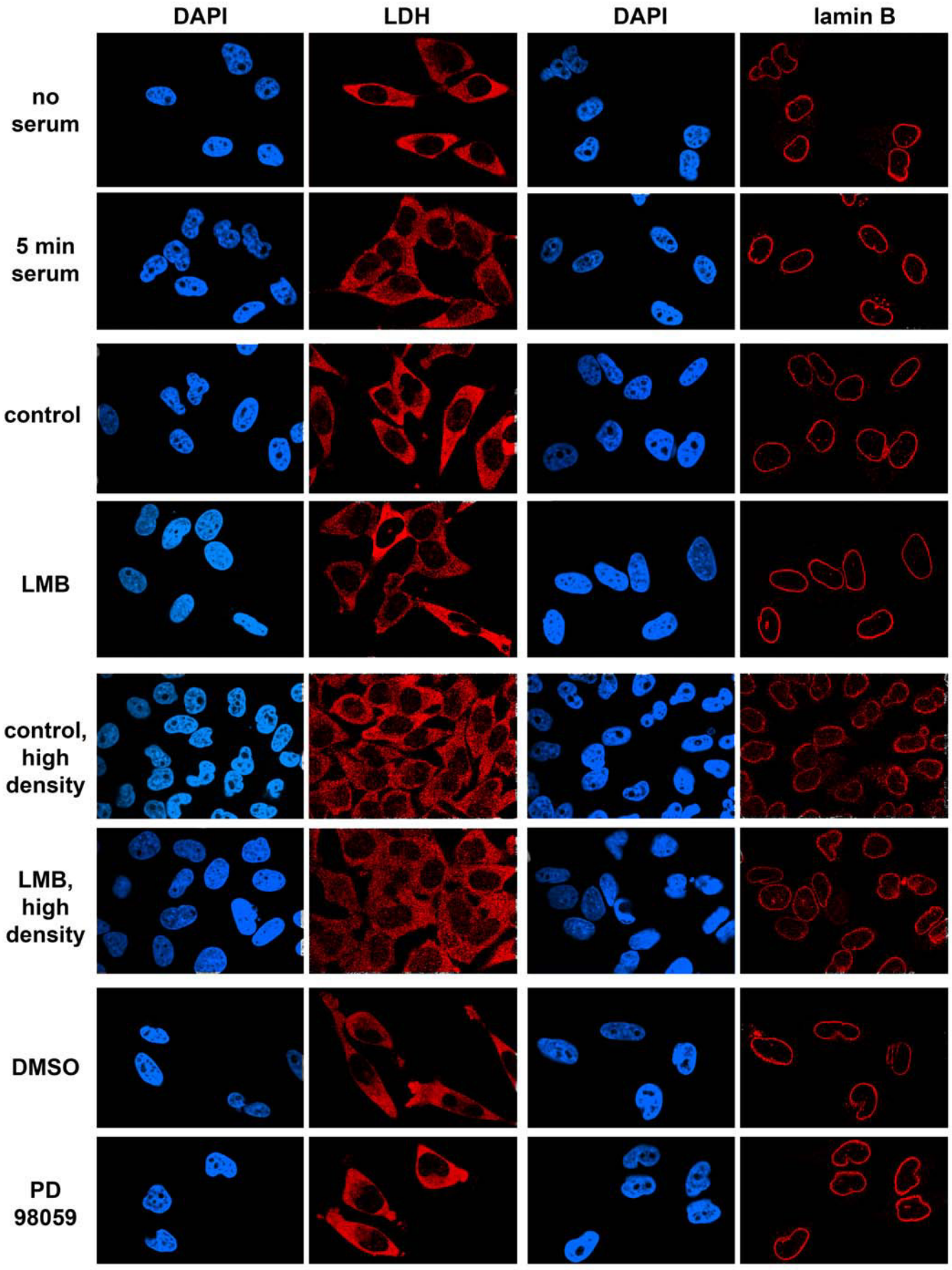

Suppl. Figure 3.3 Effect of serum starvation, LMB, high cell density or inhibition of ERK1/2 activation on the localization of LDH and lamin B

The distribution of LDH and lamin B was determined as described for Suppl. Fig. 3.2. HeLa cells grown to 70% confluency were treated with serum, LMB or PD980059, and high density HeLa cultures were incubated with LMB.

CHAPTER 4

Stress Inhibits Nucleocytoplasmic Shuttling of Heat Shock Protein Hsc70

Mohamed Kodiha, Angel Chu, Omar Lazrak and Ursula Stochaj.

Department of Physiology, McGill University, 3655 Promenade Sir William Osler, Montreal, PQ, H3G 1Y6, Canada

4.1 Connecting text to chapter 4

In addition to signaling molecules, heat shock proteins of the hsp/hsc70 family are essential chaperones that play a key role in the stress response. Under normal growth conditions hsc70s are required for the proper folding and intracellular targeting as well as the regulation of apoptosis. Heat shock protein 70 (hsc70), is an essential component of the chaperoning machinery and indispensable for the repair of stress-induced damage. Hsc70 plays a critical role in restoring cell function upon heat and other stresses. The chaperone shuttles between the nucleus and cytoplasm and is found in both compartments of unstressed cells. However, following stress exposure, hsc70 accumulates in nuclei, but relocates to the cytoplasm when cells recover from stress. As the general goal of my thesis is to characterize the effect of stress on different aspects of cell physiology, I investigated how stress impinges on the cellular chaperoning system as a key player in maintaining cellular homeostasis. The objective of the research work presented in chapter 4 is to define the molecular mechanisms that underlie the stress-induced nuclear accumulation of hsc70s. Specifically, I have characterized at the molecular level how shuttling of hsc70 is regulated under normal and stress conditions. My results demonstrate a potential role of the actin cytoskeleton in regulating hsc70 distribution under normal and stress conditions. In addition, using human/mouse heterokaryons, I have shown that heat shock inhibits hsc70 shuttling and sequesters the chaperone in nuclei. The inhibition of shuttling in response to stress is transient only, and transport is re-established when cells recover from stress. Furthermore, I have identified nuclear retention as a novel

mechanism that prevents hsc70 to move in and out of the nucleus upon stress. In depth analysis revealed that this retention depends on two distinct processes, ATP-sensitive binding of hsc70 to chaperone substrates and an ATP-insensitive association with nucleoli. My studies identified the nucleolar protein fibrillarin and ribosomal protein rpS6 as interacting partners that show increased association with hsc70 in nuclei of stressed cells. This supports the idea that hsp/hsc70 play a pivotal role in restoring nucleolar functions after heat shock. Chapter 4 demonstrates in details the results obtained from this research which are published in the paper entitled: "Stress inhibits nucleocytoplasmic shuttling of heat shock protein hsc70" by ***Mohamed Kodiha****, Angel Chu, Omar Lazrak, and Ursula Stochaj*.

4.2 Abstract

Heat shock proteins of the hsp/hsc70 family are essential chaperones, implicated in the stress response, aging, and a growing number of human diseases. At the molecular level, hsc70s are required for the proper folding and intracellular targeting of polypeptides as well as the regulation of apoptosis. Cytoplasmic members of the hsp/hsc70 family are believed to shuttle between nuclei and cytoplasm; they are found in both compartments of unstressed cells. Our experiments demonstrate that actin filament-destabilizing drugs trigger the nuclear accumulation of hsc70s in unstressed and heat-shocked cells recovering from stress. Using human/mouse heterokaryons we show that stress inhibits shuttling and sequesters the chaperone in nuclei. The inhibition of hsc70 shuttling upon heat shock is transient only and transport is re-established when cells recover from stress. Hsc70 shuttling is controlled by hsc70 retention in the nucleus, a process that is mediated by two distinct mechanisms, ATP-sensitive binding of hsc70s to chaperone substrates and furthermore the association with nucleoli. The nucleolar protein fibrillarin and ribosomal protein rpS6 were identified as components that show an increased association with hsc70s in the nucleus upon stress exposure. Taken together, our data suggest that stress abolishes the exit of hsc70s from the nucleus to the cytoplasm, thereby limiting their function to the nuclear compartment. We propose that during recovery from stress hsc70s are released from nuclear and nucleolar anchors, which is a prerequisite to restore shuttling.

Keywords: Heat shock proteins, hsc70, stress, nuclear transport

4.3 Introduction

Heat shock proteins are involved in numerous cellular functions, including folding of newly synthesized polypeptides and targeting of proteins to their proper cellular location. In particular, chaperones of the hsp/hsc70 family are essential to these processes (258, 262, 263). Hsp/hsc70s play a crucial role in the appropriate response to stress and the survival of stress-induced damage, processes that are relevant to a large number of human diseases and pathophysiological conditions (256). Moreover, hsp/hsc70s are implicated in the regulation of apoptosis, tumorigenesis and aging (255, 259, 261). In eukaryotic cells under normal growth conditions cytoplasmic hsp/hsc70s are believed to move in and out of the nucleus, and it was demonstrated in *Xenopus* oocytes that they shuttle between nucleus and cytoplasm (265). Unlike other members of the hsp70/hsc70 family, hsc70 (also referred to as hsp73 or hsp70-8) is essential for the survival of normal and tumor cells (269). Hsc70s concentrate in nuclei when cells are exposed to stress and heat shock is the most efficient treatment to induce their accumulation in nuclei (225). Although heat increases the steady-state concentration of hsc70s in nuclei, it is not known whether stress also controls their movement between nucleus and cytoplasm. However, this knowledge is required to understand the dynamics of hsc70 localization under different physiological conditions. To address this question, we have monitored the distribution of endogenous hsc70s and the reporter protein EGFP-hsc70 in human cultured cells. Our results demonstrate that exit of hsc70s from the nucleus upon recovery from stress is an active process and that heat shock restricts the nucleocytoplasmic trafficking of hsc70s.

Following heat exposure hsc70 shuttling is prevented, but restored when cells recover from this environmental insult. We have identified the stress-induced nuclear retention of hsc70 as a mechanism that controls shuttling of the chaperone.

4.4 Materials and methods

4.4.1 Nuclear reporter proteins

The fluorescent protein NLS-NES-GFP2 carries SV40 nuclear localization sequence (NLS) and the nuclear export sequence (NES) of PKI fused to two copies of GFP (270). The NLS-NES-GFP2 coding sequence was transferred to a vector that mediates inducible expression in mammalian cells (206). A plasmid encoding hsc70 (kindly provided by Drs. S. Wax and N. Kedersha, Boston) was used to generate a fusion between enhanced GFP (EGFP) and hsc70. To this end, the hsc70 coding sequence was cloned into the BamHI site of vector pEGFP-C1 (Clontech, Palo Alto). The correctness of the construct was verified by DNA-sequencing; the fusion protein is referred to as EGFP-hsc70. EGFP-hsc70 shows the same distribution as authentic hsc70 when analyzed in control and stressed cells (Fig. 4.4 and data not shown). A schematic representation of the constructs used for transfection is shown in Fig. 4.1.

4.4.2 Transfection of HeLa cells

At a confluency of ~70% HeLa cells were transfected in 6-well plates with Effectene (Qiagen, Mississauga, ON) following the manufacturer's recommendations. Transient gene expression in HeLa using a dexamethasone-

inducible system has been described in detail (206, 225). Transfected cells were grown for 24 hours on polylysine-coated cover slips in 6-well plates or on multiwell slides before exposure to stress.

4.4.3 Treatment with leptomycin B, latrunculin B and cytochalasin B

To analyze the potential role of the importin-β family member Crm1, we have tested the effect of leptomycin B (LMB), a compound that selectively inhibits this exporter (264). To this end, cells were incubated with 10 ng/ml LMB (gift of M. Yoshida, Tokyo), dissolved in ethanol, or with the solvent ethanol for 15 hours at 37°C following heat stress. Unstressed cells were incubated with LMB for up to 24 hours at 37°C. Latrunculin B and cytochalasin B (Calbiochem, San Diego, CA) were dissolved in DMSO. Cells recovering from stress were incubated for 15 hours at 37°C with 1 mM latrunculin B, 10 μM cytochalasin B or the solvent DMSO. Unstressed cells were treated with latrunculin B, cytochalasin B or DMSO for 3 h at 37°C as indicated in the figure legends. In control experiments the effect of latrunculin B or cytochalasin B on actin polymerization was tested with FITC-labeled phalloidin following the supplier's protocol (Sigma, Oakville, ON).

4.4.4 Immunofluorescence.

All steps were carried out at room temperature essentially as described (225). In brief, cells were washed in PBS and fixed for 25 min at room temperature in 3.7% formaldehyde/PBS. Fixed cells were rinsed in PBS and permeabilized with 0.1 % Triton X-100 in PBS/ 2 mg/ml BSA (5 min, room temperature). All subsequent steps were carried out in PBS/ 2 mg/ml BSA/0.05% Tween 20. Samples were

incubated overnight with primary antibodies against hsc70s or fibrillarin (SPA-815, StressGen, Victoria, BC, diluted 1:1,000; Santa Cruz Biotechnology, sc-11335, diluted 1:1,000); primary antibodies were detected with 1.5 μg/ml Cy3-conjugated secondary antibodies (Jackson ImmunoResearch, West Grove, PA). NLS-NES-GFP2 was visualized with polyclonal rabbit antibodies to GFP (Clontech, Palo Alto, diluted 1:200) and 5 μg/ml secondary antibodies conjugated to Alexa-488 (Molecular Probes, Eugene, OR). To detect rpS6 (Santa Cruz Biotechnology, sc-13007, diluted 1:500) cells were fixed in methanol/acetone (1:1, vol/vol) for 30 min at -20°C. All subsequent incubations and washes were carried out in PBS/BSA. DNA was located with 4',6-diamidino-2-phenylindole (DAPI) and samples were mounted in Vectashield (Vector Laboratories, Burlingame, CA). Cells were analyzed with a Nikon Optiphot at 400X magnification and photographed with Kodak T-MAX 400 films. Negatives were scanned and processed with Photoshop 5.5 and 8.0.

4.4.5 Human/mouse heterokaryons

Heterokaryons between HeLa and mouse NIH3T3 cells were generated by a modification of published procedures (257). In brief, HeLa cells transiently synthesizing EGFP-hsc70 were trypsinized and seeded on cover slips 24 hours post transfection to reach ~60% confluency on the next day. HeLa cells were then exposed to 1-hour heat stress at 45.5°C and $3x10^5$ NIH3T3 cells were added to each well of a six well plate. After 1.5 hours mouse cells adhered to the cover slips and cycloheximide was added to 75 μg/ml for 30 min. Cells were fused subsequently for 2 min with 50% PEG 3350. After removal of PEG, samples were

washed three times with PBS and incubated at 37°C in growth medium containing 100 µg/ml cycloheximide. Cells were fixed 3, 5 and 15 hours after heat stress, nuclei stained with DAPI and heterokaryons or homokaryons were monitored for the distribution of EGFP-hsc70.

4.4.6 Analysis of nuclear retention

Nontransfected HeLa cells were exposed for 1 hour to 45.5°C and subsequently treated for 5 min with 40 µg/ml digitonin in buffer B on ice (271). Digitonin-extracted cells were incubated with buffer B, containing 5 mg/ml BSA and 0.05% Nonidet-40 (NP-40) for 15 min at room temperature. The buffer was supplemented with 2.5 mM ATP, 2.5 mM ADP or 1 mM of the non-hydrolyzable ATP-analog AMP-PNP as indicated in the figure legends. Samples were washed extensively in buffer B/BSA/NP-40, buffer B, twice in PBS, fixed and processed for indirect immunofluorescence with anti-hsc70 antibodies as described above. To monitor the intactness of nuclear envelopes cells were extracted with digitonin, treated with buffer B/BSA/NP-40 and washed as described above. Washed samples were fixed, blocked with PBS/2 mg/ml BSA and incubated with anti-lamin B antibodies (0.5µg/ml; Santa Cruz Biotechnology, sc-6217). Control cells were treated with digitonin only before blocking and incubation with antibodies.

4.4.7 Protein cross-linking and immunoprecipitation

Control, stressed and recovering cells were grown on 100 mm tissue culture dishes, washed with cold PBS and extracted with 40µg/ml digitonin in PBS for 5 min on ice. Samples were washed with PBS and incubated with 0.2 mM 3,3'-

Dithiobis(sulfosuccinimidylpropionate) in PBS for 1 hour on ice. Dishes were washed with cold PBS and stored at -70°C until use. For immunoprecipitation, plates were incubated for 10 min on ice with IP-buffer (20 mM Tris-HCl, pH 8.0, 5 mM EDTA, 150 mM NaCl, 1 % NP-40, 10 % glycerol, protease inhibitors [aprotinin, antipain, chymostatin, leupeptin, pepstatin, each at 1µg/ml; 1 mM PMSF]). Samples were vortexed with glass beads, cleared by centrifugation (5 min, 13,000 rpm, 4°C) and incubated with protein 50 µl G-sepharose (Amersham Biosciences; 30 min, 4°C with gentle agitation). Resin was removed by centrifugation and supernatants were incubated with 5 µg anti-hsc70 for 2 hours at 4°C, followed by addition of 50 µl G-sepharose and overnight incubation at 4°C. Beads were collected by centrifugation, washed three times in IP-buffer, and incubated with gel sample buffer containing 1.4 M β-mercaptoethanol (15 min, 95°C). Material released from the resin was analyzed by Western blotting.

4.4.8 Western blot analysis

Western blotting and ECL detection was carried out essentially as described (225) using a Lumigen™ PS-3 detection kit (Amersham Biosciences.).

4.5 Results and discussion

4.5.1 During recovery from heat stress nuclear hsc70s relocate to the cytoplasm in a temperature-dependent fashion that does not require de novo protein synthesis

Heat shock induces the rapid nuclear accumulation of hsc70s in HeLa cells, and a 1-hour exposure to 45.5°C (severe heat shock) is sufficient to concentrate hsc70s

in nuclei (Fig. 4.2). Following heat stress, hsc70s relocate from nuclei to the cytoplasm when cells recover at 37°C as monitored for different time points in Fig. 4.2. Several hours after heat treatment, hsc70s began to exit the nucleus; after 15 hours of recovery they distributed throughout the cell. This relocation of hsc70s was temperature-dependent, and abolished when cells were incubated at 4°C, consistent with an active transport process (Fig. 4.2, and not shown). Interestingly, when cells were kept at 4°C, hsc70s not only failed to relocate to the cytoplasm, but they also concentrated in nucleoli. During recovery at 37°C, nuclear export of hsc70s did not depend on *de novo* protein synthesis, as it was not abolished by cycloheximide (Fig. 4.2, + CHX).

4.5.2 Hsc70 nuclear export does not require the transporter Crm1/exportin-1 in unstressed cells or during recovery from heat shock

Shuttling depends on nuclear import and export of proteins, and neither of these processes has been defined on a molecular level for members of the hsp/hsc70 family. The nuclear exporter Crm1/exportin-1 is involved in transport of a large number of cargos, most of which contain a leucine-rich NES. This export pathway can be inhibited efficiently with leptomycin B (LMB), a drug that covalently modifies the transporter Crm1/exportin-1 (264). Members of the hsc70/hsp70 families contain a conserved sequence element (i.e., position 164 to 173 of mouse hsc70) that fits the consensus sequence for a hydrophobic NES recognized by Crm1. However, LMB did not prevent hsc70 export in cells recovering from heat stress (Fig. 4.3A). The same result was obtained when both LMB and cycloheximide were added during the recovery period. Likewise, LMB did not

change the distribution of hsc70s in unstressed cells, even if the drug was present for up to 24 hours (Fig. 4.3C).

In control experiments, LMB efficiently inhibited shuttling of NLS-NES-GFP2. This reporter protein carries a signal for nuclear localization (SV40-NLS) as well as nuclear export (PKI-NES); the PKI-NES is recognized by Crm1. NLS-NES-GFP2 was both cytoplasmic and nuclear in the absence of LMB, but accumulated in nuclei when LMB was added to the growth medium. Taken together, these results show that hsc70 nuclear export upon recovery from heat or under nonstress conditions does not rely on Crm1.

4.5.3 The actin filament destabilizing drugs latrunculin B and cytochalasin B inhibit nuclear export of hsc70s in stressed and control cells

To further define hsc70 nuclear transport we tested the effect of latrunculin B and cytochalasin B. These compounds are believed to affect actin located at the nuclear pore complex (NPC), thereby preventing nuclear export of various components (260). Incubation with latrunculin B or cytochalasin B drastically reduced the amount of actin filaments, which became obvious by the loss of phalloidin-binding (not shown). Importantly, in cells recovering from heat shock either drug prevented hsc70 export from the nucleus (Fig. 4.3A; Lat B, Cyt B). Similarly, when unstressed cells were treated with latrunculin B or cytochalasin B, hsc70s concentrated in nuclei, and nuclear accumulation was apparent after a 3-hour treatment. These results support the idea that under normal physiological conditions, i.e. in the absence of stress, hsc70s shuttle between nucleus and cytoplasm in human culture cells. Furthermore, hsc70 export is abolished by the

destabilization of filamentous actin, suggesting a role of actin in the translocation of nuclear hsc70s to the cytoplasm. In particular, actin located at the NPC could play a crucial role, as it seems to be involved in nuclear export of multiple cargos (260).

4.5.4 Hsc70 shuttling is inhibited by heat shock and restored when cells recover from stress

Heterokaryons have been used to analyze the shuttling of proteins that are concentrated in nuclei at steady-state under normal growth conditions. However, this approach has not been applied previously to monitor shuttling in heat-stressed cells. To achieve this, we have used the fluorescent reporter protein EGFP-hsc70, which shares the same biological properties with endogenous hsc70s when tested under a variety of stress conditions (Fig. 4.4A; Kodiha and Stochaj, unpublished). In unstressed cells, EGFP-hsc70 was distributed throughout nuclei and cytoplasm (Fig. 4.4A). Like endogenous hsc70s, EGFP-hsc70 accumulated in nuclei when cytochalasin B or latrunculin B was added to the growth medium (Fig. 4.4A).

Human/mouse heterokaryons were employed to evaluate EGFP-hsc70 shuttling after stress exposure; these heterokaryons contain nuclei from both species, which share the same cytoplasm (257). EGFP-hsc70 was first concentrated in nuclei of HeLa cells by heat shock for 1-hour at 45.5°C. HeLa cells were returned subsequently to the normal growth temperature and fused to mouse cells. In these heterokaryons, we localized EGFP-hsc70 at different time points during their recovery from heat exposure. [Note that EGFP-hsc70 synthesized in HeLa cells is the only source of fluorescence seen in Fig. 4.4B, as

cycloheximide prevents *de novo* synthesis of EGFP-hsc70 in heterokaryons.] Three hours after heat shock, EGFP-hsc70 remained restricted to human nuclei in human/mouse heterokaryons (Fig. 4.4B, mouse nuclei in heterokaryons are labeled with arrowheads). By contrast, EGFP-hsc70 was absent from mouse nuclei and the common cytoplasm, demonstrating that the translocation from human nuclei to the cytoplasm was prevented at this point. To determine whether this export inhibition and thereby the block in shuttling was reversible, heterokaryons were allowed to recover for a longer period of time. At 5 hours post heat shock, EGFP-hsc70 began to migrate out of the human nucleus and appeared in the common cytoplasm. After a 15-hour recovery period human and mouse nuclei displayed comparable signals for EGFP-hsc70, showing that shuttling of the chaperone had resumed.

The absence of EGFP-hsc70 from mouse nuclei at early time points after cell fusion is not simply a failure of the non-stressed mouse nuclei to import the chaperone. While generating heterokaryons, we also obtained fusions originating from a mixture of transfected and non-transfected HeLa cells; the latter were not synthesizing EGFP-hsc70. In these multinucleated cells, or homokaryons, we detected 3 h after heat shock nuclei that did not contain EGFP-hsc70 (Fig. 4.4B, nuclei of non-transfected HeLa cells marked with arrows). As observed for heterokaryons, EGFP-hsc70 appeared in the common cytoplasm of homokaryons 5 h upon heat exposure and began to migrate into all of the nuclei present. At 15 post heat shock EGFP-hsc70 was present in all of the nuclei of multinucleated

cells and nuclei from transfected and non-transfected cells could no longer be distinguished.

To compare shuttling in heat-treated with control cells, heterokaryons were generated using unstressed HeLa cells and inspected at times that are equivalent to 3 and 5 hours post heat shock. For both time points EGFP-hsc70 was detected in mouse nuclei (labeled with arrowheads). At the earlier time point the amount of EGFP-hsc70 in mouse nuclei was somewhat variable between different heterokaryons (Fig. 4.4C, "equivalent to 3 h after heat shock"). At the time equivalent to 5 hours after heat exposure in stressed cells all of the mouse nuclei in heterokaryons clearly contained EGFP-hsc70. Taken together, data obtained for heterokaryons support the idea that EGFP-hsc70 appears faster in mouse nuclei when unstressed HeLa cells are the source of the fusion protein.

4.5.5 Hsc70s are retained in nuclei of heat-shocked cells

Shuttling between nucleus and cytoplasm can be regulated on different levels; this includes import, export and retention of the shuttling protein. As such, the movement of nuclear hsc70s to the cytoplasm could be controlled by retention in the nucleus. The liberation from nuclear anchors would be a rate-limiting step for shuttling, as this release is a prerequisite for subsequent export to the cytoplasm.

Heat shock is likely to trigger hsc70 binding to a large number of nuclear proteins that require chaperone activity, a process that may contribute to nuclear retention of hsc70s. To test this hypothesis, we have developed an assay for hsc70 release from nuclear anchors, which is not complicated by transport across the nuclear envelope (see Materials and Methods for details). To this end, control and

heat-shocked HeLa cells were first extracted with digitonin, which permeabilizes the plasma membrane and removes most of the cytoplasmic proteins, but leaves the nuclear membranes intact. Following digitonin extraction, the non-ionic detergent NP-40 was used to solubilize the nuclear envelope, which will no longer restrict the movement of proteins. The proper permeabilization of membranes in our assays was verified in control experiments (Fig. 4.5A). As expected, anti-lamin B antibodies do not have access to the nuclear lamina in digitonin-treated cells, but subsequent incubation with NP-40 led to antibody binding.

We next used this assay to determine whether hsc70s are retained in nuclei of control and heat-shocked cells (Fig. 4.5B, C). Samples were treated with digitonin followed by incubation in the absence or presence of NP-40. Heat-shocked samples retained most of the hsc70s even in the presence of NP-40, suggesting that binding to nuclear anchors contributes to hsc70 accumulation in nuclei. By contrast, little hsc70 was found in nuclei of unstressed cells under any of the conditions tested (Fig. 4.5B and Table 4.1).

4.5.6 ATP and the non-hydrolyzable analog AMP-PNP release hsc70s from nuclear anchors

One way to retain hsc70s in nuclei is their binding to substrates that need to be refolded. This chaperone/substrate interaction is known to be stabilized by ADP, whereas ATP induces the rapid dissociation and binding of substrates (reviewed in 258, 267). Digitonin-extracted cells were incubated for 15 min in NP-40 containing buffer supplemented with ATP, AMP-PNP or ADP followed by localization of hsc70s (Fig. 4.5C). Unlike ADP, both ATP and AMP-PNP

efficiently released the chaperone from nuclei, suggesting that ATP-binding, but not cleavage, is required to liberate hsc70s from nuclear anchors. Interestingly, ATP failed to release hsc70 completely from nucleoli, suggesting that binding to nucleolar components is more complex than a chaperone/unfolded protein interaction.

4.5.7 Nuclear retention of hsc70s changes during recovery from heat shock

We next monitored hsc70 nuclear retention in cells recovering from stress. To this end, HeLa cells exposed to heat were analyzed after 3, 5 and 15 hours incubation at 37°C. The amount of hsc70s present in the nucleoplasm decreased during recovery, and nucleoplasmic chaperone could be liberated with ATP or AMP-PNP (Fig. 4.6). In addition, hsc70s transiently concentrated in nucleoli, albeit with kinetics different from their accumulation in the nucleoplasm. Upon a 3-hour recovery period hsc70 levels increased in nucleoli of most cells, but only in few nucleoli after 5 hours (Fig. 4.6, Table 4.1). As observed after heat exposure, hsc70 associated with nucleoli was not fully liberated by incubation with ATP or AMP-PNP. At 15 hours post-heat shock, hsc70 distribution was similar to unstressed controls, and no accumulation was seen in nuclei or nucleoli. Results of these *in vitro* experiments (summarized in Table 4.1) suggest that hsc70 binding to chaperone substrates contributes to its nuclear retention immediately after heat treatment and at early stages of recovery.

4.5.8 Binding of hsc70s to nuclei of stressed cells

Members of the hsp/hsc70 family are involved in multiple interactions in the nucleus, and in response to heat stress hsc70s can be expected to interact with a

large variety of nuclear components. For instance, the importance of hsc70s for the organization of nucleoli is well established, and chaperones are implicated in restoring nucleolar function upon stress (265, 268). Based on these earlier observations, nucleolar proteins were candidates for the interaction with hsc70s in heat-treated cells. To test this idea, we have examined fibrillarin, a *bona fide* component of nucleoli, and the ribosomal protein rpS6, which is assembled into the small ribosomal subunits in nucleoli. When analyzed by indirect immunofluorescence (Fig. 4.7A) fibrillarin was concentrated in nucleoli of control cells, but redistributed throughout nucleus and cytoplasm in response to heat exposure. During recovery fibrillarin relocated to nucleoli, and after 15 h at 37°C its distribution was similar to unstressed controls. In parallel, nuclear proteins were immunoprecipitated with antibodies against hsc70s, and immunoprecipitates that contained comparable amounts of hsc70 were probed with antibodies against fibrillarin (Fig. 4.7B). Although the nucleolar protein co-purified with hsc70s for control, stressed and recovering cells, clearly the highest amount of fibrillarin associated with hsc70s in heat-shocked cells.

Like fibrillarin, rpS6 redistributed after heat stress. As part of the 40S ribosomal subunit, rpS6 is mostly cytoplasmic under control conditions; however, heat treatment resulted in the formation of large structures containing rpS6 at the cytoplasmic side of the nuclear periphery. As well, increased amounts of rpS6 were detected in the nucleus. During stress recovery rpS6 relocated and after 15 h its distribution was similar to unstressed cells (Fig. 4.7A). Similar to fibrillarin, the association of rpS6 with hsc70 in nuclei was enhanced transiently after heat

stress, as demonstrated by the co-immunoprecipitation of both proteins (Fig. 4.7B).

Taken together, data obtained for the interaction of nuclear hsc70s with fibrillarin and rpS6 are consistent with a role of the chaperone in restoring nucleolar function after heat exposure.

4.6 Conclusions

Our study demonstrates that the nucleocytoplasmic shuttling of chaperones of the hsp/hsc70 family is inhibited by heat shock, but restored when cells recover from stress-induced damage. Importantly, stress not only alters the steady-state distribution, but also the movement of hsc70s between nucleus and cytoplasm. Here we show that hsc70 retention in the nucleus is drastically increased in response to heat exposure, a process that will prevent export of the chaperone to the cytoplasm and thereby shuttling. We have identified two different forms of hsc70 interaction with nuclear anchors, both of which can be expected to contribute to the sequestration of chaperone in nuclei. First, hsc70s bind to nuclear proteins in an ATP-sensitive fashion, which most likely represents binding of the chaperone to folding substrates. Second, hsc70s associate with nucleoli and at least a portion of the nucleolar chaperone cannot be liberated by the addition of ATP. This could indicate an association of hsc70s with nucleolar components in a fashion that is distinct from a chaperone/folding protein interaction. Independent of the type of association that underlies hsc70s retention in nuclei, we have shown that this retention is low in control cells, high after heat

shock and gradually reduced during recovery from stress. These changes in nuclear retention of hsc70s upon stress and during recovery can be expected to affect a variety of biological processes that require chaperone activity. For instance, immediately following stress, the proper folding of chaperone substrates in the cytoplasm may be impaired, until *de novo* synthesis or shuttling of hsp/hsc70s resume. Moreover, stress may interfere with the chaperone-dependent targeting of cytoplasmic proteins to various organelles, including mitochondria and peroxisomes, both of which require cytoplasmic hsp/hsc70s for protein import.

Based on the results described here we have developed a simplified model for hsc70 shuttling (Fig. 4.8). Hsc70s accumulate in nuclei of heat-stressed cells where they are initially retained in the nucleoplasm by binding to chaperone substrates in an ATP-sensitive fashion. During recovery from heat hsc70s relocate within the nucleus and transiently concentrate in nucleoli, this interaction cannot be prevented by the addition of ATP. As recovery progresses, hsc70s are liberated from nuclear and nucleolar anchors, which precedes their relocation to the cytoplasm. We propose that the release from nuclear anchors is a limiting factor that regulates hsc70 nuclear export and thereby shuttling of the chaperone in cells exposed to heat.

Taken together, the stress-induced sequestration of hsc70s in nuclei possibly affects repair processes in the cytoplasm as well as the proper assembly and maintenance of several organelles. These consequences of stress exposure are

likely to impinge on different aspects of physiology and ultimately survival of each cell.

4.7 Acknowledgements

We thank Drs. M.Yoshida, (Tokyo), S. Wax and N. Kedersha (Boston) and K. Weis (Berkeley) for generous gifts of LMB and plasmids. We are grateful to Neola Matusiewicz for expert technical assistance and in particular to I. Gallouzi (Montreal) for help with heterokaryon assays.

4.8 GRANTS

This work was supported by grants from CIHR, NSERC and Heart and Stroke Foundation of Quebec to US. US is a chercheur national of FRSQ. MK and AC were supported by predoctoral fellowships from McGill University, FRSQ and NSERC.

Table 4.1 Hsc70s are retained in nucleoplasm of heat-shocked cells

		1-h Heat			
	Control	No recovery	3-h Recovery	5-h Recovery	15-h Recovery
No nucleotide added	(+)	+++*	++ Nucleoli	+ Nucleoli for some cells	(+)
ATP	(+)	(+) Nucleoli	(+) Nucleoli	(+) Nucleoli for some cells	(+)
AMP-PNP	(+)	(+) Nucleoli	(+) Nucleoli	(+) Nucleoli for some cells	(+)
ADP	(+)	+++*	++ Nucleoli	+ Nucleoli for some cells	(+)

Table 4.1 Hsc70s are retained in the nucleoplasm of heat-shocked cells

Results for the experiments shown in Fig. 4.5 and 4.6 are summarized. Control, heat-stressed and recovering cells were extracted with digitonin and incubated in buffer containing the nonionic detergent NP-40 and the different nucleotides shown in the table. The presence of hsc70s was monitored by indirect immunofluorescence. Similar results were obtained for at least three independent experiments. The signals for hsc70s in the nucleoplasm are shown as +++, strong; ++, intermediate; or (+), weak signal. For some of the conditions, hsc70s could be detected in nucleoli. [(i)]The strong fluorescence in the nucleoplasm of stressed cells could mask the presence of hsc70s in nucleoli.

Figure 4.1

Figure 4.1 Nuclear reporter proteins used in this study

NLS-NES-GFP2 is a fluorescent protein that contains two copies of GFP fused to NLS of SV40 T-antigen and NES of the inhibitor of cAMP-dependent protein kinase. The reporter protein shuttles and at steady-state is concentrated in the cytoplasm. The reporter protein EGFP-hsc70 was generated by in frame fusion of EGFP to the 5'-end of the hsc70 coding sequence. The synthesis of NLS-NES-GFP2 is controlled by a regulatable promoter that contains 5 copies of glucocorticoid response elements (GRE). Addition of dexamethasone to the growth medium will induce gene expression. Expression of the EGFP-hsc70 gene is driven by a CMV IE promoter (P_{CMV}). Both plasmids carry an SV40 polyadenylation signal (SV40 polyA).

Figure 4.2

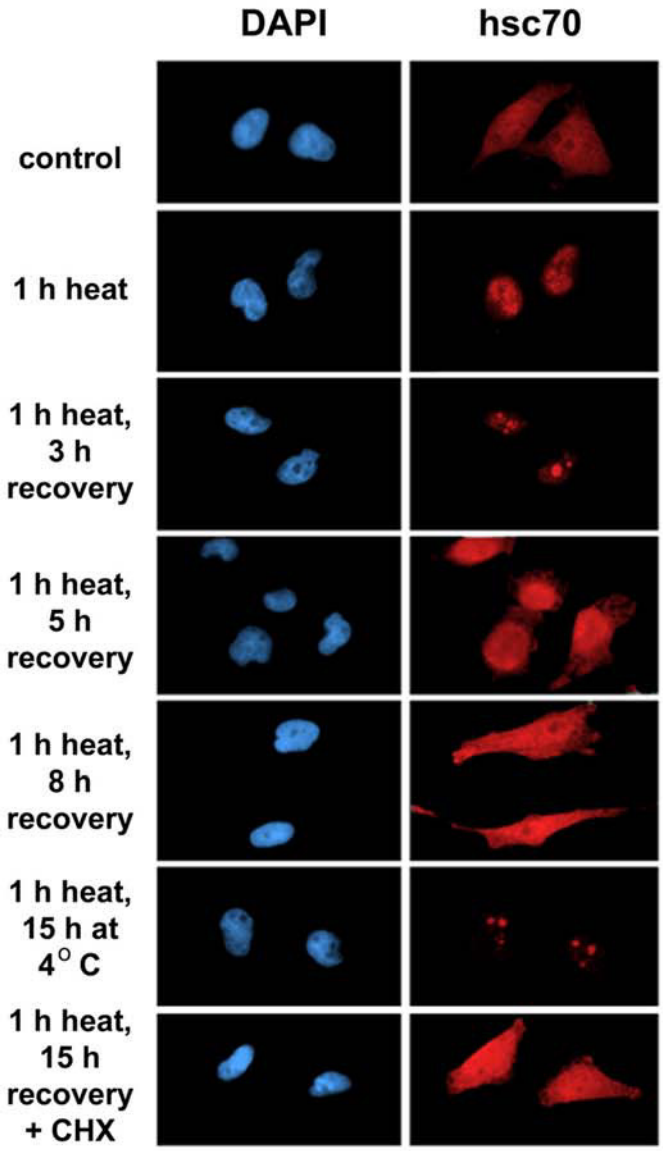
DAPI
hsc70
control
1 h heat
1 h heat, 3 h recovery
1 h heat, 5 h recovery
1 h heat, 8 h recovery
1 h heat, 15 h at 4° C
1 h heat, 15 h recovery + CHX

Figure 4.2 Nuclear hsc70s relocation to the cytoplasm during recovery from heat shock is temperature-dependent, but does not require *de novo* protein synthesis

Hsc70s were localized by indirect immunofluorescence in unstressed cells (control) or upon exposure to severe heat shock (1 hour at 45.5ºC). Following heat stress, cells recovered at 37°C for the times indicated. In addition, heat-shocked cells were kept for 15 hours at 4°C or incubated at 37°C in the presence of 100 μg/ml cycloheximide. Nuclei were stained with DAPI.

Figure 4.3

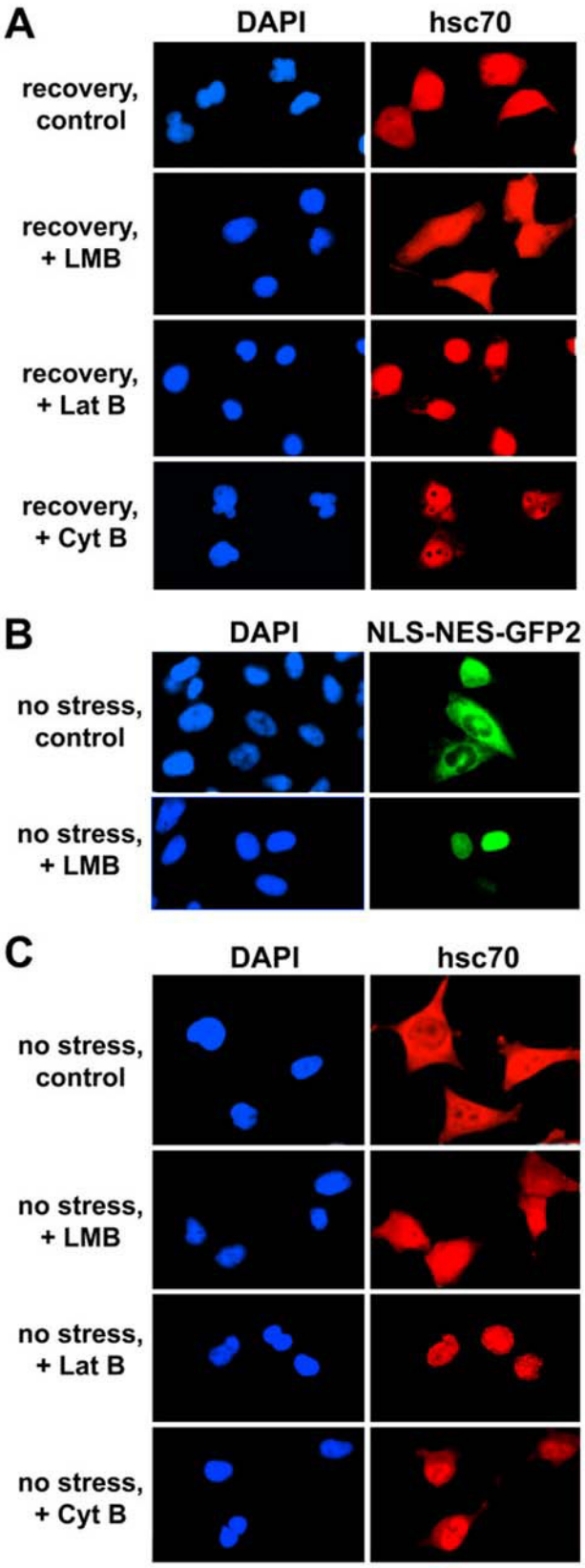
A
DAPI
hsc70
recovery, control
recovery, + LMB
recovery, + Lat B
recovery, + Cyt B
B
DAPI
NLS-NES-GFP2
no stress, control
no stress, + LMB
C
DAPI
hsc70
no stress, control
no stress, + LMB
no stress, + Lat B
no stress, + Cyt B

Figure 4.3 Effect of leptomycin B, latrunculin B and cytochalasin B on nuclear export of hsc70s and NLS-NES-GFP2

(A) Hsc70s were located in HeLa cells exposed to severe heat shock followed by 15 hours recovery at 37°C. Leptomycin B (LMB), latrunculin B (Lat B) and cytochalasin B (Cyt B) were present throughout the recovery period as described in Materials and Methods. **(B)** HeLa cells transiently synthesizing NLS-NES-GFP2 were incubated for 15 hours without or with 10 ng/ml LMB. **(C)** Unstressed cells were kept at 37°C and treated for 24 hours with 10 ng/ml LMB. Alternatively, cells were incubated for 3 hours at 37°C with 1 mM Lat B or 0.1 mM Cyt B. Hsc70s and NLS-NES-GFP2 were located by indirect immunofluorescence. Nuclei were visualized with DAPI.

Figure 4.4

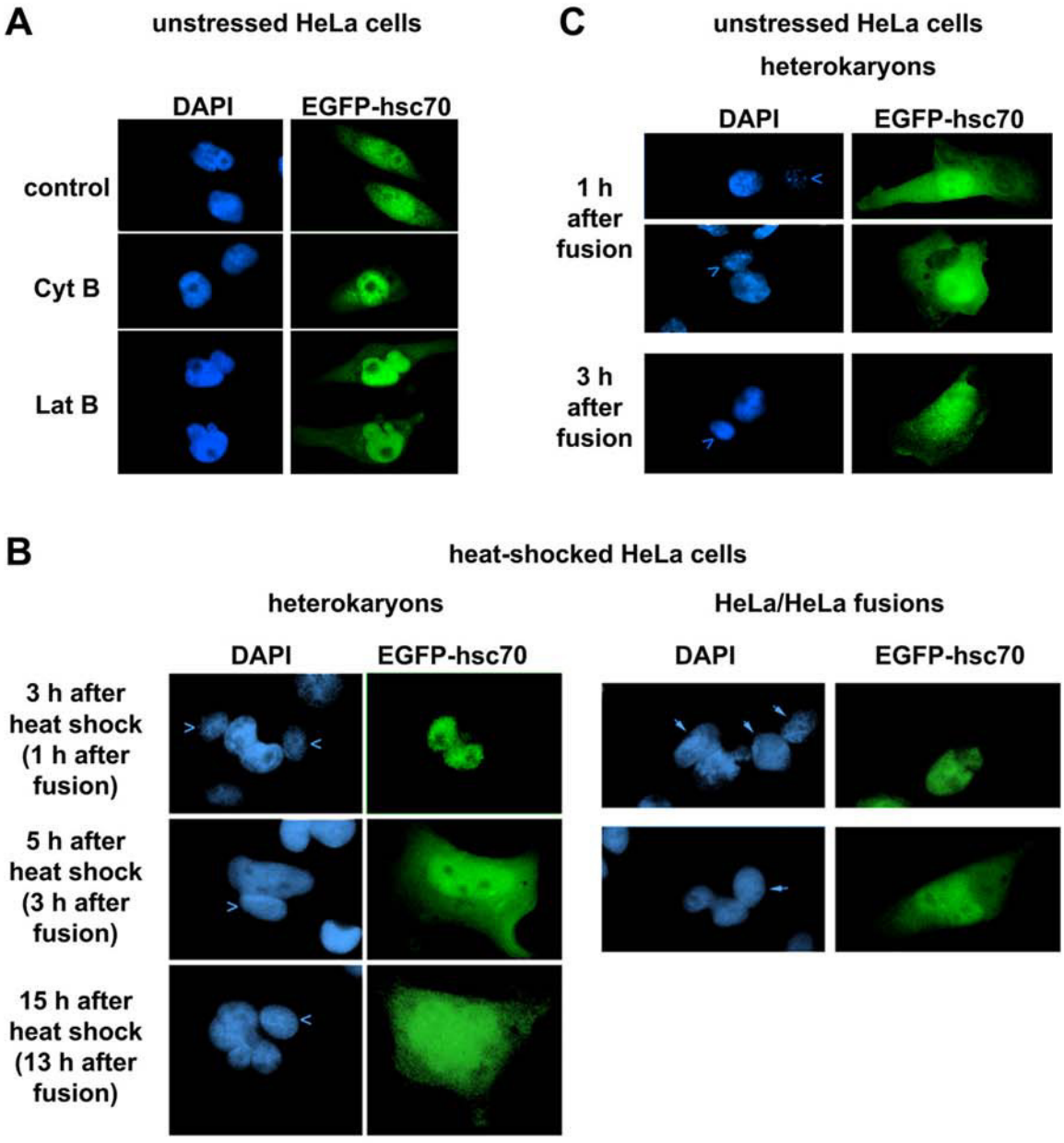
A
unstressed HeLa cells
DAPI
EGFP-hsc70
control
Cyt B
Lat B
C
unstressed HeLa cells
heterokaryons
DAPI
EGFP-hsc70
1 h after fusion
3 h after fusion
B
heat-shocked HeLa cells
heterokaryons
HeLa/HeLa fusions
DAPI
EGFP-hsc70
DAPI
EGFP-hsc70
3 h after heat shock (1 h after fusion)
5 h after heat shock (3 h after fusion)
15 h after heat shock (13 h after fusion)

Figure 4.4 Hsc70 shuttles in unstressed, but not in heat-shocked cells

(A) HeLa cells synthesizing EGFP-hsc70 were incubated with the solvent DMSO, cytochalasin B or latrunculin B for 3 hours at 37°C. In fixed cells, EGFP-hsc70 and nuclei (DAPI) were located by fluorescence microscopy. **(B)** HeLa cells synthesizing EGFP-hsc70 were heat-shocked and fused to mouse NIH3T3 cells. EGFP-hsc70 was localized in fixed heterokaryons following heat treatment at the time points indicated. Homokaryons generated by fusion of several HeLa cells were analyzed in parallel. Arrowheads mark the position of mouse nuclei in heterokaryons and arrows point to the nuclei of non-transfected HeLa cells in homokaryons. **(C)** Heterokaryons obtained after fusion with unstressed HeLa cells were fixed at time points that are comparable to 3 and 5 hours post heat shock. Mouse nuclei are labeled with arrowheads.

Figure 4.5

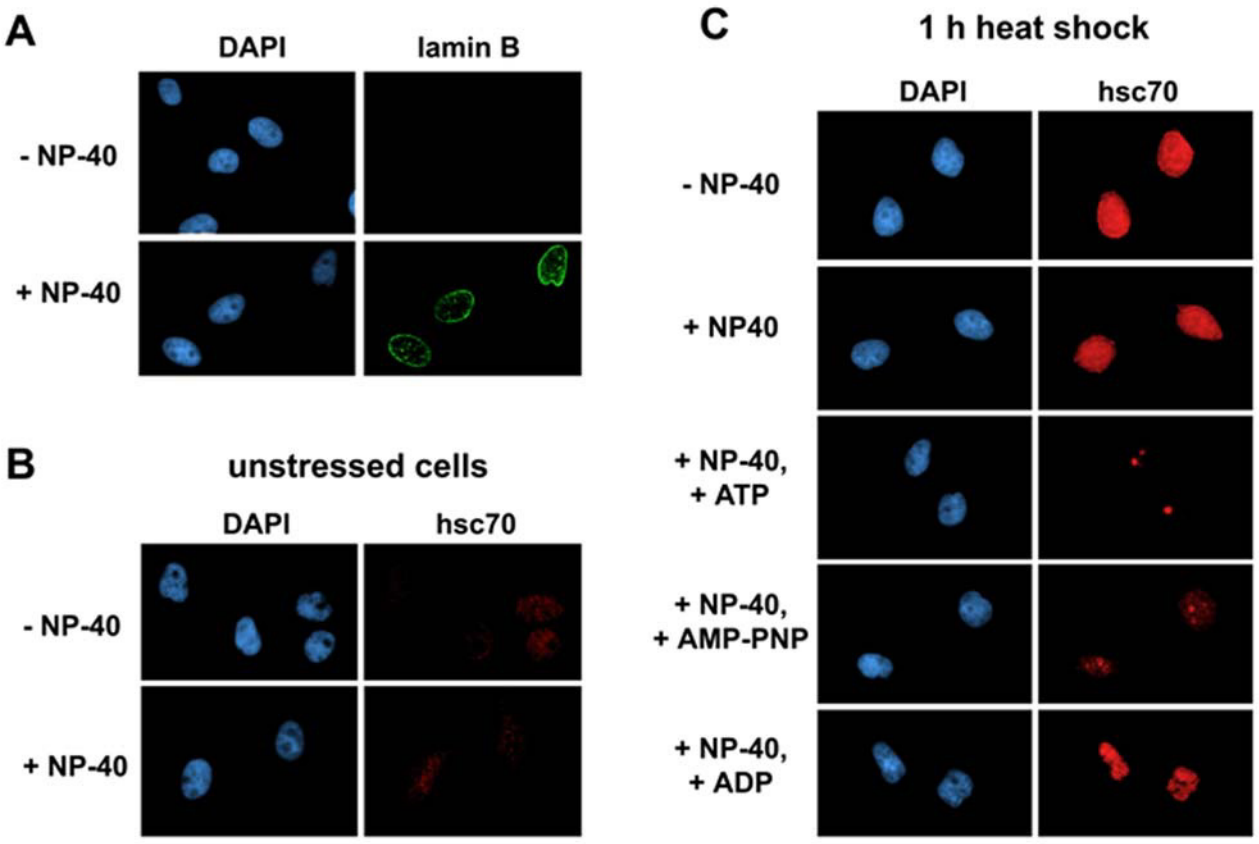
A
DAPI
lamin B
- NP-40
+ NP-40
B
unstressed cells
DAPI
hsc70
- NP-40
+ NP-40
C
1 h heat shock
DAPI
hsc70
- NP-40
+ NP40
+ NP-40,
+ ATP
+ NP-40,
+ AMP-PNP
+ NP-40,
+ ADP

Figure 4.5 Hsc70s are retained in nuclei of heat-stressed cells

(A) The nuclear envelope of digitonin-treated cells is permeabilized with NP-40. Heat-shocked HeLa cells extracted with digitonin were incubated in the absence or presence of NP-40. Cells were fixed and binding of anti-lamin B antibodies was tested by indirect immunofluorescence. Unstressed controls **(B)** and heat-shocked cells **(C)** were treated with digitonin. Samples were incubated subsequently with buffer containing NP-40 and ATP, AMP-PNP or ADP as indicated. Specimens were fixed and hsc70s detected by indirect immunofluorescence.

Figure 4.6

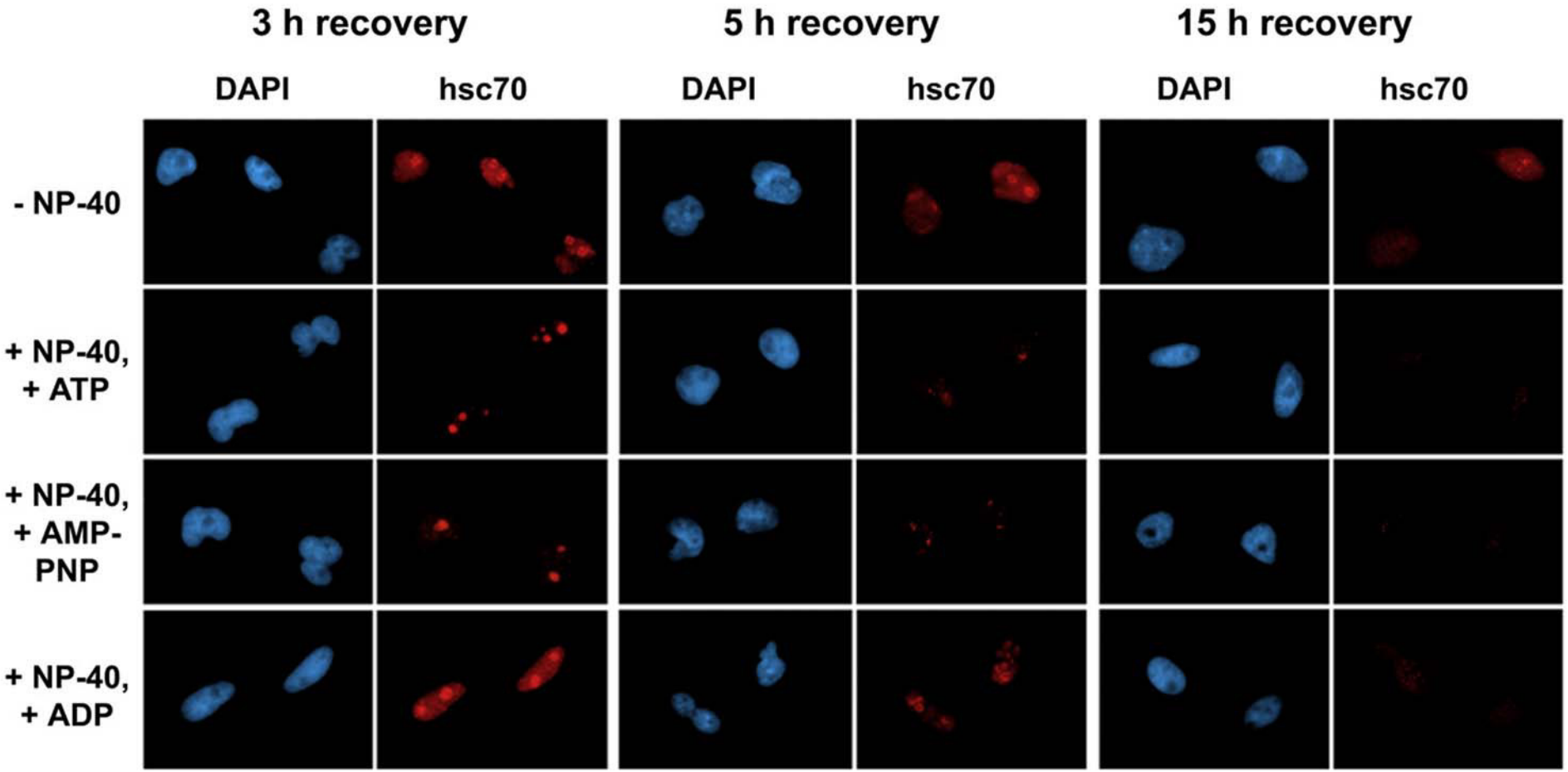
3 h recovery
5 h recovery
15 h recovery
DAPI
hsc70
DAPI
hsc70
DAPI
hsc70
- NP-40
+ NP-40, + ATP
+ NP-40, + AMP-PNP
+ NP-40, + ADP

Figure 4.6 Nuclear retention of hsc70s changes in cells recovering from heat stress

Heat-shocked cells were allowed to recover for 3, 5 and 15 hours before digitonin extraction and incubation with NP40-containing buffer in the presence of ATP, AMP-PNP or ADP. Hsc70s were located by indirect immunofluorescence as described for Fig. 4.5.

Figure 4.7

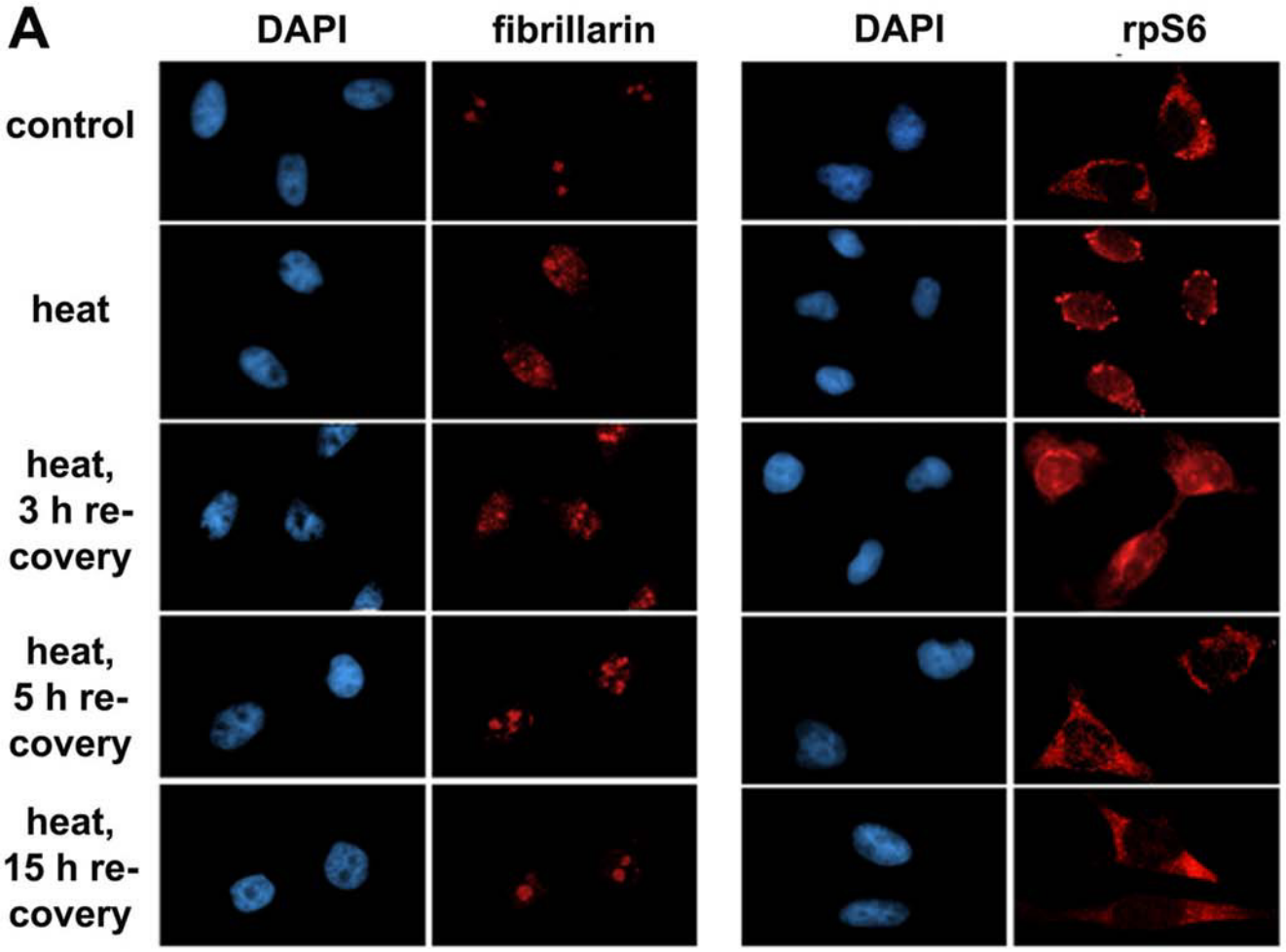
A
DAPI
fibrillarin
DAPI
rpS6
control
heat
heat, 3 h recovery
heat, 5 h recovery
heat, 15 h recovery

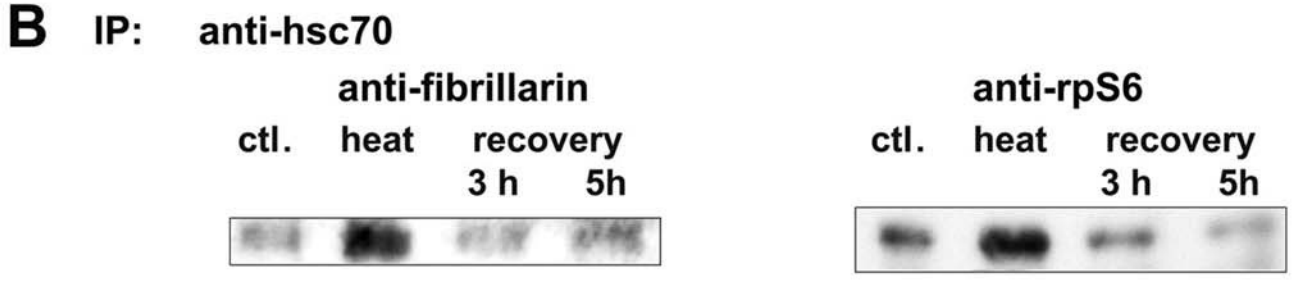
B
IP: anti-hsc70
anti-fibrillarin
ctl.
heat
recovery
3 h
5h
anti-rpS6
ctl.
heat
recovery
3 h
5h

Figure 4.7 The nucleolar protein fibrillarin and ribosomal protein rpS6 redistribute in stressed cells and associate with hsc70 upon heat shock

(A) Fibrillarin and rpS6 were localized by indirect immunofluorescence in unstressed, heat-shocked and recovering HeLa cells. **(B)** Nuclear proteins were immunoprecipitated with antibodies against hsc70. Samples containing comparable amounts of hsc70 were tested for the presence of fibrillarin and rpS6 by Western blotting.

Figure 4.8

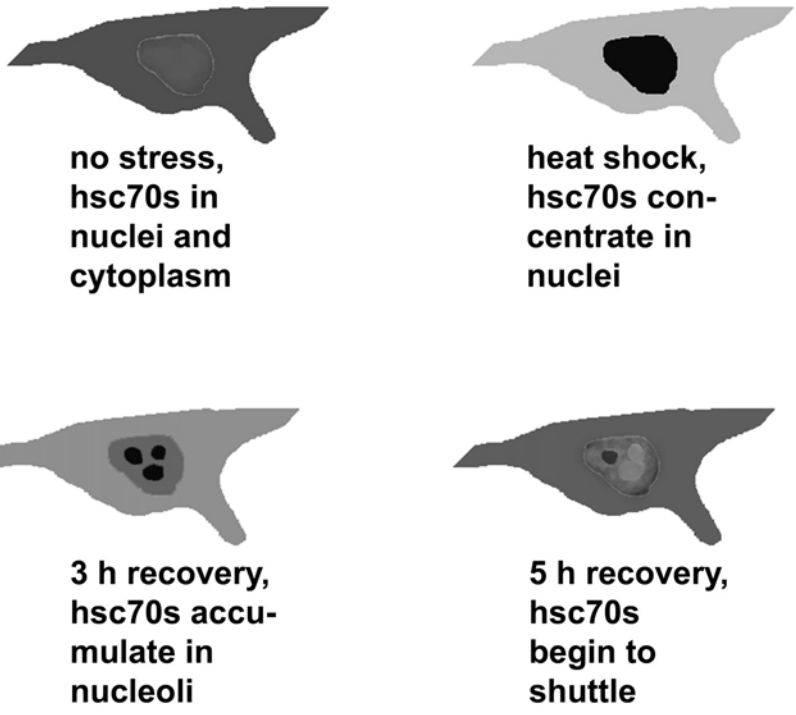
no stress, hsc70s in nuclei and cytoplasm
heat shock, hsc70s concentrate in nuclei
3 h recovery, hsc70s accumulate in nucleoli
5 h recovery, hsc70s begin to shuttle

Figure 4.8 Simplified model for the changes in nucleocytoplasmic shuttling of hsc70s upon heat shock and during recovery from stress

See text for details.

CHAPTER 5

Analysis of Signaling Events by Combining High-Throughput Screening Technology with Computer- Based Image Analysis

Mohamed Kodiha[1], Claire M. Brown[2] and Ursula Stochaj[1]

[1]Department of Physiology, [2]Department of Biochemistry and Life Sciences
Complex Imaging Facility, McGill University, Montreal, H3G 1Y6, Canada

5.1 Connecting text to chapter 5

Many of my experiments depend on imaging techniques, some of which were initially too insensitive, tedious and slow to provide dependable results in a timeless fashion. As part of my graduate research I therefore designed new powerful tools to detect and quantify fluorescence signals in different subcellular compartments. The strategy of these tools depends on combining the high throughput screening, imaging and computer based image analysis to develop a fast, accurate and reliable quantitative immunofluorescence approach which can be employed to study protein translocation in cells.

My work established new methods that contribute to the advancement in the field of image acquisition and analysis. As such, I adapted the high throughput image acquisition unit to obtain images for cells grown on cover slips. On the level of image analysis, I configured different analysis modules to quantify fluorescent signals in specific subcellular compartments such as nucleus, cytoplasm, and nuclear envelope. I show, for the first time, how to quantify fluorescence intensity of a probe that localizes to the nuclear envelope. To the best of my knowledge, there are no other quantitative immunofluorescence tools that can precisely detect and quantify nuclear envelope fluorescence.

I applied these techniques to define the mechanisms that control the distribution of nuclear transport factors as well as signaling molecules under normal and stress conditions. The flexibility of the protocols described in chapter 5 is demonstrated by the presence of different alternatives that can be used to measure fluorescence intensities in different cellular locations. This gives the user

a wide range of choices according to the need of different experimental settings as well as distinct distribution patterns of cellular proteins.

The different protocols generated by us, together with the advantages of each protocol and potential pitfalls, were published in Science Signaling: "Analysis of signaling events by combining high-throughput screening technology with computer-based image analysis"by ***Mohamed Kodiha***, *Claire M. Brown, and Ursula Stochaj*. This publication is presented in chapter 5.

5.2 Table of contents

5.3 Abstract

Intracellular signaling and cell-to-cell communication depend on the coordination of numerous signaling events, and this large flow of information has to be properly organized in space and time. Common and critical to all of these processes and the ultimate cellular response is the correct spatial distribution of signaling components and their targets. This fundamental concept applies to a large number of signaling processes. It is frequently important to quantify the localization of signaling molecules within different cellular compartments to detect subtle changes or to define threshold levels of signaling molecules in a certain location that are necessary to trigger subsequent events. Of particular importance is the separation of nuclear and cytoplasmic events, and sensitive methods are required to measure their contribution to signal transduction. Procedures described here allow the quantification of fluorescence signals located in the nucleus, cytoplasm, or at the nuclear envelope. The methods rely on high-throughput imaging equipment, confocal microscopy, and software modules that measure the fluorescence intensity in the compartment of interest. We discuss the rationale for selecting the appropriate equipment for image acquisition and the proper software modules to quantify fluorescence in distinct cellular compartments. Initially, high-throughput technology for high-speed image acquisition was developed for multiwell plates. We adapted high-throughput technology for image acquisition for cells grown on coverslips. Images of higher spatial resolution along the z-axis were acquired by confocal microscopy. For

subsequent analyses, the choice of appropriate software modules is critical for rapid and reliable quantification of fluorescence intensities.

5.4 Introduction

Most eukaryotic cells are characterized by the presence of multiple organelles, some of which are further organized into distinct compartments with unique functions. A prominent example is the nucleus, an organelle with complex and dynamic organization (272, 273). The nuclear envelope (NE) provides a physical barrier between the cytoplasm and the nucleus. This barrier separates vital cellular processes, such as DNA replication and RNA biogenesis in the nucleus, from cytoplasmic events, such as protein synthesis. The spatial segregation of cellular reactions provides a powerful mechanism for controlling numerous biological processes that have to be adjusted rapidly in response to environmental or physiological changes. In particular, a large number of signaling events alter the intracellular distribution of kinases, phosphatases, and other key components that control signaling (274-277). Moreover, subcellular compartmentalization separates distinct branches of cellular metabolism and contributes to control of gene expression.

Many signaling and metabolic processes are dynamic and enable cells to adapt to changes in environmental conditions and physiology. This dynamic state is exemplified by the bidirectional exchange of thousands of macromolecules between the nuclear and cytoplasmic compartments. For instance, nuclear proteins synthesized in the cytoplasm, such as transcription factors, polymerases, and histones, have to reach their final destination in the nucleus, whereas various RNAs and ribosomal subunits are initially generated in the nucleus and subsequently moved to the cytoplasm (246, 278, 279). All nucleocytoplasmic

transport of proteins and RNA is mediated by nuclear pore complexes (NPCs), large proteinacious assemblies embedded in the NE, which are the only gates for exchange of macromolecules between the nucleus and the cytoplasm.

Nucleocytoplasmic trafficking plays an important role in maintaining the cellular homeostasis, as it regulates various aspects of cell physiology, including gene expression, cell cycle progression, growth and proliferation, and many signaling events, as well as apoptosis (275-277, 280, 281). Two distinct mechanisms underlie the movement of molecules through NPCs: Small molecules with a mass of 40 kD or less can diffuse passively through nuclear pores, whereas larger molecules rely on active transport to move into or out of the nucleus. Nuclear transport requires several soluble factors, many of which shuttle between the nucleus and the cytoplasm. The availability of transport factors in the nuclear and cytoplasmic compartment or their association with the NE may control the efficiency of nuclear trafficking. This includes nuclear carriers that move proteins and RNA in and out of the nucleus (246, 282, 283). Like nuclear transport factors, many cargos shuttle between the nucleus and the cytoplasm, and their relative distributions can regulate their function (277, 280, 281). Prominent examples that are subject to this type of localization-mediated regulation are protein kinases and phosphatases, transcriptional regulators, and nuclear transporters for proteins or RNA (277, 280, 282, 290).

The correct localization of signaling molecules and their downstream targets is critical to produce the proper physiological response, and the dynamic distribution of these components may affect signaling on several levels. First, depending on

their subcellular location kinases and phosphatases may associate with distinct scaffolding modules, a process that can alter their substrate specificity (287, 288). Upon relocation within the cell, enzymes involved in signaling will obtain access to a unique set of substrates that is defined by the composition of the organelle or compartment. This scenario not only applies to kinases and phosphatases, but also to a large number of enzymes that regulate other posttranslational modifications, including farnesylation, acetylation, methylation, ubiquitination, and SUMOylation. On a second level, the localization of targets or substrates may be regulated. Such target molecules are exemplified by a large number of transcription factors and regulators, RNA-binding proteins, or carriers involved in intracellular trafficking.

Not only is the distribution between organelles and the cytoplasm essential for accurate signal transduction, but the proper localization to compartments within a particular organelle is crucial as well. For instance, distinct compartments within the nucleus have defined roles in signal transduction, and the NE, in particular, is emerging as an essential structure that regulates chromatin organization and gene expression (274- 276).

To obtain a better understanding of the diverse cellular activities and functions of a particular molecule, it is important to develop strategies that can be used to reliably quantify the abundance of this molecule in the organelle or suborganellar compartment of interest. Cell fractionation is a widely used procedure to separate subcellular compartments, especially organellar constituents from each other and from the cytoplasmic constituents. Although cell fractionation is useful for the

analysis of many proteins, it is prone to artifacts. For instance, small proteins that are concentrated in the nucleus of growing cells may leak out into the cytoplasm during cell fractionation. This is exemplified by the small guanosine triphosphatase (GTPase) Ran, a predominantly nuclear protein in intact cells. However, when organelles are purified by biochemical methods Ran diffuses across the NE and is obtained in substantial amounts in cytoplasmic fractions (122). Similarly, components that are dynamically or loosely, but stably, associated with the cytoplasmic side of the NE may be released into the cytoplasm when cells are lysed. In addition to problems with release and redistribution of proteins during cell fractionation, the isolation and purification of nuclear subcompartments like NEs and NPCs are laborious and time-consuming (20) and not always useful for accurately determining the concentrations of proteins present at this location.

The developments in high-throughput screening and the commercial availability of high content screening (HCS) automated fluorescence imaging platforms offer new options for rapidly performing cellular sampling and quantification of the cellular localization of molecules. Here, we describe detailed protocols to measure the distribution of fluorescent signals within different locations of the cell. We have focused on procedures for determining the nuclear or cytoplasmic location or the NE association of proteins. The methodologies can be adapted for fixed or live cells and may be used with fluorescent proteins, labeled antibodies, oligonucleotides, or any other molecule that can be detected with reasonable signal-to-noise ratio by HCS or confocal microscopy.

5.5 Materials

6-well dishes

Bovine serum albumin (BSA)

Cells engineered to produce fluorescent reporter molecules or primary and secondary antibodies against the proteins of interest.

Note: We describe experiments with Cy3-labeled secondary antibodies, but any other label that can be detected by the filters of the microscope can be used.

Dapi (Sigma)

Formaldehyde, 37%

Glass coverslips; 18 × 18 mm size 1 coverslips

Growth media appropriate for the cells under investigation

Microscope slides, such as pre-cleaned Fisherbrand slides (size 25 × 75 × 1 mm)

Phosphate-buffered saline (PBS), pH 7.4

Triton-X-100

Tween 20

5.6 Equipment

5.6.1 Cell Culture

CO_2 incubator

Laminar flow hood

Water bath

5.6.2 Microscopy

ImageXpress Micro automated imaging system (Molecular Devices, Sunnydale, CA) or a Zeiss LSM 510 confocal microscope equipped with a 200 M microscope.

Note: We collect images with the ImageXpress Micro with a 40× magnification objective [numerical aperture (NA) = 0.60)] and a CoolSnap HQ camera. Exposure times were 20 ms for Dapi and between 1.5 and 3.2 sec for TRITC and FITC. We collect images with the Zeiss LSM 510 with a 63× magnification (NA = 1.4) at scan speed 5, with 4-line averaging and a pixel resolution of 0.65 µm.

5.6.3 Software

MetaXpress (Molecular Devices, Sunnydale, CA) software

Note: The modules in MetaXpress need to be configured for the fluorescence quantification of the compartment of interest.

5.7 Recipes

Recipe 1: Formaldehyde Fix

Prepare a fresh solution of 3.7% formaldehyde in PBS by diluting a 37% formaldehyde stock solution into PBS. Prepare 9 ml for 6 samples.

Recipe 2: Permeabilization Buffer

Add 2 mg/ml of BSA to a solution of 0.1% Triton-X-100 in PBS. Prepare 9 ml for 6 samples.

Recipe 3: Wash Buffer

Add 2 mg/ml BSA to a solution of 0.05% Tween 20 in PBS. Prepare 22.5 ml for 6 samples.

Recipe 4: Primary and Secondary Antibodies

Dilute primary and secondary antibodies in Wash Buffer (Recipe 3).

Note: The optimal dilution of primary antibodies must be determined empirically for each antibody. Fluorescently labeled secondary antibodies should be used at a concentration of 0.5 to 1.5 μg/ml.

Recipe 5: Dapi Stain

Dissolve 1 μg/ml Dapi in Wash Buffer (Recipe 3). Prepare 1.5 ml for 6 samples.

5.8 Instructions

The relative abundance of a protein of interest that is present in the NE, nucleus, cytoplasm or all compartments is determined with different software modules in MetaXpress. We describe how to acquire images and adapt the software programs to quantify the amount of protein in each location, as well as the advantages and potential pitfalls of the procedures.

5.8.1 Cell preparation for imaging

This method may be applied to cells that adhere to glass coverslips or coated glass coverslips. We provide the general instructions for cells that grow on poly-lysine-coated glass coverslips. Prior to image acquisition with ImageXpress Micro, it is important to inspect the coverslips and determine the distribution of cells. This can be done by examining samples with a phase contrast microscope or examining samples that are Dapi stained with a fluorescence microscope.

Coverslips with very high cell density should not be used for image segmentation with certain modules because individual cell identification by image segmentation can be difficult. Coverslips with very low density of cells may not provide a large enough sampling of cells for appropriate statistical representation of the data. Based on our experiments with HeLa cells, we recommend 1.3×10^6 cells/coverslips (18 × 18 mm size 1).

1. Grow cells on 18 × 18 mm size 1coverslips in multiwell dishes (6-well dishes; each well with 9.6 cm^2 growth area) in the appropriate growth medium.
2. Fix cells for 20 min with 1.5 ml of 3.7% Formaldehyde in PBS (Recipe 1) at room temperature and wash with PBS.

Note: If the cells synthesize fluorescent reporter proteins, fix for only 10 min, wash with PBS, then proceed directly to step 9 for Dapi staining (282, 283).

3. To detect antigens by indirect immunofluorescence, permeabilize cells for 5 min at room temperature with Permeabilization Buffer (Recipe 2).
4. Block for 1 hour at room temperature in Wash Buffer (Recipe 3).
5. Remove coverslips from multiwell dish and incubate overnight at room temperature in a humid environment with Primary Antibodies (Recipe 4).
6. Wash cells at least 3 times for 10 min each wash in 250 µl Wash Buffer (Recipe 3).
7. Incubate with Secondary Antibodies (Recipe 4) for 2 hours at room temperature.
8. Wash cells at least 3 times for 10 min each wash in 250 µl Wash Buffer (Recipe 3).

9. Stain the nuclei with 250 µl volume of Dapi Stain (Recipe 5) for 2 minutes at room temperature.

10. Mount the coverslips on a slide in the appropriate position for image acquisition.

11. Examine the cells on the coverslip with a conventional (for phase contrast analysis) or fluorescence microscope and only use those coverslips with an appropriate density of cells for image acquisition with ImageXpress Micro or confocal microscopy.

Note: HeLa cells at 1 to 1.5x10^6 cells/coverslip worked well in our hands. With this confluency we obtained accurate segmentation with different analysis modules.

5.8.2 Image acquisition with ImageXpress Micro of cells grown on coverslips

The MetaXpress software was developed for plate formats, which cannot be used, without modification of the modules, for specimens on coverslips. For many applications cells are routinely grown on coverslips and mounted on slides, and we designed the protocol below specifically to adapt the image acquisition unit to these experimental settings (Fig. 5.1). In the descriptions below we kept the term "plate" as it is used by the software, even though the experiments were carried out with coverslips. The steps that are critical to acquire such images are described in detail; we have omitted general information that can be found in the MetaXpress manual. ImageXpress Micro has the advantage that images can be acquired rapidly. A disadvantage with this equipment is that fluorescence will be collected from the whole cell and images will contain a large amount of out of focus light.

If high concentrations of the molecule of interest are present in the cytoplasm, as well as in the nucleus, measuring the intranuclear or NE fluorescence may require image acquisition by confocal microscopy. Although confocal microscopy is more time consuming, this procedure will provide a more accurate quantification for the localization of some molecules.

A few settings in the "Plate Acquisition Setup" menu are worth noting (Fig. 5.2). Camera binning can be set to provide the best signal-to-noise ratio. Without binning, the images will be at the highest resolution; however with binning there is an increase in the signal-to-noise ratio, resulting in better image quality and shorter exposure times. Camera gain can also be used, but the same gain setting should be used if data are to be compared across different experiments. When binning is set, the signal for an array of pixels is summed and this value is read out as a single pixel. For instance, with a 2×2 binning the 4 pixels in a 2×2 array are added together and read out as a single pixel value. This results in lower noise within the images. In some pixels, noise will be higher than average and in some it will be lower; however the total signal will always be a positive value above background. Binning is especially important when the label provides a low intensity signal, when living cells are analyzed, or if image acquisition must occur quickly. For our experiments with HeLa cells, a binning of 2 was optimal and represented a pixel size of 0.3225 μm/pixel.

The second setting that is particularly important provides the parameters that generate a map of the "plate" (now a slide), which the software uses to locate each “well” (now a coverslip) on the plate. The well location is the point of intersection

between column and row. Measurements, such as the number of rows and columns in the plate, column and row offsets, spacing, well diameter and depth, plate dimensions, and the physical thickness of the plate bottom, have to be provided prior to acquisition. Because the software is designed to read special plate formats, a new plate configuration for microscope slides must be set. The new parameters for microscope slides should be added to the plate library. The configuration described below identifies the slide as a plate with 2 rows (A and B) and 2 columns (1 and 2), resulting in a total of 4 wells. Wells A01 and A02 represent the two coverslips on the slide (Fig. 5.3A, B). The software requires that the distance between rows is specified, therefore B01 and B02 were assigned to create a 2×2 array but are not representative of the actual sample. To be able to reuse the plate map for different experiments, the coverslips have to be mounted in the same position on every slide. In particular, the distance between the two coverslips and the offsets from the slide margins should be kept constant.

Another parameter that is important to understand is the autofocus setting and there are two options: Laser-based focusing and image-based focusing. Laser-based focusing on the ImageXpress Micro uses a red laser to detect light reflections at the air-slide interface and the slide-mounting media interface. If mounting media is matched well to the coverslip (following the specifications recommended by the manufacturer), the air-slide interface is usually detected more easily.

The laser-based focusing uses a red laser and a position sensitive detector to measure the reflection of the laser at the focal plane. The reflection of the laser

relies on there being a difference in the refractive index between two substances. For instance, with a dry objective there is an air-glass interface between the lens and the coverslip and this can be easily detected. Then the focus can be offset by entering the thickness of the coverslip (0.13 to 0.17 mm for #1.0 coverslips). The actual coverslip thickness can be measured with the software using the autofocus feature as the difference in the z position of the coverslip bottom and coverslip – media interfaces. For an immersion lens where the oil has essentially the same refractive index as glass the interface between the oil and the glass is optically transparent and does not give rise to a reflection. In this case the interface between the top surface of the coverslip and the aqueous media can be detected.

The image-based focus, which is based on image-contrast algorithms, can be used in addition to laser-based autofocus. The disadvantage of image-based focusing is that it requires additional time and exposes the sample to additional light. However, if the samples are fixed, have mounting medium with an antifade agent, and the data set is not excessively large, this is a good option. For large data sets or living cells, this feature is not recommended. Because our samples were fixed and the data sets were not too large, we used both laser-based and image-based focusing.

1. Add microscope slide as a new plate type to the plate library of the MetaXpress software by going to the MetaXpress Main Screen and choosing "Screening," select "Plate Acquisition Setup", then choose "Plate."

2. Load the microscope slide on the slide adaptor such that the slide is inverted with the coverslip face down. The frosted end of the slide should be oriented toward the cut corner of the slide adaptor (Fig. 5.1).

Note: Coverslips should always be mounted in the same position on the slide in order for the plate acquisition settings (specified in the next steps) to be reused.

3. On the MetaXpress main screen click the "eject" icon to open the plate stage door, load the slide adaptor on the plate stage, and then close the door.

4. On the MetaXpress main screen choose "Screening", select "Plate Acquisition Setup", then choose "Create new settings" (Fig. 5.2).

Note: Once the settings are established, then you can choose "Load existing settings file."

5. Provide a name, date, and a brief description of the experiment. The acquired images can be retrieved under this name for subsequent analyses.

6. Select the objective appropriate for screening the samples. We recommend the following objectives: For simply counting cells or looking for a positive or negative intensity of a given marker a 10× or 20× lens can be used. However, a 20× or 40× lens with a numerical aperture (NA) of >0.5 would be preferred to measure subcellular localization. To quantify correctly subcellular structures such as NEs, endosomes, focal adhesions, or peroxisomes a 60× with an NA>0.7 may be needed. When working with high NA lenses it is best to use coverslips or glass bottom plates.

7.Select the camera binning, keeping the following in mind: For fixed cells camera binning is not required because more light can be put into the system. However, if high resolution data are not required using a 2x2 binning setting will reduce file sizes by four times and speed up acquisition. The 2x2 binning setting is always suggested for live cell acquisition to increase signal-to-noise so that exposure times can be kept to a minimum (291). We recommend to use 2x2 binning as a starting point and then optimize binning taking into consideration the speed necessary for image acquisition and the desired resolution (see above).

8.Specify the details of the plate in the "Plate Acquisition Setup-Plate" screen (Fig. 5.3A).

Note: For 18x18 mm size coverslips on pre-cleaned Fisherbrand slides (size 25x75x1mm) set 2.5 cm apart (Fig. 5.1), the settings shown in Fig. 5.3A can be used.

9.Specify for which coverslips to acquire images using the "Wells to Visit" screen (Fig. 5.3B).

Note: Each coverslip on the slide is represented as a well. Wells can be selected individually (left clicking on well) or data can be acquired for both wells

10.Specify the positions and number of images to collect on each coverslip using the "Sites to Visit" screen (Fig. 5.4A).

Note: Images can be collected from each well at multiple sites and these are determined by the specified number of columns and rows. Spacing between the columns and rows can be set to ensure sampling of the entire coverslip. Images

from multiple sites distributed throughout the coverslip should be collected to provide a nonbiased representation of the sample. We collected images from 16 to 25 sites with a minimum of 70 cells for each coverslip. This was sufficient to obtain at least 50 cells with proper segmentation after segmentation results were inspected and poorly segmented cells were eliminated from the analysis.

11. Set the appropriate wavelengths for image acquisition.

Note: We set Dapi as W1 with 350/460 nm excitation/emission wavelength and an exposure time of 20 msec (Fig. 5.4B). We set W2 as either EGFP/FITC/Alexa488 (470/525 nm excitation/emission wavelength, 3182 msec exposure time, target maximum intensity 3000, and Z offset from W1 of 1.1 µm) or TRITC/Cy3 (545/620 nm excitation/emission wavelength, 3182 msec exposure time, target maximum intensity 3000, and Z offset from W1 of 1.1 µm). Shorter exposure times, ~100 to 500 msec, can be used if the signal-to-noise ratio is two or higher and must be used for live-cell imaging.

12. Set the autofocus to either laser-based or image-based or both.

Note: For fixed samples with antifade mounting medium, we used laser-based focus, enabled the image-based focus, and selected a binning of 2. For the laser-based focus, the following settings were used: Exposure on the plate bottom – 50 µsec; exposure on the well bottom – 300 µsec; course step – 3µm; fine step – 0.5µm; laser power, 100. We selected to focus on the plate bottom and then offset by the bottom thickness.

5.8.3 Image acquisition with confocal microscopy for cells grown on coverslips

1. Place microscope slide on the stage of the confocal microscope.
2. Using a 63× oil immersion objective (NA 1.4) set the confocal microscope to a resolution of 1024 × 1024 and 12 bits.
3. Choose optical slices through the center of the nucleus for quantification and obtain optical sections of 0.65 μm.
4. Save images as .lsm files, which are recognized by the MetaXpress software.

5.8.4 Image analysis with MetaXpress

Three MetaXpress software modules may be used for analysis. "Multi wavelength cell scoring," "translocation enhanced," and "multi wavelength translocation" modules (Table 1) were adapted to quantify the localization of molecules of interest. For all modules Dapi staining was used as a reference to distinguish nuclear and cytoplasmic compartments. A second fluorescent marker stained the molecule of interest, which may localize to the nucleus, cytoplasm, both compartments, or the NE. These software modules can be used with images acquired with the ImageXpress Micro instrument, with a confocal microscope, or any images acquired with a microscope that can save the images in a format that can be read by MetaXpress. Different procedures are required to analyze images based on the acquisition method and these are detailed for each module. Following configuration, data acquisition and export follows a common set of steps, which are presented once.

5.8.4.1 Configuring the multi wavelength cell scoring module to quantify nuclear and cytoplasmic distribution

The multi wavelength cell scoring module measures the fluorescence intensities of at least two markers with different wavelengths. The application of this module to quantification of nuclear and cytoplasmic distribution depends on a defined set of parameters that identify each cell and relies on the presence of a nuclear marker. The nuclear marker is required to identify cells. The software creates segments (regions) that co-localize with the compartment of interest. The exact match between the region (segment) and the compartment margin is achieved by selecting segmentation parameters (minimum and maximum width, intensity above background). The software measures the fluorescence intensity in the region defined by the settings. The minimum and maximum width of the nuclei and the intensity above local background of the nuclear marker are used to identify the nuclear compartment (minimum width = 8 μm, maximum width = 30 μm) (Fig. 5.5A; numbers in red). These are the first segmentation criteria. Similarly, segmentation settings for the second marker denote the second compartment of interest. In the example shown in Fig. 5.5, the protein of interest was stained with Cy3-labeled secondary antibodies and is present in both nuclear and cytoplasmic compartments. The same filter is used to measure fluorescence obtained for TRITC or Cy3-labeled molecules, which is shown as "TRITC" in the software window (Fig. 5.5). For segmentation of a cytoplasmic marker, the software analyzes intensities going out from the nuclear segmentation until an edge is found where fluorescence intensities are no longer above the minimum

threshold or a large drop in intensity between two neighboring pixels occurs. Care must be taken in selecting settings for segmentation in order to get a proper identification of cellular compartments. The cytoplasmic area is defined as the region where the second marker, but not the nuclear marker (in this example, Dapi), can be detected. The total intensity of Cy3 labeling in the nucleus is measured according to the segmentation obtained with Dapi staining. The intensity of Cy3 labeling of the entire cell is calculated for the region that shows Cy3 labeling above the minimum threshold set in the initial parameters. The difference between whole cell intensity (nucleus plus cytoplasm) minus the nuclear intensity provides a measure of the cytoplasmic fraction of the protein.

It is essential to visually inspect the overlay between the segments generated and the boundaries of nuclei and the cells in the original image. This step ensures that segments produced by the software colocalize with the desired regions. The settings may need to be revised to establish an accurate demarcation of the regions of interest (Fig. 5.5A, B).

Changes in the settings for minimum and maximum width or in the intensity above background affect segmentation (Fig. 5.6A-C). For instance, values too low for the approximate minimum width of the nuclear segmentation parameters underestimate the nuclear size, whereas nuclei are missed when values are too high (Fig. 5.6B; top and middle panels). Moreover, inappropriate values for the intensity above local background interfere with the proper identification of nuclei (Fig. 5.6B; lower panel). In addition, values of the cellular segmentation parameters that are too high for either the approximate minimum width or

intensity above local background underestimate the cell size (Fig. 5.6C; top and lower panels), whereas values too low for the intensity above local background overestimate the cellular size (Fig. 5.6C; middle panel).

If the cytoplasmic fluorescence is low, the boundaries of the cell may not be detected properly. In this case, the nuclear and cytoplasmic distributions can be measured using the translocation enhanced or multi wavelength translocation modules described in the later sections.

Here, we provide a step-by-step protocol using the multi wavelength cell scoring module in MetaXpress for the quantification of data obtained for fixed HeLa cells for which the protein of interest was detected by indirect immunofluorescence with Cy3-labeled secondary antibodies and DNA was stained with Dapi.

1. From the MetaXpress main screen select "Screening".
2. From the drop-down menu select "Review Plate Data".
3. In the Review Plate Data dialog box, press the "Select Plate" button in the upper left to retrieve acquired plate data (Fig. 5.7A).
4. In the Review Plate Data dialog box, select the well to be displayed under "Data view: Well arrangement" (Fig. 5.7A).

Note: For instance for A01 shown in Figure 5.7A, choose all sites from the table cell to view all the acquired fields (each field = one image).

5. Select the wavelengths to be displayed. Once selected, an HCS-image array of thumbnails for each wavelength opens showing all images acquired for each coverslip or well (Fig. 5.7B)

6.Click on a thumbnail for a site to analyze and two separate full-resolution images representing the two wavelengths open. Each one displays the name of the wavelength at the top (Fig. 5.7B; Dapi, TRITC. Note that “TRITC” shows the image obtained with the TRITC/Cy3 filter.).

7.Correct the background for the full-resolution images, by subtracting from each image pixel the average intensity of a manually selected region of the image that does not contain cells. At this point, background-corrected images can be saved. This is desirable if the same images will be processed with a different module.

Note: Because background intensities vary between different images, the background for each individual image must be determined and subtracted.

8.To begin configuring new settings, in the Review Plate Data dialog box choose "Multi Wavelength Cell Scoring" under the "Run Analysis" tab, then press the "Configure Settings" button (Fig. 5.7A).

Note: Once the new settings are configured, the stored configuration settings can be retrieved by selecting the multi wavelength cell scoring module from the application module list or from the Review Plate Data dialog box under the Run analysis tab, using “Analysis” and “Settings” lists to open the dialog box for the multi wavelength cell scoring module (Fig.5.7A).

9.In the multi wavelength cell scoring dialog box, enter the total number of wavelengths in the experiment. Separate tabs for each wavelength will be displayed.

Note: In the example in Fig. 5.5, the "All nuclei" tab corresponds to the nuclear marker Dapi and the "W2" tab represents the second marker, in this case TRITC/Cy3.

10. Open the wavelength tab for "All nuclei" and set the parameters for nuclear segmentation.

Note: Figure 5.5A (Dapi) shows the actual values used to segment the nuclei of HeLa cells.

11. Open the wavelength tab for W2 and set the parameters for cellular segmentation.

Note: For our experiments, we generated two settings. The first setting had the same parameters as that for the Dapi wavelength to identify the intensity in the nuclei (Fig. 5.5A, Nucleus, TRITC). The second setting was based on segmentation of the entire cell to determine the intensity in the nucleus and cytoplasm (Fig. 5A, Nucleus and Cytoplasm, TRITC).

12. Press the "Preview" or "Test Run" button to display the original images with the segmentation overlaid (Fig. 5.5B). Cells that are not well segmented should be excluded from the analysis.

Note: Two cells in Fig. 5.5B (marked with arrowheads) were not segmented well and are representative of the types of cells that would be excluded from the analysis by manual inspection of the data.

13. Proceed to Data Acquisition and Export.

5.8.4.2 Configuring the translocation enhanced module to quantify nuclear and cytoplasmic distribution

The translocation enhanced module determines the localization of a fluorescent probe with respect to a specific cellular compartment, such as the nucleus. It quantifies the fluorescence signal inside, as well as outside, of a defined compartment. The compartment of interest is identified with a fluorescent marker that is distinct from the fluorescent marker to be measured. In the example described, Dapi is used to stain nuclei and GFP with a nuclear localization sequence (NLS) (NLS-GFP[13]) is the protein of interest (Fig. 5.8). The software uses the Dapi image to define the margins of the compartment (Fig. 5.8A) based on several criteria that are configured in the dialog box option settings (Fig. 5.8B). The criteria are similar to those for the multi wavelength cell scoring module with the addition of the approximate width of the compartment, and the use of minimum and maximum area rather than diameter of the stained area**.** After identifying the compartment edge, the software creates two regions (segments) that are ring shaped either within or outside of the compartment. This segmentation is applied to the image of the protein of interest (in this case, NLS-GFP[13]) to measure the fluorescence intensity in both regions (Fig. 5.8C).

The translocation enhanced module should be used when quantifying the relative distribution of a molecule between the nucleus and cytoplasm instead of the multi wavelength cell scoring module when the cellular segmentation for the molecule of interest is problematic. Examples where segmentation may be problematic include: (i) situations in which the fluorescence intensity of the molecule of

interest is not very high above background, making it difficult to identify the cell edges, that is the plasma membrane; (ii) cells in which the molecule of interest concentrates in nuclei or near the nuclear periphery; (iii) samples in which the density of the cells is high, making it difficult to adequately resolve individual cells.

However, there are conditions for which the translocation enhanced module cannot be used. If the fluorescence intensity is not evenly distributed throughout the cytoplasmic compartment, then the selected outer area near the nuclear rim may not accurately represent the cytoplasmic distribution of the probe (see HuR as an example, below).

In the translocation enhanced module a background estimation method for background subtraction is available. However, this feature of the software is not well-characterized and was therefore not applied in our studies.

Below are detailed instructions for configuring MetaXpress and analyzing images acquired with ImageXpress Micro using the translocation enhanced module to quantify proteins localized in the nucleus and cytoplasm.

1. From the MetaXpress main screen select "Screening".
2. From the drop-down menu select "Review Plate Data".
3. In the Review Plate Data dialog box, press the "Select Plate" button in the upper left to retrieve acquired plate data (Fig. 5.7A).
4. In the Review Plate Data dialog box, select the well to be displayed under "Data view: Well arrangement" (Fig. 5.7A).

5.Select the wavelengths to be displayed. Once selected, an HCS-image array of thumbnails for each wavelength opens showing all images acquired for each coverslip or well (Fig. 5.7B)

6.Click on a thumbnail for a site to analyze and two separate full-resolution images representing the two wavelengths open. Each one displays the name of the wavelength at the top (Fig. 5.7B; Dapi, TRITC).

7.Correct the background for the full-resolution images, by subtracting from each image pixel the average intensity of a manually selected region of the image that does not contain cells. At this point, background-corrected images can be saved.

8.To begin configuring new settings, in the Review Plate Data dialog box choose "Translocation enhanced" under the "Run Analysis" tab, then press the "Configure Settings" button (Fig. 5.7A).

9. In the translocation enhanced dialog box (Fig. 5.8B), select the wavelengths of the compartment marker and the translocation probe, Dapi and FITC in the given example. Set the measurements to identify the compartment of interest (for instance, nucleus), and select to automatically separate touching compartments; this will ensure the accurate separation of adjacent compartments (in the example, nucleus and cytoplasm).

10. Define the inner and outer regions; this includes the region width and distance from the compartment edge (in our example the boundary of the nucleus which is delineated by the NE; dashed orange line in Fig. 5.8A).

11. Press the "Test Run" button to display the original images with the segmentation overlaid (Fig. 5.8C). Cells that are not well segmented should be excluded from the analysis.

12. Proceed to "Data Acquisition and Export".

5.8.4.3 Configuring the translocation enhanced module to quantify nuclear envelope (NE) fluorescence

By modifying the parameter settings that define the inner and outer regions, we adapted the translocation enhanced module and used it to measure the intensity of a fluorescent probe at the NE (Fig. 5.9A). This new application of the module was generated by creating two different configurations for inner and outer regions (Fig. 5.9B, C). The data from these two configurations are combined to quantify NE staining.

In the first configuration, two regions (region 1 and 2) are created that represent the fluorescence intensity in a small area around the nucleus and a portion of the NE facing the cytoplasm (region 1) as well as the nucleus and the rest of the NE (region 2). Both regions are adjoining at the edge of the compartment, with no space between inner and the outer regions. Fig. 5.9B shows the settings used to produce these regions and the overlay on the image.

In the second configuration, the inner and outer regions are produced in the same positions as above; however, a space is generated between the inner and the outer region by defining the distance from the edge. For the example in Fig. 5.9C, the inner region ends 0.9 μm from the edge and the outer region begins 1 μm from

the edge of the compartment (the nucleus in our example). These settings produce regions 3 and 4; the gap between these regions coincides with the NE.

The measurements obtained for regions 1, 2, 3, and 4 can now be combined manually to determine the fluorescence intensity at the NE: Regions (1+2) minus regions (3+4) will provide a quantification of the fluorescence signals located at the NE (Fig. 5.9D). A schematic representation of the critical parameters used to define the size and position of different regions is depicted in Fig. 5.9E.

Below are detailed instructions for configuring MetaXpress and analyzing images acquired with ImageXpress Micro using the translocation enhanced module to quantify NE localized proteins.

1.From the MetaXpress main screen select "Screening".

2.From the drop-down menu select "Review Plate Data".

3.In the Review Plate Data dialog box, press the "Select Plate" button in the upper left to retrieve acquired plate data (Fig. 5.7A).

4.In the Review Plate Data dialog box, select the well to be displayed under "Data view: Well arrangement" (Fig. 5.7A).

5.Select the wavelengths to be displayed. Once selected, an HCS-image array of thumbnails for each wavelength opens showing all images acquired for each coverslip or well (Fig. 5.7B)

6.Click on a thumbnail for a site to analyze and two separate full-resolution images representing the two wavelengths open. Each one displays the name of the wavelength at the top (Fig. 5.7B; Dapi, TRITC).

7.Correct the background for the full-resolution images, by subtracting from each image pixel the average intensity of a manually selected region of the image that does not contain cells. At this point, background-corrected images can be saved.

8.To begin configuring new settings, in the Review Plate Data dialog box choose "Translocation enhanced" under the "Run Analysis" tab, then press the "Configure Settings" button (Fig. 5.7A).

9. In the translocation enhanced dialog box (Fig. 5.8B), select the wavelengths of the compartment marker and the translocation probe, Dapi and FITC in the given example. Set the measurements to identify the compartment of interest (for instance, nucleus), and select to automatically separate touching compartments; this will ensure the accurate separation of adjacent compartments (i.e., nucleus and cytoplasm).

10. Define the inner and outer regions; this includes the region width and distance from the compartment edge (in our example the boundary of the nucleus which is delineated by the NE; dashed orange line in Fig. 5.8A). For the NE quantification you need to create 2 sets of inner and outer regions, use the configuration settings in Fig. 5.9B, C to obtain appropriate segmentation.

11. Press the "Test Run" button to display the original images with the segmentation overlaid (Fig. 5.9B, C). Cells that are not well segmented should be excluded from the analysis.

12.Proceed to Data Acquisition and Export and calculate the intensity for NE fluorescence (Fig. 5.9D).

5.8.4.4 Configuring the multi wavelength translocation module

This module is a simplified version of the translocation enhanced module; it uses the same principle as the translocation enhanced module to identify the nuclei and regions, both inside and outside of the nuclear area. The module contains one key component for NE analysis; it allows the assignment of negative values for the distance of the outer region from the compartment. We took advantage of this feature and developed configuration settings that create an outer region that colocalizes with the NE. This enabled us to measure the fluorescence intensity at the NE in one step (Fig. 5.10A-C). Nevertheless, measuring the NE intensity with the translocation enhanced module can be used to verify the results obtained by the multi wavelength translocation module. Both modules give similar results for the NE fluorescence intensity (Fig. 5.11). Although the main application of the multi wavelength translocation module in our experiments is to quantify NE intensity, it can also be used to determine fluorescence intensities in the nucleus and other areas of the cell.

Below are detailed instructions for configuring MetaXpress and analyzing images acquired with ImageXpress Micro using the multi wavelength translocation module.

1. From the MetaXpress main screen select "Screening".
2. From the drop-down menu select "Review Plate Data".
3. In the Review Plate Data dialog box, press the "Select Plate" button in the upper left to retrieve acquired plate data (Fig. 5.7A).

4.In the Review Plate Data dialog box, select the well to be displayed under "Data view: Well arrangement" (Fig. 5.7A).

5. Select the wavelengths to be displayed. Once selected, an HCS-image array of thumbnails for each wavelength opens showing all images acquired for each coverslip or well (Fig. 5.7B)

6. Click on a thumbnail for a site to analyze and two separate full-resolution images representing the two wavelengths open. Each one displays the name of the wavelength at the top (Fig. 5.7B; Dapi, TRITC).

7. Correct the background for the full-resolution images, by subtracting from each image pixel the average intensity of a manually selected region of the image that does not contain cells. At this point, background-corrected images can be saved.

8. To begin configuring new settings, in the Review Plate Data dialog box choose "Multi Wavelength Translocation" under the "Run Analysis" tab, then press the "Configure Settings" button (Fig. 5.7A).

9. In the multi wavelength translocation dialog box, select compartments and configure the parameters to identify the compartment of interest; the nucleus in our example (Fig. 5.10B).

10. Select the W2 tab, then set the parameters to identify the inner and outer regions (Fig. 5.10C).

Note: that the outer region distance from edge has a negative value, and the segment generated colocalizes well with the NE. The inner region is set to be

small; this simplifies the visual inspection to monitor an accurate match between the outer region and the NE.

11. Press the "Preview" or "Test Run" button to display the original images with the segmentation overlaid (Fig. 5.10B, C). Cells that are not well segmented should be excluded from the analysis.

12.Proceed to Data Acquisition and Export.

5.8.4.5 Analysis for images acquired by confocal microscopy

For each of the modules, images acquired by confocal microscopy may also be analyzed. The settings and parameters would be based on the same considerations as for those used for images acquired with Image Xpress Micro and so only the basic procedures are outlined here.

1. To analyze images acquired by confocal microscopy, open the image saved as an .lsm file in the MetaXpress main screen.

2. Correct the background by subtracting the average intensity from each image pixel of a manually selected region of the image that does not contain cells.

3. Select the "multi wavelength cell scoring" module, the "translocation enhanced module" box, or the "multi wavelength translocation" module from the "applications" tab in the main screen; the corresponding dialog box will open.

4. Configure new settings.

5. Press the "Preview" or "Test Run" button to examine the segmentation accuracy, and modify the segmentation settings if necessary.

6. Proceed to "Data Acquisition and Export".

5.8.5 Data acquisition and export

1.Once the segmentation settings are accurate, open “log files” to save results in the format of Excel files: On the MetaXpress main screen choose "Log", then select "Open Data Log", then "Open Data Log" window, then select "Dynamic Data Exchange (DDE)" and press "OK".

2. In the "Export Data Log" window select "Microsoft Excel" and save the file, specifying the filename.

3.Select the measurements that should be saved in the file by opening the "Configure Summary Log" and "Configure Data Log" tabs in the "multi wavelength cell scoring" dialog box, or the "translocation enhanced" dialog box, or the "multi wavelength translocation" dialog box, choose the data to be logged to the file, and close the tabs.

4.Press the "Test Run" button and review the measurements for each cell in the image in the cellular data window that opens.

Note: For each image analyzed the cellular data will be logged automatically to the Excel file specified in the previous step.

5.Click on each individual cell in the image to highlight the data line corresponding to the selected cell. Each cell is identified by a number, which appears as “Label #” in the Excel file.

6.Visually verify the accuracy of the segmentation and exclude cells with incorrect segmentation from further analysis. This can be done by identifying the improperly segmented cells using their “Label #” and highlighting the corresponding line on the Excel data sheet.

Note: We routinely save results for correctly and incorrectly segmented cells, but delete data lines for cells that were not properly segmented before analyzing the numbers.

5.9 Notes and remarks

The methods described here provide quantitative approaches for measuring the intensities of fluorescent probes in different cellular compartments, including, but not limited to, the nucleus, cytoplasm, and nuclear envelope. We illustrate methods for image acquisition and analysis with three different software modules in MetaXpress (Table 5.1), which have been adapted to measure the fluorescence intensities in these compartments. Choosing the appropriate module will depend on the distribution of the fluorescent molecule to be quantified, the strength of the fluorescent signal in the cytoplasm, the experimental conditions (for example, transfected versus nontransfected cells), and the localization of the molecule of interest.

We have employed these strategies successfully to study the subcellular localization in mammalian cells of several proteins that are involved in different aspects of signaling (Fig. 5.11-5.13). The multi wavelength cell scoring module was used to quantify the distribution of the protein HuR (Fig. 5.12), for which a larger portion is detected in the cytoplasm upon oxidative stress (283). The stress-induced relocation caused a decrease in the ratio of average nuclear to cytoplasmic (nuc/cyt) fluorescence (Fig. 5.12). The uneven distribution pattern of HuR in the cytoplasm of stressed cells requires that the fluorescence of the whole

cytoplasmic compartment is measured to obtain an accurate quantification. This is achieved by applying the multi wavelength cell scoring module. Due to the irregular distribution of HuR in stressed cells, neither the translocation enhanced nor the multi wavelength translocation module will provide a correct measurement for HuR in the cytoplasm.

The multi wavelength cell scoring module depends on the labeled protein to identify the cell boundaries. Depending on the protein studied other software modules may be more appropriate to quantify the nuclear and cytoplasmic fluorescence. For instance, cell boundaries can overlap for samples with densely plated cells, resulting in inaccurate cellular segmentation. Furthermore, in experiments with transiently transfected cells, signals may be variable or too low to define cell edges. The same problem arises if the protein of interest is restricted to the nucleus under certain conditions. In these cases, the translocation enhanced module provides the method of choice for quantification. For example, in HeLa cells that transiently synthesize NLS-GFP (Fig. 5.13, green), which is a reporter protein that localizes to the nucleus under normal conditions (control), the abundance of NLS-GFP in the cytoplasm is low, compromising cellular segmentation with the multi wavelength cell scoring module. Therefore, the translocation enhanced module is a better choice for measuring the nuclear and cytoplasmic fluorescence intensities of NLS-GFP, because the cell boundaries do not need to be identified. The appearance of green fluorescence in the cytoplasm of cells exposed to oxidative stress, quantified as a decrease in the nuc/cyt ratio

(Fig. 5.13), indicates that nuclear import is less efficient under these conditions (283).

One of the major challenges in quantifying subcellular distribution of molecules is the quantification of fluorescence signals located at the NE. First, there are no modules provided by the MetaXpress software to quantify the signals located at the NE. Second, the nuclear envelope area is very small compared to the nucleus and cytoplasm, which makes it difficult for the analysis software to define precisely the NE compartment. We adapted the translocation enhanced and the multi wavelength translocation modules to measure fluorescence intensities at the NE (Fig. 5.11) (282). Employing the translocation enhanced module to quantify fluorescence signals at the NE requires the configuration of two settings and some post analysis data processing, whereas the multi wavelength translocation module is simpler because it makes the measurements in a single step. One advantage to the translocation enhanced module is that it can be used to quantify fluorescence intensities for nuclear, NE, and cytoplasmic compartments in the same analysis, which may be required for more complex applications. For measurements of fluorescence located at the NE, results obtained with the translocation enhanced module can be verified by the multi wavelength translocation module and vice versa (Fig. 5.11). Other modules of the MetaXpress software can be used to quantify the association of molecules with the plasma membrane or different cellular compartments. Some of these modules rely on a fluorescent marker that is used to identify the compartment of interest.

This protocol details the procedures for acquiring images for cells conventionally grown on coverslips and quantifying the fluorescence intensities in defined cellular compartments. This is achieved by combining HCS for high-throughput image acquisition and adapting different software modules from MetaXpress for analyses. The methods described here provide resources to detect minor changes in the subcellular localization of proteins and other molecules that can be detected with fluorescent probes. The convenience, ease of use, and accuracy of these techniques make them powerful tools for the quantification of numerous biological processes. The procedures described here are ideal to explore in a quantitative fashion the various aspects of signal transduction cascades and their regulatory circuits, a major challenge given the complexity of these pathways. The ability to analyze single cells also provides the potential to determine subtle changes in subpopulations of cells rather than obtaining single measurements for whole cell populations.

5.10 Acknowledgements

This research was supported by grants from CIHR and NSERC to US. Images were collected in the HTS/HCS and the Imaging Facility both part of the McGill Life Sciences Complex funded by the CFI. MK was supported by fellowships from FRSQ and the Heart and Stroke Foundation of Canada. We are in particular grateful for the continuous support by Dr. Jing Liu and the HTS/HCS group in the Department of Biochemistry at McGill University.

Table 5.1 Comparison between different software modules for the quantification of nuclear, cytoplasmic and nuclear envelope fluorescence

Software module	Application	Disadvantages
Multiwavelength cell-scoring	Strong signal in cytoplasm; uneven distribution of signal in cytoplasm	Not useful if signal in cytoplasm is faint or cell edges not discernible; cannot be used to measure NE or other membrane-associated fluorescence
Translocation-enhanced	Strong or weak signals in cytoplasm; NE fluorescence	Not useful if uneven distribution of signal in cytoplasm
Multiwavelength translocation	Strong or weak signals in cytoplasm; NE fluorescence measured in one step	Not useful if uneven distribution of signal in cytoplasm

Figure 5.1

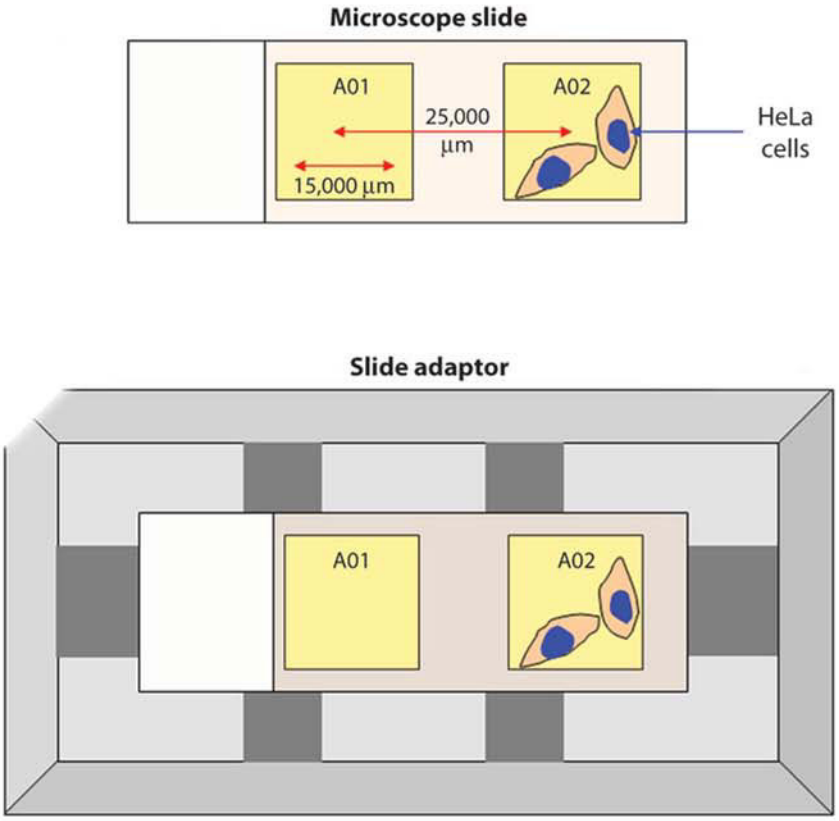
Microscope slide
A01
A02
25,000
µm
15,000 µm
HeLa
cells
Slide adaptor
A01
A02

Figure 5.1 Image acquisitions with ImageXpress micro for cells grown on poly-lysine coated coverslips

Coverslips were mounted on a microscope slide for image acquisition and loaded on the slide adaptor with the coverslips face down. Optimal positions for the mounting of coverslips are shown.

Figure 5.2

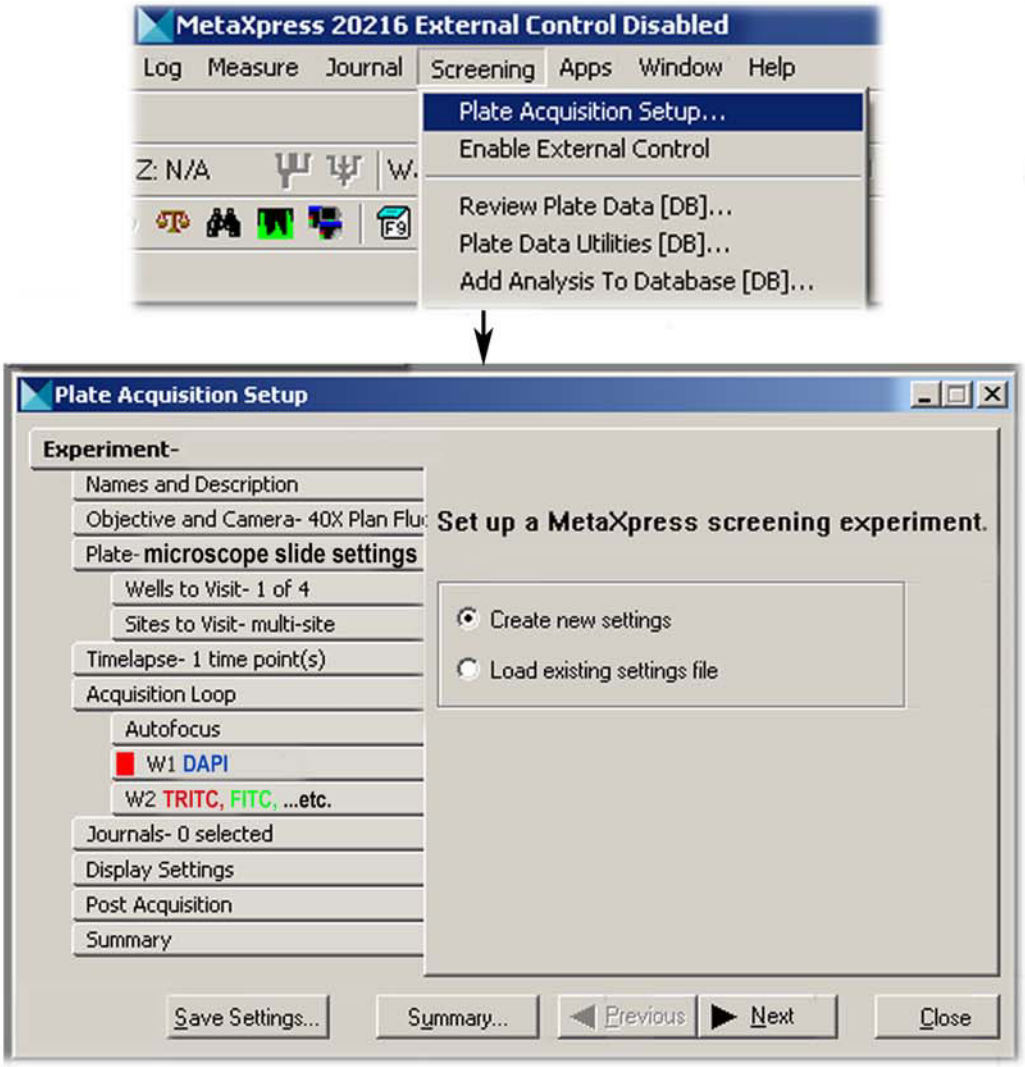
MetaXpress 20216 External Control Disabled
Log
Measure
Journal
Screening
Apps
Window
Help
Plate Acquisition Setup...
Enable External Control
Review Plate Data [DB]...
Plate Data Utilities [DB]...
Add Analysis To Database [DB]...
Z: N/A
Plate Acquisition Setup
Experiment-
Names and Description
Objective and Camera- 40X Plan Flu
Plate- microscope slide settings
Wells to Visit- 1 of 4
Sites to Visit- multi-site
Timelapse- 1 time point(s)
Acquisition Loop
Autofocus
W1 DAPI
W2 TRITC, FITC, ...etc.
Journals- 0 selected
Display Settings
Post Acquisition
Summary
Set up a MetaXpress screening experiment.
Create new settings
Load existing settings file
Save Settings...
Summary...
Previous
Next
Close

Figure 5.2 Configuration of parameters for image acquisition

Settings for the plate acquisition are generated for a new application or loaded from previous experiments (existing settings). The tabs on the left side are used to configure the different parameters for a new acquisition.

Figure 5.3

A

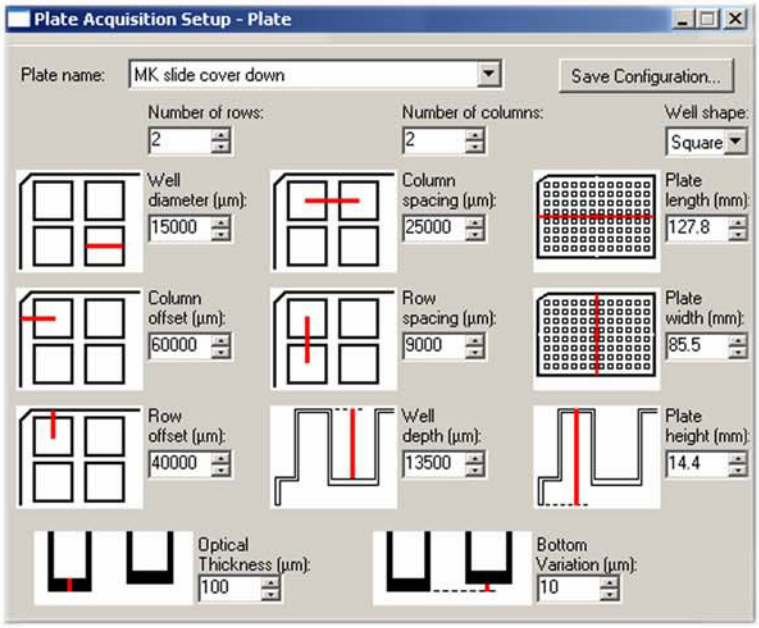
Plate Acquisition Setup - Plate
Plate name:
MK slide cover down
Save Configuration...
Number of rows:
2
Number of columns:
2
Well shape:
Square
Well diameter (µm):
15000
Column spacing (µm):
25000
Plate length (mm):
127.8
Column offset (µm):
60000
Row spacing (µm):
9000
Plate width (mm):
85.5
Row offset (µm):
40000
Well depth (µm):
13500
Plate height (mm):
14.4
Optical Thickness (µm):
100
Bottom Variation (µm):
10

B

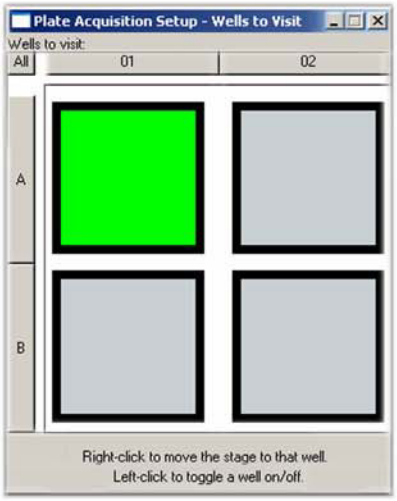
Plate Acquisition Setup - Wells to Visit
Wells to visit:
All
01
02
A
B
Right-click to move the stage to that well.
Left-click to toggle a well on/off.

Figure 5.3 Addition of a microscope slide to the plate library of the MetaXpress software

(**A**) New configuration settings for the microscope slide are added to the plate library; these settings identify the slide as a 4-well plate, the first row represents the 2 coverslips for which images will be acquired. Wells B01 and B02 are required for the plate set up, but are not actually on the slide. (**B**) Images for wells (coverslips) can be acquired separately or both in the same acquisition with one coverslip after the other.

Figure 5.4

A

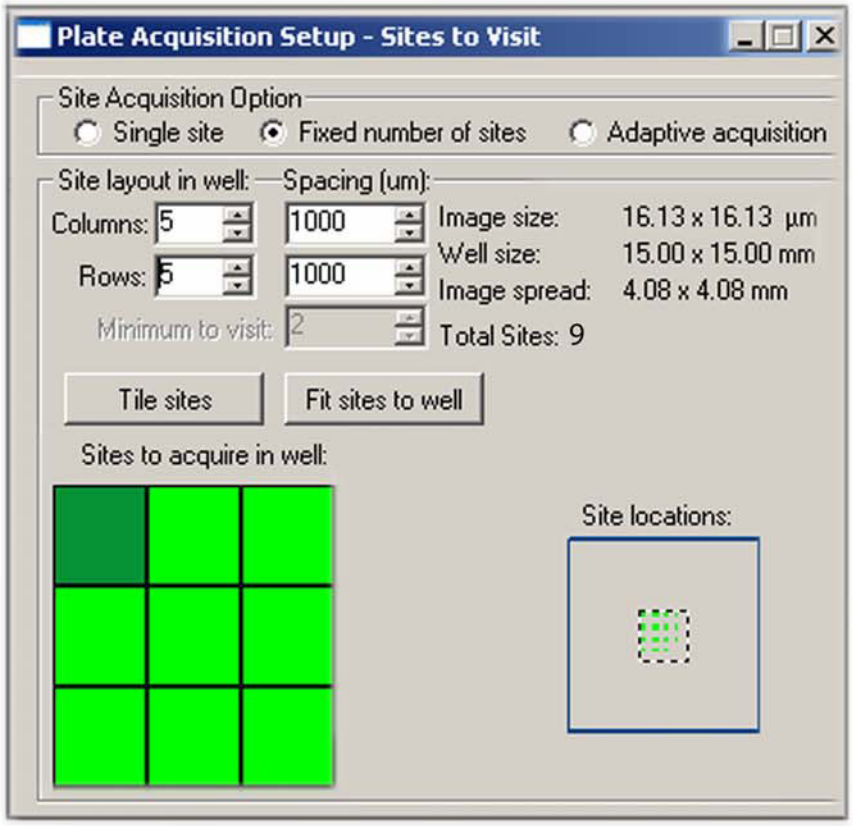
Plate Acquisition Setup - Sites to Visit
Site Acquisition Option
Single site
Fixed number of sites
Adaptive acquisition
Site layout in well:
Spacing (um):
Columns: 5
1000
Rows: 5
1000
Minimum to visit: 2
Image size: 16.13 x 16.13 µm
Well size: 15.00 x 15.00 mm
Image spread: 4.08 x 4.08 mm
Total Sites: 9
Tile sites
Fit sites to well
Sites to acquire in well:
Site locations:

B

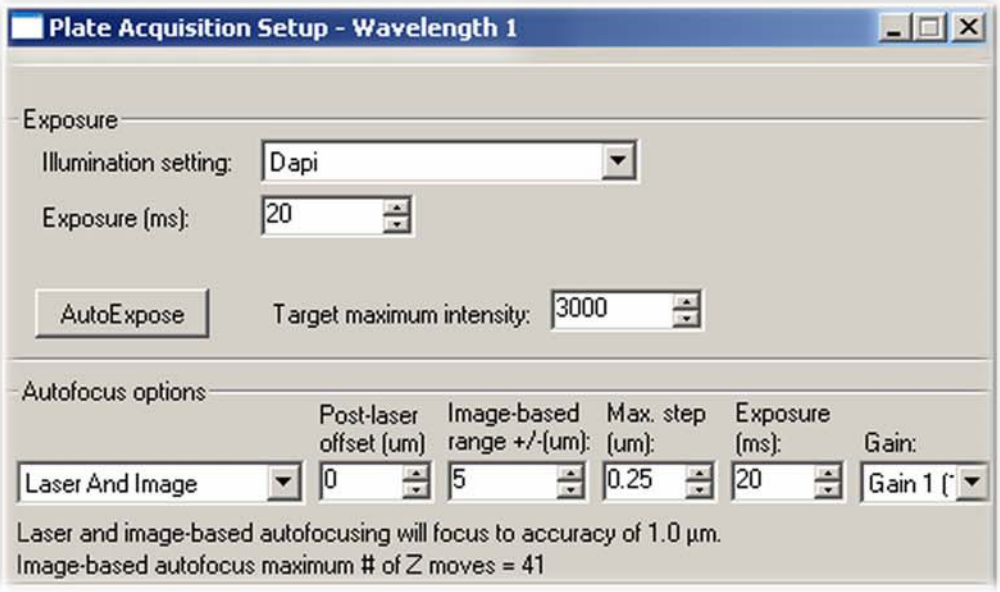
Plate Acquisition Setup - Wavelength 1
Exposure
Illumination setting: Dapi
Exposure (ms): 20
AutoExpose
Target maximum intensity: 3000
Autofocus options
Post-laser offset (um)
Image-based range +/-(um):
Max. step (um):
Exposure (ms):
Gain:
Laser And Image
0
5
0.25
20
Gain 1
Laser and image-based autofocusing will focus to accuracy of 1.0 µm.
Image-based autofocus maximum # of Z moves = 41

Figure 5.4 Defining the sites for image acquisition and wavelength-1

(**A**) Configuration settings define 9 sites for acquisition; note that the site distribution is determined by the spacing between rows and columns. (**B**) Configuration settings to acquire wavelength-1 image (Dapi). Combined laser- and image-based focus option is selected to enhance image resolution. See text for details.

Figure 5.5

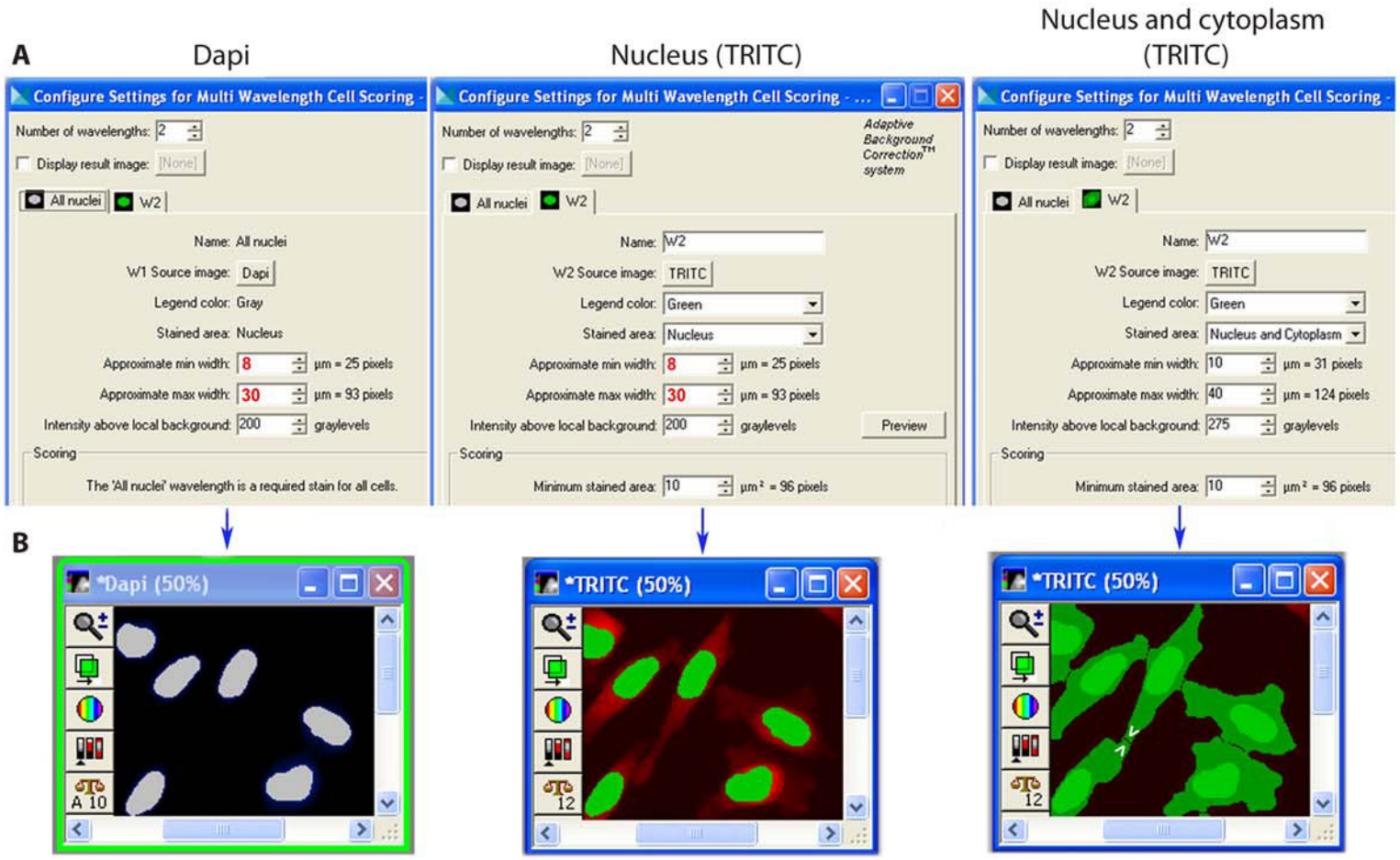
A
Dapi
Nucleus (TRITC)
Nucleus and cytoplasm (TRITC)
Configure Settings for Multi Wavelength Cell Scoring
Number of wavelengths: 2
Display result image: [None]
All nuclei
W2
Name: All nuclei
W1 Source image: Dapi
Legend color: Gray
Stained area: Nucleus
Approximate min width: 8 µm = 25 pixels
Approximate max width: 30 µm = 93 pixels
Intensity above local background: 200 graylevels
Scoring
The 'All nuclei' wavelength is a required stain for all cells.
Configure Settings for Multi Wavelength Cell Scoring - ...
Adaptive Background Correction™ system
Name: W2
W2 Source image: TRITC
Legend color: Green
Stained area: Nucleus
Approximate min width: 8 µm = 25 pixels
Approximate max width: 30 µm = 93 pixels
Intensity above local background: 200 graylevels
Preview
Minimum stained area: 10 µm² = 96 pixels
Configure Settings for Multi Wavelength Cell Scoring -
Name: W2
W2 Source image: TRITC
Legend color: Green
Stained area: Nucleus and Cytoplasm
Approximate min width: 10 µm = 31 pixels
Approximate max width: 40 µm = 124 pixels
Intensity above local background: 275 graylevels
Minimum stained area: 10 µm² = 96 pixels
B
*Dapi (50%)
*TRITC (50%)
*TRITC (50%)

Figure 5.5 Quantification of fluorescence intensities with the multi wavelength cell scoring module, defining the values for segmentation

(**A**) Settings are shown to generate segments that co-localize with the nucleus in the Dapi image (Dapi), the nucleus in the TRITC image (Nucleus-TRITC) or with the whole cell in the TRITC image (Nucleus and Cytoplasm, TRITC). (**B**) The overlays between the created segments and the cellular compartment (nucleus) or the entire cell are depicted. The overlay images are necessary to adjust and verify the accuracy of segmentation settings. Cells marked with arrowheads show incorrect segmentation of the cytoplasm and are excluded from further analyses.

Figure 5.6

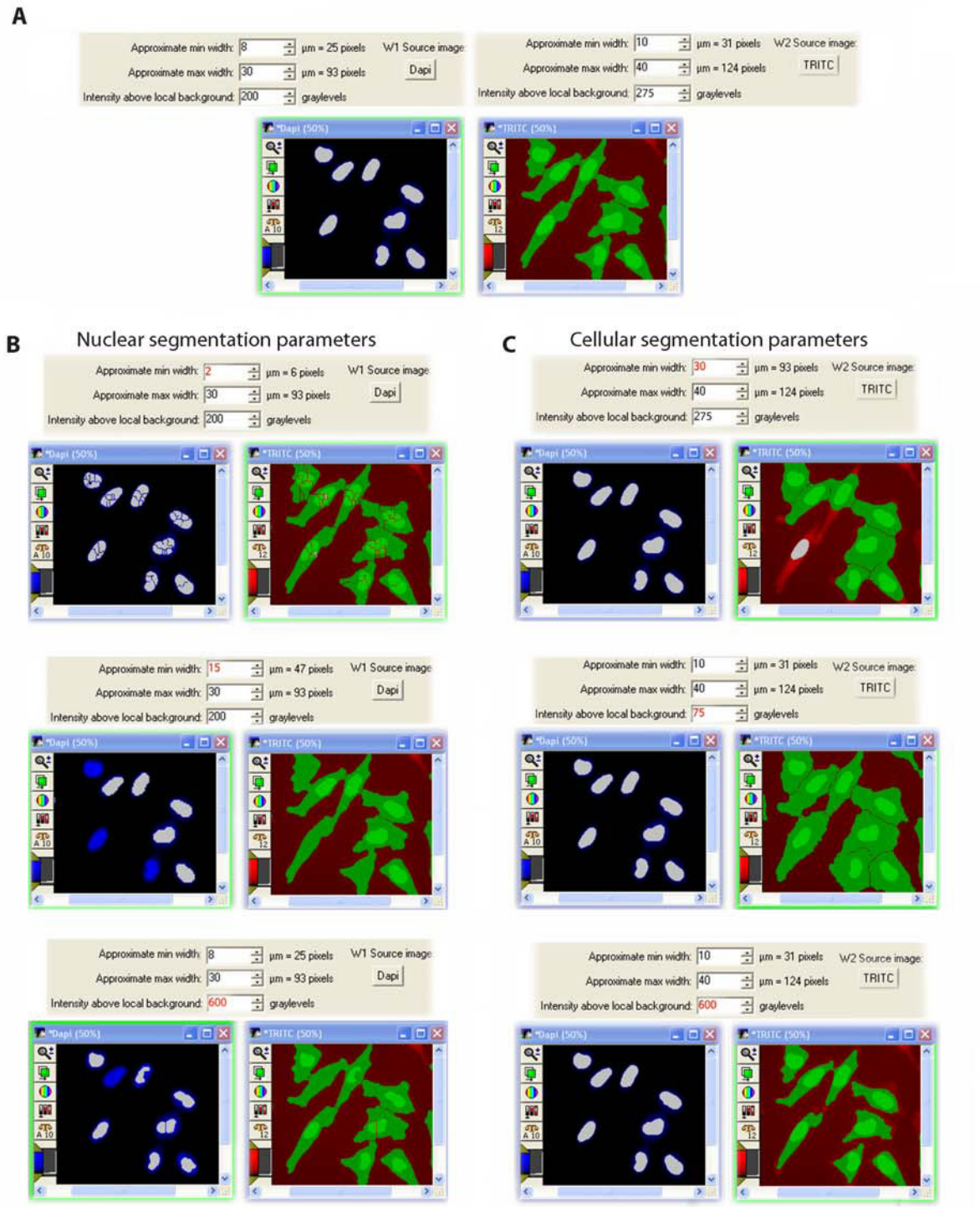
A
Approximate min width: 8 µm = 25 pixels W1 Source image:
Approximate max width: 30 µm = 93 pixels Dapi
Intensity above local background: 200 graylevels
Approximate min width: 10 µm = 31 pixels W2 Source image:
Approximate max width: 40 µm = 124 pixels TRITC
Intensity above local background: 275 graylevels
B
Nuclear segmentation parameters
Approximate min width: 2 µm = 6 pixels W1 Source image:
Approximate max width: 30 µm = 93 pixels Dapi
Intensity above local background: 200 graylevels
Approximate min width: 15 µm = 47 pixels W1 Source image:
Approximate max width: 30 µm = 93 pixels Dapi
Intensity above local background: 200 graylevels
Approximate min width: 8 µm = 25 pixels W1 Source image:
Approximate max width: 30 µm = 93 pixels Dapi
Intensity above local background: 600 graylevels
C
Cellular segmentation parameters
Approximate min width: 30 µm = 93 pixels W2 Source image:
Approximate max width: 40 µm = 124 pixels TRITC
Intensity above local background: 275 graylevels
Approximate min width: 10 µm = 31 pixels W2 Source image:
Approximate max width: 40 µm = 124 pixels TRITC
Intensity above local background: 75 graylevels
Approximate min width: 10 µm = 31 pixels W2 Source image:
Approximate max width: 40 µm = 124 pixels TRITC
Intensity above local background: 600 graylevels

Figure 5.6 Settings for nuclear and cellular segmentation parameters are crucial to generate segments that accurately match the nuclei and cell margins

(**A**) Appropriate values were selected for segmentation. (**B**) Incorrect values for any of the parameters (red numbers) to identify the nuclei (left panels) may result in under- or overestimation of the nuclear size. This may generate segments that do not match the cellular margins or may eliminate some nuclei. (**C**) Similarly, inappropriate parameters to identify the cell margins (right panels) will produce segments that do not properly co-localize with the cellular boundaries. See text for details.

Figure 5.7

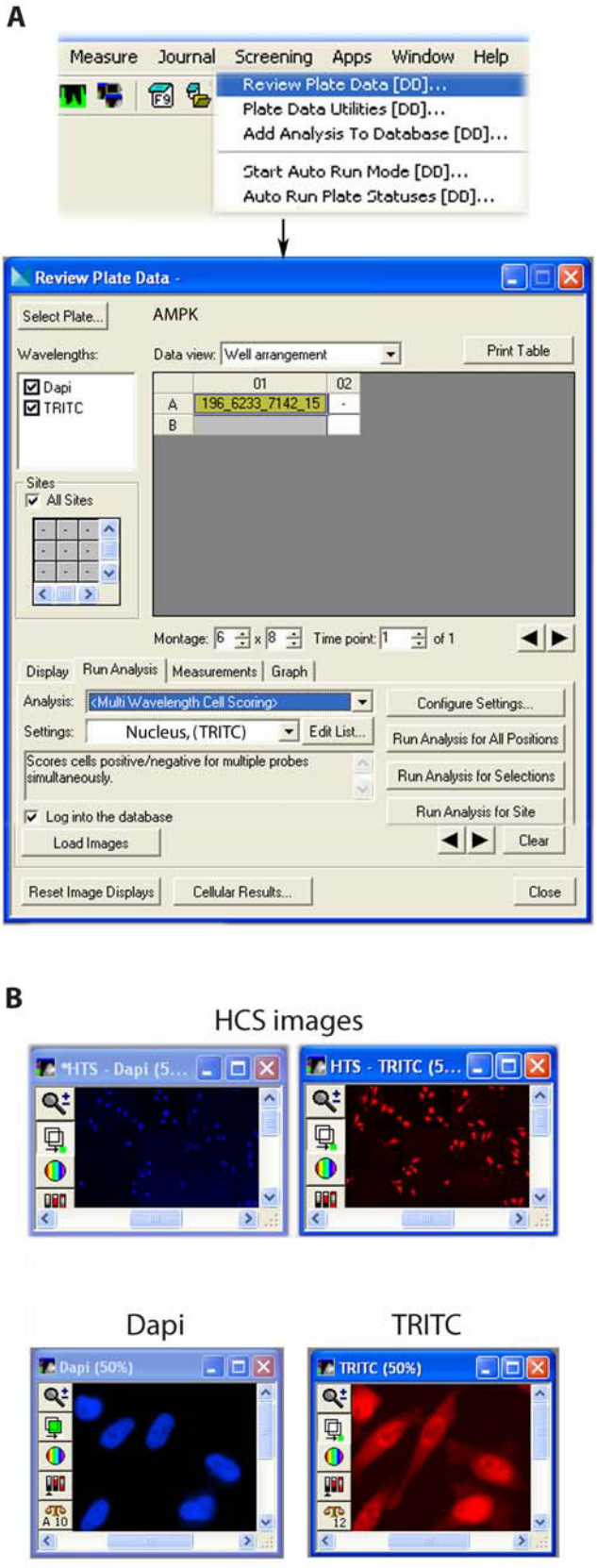
A
Measure
Journal
Screening
Apps
Window
Help
Review Plate Data [DD]...
Plate Data Utilities [DD]...
Add Analysis To Database [DD]...
Start Auto Run Mode [DD]...
Auto Run Plate Statuses [DD]...
Review Plate Data -
Select Plate...
AMPK
Wavelengths:
Data view: Well arrangement
Print Table
Dapi
TRITC
01
02
A
196_6233_7142_15
B
Sites
All Sites
Montage: 6 x 8
Time point: 1 of 1
Display
Run Analysis
Measurements
Graph
Analysis: <Multi Wavelength Cell Scoring>
Configure Settings...
Settings: Nucleus, (TRITC)
Edit List...
Run Analysis for All Positions
Scores cells positive/negative for multiple probes simultaneously.
Run Analysis for Selections
Log into the database
Run Analysis for Site
Load Images
Clear
Reset Image Displays
Cellular Results...
Close
B
HCS images
*HTS - Dapi (5...
HTS - TRITC (5...
Dapi
TRITC
Dapi (50%)
TRITC (50%)

Figure 5.7 Opening of images acquired with ImageXpress Micro and configuration of the analysis module

(**A**) The review plate data dialog box option is used to retrieve the acquired plate, open the image and select the analysis module. The analysis module settings can be configured with the Configure Settings tab. (**B**) The HCS-images show thumbnails of all the individual images which were acquired for the specified sites. After clicking on a single site full resolution Dapi and TRITC images are displayed simultaneously. On these images analysis is carried out after correcting for the contribution of background fluorescence.

Figure 5.8

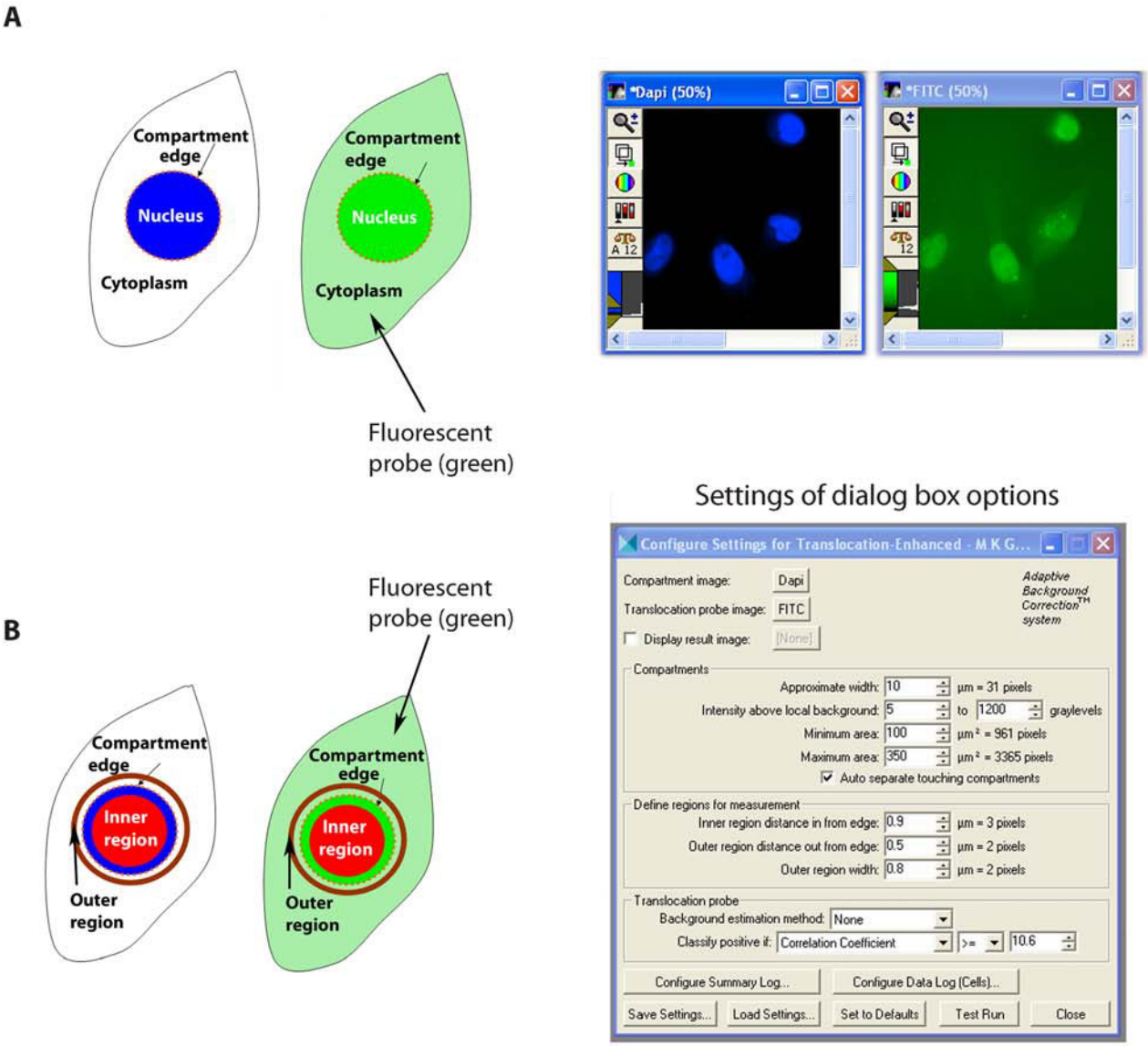
A
Compartment edge
Nucleus
Cytoplasm
Compartment edge
Nucleus
Cytoplasm
Fluorescent probe (green)
*Dapi (50%)
*FITC (50%)
B
Compartment edge
Inner region
Outer region
Fluorescent probe (green)
Compartment edge
Inner region
Outer region
Settings of dialog box options
Configure Settings for Translocation-Enhanced - M K G...
Compartment image: Dapi
Translocation probe image: FITC
Display result image: [None]
Adaptive Background Correction™ system
Compartments
Approximate width: 10 µm = 31 pixels
Intensity above local background: 5 to 1200 graylevels
Minimum area: 100 µm² = 961 pixels
Maximum area: 350 µm² = 3365 pixels
Auto separate touching compartments
Define regions for measurement
Inner region distance in from edge: 0.9 µm = 3 pixels
Outer region distance out from edge: 0.5 µm = 2 pixels
Outer region width: 0.8 µm = 2 pixels
Translocation probe
Background estimation method: None
Classify positive if: Correlation Coefficient >= 10.6
Configure Summary Log...
Configure Data Log (Cells)...
Save Settings...
Load Settings...
Set to Defaults
Test Run
Close
C
Segment overlay
*Dapi (50%)
*FITC (50%)

Figure 5.8 The translocation enhanced module is applied to analyze nuclear transport

(**A**) Dapi staining identifies the compartment of interest (nucleus); NLS-GFP is a nuclear reporter protein for which the nuclear and cytoplasmic fluorescence will be quantified (see also Fig. 5.13). (**B**) The dialog box for the translocation enhanced module shows the settings that define the nuclear compartment, as well as the inner and outer regions that were selected for quantification. The cartoon depicts the position of the inner and outer regions with respect to the nucleus, as well as the edge of the nuclear compartment (orange dashed line). (**C**) Overlays were produced for the inner and outer regions either with the Dapi or the FITC (NLS-GFP) image to visualize the segmentation for acquired images.

Figure 5.9

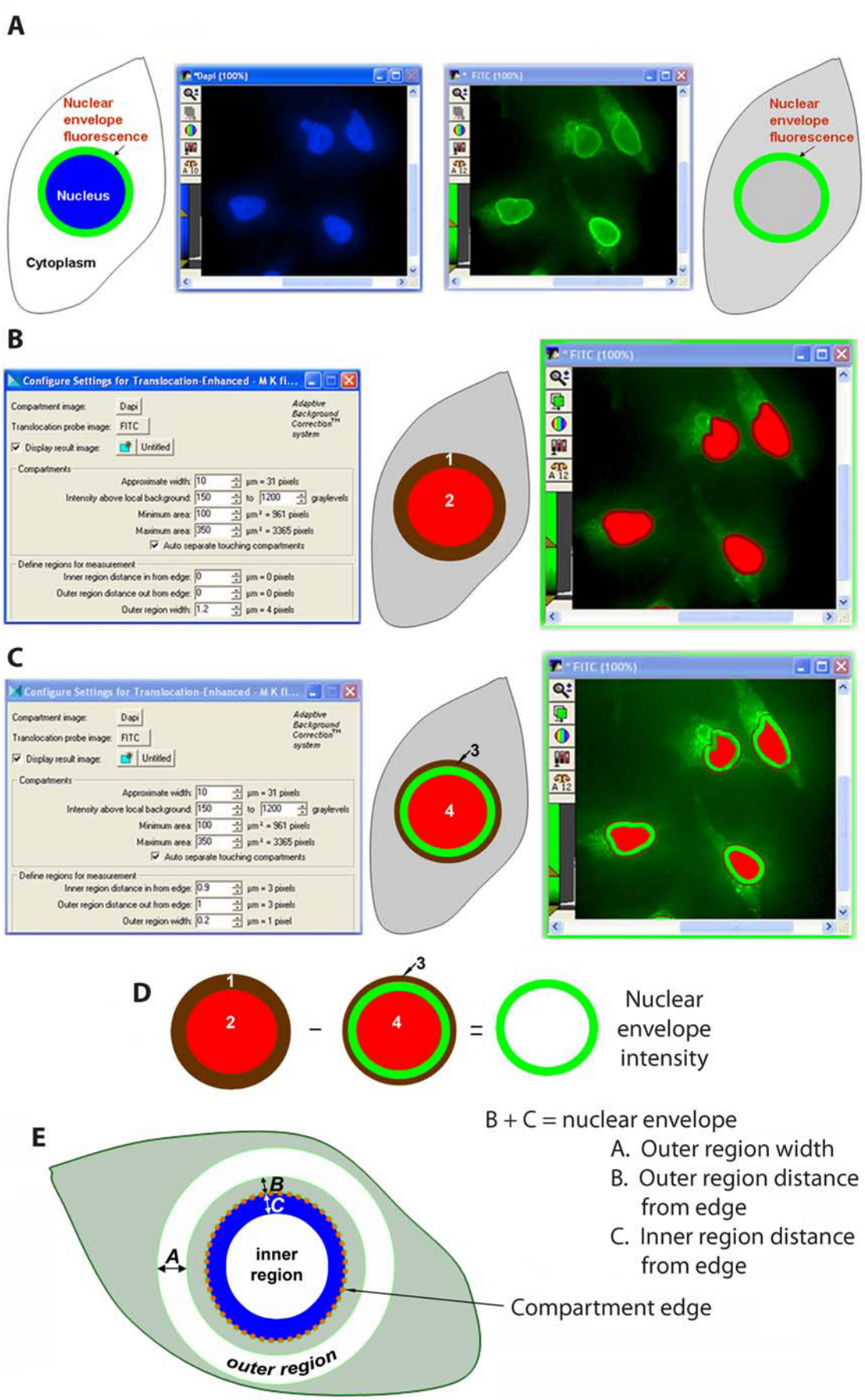
A
Nuclear envelope fluorescence
Nucleus
Cytoplasm
Dapi (100%)
FITC (100%)
Nuclear envelope fluorescence
B
Configure Settings for Translocation-Enhanced - M K fi...
Compartment image: Dapi
Translocation probe image: FITC
Display result image: Untitled
Adaptive Background Correction™ system
Compartments
Approximate width: 10 µm = 31 pixels
Intensity above local background: 150 to 1200 graylevels
Minimum area: 100 µm² = 961 pixels
Maximum area: 350 µm² = 3365 pixels
Auto separate touching compartments
Define regions for measurement
Inner region distance in from edge: 0 µm = 0 pixels
Outer region distance out from edge: 0 µm = 0 pixels
Outer region width: 1.2 µm = 4 pixels
1
2
FITC (100%)
C
Configure Settings for Translocation-Enhanced - M K fi...
Compartment image: Dapi
Translocation probe image: FITC
Display result image: Untitled
Adaptive Background Correction™ system
Compartments
Approximate width: 10 µm = 31 pixels
Intensity above local background: 150 to 1200 graylevels
Minimum area: 100 µm² = 961 pixels
Maximum area: 350 µm² = 3365 pixels
Auto separate touching compartments
Define regions for measurement
Inner region distance in from edge: 0.9 µm = 3 pixels
Outer region distance out from edge: 1 µm = 3 pixels
Outer region width: 0.2 µm = 1 pixel
3
4
FITC (100%)
D
1
2
–
3
4
=
Nuclear envelope intensity
E
B
C
A
inner region
outer region
B + C = nuclear envelope
A. Outer region width
B. Outer region distance from edge
C. Inner region distance from edge
Compartment edge

Figure 5.9 The translocation enhanced module was adapted to quantify fluorescence at the nuclear envelope (NE)

(**A**) Nuclei are stained with Dapi (blue) and a nuclear envelope protein is detected by green fluorescence. (**B**) Settings used to generate regions 1 and 2 and the overlay between the segments and the FITC image are shown. Note that there is no space between the inner and outer regions, i.e. regions 1 and 2. (**C**) Regions 3 and 4 are generated at the same position as regions 1 and 2. However, the settings introduce a gap between regions 3 and 4; this gap represents the NE. The overlay image for regions 3 and 4 should be compared with the overlay image in part B for regions 1 and 2. (**D**) The fluorescence intensity at the NE can be calculated by the simple formula: Intensities of regions (1 + 2) minus intensities of regions (3 + 4). (**E**) The positions of the outer, inner region and the compartment edge (orange dashed line) are illustrated.

Figure 5.10

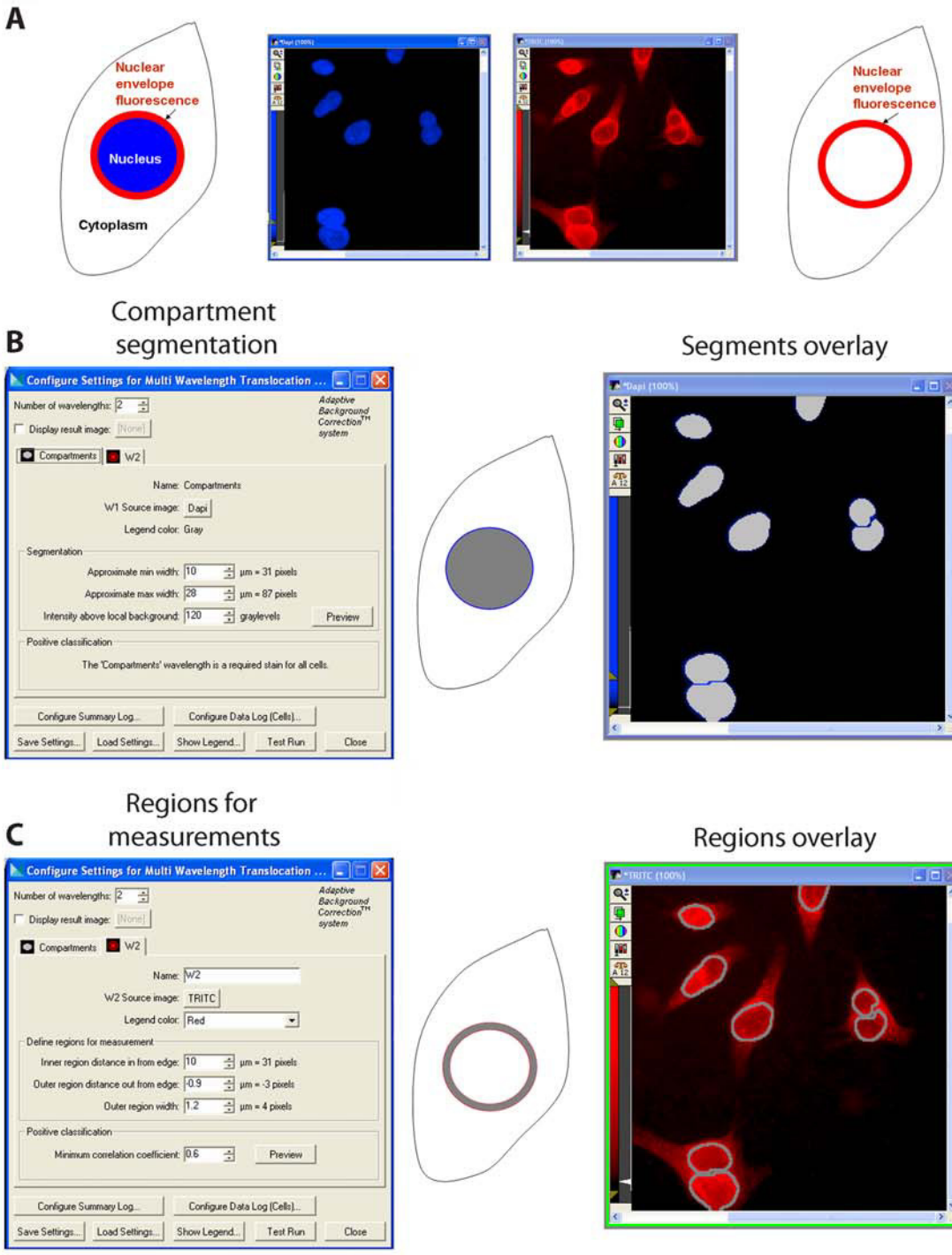
A
Nuclear envelope fluorescence
Nucleus
Cytoplasm
Nuclear envelope fluorescence
B
Compartment segmentation
Segments overlay
Configure Settings for Multi Wavelength Translocation ...
Number of wavelengths: 2
Display result image: [None]
Adaptive Background Correction™ system
Compartments
W2
Name: Compartments
W1 Source image: Dapi
Legend color: Gray
Segmentation
Approximate min width: 10 µm = 31 pixels
Approximate max width: 28 µm = 87 pixels
Intensity above local background: 120 graylevels
Preview
Positive classification
The 'Compartments' wavelength is a required stain for all cells.
Configure Summary Log...
Configure Data Log (Cells)...
Save Settings...
Load Settings...
Show Legend...
Test Run
Close
C
Regions for measurements
Regions overlay
Configure Settings for Multi Wavelength Translocation ...
Number of wavelengths: 2
Display result image: [None]
Adaptive Background Correction™ system
Compartments
W2
Name: W2
W2 Source image: TRITC
Legend color: Red
Define regions for measurement
Inner region distance in from edge: 10 µm = 31 pixels
Outer region distance out from edge: -0.9 µm = -3 pixels
Outer region width: 1.2 µm = 4 pixels
Positive classification
Minimum correlation coefficient: 0.6
Preview
Configure Summary Log...
Configure Data Log (Cells)...
Save Settings...
Load Settings...
Show Legend...
Test Run
Close

Figure 5.10 The multi wavelength translocation module was adapted to quantify fluorescence at the nuclear envelope (NE)

(**A**) The nuclear compartment is stained with Dapi and a nuclear envelope protein is detected with a red fluorescent probe (TRITC) (282). (**B**) Settings to generate segments that define the nuclei and the overlay of segments and the Dapi image are illustrated. (**C**) Parameters are set to define the inner and outer regions. Note that the outer region coincides with the NE while the inner region is set to be small to facilitate the visual inspection of overlay images. See text for details.

Figure 5.11

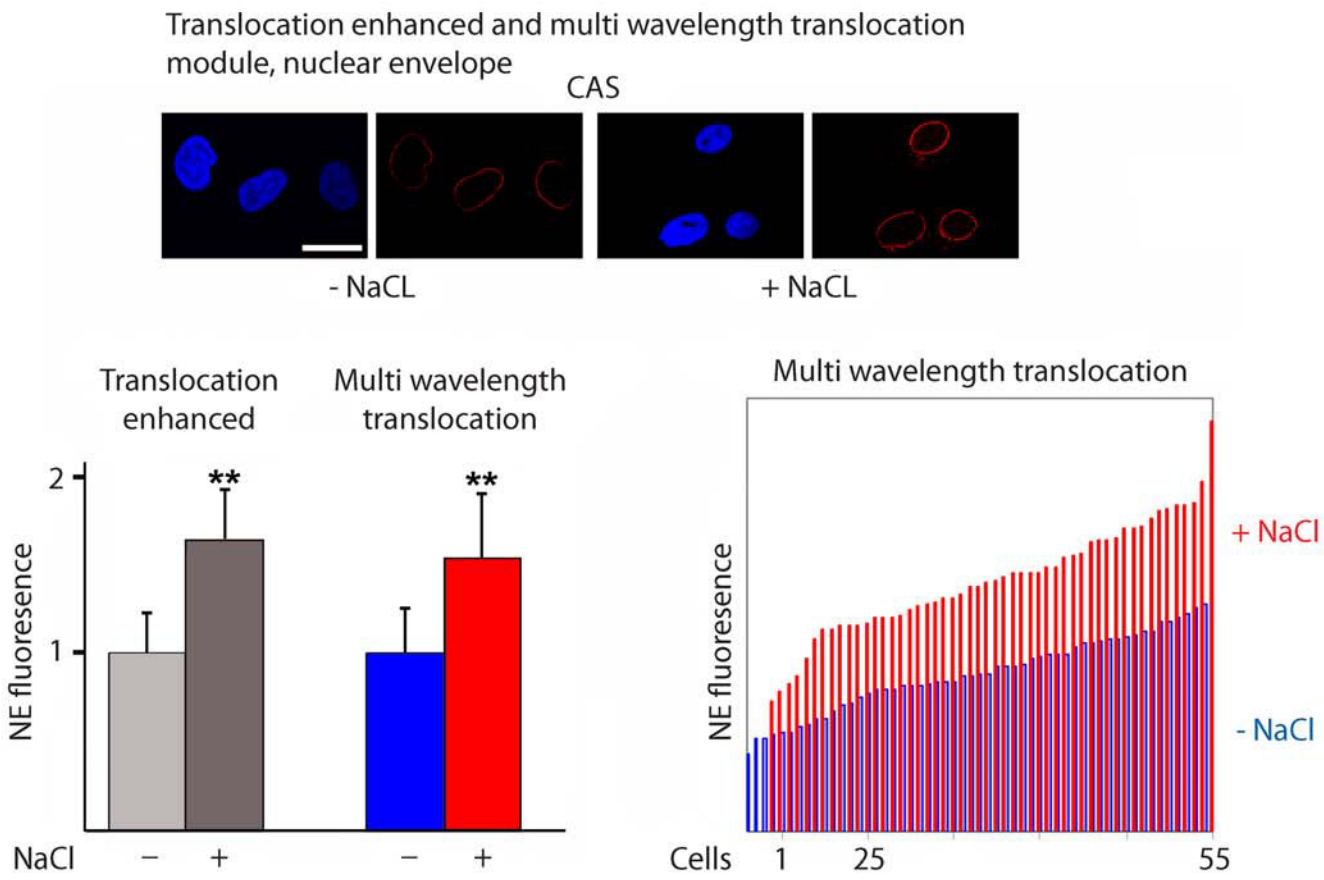
Translocation enhanced and multi wavelength translocation module, nuclear envelope
CAS
- NaCL
+ NaCL
Translocation enhanced
Multi wavelength translocation
NE fluoresence
2
1
**
**
NaCl
–
+
–
+
Multi wavelength translocation
NE fluoresence
+ NaCl
- NaCl
Cells
1
25
55

Figure 5.11 Application of the translocation enhanced and multi wavelength translocation modules to measure fluorescence located at the nuclear envelope

NE binding of the fluorescently labeled nuclear carrier CAS (282) was analyzed in HeLa cells for controls (-NaCl) or salt-extracted specimen (+NaCl). Images were acquired by confocal microscopy and NE fluorescence intensity quantified with the translocation enhanced or multi wavelength translocation module. Fluorescence intensities for samples –NaCl were defined as 1. Data obtained with the multi wavelength translocation module are also depicted on the right side for individual cells –NaCl (blue) and +NaCl (red). Size bar is 25 μm; $^{**}P<0.01$. See text for details. Parts of Fig. 5.11 were reprinted from (282) with permission from Birkhäuser Verlag AG.

Figure 5.12

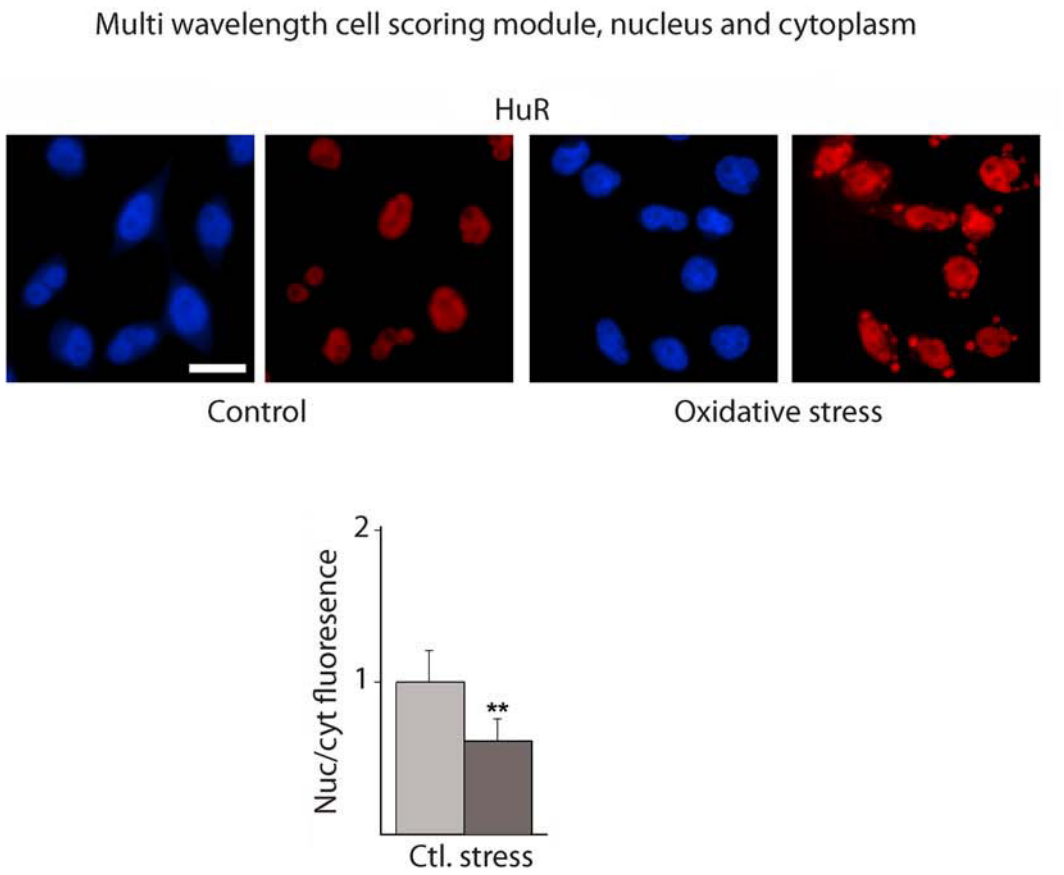
Multi wavelength cell scoring module, nucleus and cytoplasm
HuR
Control
Oxidative stress
Nuc/cyt fluoresence
2
1
**
Ctl. stress

Figure 5.12 Application of the multi wavelength cell scoring module

The multi wavelength cell scoring module is employed to measure the nuc/cyt fluorescence of HuR protein (red) under normal (control) and oxidative stress conditions (HuR) (283). Note that the irregular distribution of HuR in the cytoplasm of stressed cells requires the quantification of fluorescence in the whole cytoplasm. A γ-factor of 2 was applied to visualize the weak cytoplasmic signal, but the same image display settings are applied for all images in the same panel. Since the cytoplasmic fluorescence was weak, a low value of intensity above local background was selected to properly identify the cell edges. Changes in the ratio of average nuclear/cytoplasmic (nuc/cyt) fluorescence were determined for HCS-images. The ratio of nuc/cyt fluorescence in unstressed control cells was defined as 1. Parts of Fig. 5.12 and 5.13 were reprinted from (283) with permission from Elsevier.

Figure 5.13

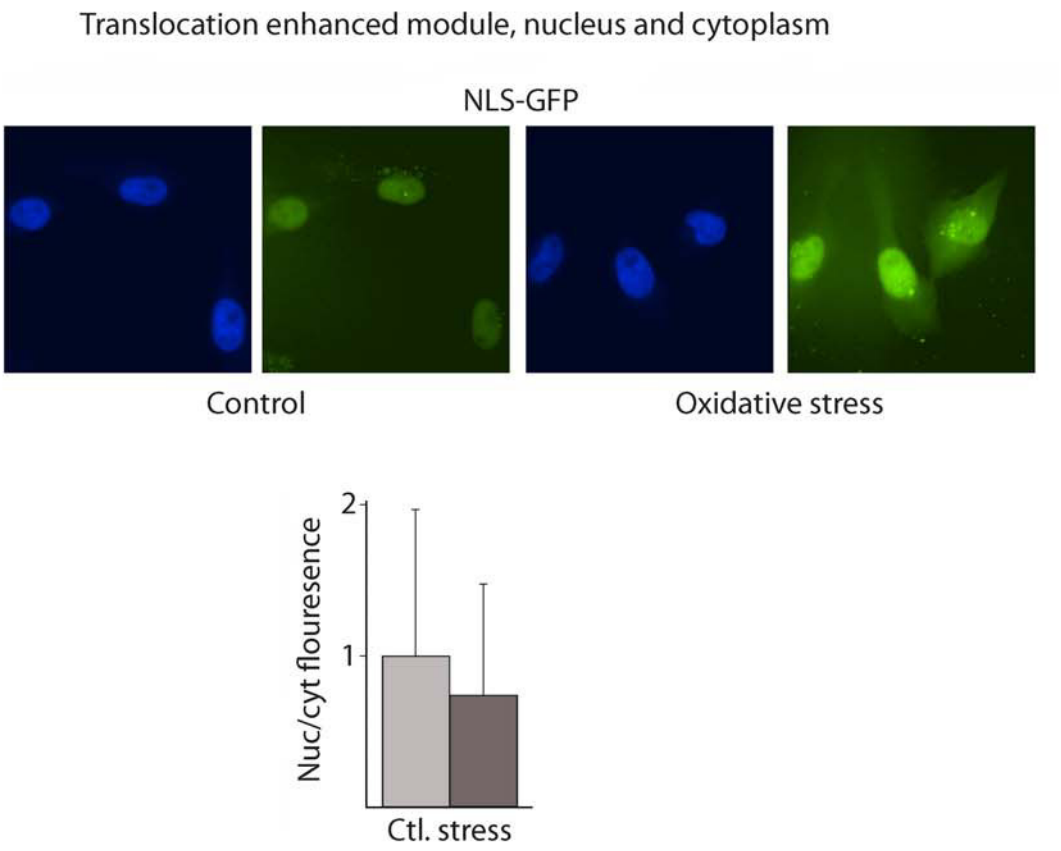
Translocation enhanced module, nucleus and cytoplasm
NLS-GFP
Control
Oxidative stress
Nuc/cyt flouresence
2
1
Ctl. stress

Figure 5.13 Application of the translocation enhanced module

The translocation enhanced module is used to measure the nuc/cyt fluorescence of NLS-GFP (green) in transiently transfected HeLa cells under normal and oxidative stress conditions (283). Note that the weak cytoplasmic signal would prevent the accurate cellular segmentation with the multi wavelength cell scoring module (see text). Parts of Fig. 5.12 and 5.13 were reprinted from (283) with permission from Elsevier.

6. Discussion

Nucleocytoplasmic trafficking of macromolecules is essential to maintain cellular homeostasis as it regulates many features of eukaryotic cell physiology. Gene expression, cell signalling, growth and proliferation, apoptosis, cell cycle control and in particular the communication between different organelles can be regulated by changing the subcellular localization of specific proteins. This includes components of the nuclear transport machinery, molecular chaperones, and a wide range of signalling molecules such as protein kinases and phosphatases. Furthermore, altering nucleocytoplasmic transport is one of the cellular strategies to respond to different forms of stress. It is well established that stress can modulate the transport of distinct molecules or completely inhibits certain transport routes (201, 202).

Several observations substantiate the effect of stress on nuclear trafficking. As such, the transcription factor NF-κB redistributes to the nuclei of cultured rat mesencephalic neurons in response to free-radical production that is accompanying C_2-ceramide induced apoptosis. NF-κB nuclear accumulation is thought to be the underlying mechanism that mediates oxidative stress-induced apoptotic cell death of the dopaminergic neurons in patients with Parkinson disease (292, 293). In addition, heat stress has been shown to accumulate mRNAs in nuclei of stressed *Saccharomyces cerevisiae* cells, while it favors the export of heat shock-mRNAs via distinct non-classical mechanism that do not require Yra1p and Npl3p (294). A prominent example that demonstrates how stress can

impinge on nucleocytoplasmic transport is the inhibition of classical nuclear import pathway following exposure to heat or oxidative stress (87, 201).

Oxidative stress has been implicated in the pathophysiology of a variety of human diseases. For example, the damage of cellular proteins induced by the accumulation of reactive oxygen species ROS is the underlying cause of cellular death in neurodegenerative diseases, ischemia/reperfusion injuries of the heart, as well as the complications associated with type-2 diabetes (reviewed in 295, 296).

Oxidative stress impinges on distinct aspects of eukaryotic cell physiology via different mechanisms. These may include the stress-induced damage of proteins that are essential for maintaining cellular homeostasis such as enzymes, transcription factors, signalling molecules, tumor suppressors and molecular chaperones. In a different scenario, oxidative stress may alter the main cellular processes such as DNA transcription, protein synthesis, or apoptotic cell death. Central to the control of all these processes is the regulation of nucleocytoplasmic transport which coordinates many vital activities within the cell. A prominent example is the modification of the transport machinery that is accompanying apoptotic cell death. This is evident by the apoptosis-induced mislocalization of several transport factors, for instance importin-α, importin-β and Ran. Furthermore, induction of apoptosis alters the permeability of the NPC. As apoptosis proceeds, the transport function of the NPC is lost due to the degradation of several nucleoporins that are essential to nuclear trafficking, including Nup153, Nup50, Nup358 and Nup214 (reviewed in 281, 297). Indeed,

the nucleocytoplasmic transport apparatus is one of the cellular targets that is highly sensitive to stress exposure.

Given the diverse structural and functional components of this transport system, stress may modify the nucleocytoplasmic transport on multiple levels which include soluble transport receptors, NPCs and transport cargoes. Several, not mutually exclusive mechanisms may contribute to this inhibition. As such, altering the function of the transport receptors as well as the different nucleoporins by mislocalization and/or degradation can play a key role in nuclear transport inhibition. On a different level, stress may modify the nucleocytoplasmic transport of specific cargoes via posttranslational modifications which can lead to masking or exposing their transport signals. All of these stress-dependent changes are a down-stream effect that is triggered by the initial stress-induced activation of different signalling cascades. These signalling events ultimately define the cellular response to stress.

In an initial attempt to explore the effect of oxidative stress on the cellular transport machinery, I have shown that severe oxidative stress elicited by the hydrogen peroxide treatment inhibits classical nuclear import in growing HeLa cells (87). Furthermore, my results revealed that the stress-induced inhibition of classical nuclear import is mediated by multiple mechanisms. These include the collapse of the Ran concentration gradient as well as the relocation and degradation of components of the nuclear transport apparatus. For instance, Nup153 and importin-β are relocated by stress. Furthermore, the docking of importin-β at the NE is inhibited in stressed cells. Interestingly, although Ran,

Nup153 and importin-β showed increased susceptibility to proteolysis upon exposure to severe oxidative stress, their degradation was mediated by different proteolytic pathways. This work has advanced our understanding of how severe oxidative stress affects the nucleocytoplasmic trafficking at the molecular level. However, it did not address the question of how milder forms of oxidative stress will impact the nuclear trafficking. This is of particular importance as the mild oxidative stress is more likely to mimic the physiological stresses associated with different human diseases. To this end, I investigated the effect of oxidative stress induced by diethyl maleate (DEM) treatment on nuclear transport function as well as the individual component of the transport apparatus (283). My goal was to understand how stress impinges on the localization of two essential components of the transport apparatus, nuclear transport receptors and nucleoporins. Using HeLa cells as model system, my research demonstrated that oxidant treatment redistributes the nuclear receptor importin-α and its exporter CAS, both transport factors concentrated in nuclei of stressed cells. Similarly, nucleoporins Nup153, Nup88, Nup50, all of which are implicated in different aspects of nuclear transport, mislocalized to the nucleus upon exposure to oxidative stress.

The nuclear accumulation of the transport receptors and nucleoporins observed by the experiments described above could be the consequence of different changes in nuclear function. These include increased nuclear import, decreased nuclear export, nuclear retention or a combination of all these events. My results have identified nuclear retention as one of the underlying mechanisms that increase the nuclear content of importin-α, CAS, Nup153, Nup88 and Nup50 upon stress.

Furthermore, I have shown that the nuclear retention of importin-α, Nup153 and Nup88 is in part due to their increased association with large molecular mass complexes in nuclei. My analysis of the classical import pathway demonstrated that exposure to mild oxidative stress renders this transport route less efficient. This is thought to be a direct consequence of the mislocalization and retention of the transport receptors and nucleoporins in stressed cells. Taken together, my work defined the mechanisms that mediate the nuclear import inhibition upon mild oxidative stress. Interestingly, unlike severe oxidative stress, neither the collapse of Ran concentration gradient nor the degradation of transport factors importin-β, Nup153 or Ran contribute to the import inhibition caused by DEM treatment. My research identified the nuclear accumulation and retention of importin-α, CAS, Nup153, Nup88, and Nup50 as well as changes in their interaction in stressed nuclei as the leading mechanisms that mediate classical import inhibition upon exposure to mild oxidative stress. Thus, diverse mechanisms promote classical import inhibition upon mild and severe oxidative stress. This indicates that a particular transport route may be regulated differently according to the type of stress that triggered a cellular response.

Nuclear transport inhibition has direct consequences for a large number of human diseases. Several studies have shown that stress-induced inhibition of classical nuclear import contributes to the accumulation of transcription factors in the cytoplasm of degenerating neurons which is a characteristic feature of numerous neurodegenerative diseases, including Alzheimer's disease and Parkinson disease (277). A prominent example is the mislocalization of the

nuclear factor E2-related factor 2 (Nrf2) to the cytoplasm of hippocampal neurons of Parkinson patients. Furthermore, Nrf2 fails to accumulate in nuclei of cultured fibroblasts from patients with Friedreich ataxia upon oxidative stress. The nuclear translocation of Nrf2 is necessary for the induction of phase II antioxidants which protect neurons from oxidative stress. Therefore, the inhibition of nuclear import of Nrf2 diminishes the cellular response to oxidative stress and is thought to be a major underlying cause that contributes to neuronal damage in Friedreich ataxia patients (298, 299)**.** Understanding the molecular basis of the stress-induced changes in nuclear transport is of fundamental importance as it opens the door for the discovery of novel pathways that can be targeted to rescue the function of the transport apparatus. Ultimately this could ameliorate the different pathophysiologies which are attributed to stress-induced impairment of nuclear trafficking.

Results obtained from the analysis of classical nuclear import in oxidant treated cells substantiate the hypothesis that soluble transport receptors are primary targets for stress-induced modifications. Stress can modulate the function of the transport receptors and consequently the nuclear trafficking in different ways. For example, disrupting the proper intracellular distribution of one or more of these transport receptors renders them unavailable to bind and translocate their cargo substrates. In a different scenario, the stress-induced post-translational modification of transport receptors may affect the function of a particular transport factor by altering its substrate binding affinity or promoting its anchoring to nuclear or cytoplasmic proteins which ultimately hinder its mobility.

Modifying transport factor location, expression, or substrate-binding has been associated with a large number of malignancies and aging-related changes (reviewed in 280). A prominent example of such a link is the striking correlation between tumorigenesis and a truncated form of importin-α found in breast cancer cells (reviewed in 280, 300). The mutation in the NLS-binding domain of the truncated importin-α impairs its ability to bind the tumor suppressor p53, which then concentrates in the cytoplasm of breast cancer cells. The impaired nuclear import of p53 diminishes its antitumour activity and promotes tumor progression. Interestingly, the impaired import functions of truncated importin-α was accompanied by its preferential localization to the cytoplasm (300). In addition, the upregulation of CAS expression has been demonstrated in a variety of tumors, such as colon cancer, breast cancer and liver neoplasms. As CAS exports importin-α, overexpression of CAS may affect the subcellular distribution of importin-α which subsequently impinges on the importin-α mediated transport of important key players in the tumorigenesis such as tumor suppressors. Interestingly, not only tumor-associated overexpression of CAS may affect the subcellular distribution of importin-α. Relocation of CAS within the cell in response to different forms of stress may also impinge on the localization of importin-α. As such, I have shown that heat shock stimulates the translocation of CAS into the nuclear interior. This may contribute to the nuclear accumulation of importin-α upon heat stress. I have further demonstrated that increased docking at the NE as well as nuclear retention mediates the heat-induced nuclear accumulation of importin-α (282). This reflects the diverse mechanisms that can

modulate the subcellular localization of a specific transport receptor which further adds to the complexity of the regulation of nucelocytoplasmic transport under different physiological and pathophysiological conditions. The prominent role of transport receptors in maintaining cellular homeostasis is further substantiated by a study that demonstrated the decreased import efficiency in old fibroblasts due to diminished concentrations of importin-α and CAS (301). This may link the function of nuclear transport receptors to the major changes related to the aging process.

Another component of the transport system which can be modified by stress is the NPC, the sole gate that mediates macromolecular exchange between the nucleus and cytoplasm (reviewed in 14, 15). The pivotal role of nucleoporins in maintaining cellular homeostasis is now emerging. For example, fusion of the Nup98 gene to homeobox family members can lead to the production of Nup98-HOXA9 fusion proteins. A mislocalization of Nup98 fusion proteins correlates frequently with human leukemia. Fusion proteins containing other nucleoporins, for instance CAN/Nup214, have been demonstrated as well to play a role in acute mylogenous leukaemia (reviewed in 302). Wild type Nup98 is a mobile nucleoporin that localizes to multiple subcellular compartments. As the dynamic nature and the multiple subcellular localizations of Nup98 will likely impinge on its function, and given its importance in cancer cell research, I have optimized IF staining protocols that are optimal to visualize Nup98 in different compartments of interest, including nucleoli, nuclear bodies and the cytoplasm (303). The

protocols developed set the stage to analyze the effect of oxidative stress on Nup98 and other transport components (304).

Other examples substantiate the importance of NPC function in maintaining cell physiology, for instance recent reports have linked aging process to defects in the structural and functional integrity of the NPCs; these defects are characterized by the loss of the structural nucleoporin Nup93. This deterioration in NPC function compromises the permeability barrier of the NE and collapses nucleocytoplasmic transport (305). In line with these findings, my results demonstrated that oxidative stress exerts its effects in part by modifying the subcellular localization of several nucleoporins such as Nup153, Nup88 and Nup50. In addition, the posttranslational modification of these nucleoporins as well as their association with the nuclear proteins is altered upon stress (306).

On the basis of my results, nuclear transport receptors and nucleoporins are good candidates that can be targeted to rescue the function of the nuclear transport apparatus which has been altered due to different pathophysiologies or as a result of aging. A striking example consistent with this idea is the regaining of functional activity of p53 as a tumor suppressor by overexpression of wild type importin-α in breast cancer cells (300). Future directions will have to focus on designing molecular strategies that can redirect the mislocalized transport receptors and nucleoporins to their proper subcellular localization. Screening libraries for small molecules using high throughput technology may help to identify new candidates that can bind and modulate the subcellular localization of the different transport receptors (307). *Kau et al* (308) have successfully

employed this strategy to identify compounds that inhibit Foxo1a nuclear export in PTEN deficient tumor cells. Absence of PTEN activity in tumor cells leads to Akt-mediated phosphorylation of Foxo1a, which localizes Foxo1a to the cytoplasm. Thus, relocating Foxo1a to the nucleus via export inhibition may help to overcome the consequences of PTEN absence in tumor cells (308). This approach is not restricted to Foxo1a, but will be applicable to other cargoes of the nuclear transport apparatus as well. A prerequisite for these experiments are the screening and reliable evaluation of large numbers of compounds. Toward this goal, I have designed new methods that combine high throughput screening technologies with computer-based image analysis to study the changes in the subcellular distribution of different cellular proteins. These protocols have been successfully used for the precise detection and quantification of multiple components of the transport machinery as well as signalling molecules that are localized to different subcellular compartment (309) (see below).

Nucleocytoplasmic transport is of fundamental importance to generate a specific response to diverse environmental stimuli. Nuclear transport factors are also targets of multiple cellular signalling events. For instance, following oxidant exposure, cells respond by activating different signalling cascades, a process that is required for cell survival and repair of stress-induced damage. Changes in signalling and therefore the appropriate cellular response to a stimulus relies on several factors. This includes the activation or inactivation of signalling molecules, including kinases and phosphatases. Of pivotal importance for the specificity and duration of signalling is the proper location of signalling

molecules within the cell. Thus, redistribution of signalling molecules provides an additional tool to regulate the outcome of the signalling cascade and ultimately control the cellular response to stress. Confining the signalling molecule to a specific subcellular compartment limits its access to certain substrates which subsequently determine the modification of the downstream targets. This compartmentalization may lead to signalling in the cytoplasm, the nucleus or at the plasma membrane. To further explore the importance of subcellular localization in the control of signalling under normal and stress conditions, I have studied how the distribution of AMP-activated protein kinase (AMPK) in mammalian cells is regulated in response to stress. AMPK is a key component controlling cellular metabolism; its pivotal role in the regulation of glucose homeostasis and lipid metabolism makes AMPK an important therapeutic target in type-2 diabetes and obesity (reviewed in 134, 137). Under normal conditions, the heterotrimeric enzyme is present in the cytoplasm and nucleus and the levels of kinase in either compartment are likely to control the phosphorylation of downstream targets. To better understand the effects of different types of stress on the subcellular distribution of the enzyme subunits, I have analyzed the distribution of AMPK subunits under different conditions (210). My research demonstrated that in response to stress, such as heat, oxidative stress and depletion of metabolic energy, the nuclear levels of the enzyme α and β subunits increase. This can be explained by the need to phosphorylate distinct nuclear AMPK substrates, like transcription factors, or to downregulate the phosphorylation of cytoplasmic targets. Conversely, both AMPK subunits were

confined to the cytoplasm in cells growing in high density cultures. Extracellular signalling cascades might be activated upon high confluency, thereby altering the AMPK distribution. This is in line with the idea that the nuclear transport of signalling molecules may be modified differently according to the different physiological conditions. Ultimately, this will determine the proper cellular response. Furthermore, my results showed that AMPK shuttles between the nucleus and cytoplasm under normal conditions, and that this process is dependent on the exporter Crm1. This favors the dynamic nature of AMPK distribution rather than the existence of fixed nuclear and cytoplasmic pools of the kinase. Such a dynamic organization provides the cell with more flexibility to regulate the enzyme activity. Analyzing the effect of stress on the phosphorylation state of the AMPK-α subunits revealed an inverse correlation with the activation of the MAPKs ERK1/2. As such, several different stressors led to dephosphorylation and thereby inactivation of the AMPK-α1/2 subunits on Thr172. Furthermore, my results demonstrated that signaling through the MEK→ERK1/2 cascade plays a crucial role in controlling the localization of AMPK; pharmacological inhibitors that interfere with this pathway alter the AMPK distribution under non-stress conditions. This identified novel links between the physiological state of the cell, the activation of MEK→ERK1/2 signaling and the nucleocytoplasmic distribution of AMPK. These findings are important, as they set the stage to identify specific AMPK functions in either the nuclear or cytoplasmic compartment that are dictated by changes in cell physiology. For instance, it is speculated that the stress-induced nuclear

localization of the AMPK may be necessary to modify certain enzymes as well as transcription factors which activate the expression of stress-related genes. For example, acetylation of multiple transcription factors, such as the modification of members of the Foxo family by p300/CBP, requires p300/CBP phosphorylation by AMPK (249). The control of AMPK distribution by the activity of the MEK→ERK1/2 signalling pathway adds a new dimension to the complexity of the regulatory processes that govern signaling events. Moreover, these results further substantiate the importance of the subcellular distribution of signaling molecules.

Taken together, my studies demonstrated the highly dynamic localization of AMPK within the cell. Several forms of stress, high cell density, pharmacological inhibitors of ERK1/2 kinases and the exporter Crm1 control the nucleocytoplasmic distribution of AMPK, thereby regulating its downstream effects. Understanding how stress regulates AMPK distribution between different cell compartments sets the stage to develop new therapeutic strategies to control the intracellular localization of AMPK and thereby the modification of targets that are relevant to human disease and pathophysiology, including, but not limited to type 2 diabetes and obesity.

The crosstalk between AMPK and MEK→ERK1/2, as revealed by my results, and how such crosstalk impinges on the subcellular localization as well as the activity of AMPK directed my research to further investigate the effects of oxidative stress on other signalling pathways. In particular, PI3→Akt and MEK→ERK1/2 are essential signalling cascades that are activated upon exposure

to stress. Signalling through these two modules is of fundamental importance as it determines the cellular response to various stimuli via phosphorylation of different nuclear and cytoplasmic targets. My analysis of the subcellular distribution of individual components of these signalling modules showed that oxidative stress drastically alters the localization of phospho-ERK1/2 and phospho-Akt(Ser473) (310 and references therein). This supports the idea that specific downstream nuclear and/or cytoplasmic targets need to be modified upon stress and that their modification relies on the proper localization of both kinases. Furthermore, my research demonstrated that the interplay between MEK and PI3 kinase signalling affects the subcellular distribution of kinases in both cascades. As such, pharmacological inhibition of PI3 kinase modulates the subcellular localization of phospho-ERK-1/2, whereas MEK inhibition affects the distribution of phospho-Akt(thr308) and phospho-Akt(ser473) (310). These findings highlight a possible cross-talk between nucleocytoplasmic transport and signalling events which can occur in different ways. For example, the activation of signalling cascades may lead to the posttranslational modification of individual components of the transport apparatus, like transport receptors and nucleoporins. Such modifications could then alter nucleocytoplasmic transport. At the same time, changes in the transport apparatus can modify the subcellular distribution of various kinases or phosphatases which ultimately leads to a change in the posttranslational modification of their downstream targets. A combination of these two scenarios may enable the cell to cope with stress. It is noteworthy that the interplay between the transport machinery and signalling cascade is not

limited to a particular signalling pathway. Rather, my results demonstrate that several kinases which are involved in several distinct signalling cascades are subject to regulation by changing their subcellular distribution. This indicates a general role for nucleocytoplasmic transport in controlling cellular signalling under normal and stress conditions. Indeed, my preliminary data support both models (306).

One of the basic systems which cells rely on to cope with different stressors is the molecular chaperone machinery. Hsp70s are essential components of the cellular chaperone system and play a fundamental role in protecting cells against damage. It is well established that stress exposure upregulates the synthesis of certain members of hsp70s family, such as the inducible hsp70. Furthermore, hsc70 has been shown by us and others to accumulate in nuclei of stressed cells (202). This accumulation is only transient and hsc70 redistributes to the nucleoli and then to the cytoplasm upon recovery from stress, indicating a crucial role for hsc70 in the nuclei of stressed cells. However, the mechanisms that underlie the stress-induced nuclear accumulation of hsc70 have yet to be defined. This is of fundamental importance as it impinges on the functions of hsc70 in different cellular compartments. The nuclear functions of hsc70 are most likely to be distinct from its cytoplasmic role in folding newly synthesized proteins and intracellular transport. To better understand these mechanisms, I have analyzed the subcellular distribution of hsc70 under normal and stress conditions (208). My research revealed that hsc70 shuttles between the nucleus and cytoplasm under normal conditions which supports the idea that the chaperone has crucial

functions in both compartments. Using human-mouse heterokaryons, my studies demonstrated that upon heat shock this shuttling process is inhibited and hsc70 is retained in the nuclei of stressed cells. Further analysis showed that the nuclear retention of hsc70 is mediated by two different mechanisms. First, the binding of hsc70 to damaged nuclear proteins which require chaperoning activity. Second, its association with nucleolar proteins such as fibrillarin and ribosomal protein rpS6, which increased upon stress, substantiates a key role for hsc70 to restore nucleolar function. The role of hsc70 and other chaperones in maintaining the functional integrity of nucleoli has been proposed based on the accumulation of hsc70 in the dense fibrillar components (DFC) of nucleoli upon heat shock (311). Despite this initial finding, the molecular basis of hsc70 functions in the nucleoli remained obscure. My research identified the molecular targets for hsc70 function in the nucleolus. Fibrillarin and ribosomal protein rpS6 are two fundamental components of the nucleolus that showed an increased association with hsc70 upon exposure to heat stress. The redistribution of these proteins in response to stress, together with their increased association with hsc70, may indicate that hsc70 is necessary to restore their proper localization upon recovery from stress. Furthermore, I demonstrated that the molecular mechanisms that govern the interaction of hsc70 with its nucleolar binding partners are distinct from those which mediate chaperone-substrate binding. This sets the stage to design strategies that aim to rescue the nucleolar functions that are impaired by stress.

Hsp70s play a fundamental role in different aspects of eukaryotic cell physiology. This is well established by the large number of human diseases and

disorders which are associated with improper function of chaperones. A prominent example is their implication in neurodegenerative diseases such as Alzheimer and Parkinson diseases. Interestingly, the onset of Parkinson disease has been attributed at least in part to defects in protein folding, the main function of the molecular chaperones (reviewed in 312). Furthermore, the pivotal role of hsp70s in protecting heart cells from ischemia/reperfusion injuries is well established. As such, increased levels of hsp70 correlated with increased heart protection from ischemia in transgenic mice. This is demonstrated by the decreased susceptibility of the heart cells to ischemia-induced damage in mice that overexpress hsp70s (reviewed in 313). The protective role of hsp70s is mediated by their ability to inhibit multiple apoptotic pathways thereby promoting cell survival (reviewed in 314). On the other hand, overexpression of hsp70s increases the probability of cellular transformation and enhances tumorigenesis (reviewed in 315, 316). As such, high levels of hsp70s correlate with tumor development and progression in animal models for breast cancer tumor as well as T-cell lymphomas. Thus, the expression level of hsp70s should be kept in balance in order to maintain cellular homeostasis.

However, chaperone function is not only an important factor in human disease. Furthermore, aging process is correlated with a reduction in the levels of hsp70s. *In vitro* studies demonstrated that the levels of hsp70 in human lung fibroblasts decrease as cells were aging (reviewed in 317). Another study has shown that aging reduces the chaperoning activity as well as hsp90 levels in rat hepatocytes (reviewed in 318). The increased amount of damaged proteins due to

oxidative stress upon aging together with the aberrant induction of heat shock proteins is considered to be the cause of many age-related pathophysiologies.

Understanding the molecular mechanisms that regulate the dynamic nature of heat shock proteins under stress conditions sets the stage to design strategies that regulate its function and enhance the cellular stress response. For instance, increasing the cytoplasmic retention of hsc70 may help to dissolve the protein aggregates associated with neurodegenerative diseases. Toward this goal my study defined the nuclear retention as one of the mechanisms that modify the nucleocytoplasmic transport of hsc70 upon stress; however, other processes such as import and export may also participate in determining the final destination of the chaperone. Future studies will have to focus on how these pathways are regulated under normal and stress conditions. This will add further dimensions to the regulation of the subcellular localization of hsc70 and lead the way for more possible interventions that aim to direct the chaperone to specific cellular locations.

Thus far, my research has demonstrated that the subcellular localization of many cellular components is a dynamic process which is regulated by different internal and external stimuli. This dynamic nature provides the cell with powerful tools to regulate the functions of many cellular proteins by changing their distribution between the different subcellular compartments. The close correlation between the function of these proteins and their proper localization within the cell requires efficient and reliable tools to quantify precisely their amounts in a specific subcellular location. Immunofluorescent staining has been extensively

used to visualize molecules inside the cell. Despite the wide application of this technique, it remains a rather qualitative than quantitative method. Other techniques, such as cell fractionation followed by Western blot analysis, may be used to quantify protein abundance or distribution within different cellular compartments. However, these procedures are frequently laborious, time consuming, inefficient and prone to error. As part of my studies, I developed new strategies to analyze the subcellular localization of fluorescent molecules in a quantitative fashion (309). To achieve this, I took advantage of the recent developments in technologies that combine high throughput screening with imaging and computer-based image analysis. I have developed protocols to detect and quantify fluorescent signals in specific subcellular compartments such as nucleus, cytoplasm, and for the first time, at the nuclear envelope (309). A particular challenge is the quantification of the fluorescent signals at the NE. The small area of the NE renders this process very difficult. However, this is of fundamental importance as many cellular proteins, including the transport receptor importin-α, transcription regulators, as well as several nucleoporins change their association with the NE in response to different stressors. These new protocols have been employed successfully to accurately detect the subtle changes in the association of importin-α, Nup153 and Nup88 with the NE upon exposure to stress. Furthermore, the protocols described for fluorescent signal quantification in nuclear and cytoplasmic compartments have been used to analyze the changes in the nucleocytoplasmic distribution of three signaling molecules AMPK, AKT, ERK1/2 under different stress conditions. The accuracy

as well as the ease of use of these protocols encouraged me to explore the complex signaling events of two main pathways, PI3K→AKT and MEK→ERK1/2, I determined how these signaling cascades impinge on the subcellular localization of the individual components of the two signaling routes. The results of my experiments revealed a crosstalk between PI3K →AKT and MEK→ERK1/2 signaling pathways which ultimately define the subcellular distribution of their components under normal and stress conditions (310). Furthermore, using these protocols, the effect of this interplay on the subcellular distribution of the downstream target Foxo3a has been analyzed in a quantitative fashion. These studies provided new insights into the dynamic distribution of Foxo3a transcription factor.

The flexibility of the protocols developed here is demonstrated by the presence of different alternatives that can be used to measure the intensities of the fluorescent molecule in the same cellular compartment. This gives the user a wide variety of solutions that can fit with the different experimental settings as well as the distinct distribution patterns of cellular proteins.

Future studies will have to develop new protocols that can be used to quantify signals in other subcellular locations such as nucleoli and cellular membranes. Taken together, the methods described in chapter 5 provide for the first time novel powerful tools to detect and quantify fluorescence signals in different cellular organelles. These tools are valuable to the scientific community as their applications are not limited to research in the area of nuclear transport. As such, these protocols can be employed on a broader scale to study different cellular

activities, for instance, transcription regulation, signaling events, receptor internalization and apoptosis. The accuracy, ease of use and convenience of these methods open new avenues to study a wide variety of biological processes.

7. Summary

In this contribution, I have analyzed the effect of stress on different aspects of eukaryotic cell physiology. My research is directed towards a better understanding of how environmental changes and insults affect cellular functions, with particular focus on how stress modulates nucleocytoplasmic transport, the molecular chaperone system and the signalling events in mammalian cells. My studies defined at the molecular level the stress-induced changes in the intracellular distribution of key players of the nuclear transport machinery (transport receptors and nucleoporins), the signalling molecule AMPK as well as hsc70, the essential component of the chaperone system in mammalian cells. Furthermore, I have developed new techniques to quantify fluorescence signals in different cellular compartments. These quantitative assays facilitate the analysis of cell signalling events and protein trafficking in mammalian cells. Understanding how the molecular transport apparatus works under different conditions and how signalling events are organized in a spatio-temporal fashion may help to design novel therapeutic strategies for the defects seen under stress conditions. These strategies could aim at the rescue of functions of the transport machinery as well as the correct distribution of fundamental proteins in the cells like signalling molecules and molecular chaperones.

8. References

1. **Vellai T and Vida G.** The origin of eukaryotes: the difference between prokaryotic and eukaryotic cells. *Proceedings of the Royal Society of London Series B: Biological Sciences* 266: 1571-1577, 1999.

2. **D'Angelo M and Hetzer M.** The role of the nuclear envelope in cellular organization. *Cellular and Molecular Life Sciences (CMLS)* 63: 316-332, 2006.

3. **Weis K.** Regulating access to the genome: nucleocytoplasmic transport throughout the cell cycle. *Cell* 112: 441-451, 2003.

4. **Gerace L and Burke B.** Functional organization of the nuclear envelope. *Annual Review of Cell Biology* 4: 335-374, 1988.

5. **Görlich D and Kutay U.** Transport between the cell nucleus and the cytoplasm. *Annual Review of Cell and Developmental Biology* 15: 607-660, 1999.

6. **Feldherr CM, Kallenbach E, and Schultz N.** Movement of a karyophilic protein through the nuclear pores of oocytes. *J Cell Biol* 99: 2216-2222, 1984.

7. **Salina D, Bodoor K, Enarson P, Raharjo WH, Burke B.** Nuclear envelope dynamics. *Biochem Cell Biol* 79: 533-542, 2001.

8. **Goldberg MW and Allen TD.** Structural and functional organization of the nuclear envelope. *Current Opinion in Cell Biology* 7: 301-309, 1995.

9. **Gerace L and Foisner R.** Integral membrane proteins and dynamic organization of the nuclear envelope. *Trends in Cell Biology* 4: 127-131, 1994.

10. **Gerace L, Blum A, and Blobel G.** Immunocytochemical localization of the major polypeptides of the nuclear pore complex-lamina fraction. Interphase and mitotic distribution. *J Cell Biol* 79: 546-566, 1978.

11. **Dechat T, Pfleghaar K, Sengupta K, Shimi T, Shumaker DK, Solimando L, and Goldman RD.** Nuclear lamins: major factors in the structural organization and function of the nucleus and chromatin. *Genes & Development* 22: 832-853, 2008.

12. **Wilhelmsen K, Ketema M, Truong H, and Sonnenberg A.** KASH-domain proteins in nuclear migration, anchorage and other processes. *J Cell Sci* 119: 5021-5029, 2006.

13. **Gruenbaum Y, Wilson KL, Harel A, Goldberg M, and Cohen M.** Review: Nuclear lamins--structural proteins with fundamental functions. *Journal of Structural Biology* 129: 313-323, 2000.

14. **Davis LI.** The nuclear pore complex. *Annual Review of Biochemistry* 64: 865-896, 1995.

15. **Stewart M and Clarkson WD.** Nuclear pores and macromolecular assemblies involved in nucleocytoplasmic transport. *Current Opinion in Structural Biology* 6: 162-165, 1996.

16. **Yang Q, Rout MP, and Akey CW.** Three-dimensional architecture of the isolated yeast nuclear pore complex: functional and evolutionary implications. *Molecular Cell* 1: 223-234, 1998.

17. **Reichelt R, Holzenburg A, Buhle EL, Jr., Jarnik M, Engel A, and Aebi U.** Correlation between structure and mass distribution of the nuclear pore complex and of distinct pore complex components. *J Cell Biol* 110: 883-894, 1990.

18. **Rout MP and Blobel G.** Isolation of the yeast nuclear pore complex. *J Cell Biol* 123: 771-783, 1993.

19. **Cordes VC, Reidenbach S, and Franke WW.** High content of a nuclear pore complex protein in cytoplasmic annulate lamellae of Xenopus oocytes. *Eur J Cell Biol* 68: 240-255, 1995.

20. **Cronshaw JM, Krutchinsky AN, Zhang W, Chait BT, and Matunis MJ.** Proteomic analysis of the mammalian nuclear pore complex. *J Cell Biol* 158: 915-927, 2002.

21. **Hinshaw JE, Carragher BO, and Milligan RA.** Architecture and design of the nuclear pore complex. *Cell* 69: 1133-1141, 1992.

22. **Rout MP and Wente SR.** Pores for thought: nuclear pore complex proteins. *Trends in Cell Biology* 4: 357-365, 1994.

23. **Schwartz TU.** Modularity within the architecture of the nuclear pore complex. *Current Opinion in Structural Biology* 15: 221-226, 2005.

24. **Bayliss R, Corbett AH, and Stewart M.** The molecular mechanism of transport of macromolecules through nuclear pore complexes. *Traffic* 1: 448-456, 2000.

25. **Powers MA, Forbes DJ, Dahlberg JE, and Lund E.** The vertebrate GLFG nucleoporin, Nup98, is an essential component of multiple RNA export pathways. *J Cell Biol* 136: 241-250, 1997.

26. **Kraemer D, Wozniak RW, Blobel G, and Radu A.** The human CAN protein, a putative oncogene product associated with myeloid leukemogenesis, is a nuclear pore complex protein that faces the cytoplasm. *Proc Natl Acad Sci* 91: 1519–1523, 1994.

27. **Wu J, Matunis MJ, Kraemer D, Blobel G, and Coutavas E.** Nup358, a cytoplasmically exposed nucleoporin with peptide repeats, Ran-GTP binding sites, Zinc fingers, a cyclophilin a homologous domain, and a leucine-rich region. *J Biol Chem* 270: 14209-14213, 1995.

28. **Bodoor K, ShaikhS, Enarson P, Chowdhury S, Salina D, Raharjo WH, and Burke B.** Function and assembly of nuclear pore complex proteins. *Biochem Cell Biol* 77: 321-329, 1999.

29. **D'Angelo MA and Hetzer MW.** Structure, dynamics and function of nuclear pore complexes. *Trends in Cell Biology* 18: 456-466, 2008.

30. **Tran EJ and Wente SR.** Dynamic nuclear pore complexes: life on the edge. *Cell* 125: 1041-1053, 2006.

31. **Beck M, Forster F, Ecke M, Plitzko JM, Melchior F, Gerisch G, Baumeister W, and Medalia O.** Nuclear pore complex structure and dynamics revealed by cryoelectron tomography. *Science* 306: 1387-1390, 2004.

32. **Rabut G, Doye V, and Ellenberg J.** Mapping the dynamic organization of the nuclear pore complex inside single living cells. *Nat Cell Biol* 11: 1114-1121, 2004.

33. **Hetzer MW, Walther TC, and Mattaj IW.** Pushing the envelope: structure, function, and dynamics of the nuclear periphery. *Annual Review of Cell and Developmental Biology* 21: 347-380, 2005.

34. **Paulillo SM, Phillips EM, Köser J, Sauder U, Ullman KS, Powers MA, and Fahrenkrog B.** Nucleoporin domain topology is linked to the transport status of the nuclear pore complex. *Journal of Molecular Biology* 351: 784-798, 2005.

35. **Fahrenkrog B, Maco B, Fager AM, Köser J, Sauder U, Ullman KS, and Aebi U.** Domain-specific antibodies reveal multiple-site topology of Nup153 within the nuclear pore complex. *Journal of Structural Biology* 140: 254-267, 2002.

36. **Nakielny S, Shaikh S, Burke B, and Dreyfuss G.** Nup153 is an M9-containing mobile nucleoporin with a novel Ran-binding domain. *EMBO J* 18: 1982-1995, 1999.

37. **Griffis ER, Altan N, Lippincott-Schwartz J, and Powers MA.** Nup98 is a mobile nucleoporin with transcription-dependent dynamics. *Mol Biol Cell* 13: 1282-1297, 2002.

38. **Paine PL, Moore LC, and Horowitz SB.** Nuclear envelope permeability. *Nature* 13: 109-114, 1975.

39. **Keminer O and Peters R.** Permeability of single nuclear pores. *Biophysical Journal* 77: 217-228, 1999.

40. **Wagner P, Kunz J, Koller A, and Hall MN.** Active transport of proteins into the nucleus. *FEBS Letters* 275: 1-5, 1990.

41. **Ribbeck K and Görlich D.** Kinetic analysis of translocation through nuclear pore complexes. *EMBO J* 20: 1320–1330, 2001.

42. **De Robertis EM, Longthorne RF, and Gurdon JB.** Intracellular migration of nuclear proteins in Xenopus oocytes. *Nature* 16: 254-256, 1978.

43. **Dingwall C, Sharnick SV, and Laskey RA.** A polypeptide domain that specifies migration of nucleoplasmin into the nucleus. *Cell* 30: 449-458, 1982.

44. **Peters R.** Translocation through the nuclear pore complex: selectivity and speed by reduction of dimensionality. *Traffic* 6: 421-427, 2005.

45. **Sorokin AV, Kim ER, and Ovchinnikov LP.** Nucleocytoplasmic transport of proteins. *Biochemistry (Mosc)* 72: 1439-1457, 2007.

46. **Panté N and Kann M.** Nuclear pore complex is able to transport macromolecules with diameters of ~39 nm. *Mol Biol Cell* 13: 425-434, 2002.

47. **Görlich D and Mattaj IW.** Nucleocytoplasmic transport. *Science* 271(5255): 1513-1518, 1996.

48. **Kuersten S, Ohno M, and Mattaj IW.** Nucleocytoplasmic transport: Ran, β and beyond. *Trends in Cell Biology* 11: 497-503, 2001.

49. **Gama-Carvalho M and Carmo-Fonseca M.** The rules and roles of nucleocytoplasmic shuttling proteins. *FEBS Letters* 498: 157-163, 2001.

50. **Feldherr CM and Akin D.** The location of the transport gate in the nuclear pore complex. *J Cell Sci* 110: 3065-3070, 1997.

51. **Hegde RS and Bernstein HD**. The surprising complexity of signal sequences. *Trends Biochem. Sci.* 31: 563-571, 2006.

52. **Kalderon D, Richardson WD, Markham AF, andSmith AE.** Sequence requirements for nuclear location of simian virus 40 large-T antigen. *Nature* 11: 33-38, 1984.

53. **Kalderon D, Roberts BL, Richardson WD, and Smith AE.** A short amino acid sequence able to specify nuclear location. *Cell* 39: 499-509, 1984.

54. **Robbins J, Dilwortht SM, Laskey RA, and Dingwall C.** Two interdependent basic domains in nucleoplasmin nuclear targeting sequence: Identification of a class of bipartite nuclear targeting sequence. *Cell* 64: 615-623, 1991.

55. **Christophe D, Christophe-Hobertus C, and Pichon B.** Nuclear targeting of proteins: how many different signals? *Cellular Signalling* 12: 337-341, 2000.

56. **Palmeri D and Malim MH.** Importin β can mediate the nuclear import of an arginine-rich nuclear localization signal in the absence of importin alpha. *Mol Cell Biol* 19: 1218-1225, 1999.

57. **Truant R and Cullen BR.** The arginine-rich domains present in human immunodeficiency virus type 1 tat and rev function as direct importin β - dependent nuclear localization signals. *Mol Cell Biol* 19: 1210-1217, 1999.

58. **Boulikas T.** Putative nuclear localization signals (NLS) in protein transcription factors. *J Cell Biochem* 55: 32-58, 1994.

59. **Pollard VW, Michael WM, Nakielny S, Siomi MC, Wang F, and Dreyfuss G.** A novel receptor-mediated nuclear protein import pathway. *Cell* 86: 985-994, 1996.

60. **Hall MN, Craik C, and Hiraoka Y.** Homeodomain of yeast repressor alpha 2 contains a nuclear localization signal. *Proc Natl Acad Sci* 87: 6954-6958, 1990.

61. **Jans DA, Xiao CY, and Lam MH.** Nuclear targeting signal recognition: a key control point in nuclear transport? *BioEssays* 22: 532-544, 2000.

62. **Dang CV and Lee WM.** Identification of the human c-myc protein nuclear translocation signal. *Mol Cell Biol* 8: 4048-4054, 1988.

63. **Makkerh JPS, Dingwall C, and Laskey RA.** Comparative mutagenesis of nuclear localization signals reveals the importance of neutral and acidic amino acids. *Current Biology* 6: 1025-1027, 1996.

64. **Nadler SG, Tritschler D, Haffar OK, Blake J, Bruce AG, and Cleaveland JS.** Differential expression and sequence-specific interaction of karyopherin alpha with nuclear localization sequences. *J Biol Chem* 272: 4310-4315, 1997.

65. **Briggs LJ, Stein D, Goltz J, Corrigan VC, Efthymiadis A, Hubner S, and Jans DA.** The cAMP-dependent protein kinase site (Ser312) enhances dorsal nuclear import through facilitating nuclear localization sequence/importin interaction. *J Biol Chem* 273: 22745-22752, 1998.

66. **Hood JK and Silver PA.** In or out? Regulating nuclear transport. *Current Opinion in Cell Biology* 11: 241-247, 1999.

67. **Henkel T, Zabel U, van Zee K, Müller JM, Fanning E, and Baeuerle PA.** Intramolecular masking of the nuclear location signal and dimerization domain in the precursor for the p50 NF-kappa B subunit. *Cell* 68: 1121-1133, 1992.

68. **Wen W, Meinkotht JL, Tsien RY, and Taylor SS.** Identification of a signal for rapid export of proteins from the nucleus. *Cell* 82: 463-473, 1995.

69. **Fischer U, Huber J, Boelens WC, Mattajt LW, and Lührmann R.** The HIV-1 Rev activation domain is a nuclear export signal that accesses an export pathway used by specific cellular RNAs. *Cell* 82: 475-483, 1995.

70. **Fried H and Kutay U.** Nucleocytoplasmic transport: taking an inventory. *Cellular and Molecular Life Sciences (CMLS)* 60: 1659-1688, 2003.

71. **la Cour T, Gupta R, Rapacki K, Skriver K, Poulsen FM, and Brunak S.** NESbase version 1.0: a database of nuclear export signals. *Nucl Acids Res* 31: 393-396, 2003.

72. **Adam SA.** Transport pathways of macromolecules between the nucleus and the cytoplasm. *Current Opinion in Cell Biology* 11: 402-406, 1999.

73. **Mosammaparast N and Pemberton LF.** Karyopherins: from nuclear-transport mediators to nuclear-function regulators. *Trends in Cell Biology* 14: 547-556, 2004.

74. **Kutay U, Hartmann E, Treichel N, Calado A, Carmo-Fonseca M, Prehn S, Kraft R, Gorlich D, and Bischoff FR.** Identification of two novel RanGTP-binding proteins belonging to the importin β superfamily. *J Biol Chem* 275: 40163-40168, 2000.

75. **Strom AC and Weis K.** Importin-β-like nuclear transport receptors. *Genome Biology* 2: 3008.1 - 3008.9, 2001.

76. **Cingolani G, Petosa C, Weis K, and Muller CW.** Structure of importin-β bound to the IBB domain of importin-alpha. *Nature* 399: 221-229, 1999.

77. **Chook YM and Blobel G.** Structure of the nuclear transport complex karyopherin-β2-Ran x GppNHp. *Nature* 399: 230-237, 1999.

78. **Kutay U, Izaurralde E, Bischoff FR, Mattaj IW, and Görlich D.** Dominant-negative mutants of importin-β block multiple pathways of import and export through the nuclear pore complex. *EMBO J* 16: 1153-1163, 1997.

79. **Chi NC and Adam SA.** Functional domains in nuclear import factor p97 for binding the nuclear localization sequence receptor and the nuclear pore. *Mol Biol Cell* 8: 945-956, 1997.

80. **Bayliss R, Littlewood T, and Stewart M.** Structural basis for the interaction between FxFG nucleoporin repeats and importin-β in nuclear trafficking. *Cell* 102: 99-108, 2000.

81. **Cingolani G, Bednenko J, Gillespie MT, and Gerace L.** Molecular basis for the recognition of a non classical nuclear localization signal by importin β. *Molecular Cell* 10: 1345-1353, 2002.

82. **Lee SJ, Sekimoto T, Yamashita E, Nagoshi E, Nakagawa A, Imamoto N, Yoshimura M, Sakai H, Chong KT, Tsukihara T, and Yoneda Y.** The structure of importin-β Bound to SREBP-2: Nuclear Import of a Transcription Factor. *Science* 302: 1571-1575, 2003.

83. **Görlich D, Vogel F, Mills AD, Hartmann E, and Laskey RA.** Distinct functions for the two importin subunits in nuclear protein import. *Nature* 377: 246-248, 1995.

84. **Huber J, Cronshagen U, Kadokura M, Marshallsay C, Wada T, Sekine M, and Lührmann R.** Snurportin1, an m3G-cap-specific nuclear import receptor with a novel domain structure. *EMBO J* 17: 4114-4126, 1998.

85. **Jullien D, Görlich D, Laemmli UK, and Adachi Y.** Nuclear import of RPA in Xenopus egg extracts requires a novel protein XRIPalpha but not importin alpha. *EMBO J* 18: 4348-4358, 1999.

86. **Lam MHC, Briggs LJ, Hu W, Martin TJ, Gillespie MT, and Jans DA.** Importin β recognizes parathyroid hormone-related protein with high affinity and mediates its nuclear import in the absence of importin alpha. *J Biol Chem* 274: 7391-7398, 1999.

87. **Kodiha M, Chu A, Matusiewicz N, and Stochaj U.** Multiple mechanisms promote the inhibition of classical nuclear import upon exposure to severe oxidative stress. *Cell Death Differ* 11: 862-874, 2004.

88. **Conti E, Müller CW, and Stewart M.** Karyopherin flexibility in nucleocytoplasmic transport. *Current Opinion in Structural Biology* 16: 237-244, 2006.

89. **Fornerod M and Ohno M.** Exportin-mediated nuclear export of proteins and ribonucleoproteins. *Results Probl Cell Differ* 35: 67-91, 2002.

90. **Kutay U and Güttinger S.** Leucine-rich nuclear-export signals: born to be weak. *Trends in Cell Biology* 15: 121-124, 2005.

91. **Bohnsack MT, Regener K, Schwappach B, Saffrich R, Paraskeva E, Hartmann E, Görlich D.** Exp5 exports eEF1A via tRNA from nuclei and synergizes with other transport pathways to confine translation to the cytoplasm. *EMBO J* 21: 6205-6215, 2002.

92. **Kutay U, Lipowsky G, Izaurralde E, Bischoff FR, Schwarzmaier P, Hartmann E, and Görlich D.** Identification of a tRNA-Specific Nuclear Export Receptor. *Molecular Cell* 1: 359-369, 1998.

93. **Fornerod M, Ohno M, Yoshida M, and Mattaj IW.** CRM1 is an export receptor for leucine-rich nuclear export signals. *Cell* 90: 1051-1060, 1997.

94. **Johnson AW, Lund E, and Dahlberg J.** Nuclear export of ribosomal subunits. *Trends in Biochemical Sciences* 27: 580-585, 2002.

95. **Englmeier L, Fornerod M, Bischoff FR, Petosa C, Mattaj IW, and Kutay U.** RanBP3 influences interactions between CRM1 and its nuclear protein export substrates. *EMBO Rep* 2: 926-932, 2001.

96. **Kutay U, Bischoff FR, Kostka S, Kraft R, and Görlich D.** Export of importin alpha from the nucleus is mediated by a specific nuclear transport factor. *Cell* 90: 1061-1071, 1997.

97. **Goldfarb DS, Corbett AH, Mason DA, Harreman MT, and Adam SA.** Importin alpha: a multipurpose nuclear-transport receptor. *Trends in Cell Biology* 14: 505-514, 2004.

98. **Chook Y and Blobel G.** Karyopherins and nuclear import. *Current Opinion in Structural Biology* 11: 703-715, 2001.

99. **Conti E, Uy M, Leighton L, Blobel G, and Kuriyan J.** Crystallographic analysis of the recognition of a nuclear localization signal by the nuclear import factor karyopherin alpha. *Cell* 94: 193-204, 1998.

100. **Conti E and Kuriyan J.** Crystallographic analysis of the specific yet versatile recognition of distinct nuclear localization signals by karyopherin alpha. *Structure* 8: 329-338, 2000.

101. **Fontes MR, Teh T, and Kobe B.** Structural basis of recognition of monopartite and bipartite nuclear localization sequences by mammalian importin-alpha. *Journal of Molecular Biology* 297: 1183-1194, 2000.

102. **Moroianu J Blobel G, and Radu A.** The binding site of karyopherin alpha for karyopherin β overlaps with a nuclear localization sequence. *Proc Natl Acad Sci* 93: 6572-6576, 1996.

103. **Kobe B.** Autoinhibition by an internal nuclear localization signal revealed by the crystal structure of mammalian importin alpha. *Nat Struct Biol* 6: 388-397, 1999.

104. **Fanara P, Hodel MR, Corbett AH, and Hodel AE.** Quantitative analysis of nuclear localization signal (NLS)-importin alpha interaction through fluorescence depolarization. Evidence for auto-inhibitory regulation of NLS binding. *J Biol Chem* 275: 21218-21223, 2000.

105. **Matsuura Y, Lange A, Harreman MT, Corbett AH, Stewart M.** Structural basis for Nup2p function in cargo release and karyopherin recycling in nuclear import. *EMBO J* 22: 5358-5369, 2003.

106. **Stochaj U and Rother KL.** Nucleocytoplasmic trafficking of proteins: With or without Ran? *BioEssays* 21: 579-589, 1999.

107. **Melchior F, Paschal B, Evans J, and Gerace L.** Inhibition of nuclear protein import by nonhydrolyzable analogues of GTP and identification of the small GTPase Ran/TC4 as an essential transport factor [published erratum appears in J Cell Biol 1994 Jan;124(1-2):217]. *J Cell Biol* 123: 1649-1659, 1993.

108. **Moore MS and Blobel G.** The GTP-binding protein Ran/TC4 is required for protein import into the nucleus. *Nature* 365: 661-663, 1993.

109. **Macara IG.** Transport into and out of the Nucleus. *Microbiol Mol Biol Rev* 65: 570-594, 2001.

110. **Rexach M and Blobel G.** Protein import into nuclei: association and dissociation reactions involving transport substrate, transport factors, and nucleoporins. *Cell* 83: 683-692, 1995.

111. **Görlich D, Panté N, Kutay U, Aebi U, and Bischoff FR.** Identification of different roles for RanGDP and RanGTP in nuclear protein import. *EMBO J* 15: 5584-5594, 1996.

112. **Nicolas FJ, Zhang C, Hughes M, Goldberg M, Watton S, and Clarke P.** Xenopus Ran-binding protein 1: molecular interactions and effects on nuclear assembly in Xenopus egg extracts. *J Cell Sci* 110: 3019-3030, 1997.

113. **Moore MS.** Ran and nuclear transport. *J Biol Chem* 273: 22857-22860, 1998.

114. **Izaurralde E, Kutay U, von Kobbe C, Mattaj IW, and Görlich D.** The asymmetric distribution of the constituents of the Ran system is essential for transport into and out of the nucleus. *1997* 16: 6535-6547, 1997.

115. **Bischoff FR, Klebe C, Kretschmer J, Wittinghofer A, and Ponstingl H.** RanGAP1 induces GTPase activity of nuclear Ras-related Ran. *Proc Natl Acad Sci* 91: 2587-2591, 1994.

116. **Becker J, Melchior F, Gerke V, Bischoff FR, Ponstingl H, and Wittinghofer A.** RNA1 encodes a GTPase-activating protein specific for Gsp1p, the Ran/TC4 homologue of Saccharomyces cerevisiae. *J Biol Chem* 270: 11860-11

117. **Mahajan R, Delphin C, Guan T, Gerace L, and Melchior F.** A small ubiquitin-related polypeptide involved in targeting RanGAP1 to nuclear pore complex protein RanBP2. *Cell* 88: 97-107, 1997.

118. **Bischoff FR, Krebber H, Smirnova E, Dong W, and Ponstingl H.** Co-activation of RanGTPase and inhibition of GTP dissociation by Ran-GTP binding protein RanBP1. *EMBO J* 14: 705-715, 1995.

119. **Kunzler M, Gerstberger T, Stutz F, Bischoff FR, and Hurt E.** Yeast Ran-binding protein 1 (Yrb1) shuttles between the nucleus and cytoplasm and is exported from the nucleus via a CRM1 (XPO1)-dependent pathway. *Mol Cell Biol* 20: 4295-4308, 2000.

120. **Plafker K and Macara IG.** Facilitated nucleocytoplasmic shuttling of the Ran binding protein RanBP1. *Mol Cell Biol* 20: 3510-3521, 2000.

121. **Bischoff FR and Ponstingl H.** Catalysis of guanine nucleotide exchange on Ran by the mitotic regulator RCC1. *Nature* 354: 80-82, 1991.

122. **Bischoff FR and Ponstingl H.** Mitotic regulator protein RCC1 is complexed with a nuclear ras-related polypeptide. *Proc Natl Acad Sci* 88: 10830-10834, 1991.

123. **Nemergut ME and Macara IG.** Nuclear import of the Ran exchange factor, RCC1, Is Mediated by at Least Two Distinct Mechanisms. *J Cell Biol* 149: 835-850, 2000.

124. **Nemergut ME, Lindsay ME, Brownawell AM, and Macara IG.** Ran-binding protein 3 links crm1 to the Ran guanine nucleotide exchange factor. *J Biol Chem* 277: 17385-17388, 2002.

125. **Nemergut ME, Mizzen CA, Stukenberg T, Allis CD, and Macara IG.** Chromatin docking and exchange activity enhancement of RCC1 by Histones H2A and H2B. *Science* 292: 1540-1543, 2001.

126. **Corbett AH, Koepp DM, Schlenstedt G, Lee MS, Hopper AK, and Silver PA.** Rna1p, a Ran/TC4 GTPase activating protein, is required for nuclear import. *J Cell Biol* 130: 1017-1026, 1995.

127. **Schlenstedt G Wong DH, Koepp DM, and Silver PA.** Mutants in a yeast Ran binding protein are defective in nuclear transport. *EMBO J* 1995: 5367-5378, 1995.

128. **Ribbeck K, Lipowsky G, Kent HM, Stewart M, and Görlich D.** NTF2 mediates nuclear import of Ran. *EMBO J* 17: 6587-6598

129. **Rout MP, Aitchison JD, Magnasco MO, and Chait BT.** Virtual gating and nuclear transport: the hole picture. *Trends in Cell Biology* 13: 622-628, 2003.

130. **Lage R, Diéguez C, Vidal-Puig A, and López M.** AMPK: a metabolic gauge regulating whole-body energy homeostasis. *Trends in Molecular Medicine* 14: 539-549, 2008.

131. **Hardie DG.** AMPK: a key regulator of energy balance in the single cell and the whole organism. *Int J Obe* 8: S7-S12, 2008.

132. **Hardie DG.** Minireview: The AMP-activated protein kinase cascade: the key sensor of cellular energy status. *Endocrinology* 144: 5179-5183, 2003.

133. **Hardie DG.** Roles of the AMP-activated/SNF1 protein kinase family in the response to cellular stress. *Biochem Soc Symp* 64: 13-27, 1999.

134. **Hardie DG and Pan DA.** Regulation of fatty acid synthesis and oxidation by the AMP-activated protein kinase. *Biochem Soc Trans* 30: 1064-1070, 2002.

135. **Towler MC and Hardie DG.** AMP-activated protein kinase in metabolic control and insulin signaling. *Circ Res* 100: 328-341, 2007.

136. **Holmes BF, Kurth-Kraczek EJ, and Winder WW.** Chronic activation of 5'-AMP-activated protein kinase increases GLUT-4, hexokinase, and glycogen in muscle. *J Appl Physiol* 87: 1990-1995, 1999.

137. **Viollet B, Lantier L, Devin-Leclerc J, Hebrard S, Amouyal C, Mounier R, Foretz M, and Andreelli F.** Targeting the AMPK pathway for the treatment of type 2 diabetes. *Front Biosci* 14: 3380-3400, 2009.

138. **Scott JW, Oakhill J, and van Denderen BJ.** AMPK/SNF1 structure: a menage a trois of energy-sensing. *Front Biosci* 14: 596-610, 2009.

139. **Witczak C, Sharoff C, and Goodyear L**. AMP-activated protein kinase in skeletal muscle: From structure and localization to its role as a master regulator of cellular metabolism. *Cellular and Molecular Life Sciences (CMLS)* 65: 3737-3755, 2008.

140. **Hardie DG.** AMP-activated/SNF1 protein kinases: conserved guardians of cellular energy. *Nat Rev Mol Cell Biol* 8: 774-785, 2007.

141. **Sanders MJ, Grondin PO, Hegarty BD, Snowden MA, and Carling D.** Investigating the mechanism for AMP activation of the AMP-activated protein kinase cascade. *Biochem J* 403: 139-148, 2007.

142. **McGee SL, Howlett KF, Starkie RL, Cameron-Smith D, Kemp BE, and Hargreaves M.** Exercise increases nuclear AMPK alpha in human skeletal muscle. *Diabetes* 52: 926-928, 2003.

143. **Ritossa F.** A new puffing pattern induced by temperature shock and DNP in drosophila. *Cellular and Molecular Life Sciences (CMLS)* 18: 571-573, 1962.

144. **Freeman ML, Borrelli MJ, Meredith MJ, and Lepock JR.** On the path to the heat shock response: destabilization and formation of partially folded protein intermediates, a consequence of protein thiol modification. *Free Radical Biology and Medicine* 26: 737-745, 1999.

145. **Tavaria M, Gabriele T, Kola I, and Anderson RL.** A hitchhiker's guide to the human Hsp70 family. *Cell Stress Chaperones* 1: 23-28, 1996.

146. **Vos MJ, Hageman J, Carra S, Kampinga HH.** Structural and functional diversities between members of the human HSPB, HSPH, HSPA, and DNAJ chaperone families. *Biochemistry* 47(27):7001-11, 2008

147. **Young JC, Agashe VR, Siegers K, and Hartl FU.** Pathways of chaperone-mediated protein folding in the cytosol. *Nat Rev Mol Cell Biol* 5: 781-791, 2004.

148. **Becker J and Craig EA.** Heat-shock proteins as molecular chaperones. *European Journal of Biochemistry* 219: 11-23, 1994.

149. **Meimaridou E, Gooljar SB, and Chapple JP.** From hatching to dispatching: the multiple cellular roles of the Hsp70 molecular chaperone machinery. *J Mol Endocrinol* 42: 1-9, 2009.

150. **Nollen EAA and Morimoto RI.** Chaperoning signaling pathways: molecular chaperones as stress-sensing `heat shock' proteins. *J Cell Sci* 115: 2809-2816, 2002.

151. **Agashe VR and Hartl FU.** Roles of molecular chaperones in cytoplasmic protein folding. *Seminars in Cell & Developmental Biology* 11: 15-25, 2000.

152. **Mayer M and Bukau B.** Hsp70 chaperones: Cellular functions and molecular mechanism. *Cellular and Molecular Life Sciences (CMLS)* 62: 670-684, 2005.

153. **Pilon M and Schekman R.** Protein translocation: how hsp70 pulls it off. *Cell* 97: 679-682, 1999.

154. **Zhu X, Zhao X, Burkholder WF, Gragerov A, Ogata CM, Gottesman ME, and Hendrickson WA.** Structural analysis of substrate binding by the molecular chaperone DnaK. *1996* 272: 1606-1614, 1996.

155. **Morshauser RC, Hu W, Wang H, Pang Y, Flynn GC, and Zuiderweg ERP.** High-resolution solution structure of the 18 kDa substrate-binding domain of the mammalian chaperone protein Hsc70. *Journal of Molecular Biology* 289: 1387-1403, 1999.

156. **Mayer MP, Schröder H, Rüdiger S, Paal K, Laufen T, and Bukau B.** Multistep mechanism of substrate binding determines chaperone activity of Hsp70. *Nat Struct Biol* 7: 586-593, 2000.

157. **Kelley WL.** Molecular chaperones: How J domains turn on Hsp70s. *Current Biology* 9: R305-R308, 1999.

158. **Qiu X, Shao Y, Miao S, and Wang L.** The diversity of the DnaJ/Hsp40 family, the crucial partners for Hsp70 chaperones. *Cellular and Molecular Life Sciences (CMLS)* 63: 2560-2570, 2006.

159. **Höfeld J, Minami Y, and Hartl F-U.** Hip, a novel cochaperone involved in the eukaryotic hsc70/hsp40 reaction cycle. *Cell* 83: 589-598, 1995.

160. **Alberti S, Esser C, and Höhfeld J.** BAG-1--a nucleotide exchange factor of Hsc70 with multiple cellular functions. *Cell Stress Chaperones* 8: 225-231, 2003.

161. **Ballinger CA, Connell P, Wu Y, Hu Z, Thompson LJ, Yin L-Y, and Patterson C.** Identification of CHIP, a novel tetratricopeptide repeat-containing protein that interacts with heat shock proteins and negatively regulates chaperone functions. *Mol Cell Biol* 19: 4535-4545, 1999.

162. **McDonough H and Patterson C.** CHIP: a link between the chaperone and proteasome systems. *Cell Stress Chaperones* 8: 303-308, 2003.

163. **Murata S, Chiba T, and Tanaka K.** CHIP: a quality-control E3 ligase collaborating with molecular chaperones. *The International Journal of Biochemistry & Cell Biology* 35: 572-578, 2003.

164. **Nicolet CM and Craig EA.** Isolation and characterization of STI1, a stress-inducible gene from Saccharomyces cerevisiae. *Mol Cell Biol* 9: 3638-3646, 1989.

165. **Odunuga OO, Longshaw VM, and Blatch GL.** Hop: more than an Hsp70/Hsp90 adaptor protein. *BioEssays* 26: 1058-1068, 2004.

166. **Smith DF, Sullivan WP, Marion TN, Zaitsu K, Madden B, McCormick DJ, and Toft DO.** Identification of a 60-kilodalton stress-related protein, p60, which interacts with hsp90 and hsp70. *Mol Cell Biol* 13: 869-876, 1993.

167. **Scheufler C, Brinker A, Bourenkov G, Pegoraro S, Moroder L, Bartunik H, Hartl FU, and Moarefi I.** Structure of TPR domain-peptide complexes: critical elements in the assembly of the Hsp70-Hsp90 multichaperone machine. *Cell* 101: 199-210, 2000.

168. **Chen S and Smith DF.** Hop as an adaptor in the heat shock protein 70 (Hsp70) and Hsp90 chaperone machinery. *J Biol Chem* 273: 35194-35200, 1998

169. **Demand J, Luders J, and Hohfeld J.** The carboxy-terminal domain of hsc70 provides binding sites for a distinct set of chaperone cofactors. *Mol Cell Biol* 18: 2023-2028, 1998.

170. **Gebauer M, Zeiner M, and Gehring U.** Proteins interacting with the molecular chaperone hsp70/hsc70: physical associations and effects on refolding activity. *FEBS Letters* 417: 109-113

171. **Johnson BD, Schumacher RJ, Ross ED, and Toft DO.** Hop modulates hsp70/hsp90 interactions in protein folding. *J Biol Chem* 273: 3679-3686, 1998.

172. **Prodromou C, Siligardi G, O'Brien R, Woolfson DN, Regan L, Panaretou B, Ladbury JE, Piper PW and Pearl LH.** Regulation of Hsp90

ATPase activity by tetratricopeptide repeat (TPR)-domain co-chaperones. *EMBO J* 18: 754-762 1999.

173. **Gross M and Hessefort S.** Purification and characterization of a 66-kDa Protein from rabbit reticulocyte lysate which promotes the recycling of Hsp 70. *J Biol Chem* 271: 16833-16841, 1996.

174. **Pratt WB and Toft DO.** Regulation of signaling protein function and trafficking by the hsp90/hsp70-based chaperone machinery. *Experimental Biology and Medicine* 228: 111-133, 2003.

175. **Murphy PJ, Kanelakis KC, Galigniana MD, Morishima Y, and Pratt WB.** Stoichiometry, abundance, and functional significance of the hsp90/hsp70-based multiprotein chaperone machinery in reticulocyte lysate. *J Biol Chem* 276: 30092-30098, 2001.

176. **Frydman J and Höhfeld J.** Chaperones get in touch: the Hip-Hop connection. *Trends in Biochemical Sciences* 22: 87-92, 1997.

177. **Finkel T and Holbrook NJ.** Oxidants, oxidative stress and the biology of ageing. *Nature* 408: 239-247, 2000.

178. **Jennifer L. Martindale NJH.** Cellular response to oxidative stress: Signaling for suicide and survival. *Journal of Cellular Physiology* 192: 1-15, 2002.

179. **Cadenas E and Davies KJA.** Mitochondrial free radical generation, oxidative stress, and aging. *Free Radical Biology and Medicine* 29: 222-230, 2000.

180. **Rhee SG, Bae YS, Lee S-R, and Kwon J.** Hydrogen peroxide: A key messenger that modulates protein phosphorylation through cysteine oxidation. *Sci STKE* 2000: pe1-, 2000.

181. **Dhalla NS, Elmoselhi AB, Hata T, and Makino N.** Status of myocardial antioxidants in ischemia-reperfusion injury. *Cardiovasc Res* 47: 446-456, 2000.

182. **Kumar D, Lou H, and Singal PK.** Oxidative stress and apoptosis in heart dysfunction. *Herz* 27: 662-668, 2002.

183. **Droge W.** Free radicals in the physiological control of cell function. *Physiol Rev* 82: 47-95, 2002.

184. **Mariani E, Polidori MC, Cherubini A, and Mecocci P.** Oxidative stress in brain aging, neurodegenerative and vascular diseases: An overview. *Journal of Chromatography B* 827: 65-75, 2005.

185. **Crack PJ and Taylor JM.** Reactive oxygen species and the modulation of stroke. *Free Radical Biology and Medicine* 38: 1433-1444, 2005.

186. **Sitia R and Molteni SN.** Stress, protein (mis)folding, and signaling: The redox connection. *Sci STKE* 2309: pe27, 2004.

187. **Townsend DM, Tew KD, and Tapiero H.** The importance of glutathione in human disease. *Biomedecine & Pharmacotherapy* 57: 145-155, 2003.

188. **Bizzozero OA, Ziegler JL, De Jesus G, and Bolognani F.** Acute depletion of reduced glutathione causes extensive carbonylation of rat brain proteins. *Journal of Neuroscience Research* 83: 656-667, 2006.

189. **Cruz-Aguado R, Almaguer-Melian W, Díaz CM, Lorigados L, and Bergado J.** Behavioral and biochemical effects of glutathione depletion in the rat brain. *Brain Research Bulletin* 55: 327-333, 2001.

190. **Kaur P, Kalia S, and Bansal MP.** Effect of diethyl maleate induced oxidative stress on male reproductive activity in mice: Redox active enzymes and transcription factors expression. *Molecular and Cellular Biochemistry* 291: 55-61, 2006.

191. **Esposito F, Russo L, Chirico G, Ammendola R, Russo T, and Cimino F .** Regulation of p21 waf1/cip1 expression by intracellular redox conditions. *IUBMB Life* 52: 67-70, 2001.

192. **Harel A and Forbes DJ.** Importin B: Conducting a much larger cellular symphony. *Molecular Cell* 16: 319-330, 2004.

193. **Matsuura Y and Stewart M.** Structural basis for the assembly of a nuclear export complex. *Nature* 432: 872-877, 2004.

194. **Otis KO, Thompson KR, and Martin KC.** Importin-mediated nuclear transport in neurons. *Current Opinion in Neurobiology* 16: 329-335, 2006.

195. **Behrens P, Brinkmann U, and Wellmann A.** CSE1L/CAS: Its role in proliferation and apoptosis. *Apoptosis* 8: 39-44, 2003.

196. **Bastos R, Lin A, Enarson M, and Burke B.** Targeting and function in mRNA export of nuclear pore complex protein Nup153. *J Cell Biol* 134: 1141-1156, 1996.

197. **Moore MS.** Npap60: a new player in nuclear protein import. *Trends in Cell Biology* 13: 61-64, 2003.

198. **Stewart M and Matsuura Y.** Nup50/Npap60 function in nuclear protein import complex disassembly and importin recycling. *EMBO J* 24: 3681-3689, 2005.

199. **Hutten S and Kehlenbach RH.** CRM1-mediated nuclear export: to the pore and beyond. *Trends in Cell Biology* 17: 193-201, 2007.

200. **Liu H-l, Chen Y, Cui G-h, Wu Q-l, He J, Chen W-h, and Zhou J-f.** Deguelin regulates nuclear pore complex proteins Nup98 and Nup88 in U937 cells in vitro. *Acta Pharmacol Sin* 26: 1265-1273, 2005.

201. **Stochaj U, Rassadi R, and Chiu J.** Stress-mediated inhibition of the classical nuclear protein import pathway and nuclear accumulation of the small GTPase Gsp1p. *FASEB J*: 99-0751fje, 2000.

202. **Chu A, Matusiewicz N, and Stochaj U.** Heat-induced nuclear accumulation of hsc70 proteins is regulated by phosphorylation and inhibited in confluent cells. *FASEB J*: 00-0680fje, 2001.

203. **Miyamoto Y, Saiwaki T, Yamashita J, Yasuda Y, Kotera I, Shibata S, Shigeta M, Hiraoka Y, Haraguchi T, and Yoneda Y.** Cellular stresses induce the nuclear accumulation of importin alpha and cause a conventional nuclear import block. *J Cell Biol* 165: 617-623, 2004.

204. **Boyland E and Chasseaud LF.** Enzyme-catalysed conjugations of glutathione with unsaturated compounds. *Biochem J* 104: 95-102, 1967.

205. **Plummer JL, Smith BR, Sies H, Bend JR, and William BJ.** Chemical depletion of glutathione in vivo. *Methods in Enzymology*: Academic Press, 1981, p. 50-59.

206. **Chatterjee S and Stochaj U.** Diffusion of proteins across the nuclear envelope of HeLa cells. *Biotechniques* 24: 668-674, 1998.

207. **Carey KL, Richards SA, Lounsbury KM, and Macara IG.** Evidence using a green fluorescent protein-glucocorticoid receptor chimera that the Ran/TC4 GTPase mediates an essential function independent of nuclear protein import. *J Cell Biol* 133: 985-996, 1996.

208. **Kodiha M, Chu A, Lazrak O, and Stochaj U.** Stress inhibits nucleocytoplasmic shuttling of heat shock protein hsc70. *Am J Physiol Cell Physiol* 289: C1034-1041, 2005.

209. **Cordes VC, Reidenbach S, Kohler A, Stuurman N, van Driel R, and Franke WW.** Intranuclear filaments containing a nuclear pore complex protein. *J Cell Biol* 123: 1333-1344, 1993.

210. **Kodiha M, Rassi JG, Brown CM, and Stochaj U.** Localization of AMP kinase is regulated by stress, cell density, and signaling through the MEK->ERK1/2 pathway. *Am J Physiol Cell Physiol* 293: C1427-1436, 2007.

211. **Truant R, Fridell RA, Benson ER, Herold A, and Cullen BR.** Nucleocytoplasmic shuttling by protein nuclear import factors. *Eur J Cell Biol* 77: 269-275, 1998.

212. **Staufenbiel M and Deppert W.** Preparation of nuclear matrices from cultured cells: Subfractionation of nuclei in situ. *J Cell Biol* 98: 1886-1894, 1984.

213. **Sánchez L, Kodiha M,and Stochaj U.** Monitoring the disruption of nuclear envelopes in interphase cells with GFP-β-galactosidase. *J Biomol Tech* 16: 235-238, 2005.

214. **Freedman ND and Yamamoto KR.** Importin 7 and importin alpha/importin β are nuclear import receptors for the glucocorticoid receptor. *Mol Biol Cell* 15: 2276-2286, 2004.

215. **Wang W, Yang X, Kawai T, de Silanes IL, Mazan-Mamczarz K, Chen P, Chook YM, Quensel C, Kohler M, and Gorospe M.** AMP-activated protein kinase-regulated phosphorylation and acetylation of importin alpha1: involvement in the nuclear import of rna-binding protein HuR. *J Biol Chem* 279: 48376-48388, 2004.

216. **Nakahara S, Hogan V, Inohara H, and Raz A.** Importin-mediated nuclear translocation of Galectin-3. *J Biol Chem* 281: 39649-39659, 2006.

217. **Miyamoto Y, Hieda M, Harreman MT, Fukumoto M, Saiwaki T, Hodel AE, Corbett AH, and Yoneda Y.** Importin alpha can migrate into the nucleus in an importin β- and Ran-independent manner. *EMBO J* 21: 5833-5842, 2002.

218. **Mattson MP and Meffert MK.** Roles for NF- kappa B in nerve cell survival, plasticity, and disease. *Cell Death Differ* 13: 852-860, 2006.

219. **Van Der Heide LP, Hoekman MFM, and Smidt MP.** The ins and outs of FoxO shuttling: mechanisms of FoxO translocation and transcriptional regulation. *Biochem J* 380: 297-309, 2004.

220. **Jaiswal AK.** Nrf2 signaling in coordinated activation of antioxidant gene expression. *Free Radical Biology and Medicine* 36: 1199-1207, 2004.

221. **Cronshaw JM and Matunis MJ.** The nuclear pore complex protein ALADIN is mislocalized in triple A syndrome. *Proceedings of the National Academy of Sciences of the United States of America* 100: 5823-5827, 2003.

222. **Hirano M, Furiya Y, Asai H, Yasui A, and Ueno S.** ALADINI482S causes selective failure of nuclear protein import and hypersensitivity to oxidative stress in triple A syndrome. *Proceedings of the National Academy of Sciences of the United States of America* 103: 2298-2303, 2006.

223. **Ashrafian H**. Cancer's sweet tooth: the Janus effect of glucose metabolism in tumorigenesis. *Lancet* 367:618-521, 2006.

224. **Birnbaum MJ.** Activating AMP-activated protein kinase without AMP. *Mol. Cell* 19:289-290, 2005.

225. **Chu A, Matusiewicz N, and Stochaj U.** Heat-induced nuclear accumulation of hsc70s is regulated by phosphorylation and inhibited in confluent cells. *FASEB J.* 10.1096/fj.00-0680jje, 2001.

226. **Dagon Y, Avraham Y, Magen I, Gertler A, Ben-Hur T, and Berry EM.** Nutritional status, cognition, and survival. *J. Biol. Chem.* 280:42142-42148, 2005.

227. **Daval M, Foufelle F, and Ferré P.** Functions of AMP-activated protein kinase in adipose tissue. *J. Physiol.* 574:55-62, 2006.

228. **Eberhardt W, Doller A, Akool E, and Pfeilschifter J.** Modulation of mRNA stability as a novel therapeutic approach. *Pharmac. & Therap.* 114:56-73, 2007.

229. **Hardie DG, Hawley SA, and Scott JW.** AMP-activated protein kinase - development of the energy sensor concept. *J. Physiol.* 574: 7-15, 2006.

230. **Harel A, and Forbes DJ.** Importin beta: conducting a much larger cellular symphony. *Mol. Cell* 16: 319-330, 2004.

231. **Hurley RL, Anderson KA, Franzone JM, Kemp BE, Means AR, and Witters LA**. The Ca2+/calmodulin protein kinase kinases are AMP-activated protein kinase kinases. *J. Biol. Chem.* 280:29060-29066, 2005

232. **Ikuta T, Kobayashi Y, and Kawajiri K.** Cell density regulates intracellular localization of aryl hydrocarbon receptor. *J. Biol. Chem.* 279:19209-19216, 2004.

233. **Kelemen BR, Hsiao, and Goueli SA.** Selective in vivo inhibition of mitogen-activated protein kinase activation using cell-permeable peptides. *J. Biol. Chem.* 277:8741-8748, 2002.

234**. Kim J, Yoon M, Choi S, Kang I, Kim S, Kim Y, Choi Y, and Ha J**. Effects of stimulation of AMP-activated protein kinase on insulin-like growth factor 1- and epidermal growth factor-dependent extracellular signal-regulated kinase pathway. *J. Biol. Chem.* 276:19102-19110, 2001.

235. **Kuda N, Matsumori N, Taoka H, Fukiwara D, Schreiner EP, Wolff B, Yoshida M, and Horinouchi S.** Leptomycin B inactivates CRM1/exportin1 by covalent modification at a cysteine residue in the central conserved region. *Proc Natl. Acad. Sci USA* 75: 9112–9117, 1999.

236. **Kutay U and Güttinger S.** Leucine-rich nuclear export signals: born to be weak. *Trends Cell Biol.* 15:121-124, 2005.

237. **Lee JH, Koh H, Kim M, Kim Y, Lee SY, Karess RE, Lee S, Shong J, Kim J, and Chung J.** Energy-dependent regulation of cell structure by AMP-activated protein kinase. *Nature* 447:1017-1021.

238. **Long YC and Zierath JR.** AMP-activated protein kinase signaling in metabolic regulation. *J. Clin. Invest.* 116:1776-1783, 2006.

239. **Marshall S.** Role of insulin, adipocyte hormones, and nutrient-sensing pathways in regulating fuel metabolism and energy homeostasis: a nutritional perspective of diabetes, obesity, and cancer. *Science's STKE* 2006, re7 (2006).

240. **Mu J, Barton ER, and Birnbaum MJ.** Selective suppression of AMP-activated protein kinase in skeletal muscle: update on 'lazy mice'. *Biochem. Soc. Trans.* 32:236-241, 2003.

241. **Quan X, Tsoulos P, Kuritzky A, Zhang R, and Stochaj U**. The carrier Msn5p/Kap142p promotes nuclear export of the hsp70 Ssa4p and relocates in response to stress. *Mol. Microbiol.* 62:592-609, 2006.

242. **Rask-Madsen C and King GL.** Mechanisms of disease: endothelial dysfunction in insulin resistance and diabetes. *Nature Clin. Practice. Endocrinol. & Metabolism* 3:46-56, 2007.

243. **Rutter GA, Silva Xavier G, and Leclerc I.** Roles of 5'-AMP-activated protein kinase (AMPK) in mammalian glucose homeostasis. *Biochem.* 375: 1-16, 2003.

244. **Salt I, Celler JW, Hawley SA, Prescott A, Woods A, Carling D, and Hardie DG.** AMP-activated protein kinase: greater AMP dependence, and preferential nuclear localization, of complexes containing the α2 isoform. *Biochem J.* 334:177-187, 1998.

245. **Sapkota GP, Kieloch A, Lizcano JM, Lain S, Arthur JSC, Williams MR, Morrice N, Deak M, and Alessi DR.** Phosphorylation of the protein kinase mutated in Peutz-Jeghers Cancer Syndrome, LKB1/STK11, at Ser^{431} by $p90^{RSK}$ and cAMP-dependent protein kinase, but not its farnesylation at Cys433, is essential for LKB1 to suppress cell growth. *J. Biol. Chem.* 276:19469-19482, 2001.

246. **Stewart M.** Molecular mechanism of the nuclear protein import cycle. *Nature Rev. Mol. Cell Biol.* 8: 195-208, 2007.

247. **Ström AC and Weis K.** Importin-beta-like transport receptors. *Genome Biol.* 2: REVIEWS3008, 2001.

248. **Valko M, Leibfritz D, Moncol J, Cronin MTD, Mazur M, and Telser J.** Free radicals and antioxidants in normal physiological functions and disease. *Intern. J. Biochem. & Cell Biol.* 39:44-84, 2007.

249. **Van der Heide L and Smidt MP.** Regulation of FoxO activity by CBP/p300-mediated acetylation. *Trends Biochem. Sci.* 30:81-86, 2005.

250. **Van Gaal LF, Mertens IL, and De Block CE.** Mechanisms linking obesity with cardiovascular disease. *Nature* 444:875-880, 2006.

251. **Viollet B, Foretz M, Guigas B, Horman S, Dentin R, Bertrand L, Hue L, and Andreelli F.** Activation of AMP-activated protein kinase in the liver: a new strategy for the management of metabolic hepatic disorders. *J. Physiol.* 574:41-53, 2006.

252. **Vogt PK, Jiang H, and Aoki M.** Triple Layer Control. Phosphorylation, acetylation and ubiquitination of FOXO proteins. *Cell Cycle* 4:908-913, 2005.

253. **Warden SM, Richardson C, O'Donnell J, Stapleton D, Kemp BE, and Witters LA.** Post-translational modifications of the β1 subunit of AMP-activated protein kinase affect enzyme activity and cellular localization. *Biochem. J.* 354:275-283, 2001.

254. **Yang W, Hong YH, Shen X, Frankowski C, Camp HS, and Leff T.** Regulation of transcription by AMP-activated protein kinase. *J. Biol. Chem.* 276:38341-38344, 2001.

255. **Beere HM.** 'The stress of dying': the role of heat shock proteins in the regulation of apoptosis. *J. Cell Sci.* 117:2641-2651.

256. **Benjamin IJ and Williams RS**. Expression and function of stress proteins in the ischemic heart. In: *The Biology of heat shock proteins and molecular chaperones*, pp 533-552. Cold Spring Harbor, NY: Cold Spring Harbor Laboratory Press, 1994

257. **Fan XC and Steitz JA.** Overexpression of HuR, a nuclear-cytoplasmic shuttling protein, increases the in vivo stability of ARE-containing mRNAs. *EMBO J.* 17: 3448-3460, 1998.

258. **Frydman J.** Folding of newly translated proteins in vivo: the role of molecular chaperones. *Ann Rev. Biochem.* 70: 6003-647, 2001.

259. **Garrido C, Gurbuxani S, Ravagnan L, and Kroemer G.** Heat shock proteins: Endogenous modulators of apoptotic cell death. *Biochim. Biophys. Res. Comm.* 286: 433-442, 2001.

260. **Hofmann W, Reichart B, Ewald A, Müller E., Schmitt I, Stauber RH, Lottspeich F, Jockusch BM, Scheer U, Hauber J, and Dabauvalle MC.** Cofactor requirements for nuclear export of Rev response element (RRE)- and constitutive transport element(CTE)-containing retroviral RNAs: an unexpected role for actin**.** *J. Cell Biol.* 152: 895-910, 2001.

261. **Jäättelä M.** Escaping death: Survival proteins in cancer. *Exp. Cell. Res.* 248: 30-43, 1999.

262. **Kiang JG, and Tsokos GC.** Heat shock protein 70 kDa: Molecular biology, biochemistry and physiology. *Pharmacol. Ther*. 80: 183-201, 1998.

263. **Kregel KC.** Heat shock proteins: modifying factors in physiological stress responses and acquired thermotolerance. *J. Appl. Physiol.* 92: 2177-2186, 2002.

264. **Kudo, N, Matsumori N, Taoka H, Fukiwara D, Schreiner EP, Wolff B, Yoshida M, and Horinouchi S.** Leptomycin B inactivates CRM1/exportin 1 by covalent modification at a cysteine residue in the central conserved region**.** *Proc. Natl. Acad. Sci. U.S.A.* 75: 9112-9117, 1999.

265. **Mandell RB and Feldherr CM**. Identification of two HSP70-related Xenopus oocyte proteins that are capable of recycling across the nuclear envelope. *J. Cell Biol.* 111**:** 1775-1783, 1990.

266. **Morcillo G, Gorab E, Tanguay RM, and Dietz JL.** Specific intranuclear distribution of hsp70 during heat shock in polytene cells. *Exp. Cell Res.* 236**:** 361-370, 1997.

267. **Nollen EAA and Morimoto RI.** Chaperoning signaling pathways: molecular chaperones as stress-sensing 'heat shock' proteins. *J. Cell Sci.* 115**:** 2809-2816, 2002.

268. **Pelham HRB.** Hsp70 accelerates the recovery of nucleolar morphology after heat shock. *EMBO J.* 3:3095-3100, 1984.

269. **Rohde M, Daugaard M, Jensen MH, Helin K, Nylandsted J, and Jäättelä M.** Members of the heat-shock protein 70 family promote cancer cell growth by distinct mechanisms. *Genes & Developm.* 19: 570-582, 2005.

270. **Stade K., Ford CS, Guthrie C, and Weis K.** Exportin 1 (Crm1) is an essential nuclear export factor. *Cell* 90: 1041-1050, 1997.

271. **Stochaj U and Silver P.** A conserved phosphoprotein that specifically binds nuclear localization sequences is involved in nuclear import. *J. Cell. Biol.* 117: 473-482, 1992.

272. **Zimber A, Nguyen Q-D, and Gespach C.** Nuclear bodies and compartments: functional roles and cellular signalling in health and disease. *Cellular Signalling* 16: 1085-1104, 2004.

273. **Boisvert F-M, van Koningsbruggen S, Navascues J, and Lamond AI.** The multifunctional nucleolus. *Nat Rev Mol Cell Biol* 8: 574-585, 2007.

274. **Akhtar A and Gasser SM.** The nuclear envelope and transcriptional control. *Nat Rev Genet* 8: 507-517, 2007.

275. **Brown CR, Kennedy CJ, Delmar VA, Forbes DJ, and Silver PA.** Global histone acetylation induces functional genomic reorganization at mammalian nuclear pore complexes. *Genes Dev* 22: 627-639, 2008.

276. **Reddy KL, Zullo JM, Bertolino E, and Singh H.** Transcriptional repression mediated by repositioning of genes to the nuclear lamina. *Nature* 452: 243-247, 2008.

277. **Chu CT, Plowey ED, Wang Y, Patel V, and Jordan-Sciutto KL.** Location, location, location: altered transcription factor trafficking in neurodegeneration. *J Neuropathol Exp Neurol* 66: 873-883, 2007.

278. **Terry LJ, Shows EB, and Wente SR.** Crossing the nuclear envelope: hierarchical regulation of nucleocytoplasmic transport. *Science* 318: 1412-1416, 2007.

279. **Kohler A and Hurt E.** Exporting RNA from the nucleus to the cytoplasm. *Nat Rev Mol Cell Biol* 8: 761-773, 2007.

280. **Poon IK**, **and Jans DA .** Regulation of nuclear transport: Central role in development and transformation? *Traffic* 6: 173-186, 2005.

281. **Grote P, Schaeuble K, and Ferrando-May E.** Commuting (to) suicide: An update on nucleocytoplasmic transport in apoptosis. *Archives of Biochemistry and Biophysics* 462: 156-161, 2007.

282. **Kodiha M, Bański P, Ho-Wo-Cheong D, and Stochaj U.** Dissection of the molecular mechanisms that control the nuclear accumulation of transport factors importin-α and CAS in stressed cells. *Cellular and Molecular Life Sciences (CMLS)* 65: 1756-1767, 2008.

283. **Kodiha M, Tran D, Qian C, Morogan A, Presley JF, Brown CM, and Stochaj U.** Oxidative stress mislocalizes and retains transport factor importin-alpha and nucleoporins Nup153 and Nup88 in nuclei where they generate high molecular mass complexes. *Biochimica et Biophysica Acta (BBA) - Molecular Cell Research* 1783: 405-418, 2008.

284. **Li Q, Falsey RR, Gaitonde S, Sotello V, Kislin K, and Martinez JD.** Genetic analysis of p53 nuclear importation. *Oncogene* 26: 7885-7893, 2007.

285. **Huang H and Tindall DJ.** Dynamic FoxO transcription factors. *J Cell Sci* 120: 2479-2487, 2007.

286. **Tanaka T, Ohkubo S, Tatsuno I, and Prives C.** hCAS/CSE1L associates with chromatin and regulates expression of select p53 target genes. *Cell* 130: 638-650, 2007.

287. **Turjanski AG, Vaque JP, and Gutkind JS.** MAP kinases and the control of nuclear events. *Oncogene* 26: 3240-3253.

288. **Shaul YD and Seger R.** The MEK/ERK cascade: From signaling specificity to diverse functions. *Biochimica et Biophysica Acta (BBA) - Molecular Cell Research* 1773: 1213-1226, 2007.

289. **Hedbacker K and Carlson M.** SNF1/AMPK pathways in yeast. *Front Biosci* 13: 2408-2420, 2008.

290. **Ashery U, Yizhar O, Rotblat B, and Kloog Y.** Nonconventional trafficking of Ras associated with Ras signal organization. *Traffic* 7: 1119-1126, 2006.

291. **Brown CM.** Fluorescence microscopy - avoiding the pitfalls. *J Cell Sci* 120: 1703-1705, 2007.

292. **Hunot S, Brugg B, Ricard D, Michel PP, Muriel M-P, Ruberg M, Faucheux BA, Agid Y, and Hirsch EC.** Nuclear translocation of NF-kappaB is increased in dopaminergic neurons of patients with Parkinson disease. *Proceedings of the National Academy of Sciences of the United States of America* 94: 7531-7536, 1997.

293. **Brugg B, Michel PP, AgidY, and Ruberg M.** Ceramide induces apoptosis in cultured mesencephalic neurons. *Journal of Neurochemistry* 66: 733-739, 1996.

294. **Rollenhagen C, Hodge CA, and Cole CN.** Following temperature stress, export of heat shock mRNA occurs efficiently in cells with mutations in genes normally important for mRNA export. *Eukaryotic Cell* 6: 505-513, 2007.

295. **Emerit J, Edeas M, and Bricaire F.** Neurodegenerative diseases and oxidative stress. *Biomedecine & Pharmacotherapy* 58: 39-46, 2004.

296. **Roberts CK and Sindhu KK.** Oxidative stress and metabolic syndrome. *Life Sciences* 84: 705-712, 2009.

297. **Ferrando-May E.** Nucleocytoplasmic transport in apoptosis. *Cell Death Differ* 12: 1263-1276, 2005.

298. **Calabrese V, Lodi R, Tonon C, D'Agata V, Sapienza M, Scapagnini G, Mangiameli A, Pennisi G, Stella AMG, and Butterfield DA.** Oxidative stress, mitochondrial dysfunction and cellular stress response in Friedreich's ataxia. *Journal of the Neurological Sciences* 233: 145-162, 2005.

299. **Li W and Kong AN.** Molecular mechanisms of Nrf2-mediated antioxidant response. *Molecular Carcinogenesis* 48: 91-104, 2009.

300. **Kim IS, Kim DH, Han SM, Chin MU, Nam HJ, Cho HP, Choi SY, Song BJ, Kim ER, Bae YS, and Moon YH.** Truncated form of importin alpha identified in breast cancer cell inhibits nuclear import of p53. *J Biol Chem* 275: 23139-23145, 2000.

301. **Pujol G, Söderqvist H, and Radu A.** Age-associated reduction of nuclear protein import in human fibroblasts. *Biochemical and Biophysical Research Communications* 294: 354-358, 2002.

302. **Kau TR, Way JC, and Silver PA.** Nuclear transport and cancer: from mechanism to intervention. *Nat Rev Cancer* 4: 106-117, 2004.

303. **Kodiha M, Umar R, and Stochaj U.** Optimized immunofluorescence staining protocol to detect the nucleoporin Nup98 in different subcellular compartments. *Nature protocols* DOI**:** 10.1038/nprot.2009.16, 2009.

304. **Crampton N, Kodiha M, Umar R, and Stochaj U**. Oxidative stress inhibits nuclear protein export by multiple mechanisms which target FG nucleoporins and Crm1. *Molecular Biology of the Cell* in revision 2009

305. **D'Angelo MA, Raices M, Panowski SH, and Hetzer MW.** Age-dependent deterioration of nuclear pore complexes causes a loss of nuclear integrity in postmitotic cells. *Cell* 136: 284-295, 2009.

306. **Kodiha M, Tran D, Morogan A, Qian C, and Stochaj U**. Dissecting the Signaling Events that Control Classical Nuclear Import and Target Nuclear Transport Factors. *PLoS* submitted 2009

307. **Smukste I and Stockwell BR.** Restoring functions of tumor suppressors with small molecules. *Cancer Cell* 4: 419-420, 2003.

308. **Kau TR, Schroeder F, Ramaswamy S, Wojciechowski CL, Zhao JJ, Roberts TM, Clardy J, Sellers WR, and Silver PA.** A chemical genetic screen identifies inhibitors of regulated nuclear export of a forkhead transcription factor in PTEN-deficient tumor cells. *Cancer Cell* 4: 463-476, 2003.

309. **Kodiha M, Brown CM, and Stochaj U.** Analysis of signaling events by combining high-throughput screening technology with computer-based image analysis. *Sci Signal* 1: pl2-, 2008.

310. **Kodiha M, Banski P, and Stochaj U.** Interplay between MEK and PI3 kinase signaling regulates the subcellular localization of protein kinases ERK1/2 and Akt upon oxidative stress. *FEBS Letters* In Press, Corrected Proof.

311. **Morcillo G, Gorab E, Tanguay RM, and Díez JL.** Specific intranucleolar distribution of hsp70 during heat shock in polytene cells. *Experimental Cell Research* 236: 361-370, 1997.

312. **Söti C and Csermely P.** Chaperones and aging: role in neurodegeneration and in other civilizational diseases. *Neurochemistry International* 41: 383-389, 2002.

313. **Latchman DS.** Heat shock proteins and cardiac protection. *Cardiovasc Res* 51: 637-646, 2001.

314. **Beere HM.** Stressed to death: regulation of apoptotic signaling pathways by the heat shock proteins. *Sci STKE* 2001: re1-, 2001.

315. **Jolly C and Morimoto RI.** Role of the heat shock response and molecular chaperones in oncogenesis and cell death. *J Natl Cancer Inst* 92: 1564-1572, 2000.

316. **Nylandsted J, Brand K, and Jäättelä M.** Heat shock protein 70 is required for the survival of cancer cells. *Annals of the New York Academy of Sciences* 926: 122-125, 2000.

317. **Macario AJ and Conway de Macario E.** Sick chaperones, cellular stress, and disease. *N Engl J Med* 353: 1489-1501, 2005.

318. **Nardai G, Csermely P, and Söti C.** Chaperone function and chaperone overload in the aged. A preliminary analysis. *Experimental Gerontology* 37: 1257-1262, 2002.

9. Appendix

Please find attached reprints of additional first-authorship papers that I published during my PhD program.

Available online at www.sciencedirect.com
ScienceDirect
Biochimica et Biophysica Acta 1783 (2008) 405–418
Biochimica et Biophysica Acta
BBA
www.elsevier.com/locate/bbamcr

Oxidative stress mislocalizes and retains transport factor importin-α and nucleoporins Nup153 and Nup88 in nuclei where they generate high molecular mass complexes

Mohamed Kodiha [a], Dan Tran [a], Cynthia Qian [a], Andreea Morogan [a], John F. Presley [b], Claire M. Brown [c], Ursula Stochaj [a,*]

[a] *Department of Physiology, McGill University, Montreal, PQ, Canada H3G 1Y6*
[b] *Department of Anatomy and Cell Biology, McGill University, Montreal, PQ, Canada H3A 2B2*
[c] *Department of Biochemistry and Life Sciences Imaging Facility, McGill University, Montreal, PQ, Canada H3G 1Y6*

Received 16 July 2007; received in revised form 30 October 2007; accepted 31 October 2007
Available online 17 November 2007

Abstract

Nuclear trafficking of proteins requires the cooperation between soluble transport components and nucleoporins. As such, classical nuclear import depends on the dimeric carrier importin-α/β1, and CAS, a member of the importin-β family, which exports importin-α to the cytoplasm. Here we analyzed the effect of oxidative stress elicited by diethyl maleate (DEM) on classical nuclear transport. Under conditions that do not induce death in the majority of cells, DEM has little effect on the nucleocytoplasmic concentration gradient of Ran, but interferes with the nuclear accumulation of several reporter proteins. Moreover, DEM treatment alters the distribution of soluble transport factors and several nucleoporins in growing cells. We identified nuclear retention of importin-α, CAS as well as nucleoporins Nup153 and Nup88 as a mechanism that contributes to the nuclear concentration of these proteins. Both nucleoporins, but not CAS, associate with importin-α in the nuclei of growing cells and *in vitro*. Importin-α generates high molecular mass complexes in the nucleus that contain Nup153 and Nup88, whereas CAS was not detected. The formation of high molecular mass complexes containing importin-α, Nup153 and Nup88 is increased upon oxidant treatment, suggesting that complex formation contributes to the anchoring of importin-α in nuclei. Taken together, our studies link oxidative stress to the proper localization of soluble transport factors and nucleoporins and to changes in the interactions between these proteins.

Keywords: Stress; Oxidant; Nucleus; Nuclear transport

1. Introduction

The appropriate response to stress is fundamental to cell survival and the recovery from different insults, such as oxidant exposure [1–4]. Oxidative stress generated by the increase in reactive oxygen species (ROS) is the most prominent insult that causes ischemia/reperfusion injury, which can lead to apoptotic or necrotic cell death [5–8]. ROS-mediated stress contributes to cell death not only in cardiovascular diseases and stroke, but also in Alzheimer's disease and many other neurodegenerative disorders and syndromes [7–9]. The glutathione/glutathione disulfide (GSH/GSSG) system is one of the major contributors to redox homeostasis and of particular importance to the intracellular redox state [5–8,10]. Changes in the GSH/GSSG ratio have been observed for several human diseases, pathologies and during aging (reviewed in [11]). Oxidative stress affects many intracellular processes, and DEM treatment may affect protein modification, cell biochemistry, physiology and even behavior of an organism [12–15]. At present, not all of the consequences of oxidative stress are understood at the molecular level. In particular, the impact on nuclear transport is only beginning to emerge.

Abbreviations: BSA, bovine serum albumin; cNLS, classical NLS; DAPI, 4′,6-diamidino-2-phenylindole; GFP, green fluorescent protein; GFP-β-gal, GFP-β-galactosidase; GR, glucocorticoid receptor; NE, nuclear envelope; NLS, nuclear localization sequence; NPC, nuclear pore complex; NP40, Nonidet P-40

* Corresponding author. Tel.: +1 514 398 2949; fax: +1 514 398 7452.
E-mail address: ursula.stochaj@mcgill.ca (U. Stochaj).

0167-4889/$ - see front matter © 2007 Elsevier B.V. All rights reserved.
doi:10.1016/j.bbamcr.2007.10.022

Many of the proteins transported in or out of the nucleus require a specialized transport apparatus which includes members of the importin-β family [16,17]. For instance, classical nuclear import relies on importin-β1 and the adaptor importin-α. Together, importin-α/β1 generate a dimeric nuclear import receptor that recognizes classical nuclear localization sequences (cNLS) in the cytoplasm, transports cNLS-containing cargo across the nuclear pore complex (NPC) and delivers this cargo to the nuclear side of the NPC. Once in the nucleus, binding of RanGTP to importin-β1 dissociates the importin-α/β1/cargo complex. Upon delivery of the cargo to the nucleus, importin-α and importin-β1 return independently to the cytoplasm. Importin-α is exported to the cytoplasm by CAS (cellular apoptosis susceptibility protein), a carrier of the importin-β family, and RanGTP is necessary to generate trimeric export complexes [18]. Importin-α and CAS are not only involved in nuclear transport, but also in other cellular processes (reviewed in [19–21]).

Like nuclear carriers, nucleoporins play a key role in moving cargo across the NPC, as they provide sites for the translocation of import and export complexes. Nucleoporins are organized into modules that generate defined components of the NPC [22]; they may be involved in nuclear import and/or export of macromolecules. Some nucleoporins are stably bound to NPCs, whereas others play a more dynamic role and reversibly interact with the nuclear pore [23]. Nup153 and Nup50 are dynamic nucleoporins predominantly located on the nuclear side of the NPC, where they participate in nuclear trafficking. As such, Nup153 is implicated in nuclear import and export of protein and RNA [24], whereas Nup50 plays a role in the final step of classical nuclear import by interacting with the adaptor importin-α (reviewed in [25]). Nup50 may increase the efficiency of classical protein import by promoting the disassembly of transport complexes at the nuclear side of the NPC [26]. On the cytoplasmic side, nucleoporins Nup214 and Nup88 contribute to CRM1-mediated nuclear export of proteins, ribosomal and other types of RNA (reviewed in [27]). Together with Nup214, the nucleoporin Nup88 is a structural component of cytoplasmic NPC filaments, but also present on the nuclear side of the NE, suggesting functions inside the nucleus [28].

Classical nuclear import in higher eukaryotes and yeast is sensitive to various forms of stress [29–32]. Ultimately, severe stress conditions inhibit nuclear transport and may also lead to cell death [31]. The molecular mechanisms that link oxidative stress to changes in nuclear trafficking are presently not understood, and little is known about the impact of stress and oxidants in particular on nucleoporin localization. This prompted us to analyze how non-lethal oxidative stress, conditions that are likely to mimic the oxidant-induced physiological changes observed upon ischemia/reperfusion injury and other pathologies, affects the classical nuclear import apparatus. To gain further insight into these questions, we exposed human culture cells to the oxidant diethyl maleate (DEM). DEM is a weak electrophile that can deplete GSH pools by alkylation of its SH-group [33,34] and has been used widely to generate oxidative stress. Our studies now demonstrate that the exposure to DEM interferes with classical nuclear import, redistributes transport components, induces the formation of high molecular mass complexes in nuclei and the nuclear retention of several soluble transport components and nucleoporins that participate in nuclear protein import and export.

2. Materials and methods

2.1. Growth and stress exposure of HeLa cells

HeLa cells were grown in multiwell chambers to 50 to 70% confluency [35] and subjected to incubation with DEM or the solvent ethanol as indicated. All of the results were obtained for at least three independent experiments.

2.2. Flow cytometry

Cell death was analyzed by staining with annexin-V-fluorescein combined with propidium iodide. In brief, two 100-mm dishes were incubated with ethanol or 2 mM DEM for 4 h at 37 °C. Attached cells and cells in the medium were washed with PBS and together incubated overnight in fresh medium. The next day, cells attached to the dish were collected by trypsination and combined with cells in the medium. After washing in PBS, cells were incubated with annexin-V-fluorescein and propidium iodide according to the manufacturer (Roche, Germany). Binding of annexin-V-fluorescein and propidium iodide was quantified by flow cytometry.

2.3. Analysis of nuclear protein import in growing cells

Nuclear protein import was analyzed with NLS-GFP as previously described [31] and with GFP-tagged glucocorticoid receptor essentially as in reference [36]. Endogenous import cargos HuR and galectin-3 were located as described in Section 2.4.

2.4. Immunofluorescent staining

All steps were carried out essentially as described [37]. Antibodies against the following proteins were used: Ran (sc-1156, Santa Cruz Biotechnology, CA), HuR, importin-α1, CAS and α-tubulin (sc-5261, sc-6917, sc-1708, sc-5286), galectin-3 (Thermo Fisher, Fremont, CA), 7A8 is specific for Nup153 [38] (gift of Dr. Franke, Heidelberg). Primary antibodies were used as suggested by the suppliers; supernatant 7A8 was diluted 1:100. Anti-Nup50 was a gift of Dr. Gerace, La Jolla. Bound primary antibodies were detected with Cy3-conjugated secondary antibodies (1:500, Jackson ImmunoResearch, West Grove, PA). DNA was visualized with 4′,6-diamidino-2-phenylindole (DAPI) and samples were mounted in Vectashield (Vector Laboratories, Burlingame, CA). Cells were analyzed with a Zeiss 510 LSM or a Nikon Optiphot and photographed with Kodak T-MAX 400 films. Images were processed with Photoshop 5.5 and 8.0.

2.5. Data analysis

Images were collected using the ImageXpress Micro automated imaging system from Molecular Devices (Sunnyvale, CA) using excitation from a 300 W Xenon light source and a CoolSnapHQ CCD camera (Photometrics, Tucson, AZ). Images were collected using 2×2 camera binning with a Nikon ×40 PlanFluor ELWD (0.60 NA) objective using the automated focusing option in the MetaXpress software to find the cover slip-mounting media interface and then offset by a fixed amount to image the nuclear DAPI staining (Chroma Technologies Corp, Rockingham, VT, #49000) with 20 ms exposure times. Images were than taken in the same image plane for either NLS-GFP or GR-GFP using the FITC cube with 3182 ms exposure times (Chroma Technologies Corp, Rockingham, VT, #49002) or endogenous HuR and galectin-3 using the Cy3 cube with 3182 exposure times (Chroma Technologies Corp, Rockingham, VT, #49005). Between 55 and 100 cells were analyzed for each condition. Image analysis was performed using the MetaXpress software and the Multi-wavelength Cell Scoring module as described [39] or the Translocation Enhanced Module. For the Translocation Enhanced Module nuclei were

identified as 100–350 μm^2 area with a width of ~10 μm and an intensity of DAPI staining over local background of >5 intensity units. The segmentation regions identified by DAPI staining were then used to measure intensities of the GFP or Cy3 images. An inner region corresponding to the nuclear intensity was identified as the area 0.9 μm from the edge of the segmentation identified by DAPI staining. The outer region was identified as a ring 0.5 μm from the edge of the segmentation identified by DAPI staining with a width of 0.8 μm, corresponding to the cytosolic intensity. All images were corrected for contributions from background intensity using regions of the images that did not contain cells. Ratios of the average intensities of nuclear/cytosolic regions were calculated for individual cells. All segmentation data sets were inspected manually to ensure accuracy of the data and cells with inaccurate segmentation were removed from the analysis.

2.6. Purification of proteins synthesized in Escherichia coli and labeling with tetramethylrhodamine

Tagged proteins were synthesized in *E. coli* and purified under native conditions following standard procedures. Purified importin-α or CAS was labeled with tetramethylrhodamine-maleimide (TMR, Molecular Probes) overnight on ice as recommended by the supplier. Non-incorporated dye was removed by gel exclusion chromatography with Sephadex G-25.

2.7. In vitro nuclear import of importin-α and CAS

Import of TMR-labeled importin-α or CAS was analyzed in semi-intact HeLa cells at a final concentration of 400 nM in transport buffer [40]. Import assays were supplemented with 3 mg/ml cytosol prepared from control or DEM-treated HeLa cells (4 h, 2 mM DEM) as indicated. After 5 min at 30 °C, samples were fixed and stained with DAPI. Transport factors were localized by fluorescence microscopy and intranuclear fluorescence was quantified.

2.8. Measurement of mean intranuclear fluorescence for in vitro import assays

To quantify intranuclear fluorescence of TMR-labeled importin-α or CAS, cells were optically sectioned using a Zeiss 510 LSM laser-scanning confocal microscope with a ×63 objective (NA 1.4, full width half maximum of 0.65 μm for the optical slice at the pinhole setting used). A single optical slice through the center of the nucleus was chosen for quantitation. The effective nuclear thickness is much greater than the optical slice thickness under our imaging conditions, therefore cytosolic fluorescence should not contribute to the measured intensity. Average pixel intensities over the nuclei were quantified using Metamorph software (Universal Imaging). Fluorescent signals for 53 to 59 individual cells and background intensities were determined for each of the conditions. All images to be directly compared were taken under identical microscope settings using appropriate rhodamine optics.

2.9. Statistics

To measure fluorescence signals in nuclei and cytoplasm, data for at least 50 cells were acquired for each of the different conditions. Data were obtained for at least three independent experiments. Results are shown as means±STDEV and Student's *t* test (two-tailed) for unpaired samples was carried out to identify significant differences.

2.10. Western blot analysis

HeLa cells were grown on dishes to 50 to 70% confluency. Cells were stressed as described above, washed with PBS and stored at −70 °C until use. Crude extracts were prepared by solubilizing proteins in gel sample buffer, pH 8.0, containing protease inhibitors (aprotinin, leupeptin, pepstatin, each at 1 μg/ml; 1 mM PMSF), 20 mM β-glycerophosphate, 1 mM NaN_3, 2.5 mM NaF. Samples were incubated for 10 min at 95 °C and vortexed with glass beads to shear DNA. After centrifugation (5 min, 13,000 rpm, microfuge) equal amounts of protein were separated by SDS-PAGE. Proteins were blotted to nitrocellulose and blots processed as described [31]. Antibodies were used at the following dilutions: Nup153, (1:200); mab414 (1:5,000; BabCo, Richmond, CA), Nup88 (1:100; Novocastra, Newcastle, UK, or 1:1,000; BD Biosciences; Mississauga, ON); hsc70 (1:2,000; SPA-815 and SPA-816, Stressgen); actin (1:1,000, Chemicon, Temecula, CA). All other antibodies were purchased from Santa Cruz Biotechn.: importin-α1 (1:500, sc-6917), importin-β1 (1:400, sc-11367), CAS (1:200, sc-1708), Ran (1:500, sc-1156), tubulin (1:2,000, sc-5286).

2.11. Indirect immunoprecipitation

For immunoprecipitations under native conditions control and stressed cells were extracted with 40 μg/ml digitonin in PBS for 5 min on ice. All subsequent steps were carried out at 4 °C. Cells were washed with cold PBS and proteins were solubilized in PBS, 1% NP40, 2.5 mM NaF, 20 mM β-glycerophosphate, 1 mM NaN_3, and a mixture of protease inhibitors (aprotinin, leupeptin, pepstatin, each at 1 μg/ml, 1 mM PMSF). After 10-min incubation, samples were vortexed several times with glass beads, cleared by centrifugation (5 min, 15,000 rpm, microfuge) and pre-treated with protein G-Sepharose (Pharmacia Biotech, Baie d'Urfé) for 30 min with gentle agitation. Supernatants obtained after 5 min centrifugation at 13,000 rpm were incubated with antibodies against importin-α1, Nup153 or Nup88 for 1 h, followed by addition of protein-G-Sepharose and overnight incubation. Beads were collected by centrifugation (3 min, 13,000 rpm) and washed three times with PBS/1 mM NaN_3. Bound material was released by incubation in gel sample buffer for 10 min at 95 °C and supernatants (5 min, 13,000 rpm, room temperature) were subjected to Western blot analysis.

2.12. Affinity purification with immobilized importin-α

His6-tagged importin-α was purified from bacteria and dialyzed against 20 mM MOPS, 100 mM sodium acetate, 5 mM magnesium acetate, 5 mM imidazole, 2.5 mM NaF, pH 7.1 (binding buffer). Ni-TA resin (Qiagen) was preloaded with importin-α in binding buffer for 1 h at 4°C and washed three times with binding buffer. Crude extracts were generated from digitonin-treated control or stressed cells in binding buffer containing 0.5 mM DTT, 0.5% SDS and protease inhibitors (aprotinin, leupeptin, pepstatin, each at 1 μg/ml; 1 mM PMSF). Samples were diluted into binding buffer containing protease inhibitors and Triton X-100 to give a final concentration of 1% Triton X-100, 0.1% SDS and 0.1 mM DTT. Samples were vortexed with glass beads, centrifuged (3 min, 13,000 rpm) and incubated with immobilized importin-α for 1 h at 4 °C. Beads were washed three times with binding buffer containing 1% Triton X-100 and bound material was analyzed by Western blotting.

2.13. Protein crosslinking and gel chromatography

Control and DEM-treated cells were extracted with 40 μg/ml digitonin in PBS for 5 min on ice, washed with ice-cold PBS and incubated with 0.2 mM 3.3′-Dithiobis[sulfosuccinimidylproprionate] (DTSSP, Pierce, Rockford, IL) in PBS for 1 h on ice. Plates were washed with ice-cold PBS and stored at −70 °C. Proteins were solubilized in 10 mM Tris–HCl pH 7.4, 1% SDS, 2.5 mM NaF, 1 mM NaN_3, containing protease inhibitors (aprotinin, leupeptin, pepstatin, each at 1 μg/ml; 1 mM PMSF). Samples were vortexed with glass beads and cleared by centrifugation (3 min, 13,000 rpm, microfuge). Supernatants were separated on a Superose-12 column (Pharmacia) and eluted in 10 mM Tris–HCl pH 7.4, 0.1% SDS. A total of 25 fractions (1 ml) were collected and aliquots of each fraction were analyzed by Western blotting. For indirect immunoprecipitation, peak fractions were pooled and concentrated with Amicon centrifugal filters (Molecular weight cut off 10 kDa). Samples containing 10 mM Tris–HCl pH 7.4, 150 mM NaCl, 0.1% SDS, 1% NP40, 2.5 mM NaF, 20 mM β-glycerophosphate, 1 mM NaN_3, and a mixture of protease inhibitors (aprotinin, leupeptin, pepstatin, each at 1 μg/ml; 1 mM PMSF) were pre-treated with protein G-Sepharose and incubated with anti-Nup153 or anti-Nup88 antibodies as in Section 2.11.

2.14. Extraction of unfixed HeLa cells

Samples were treated with buffer, detergent, DNase, NaCl, DNase+RNase essentially as described in ref. [41]. After each step samples were processed for

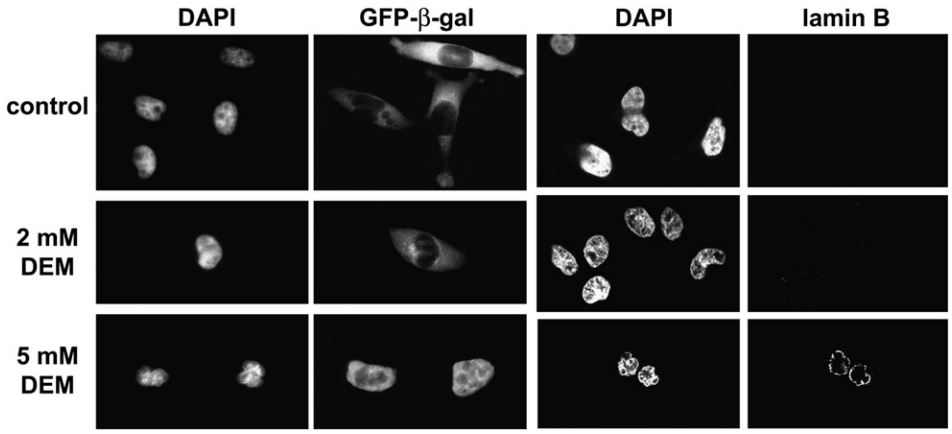

Fig. 1. Effect of DEM on nuclear envelope integrity. HeLa cells transiently synthesizing GFP-β-galactosidase were incubated for 4 h with ethanol (control) or DEM as indicated. Cells were fixed and the reporter protein localized by fluorescence microscopy (GFP-β-gal). Nontransfected HeLa cells were incubated with ethanol, 2 mM or 5 mM DEM. Fixed cells were semi-permeabilized with digitonin and incubated with anti-lamin B antibodies [42]. Nuclei were located with DAPI. Note that GFP-β-gal appears in nuclei and lamin B is accessible to antibodies only after treatment with 5 mM, but not 2 mM DEM.

indirect immunofluorescence. Confocal imaging for each antigen was carried out at identical settings for all extraction steps.

3. Results

3.1. The effect of diethyl maleate (DEM) on nuclear envelope integrity

To determine whether DEM treatment alters the permeability barrier of nuclear envelopes (NEs), we incubated HeLa cells with 1, 2 and 5 mM DEM or the solvent ethanol for 4 h at 37 °C (Fig. 1). Changes in nuclear membrane integrity were monitored with two independent assays [42]. First, HeLa cells were transiently transfected with a plasmid encoding GFP-β-galactosidase, a fusion protein that is excluded from the nucleus. The absence of GFP-β-galactosidase from the nucleus indicates that the NE is intact (Fig. 1). Second, we tested whether antibodies against lamin B have access to the nuclear lamina when cells were fixed and treated with the detergent digitonin [42]. Digitonin permeabilizes the plasma membrane, but leaves the NE intact, and staining with anti-lamin B antibodies is only observed when NEs have been disrupted. Both the localization of GFP-β-galactosidase and binding of antibodies against lamin B revealed that after 2 mM DEM treatment nuclear membranes remained intact, but became permeable upon incubation with 5 mM DEM (Fig. 1 and reference [42]).

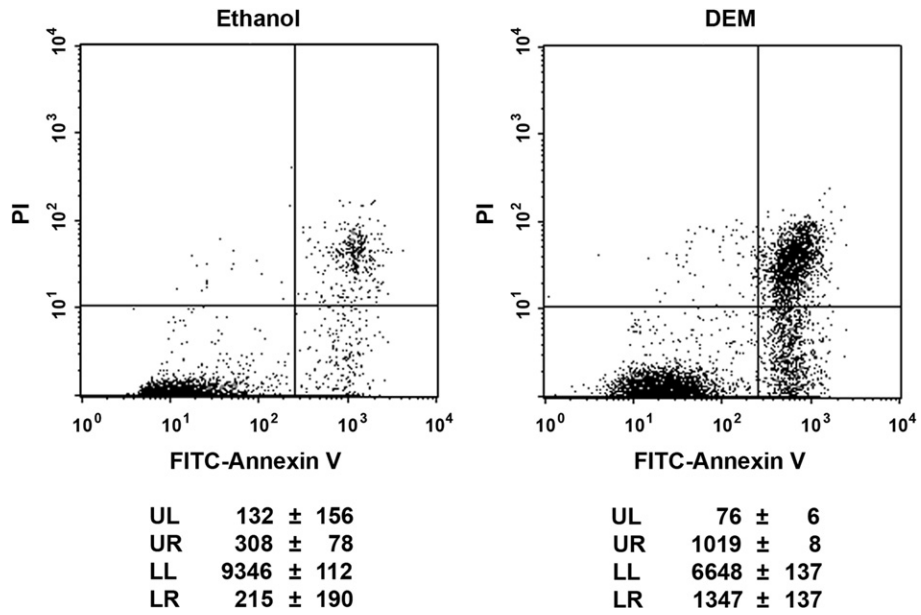

Fig. 2. Flow cytometry. HeLa cells were incubated with ethanol or 2 mM DEM for 4 h and further treated as described in Materials and methods. Binding of FITC-Annexin V or propidium iodide (PI) was quantified for 10,000 cells. Means and standard deviations are depicted for two separate experiments.

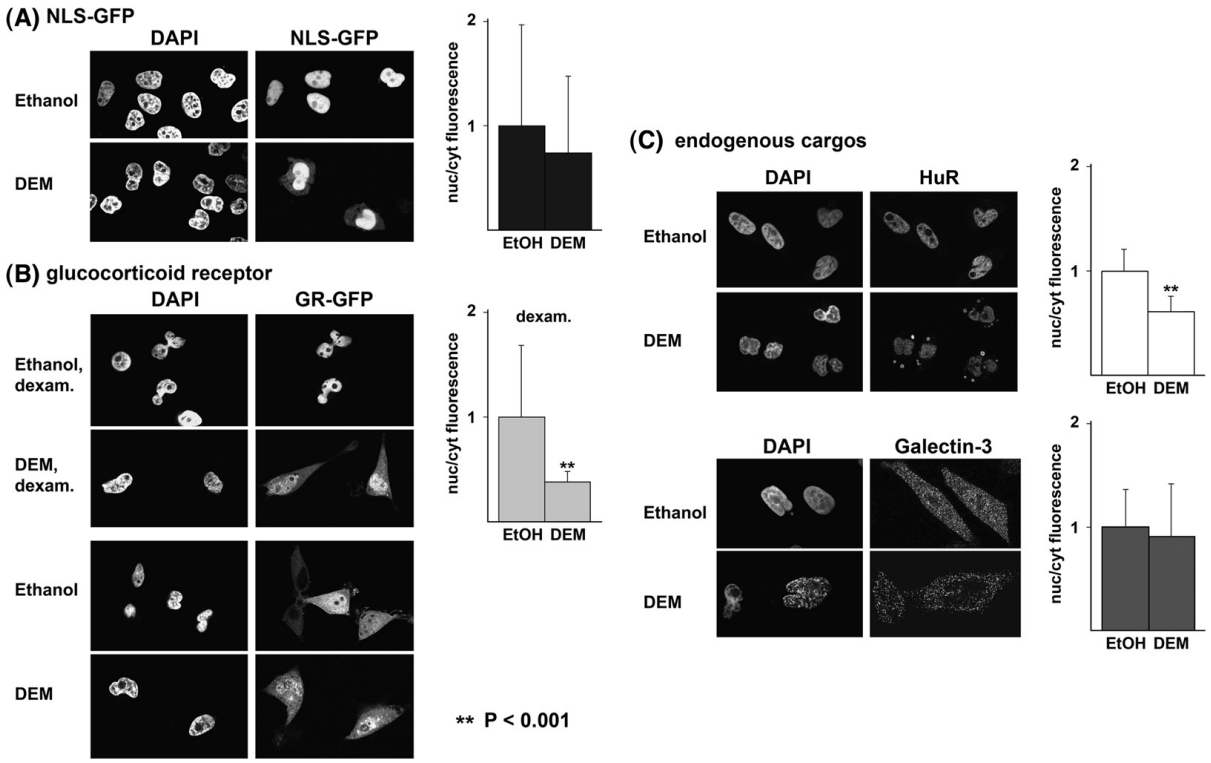

Fig. 3. The oxidant DEM interferes with nuclear import in growing HeLa cells. Transiently synthesized reporter proteins (A, B) and endogenous cargos (C) were localized in HeLa cells grown for 4 h under non-stress (ethanol) or stress conditions (DEM). NLS-GFP import is constitutively active; GR-GFP is transported into nuclei upon addition of dexamethasone (dexam.). (C) Endogenous proteins HuR and galectin-3 were located by indirect immunofluorescence. DAPI staining of the nuclei and signals for fluorescent reporter proteins are shown. The nuclear/cytoplasmic ratio (nuc/cyt) of fluorescence was quantified for each cargo. The ratio for control cells incubated with ethanol was defined as 1. Means and STDEV are shown; $^{**}P<0.01$. Note that a reduction of the nuc/cyt ratio of reporter proteins upon DEM treatment is consistent with less efficient nuclear import.

3.2. Recovery of cells from DEM-induced oxidative stress

To test the effect on cell viability, we treated cells for 4 h with 2 mM DEM, allowed them to recover overnight and quantified the percentage of apoptotic and necrotic cells. In ethanol treated controls, approximately 4% of the cells were apoptotic or necrotic, which increased to approximately 20% upon incubation with DEM (Fig. 2). However, about 70% of the DEM-treated cells were neither necrotic nor apoptotic, suggesting that the majority of cells recovered from DEM-induced stress.

3.3. DEM treatment interferes with nuclear protein import

To determine whether DEM affects nuclear import, different substrates were analyzed, including transiently synthesized reporter proteins tagged with GFP or endogenous substrates HuR and galectin-3. The nuclear/cytoplasmic (nuc/cyt) distribution was quantified for each cargo for non-stress or stress conditions, and the nuc/cyt ratio in unstressed cells was defined as 1. A reduction of the nuc/cyt ratio in stressed cells would be consistent with impaired nuclear import.

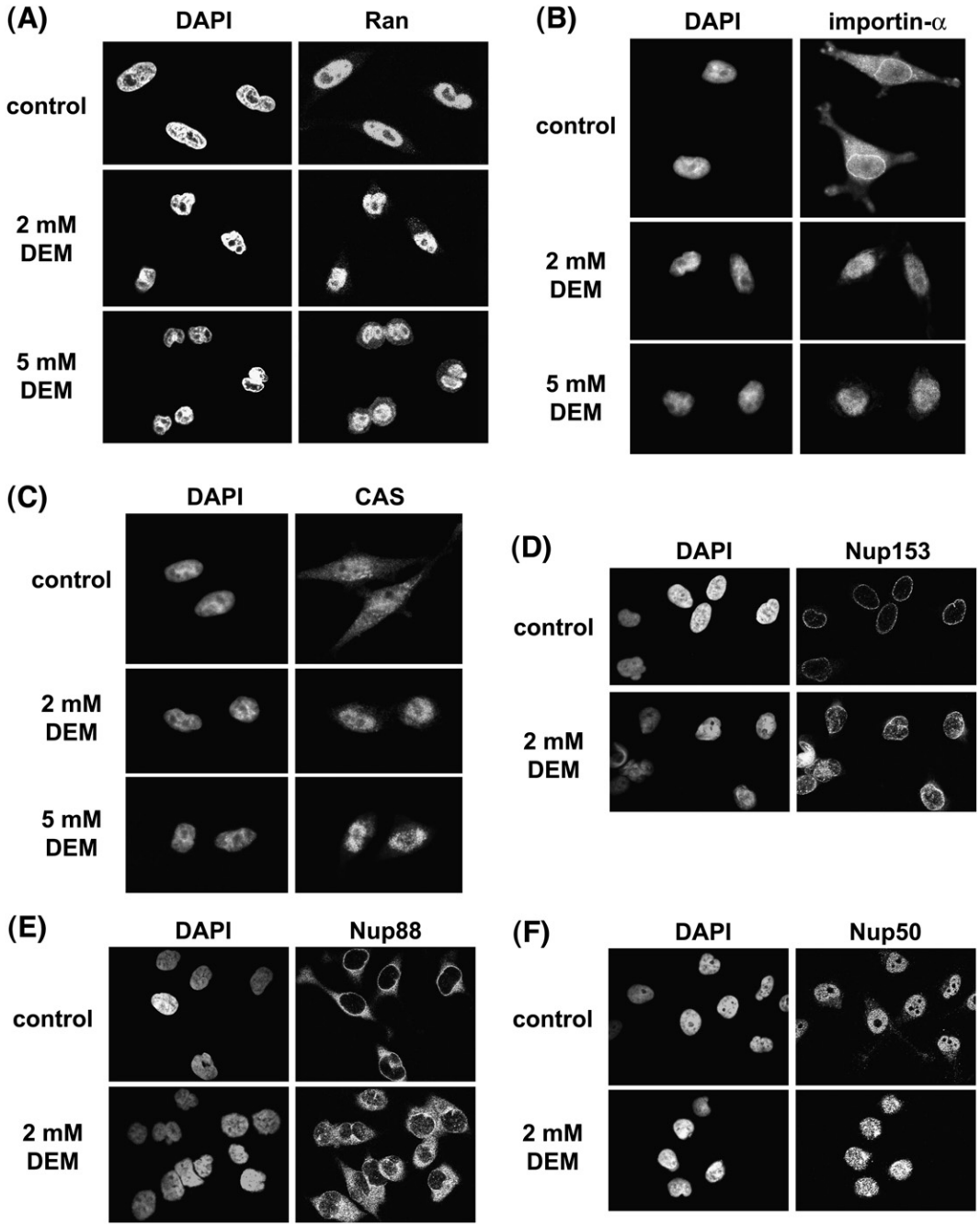

Fig. 4. Effect of DEM on the location of Ran (A), importin-α (B), CAS (C), nucleoporins Nup153 (D), Nup88 (E) and Nup50 (F). HeLa cells treated for 4 h with ethanol (control), 2 mM or 5 mM DEM were fixed and different proteins were localized by indirect immunofluorescence followed by confocal microscopy as detailed in Materials and methods. Nuclei were visualized with DAPI.

In HeLa cells transiently transfected with a plasmid encoding NLS-GFP, which carries the SV40-NLS, the fluorescent reporter accumulates in nuclei only when classical nuclear import is constantly active [31]. Upon treatment with 2 mM DEM the amount of NLS-GFP in the cytoplasm was increased, indicating that classical import was less efficient (Fig. 3A). The fluorescent tag GFP did not change its localization in the presence of DEM; GFP was nuclear and cytoplasmic under all conditions tested (not shown).

A different reporter protein, GFP-tagged glucocorticoid receptor (GFP-GR [36]) is imported into the nucleus by importin-α/β1 and importin-β7 [43]. In the absence of hormone, GFP-GR was nuclear as well as cytoplasmic (Fig. 3B). Addition of dexamethasone resulted in the rapid nuclear accumulation of GFP-GR in unstressed cells (Fig. 3B), whereas most of the DEM-treated cells failed to concentrate GFP-GR in nuclei.

Using nontransfected cells, the effect of oxidative stress on endogenous substrates HuR and galectin-3 was analyzed. Both proteins are involved in RNA transport or processing and transported into nuclei via the classical importin-α dependent pathway [44,45]. HuR is nuclear under normal conditions, whereas a significant amount is cytoplasmic in stressed cells. Galectin-3, nuclear and cytoplasmic in unstressed cells, becomes less abundant in the nuclei following DEM exposure. Taken together, DEM treatment reduces the nuc/cyt ratio of GFP-tagged reporter proteins and endogenous cargos HuR and galectin-3 when compared with controls. These results are in line with the idea that DEM-induced oxidative stress interferes with nuclear protein import under conditions that leave the nuclear envelope intact.

3.4. Ran remains concentrated in nuclei upon incubation with 2 mM DEM

Stress can affect the nucleocytoplasmic Ran gradient and severe oxidative stress leads to a collapse of the gradient, ultimately causing the inhibition of nuclear transport [31]. However, Ran did not relocate significantly at 2 mM DEM. By contrast, the GTPase concentration gradient collapsed after treatment with 5 mM DEM (Fig. 4A), conditions that permeabilize the nuclear envelope (Fig. 1). This suggested that a loss of the nucleocytoplasmic Ran concentration gradient is not the key factor that interferes with nuclear transport upon treatment with 2 mM DEM and prompted us to analyze the effect of DEM on other nuclear transport components.

3.5. Importin-α, CAS, Nup153, Nup88 and Nup50 mislocalize in DEM-treated cells

Importin-α, a subunit of the dimeric classical import receptor, is exported from the nucleus by the importin-β-like carrier CAS. In HeLa cells, both importin-α and CAS concentrated in nuclei when cells were treated with 2 mM DEM, but not with the solvent ethanol (Fig. 4B, C). Interestingly, importin-α and CAS also accumulated in nuclei after a 5 mM DEM treatment, i.e. conditions that permeabilize the NE. This suggests that nuclear retention contributes to their nuclear concentration after oxidant exposure (see Fig. 7). In contrast, the localization of importin-β1 was not drastically changed at any of the DEM concentrations tested (not shown).

In addition, nucleoporins Nup153, Nup88 and Nup50 were localized in control and stressed cells. These nucleoporins were chosen because they contribute to different aspects of nuclear trafficking (see Introduction); Nup153 participates in nuclear import and export, Nup88 is involved in export and Nup50 stimulates importin-α-dependent nuclear import. Both Nup153 and Nup88 displayed a “ring like” staining of the nuclear periphery under non-stress conditions, and Nup88 was also detected in the cytoplasm. In control cells, Nup50 associated mostly with nuclei, but was present in the cytoplasm as well (Fig. 4D, E, F). After DEM treatment changes were observed for all of the nucleoporins (summarized in Table 1). Nup153 and Nup88 were detected in the nucleoplasm, and substantially more Nup88 was located in the cytoplasm, whereas Nup50 was no longer detected in the cytoplasm (Fig. 4D, E, F). Interestingly, in stressed cells the fluorescence signals for Nup153 increased, similar to the stronger signals obtained after Western blotting (see below).

3.6. Effect of DEM exposure on in vitro nuclear accumulation of transport factors

Different mechanisms may contribute to the nuclear accumulation of importin-α and CAS in DEM-treated cells; this may include an increase in nuclear import. We therefore measured the nuclear concentration of fluorescently labeled importin-α and CAS upon incubation with semi-intact cells. Since importin-α and CAS can be transported into nuclei *in vitro* by cytosol-dependent and independent pathways [46], nuclear accumulation was tested for six different conditions (Fig. 5). First, unstressed and stressed cells were semi-permeabilized and analyzed in the absence of exogenously added cytosol (Fig. 5A,B). Second, unstressed and stressed semi-intact cells were combined with cytosol prepared from control or DEM-treated cells (Fig. 5B). To detect minor differences in nuclear accumulation, the intranuclear fluorescence was measured for all of the conditions. There was little effect on importin-α nuclear accumulation for any of the

Table 1
Location of soluble transport factors and nucleoporins in control and DEM-treated cells

Protein	Control conditions (ethanol)	Oxidative stress (2 mM DEM)
Ran	N ≫ C	N ≫ C
Importin-α	NE, N+C	N>C
CAS	N ≥ C, N+C	N>C
Nup153	NE	(NE), N>C
Nup88	NE, (N<C)	(NE), N+C
Nup50	N>C	N ≫ C

Proteins were located by indirect immunofluorescence after 4 h incubation under control (ethanol) conditions or treatment with DEM. N ≫ C, nuclear accumulation with no or little cytoplasmic staining; N>C, nuclear accumulation with cytoplasmic staining; N ≥ C, weak nuclear accumulation with well defined cytoplasmic staining; N+C, equal staining in nucleus and cytoplasm; NE, nuclear envelope.

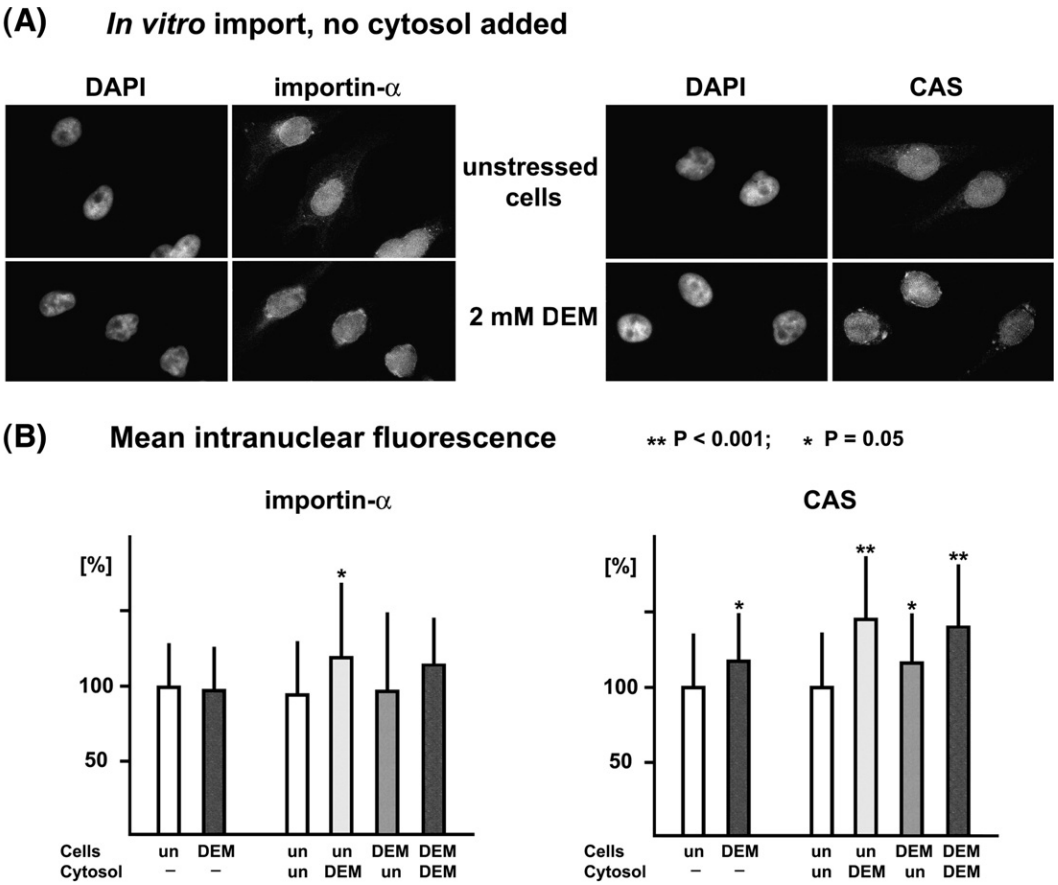

Fig. 5. Stress-induced changes in nuclear accumulation of importin-α and CAS. (A) *In vitro* nuclear import of fluorescently labeled importin-α and CAS was carried out with semi-intact HeLa cells. Nuclear import was carried out *in vitro* with fluorescently labeled importin-α or CAS in the absence (−) or presence of exogenously added cytosol. Cytosol was prepared from unstressed controls (un) or DEM-treated cells (DEM). (B) Mean intranuclear fluorescence was quantified as described in Materials and methods. Fluorescence intensities obtained for unstressed cells were defined as 100% (white bars).

conditions tested, although a small increase was seen when unstressed cells were supplemented with stressed cytosol (Fig. 5B). For CAS, nuclear import was significantly higher when cytosol and semi-intact cells or cytosol only had been treated with DEM. The strongest effect was seen with cytosol prepared from DEM-treated cells, which increased nuclear import to about 140% of control samples (Fig. 5B). Thus, oxidative stress upregulates nuclear import and/or reduces nuclear export of CAS, thereby increasing the steady-state concentration of the carrier in nuclei *in vitro*. Based on the quantification shown in Fig. 5B DEM may also stimulate the cytosol-dependent nuclear concentration of importin-α, albeit to a lesser extent when compared with CAS.

3.7. Effect of DEM on the stability of transport factors

Oxidative stress may trigger the degradation of transport factors and the effect of DEM on protein levels was analyzed in control and oxidant-treated cells that had been incubated in the absence or presence of cycloheximide (Fig. 6A). Crude extracts

Fig. 6. (A) Effect of DEM on protein abundance. HeLa cells were incubated with the solvent ethanol (-DEM) or 2 mM DEM for 4 h. Cycloheximide was present at 100 μg/ml as indicated. Equal amounts of protein from whole cell extracts were analyzed side-by-side. (B) Interaction of importin-α with other nuclear transport factors in growing cells. Nuclear extracts from control and stressed cells were used to immunoprecipitate importin-α under native conditions. Co-purified proteins were detected by Western blotting of the immunoprecipitates. Aliquots of the starting material (Input) represent 8% of the immunoprecipitates (IP). (C) Interaction of Nup153 and Nup88 with importin-α. Immunoprecipitations with anti-Nup153 and anti-Nup88 were carried out as described for part (B). Immunopurified material was analyzed for the presence of importin-α, hsc70 and actin. (D) Binding of nuclear transport factors to purified importin-α *in vitro*. His6-tagged importin-α was purified from bacteria and immobilized on Ni-NTA beads. Equal amounts of protein from nuclear extracts were added to immobilized importin-α and material bound was analyzed by Western blotting. Input shows 10% of the starting material used for affinity purification. Note that Nup153 and Nup88 were efficiently pulled down under these conditions. (E) Importin-α forms high molecular weight complexes with Nup153 and Nup88 in nuclei. Control and DEM-treated cells were extracted with digitonin and proteins were reversibly crosslinked. Equal amounts of crosslinked protein were separated by gel exclusion chromatography (FPLC) and peak fractions containing high molecular mass complexes (molecular mass of >1MD) were analyzed by Western blotting. ECL-signals for control and DEM-treated samples were obtained under identical conditions. (F) High molecular mass complexes obtained after FPLC were analyzed by immunoprecipitation with anti-Nup153 and anti-Nup88 antibodies. Input represents 8% of the starting material. Note that prolonged exposure times were required to visualize importin-β1. (G) To quantify the co-purification of importin-α with Nup153 and Nup88 peak fractions were split into three identical samples to measure the input or co-purification with Nup153 or Nup88 by quantitative Western blotting [39]. Importin-α present in the input was defined as 100%. The graph shows means and STDEV of four independent experiments.

were prepared for whole cells and comparable amounts of protein were separated in parallel. The amounts of importin-β1 were somewhat decreased by DEM, but the concentration of other proteins was not drastically reduced. Furthermore, Western blotting did not reveal the accumulation of proteolytic degradation products after DEM treatment (not shown). Interestingly, the levels of Nup153 were slightly increased upon incubation with DEM, even in the presence of cycloheximide.

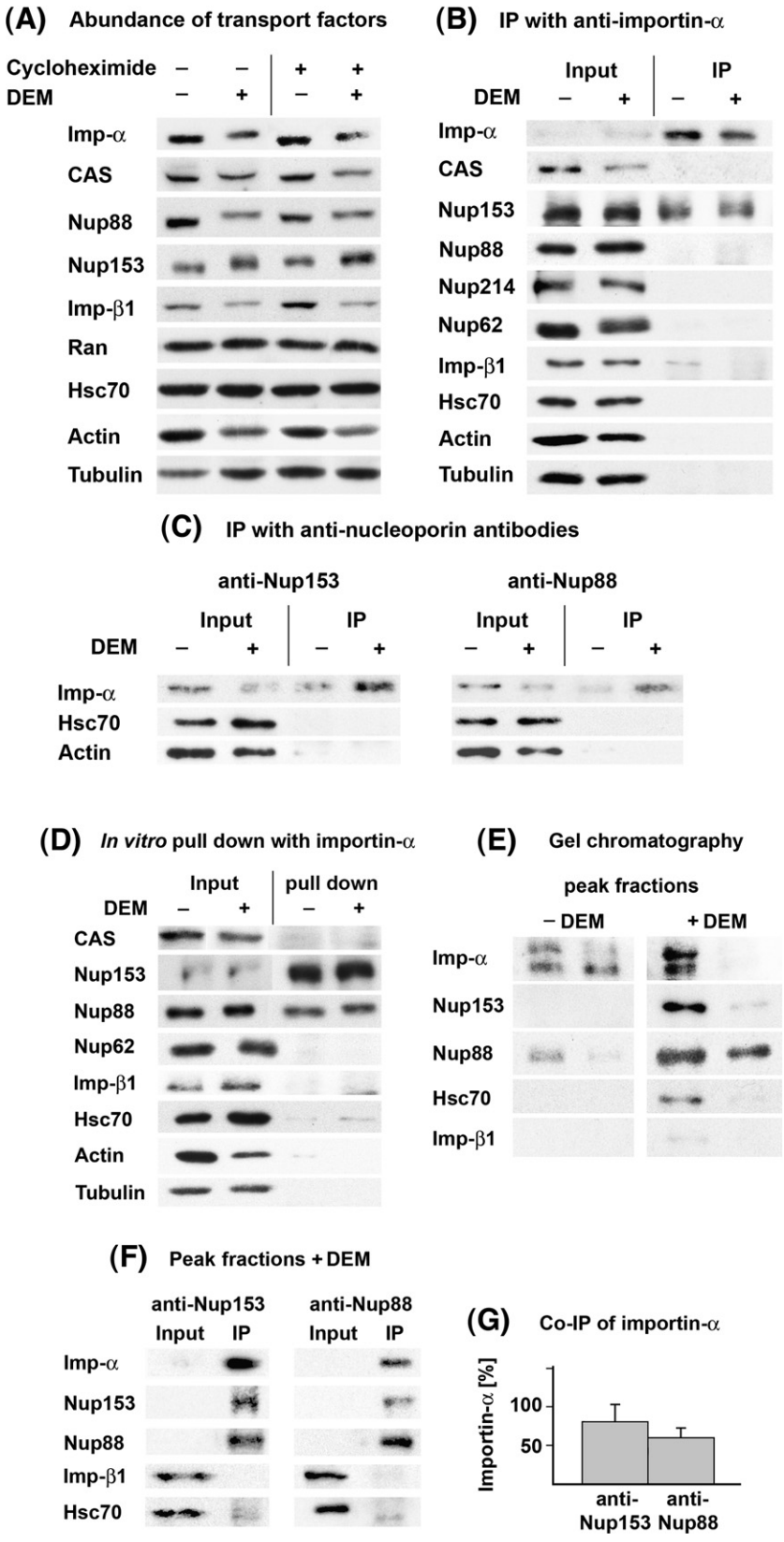

Together with the data described for Nup153 immunolocalization (Fig. 4D) this may indicate that DEM treatment stabilizes Nup153.

In summary, Western blot analyses support the idea that the nuclear distribution of importin-α, CAS, Nup88 or Nup153 in oxidant-treated cells represents the relocation of intact proteins and not simply a mislocalization of their proteolytic products generated upon stress.

3.8. Importin-α stably associates with Nup153 and Nup88 in nuclei of growing cells

The nuclear localization of importin-α could be controlled by its interaction with other components in the nucleus. To address this question, we immunoprecipitated importin-α from crude nuclear extracts under native conditions and monitored the co-purification of transport factors. This approach identifies stable associations, whereas transient or unstable interactions of importin-α as well as interactions that are disrupted by the antibody will be missed. For the experiments shown in Fig. 6B we used the same amounts of nuclear proteins from control and DEM-treated cells as starting material. Nup153 associated with importin-α under control and stress conditions, whereas Nup88 was not detected in immunoprecipitates. The absence of Nup88 from complexes isolated with anti-importin-α antibodies may suggest that this antibody interferes with the Nup88/importin-α interaction, since both proteins co-purified when anti-Nup88 antibodies were used and in pull down experiments (see below Fig. 6C, D). As expected, only little importin-β1 co-purified with importin-α in nuclear extracts of unstressed cells, as import complexes are disassembled in the nucleus. This co-purification of importin-β1 was further reduced after DEM treatment. The specificity of the interaction between Nup153 and importin-α is demonstrated by the fact that other members of the FXFG family, including Nup62 and Nup214, did not co-purify with importin-α. Likewise, CAS, hsc70, actin or tubulin did not bind to importin-α under these conditions (Fig. 6B). Furthermore, immunoprecipitation with anti-Nup153 or anti-Nup88 under native conditions both led to the co-purification of importin-α (Fig. 6C), in line with the idea that nucleoporins form complexes with this transport factor in nuclei. Neither hsc70 nor actin co-purified with Nup153 or Nup88 under these conditions.

Taken together, immunoprecipitation under native conditions indicates an association of importin-α with Nup153 and Nup88; this hypothesis is further substantiated by the results described below.

3.9. Importin-α associates with Nup153 and Nup88 in crude extracts

Immobilized importin-α was used as bait *in vitro* to purify binding partners from nuclear extracts prepared from control or DEM-treated cells (Fig. 6D). With this approach, Nup153 was efficiently pulled down, when compared to the starting material (Input, 10% of the pull down). A substantial amount of Nup88 was also affinity-purified, whereas CAS, importin-β1, actin, tubulin or the FXFG nucleoporin Nup62 did not associate with immobilized importin-α. Minor amounts of hsc70s were affinity-purified with immobilized importin-α as well.

3.10. Importin-α is present in high molecular mass complexes that contain Nup153 and Nup88

Interactions of importin-α with other proteins could be transient only, unstable under the conditions used for co-purification or promoted by *in vivo* post-translational modifications of the bait. To address this problem, we reversibly crosslinked proteins and analyzed components present in high molecular mass complexes. Since crosslinking interfered with anti-importin-α immunoprecipitation, we solubilized complexes in SDS and separated them by gel exclusion chromatography using a Superose-12 column. Individual fractions were probed for the presence of transport factors and importin-α was detected in a high molecular mass fraction, which eluted at a position similar to the marker dextran blue (Mol. mass $\sim 2 \times 10^6$). The same fraction also contained Nup153 and Nup88, whereas CAS and importin-β1 were either absent or hardly detectable (Fig. 6E and data not shown). Complexes containing importin-α could be prepared from control and DEM-treated cells; however, the relative amounts of Nup153, Nup88 and hsc70 were substantially increased in complexes of stressed cells.

It was possible that importin-α, Nup153 and Nup88 were components of distinct protein complexes that have a similar molecular mass. Since crosslinking interfered with anti-importin-α immunoprecipitation, we addressed this point with antibodies against Nup153 and Nup88. Using high molecular mass complexes as starting material, both antibodies co-precipitated importin-α, supporting the idea that importin-α/Nup153 and importin-α/Nup88 complexes were generated. For complexes containing importin-α/Nup153 or importin-α/Nup88 we did not detect importin-β1, Nup214, actin or tubulin, even after prolonged exposure of the filters (Fig. 6F, summarized in Table 2). Importantly, Nup153 and Nup88 co-purified under these conditions, indicating a Nup153/Nup88 association. These results established complexes that contained importin-α/Nup153, importin-α/Nup88 or Nup153/Nup88. However, the experiments did not determine whether complexes are generated that harbor all three components (see model, Fig. 8). To begin to address this question, we used identical samples to quantify the input (defined as 100%) and the amounts of importin-α that co-purified with anti-Nup153 or anti-Nup88 (Fig. 6G). In these experiments, 81% of importin-α was precipitated with anti-Nup153 and 68% with anti-Nup88 antibodies, suggesting that at least some of complexes contained importin-α, Nup153 and Nup88 (see Discussion and model, Fig. 8).

3.11. Stress increases the nuclear retention of importin-α, CAS, Nup153 and Nup88

The nuclear accumulation of importin-α and CAS may be explained by increased nuclear import, increased nuclear

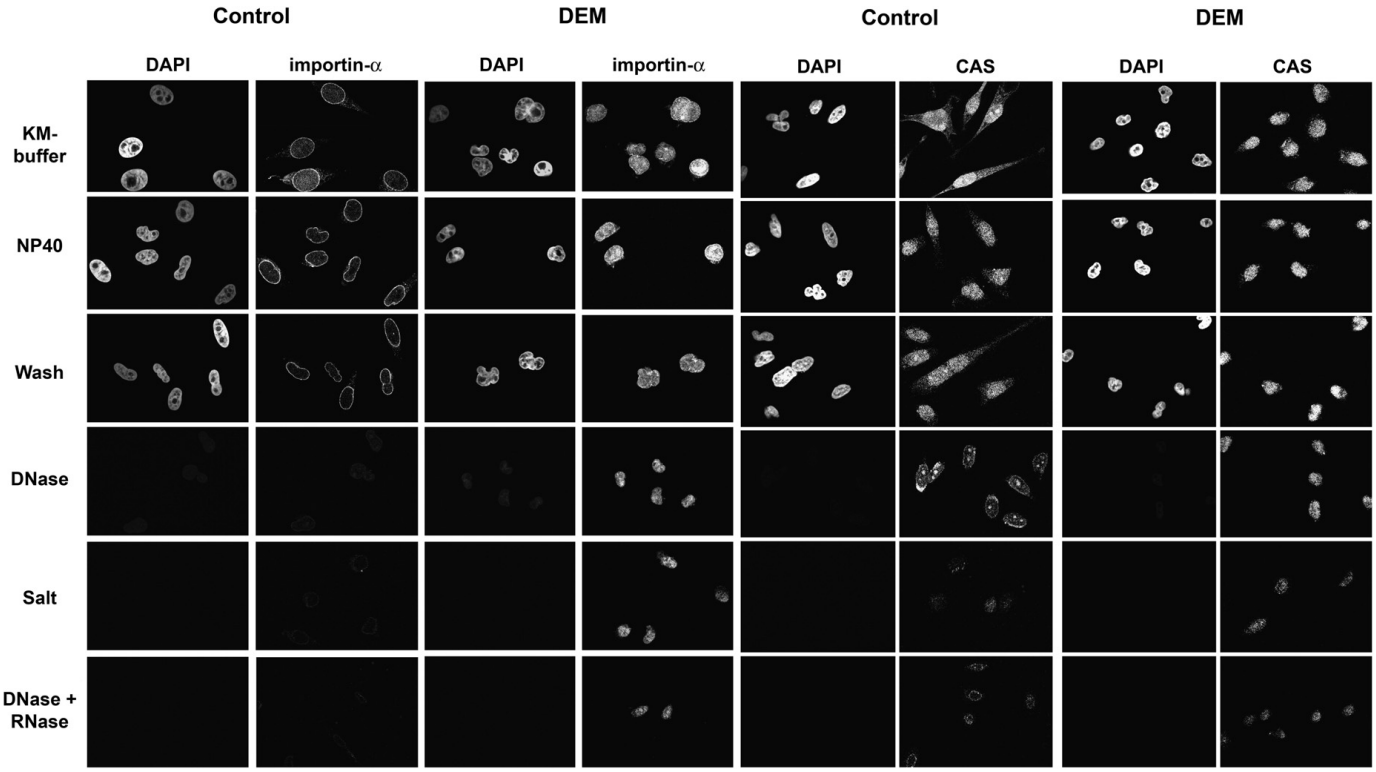

Fig. 7. Oxidative stress increases the nuclear retention of importin-α and CAS. Control and DEM-stressed cells were incubated with KM buffer followed by treatment with NP40, washing with buffer and treatment with DNase, salt as well as DNase+RNase [41]. Samples were fixed after each step and proteins were located by indirect immunofluorescence. For each protein, all samples were visualized with identical settings of the confocal microscope.

Table 2
Analysis of high molecular mass complexes in nuclei of DEM-treated cells

Protein	Anti-Nup153 IP	Anti-Nup88 IP
Importin-α	+	+
Nup153	+	+
Nup88	+	+
Nup214	−	−
Importin-β1	−	−
Hsc70	(+/−)	(+/−)
Actin	−	−
Tubulin	−	−

High molecular mass complexes obtained after FPLC were subjected to immunoprecipitation with anti-Nup153 and anti-Nup88 antibodies. Immunoprecipitates were separated by SDS-PAGE and Western blots were probed with antibodies against the proteins listed. Results are shown for at least three independent experiments. Co-purification is indicated by +, variable amounts of hsc70s co-purified with anti-Nup153 and anti-Nup88 are shown as (+/−). Proteins listed as − were not detected in immunoprecipitates.

retention, reduced nuclear export or a combination of these mechanisms. Quantitative analysis of *in vitro* nuclear trafficking of importin-α and CAS revealed that DEM treatment somewhat increased CAS and importin-α nuclear accumulation *in vitro* (Fig. 5). Since results described in the previous section suggested that the complex formation between importin-α and other proteins in the nucleus changes upon oxidant treatment, we tested whether these changes may correlate with stress-induced nuclear accumulation. To this end, control and DEM-treated cells were extracted with detergent, nucleases and salt. After each step, the presence of transport factors and nucleoporins was monitored by indirect immunofluorescence (Fig. 7, Suppl. Fig. 1, 2, 3). Individual proteins were solubilized at different steps of the procedure; however, in response to stress all of the components tested became less soluble. For instance, importin-α was readily extracted in control cells, and after DNase incubation only faint signals were observed. By contrast, upon DEM treatment a portion of importin-α remained associated with nuclei and was not extracted by any of the treatments (Fig. 7). Thus, the extraction of unfixed cells supports the interpretation that DEM-induced oxidative stress upregulated the nuclear retention of importin-α, CAS and several nucleoporins, including Nup153 and Nup88, while the formation of high molecular mass complexes containing importin-α, Nup153 and Nup88 increased.

4. Discussion

We have analyzed the effects of the oxidant DEM on nuclear trafficking and demonstrated the mislocalization and nuclear

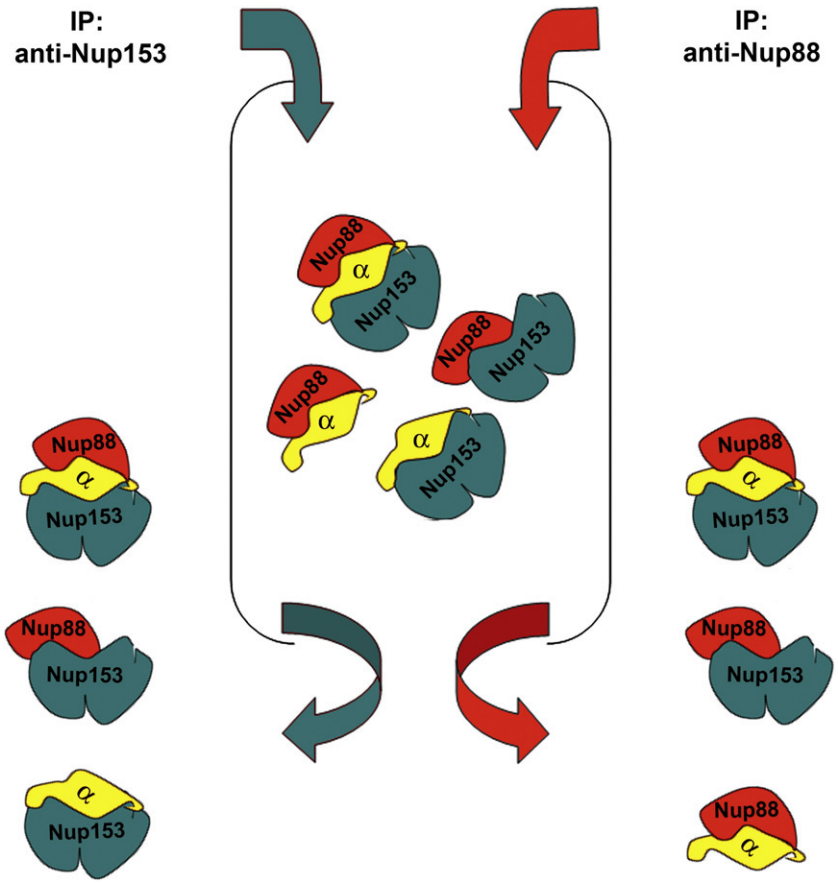

Fig. 8. Simplified model for the isolation of high molecular mass complexes containing Nup153 or Nup88. High molecular mass complexes analyzed in Fig. 6E and F may contain Nup153, Nup88 and/or importin-α as depicted. For simplicity, other subunits of the complexes which have yet to be identified were omitted. See text for details.

retention of several nuclear transport factors. Under the stress conditions used by us most of the cells remained viable, although the number of apoptotic and necrotic cells was somewhat increased. These conditions are likely to mimic exposure to physiological stresses or the pathophysiologies seen upon ischemia/reperfusion damage [5–9].

The analyses of GFP-tagged reporter proteins or endogenous substrates HuR and galectin-3 show that the nuc/cyt ratio for all proteins is reduced by DEM treatment, consistent with an oxidant-induced inhibition of nuclear import. However, it should be kept in mind that the nucleocytoplasmic distribution of HuR and galectin-3, like most endogenous cargos, is probably subject to additional regulation, including nuclear export and interactions with nuclear or cytoplasmic anchors. Our experiments do not address the question to which extent DEM alters these processes.

Our studies show for the first time that oxidant treatment not only relocates the soluble transport factors importin-α and CAS, but also nucleoporins Nup153 and Nup88. Interestingly, not all transport factors are affected by oxidative stress to the same extent, as we did not observe a strong effect on the localization of importin-β1. Moreover, we did not detect drastic changes in the nucleocytoplasmic Ran concentration gradient, which is sensitive to severe forms of stress that inhibit nuclear transport and may ultimately lead to cell death [31].

Results obtained for importin-α, CAS and nucleoporins are of particular interest with respect to nuclear protein trafficking. These components are required for nuclear transport of a wide variety of cargos, either as subunit of the classical NLS-receptor, to recycle importin-α to the cytoplasm or for the translocation of transport complexes across the NPC. Moreover, transport of proteins into the nucleus is an essential step of the stress response and necessary to cope with stress-induced damage, including exposure to oxidants. For instance, following oxidative stress transcription factors NF-κB, Nrf2 and members of the FoxO family translocate into the nucleus where they induce the expression of genes that encode antiapoptotic proteins or detoxifying enzymes [47–49]. Changes in the steady-state distribution of importin-α and CAS may inhibit these processes or render them less efficient.

Oxidative stress not only changes the distribution of soluble transport factors and nucleoporins, but also alters their interactions in the nucleus. Specifically, oxidant treatment leads to the formation of high molecular mass complexes which is accompanied by an increase in nuclear retention. Our experiments show for the first time that oxidant treatment relocates several nucleoporins to the nuclear interior, where they become components of high molecular mass complexes. These complexes contain importin-α, Nup153 and Nup88, but not CAS, suggesting that importin-α associates with a defined set of proteins in nuclei of stressed cells. Although importin-α containing high molecular mass complexes were isolated from control and stressed cells, the levels of Nup153 and Nup88 substantially increased after DEM treatment. Further analyses of high molecular mass complexes isolated from stressed cells demonstrated that importin-α associates with Nup153 as well as Nup88; furthermore, Nup153 binds to Nup88 (Fig. 8). This could be explained by the presence of different complexes containing importin-α/Nup153, importin-α/Nup88 and Nup153/Nup88, a complex harboring importin-α/Nup153/Nup88 or a mixture of all four complexes. Quantitation of immunoprecipitations showed that 81% of importin-α co-purified with Nup153 and 68% with Nup88, indicating that a portion of importin-α is likely to associate with both nucleoporins to generate importin-α/Nup153/Nup88 complexes.

Several scenarios can be proposed for the biochemical mechanisms that may link oxidative stress to the changes observed by us. For instance, oxidant treatment may lead to direct damage of soluble transport factors and nucleoporins or changes in signaling events. DEM may trigger not only the oxidation of critical residues in importin-α, CAS and nucleoporins; it may also activate signaling events that induce specific post-translational modifications of these proteins. As a consequence of oxidation or other modifications, transport across the NPC and retention within the cytoplasm or nucleus may be altered. With respect to our results one could propose that oxidative stress alters the affinity between importin-α and its binding partners in the nucleus, thereby promoting nuclear retention. The changes in affinity may result from the increased modifications of importin-α, Nup153 and Nup88, either alone or in combination. Given the molecular mass of the complexes isolated by us, they may contain additional components yet to be identified. These factors and their potential role in nuclear trafficking under normal and stress conditions will have to be defined in the future.

Little is known about stress-induced changes in the distribution and function of nucleoporins. We have shown previously that severe stress triggers the degradation of Nup153 [31]. The impact of non-lethal stress on nucleoporins is only poorly understood, but could play a role in human disease. For instance, mutations in the nucleoporin ALADIN may cause Triple A syndrome, and these mutations can also induce mislocalization of ALADIN, hypersensitivity to oxidative stress and defects in nuclear transport [50,51]. Our research demonstrates that stress modulates the localization and interactions of several nucleoporins in human cells. This sets the stage to further define the role of nucleoporins in the change of nuclear functions under stress and pathophysiological conditions.

Acknowledgements

We thank Drs. L. Gerace and W. Franke for their generous gifts of antibodies. We are grateful to Dr. J. Liu (HTS/HCS Facility at McGill University), K. McDonald and A. Srivastava for their help with ImageXpress Micro, FACS and confocal analyses. US was supported by grants from CIHR, NSERC and Heart and Stroke Foundation of Canada and is a chercheur national of FRSQ. MK was supported by a doctoral fellowship from FRSQ and the Heart and Stroke Foundation of Canada, CQ and AM by research bursaries from McGill University.

Appendix A. Supplementary data

Supplementary data associated with this article can be found, in the online version, at doi:10.1016/j.bbamcr.2007.10.022.

References

[1] T. Finkel, N. Holbrook, Oxidants, oxidative stress and the biology of ageing, Nature 408 (2000) 239–247.

[2] J.L. Martindale, N.J. Holbrook, Cellular response to oxidative stress: signaling for suicide and survival, J. Cell. Physiol. 192 (2002) 1–15.

[3] E. Cadenas, K.J. Davies, Mitochondrial free radical generation, oxidative stress, and aging, Free Radic. Biol. Med. 29 (2000) 222–230.

[4] S.G. Rhee, Y.S. Bae, S.R. Lee, J. Kwon, Hydrogen peroxide: a key messenger that modulates protein phosphorylation through cysteine oxidation, Sci. STKE (2000) 1–23.

[5] N.S. Dhalla, A.B. Elmoselhi, T. Hata, N. Makino, Status of myocardial antioxidants in ischemia-reperfusion injury, Cardiovasc. Res. 47 (2000) 446–456.

[6] D. Kumar, H. Lou, P.K. Singal, Oxidative stress and apoptosis in heart dysfunction, Herz 27 (2002) 662–668.

[7] W. Dröge, Free radicals in the physiological control of cell function, Physiol. Rev. 82 (2002) 47–95.

[8] E. Mariani, M.C. Polidori, A. Cherubini, P. Mecocci, Oxidative stress in brain aging, neurodegenerative and vascular diseases: an overview, J. Chromatogr. 827 (2005) 65–75.

[9] P.J. Crack, J.M. Taylor, Reactive oxygen species and the modulation of stroke, Free Radic. Biol. Med. 38 (2005) 1433–1444.

[10] R. Sitia, S.N. Molteni, Stress, protein (mis)folding, and signaling: the redox connection, Sci. STKE 2309 (2004) pe27.

[11] D.M. Townsend, K.D. Tew, H. Tapiero, The importance of glutathione in human disease, Biomed. Pharmacother. 57 (2003) 145–155.

[12] O.A. Bizzozero, J.L. Ziegler, G. De Jesus, F. Bolognani, Acute depletion of reduced glutathione causes extensive carbonylation of rat brain proteins, J. Neurosci. Res. 83 (2006) 656–667.

[13] R. Cruz-Aguado, W. Almaguer-Melian, C.M. Diaz, L. Lorigados, J. Bergado, Behavior and biochemical effects of glutathione depletion in the rat brain, Brain Res. Bull. 55 (2001) 327–333.

[14] P. Kaur, S. Kalia, M.P. Bansal, Effect of diethyl maleate induced oxidative stress on male reproductive activity in mice: redox active enzymes and transcription factor expression, Mol. Cell. Biochem. 291 (2006) 55–61.

[15] F. Esposito, L. Russo, G. Chirico, R. Ammendola, T. Russo, F. Cimino, Regulation of $p21^{waf1/cip1}$ expression by intracellular redox conditions, IUBMB Life 52 (2001) 67–70.

[16] K. Weis, Regulating access to the genome: nucleocytoplasmic transport throughout the cell cycle, Cell 112 (2005) 441–451.

[17] A. Harel, D.J. Forbes, Importin beta: conducting a much larger cellular symphony, Mol. Cell 16 (2004) 319–330.

[18] Y. Matsuura, M. Stewart, Structural basis for the assembly of a nuclear export complex, Nature 432 (2004) 872–877.

[19] D.S. Goldfarb, A.H. Corbett, D.A. Mason, M.T. Harreman, S.A. Adam, Importin α: a multipurpose nuclear-transport receptor, Trends Cell Biol. 14 (2004) 505–514.

[20] K.O. Otis, K.R. Thompson, K.C. Martin, Importin-mediated nuclear transport in neurons, Curr. Opin. Neurobiol. 16 (2006) 1–7.

[21] P. Behrens, U. Brinkmann, A. Wellmann, CSE1L/CAS: its role in proliferation and apoptosis, Apoptosis 8 (2003) 39–44.

[22] T.U. Schwartz, Modularity within the architecture of the nuclear pore complex, Curr. Opin. Struct. Biol. 15 (2005) 221–226.

[23] E.J. Tran, S.R. Wente, Dynamic nuclear pore complexes: life on the edge, Cell 125 (2006) 1041–1053.

[24] R. Bastos, M. Enarson, B. Burke, Targeting and function in mRNA export of nuclear pore protein Nup153, J. Cell Biol. 134 (1996) 1141–1156.

[25] M.S. Moore, Npap60: a new player in nuclear protein import, Trends Cell Biol. 13 (2003) 61–64.

[26] Y. Matsuura, M. Stewart, Nup50/Npap60 function in nuclear protein import complex disassembly and importin recycling, EMBO J. 24 (2005) 3681–3689.

[27] S. Hutten, R.H. Kehlenbach, CRM1-mediated nuclear export: to the pore and beyond, Trends Cell Biol. 17 (2007) 194–201.

[28] H. Liu, Y. Chen, G. Cui, Q. Wu, W. Chen, J. Zhou, Deguelin regulates nuclear pore complex proteins Nup98 and Nup88 in U937 cells *in vitro*, Acta Pharmacol. Sin. 26 (2005) 1265–1273.

[29] U. Stochaj, R. Rassadi, J. Chiu, Stress-mediated inhibition of classical nuclear import pathway and nuclear accumulation of the small GTPase Gsp1p, FASEB J. (2000), doi:10.1096/fj.99-0751fje.

[30] A. Chu, N. Matusiewicz, U. Stochaj, Heat-induced nuclear accumulation of hsc70s is regulated by phosphorylation and inhibited in confluent cells, FASEB J. (2001), doi:10.1096/fj.00-0680jje.

[31] M. Kodiha, A. Chu, N. Matusiewicz, U. Stochaj, Multiple mechanisms promote the inhibition of classical nuclear import upon exposure to severe oxidative stress, Cell Death Differ. 11 (2004) 862–874.

[32] Y. Miyamoto, T. Saiwaki, J. Yamashita, Y. Yasuda, I. Kotera, S. Shibata, M. Shigeta, Y. Hiraoka, T. Haraguchi, Y. Yoneda, Cellular stresses induce the nuclear accumulation of importin α and cause a conventional nuclear import block, J. Cell Biol. 165 (2004) 617–623.

[33] E. Boyland, L.F. Chasseaud, Enzyme-catalyzed conjugations with glutathione with unsaturated compounds, Biochem. J. 104 (1967) 95–102.

[34] J.L. Plummer, B.R. Smith, H. Sies, J.R. Bend, Chemical depletion of glutathione *in vivo*, Methods Enzymol. 77 (1981) 50–59.

[35] S. Chatterjee, U. Stochaj, Diffusion of proteins across the nuclear envelope of HeLa cells, BioTechniques 24 (1998) 668–674.

[36] K.L. Carey, S.A. Richards, K.M. Lounsbury, I.G. Macara, Evidence using a green fluorescent protein-glucocorticoid receptor chimera that the Ran/TC4 GTPase mediates an essential function independent of nuclear protein import, J. Cell Biol. 133 (1996) 985–996.

[37] M. Kodiha, A. Chu, O. Lazrak, U. Stochaj, Stress inhibits nucleocytoplasmic shuttling of heat shock protein hsc70, Am. J. Physiol., Cell Physiol. 289 (2005) C1034–C1041.

[38] V.C. Cordes, S. Reidenbach, A. Kohler, N. Stuurman, R. van Driel, W.W. Franke, Intranuclear filaments containing a nuclear pore complex protein, J. Cell Biol. 123 (1993) 1333–1344.

[39] M. Kodiha, J.G. Rassi, C.M. Brown, U. Stochaj, Localization of AMP kinase is regulated by stress, cell density, and signaling through the MEK-> ERK1/2 pathway, Am. J. Physiol. Cell Physiol. 293 (2007) C1427–C1436.

[40] R. Truant, R.A. Fridell, E.R. Benson, A. Herold, B.R. Cullen, Nucleocytoplasmic shuttling by protein nuclear import factors, Eur. J. Cell Biol. 77 (1998) 269–275.

[41] I.M. Staufenbiel, W. Deppert, Preparation of nuclear matrices from cultured cells: subfractionation of nuclei in situ, J. Cell Biol. 98 (1984) 1886–1894.

[42] L. Sanchez, M. Kodiha, U. Stochaj, Monitoring the disruption of nuclear envelopes in interphase cells with GFP-β-galactosidase, J. Biomol. Tech. 16 (2005) 235–238.

[43] N.D. Freedman, K.R. Yamamoto, Importin 7 and importin α/importin β are nuclear import receptors for the glucocorticoid receptor, Mol. Biol. Cell 15 (2004) 2276–2286.

[44] W. Wang, X. Yang, T. Kawai, I.L. Silanes, K. Mazan-Mamczarz, P. Chen, Y.M. Chook, C. Quensel, M. Köhler, M. Gorospe, AMP-activated kinase-regulated phosphorylation and acetylation of importin-α, J. Biol. Chem. 279 (2004) 48376–48388.

[45] S. Nakahara, V. Hogan, H. Inohara, A. Raz, Importin-mediated nuclear translocation of galectin-3, J. Biol. Chem. 281 (2006) 39649–39659.

[46] Y. Miyamoto, M. Hieda, M.T. Harreman, M. Fukumoto, T. Saiwaki, A.E. Hodel, A.H. Corbett, Y. Yoneda, Importin α can migrate into the nucleus in an importin β- and Ran-independent manner, EMBO J. 21 (2002) 5833–5842.

[47] M.P. Mattson, M.K. Meffert, Roles for NF-κB in nerve cell survival, plasticity, and disease, Cell Death Differ. 13 (2006) 852–860.

[48] L.P. Heide, M.F.M. Hoekman, M.P. Smidt, The ins and outs of FoxO shuttling: mechanisms of FoxO translocation and transcriptional regulation, Biochem. J. 380 (2004) 297–309.

[49] A.K. Jaiswal, Nrf2 signaling in coordinated activation of antioxidant gene expression, Free Radic. Biol. Med. 36 (2004) 1199–1207.

[50] J.M. Cronshaw, M.J. Matunis, The nuclear pore complex protein ALADIN is mislocalized in triple A syndrome, Proc. Natl. Acad. Sci. U. S. A. 100 (2003) 5823–5827.

[51] M. Hirano, Y. Furiya, H. Asai, A. Yasui, S. Ueno, $ALADIN^{I2825}$ causes selective failure of nuclear protein import and hypersensitivity to oxidative stress in triple A syndrome, Proc. Natl. Acad. Sci. U. S. A. 103 (2006) 2298–2302.

Localization of AMP kinase is regulated by stress, cell density, and signaling through the MEK->ERK1/2 pathway

Mohamed Kodiha, James G. Rassi, Claire M. Brown and Ursula Stochaj

Am J Physiol Cell Physiol 293:1427-1436, 2007. First published Aug 29, 2007;
doi:10.1152/ajpcell.00176.2007

AJP - Cell Physiology is dedicated to innovative approaches to the study of cell and molecular physiology. It is published 12 times a year (monthly) by the American Physiological Society, 9650 Rockville Pike, Bethesda MD 20814-3991. Copyright © 2005 by the American Physiological Society. ISSN: 0363-6143, ESSN: 1522-1563. Visit our website at http://www.the-aps.org/.

Am J Physiol Cell Physiol 293: C1427–C1436, 2007.
First published August 29, 2007; doi:10.1152/ajpcell.00176.2007.

CALL FOR PAPERS | *Protein and Vesicle Trafficking, Cytoskeleton*

Localization of AMP kinase is regulated by stress, cell density, and signaling through the MEK→ERK1/2 pathway

Mohamed Kodiha,[1] James G. Rassi,[1] Claire M. Brown,[2] and Ursula Stochaj[1]

[1]*Department of Physiology,* [2]*Department of Biochemistry and Life Sciences Imaging Facility, McGill University, Montreal H3G 1Y6, Canada*

Submitted 26 April 2007; accepted in final form 10 August 2007

Kodiha M, Rassi JG, Brown CM, Stochaj U. Localization of AMP kinase is regulated by stress, cell density, and signaling through the MEK→ERK1/2 pathway. *Am J Physiol Heart Circ Physiol* 293: C1427–C1436, 2007. First published August 29, 2007; doi:10.1152/ajpcell.00176.2007.—5′-AMP-activated protein kinase (AMPK) serves as an energy sensor and is at the center of control for a large number of metabolic reactions, thereby playing a crucial role in Type 2 diabetes and other human diseases. AMPK is present in the nucleus and cytoplasm; however, the mechanisms that regulate the intracellular localization of AMPK are poorly understood. We have now identified several factors that control the distribution of AMPK. Environmental stress regulates the intracellular localization of AMPK, and upon recovery from heat shock or oxidant exposure AMPK accumulates in the nuclei. We show that under normal growth conditions AMPK shuttles between the nucleus and the cytoplasm, a process that depends on the nuclear exporter Crm1. However, nucleocytoplasmic shuttling does not take place in high-density cell cultures, for which AMPK is confined to the cytoplasm. Furthermore, we demonstrate that signaling through the mitogen-activated protein kinase kinase (MEK)→extracellular signal-regulated kinase 1/2 (ERK1/2) cascade plays a crucial role in controlling the proper localization of AMPK. As such, pharmacological inhibitors that interfere with this pathway alter AMPK distribution under non-stress conditions. Taken together, our studies identify novel links between the physiological state of the cell, the activation of MEK→ERK1/2 signaling, and the nucleocytoplasmic distribution of AMPK. This sets the stage to develop new strategies to regulate the intracellular localization of AMPK and thereby the modification of targets that are relevant to human disease.

5′-AMP-activated protein kinase; nuclear transport

THE PRESENCE OF NUTRIENTS, such as the carbon source, regulates protein synthesis, gene expression, and the activity of a large number of proteins. 5′-AMP-activated protein kinase (AMPK) is a key player in these processes; the enzyme not only controls cell growth and transcription but also the response to nutrient limitation and stress (reviewed in Refs. 1, 4, 5, 7, 19, 23, 28, 32). AMPK is a central regulator of cellular metabolism for which it serves as an energy sensor; the enzyme is activated by a reduction of ATP/AMP levels, changes in intracellular calcium, and other forms of stress, including ischemia and hypoxia (18). Based on its central role in the control of glucose homeostasis and lipid metabolism, AMPK is an important therapeutic target in Type 2 diabetes and obesity. In particular, low-level activation of AMPK is likely to contribute to the global rise in obesity and diabetes (7). In addition to its regulatory function in metabolism, more recent studies demonstrate that AMPK is also crucial for cell polarity and mitosis (17).

The heterotrimeric AMPK contains a catalytic α-subunit, encoded by two genes (α_1 and α_2). The regulatory β- and γ-subunits are encoded by two and three genes, respectively (reviewed in Ref. 7). Activation of AMPK includes the phosphorylation of Thr172 of the α-subunit, which can be mediated by one of the two upstream regulatory kinases LKB1 and Ca^{2+}/calmodulin-dependent kinase kinase (CaMKK) (2, 9, and references therein). Previous reports suggest that the α_2-subunit of AMPK maybe somewhat enriched in the nucleus (24), and mutations in the β_1-subunit can increase its amount in nuclei (34).

The only direct means of communication between the nucleoplasm and cytoplasm is through nuclear pore complexes (NPCs, reviewed in Refs. 8, 26, and 27). There are several mechanisms of macromolecular translocation along NPCs, molecules with a mass of 40 kDa or less may diffuse across the NPC. By contrast, larger macromolecules rely on active transport and, in most cases, on specific carriers that promote transport across the NPC (8, 26, 27). Members of the importin-β family in particular play a crucial role in protein trafficking in and out of the nucleus. For instance, the nuclear exporter Crm1 recognizes hydrophobic leucine-rich signals that target a protein for export to the cytoplasm (16). Crm1-mediated nuclear export is inhibited by the drug leptomycin B (LMB), which covalently modifies the carrier (15).

To date, little is known about the nuclear and cytoplasmic pools of AMPK and how its intracellular distribution is controlled. Such a regulated localization to different cell compartments should be critical for the proper response to extra- and intracellular stimuli, leading to the phosphorylation of distinct AMPK targets. Although AMPK phosphorylates proteins in both the nucleus and the cytoplasm, it has not been determined whether its distribution is sensitive to stress or other changes in cell physiology. This knowledge is important, because it will set the stage to identify specific AMPK functions in either compartment that are dictated by physiological changes. This includes oxidative stress, a key factor that adds to the patho-

Address for reprint requests and other correspondence: U. Stochaj, Physiology Dept., 3655 Promenade Sir William Osler, McGill Univ., Montreal H3G 1Y6, Canada (e-mail: ursula.stochaj@mcgill.ca).

The costs of publication of this article were defrayed in part by the payment of page charges. The article must therefore be hereby marked "*advertisement*" in accordance with 18 U.S.C. Section 1734 solely to indicate this fact.

physiologies in diabetic patients (22, 29, 31). To begin to answer these questions, we analyzed AMPK phosphorylation and localization in human culture cells. Since LKB1 has been associated with the activation and actions of AMPK (reviewed in Ref. 7), we used HeLa cells, which do not synthesize LKB1 (9), as well as HEK293 cells, a human kidney cell line that does express LKB1 (25). Our studies demonstrate that stress, cell density, and signaling through the extracellular signal-regulated kinase 1/2 (ERK1/2)-mitogen-activated protein kinase (MAPK) module control the subcellular distribution of AMPK. Moreover, we show that AMPK shuttles between the nucleus and the cytoplasm and identified Crm1 as the nuclear carrier that translocates AMPK to the cytoplasm. Together, this multilayered control of intracellular localization provides a unique set of tools to rapidly adjust the distribution of AMPK to changes in cell physiology.

MATERIALS AND METHODS

Cell culture and exposure to stress. HeLa and HEK293 cells were cultured essentially as described (3, 13). In brief, cells were grown on poly-L-lysine-coated coverslips in six-well dishes to ~70% confluency or high density (>100% confluency). This correlates with ~4 × 10^5 and >2 × 10^6 cells/cm^2, respectively. Heat shock was for 1 h at 45.5°C followed by recovery at 37°C for 2, 3, and 5 h. All other treatments were at 37°C. Incubation with 2 mM diethyl maleate was for 4 h.

Pharmacological tools. Energy depletion was performed with 50 mM deoxyglucose combined with 10 mM NaN_3 for 30 min. For inhibition of the ERK1/2 pathway, cells were incubated with 25 μM PD98059 (Calbiochem) for 5 h or 50 μg/ml ERK peptide inhibitor II (Calbiochem) for 1 h. PD98059 inhibits the MAPK kinase (MEK) thereby preventing the activation of the downstream kinase ERK1/2. The ERK peptide inhibitor II contains 13 residues derived from the NH_2-terminal portion of MEK1, binds to ERK, and prevents its activation by inhibiting the binding of MEK1 (11). LMB (LC laboratories, Woburn, MA) has multiple actions, which includes inhibition of the nuclear exporter Crm1, inhibition of cell cycle progression, and antitumor activity. LMB was present at 10 ng/ml for 21 h, and controls were treated with the solvent only under identical conditions. For serum starvation, cultures were grown for 18 h without serum followed by 5 min incubation with fresh medium with or without 8% serum. After stress exposure or drug treatment, cells were immediately fixed for immunofluorescence or stored at −70°C.

Indirect immunofluorescence and microscopy. All steps were carried out at room temperature following published procedures (14). Primary antibodies were used at the following concentrations: AMPK-α1/2 (Cell Signaling Techn no. 2532), 1:200; AMPK-β1/2 (Cell Signaling Techn no. 4150), 1:200; and Cy3-coupled secondary antibodies (Jackson ImmunoResearch) were diluted 1:500. No signals were obtained when primary antibodies were omitted (not shown). Images were either acquired for 1-μm slices with a Zeiss LSM510 inverted microscope using a ×63 oil-immersion objective with 1.4 numerical aperature or with the Molecular Devices (Sunnyvale, CA) ImageXpress Micro equipped with a 300-W Xenon light source and a CoolSnapHQ (Photometrics, Tucson, AZ). For the ImageXpress, Micro images of 4′,6-diamidino-2-phenylindole (DAPI, cube no. 49000) or Cy3 (no. 49005) were collected with cubes from Chroma Technology (Rockingham, VT). Cells were grown on glass coverslips before being labelled and mounted with Vectashield (Vector Laboratories, Burlingame, CA) after labeling was completed. Up to 64 fields of view were imaged at ×40 (PlanFluor ELWD 0.6NA) using 2 × 2 binning and ensuring at least 55 cells were sampled for each experimental condition. Image analysis was done with MetaXpress software. DAPI labeling was used to identify the number of cells in each field of view; protein staining with Cy3 was used to identify the entire cell. Care was taken to adjust the threshold level used to ensure that all cells were detected accurately even for lower expressing samples. The total intensity of antibody labeling in the nucleus was measured based on segmentation using DAPI staining, and the intensity of the entire cell was calculated based on segmentation with the Cy3 labeling. The difference between these two intensities was taken as the total intensity of the cytosolic fraction of the protein. All images were corrected for contributions due to background intensity based on intensity measurements off of the cells for each image field. Finally, the ratio of the total intensity in the nucleus versus the total intensity of the cytosol was measured for each sample. Images were processed in Adobe Photoshop 8.0 for publication.

Western blot analysis. Cells grown on 10-cm culture dishes to ~70% confluency or at high density were exposed to stress or pharmacological inhibitors as described above. After treatment, plates were rinsed with phosphate-buffered saline and stored at −70°C until use. Crude extracts were prepared by solubilizing proteins in gel sample buffer, pH 8.0, containing protease inhibitors (1 mM phenylmethylsulfonyl fluoride; aprotinin, leupeptin, and pepstatin, each at 1 μg/ml), 20 mM β-glycerophosphate, 1 mM NaN_3, and 2.5 mM NaF. Samples were incubated for 15 min at 95°C and vortexed with glass beads to shear DNA. After centrifugation (5 min, 13,000 rpm, microfuge), equal amounts of protein were separated in SDS-PA gels. Proteins were blotted to nitrocellulose and filters were processed as described (3). Antibodies against AMPK and dually phospho-ERK1/2 (Cell Signaling, no. 9106) were diluted 1:1,000; anti-ERK1/2 (StressGen, KAP-MA001C) was used at 1:2,000, anti-LDH (100–1173, Rockland, Gilbertsville, PA) at 1:2,000, and anti-lamin B (SC-6217, Santa Cruz Biotechnology, CA) at 1:2,000. ECL signals (Amersham Biosciences) were quantified by densitometry (21). Results are shown as means ± SD of at least three independent experiments.

Cell fractionation. To isolate cytoplasmic and nuclear fractions, cells were incubated in lysis buffer [10 mM HEPES, pH 7.9, 10 mM KCl, 1.5 mM $MgCl_2$, 1 mM DTT, 1 mM NaN_3, and a mixture of protease inhibitors (Roche)] for 15 min on ice. Cells were drawn through a 26-gauge needle and centrifuged 10 min at 2,000 *g*. Sediments were resuspended in lysis buffer, centrifuged, and washed once in lysis buffer containing 0.005% Nonidet-40. After 1 min centrifugation at 20,000 *g*, nuclear proteins were obtained in the sediments. Combined supernatants contained the cytoplasmic marker protein LDH, whereas lamin B was restricted to nuclear fractions. For comparison, one equivalent of cytoplasmic proteins and two equivalents of nuclear proteins were analyzed side-by-side by Western blot analysis with different antibodies. ECL signals were quantified for AMPK-α1/2 phosphorylated on Thr172 (p-AMPK-α1/2), total AMPK-α1/2 (t-AMPK-α1/2), and AMPK-β1/2, and nuclear-to-cytoplasmic ratios (nuc/cyt) were calculated. Based on AMPK-α1/2 Thr172 phosphorylation and the nuc/cyt distribution of p-AMPK-α1/2, we determined the net nuclear levels of p-AMPK-α1/2. Note that the amount of t-AMPK-α1/2 was not drastically altered by the different stressors. For all conditions the net nuclear levels of controls were defined as 1.

Statistics. For Western blot analysis, ECL signals were quantified as described in Ref. 21. Data were acquired for at least three independent experiments. Results are shown as means ± SD. Bonferroni tests for multiple statistical comparisons (Figs. 1 and 2 and online supplment Fig. 1) and Student's *t*-test (two-tailed) for unpaired samples were carried out to identify significant differences. For each experiment, all test results were compared with the control.

RESULTS

AMPK accumulates in nuclei upon stress. Quantitative immunofluorescence and Western blot analysis were used to detect AMPK-α1/2 and -β1/2-subunits in cultured human

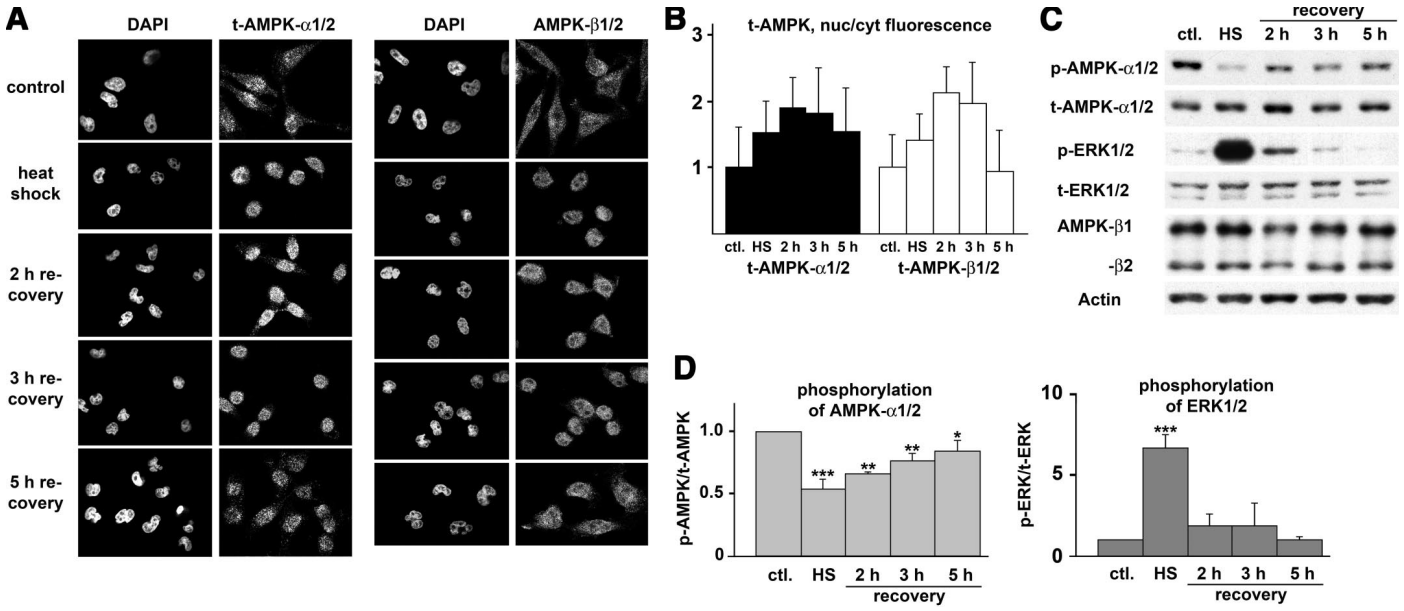

Fig. 1. Heat stress relocates 5′-AMP-activated protein kinase (AMPK) to the nucleus of HeLa cells. Cells grown to ~70% confluency were exposed to 1 h heat stress (HS) and allowed to recover at 37°C for the times indicated. *A*: total AMPK-α1/2 (t-AMPK-α1/2) and AMPK-β1/2 were detected by indirect immunofluorescence. DAPI, 4′,6-diamidino-2-phenylindole. *B*: quantification of fluorescence signals was carried out as detailed in MATERIALS AND METHODS. *C*: for Western blot analysis equal amounts of proteins were analyzed with antibodies against AMPK-α1/2 phosphorylated on Thr172 (p-AMPK-α1/2), t-AMPK-α1/2, dually phosphorylated ERK1/2 (p-ERK1/2), total ERK1/2 (t-ERK1/2), AMPK-β1/2, and actin. *D*: ECL signals were quantified for at least three independent experiments. Means and SD are shown for changes in AMPK-α1/2 Thr172 (p-AMPK/t-AMPK) and ERK1/2 phosphorylation (p-ERK/t-ERK). Untreated controls served as reference for heat-shocked and recovering cells. $***P < 0.001$; $**P < 0.01$, $*P < 0.05$.

cells. The results are shown here for HeLa (Figs. 1–10, online supplemental Figs. 2 and 3) and HEK293 cells (online supplemental Fig. 1). When analyzed by indirect immunofluorescence, α- and β-subunits of AMPK were nuclear and cytoplasmic in HeLa cells under nonstress conditions, with α-subunits somewhat concentrated in nuclei. When cells were exposed to heat, energy depletion, or oxidative stress, the levels of α- and β-subunits in nuclei increased (Figs. 1, *A* and *B*, and 3, *A* and *B*). In control experiments, the cytoplasmic enzyme lactate dehydrogenase (LDH) did not relocate to the nucleus for any of the stresses analyzed. Furthermore, the nuclear marker protein lamin B was confined to the nucleus under all conditions tested (online supplemental Figs. 2 and 3).

Nuclear accumulation of AMPK-α1/2 and -β1/2 was particularly prominent after heat stress and when cells were allowed to recover at 37°C for 2 to 3 h; after 5 h recovery nuclear levels

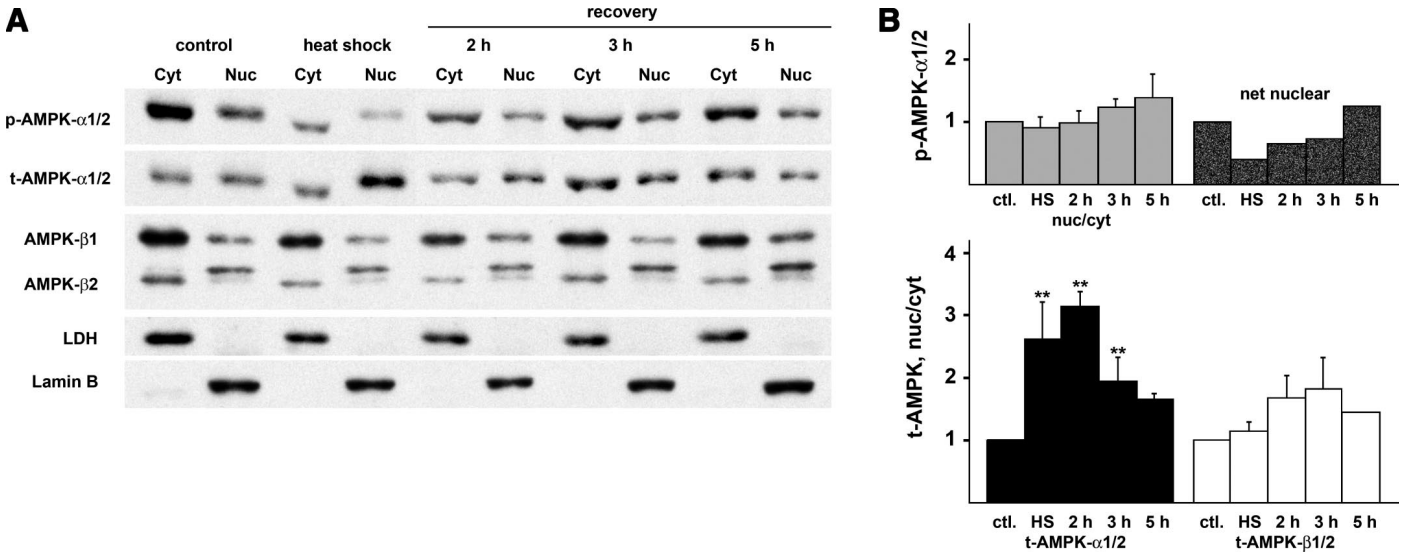

Fig. 2. Analysis of AMPK distribution in heat-stressed HeLa cells by cell fractionation. *A*: control and stressed cells were fractionated followed by Western blot analysis of cytoplasmic (Cyt) and nuclear (Nuc) fractions. One equivalent of cytoplasmic and two equivalents of nuclear proteins were analyzed side by side. *B*: for p-AMPK-α1/2, nuclear-to-cytoplasmic ratios (nuc/cyt) and the net nuclear content were determined (MATERIALS AND METHODS). Nuc/cyt ratios were calculated for t-AMPK-α1/2 and t-AMPK-β1/2. As controls, filters were probed for lactate dehydrogenase (LDH) and lamin B. ECL signals were quantified for AMPK as in Fig. 1. All test results were compared with the untreated control. $**P < 0.01$, $*P < 0.05$.

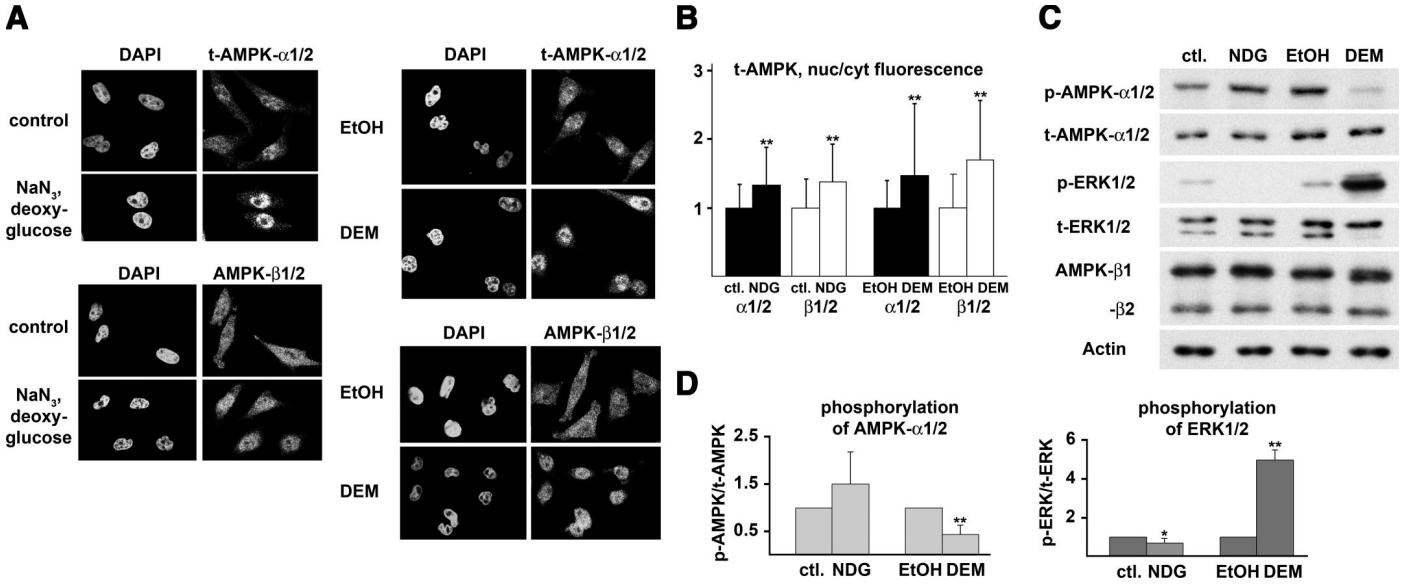

Fig. 3. Energy depletion and oxidative stress alter the distribution of AMPK in HeLa cells. Cultured cells at ~70% confluency were energy depleted with NaN_3-deoxyglucose (NDG) or treated with the oxidant diethyl maleate (DEM) as described in MATERIALS AND METHODS. Controls were incubated with solvent only. *A–D*: localization of proteins by indirect immunofluorescence and Western blot analysis were carried out as described for Fig. 1, *A–D*. Control samples served as reference for all test results. $^{**}P < 0.01$; $^{*}P < 0.05$.

of AMPK began to decrease again. The distribution of AMPK subunits under different conditions was quantified by determining nuclear and cytoplasmic fluorescence (see MATERIALS AND METHODS) and calculating the nuc/cyt ratio of fluorescence (Fig. 1*B*). Since the nucleus occupies less than 10% of the mammalian cell volume, a small increase in the nuc/cyt ratio of AMPK represents a drastic change in the nuclear concentration of the protein.

The results obtained for immunolocalization were further substantiated by cell fractionation (Figs. 2*A* and 4*A*). Cytoplasmic and nuclear fractions were analyzed by quantitative Western blot analysis and quantification of ECL signals (Figs. 2*B* and 4*B*). (Note that for all cell fractionations one equivalent of cytoplasmic and two equivalents of nuclear proteins were separated side-by-side.) As observed for immunolocalization, the nuc/cyt ratio of total AMPK-α1/2 and -β1/2 increased upon heat shock and started to decline upon 5 h of recovery.

A different scenario, however, emerged for cell fractionation followed by Western blot analysis with antibodies that recognize phosphorylated Thr172 in α-subunits (Figs. 2, 4, and 6; p-AMPK-α1/2). In crude extracts, heat stress significantly reduced the modification of Thr172 (Fig. 1, *C* and *D*). By contrast, the nuc/cyt ratio of p-AMPK-α1/2 did not drastically change and slightly increased at 3 and 5 h of recovery (Fig. 2*B*). Thus the heat-induced changes in the nuc/cyt distribution

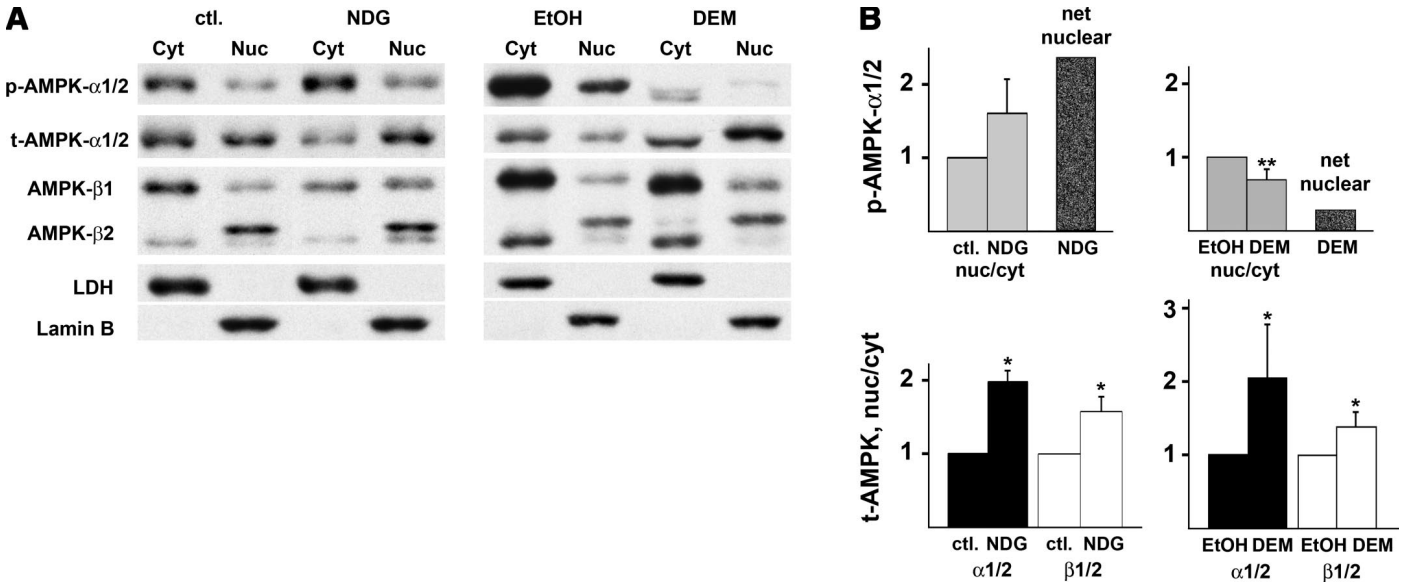

Fig. 4. *A* and *B*: effect of energy depletion and oxidant exposure on the distribution of AMPK in HeLa cells. Cell fractionation and quantification of ECL signals for cytoplasmic and nuclear AMPK were as in Fig. 2, *A* and *B*. All test results were compared with control samples. $^{**}P < 0.01$; $^{*}P < 0.05$.

Table 1. *Distribution of AMPK-α1/2 phosphorylated on Thr172 and activation of ERK1/2. Results for nuc/cyt ratio, net nuclear content of p-AMPK-α1/2, and ERK1/2 activation are summarized*

	p-AMPK-α1/2		
Treatment	Nuc/cyt ratio	Net nuclear content	ERK1/2 Activation
Heat shock	↔	↓	↑
NDG	↑	↑	↓
DEM	↓	↓	↑
Serum	↓	↓	↑
PD98059	↑	↑	↓

Effects of stress exposure, serum starvation, and incubation with the MAPK kinase (MEK) inhibitor PD98059 are shown. Arrows indicate no change (↔), reduction (↓), or increase (↑). p-AMPK-α1/2, 5′-AMP-activated protein kinase phosphorylated on Thr172; ERK1/2, extracellular signal-regulated kinase 1/2; NDG, deoxyglucose/NaN_3; DEM, diethyl maleate.

of t-AMPK-α1/2 and p-AMPK-α1/2 were clearly different (Fig. 2*B*).

A change in the nuc/cyt ratio of p-AMPK-α1/2 does not necessarily lead to a change in the net amount of p-AMPK-α1/2 in the nucleus. To address this point, we calculated how the net amount of p-AMPK-α1/2 in nuclei changes upon exposure to heat and during recovery (see MATERIALS AND METHODS). After heat shock and after 2 or 3 h of recovery, net nuclear levels of p-AMPK-α1/2 were reduced compared with unstressed cells (Fig. 2*B*, net nuclear).

Like heat, energy depletion with deoxyglucose-NaN_3 (NDG) or oxidative stress triggered by diethyl maleate (DEM) induced t-AMPK nuclear accumulation as determined by quantitative immunolocalization and Western blot analysis (Figs. 3*B* and 4). Energy depletion increased the phosphorylation of AMPK-α1/2 on Thr172 as well as the nuc/cyt ratio of p-AMPK-α1/2. By contrast, DEM treatment reduced Thr172 phosphorylation and the nuc/cyt ratio of p-AMPK-α1/2 (Figs. 3, *C* and *D*, and 4*B*). Taken together, changes in the distribution of AMPK-α1/2 phosphorylated on Thr172 did not correlate with the redistribution of t-AMPK-α1/2. Table 1 summarizes the results obtained for AMPK phosphorylation and distribution and ERK1/2 activation under different experimental conditions.

Stress-induced dephosphorylation of AMPK-α1/2 Thr172 correlates with the activation of ERK1/2. Crosstalk between AMPK and ERK1/2 may involve positive as well as negative signaling events (29). In our experiments with HeLa cells, heat and DEM significantly activated ERK1/2, as evident from its dual phosphorylation (Figs. 1, *C* and *D*, and 3, *C* and *D*; p-ERK1/2). At the same time, the phosphorylation of AMPK-α1/2 Thr172 (p-AMPK-α1/2) was reduced. By contrast, deoxyglucose-NaN_3 elevated Thr172 and decreased ERK1/2 phosphorylation. In HEK293 cells upon DEM treatment, we detected neither an increase in the dual phosphorylation of ERK1/2 nor significant changes in the modification of AMPKα1/2. Nevertheless, for all stress conditions analyzed there was an inverse relationship between AMPK-α1/2 Thr172 phosphorylation and the dual modification of ERK1/2 in both HeLa and HEK293 cells (Figs. 1, 3, and 5 and online supplemental Fig. 1), suggesting that this effect is not restricted to a specific cell line.

Addition of serum to starved HeLa cells increases the amount of AMPK in nuclei. Experiments above showed that in stressed cells the increase in ERK1/2 activation may be linked to a reduction in the net amount of p-AMPK-α1/2 in nuclei. We further addressed this point using serum-deprived cells. After 18 h incubation in serum-free medium, the addition of serum to HeLa cells rapidly induced ERK1/2 phosphorylation. Concomitantly, there was a small but significant decrease of AMPK-α1/2 Thr172 phosphorylation as well as a reduction of the net amount of nuclear p-AMPK1/2. Unlike p-AMPK1/2, t-AMPK-α1/2 and -β1/2 subunits accumulated in nuclei (Figs. 5 and 6).

AMPK shuttles between the nucleus and the cytoplasm and is exported from nuclei by the carrier Crm1. Results for the relocation of AMPK-α and β-subunits upon stress and the

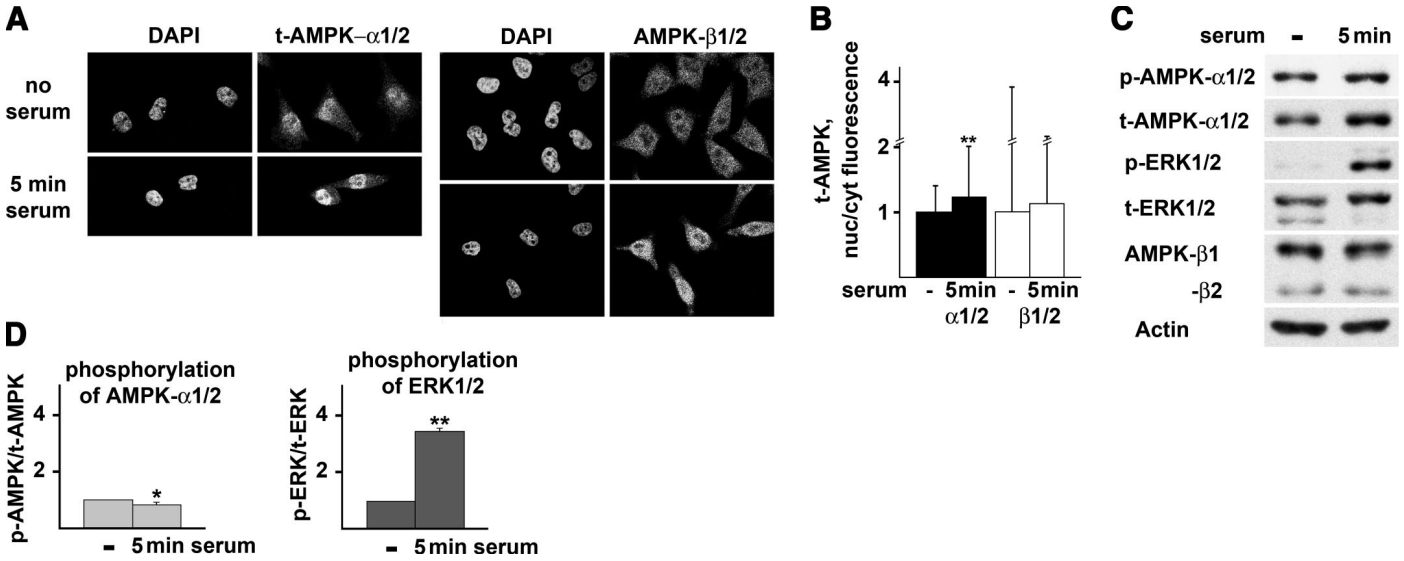

Fig. 5. *A–D*: addition of serum to starved cells raises the nuclear levels of AMPK. HeLa cells were serum starved for 18 h and subsequently incubated with fresh medium without or with serum for 5 min. Indirect immunofluorescence and Western blot analysis were as detailed for Fig. 1, *A–D*. All experimental results were compared with the untreated control. $^{**}P < 0.01$; $^{*}P < 0.05$.

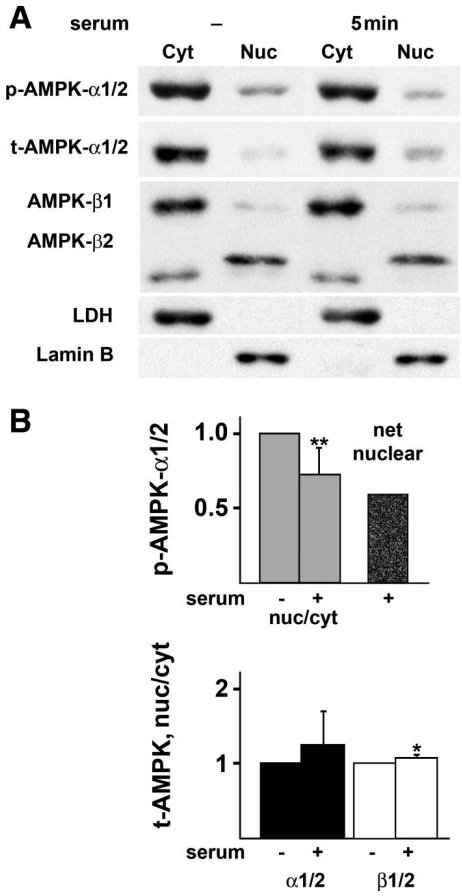

Fig. 6. *A* and *B*: serum addition affects AMPK distribution in starved cells. HeLa cells were incubated with medium in the absence or presence of serum as described for Fig. 5. Cell fractionation and quantification of cytoplasmic and nuclear AMPK were as in Fig. 2. The untreated control was used as reference for all test results. $^{**}P < 0.01$; $^{*}P < 0.05$.

reversal during recovery may suggest that they shuttle between the nucleus and the cytoplasm using unknown transporters. The carrier Crm1 is involved in the export of a large number of proteins and efficiently inhibited by the drug LMB. As shown for quantitative immunofluorescence (Fig. 7, *A* and *B*) and Western blot analysis (Fig. 7, *C* and *D*), incubation with LMB resulted in the nuclear accumulation of t-AMPK-α and β-subunits in unstressed HeLa cells, in line with the idea that the subunits shuttle and Crm1 serves as their nuclear exporter. No significant changes were detected for the distribution of p-AMPK-α1/2 (Fig. 7, *C* and *D*).

Cell density controls the distribution and shuttling of AMPK. Nuclear trafficking of proteins can be controlled by the density of the culture, and high confluency may interfere with nuclear transport of proteins (3, 10). Both α- and β-subunits of the kinase were nuclear and cytoplasmic at 70% confluency in unstressed HeLa cells (Figs. 1, 3, 5, and 7) but were restricted to the cytoplasm in high-density cultures when analyzed by indirect immunofluorescence or cell fractionation (Fig. 8, *A*, *C*, *D*). Moreover, in high-density HeLa cultures treated with the inhibitor LMB, AMPK failed to accumulate in nuclei, indicating that shuttling does not take place under these conditions (Fig. 8, *A*, *C*, *D*). This density-dependent redistribution of AMPK is not simply an effect of changes in the medium of high-density cultures, since AMPK was nuclear as well as cytoplasmic and able to shuttle for cells growing in less dense areas of the same coverslip (data not shown). Interestingly, in high-density cells we detected little phosphorylation of AMPK-α1/2 Thr172 or activation of ERK1/2 (Fig. 8*B*). This could be in part attributed to changes in protein levels, as the total amount of AMPK-α1/2 and ERK1/2 was somewhat reduced in high-density cultures. By contrast, the levels of AMPK-β1/2 were somewhat increased (Fig. 8*B*). It is not known why the nuc/cyt ratio of AMPK-β1/2 decreases in the presence of LMB (Fig. 8*D*).

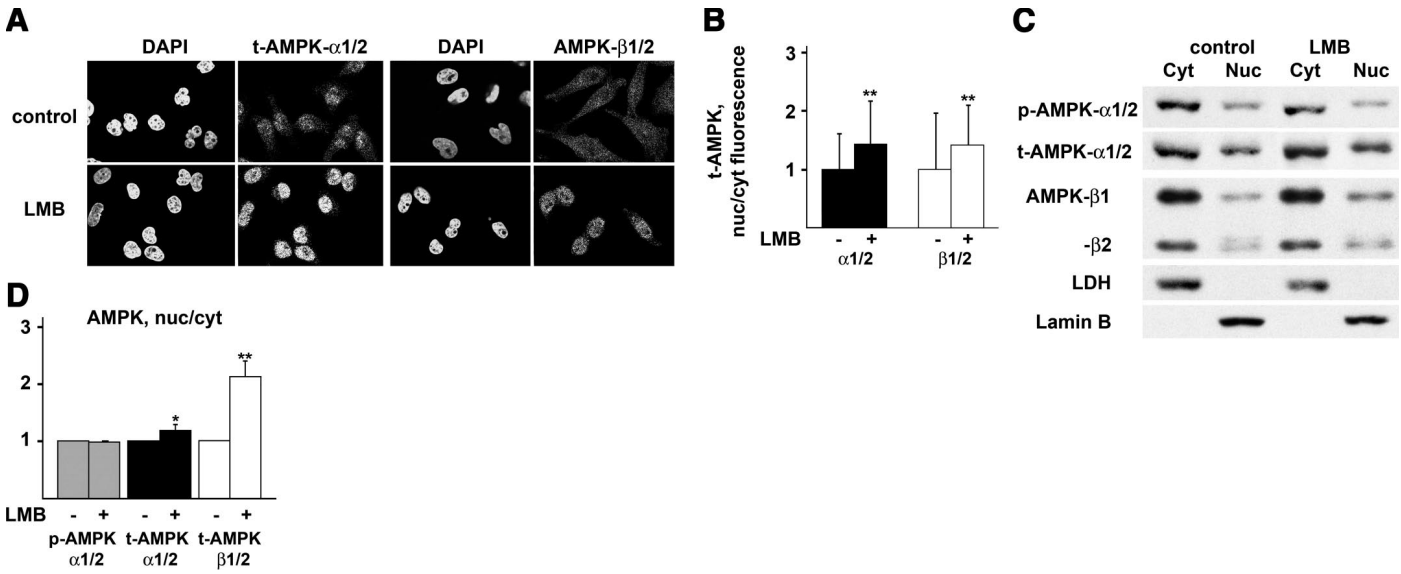

Fig. 7. AMPK shuttles between the nucleus and the cytoplasm using Crm1 as the nuclear exporter. HeLa cells at 70% confluency were incubated with solvent only (control) or leptomycin B (LMB). Indirect immunofluorescence and Western blot analysis was carried out as in Figs. 1 and 2. *A*: AMPK-α1/2 and -β1/2 were located by indirect immunofluorescence. *B*: ratio of nuc to cyt fluorescence was quantified. *C* and *D*: Western blot analysis of cytoplasmic and nuclear fraction and quantitation of ECL signals are shown. All test results were compared with the untreated control. $^{**}P < 0.01$; $^{*}P < 0.05$.

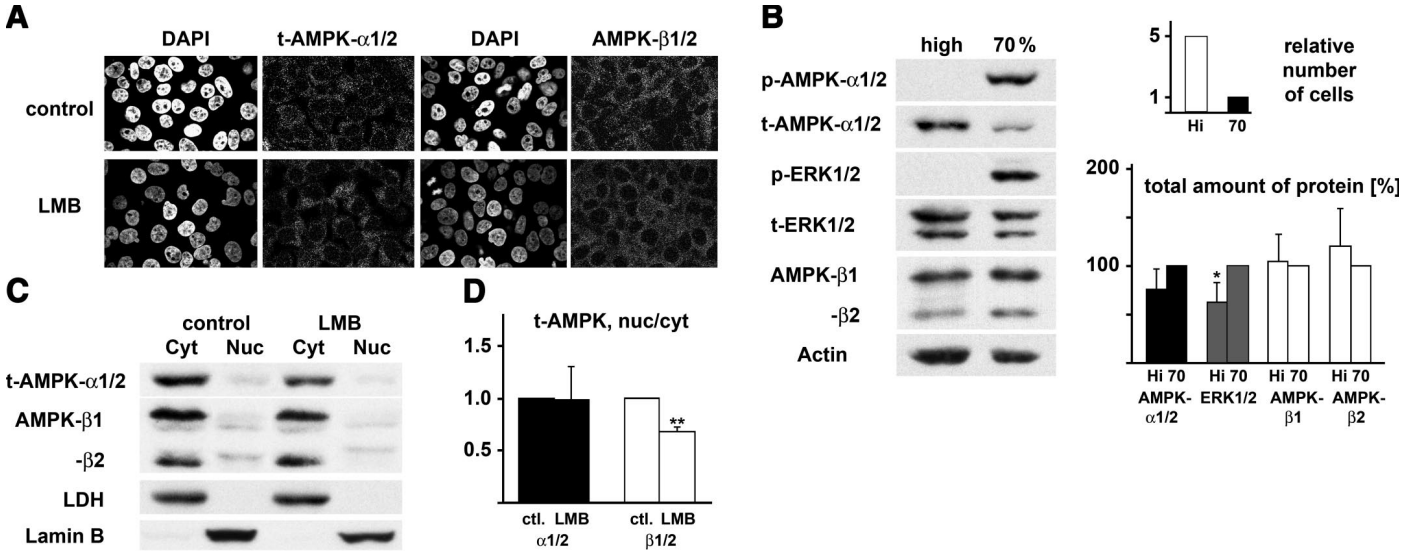

Fig. 8. Cell density controls the nucleocytoplasmic distribution of AMPK. High-density HeLa cell cultures were treated with solvent or LMB as in Fig. 7. *A*: AMPK was located by indirect immunofluorescence. *B*: Western blot analysis showed no or little p-AMPK-α1/2 or dually phosphorylated ERK1/2 in high-density cells. Note that a higher amount of total protein (140%) was loaded for high-density cultures to detect weak ECL signals. Changes in the total concentrations of AMPK and ERK1/2 in high-density cultures were determined with actin as a reference. Results obtained for 70% confluency (70) were used as a reference for high-density cultures (Hi). $*P < 0.05$. *C* and *D*: cytoplasmic and nuclear fractions were analyzed by Western blot analysis, and ECL signals were quantified as described for Fig. 2. All test results were compared with the control samples. $**P < 0.01$.

Signaling through MAPKs ERK1/2 controls the nucleocytoplasmic distribution of AMPK. Experiments with stressed cells suggested that decreasing the activity of ERK1/2 may correlate with the nuclear accumulation of p-AMPK-α1/2 (Table 1). Previous experiments by others indicate a complex crosstalk between AMPK activation and ERK1/2 activation, with positive as well as negative feedback between the two pathways (12). No previous studies have analyzed the possible role of MEK→ERK1/2 signaling in the intracellular localization of AMPK. In particular, it is not known whether ERK1/2 has any effect on the distribution of AMPK subunits under nonstress conditions. To begin to understand

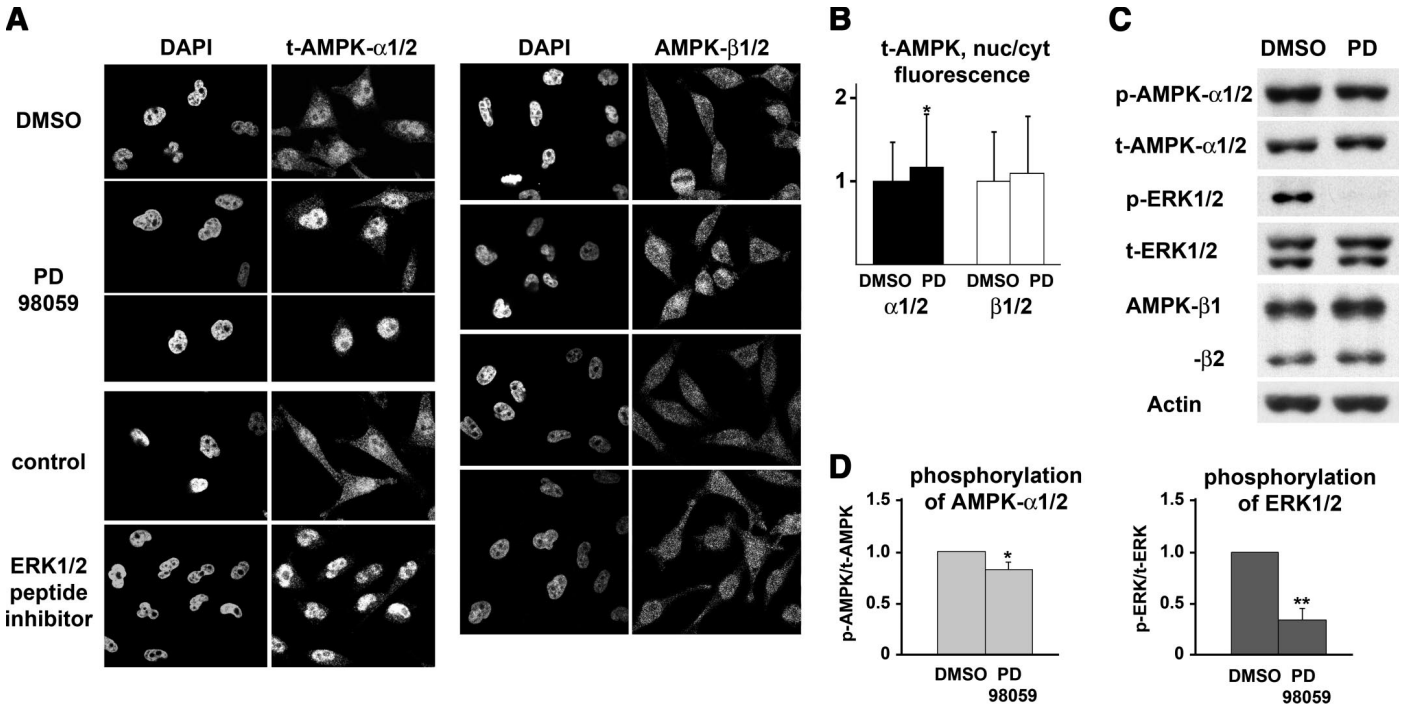

Fig. 9. Signaling through MEK→ERK1/2 regulates the nucleocytoplasmic distribution of AMPK in HeLa cells. Cultures were incubated with PD98059 (PD) or ERK1/2 peptide inhibitor as described in MATERIALS AND METHODS. *A* and *B*: AMPK subunits were visualized by indirect immunofluorescence and fluorescence signals were quantified. $*P < 0.05$. *C* and *D*: changes in the phosphorylation of AMPK-α1/2 Thr172 or ERK1/2 were determined by Western blot analysis and quantification of ECL signals. Indirect immunofluorescence, Western blot analysis, and statistical analyses were carried out as described for Fig. 3, *A–D*. $**P < 0.01$; $*P < 0.05$.

the events that control the nucleocytoplasmic distribution of AMPK in unstressed cells, we tested a potential role of MEK→ERK1/2 signaling in this process. Two different pharmacological inhibitors, PD98059, which inhibits the upstream kinase MEK, and peptide inhibitor II, which prevents ERK binding to MEK (11), induced the nuclear accumulation of AMPK-α1/2 and β1/2 (Figs. 9 and 10). Although the phosphorylation of AMPK-α1/2 Thr172 was slightly reduced, the nuc/cyt ratio of p-AMPK-α1/2 increased upon treatment with PD98059 (Figs. 9*D* and 10*B*).

DISCUSSION

AMPK is central to the control of glucose and lipid metabolism and the rapid adaptation to changes in cell physiology. As such, the kinase modifies a variety of substrates that are involved in carbohydrate or fatty acid synthesis or degradation and protein synthesis (32). Furthermore, AMPK regulates the expression of a large number of genes, the stability of several mRNAs, cell polarity, and mitosis (6, 17, 20, 35). These previous studies showed that AMPK recognizes a growing number of proteins, both in the nucleus and cytoplasm. Access to and modification of these substrates requires the proper localization of AMPK.

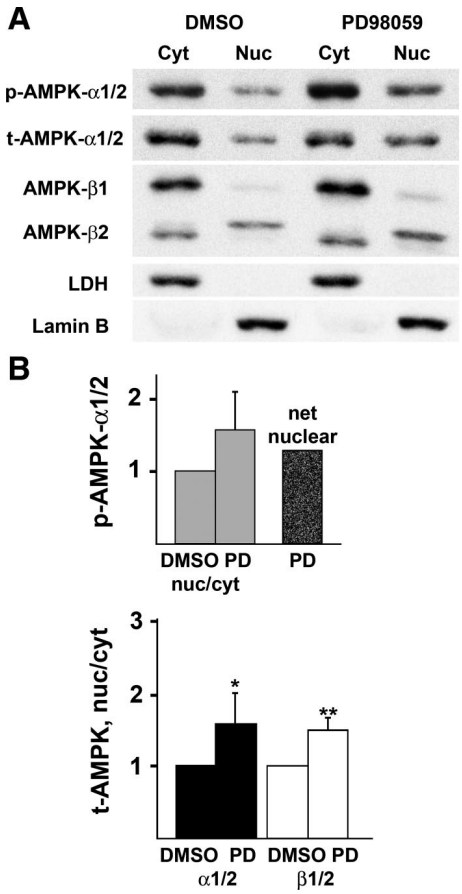

Fig. 10. Inhibition of the MEK→ERK1/2 pathway alters the nuclear levels of AMPK. *A*: distribution of p-AMPK-α1/2, t-AMPK-α1/2, and AMPK-β1/2 was monitored by cell fractionation and Western blot analysis. *B*: ECL signals were quantified as for Fig. 2. The untreated control served as reference for cells incubated with PD98059. $^{**}P < 0.01$; $^{*}P < 0.05$.

Our studies provide new insights into the complex regulatory processes that determine the modification and subcellular distribution of AMPK. Changes in the phosphorylation of AMPK-α1/2 Thr172 were inversely related to changes in the activation of ERK1/2. This is not restricted to HeLa cells, which are lacking the upstream activating kinase LKB1, but was also observed with HEK293 cells, which contain LKB1.

Our results demonstrate that various forms of stress, including heat, energy depletion, and oxidants, not only alter the phosphorylation state of AMPK-α1/2, but also concentrate AMPK in nuclei. The simplified model in Fig. 11 summarizes how different physiological conditions regulate the intracellular distribution of AMPK. In unstressed cells (Fig. 11*A*), AMPK-α and -β shuttle between the nucleus and the cytoplasm, using the carrier Crm1 for export from the nucleus. Upon exposure to stress both α- and β-subunits accumulate in nuclei (Fig. 11*B*). This redistribution could be achieved by upregulation of AMPK nuclear import, increase in nuclear retention, reduced export, or a combination of these events. High cell density confines AMPK-α and β-subunits to the cytoplasm and prevents them from shuttling (Fig. 11*C*). It is possible that contacts between neighboring cells regulate the distribution of AMPK; signaling events based on high culture density could prevent nuclear import or induce cytoplasmic anchoring of AMPK subunits. Finally, our results demonstrate a complex role for MEK→ERK1/2 signaling in the control of AMPK localization. Under nonstress conditions, inhibition of the MEK→ERK1/2 pathway triggered nuclear accumulation of AMPK α- and β-subunits (Fig. 11*D*).

Interestingly, the localization of p-AMPK-α1/2 and t-AMPK-α1/2 may be controlled differently. Our results indicate that there is no direct link between the phosphorylation of Thr172 of AMPK-α1/2 and the distribution of t-AMPK-α1/2. However, the changes in net nuclear p-AMPK-α1/2 are negatively correlated with ERK1/2 activation; whenever the net nuclear levels of p-AMPK-α1/2 were reduced, we observed an increase in ERK1/2 activation, and vice versa (summarized in Table 1).

Taken together, our results support the hypothesis that p-AMPK-α1/2 localization can be linked to the activation status of ERK1/2, whereas a more complex regulation directs the distribution of t-AMPK-α1/2 and β1/2 in stressed cells. Future experiments will have to determine whether the localization of the MAPK ERK1/2, in addition to its activation, plays a role in the nucleocytoplasmic distribution of AMPK.

At this point, we can only speculate how AMPK redistribution participates in the response to different stressors. One effect of AMPK redistribution could be changing its interactions with kinase substrates. For example, raising the nuc/cyt ratio of activated AMPK in nuclei may increase the phosphorylation of nuclear or reduce the modification of cytoplasmic targets. AMPK controls cell physiology not only by the direct phosphorylation of various metabolic enzymes but also via transcriptional regulation (reviewed in Ref. 28). Many genes change their expression levels when a dominant-negative allele of AMPK-α2 is highly overexpressed over the endogenous wild-type α-subunit in skeletal muscles of transgenic mice (20). Proteins encoded by these genes participate in various functions, including energy metabolism, cell signaling, tran-

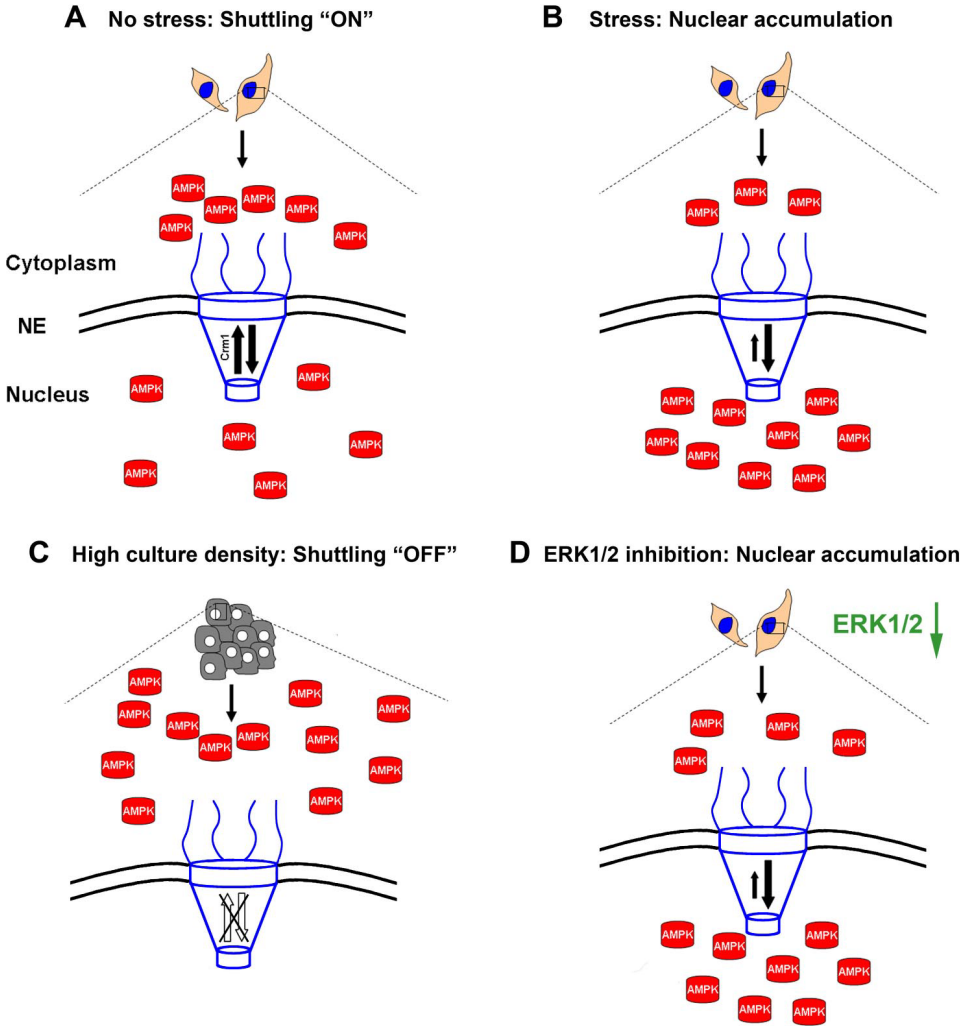

Fig. 11. Simplified model for the control of AMPK localization under normal and stress conditions. *A*: in unstressed cells AMPK shuttles between the nucleus and the cytoplasm and is present in both compartments. Nuclear export is mediated by the carrier Crm1. *B*: several forms of stress, including heat, energy depletion, and oxidants, increase the levels of AMPK-α1/2 and -β1/2 in nuclei. *C*: in high-density cultures, AMPK fails to shuttle and is located in the cytoplasm. *D*: signaling through MEK→ERK1/2 regulates the intracellular distribution of AMPK. Inhibition of the MEK→ERK1/2 pathway leads to AMPK nuclear accumulation of AMPK subunits. The redistribution of AMPK under different physiological conditions may be triggered by changes in transport across the nuclear envelope, retention in the nucleus and cytoplasm, or a combination of these events.

scription, and translation. Furthermore, AMPK activity contributes to the regulation of mRNA stability as the kinase controls the half-lives of p21, cyclin A, B1, and VEGF mRNAs (reviewed in Ref. 6).

A possible connection between the multiple processes that AMPK affects and the results reported here could be the transcriptional regulator p300/CBP and several transcription factors that are acetylated by p300/CBP. These include members of the FOXO family, p53 and NF-κB. AMPK phosphorylates p300/CBP on Ser89 (35) thereby modulating the interactions of p300/CBP with transcriptional regulators (reviewed in Ref. 28). Upon oxidative stress, FOXO proteins move to the nucleus to be bound and acetylated by p300/CBP (reviewed in Refs. 30 and 33). The acetylation state of FOXO proteins seems to control which genes are selected for transcription. A simplified model may propose a link between AMPK activation, p300/CBP phosphorylation, and FOXO protein acetylation; and the cascade AMPK→p300/CBP→FOXO proteins could contribute to the specific gene expression following oxidative stress. Since we observed a reduction in p-AMPK-α1/2 in nuclei upon oxidant exposure, this model would predict that p300/CBP phosphorylation on Ser89 is reduced, which could modulate the subsequent interaction between p300/CBP and FOXO proteins and ultimately gene expression.

Our data show that the nucleocytoplasmic distribution of total and phosphorylated AMPK is regulated differently; AMPK subunits accumulate in nuclei upon stress independent of kinase activation. There are several possible scenarios that could explain this redistribution: *1*) the redistribution of AMPK to nuclei controls its accessibility to activating upstream kinases; *2*) AMPK nuclear accumulation is caused by inhibition of nuclear export in stressed cells; and *3*) alternatively, AMPK subunits have additional functions that are unrelated to the kinase activity but required in nuclei of stressed cells for other processes. Future experiments will have to explore these possibilities.

ACKNOWLEDGMENTS

We thank P. Banski for critical reading of the manuscript and Dr. J. Liu (HTS/HCS Facility at McGill University) for help with ImageExpress Micro.

GRANTS

This work was supported by grants from Canadian Institutes of Health Research, National Sciences and Engineering Research Council, and Heart and Stroke Foundation of Quebec to U. Stochaj. U. Stochaj is a chercheur national of Fonds de la Recherche en Santé du Québec. M. Kodiha was supported by doctoral fellowships from Fonds de la Recherche en Santé du Québec and the Heart and Stroke Foundation of Canada.

REFERENCES

1. **Ashrafian H.** Cancer's sweet tooth: the Janus effect of glucose metabolism in tumorigenesis. *Lancet* 367: 618–521, 2006.
2. **Birnbaum MJ.** Activating AMP-activated protein kinase without AMP. *Mol Cell* 19: 289–290, 2005.
3. **Chu A, Matusiewicz N, Stochaj U.** Heat-induced nuclear accumulation of hsc70s is regulated by phosphorylation and inhibited in confluent cells. *FASEB J.* 10.1096/fj.00-0680jje, 2001.
4. **Dagon Y, Avraham Y, Magen I, Gertler A, Ben-Hur T, Berry EM.** Nutritional status, cognition, survival. *J Biol Chem* 280: 42142–42148, 2005.
5. **Daval M, Foufelle F, Ferré P.** Functions of AMP-activated protein kinase in adipose tissue. *J Physiol* 574: 55–62, 2006.
6. **Eberhardt W, Doller A, Akool E, Pfeilschifter J.** Modulation of mRNA stability as a novel therapeutic approach. *Pharmacol Ther* 114: 56–73, 2007.
7. **Hardie DG, Hawley SA, Scott JW.** AMP-activated protein kinase–development of the energy sensor concept. *J Physiol* 574: 7–15, 2006.
8. **Harel A, Forbes DJ.** Importin beta: conducting a much larger cellular symphony. *Mol Cell* 16: 319–330, 2004.
9. **Hurley RL, Anderson KA, Franzone JM, Kemp BE, Means AR, Witters LA.** The Ca2+/calmodulin protein kinase kinases are AMP-activated protein kinase kinases. *J Biol Chem* 280: 29060–29066, 2005.
10. **Ikuta T, Kobayashi Y, Kawajiri K.** Cell density regulates intracellular localization of aryl hydrocarbon receptor. *J Biol Chem* 279: 19209–19216, 2004.
11. **Kelemen BR, Hsiao, Goueli SA.** Selective in vivo inhibition of mitogen-activated protein kinase activation using cell-permeable peptides. *J Biol Chem* 277: 8741–8748, 2002.
12. **Kim J, Yoon M, Choi S, Kang I, Kim S, Kim Y, Choi Y, Ha J.** Effects of stimulation of AMP-activated protein kinase on insulin-like growth factor 1- and epidermal growth factor-dependent extracellular signal-regulated kinase pathway. *J Biol Chem* 276: 19102–19110, 2001.
13. **Kodiha M, Chu A, Matusiewicz N, Stochaj U.** Multiple mechanisms promote the inhibition of classical nuclear import upon exposure to severe oxidative stress. *Cell Death Differ* 11: 862–874, 2004.
14. **Kodiha M, Chu A, Lazrak O, Stochaj U.** Stress inhibits nucleocytoplasmic shuttling of heat shock protein hsc70. *Am J Physiol Cell Physiol* 289: C1034–C1041, 2005.
15. **Kuda N, Matsumori N, Taoka H, Fukiwara D, Schreiner EP, Wolff B, Yoshida M, Horinouchi S.** Leptomycin B inactivates CRM1/exportin1 by covalent modification at a cysteine residue in the central conserved region. *Proc Natl Acad Sci USA* 75: 9112–9117, 1999.
16. **Kutay U, Güttinger S.** Leucine-rich nuclear export signals: born to be weak. *Trends Cell Biol* 15: 121–124, 2005.
17. **Lee JH, Koh H, Kim M, Kim Y, Lee SY, Lee S, Shong J, Kim J, Chung J, Karess RE.** Energy-dependent regulation of cell structure by AMP-activated protein kinase. *Nature* 447: 1017–1021, 2007.
18. **Long YC, Zierath JR.** AMP-activated protein kinase signaling in metabolic regulation. *J Clin Invest* 116: 1776–1783, 2006.
19. **Marshall S.** Role of insulin, adipocyte hormones, and nutrient-sensing pathways in regulating fuel metabolism and energy homeostasis: a nutritional perspective of diabetes, obesity, and cancer (Review). *Sci STKE* 346: re7, 2006.
20. **Mu J, Barton ER, Birnbaum MJ.** Selective suppression of AMP-activated protein kinase in skeletal muscle: update on "lazy mice". *Biochem Soc Trans* 32: 236–241, 2003.
21. **Quan X, Tsoulos P, Kuritzky A, Zhang R, Stochaj U.** The carrier Msn5p/Kap142p promotes nuclear export of the hsp70 Ssa4p and relocates in response to stress. *Mol Microbiol* 62: 592–609, 2006.
22. **Rask-Madsen C, King GL.** Mechanisms of disease: endothelial dysfunction in insulin resistance and diabetes. *Nature Clin Pract Endocrinol Metab* 3: 46–56, 2007.
23. **Rutter GA, Silva Xavier G, Leclerc I.** Roles of 5′-AMP-activated protein kinase (AMPK) in mammalian glucose homeostasis. *Biochem J* 375: 1–16, 2003.
24. **Salt I, Celler JW, Hawley SA, Prescott A, Woods A, Carling D, Hardie DG.** AMP-activated protein kinase: greater AMP dependence, and preferential nuclear localization, of complexes containing the α2 isoform. *Biochem J* 334: 177–187, 1998.
25. **Sapkota GP, Kieloch A, Lizcano JM, Lain S, Arthur JSC, Williams MR, Morrice N, Deak M, Alessi DR.** Phosphorylation of the protein kinase mutated in Peutz-Jeghers Cancer Syndrome, LKB1/STK11, at Ser^{431} by $p90^{RSK}$ and cAMP-dependent protein kinase, but not its farnesylation at Cys433, is essential for LKB1 to suppress cell growth. *J Biol Chem* 276: 19469–19482, 2001.
26. **Stewart M.** Molecular mechanism of the nuclear protein import cycle. *Nat Rev Mol Cell Biol* 8: 195–208, 2007.
27. **Ström AC, Weis K.** Importin-beta-like transport receptors (Review). *Genome Biol* 2: 3008, 2001.
28. **Towler MC, Hardie DG.** AMP-activated protein kinase in metabolic control and insulin signaling. *Circ Res* 100: 328–341, 2007.
29. **Valko M, Leibfritz D, Moncol J, Cronin MTD, Mazur M, Telser J.** Free radicals and antioxidants in normal physiological functions and disease. *Int J Biochem Cell Biol* 39: 44–84, 2007.
30. **Van der Heide L, Smidt MP.** Regulation of FoxO activity by CBP/p300-mediated acetylation. *Trends Biochem Sci* 30: 81–86, 2005.
31. **Van Gaal LF, Mertens IL, De Block CE.** Mechanisms linking obesity with cardiovascular disease. *Nature* 444: 875–880, 2006.
32. **Viollet B, Foretz M, Guigas B, Horman S, Dentin R, Bertrand L, Hue L, Andreelli F.** Activation of AMP-activated protein kinase in the liver: a new strategy for the management of metabolic hepatic disorders. *J Physiol* 574: 41–53, 2006.
33. **Vogt PK, Jiang H, Aoki M.** Triple layer control. Phosphorylation, acetylation and ubiquitination of FOXO proteins. *Cell Cycle* 4: 908–913, 2005.
34. **Warden SM, Richardson C, O'Donnell J, Stapleton D, Kemp BE, Witters LA.** Post-translational modifications of the β1 subunit of AMP-activated protein kinase affect enzyme activity and cellular localization. *Biochem J* 354: 275–283, 2001.
35. **Yang W, Hong YH, Shen X, Frankowski C, Camp HS, Leff T.** Regulation of transcription by AMP-activated protein kinase. *J Biol Chem* 276: 38341–38344, 2001.

Stress inhibits nucleocytoplasmic shuttling of heat shock protein hsc70

Mohamed Kodiha, Angel Chu, Omar Lazrak and Ursula Stochaj

Am J Physiol Cell Physiol 289:1034-1041, 2005. First published Jun 1, 2005;
doi:10.1152/ajpcell.00590.2004

AJP - Cell Physiology is dedicated to innovative approaches to the study of cell and molecular physiology. It is published 12 times a year (monthly) by the American Physiological Society, 9650 Rockville Pike, Bethesda MD 20814-3991. ISSN: 0363-6143, ESSN: 1522-1563. Visit our website at http://www.the-aps.org/.

Am J Physiol Cell Physiol 289: C1034–C1041, 2005.
First published June 1, 2005; doi:10.1152/ajpcell.00590.2004.

CALL FOR PAPERS | *Protein and Vesicle Trafficking*

Stress inhibits nucleocytoplasmic shuttling of heat shock protein hsc70

Mohamed Kodiha, Angel Chu, Omar Lazrak, and Ursula Stochaj
Department of Physiology, McGill University, Montreal, Quebec, Canada

Submitted 1 December 2004; accepted in final form 25 May 2005

Kodiha, Mohamed, Angel Chu, Omar Lazrak, and Ursula Stochaj. Stress inhibits nucleocytoplasmic shuttling of heat shock protein hsc70. *Am J Physiol Cell Physiol* 289: C1034–C1041, 2005. First published June 1, 2005; doi:10.1152/ajpcell.00590.2004.—Heat shock proteins of the hsp/hsc70 family are essential chaperones, implicated in the stress response, aging, and a growing number of human diseases. At the molecular level, hsc70s are required for the proper folding and intracellular targeting of polypeptides as well as the regulation of apoptosis. Cytoplasmic members of the hsp/hsc70 family are believed to shuttle between nuclei and cytoplasm; they are found in both compartments of unstressed cells. Our experiments demonstrate that actin filament-destabilizing drugs trigger the nuclear accumulation of hsc70s in unstressed and heat-shocked cells recovering from stress. Using human-mouse heterokaryons, we show that stress inhibits shuttling and sequesters the chaperone in nuclei. The inhibition of hsc70 shuttling upon heat shock is only transient, and transport is reestablished when cells recover from stress. Hsc70 shuttling is controlled by hsc70 retention in the nucleus, a process that is mediated by two distinct mechanisms, ATP-sensitive binding of hsc70s to chaperone substrates and, furthermore, the association with nucleoli. The nucleolar protein fibrillarin and ribosomal protein rpS6 were identified as components that show an increased association with hsc70s in the nucleus upon stress exposure. Together, our data suggest that stress abolishes the exit of hsc70s from the nucleus to the cytoplasm, thereby limiting their function to the nuclear compartment. We propose that during recovery from stress hsc70s are released from nuclear and nucleolar anchors, which is a prerequisite to restore shuttling.

nuclear transport; chaperone; nuclear retention; nucleoli

HEAT SHOCK PROTEINS ARE INVOLVED in numerous cellular functions, including folding of newly synthesized polypeptides and targeting of proteins to their proper cellular location. In particular, chaperones of the hsp/hsc70 family are essential to these processes (6, 10, 11). The hsp/hsc70s play a crucial role in the appropriate response to stress and the survival of stress-induced damage, processes that are relevant to a large number of human diseases and pathophysiological conditions (2). Moreover, hsp/hsc70s are implicated in the regulation of apoptosis, tumorigenesis, and aging (1, 7, 9). In eukaryotic cells under normal growth conditions, cytoplasmic hsp/hsc70s are believed to move in and out of the nucleus, and it was demonstrated in *Xenopus* oocytes that they shuttle between nucleus and cytoplasm (13). Unlike other members of the hsp70/hsc70 family, hsc70 (also referred to as hsp73 or hsp70-8) is essential for the survival of normal and tumor cells (17). Hsc70s concentrate in nuclei when cells are exposed to stress, and heat shock is the most efficient treatment to induce their accumulation in nuclei (4). Although heat increases the steady-state concentration of hsc70s in nuclei, it is not known whether stress also controls their movement between nucleus and cytoplasm. However, this knowledge is required to understand the dynamics of hsc70 localization under different physiological conditions. To address this question, we have monitored the distribution of endogenous hsc70s and the reporter protein EGFP-hsc70 (enhanced green fluorescent protein fused to hsc70) in human cultured cells. Our results demonstrate that exit of hsc70s from the nucleus upon recovery from stress is an active process and that heat shock restricts the nucleocytoplasmic trafficking of hsc70s. After heat exposure, hsc70 shuttling is prevented but is restored when cells recover from this environmental insult. We have identified stress-induced nuclear retention of hsc70 as a mechanism that controls shuttling of the chaperone.

MATERIALS AND METHODS

Nuclear reporter proteins. The fluorescent protein NLS-NES-GFP2 carries SV40 nuclear localization sequence (NLS) and the nuclear export sequence (NES) of inhibitor of cAMP-dependent protein kinase (PKI) fused to two copies of GFP (18). The NLS-NES-GFP2 coding sequence was transferred to a vector that mediates inducible expression in mammalian cells (3). A plasmid encoding hsc70 (kindly provided by Drs. S. Wax and N. Kedersha, Harvard Medical School, Boston, MA) was used to generate a fusion between EGFP and hsc70. To this end, the hsc70 coding sequence was cloned into the *Bam*HI site of vector pEGFP-C1 (Clontech, Palo Alto, CA). The correctness of the construct was verified by DNA sequencing; the fusion protein is referred to as EGFP-hsc70. EGFP-hsc70 shows the same distribution as authentic hsc70 when analyzed in control and stressed cells (data not shown; see Fig. 4). A schematic representation of the constructs used for transfection is shown in Fig. 1.

Transfection of HeLa cells. At a confluency of ~70%, HeLa cells were transfected in six-well plates with Effectene (Qiagen, Mississauga, ON, Canada), following the manufacturer's recommendations. Transient gene expression in HeLa cells with a dexamethasone-inducible system was described in detail previously (3, 4). Transfected cells were grown for 24 h on polylysine-coated coverslips in six-well plates or on multiwell slides before exposure to stress.

Treatment with leptomycin B, latrunculin B, and cytochalasin B. To analyze the potential role of the importin-β family member Crm1, we have tested the effect of leptomycin B (LMB), a compound that selectively inhibits this exporter (12). To this end, cells were incubated with 10 ng/ml LMB (gift of M. Yoshida, University of Tokyo, Tokyo, Japan) dissolved in ethanol or with the solvent ethanol for 15 h at 37°C after heat stress. Unstressed cells were incubated with LMB

Address for reprint requests and other correspondence: U. Stochaj, Dept. of Physiology, McGill Univ., 3655 Promenade Sir William Osler, Montreal, QC, H3G 1Y6, Canada (e-mail: ursula.stochaj@mcgill.ca).

The costs of publication of this article were defrayed in part by the payment of page charges. The article must therefore be hereby marked "*advertisement*" in accordance with 18 U.S.C. Section 1734 solely to indicate this fact.

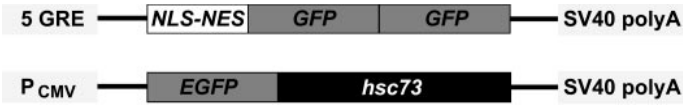

Fig. 1. Nuclear reporter proteins used in this study. NLS-NES-GFP2 is a fluorescent protein that contains two copies of green fluorescent protein (GFP) fused to nuclear localization sequence (NLS) of SV40 T-antigen and nuclear export sequence (NES) of the inhibitor of cAMP-dependent protein kinase. The reporter protein shuttles and at steady state is concentrated in the cytoplasm. The reporter protein EGFP-hsc70 was generated by in-frame fusion of enhanced GFP (EGFP) to the 5′-end of the hsc70 coding sequence. The synthesis of NLS-NES-GFP2 is controlled by a regulatable promoter that contains 5 copies of glucocorticoid response elements (GRE). Addition of dexamethasone to the growth medium will induce gene expression. Expression of the EGFP-hsc70 gene is driven by a cytomegalovirus (CMV) immediate early promoter (P_{CMV}). Both plasmids carry an SV40 polyadenylation signal (SV40 polyA).

for up to 24 h at 37°C. Latrunculin B and cytochalasin B (Calbiochem, San Diego, CA) were dissolved in DMSO. Cells recovering from stress were incubated for 15 h at 37°C with 1 mM latrunculin B, 10 μM cytochalasin B, or the solvent DMSO. Unstressed cells were treated with latrunculin B, cytochalasin B, or DMSO for 3 h at 37°C, as indicated in Figs. 3 and 4. In control experiments, the effect of latrunculin B or cytochalasin B on actin polymerization was tested with FITC-labeled phalloidin, following the supplier's protocol (Sigma, Oakville, ON, Canada).

Immunofluorescence. All steps were carried out at room temperature essentially as described previously (4). In brief, cells were washed in PBS and fixed for 25 min at room temperature in 3.7% formaldehyde-PBS. Fixed cells were rinsed in PBS and permeabilized with 0.1% Triton X-100 in PBS-2 mg/ml BSA (5 min, room temperature). All subsequent steps were carried out in PBS-2 mg/ml BSA-0.05% Tween 20. Samples were incubated overnight with primary antibodies against hsc70s or fibrillarin [SPA-815, StressGen (Victoria, BC, Canada); diluted 1:1,000; Santa Cruz Biotechnology, sc-11335, diluted 1:1,000]; primary antibodies were detected with 1.5 μg/ml Cy3-conjugated secondary antibodies (Jackson ImmunoResearch, West Grove, PA). NLS-NES-GFP2 was visualized with polyclonal rabbit antibodies to GFP (Clontech, diluted 1:200) and 5 μg/ml secondary antibodies conjugated to Alexa Fluor 488 (Molecular Probes, Eugene, OR). To detect rpS6 (Santa Cruz Biotechnology, sc-13007, diluted 1:500), cells were fixed in methanol-acetone (1:1, vol/vol) for 30 min at −20°C. All subsequent incubations and washes were carried out in PBS-BSA. DNA was located with 4′,6-diamidino-2-phenylindole (DAPI), and samples were mounted in Vectashield (Vector Laboratories, Burlingame, CA). Cells were analyzed with a Nikon Optiphot at ×400 magnification and photographed with Kodak T-MAX 400 film. Negatives were scanned and processed with PhotoShop 5.5 and 8.0.

Human-mouse heterokaryons. Heterokaryons between HeLa and mouse NIH3T3 cells were generated by a modification of published procedures (5). In brief, HeLa cells transiently synthesizing EGFP-hsc70 were trypsinized and seeded on coverslips 24 h after transfection to reach ~60% confluency on the next day. HeLa cells were then exposed to 1 h of heat stress at 45.5°C, and 3×10^5 NIH3T3 cells were added to each well of a six-well plate. After 1.5 h, mouse cells adhered to the coverslips, and cycloheximide was added to 75 μg/ml for 30 min. Cells were fused subsequently for 2 min with 50% polyethylene glycol (PEG) 3350. After removal of PEG, samples were washed three times with PBS and incubated at 37°C in growth medium containing 100 μg/ml cycloheximide. Cells were fixed 3, 5, and 15 h after heat stress, i.e., 1, 3, and 13 h after fusion. Nuclei were stained with DAPI, and heterokaryons or homokaryons were monitored for the distribution of EGFP-hsc70.

Analysis of nuclear retention. Nontransfected HeLa cells were exposed for 1 h to 45.5°C and subsequently treated for 5 min with 40 μg/ml digitonin in *buffer B* on ice (19). Digitonin-extracted cells were incubated with *buffer B* [containing 5 mg/ml BSA and 0.05% Nonidet P-40 (NP-40)] for 15 min at room temperature. The buffer was supplemented with 2.5 mM ATP, 2.5 mM ADP, or 1 mM nonhydrolyzable ATP analog adenosine 5′-(β,γ-imido)triphosphate (AMP-PNP), as indicated in Figs. 5 and 6. Samples were washed extensively in *buffer B*-BSA-NP-40, in *buffer B*, and twice in PBS and fixed and processed for indirect immunofluorescence with anti-hsc70 antibodies as described above. To monitor the intactness of nuclear envelopes, cells were extracted with digitonin, treated with *buffer B*-BSA-NP-40, and washed as described above. Washed samples were fixed, blocked with PBS-2 mg/ml BSA, and incubated with anti-lamin B antibodies (0.5 μg/ml; Santa Cruz Biotechnology, sc-6217). Control cells were treated with digitonin only before blocking and incubation with antibodies.

Protein cross-linking and immunoprecipitation. Control, stressed, and recovering cells were grown on 100-mm tissue culture dishes, washed with cold PBS, and extracted with 40 μg/ml digitonin in PBS for 5 min on ice. Samples were washed with PBS and incubated with 0.2 mM 3,3′-dithiobis(sulfosuccinimidylpropionate) in PBS for 1 h on ice. Dishes were washed with cold PBS and stored at −70°C until use. For immunoprecipitation, plates were incubated for 10 min on ice with IP buffer [in mM: 20 Tris·HCl, pH 8.0, 5 EDTA, and 150 NaCl with 1% NP-40, 10% glycerol, and protease inhibitors (aprotinin, antipain, chymostatin, leupeptin, pepstatin, each at 1 μg/ml; 1 mM PMSF)]. Samples were vortexed with glass beads, cleared by centrifugation (5 min, 13,000 rpm, 4°C), and incubated with 50 μl of protein G-Sepharose (Amersham Biosciences; 30 min, 4°C with gentle agitation). Resin was removed by centrifugation, and supernatants were incubated with 5 μg of anti-hsc70 for 2 h at 4°C, followed by addition of 50 μl of protein G-Sepharose and overnight incubation at 4°C. Beads were collected by centrifugation, washed three times in IP buffer, and incubated with gel sample buffer containing 1.4 M β-mercaptoethanol (15 min, 95°C). Material released from the resin was analyzed by Western blotting.

Western blot analysis. Western blotting and enhanced chemiluminescence detection was carried out essentially as described previously (4), using a Lumigen PS-3 detection kit (Amersham Biosciences).

RESULTS AND DISCUSSION

During recovery from heat stress, nuclear hsc70s relocate to the cytoplasm in temperature-dependent fashion that does not require de novo protein synthesis. Heat shock induces the rapid nuclear accumulation of hsc70s in HeLa cells, and a 1-h exposure to 45.5°C (severe heat shock) is sufficient to concentrate hsc70s in nuclei (Fig. 2). After heat stress, hsc70s relocate from nuclei to the cytoplasm when cells recover at 37°C, as monitored for different time points in Fig. 2. Several hours after heat treatment, hsc70s began to exit the nucleus; after 15 h of recovery, they distributed throughout the cell. This relocation of hsc70s was temperature dependent and was abolished when cells were incubated at 4°C, consistent with an active transport process (Fig. 2 and data not shown). Interestingly, when cells were kept at 4°C, hsc70s not only failed to relocate to the cytoplasm but also concentrated in nucleoli. During recovery at 37°C, nuclear export of hsc70s did not depend on de novo protein synthesis, because it was not abolished by cycloheximide (Fig. 2).

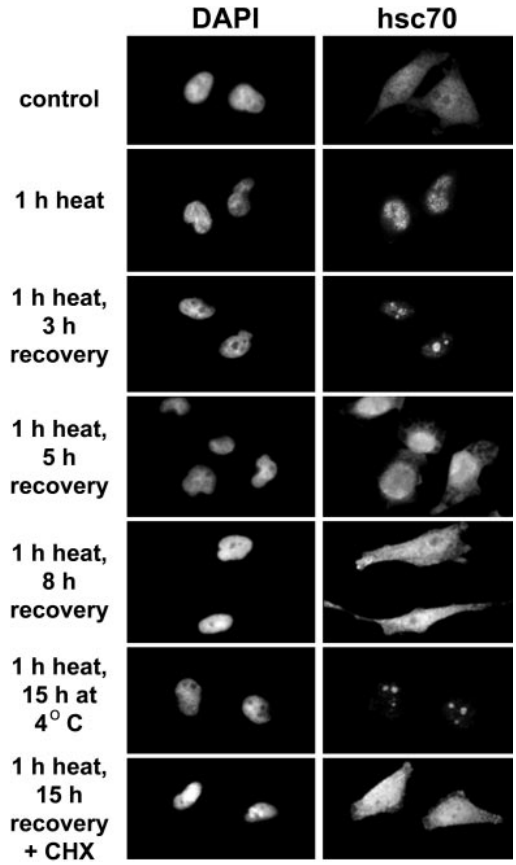

Fig. 2. Nuclear hsc70 relocation to the cytoplasm during recovery from heat shock is temperature dependent but does not require de novo protein synthesis. Hsc70s were localized by indirect immunofluorescence in unstressed cells (control) or upon exposure to severe heat shock (1 h at 45.5°C). After heat stress, cells recovered at 37°C for the times indicated. In addition, heat-shocked cells were kept for 15 h at 4°C or incubated at 37°C in the presence of 100 μg/ml cycloheximide (CHX). Nuclei were stained with 4′,6-diamidino-2-phenylindole (DAPI).

Hsc70 nuclear export does not require the transporter Crm1/exportin-1 in unstressed cells or during recovery from heat shock. Shuttling depends on nuclear import and export of proteins, and neither of these processes has been defined on a molecular level for members of the hsp/hsc70 family. The nuclear exporter Crm1/exportin-1 is involved in transport of many cargos, most of which contain a leucine-rich NES. This export pathway can be inhibited efficiently with LMB, a drug that covalently modifies the transporter Crm1/exportin-1 (12). Members of the hsc70/hsp70 families contain a conserved sequence element (i.e., positions 164–173 of mouse hsc70) that fits the consensus sequence for a hydrophobic NES recognized by Crm1. However, LMB did not prevent hsc70 export in cells recovering from heat stress (Fig. 3*A*). The same result was obtained when both LMB and cycloheximide were added during the recovery period. Likewise, LMB did not change the distribution of hsc70s in unstressed cells, even if the drug was present for up to 24 h (Fig. 3*C*).

In control experiments, LMB efficiently inhibited shuttling of NLS-NES-GFP2. This reporter protein carries a signal for nuclear localization (SV40-NLS) as well as nuclear export (PKI-NES); PKI-NES is recognized by Crm1. NLS-NES-

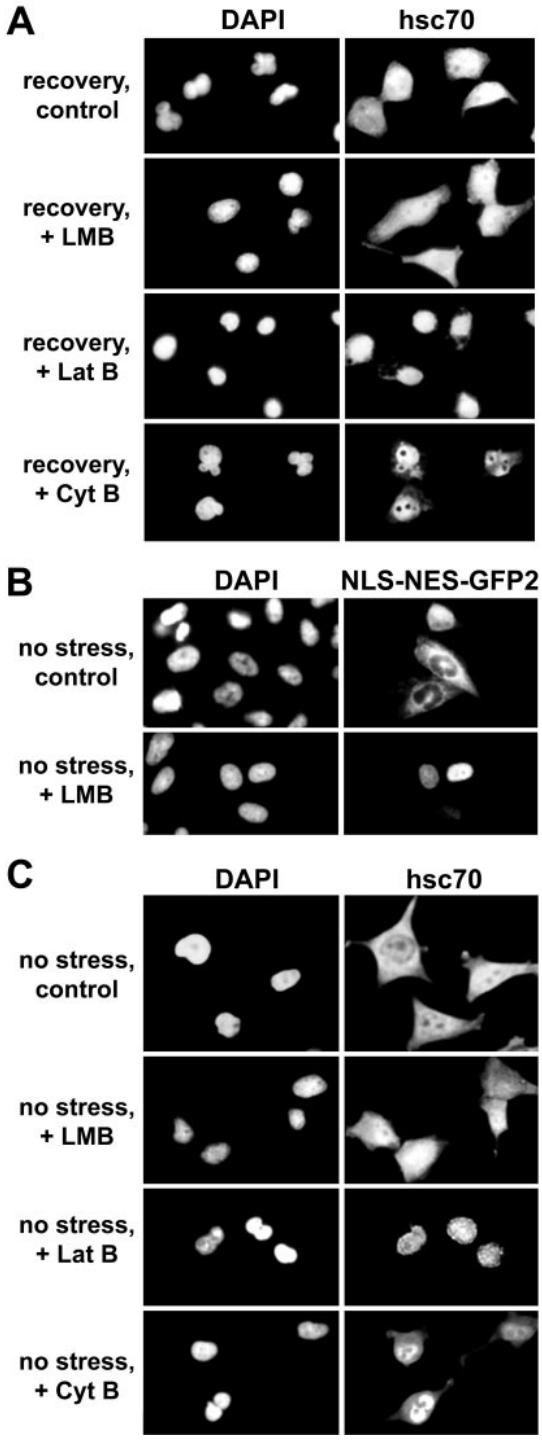

Fig. 3. Effect of leptomycin B (LMB), latrunculin B (Lat B), and cytochalasin B (Cyt B) on nuclear export of hsc70s and NLS-NES-GFP2. *A*: hsc70s were located in HeLa cells exposed to severe heat shock followed by 15-h recovery at 37°C. LMB, Lat B, and Cyt B were present throughout the recovery period as described in MATERIALS AND METHODS. *B*: HeLa cells transiently synthesizing NLS-NES-GFP2 were incubated for 15 h without or with 10 ng/ml LMB. *C*: unstressed cells were kept at 37°C and treated for 24 h with 10 ng/ml LMB. Alternatively, cells were incubated for 3 h at 37°C with 1 mM Lat B or 0.1 mM Cyt B. Hsc70s and NLS-NES-GFP2 were located by indirect immunofluorescence. Nuclei were visualized with DAPI.

GFP2 was both cytoplasmic and nuclear in the absence of LMB but accumulated in nuclei when LMB was added to the growth medium. Together, these results show that hsc70 nuclear export upon recovery from heat or under nonstress conditions does not rely on Crm1.

Actin filament-destabilizing drugs latrunculin B and cytochalasin B inhibit nuclear export of hsc70s in stressed and control cells. To further define hsc70 nuclear transport, we tested the effect of latrunculin B and cytochalasin B. These compounds are believed to affect actin located at the nuclear pore complex (NPC), thereby preventing nuclear export of various components (8). Incubation with latrunculin B or cytochalasin B drastically reduced the amount of actin filaments, which became obvious by the loss of phalloidin binding (not shown). Importantly, in cells recovering from heat shock, either drug prevented hsc70 export from the nucleus (Fig. 3*A*). Similarly, when unstressed cells were treated with latrunculin B or cytochalasin B, hsc70s concentrated in nuclei and nuclear accumulation were apparent after a 3-h treatment. These results support the idea that under normal physiological conditions, i.e., in the absence of stress, hsc70s shuttle between nucleus and cytoplasm in human culture cells. Furthermore, hsc70 export is abolished by the destabilization of filamentous actin, suggesting a role for actin in the translocation of nuclear hsc70s to the cytoplasm. In particular, actin located at the NPC could play a crucial role because it seems to be involved in nuclear export of multiple cargos (8).

Hsc70 shuttling is inhibited by heat shock and restored when cells recover from stress. Heterokaryons have been used to analyze the shuttling of proteins that are concentrated in nuclei at steady state under normal growth conditions. However, this approach has not been applied previously to monitor shuttling in heat-stressed cells. To achieve this, we used the fluorescent reporter protein EGFP-hsc70, which shares the biological properties of endogenous hsc70s when tested under a variety of stress conditions (Fig. 4*A*; M. Kodiha and U. Stochaj, unpublished observations). In unstressed cells, EGFP-hsc70 was distributed throughout nuclei and cytoplasm (Fig. 4*A*). Like endogenous hsc70s, EGFP-hsc70 accumulated in nuclei when cytochalasin B or latrunculin B was added to the growth medium (Fig. 4*A*).

Human-mouse heterokaryons were used to evaluate EGFP-hsc70 shuttling after stress exposure; these heterokaryons contain nuclei from both species, which share the same cytoplasm (5). EGFP-hsc70 was first concentrated in nuclei of HeLa cells

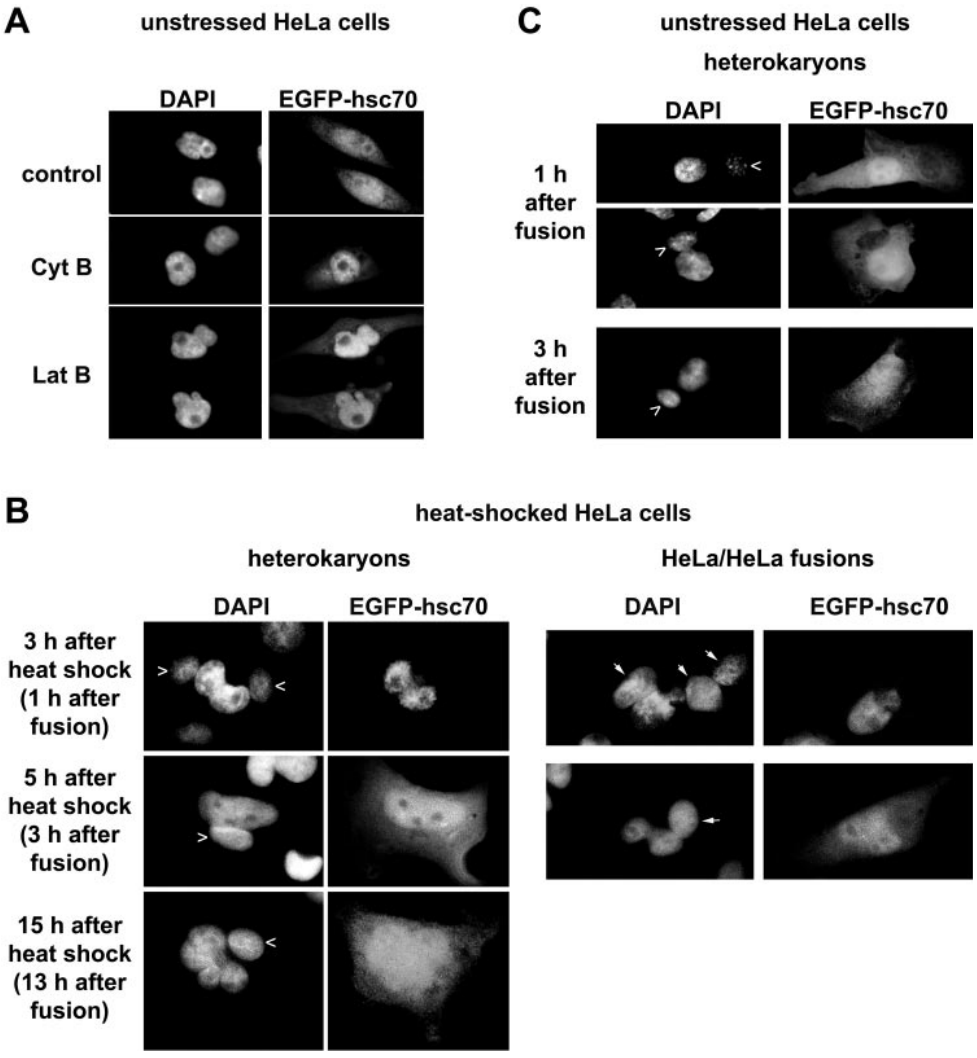

Fig. 4. Hsc70 shuttles in unstressed, but not heat-shocked, cells. *A*: HeLa cells synthesizing EGFP-hsc70 were incubated with the solvent DMSO, Cyt B, or Lat B for 3 h at 37°C. In fixed cells, EGFP-hsc70 and nuclei (DAPI) were located by fluorescence microscopy. *B*: HeLa cells synthesizing EGFP-hsc70 were heat shocked and fused to mouse NIH3T3 cells. EGFP-hsc70 was localized in fixed heterokaryons 3, 5, and 15 h after heat treatment, equivalent to 1, 3, and 13 h after fusion. Homokaryons generated by fusion of several HeLa cells were analyzed in parallel. Arrowheads mark the position of mouse nuclei in heterokaryons, and arrows point to the nuclei of nontransfected HeLa cells in homokaryons. *C*: heterokaryons obtained after fusion with unstressed HeLa cells were fixed at 1 and 3 h after fusion, comparable to samples shown for 3 and 5 h after heat shock in *B*. Mouse nuclei are labeled with arrowheads.

by heat shock for 1 h at 45.5°C. HeLa cells were returned subsequently to the normal growth temperature and fused to mouse cells. In these heterokaryons, we localized EGFP-hsc70 at different time points during their recovery from heat exposure. (It should be noted that EGFP-hsc70 synthesized in HeLa cells is the only source of fluorescence seen in Fig. 4*B*, because cycloheximide prevents de novo synthesis of EGFP-hsc70 in heterokaryons.) Three hours after heat shock, EGFP-hsc70 remained restricted to human nuclei in human-mouse heterokaryons (Fig. 4*B*). By contrast, EGFP-hsc70 was absent from mouse nuclei and the common cytoplasm, demonstrating that the translocation from human nuclei to the cytoplasm was prevented at this point. To determine whether this export inhibition, and thereby the block in shuttling, was reversible, heterokaryons were allowed to recover for a longer period of time. At 5 h after heat shock, EGFP-hsc70 began to migrate out of the human nucleus and appeared in the common cytoplasm. After a 15-h recovery period, human and mouse nuclei displayed comparable signals for EGFP-hsc70, showing that shuttling of the chaperone had resumed.

The absence of EGFP-hsc70 from mouse nuclei at early time points after cell fusion is not simply a failure of the nonstressed mouse nuclei to import the chaperone. While generating heterokaryons, we also obtained fusions originating from a mixture of transfected and nontransfected HeLa cells, the latter were not synthesizing EGFP-hsc70. In these multinucleated cells, or homokaryons, 3 h after heat shock we detected nuclei that did not contain EGFP-hsc70 (Fig. 4*B*). As observed for heterokaryons, EGFP-hsc70 appeared in the common cytoplasm of homokaryons at 5 h upon heat exposure and began to migrate into all of the nuclei present. At 15 h after heat shock, EGFP-hsc70 was present in all of the nuclei of multinucleated cells, and nuclei from transfected and nontransfected cells could no longer be distinguished.

For comparison, heterokaryons were generated with the protocol described above, but with unstressed instead of heat-treated HeLa cells. When inspected 1 and 3 h after fusion, the times equivalent to 3 and 5 h after heat shock, EGFP-hsc70 was detected at the earlier time point in all mouse nuclei present in heterokaryons (Fig. 4*C*). At 1 h after fusion, the amount of EGFP-hsc70 in mouse nuclei was somewhat variable between different heterokaryons. Three hours after fusion, the time equivalent to 5 h after heat exposure for the stressed cells shown in Fig. 4*B*, the signal for EGFP-hsc70 was comparable to that for mouse and HeLa nuclei of heterokaryons (Fig. 4*C*). Together, the data obtained for heterokaryons support the idea that EGFP-hsc70 appears faster in mouse nuclei when unstressed HeLa cells are the source of the fusion protein.

Hsc70s are retained in nuclei of heat-shocked cells. Shuttling between nucleus and cytoplasm can be regulated on different levels; this includes import, export, and retention of the shuttling protein. As such, the movement of nuclear hsc70s to the cytoplasm could be controlled by retention in the nucleus. The liberation from nuclear anchors would be a rate-limiting step for shuttling because this release is a prerequisite for subsequent export to the cytoplasm.

Heat shock is likely to trigger hsc70 binding to a large number of nuclear proteins that require chaperone activity, a process that may contribute to nuclear retention of hsc70s. To test this hypothesis, we have developed an assay for hsc70 release from nuclear anchors, which is not complicated by transport across the nuclear envelope (see MATERIALS AND METHODS for details). To this end, control and heat-shocked HeLa cells were first extracted with digitonin, which permeabilizes the plasma membrane and removes most of the cytoplasmic proteins but leaves the nuclear membranes intact. After digitonin extraction, the nonionic detergent NP-40 was used to solubilize the nuclear envelope, which would no longer restrict the movement of proteins. The proper permeabilization of membranes in our assays was verified in control experiments (Fig. 5*A*). As expected, anti-laminin B antibodies do not have

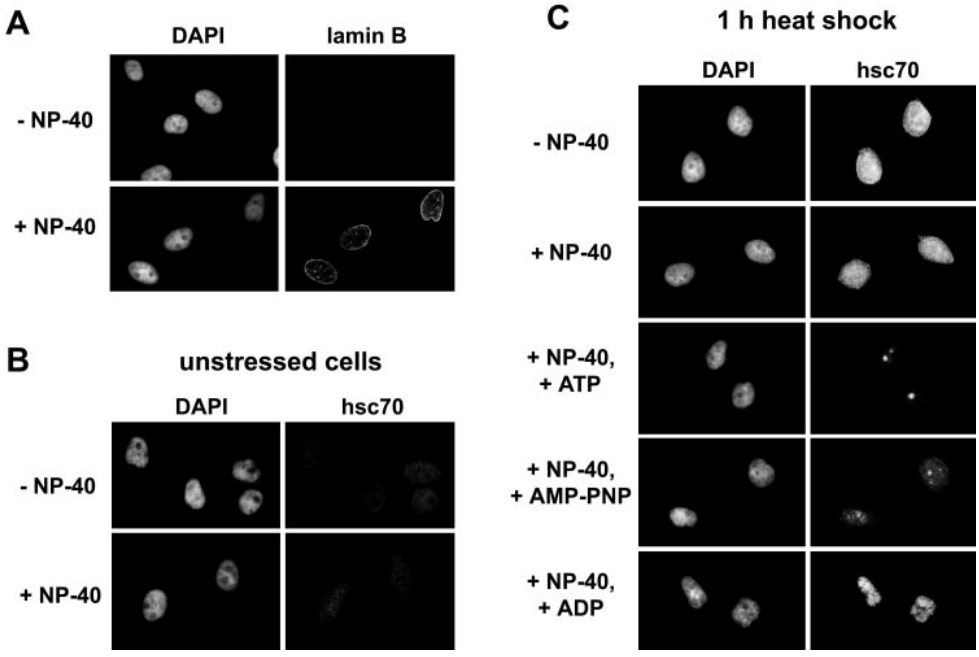

Fig. 5. Hsc70s are retained in nuclei of heat-stressed cells. *A*: the nuclear envelope of digitonin-treated cells was permeabilized with Nonidet P-40 (NP-40). Heat-shocked HeLa cells extracted with digitonin were incubated in the absence or presence of NP-40. Cells were fixed and binding of anti-laminin B antibodies was tested by indirect immunofluorescence. Unstressed controls (*B*) and heat-shocked cells (*C*) were treated with digitonin. Samples were incubated subsequently with buffer containing NP-40 and ATP, adenosine 5′-(β,γ-imido)triphosphate (AMP-PNP), or ADP as indicated. Specimens were fixed, and hsc70s were detected by indirect immunofluorescence.

Table 1. *Hsc70s are retained in nucleoplasm of heat-shocked cells*

	Control	1-h Heat			
		No recovery	3-h Recovery	5-h Recovery	15-h Recovery
No nucleotide added	(+)	+++*	++ Nucleoli	+ Nucleoli for some cells	(+)
ATP	(+)	(+) Nucleoli	(+) Nucleoli	(+) Nucleoli for some cells	(+)
AMP-PNP	(+)	(+) Nucleoli	(+) Nucleoli	(+) Nucleoli for some cells	(+)
ADP	(+)	+++*	++ Nucleoli	+ Nucleoli for some cells	(+)

AMP-PNP, adenosine 5′-(β,γ-imido)triphosphate. Results for the distribution of hsc70s in nuclei of digitonin-treated cells for the experiments shown in Figs. 5 and 6 are summarized. Control, heat-stressed, and recovering cells were extracted with digitonin and incubated in buffer containing the nonionic detergent Nonidet P-40 and the different nucleotides shown. The presence of hsc70s was monitored by indirect immunofluorescence. Similar results were obtained for at least 3 independent experiments. Signals for hsc70s in nucleoplasm: +++, strong; ++, intermediate; (+), weak. For some of the conditions, hsc70s could be detected in nucleoli. *The strong fluorescence in the nucleoplasm of stressed cells could mask the presence of hsc70s in nucleoli.

access to the nuclear lamina in digitonin-treated cells, but subsequent incubation with NP-40 led to antibody binding.

We next used this assay to determine whether hsc70s are retained in nuclei of control and heat-shocked cells (Fig. 5, *B* and *C*). Samples were treated with digitonin followed by incubation in the absence or presence of NP-40. Heat-shocked samples retained most of the hsc70s even in the presence of NP-40, suggesting that binding to nuclear anchors contributes to hsc70 accumulation in nuclei. By contrast, little hsc70 was found in nuclei of unstressed cells under any of the conditions tested (Fig. 5*B* and Table 1).

ATP and its nonhydrolyzable analog AMP-PNP release hsc70s from nuclear anchors. One way to retain hsc70s in nuclei is their binding to substrates that need to be refolded. This chaperone-substrate interaction is known to be stabilized by ADP, whereas ATP induces the rapid dissociation and binding of substrates (reviewed in Refs. 6 and 15). Digitonin-extracted cells were incubated for 15 min in NP-40-containing buffer supplemented with ATP, AMP-PNP, or ADP followed by localization of hsc70s (Fig. 5*C*). Unlike ADP, both ATP and AMP-PNP efficiently released the chaperone from nuclei, suggesting that ATP binding, but not cleavage, is required to liberate hsc70s from nuclear anchors. Interestingly, ATP failed to release hsc70 completely from nucleoli, suggesting that binding to nucleolar components is more complex than a chaperone-unfolded protein interaction.

Nuclear retention of hsc70s changes during recovery from heat shock. We next monitored hsc70 nuclear retention in cells recovering from stress. To this end, HeLa cells exposed to heat were analyzed after 3-, 5-, and 15-h incubation at 37°C. The amount of hsc70s present in the nucleoplasm decreased during recovery, and nucleoplasmic chaperone could be liberated with ATP or AMP-PNP (Fig. 6). In addition, hsc70s transiently concentrated in nucleoli, albeit with kinetics different from their accumulation in the nucleoplasm. The hsc70 levels increased in nucleoli of most cells after a 3-h recovery period, but only in few nucleoli after 5 h (Fig. 6, Table 1). As observed after heat exposure, hsc70 associated with nucleoli was not fully liberated by incubation with ATP or AMP-PNP. At 15 h after heat shock, hsc70 distribution was similar to that in unstressed controls and no accumulation was seen in nuclei or nucleoli. Results of these in vitro experiments (summarized in Table 1) suggest that hsc70 binding to chaperone substrates

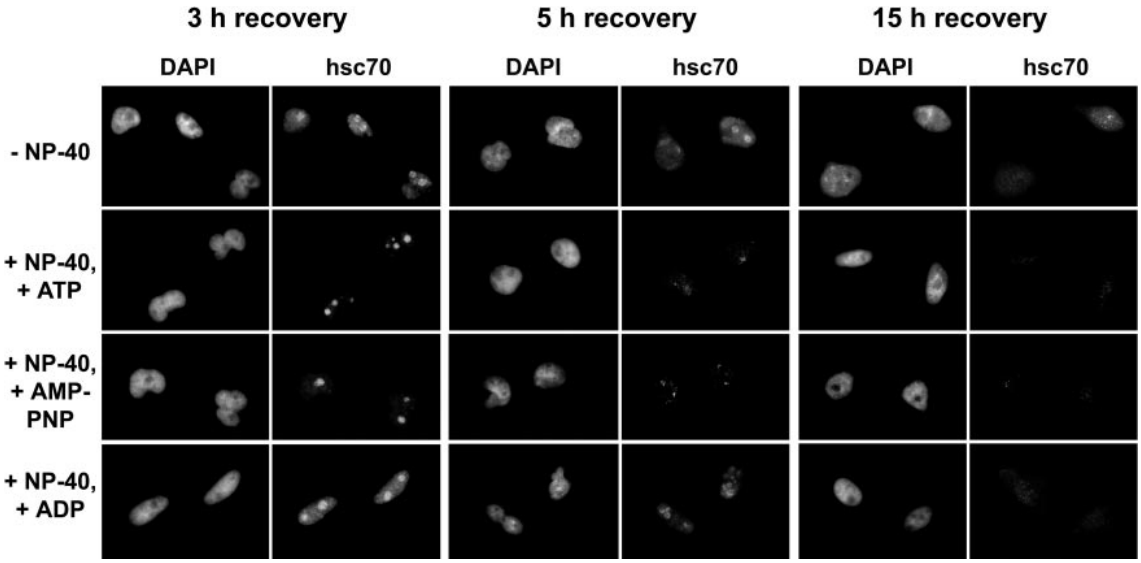

Fig. 6. Nuclear retention of hsc70s changes in cells recovering from heat stress. Heat-shocked cells were allowed to recover for 3, 5, and 15 h before digitonin extraction and incubation with NP-40-containing buffer in the presence of ATP, AMP-PNP, or ADP. Hsc70s were located by indirect immunofluorescence as described for Fig. 5.

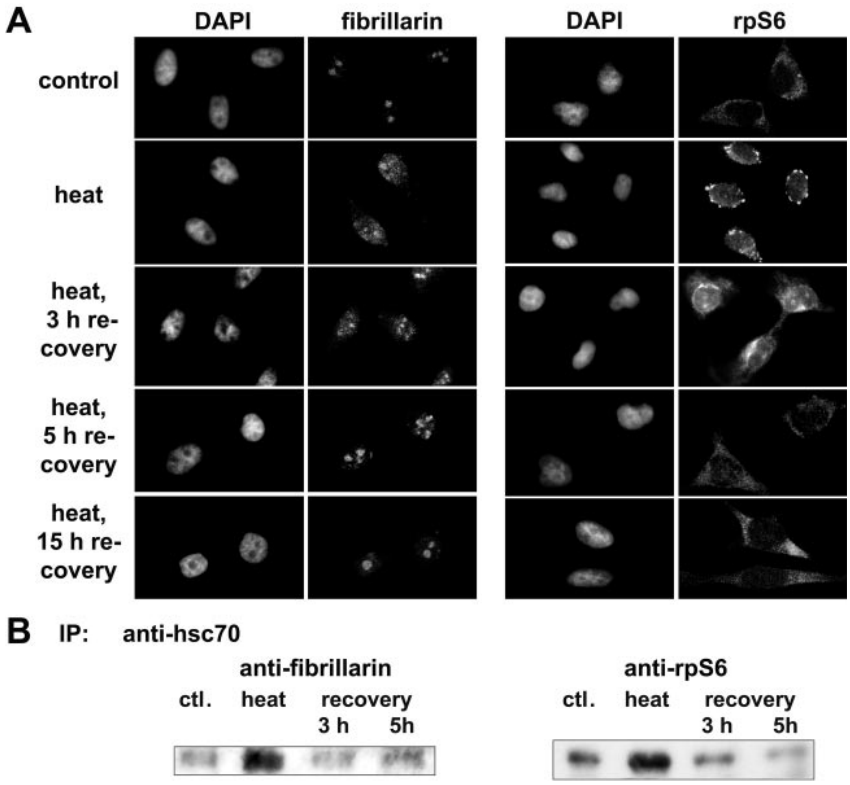

Fig. 7. Nucleolar protein fibrillarin and ribosomal protein rpS6 redistribute in stressed cells and associate with hsc70 upon heat shock. *A*: fibrillarin and rpS6 were localized by indirect immunofluorescence in unstressed, heat-shocked, and recovering HeLa cells. *B*: nuclear proteins were immunoprecipitated (IP) with antibodies against hsc70. Samples containing comparable amounts of hsc70 were tested for the presence of fibrillarin and rpS6 by Western blot analysis.

contributes to its nuclear retention immediately after heat treatment and at early stages of recovery.

Binding of hsc70s to nuclei of stressed cells. Members of the hsp/hsc70 family are involved in multiple interactions in the nucleus, and in response to heat stress hsc70s can be expected to interact with a large variety of nuclear components. For instance, the importance of hsc70s for the organization of nucleoli is well established, and chaperones are implicated in restoring nucleolar function upon stress (13, 16). On the basis of these earlier observations, nucleolar proteins were candidates for the interaction with hsc70s in heat-treated cells. To test this idea, we examined fibrillarin, a bona fide component of nucleoli, and the ribosomal protein rpS6, which is assembled into the small ribosomal subunits in nucleoli. When analyzed by indirect immunofluorescence (Fig. 7*A*), fibrillarin was concentrated in nucleoli of control cells but redistributed throughout nucleus and cytoplasm in response to heat exposure. During recovery, fibrillarin relocated to nucleoli, and after 15 h at 37°C, its distribution was similar to that in unstressed controls. In parallel, nuclear proteins were immunoprecipitated with antibodies against hsc70s, and immunoprecipitates that contained comparable amounts of hsc70 were probed with antibodies against fibrillarin (Fig. 7*B*). Although the nucleolar protein copurified with hsc70s for control, stressed, and recovering cells, clearly the highest amount of fibrillarin associated with hsc70s in heat-shocked cells.

Like fibrillarin, rpS6 redistributed after heat stress. As part of the 40S ribosomal subunit, rpS6 is mostly cytoplasmic under control conditions; however, heat treatment resulted in the formation of large structures containing rpS6 at the cytoplasmic side of the nuclear periphery. Increased amounts of rpS6 were detected in the nucleus as well. During stress recovery rpS6 relocated, and after 15 h its distribution was similar to that in unstressed cells (Fig. 7*A*). Similarly to fibrillarin, the association of rpS6 with hsc70 in nuclei was enhanced transiently after heat stress, as demonstrated by the coimmunoprecipitation of both proteins (Fig. 7*B*). Together, the data obtained for the interaction of nuclear hsc70s with fibrillarin and rpS6 are consistent with a role of the chaperone in restoring nucleolar function after heat exposure.

In conclusion, our study demonstrates that the nucleocytoplasmic shuttling of chaperones of the hsp/hsc70 family is inhibited by heat shock but restored when cells recover from

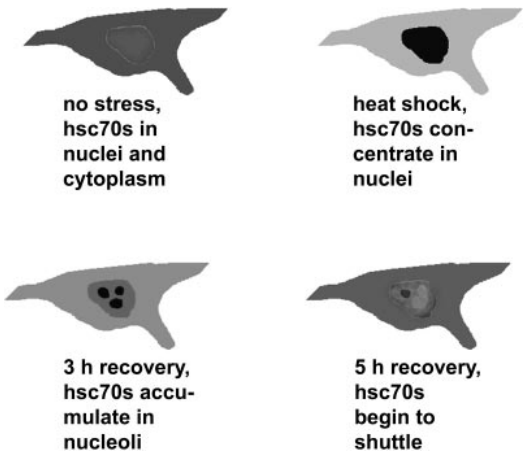

Fig. 8. Simplified model for the changes in nucleocytoplasmic shuttling of hsc70s upon heat shock and during recovery from stress. See text for details.

stress-induced damage. Importantly, stress alters not only the steady-state distribution but also the movement of hsc70s between nucleus and cytoplasm. Herein we have shown that hsc70 retention in the nucleus is drastically increased in response to heat exposure, a process that prevents export of the chaperone to the cytoplasm and thereby shuttling. We have identified two different forms of hsc70 interaction with nuclear anchors, both of which can be expected to contribute to the sequestration of chaperone in nuclei. First, hsc70s bind to nuclear proteins in an ATP-sensitive fashion, which most likely represents binding of the chaperone to folding substrates. Second, hsc70s associate with nucleoli, and at least a portion of the nucleolar chaperone cannot be liberated by the addition of ATP. This could indicate an association of hsc70s with nucleolar components in a fashion that is distinct from a chaperone-folding protein interaction. Independent of the type of association that underlies hsc70s retention in nuclei, we have shown that this retention is low in control cells, high after heat shock, and gradually reduced during recovery from stress. These changes in nuclear retention of hsc70s upon stress and during recovery can be expected to affect a variety of biological processes that require chaperone activity. For instance, immediately after stress, the proper folding of chaperone substrates in the cytoplasm may be impaired until de novo synthesis or shuttling of hsp/hsc70s resumes. Moreover, stress may interfere with the chaperone-dependent targeting of cytoplasmic proteins to various organelles, including mitochondria and peroxisomes, both of which require cytoplasmic hsp/hsc70s for protein import.

On the basis of the results described herein, we have developed a simplified model for hsc70 shuttling (Fig. 8). Hsc70s accumulate in nuclei of heat-stressed cells, where they are initially retained in the nucleoplasm by binding to chaperone substrates in an ATP-sensitive fashion. During recovery from heat, hsc70s relocate within the nucleus and transiently concentrate in nucleoli; this interaction cannot be prevented by the addition of ATP. As recovery progresses, hsc70s are liberated from nuclear and nucleolar anchors, which precedes their relocation to the cytoplasm. We propose that the release from nuclear anchors is a limiting factor that regulates hsc70 nuclear export and thereby shuttling of the chaperone in cells exposed to heat.

Taken together, the stress-induced sequestration of hsc70s in nuclei possibly affects repair processes in the cytoplasm as well as the proper assembly and maintenance of several organelles. These consequences of stress exposure are likely to impinge on different aspects of physiology and ultimately survival of each cell.

ACKNOWLEDGMENTS

We thank Drs. M. Yoshida (Tokyo, Japan), S. Wax and N. Kedersha (Boston, MA), and K. Weis (University of California, Berkeley, CA) for generous gifts of LMB and plasmids. We are grateful to Neola Matusiewicz for expert technical assistance and in particular to I. Gallouzi (Montreal) for help with heterokaryon assays.

GRANTS

This work was supported by grants from the Canadian Institutes of Health Research, National Sciences and Engineering Research Council (NSERC), and the Heart and Stroke Foundation of Quebec (to U. Stochaj). U. Stochaj is a Chercheur National of Fonds de la Recherche en Santé du Québec (FRSQ). M. Kodiha and A. Chu were supported by predoctoral fellowships from McGill University, FRSQ, and NSERC.

REFERENCES

1. **Beere HM.** "The stress of dying": the role of heat shock proteins in the regulation of apoptosis. *J Cell Sci* 117: 2641–2651, 2004.
2. **Benjamin IJ and Williams RS.** Expression and function of stress proteins in the ischemic heart. In: *The Biology of Heat Shock Proteins and Molecular Chaperones*. Cold Spring Harbor, NY: Cold Spring Harbor Laboratory Press, 1994, p. 533–552.
3. **Chatterjee S and Stochaj U.** Diffusion of proteins across the nuclear envelope of HeLa cells. *Biotechniques* 24: 668–674, 1998.
4. **Chu A, Matusiewicz N, and Stochaj U.** Heat-induced nuclear accumulation of hsc70s is regulated by phosphorylation and inhibited in confluent cells. *FASEB J* 15: 1478–1480, 2001. First published online April 27, 2001 as doi:10.1096/fj.00-0680fje.
5. **Fan XC and Steitz JA.** Overexpression of HuR, a nuclear-cytoplasmic shuttling protein, increases the in vivo stability of ARE-containing mRNAs. *EMBO J* 17: 3448–3460, 1998.
6. **Frydman J.** Folding of newly translated proteins in vivo: the role of molecular chaperones. *Annu Rev Biochem* 70: 603–647, 2001.
7. **Garrido C, Gurbuxani S, Ravagnan L, and Kroemer G.** Heat shock proteins: endogenous modulators of apoptotic cell death. *Biochem Biophys Res Commun* 286: 433–442, 2001.
8. **Hofmann W, Reichart B, Ewald A, Müller E, Schmitt I, Stauber RH, Lottspeich F, Jockusch BM, Scheer U, Hauber J, and Dabauvalle MC.** Cofactor requirements for nuclear export of Rev response element (RRE)- and constitutive transport element (CTE)-containing retroviral RNAs: an unexpected role for actin. *J Cell Biol* 152: 895–910, 2001.
9. **Jäättelä M.** Escaping death: survival proteins in cancer. *Exp Cell Res* 248: 30–43, 1999.
10. **Kiang JG and Tsokos GC.** Heat shock protein 70 kDa: molecular biology, biochemistry and physiology. *Pharmacol Ther* 80: 183–201, 1998.
11. **Kregel KC.** Heat shock proteins: modifying factors in physiological stress responses and acquired thermotolerance. *J Appl Physiol* 92: 2177–2186, 2002.
12. **Kudo N, Matsumori N, Taoka H, Fukiwara D, Schreiner EP, Wolff B, Yoshida M, and Horinouchi S.** Leptomycin B inactivates CRM1/exportin 1 by covalent modification at a cysteine residue in the central conserved region. *Proc Natl Acad Sci USA* 75: 9112–9117, 1999.
13. **Mandell RB and Feldherr CM.** Identification of two HSP70-related *Xenopus* oocyte proteins that are capable of recycling across the nuclear envelope. *J Cell Biol* 111: 1775–1783, 1990.
14. **Morcillo G, Gorab E, Tanguay RM, and Dietz JL.** Specific intranuclear distribution of hsp70 during heat shock in polytene cells. *Exp Cell Res* 236: 361–370, 1997.
15. **Nollen EAA and Morimoto RI.** Chaperoning signaling pathways: molecular chaperones as stress-sensing "heat shock" proteins. *J Cell Sci* 115: 2809–2816, 2002.
16. **Pelham HRB.** Hsp70 accelerates the recovery of nucleolar morphology after heat shock. *EMBO J* 3:3095–3100, 1984.
17. **Rohde M, Daugaard M, Jensen MH, Helin K, Nylandsted J, and Jäättelä M.** Members of the heat-shock protein 70 family promote cancer cell growth by distinct mechanisms. *Genes Dev* 19: 570–582, 2005.
18. **Stade K, Ford CS, Guthrie C, and Weis K.** Exportin 1 (Crm1) is an essential nuclear export factor. *Cell* 90: 1041–1050, 1997.
19. **Stochaj U and Silver P.** A conserved phosphoprotein that specifically binds nuclear localization sequences is involved in nuclear import. *J Cell Biol* 117: 473–482, 1992.

Science Signaling
AAAS

Analysis of Signaling Events by Combining High-Throughput Screening Technology with Computer-Based Image Analysis

Mohamed Kodiha, Claire M. Brown and Ursula Stochaj (16 September 2008)
Science Signaling **1** (37), pl2. [DOI: 10.1126/scisignal.137pl2]

Science Signaling (ISSN 1937-9145) is published weekly, except the last week in December, by the American Association for the Advancement of Science, 1200 New York Avenue, NW, Washington, DC 20005.

Analysis of Signaling Events by Combining High-Throughput Screening Technology with Computer-Based Image Analysis

Mohamed Kodiha,[1] Claire M. Brown,[2] Ursula Stochaj[1]*

Published 16 September 2008

[1]Department of Physiology, McGill University, Montreal, Quebec H3G 1Y6, Canada. [2]Department of Biochemistry and Life Sciences Complex Imaging Facility, McGill University, Montreal, Quebec H3G 1Y6, Canada.

*Corresponding author: E-mail, ursula.stochaj@mcgill.ca

Intracellular signaling and cell-to-cell communication depend on the coordination of numerous signaling events, and this large flow of information has to be properly organized in space and time. Common and critical to all of these processes and the ultimate cellular response is the correct spatial distribution of signaling components and their targets. This fundamental concept applies to a large number of signaling processes. It is frequently important to quantify the localization of signaling molecules within different cellular compartments to detect subtle changes or to define threshold levels of signaling molecules in a certain location that are necessary to trigger subsequent events. Of particular importance is the separation of nuclear and cytoplasmic events, and sensitive methods are required to measure their contribution to signal transduction. Procedures described here allow the quantification of fluorescence signals located in the nucleus, cytoplasm, or at the nuclear envelope. The methods rely on high-throughput imaging equipment, confocal microscopy, and software modules that measure the fluorescence intensity in the compartment of interest. We discuss the rationale for selecting the appropriate equipment for image acquisition and the proper software modules to quantify fluorescence in distinct cellular compartments. Initially, high-throughput technology for high-speed image acquisition was developed for multiwell plates. We adapted high-throughput technology for image acquisition for cells grown on cover slips. Images of higher spatial resolution along the *z* axis were acquired by confocal microscopy. For subsequent analyses, the choice of appropriate software modules is critical for rapid and reliable quantification of fluorescence intensities.

Introduction

Most eukaryotic cells are characterized by the presence of multiple organelles, some of which are further organized into distinct compartments with unique functions. A prominent example is the nucleus, an organelle with complex and dynamic organization (*1*, *2*). The nuclear envelope (NE) provides a physical barrier between the cytoplasm and the nucleus. This barrier separates vital cellular processes, such as DNA replication and RNA biogenesis in the nucleus, from cytoplasmic events, such as protein synthesis. The spatial segregation of cellular reactions provides a powerful mechanism for controlling numerous biological processes that have to be adjusted rapidly in response to environmental or physiological changes. In particular, a large number of signaling events alter the intracellular distribution of kinases, phosphatases, and other key components that control signaling (*3*–*6*). Moreover, subcellular compartmentalization separates distinct branches of cellular metabolism and contributes to control of gene expression.

Many signaling and metabolic processes are dynamic and enable cells to adapt to changes in environmental conditions and physiology. This dynamic state is exemplified by the bidirectional exchange of thousands of macromolecules between the nuclear and cytoplasmic compartments. For instance, nuclear proteins synthesized in the cytoplasm, such as transcription factors, polymerases, and histones, have to reach their final destination in the nucleus, whereas various RNAs and ribosomal subunits are initially generated in the nucleus and subsequently moved to the cytoplasm (*7*–*9*). All nucleocytoplasmic transport of proteins and RNA is mediated by nuclear pore complexes (NPCs), large proteinaceous assemblies embedded in the NE, which are the only gates for exchange of macromolecules between the nucleus and the cytoplasm. Nucleocytoplasmic trafficking plays an important role in maintaining the cellular homeostasis, as it regulates various aspects of cell physiology, including gene expression, cell cycle progression, growth and proliferation, and many signaling events, as well as apoptosis (*4*–*6*, *10*, *11*). Two distinct mechanisms underlie the movement of molecules through NPCs: Small molecules with a mass of 40 kD or less can diffuse passively through nuclear pores, whereas larger molecules rely on active transport to move into or out of the nucleus. Nuclear transport requires several soluble factors, many of which shuttle between the nucleus and the cytoplasm. The availability of transport factors in the nuclear and cytoplasmic compartment or their association with the NE may control the efficiency of nuclear trafficking. These factors include nuclear carriers that move proteins and RNA in and out of the nucleus (*7, 12, 13*). Like nuclear transport factors, many cargos shuttle between the nucleus and the cytoplasm, and their relative distributions can regulate their function (*6*, *10*, *11*). Prominent examples that are subject to this type of localization-mediated regulation are protein kinases and phosphatases, transcriptional regulators, and nuclear transporters for proteins or RNA (*6*, *10*, *12*–*23*).

The correct localization of signaling molecules and their downstream targets is critical to produce the proper physiological response, and the dynamic distribution of these components may affect signaling on several levels. First, depending on their subcellular location, kinases and phosphatases may associate with distinct scaffolding modules, a process that can alter their substrate specificity (*18*, *19*). After relocation within the cell, enzymes involved in signaling will obtain access to a unique set of substrates that is defined by the composition of the organelle or compartment. This scenario not only applies to kinases and phosphatases, but also to a large number of enzymes that regulate other posttranslational modifications, including farnesylation, acetylation, methylation, ubiquitination, and sumoylation. On a second level, the localization of targets or substrates may be regulated. Such target molecules are exemplified by a large number of transcription factors and regulators, RNA-binding proteins, or carriers involved in intracellular trafficking.

Not only is the distribution between organelles and the cytoplasm essential for accurate signal transduction, but the proper localization to compartments within a particular organelle is crucial as well. For instance, distinct compartments within the nucleus have defined roles in signal transduction, and the NE, in particular, is emerging as an essential structure that regulates chromatin organization and gene expression (*3*–*5*).

To obtain a better understanding of the diverse cellular activities and functions of a particular molecule, it is important to develop strategies that can be used to reliably quantify the abundance of this molecule in the organelle or suborganellar compartment of interest.

Cell fractionation is a widely used procedure to separate subcellular compartments, especially organellar constituents, from each other and from the cytoplasmic constituents. Although cell fractionation is useful for the analysis of many proteins, it is prone to artifacts. For instance, small proteins that are concentrated in the nucleus of growing cells may leak out into the cytoplasm during cell fractionation. This is exemplified by the small guanosine triphosphatase (GTPase) Ran, a predominantly nuclear protein in intact cells. However, when organelles are purified by biochemical methods, Ran diffuses across the NE and is found in substantial amounts in cytoplasmic fractions (*24*). Similarly, components that are dynamically or loosely, but stably, associated with the cytoplasmic side of the NE may be released into the cytoplasm when cells are lysed. In addition to problems with release and redistribution of proteins during cell fractionation, the isolation and purification of nuclear subcompartments like NEs and NPCs are laborious and time-consuming (*25*) and not always useful for accurately determining the concentrations of proteins present at this location.

The developments in high-throughput screening and the commercial availability of high-content screening (HCS) automated fluorescence-imaging platforms offer new options for rapidly performing cellular sampling and quantification of the cellular localization of molecules. Here, we describe detailed protocols to measure the distribution of fluorescent signals within different locations of the cell. We have focused on procedures for determining the nuclear or cytoplasmic location or the NE association of proteins. The methodologies can be adapted for fixed or live cells and may be used with fluorescent proteins, labeled antibodies, oligonucleotides, or any other molecule that can be detected with reasonable signal-to-noise ratio by HCS or confocal microscopy.

Materials

Six-well dishes

Bovine serum albumin (BSA)

Cells engineered to produce fluorescent reporter molecules or primary and secondary antibodies against the proteins of interest.

Note: We describe experiments with cyanine 3 fluorescent synthetic dye (Cy3)–labeled secondary antibodies, but any other label that can be detected by the filters of the microscope can be used.

DAPI (4′,6-diamidino-2-phenylindole) (Sigma) [Dapi in the MetaXpress software]

Formaldehyde, 37%

Glass cover slips; 18- × 18-mm size 1 cover slips

Growth medium appropriate for the cells under investigation

Microscope slides, such as precleaned Fisherbrand slides (size 25 × 75 × 1 mm)

Phosphate-buffered saline (PBS), pH 7.4

Triton X-100

Tween 20 (polysorbate detergent)

Equipment

Cell Culture

CO_2 incubator

Laminar flow hood

Water bath

Microscopy

ImageXpress Micro automated imaging system (Molecular Devices, Sunnydale, CA) or a Zeiss LSM 510 confocal microscope equipped with a 200 M microscope.

Note: We collect images with the ImageXpress Micro with a 40× magnification objective [numerical aperture (NA) = 0.60)] and a CoolSnap HQ camera. Exposure times were 20 ms for DAPI and between 1.5 and 3.2 s for tetramethyl rhodamine isothiocyanate (TRITC) and fluorescein isothiocyanate (FITC). We collect images with the Zeiss LSM 510 with a 63× magnification (NA = 1.4) at scan speed 5, with four-line averaging and a pixel resolution of 0.65 μm.

Software

MetaXpress (Molecular Devices, Sunnydale, CA) software

Note: The modules in MetaXpress need to be configured for the fluorescence quantification of the compartment of interest.

Recipes

Recipe 1: Formaldehyde Fix

Prepare a fresh solution of 3.7% formaldehyde in PBS by diluting a 37% formaldehyde stock solution into PBS. Prepare 9 ml for six samples.

Recipe 2: Permeabilization Buffer

Add 2 mg/ml of BSA to a solution of 0.1% Triton X-100 in PBS. Prepare 9 ml for six samples.

Recipe 3: Wash Buffer

Add 2 mg/ml BSA to a solution of 0.05% Tween 20 in PBS. Prepare 22.5 ml for six samples.

Recipe 4: Primary and Secondary Antibodies

Dilute primary and secondary antibodies in Wash Buffer (Recipe 3).

Note: The optimal dilution of primary antibodies must be determined empirically for each antibody. Fluorescently labeled secondary antibodies should be used at a concentration of 0.5 to 1.5 μg/ml.

Recipe 5: DAPI Stain

Dissolve 1 μg/ml DAPI in Wash Buffer (Recipe 3). Prepare 1.5 ml for six samples.

Instructions

The relative abundance of a protein of interest that is present in the NE, nucleus, cytoplasm, or all compartments is determined with different software modules in MetaXpress. We describe how to acquire images and to adapt the software programs to quantify the amount of protein in each location, as well as the advantages and potential pitfalls of the procedures.

Cell Preparation for Imaging

This method may be applied to cells that adhere to glass cover slips or coated glass cover slips. We provide the general instructions for cells that grow on poly-lysine–coated glass cover slips. Before image acquisition with ImageXpress Micro, it is important to inspect the cover slips and to determine the distribution of cells. This can be done by examining samples with a phase-contrast microscope or by examining samples that are DAPI-stained with a fluorescence microscope. Cover slips with very high cell density should not be used for image segmentation with certain modules, because individual cell identification by image segmentation can be difficult. Cover slips with cells at very low density may not provide a large enough sampling of cells for appropriate statistical representation of the data. On the basis of our experiments with HeLa cells, we recommend 1.3×10^6 cells/cover slip (18- × 18-mm size 1).

1. Grow cells on 18- × 18-mm size 1 cover slips in multiwell dishes (six-well dishes; each well with 9.6 cm^2 growth area) in the appropriate growth medium.
2. Fix cells for 20 min with 1.5 ml of 3.7% formaldehyde in PBS (Recipe 1) at room temperature and wash with PBS.

   Note: If the cells synthesize fluorescent reporter proteins, fix for only 10 min, wash with PBS, then proceed directly to step 9 for DAPI staining (12, 13).
3. To detect antigens by indirect immunofluorescence, permeabilize cells for 5 min at room temperature with Permeabilization Buffer (Recipe 2).

4. Block for 1 hour at room temperature in Wash Buffer (Recipe 3).
5. Remove cover slips from multiwell dish and incubate overnight at room temperature in a humid environment with Primary Antibodies (Recipe 4).
6. Wash cells at least three times for 10 min each wash in 250 μl Wash Buffer (Recipe 3).
7. Incubate with Secondary Antibodies (Recipe 4) for 2 hours at room temperature.
8. Wash cells at least three times for 10 min, each wash in 250 μl Wash Buffer (Recipe 3).
9. Stain the nuclei with 250 μl of DAPI Stain (Recipe 5) for 2 min at room temperature.
10. Mount the cover slips on a slide in the appropriate position for image acquisition.
11. Examine the cells on the cover slip with a conventional (for phase-contrast analysis) or fluorescence microscope, and only use those cover slips with an appropriate density of cells for image acquisition with ImageXpress Micro or confocal microscopy.

Note: HeLa cells at 1 to 1.5 × 10^6 cells/cover slip worked well in our hands. With this confluency, we obtained accurate segmentation with different analysis modules.

Image Acquisition with ImageXpress Micro of Cells Grown on Cover Slips

The MetaXpress software was developed for plate formats, which cannot be used without modification of the modules for specimens on cover slips. For many applications, cells are routinely grown on cover slips and mounted on slides, and we designed the protocol below specifically to adapt the image acquisition unit to these experimental settings (Fig. 1). In the descriptions below, we kept the term "plate" as it is used by the software, even though the experiments were carried out with cover slips. The steps that are critical to acquire such images are described in detail; we have omitted general information that can be found in the MetaXpress manual. ImageXpress Micro has the advantage that images can be acquired rapidly. A disadvantage with this equipment is that fluorescence will be collected from the whole cell, and images will contain a large amount of out-of-focus light. If high concentrations of the molecule of interest are present in the cytoplasm, as well as in the nucleus, measuring the intranuclear or NE fluorescence may require image acquisition by confocal microscopy. Although confocal microscopy is more time-consuming, this procedure will provide a more accurate quantification for the localization of some molecules.

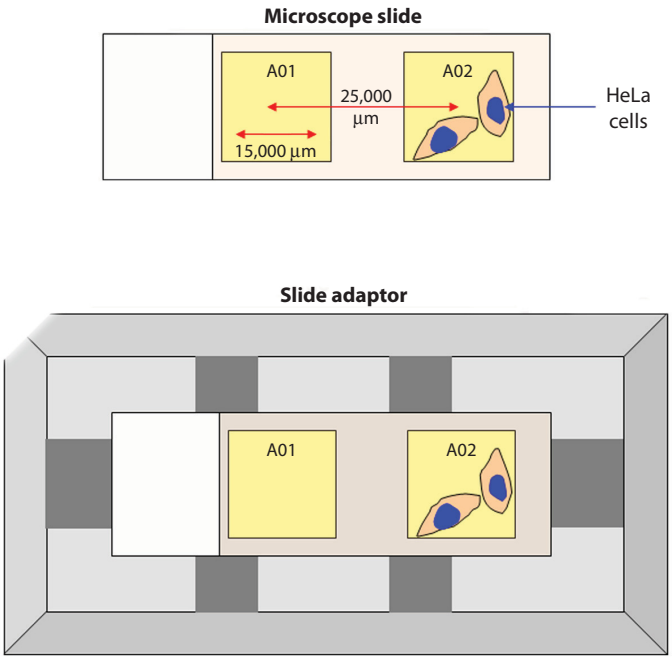

Fig. 1. Image acquisition with ImageXpress micro for cells grown on poly-lysine–coated cover slips. Cover slips were mounted on a microscope slide for image acquisition and loaded on the slide adaptor with the cover slips face down. Optimal positions for the mounting of cover slips are shown.

A few settings in the "Plate Acquisition Setup" menu are worth noting (Fig. 2). Camera binning can be set to provide the best signal-to-noise ratio. Without binning, the images will be at the highest resolution; however, with binning, there is an increase in the signal-to-noise ratio, resulting in better image quality and shorter exposure times. Camera gain can also be used, but the same gain setting should be used if data are to be compared across different experiments. When binning is set, the signal for an array of pixels is summed, and this value is read out as a single pixel. For instance, with a 2 × 2 binning, the 4 pixels in a 2 × 2 array are added together and read out as a single pixel value. This results in lower noise within the images. In some pixels, noise will be higher than average, and in some, it will be lower; however, the total signal will always be a positive value above background. Binning is especially important when the label provides a low-intensity signal, when living cells are analyzed, or if image acquisition must occur quickly. For our experiments with HeLa cells, a binning of 2 was optimal and represented a pixel size of 0.3225 μm/pixel.

The second setting that is particularly important provides the parameters that generate a map of the "plate" (now a slide), which the software uses to locate each "well" (now a cover slip) on the plate. The well location is the point of intersection between column and row. Measurements, such as the number of rows and columns in the plate, column and row offsets, spacing, well diameter and depth, plate dimensions, and the physical thickness of the plate bottom, have to be provided before acquisition. Because the software is

designed to read special plate formats, a new plate configuration for microscope slides must be set. The new parameters for microscope slides should be added to the plate library. The configuration described below identifies the slide as a plate with two rows (A and B) and two columns (1 and 2), resulting in a total of four wells. Wells A01 and A02 represent the two cover slips on the slide (Fig. 3, A and B). The software requires that the distance between rows is specified; therefore, B01 and B02 were assigned to create a 2 × 2 array but are not representative of the actual sample. To be able to reuse the plate map for different experiments, the cover slips have to be mounted in the same position on every slide. In particular, the distance between the two cover slips and the offsets from the slide margins should be kept constant.

Another parameter that is important to understand is the autofocus setting, and there are two options: laser-based focusing and image-based focusing. Laser-based focusing on the ImageXpress Micro uses a red laser to detect light reflections at the air-slide interface and the slide-mounting medium interface. If mounting medium is matched well to the cover slip (following the specifications recommended by the manufacturer), the air-slide interface is usually detected more easily.

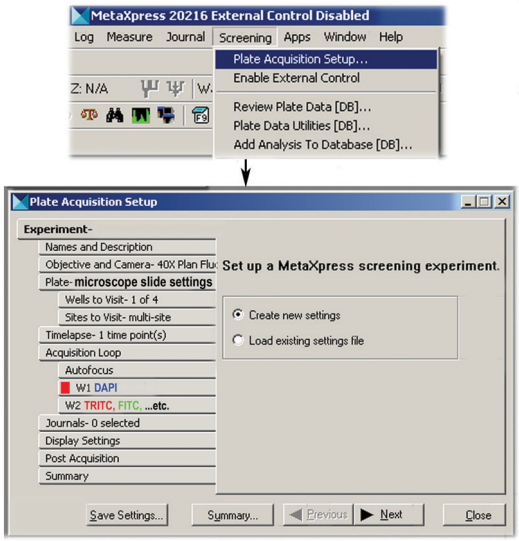

Fig. 2. Configuration of parameters for image acquisition. Settings for the plate acquisition are generated for a new application or loaded from previous experiments (existing settings). The buttons on the left side are used to configure the different parameters for a new acquisition.

The laser-based focusing uses a red laser and a position-sensitive detector to measure the reflection of the laser at the focal plane. The reflection of the laser relies on there being a difference in the refractive index between two substances. For instance, with a dry objective, there is an air-glass interface between the lens and the cover slip, and this can be easily detected. Then the focus can be offset by entering the thickness of the cover slip (0.13 to 0.17 mm for no. 1.0 cover slips). The actual cover slip thickness can be measured with the software by using the autofocus feature as the difference in the *z* position of the cover slip bottom and cover slip–medium interfaces. For an immersion lens, where the oil has essentially the same refractive index as glass, the interface between the oil and the glass is optically transparent and does not give rise to a reflection. In this case, the interface between the top surface of the cover slip and the aqueous medium can be detected.

The image-based focus, which is based on image-contrast algorithms, can be used in addition to laser-based autofocus. The disadvantage of image-based focusing is that it requires additional time and exposes the sample to additional light. However, if the samples are fixed and have mounting medium with an antifade agent, and the data set is not excessively large, this is a good option. For large data sets or living cells, this feature is not recommended. Because our samples were fixed and the data sets were not too large, we used both laser-based and image-based focusing.

1. Add microscope slide as a new plate type to the plate library of the MetaXpress software by going to the MetaXpress Main Screen and choosing "Screening," select "Plate Acquisition Setup," then choose "Plate."
2. Load the microscope slide on the slide adaptor such that the slide is inverted with the cover slip face down. The frosted end of the slide should be oriented toward the cut corner of the slide adaptor (Fig. 1).

   Note: Cover slips should always be mounted in the same position on the slide in order for the plate acquisition settings (specified in the next steps) to be reused.
3. On the MetaXpress main screen click the "eject" icon to open the plate stage door, load the slide adaptor on the plate stage, and then close the door.
4. On the MetaXpress main screen choose "Screening," select "Plate Acquisition Setup," then choose "Create new settings" (Fig. 2).

   Note: Once the settings are established, then you can choose "Load existing settings file."
5. Provide a name, date, and a brief description of the experiment. The acquired images can be retrieved under this name for subsequent analyses.
6. Select the objective appropriate for screening the samples.

   Note: We recommend the following objectives: For simply counting cells or looking for a positive or negative intensity of a given marker, a 10× or 20× pt lens can be used. However, a 20× or 40× lens with a numerical aperture (NA) of >0.5 would be preferred to measure subcellular localization. To quantify correctly subcellular structures such as NEs, endosomes, focal adhesions, or peroxisomes, a 60× with an NA > 0.7 may be needed. When working with high-NA lenses, it is best to use cover slips or glass-bottomed plates.

7. Select the camera binning; we recommend using 2 × 2 binning as a starting point and then optimizing binning, taking into consideration the speed necessary for image acquisition and the desired resolution.

Note: The following information should be considered when setting camera binning: For fixed cells, camera binning is not required because more light can be put into the system. However, if high-resolution data are not required, using a 2 × 2 binning setting will reduce file sizes by four times and speed up acquisition. The 2 × 2 binning setting is always suggested for live-cell acquisition to increase signal-to-noise so that exposure times can be kept to a minimum (26).

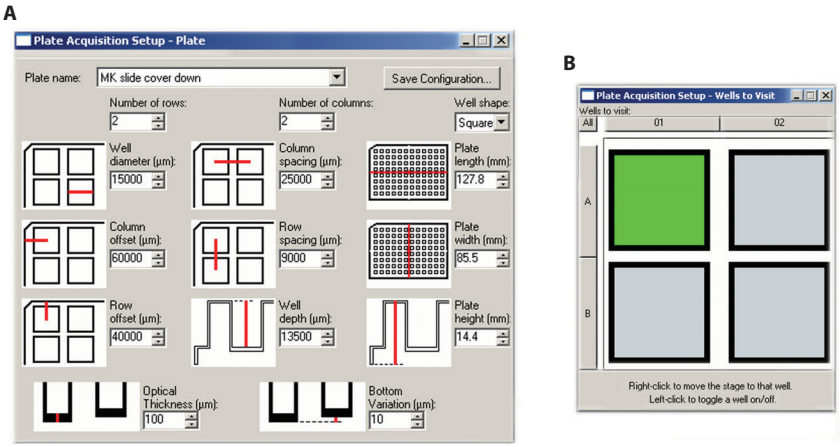

Fig. 3. Addition of a microscope slide to the plate library of the MetaXpress software. (**A**) New configuration settings for the microscope slide are added to the plate library; these settings identify the slide as a four-well plate, the first row represents the two cover slips for which images will be acquired. Wells B01 and B02 are required for the plate set up, but are not actually on the slide. (**B**) Images for wells (cover slips) can be acquired separately or both in the same acquisition with one cover slip after the other.

8. Specify the details of the plate in the "Plate Acquisition Setup-Plate" screen (Fig. 3A).

Note: For 18- × 18-mm-sized cover slips on precleaned Fisherbrand slides (size 25 × 75 × 1 mm) set 2.5 cm apart (Fig. 1), the settings shown in Fig. 3A can be used.

9. Specify which cover slips will be used to acquire images by using the "Wells to Visit" screen (Fig. 3B).

Note: Each cover slip on the slide is represented as a well. Wells can be selected individually (left-clicking on well) or data can be acquired for both wells

10. Specify the positions and number of images to collect on each cover slip by using the "Sites to Visit" screen (Fig. 4A).

Note: Images can be collected from each well at multiple sites, and these are determined by the specified number of columns and rows. Spacing between the columns and rows can be set to ensure sampling of the entire cover slip. Images from multiple sites distributed throughout the cover slip should be collected to provide a nonbiased representation of the sample. We collected images from 16 to 25 sites with a minimum of 70 cells for each cover slip. This was sufficient to obtain at least 50 cells with proper segmentation, after segmentation results were inspected and poorly segmented cells were eliminated from the analysis.

11. Set the appropriate wavelengths for image acquisition.

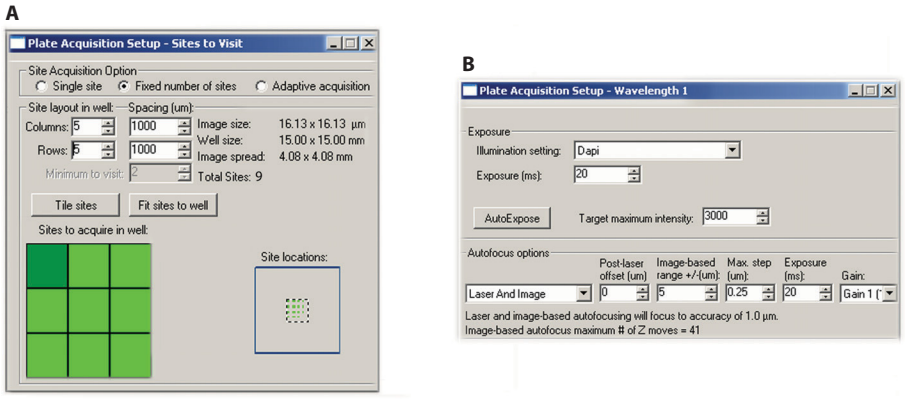

Fig. 4. Defining the sites for image acquisition and wavelength-1. (**A**) Configuration settings define nine sites for acquisition; note that the site distribution is determined by the spacing between rows and columns. (**B**) Configuration settings to acquire wavelength-1 image (Dapi). Combined laser- and image-based focus option is selected to enhance image resolution (see text for details).

Note: We set DAPI as W1 with 350/460 nm excitation/emission wavelength and an exposure time of 20 ms (Fig. 4B). We set W2 as either enhanced GFP (EGFP)/FITC/Alexa488 (470/525-nm excitation/emission wavelength, 3182-ms exposure time, target maximum intensity 3000, and Z offset from W1 of 1.1 μm) or TRITC/Cy3 (545/620-nm excitation/emission wavelength, 3182-ms exposure time, target maximum intensity 3000, and Z offset from W1 of 1.1 μm). Shorter exposure times, ~100 to 500 ms, can be used if the signal-to-noise ratio is two or higher and must be used for live-cell imaging.

12. Set the autofocus to either laser-based or image-based, or both.

Note: For fixed samples with antifade mounting medium, we used laser-based focus, enabled the image-based focus, and selected a binning of 2. For the laser-based focus, the following settings were used: Exposure on the plate bottom, 50 μs; exposure on the well bottom, 300 μs; course step, 3μm; fine step, 0.5μm; laser power, 100. We selected to focus on the plate bottom and then offset by the bottom thickness.

Image Acquisition with Confocal Microscopy for Cells Grown on Cover Slips

1. Place microscope slide on the stage of the confocal microscope.
2. Using a 63× oil immersion objective (NA 1.4), set the confocal microscope to a resolution of 1024 × 1024 and 12 bits.
3. Choose optical slices through the center of the nucleus for quantification and obtain optical sections of 0.65 μm.
4. Save images as .lsm files, which are recognized by the MetaXpress software.

Image Analysis with MetaXpress

Table 1. Comparison between different software modules for the quantification of nuclear, cytoplasmic, and NE fluorescence.

Software module	Application	Disadvantages
Multiwavelength cell-scoring	Strong signal in cytoplasm; uneven distribution of signal in cytoplasm	Not useful if signal in cytoplasm is faint or cell edges not discernible; cannot be used to measure NE or other membrane-associated fluorescence
Translocation-enhanced	Strong or weak signals in cytoplasm; NE fluorescence	Not useful if uneven distribution of signal in cytoplasm
Multiwavelength translocation	Strong or weak signals in cytoplasm; NE fluorescence measured in one step	Not useful if uneven distribution of signal in cytoplasm

Three MetaXpress software modules may be used for analysis. "Multiwavelength cell-scoring,"translocation-enhanced," and "multiwavelength translocation" modules (Table 1) were adapted to quantify the localization of molecules of interest. For all modules, DAPI staining was used as a reference to distinguish nuclear and cytoplasmic compartments. A second fluorescent marker stained the molecule of interest, which may localize to the nucleus, cytoplasm, both compartments, or the NE. These software modules can be used with images acquired with the ImageXpress Micro instrument, with a confocal microscope, or with any images acquired with a microscope that can save the images in a format that can be read by MetaXpress. Different procedures are required for analyzing images depending on the acquisition method, and these are detailed for each module. After configuration, data acquisition and export follow a common set of steps, which are presented once.

Configuring the Multiwavelength Cell-Scoring Module to Quantify Nuclear and Cytoplasmic Distribution

The multiwavelength cell-scoring module measures the fluorescence intensities of at least two markers with different wavelengths. The application of this module to quantification of nuclear and cytoplasmic distribution depends on a defined set of parameters that identify each cell and relies on the presence of a nuclear marker. The nuclear marker is required to identify cells. The software creates segments (regions) that colocalize with the compartment of interest. The exact match between the region (segment) and the compartment margin is achieved by selecting segmentation parameters (minimum and maximum width, intensity above background). The software measures the fluorescence intensity in the region defined by the settings.

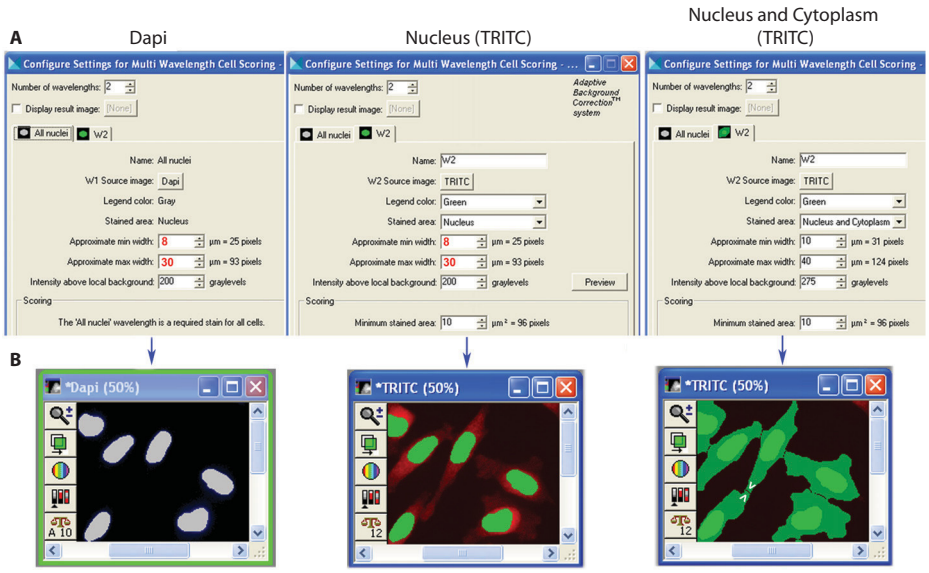

Fig. 5. Quantification of fluorescence intensities with the multiwavelength cell-scoring module, defining the values for segmentation (**A**) Settings are shown to generate segments that colocalize with the nucleus in the DAPI image (Dapi), the nucleus in the TRITC image [Nucleus (TRITC)], or with the whole cell in the TRITC image [Nucleus and Cytoplasm (TRITC)]. (**B**) The overlays between the created segments and the cellular compartment (nucleus) or the entire cell are depicted. The overlay images are necessary to adjust and verify the accuracy of segmentation settings. Cells marked with arrowheads show incorrect segmentation of the cytoplasm and are excluded from further analyses.

The minimum and maximum width of the nuclei and the intensity above local background of the nuclear marker are used to identify the nuclear compartment (minimum width = 8 μm, maximum width = 30 μm) (Fig. 5A; numbers in red). These are the first segmentation criteria. Similarly, segmentation settings for the second marker denote the second compartment of interest. In the example shown in Fig. 5, the protein of interest was stained with Cy3-labeled secondary antibodies and is present in both nuclear and cytoplasmic compartments. The same filter is used to measure fluorescence obtained for TRITC- or Cy3-labeled molecules, which is shown as "TRITC" in the software window (Fig. 5). For segmentation of a cytoplasmic marker, the software analyzes intensities going out from the nuclear segmentation until an edge is found where fluorescence intensities are no longer above the minimum threshold or a large drop in intensity between two neighboring pixels occurs. Care must be taken in selecting settings for segmentation in order to get a proper identification of cellular compartments. The cytoplasmic area is defined as the region where the second marker, but not the nuclear marker (in this example, DAPI), can be detected. The total intensity of Cy3-labeling in the nucleus is measured according to the segmentation obtained with DAPI staining. The intensity of Cy3-labeling of the entire cell is calculated for the region that shows Cy3-labeling above the minimum threshold set in the initial parameters. The difference between whole-cell intensity (nucleus plus cytoplasm) minus the nuclear intensity provides a measure of the cytoplasmic fraction of the protein.

It is essential to visually inspect the overlay between the segments generated and the boundaries of nuclei and the cells in the original image. This step ensures that segments produced by the software colocalize with the desired regions. The settings may need to be revised to establish an accurate demarcation of the regions of interest (Fig. 5, A and B).

Changes in the settings for minimum and maximum width or in the intensity above background affect segmentation (Fig. 6, A to C). For instance, values too low for the approximate minimum width of the nuclear segmentation parameters underestimate the nuclear size, whereas nuclei are missed when values are too high (Fig. 6B, top and middle). Moreover, inappropriate values for the intensity above local background interfere with the proper identification of nuclei (Fig. 6B, bottom). In addition, values of the cellular segmentation parameters that are too high for either the approximate minimum width or intensity above local background underestimate the cell size (Fig. 6C, top and bottom), whereas values too low for the intensity above local background overestimate the cellular size (Fig. 6C, middle).

If the cytoplasmic fluorescence is low, the boundaries of the cell may not be detected properly. In this case, the nuclear and cytoplasmic distributions can be measured by using the translocation-enhanced or multiwavelength translocation modules described in the later sections.

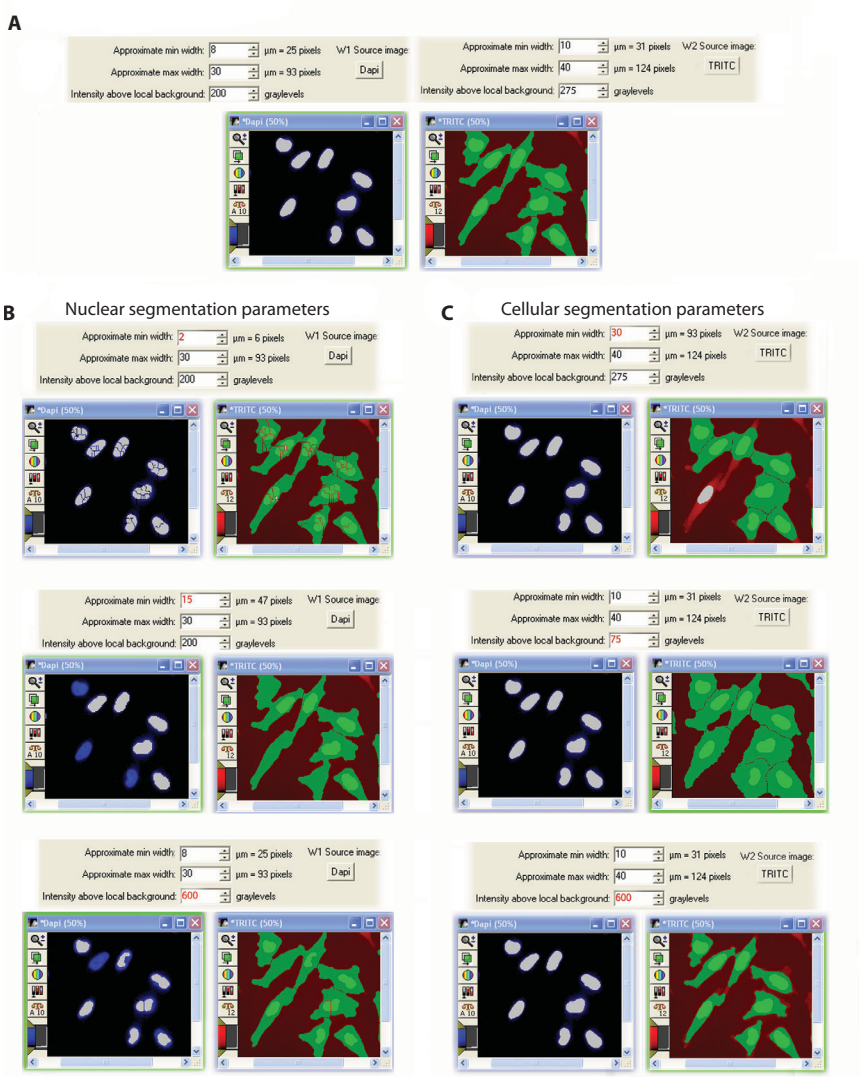

Fig. 6. Settings for nuclear and cellular segmentation parameters are crucial to generate segments that accurately match the nuclei and cell margins. (**A**) Appropriate values were selected for segmentation. (**B**) Incorrect values for any of the parameters (red numbers) to identify the nuclei (left) may result in under- or overestimation of the nuclear size. This may generate segments that do not match the cellular margins or may eliminate some nuclei. (**C**) Similarly, inappropriate parameters to identify the cell margins (right) will produce segments that do not properly colocalize with the cellular boundaries (see text for details).

Here, we provide a step-by-step protocol using the multiwavelength cell-scoring module in MetaXpress for the quantification of data obtained for fixed HeLa cells for which the protein of interest was detected by indirect immunofluorescence with Cy3-labeled secondary antibodies and DNA was stained with DAPI.

1. From the MetaXpress main screen, select "Screening."
2. From the drop-down menu, select "Review Plate Data."
3. In the Review Plate Data dialog box, press the "Select Plate" button in the upper left to retrieve acquired plate data (Fig. 7A).
4. In the Review Plate Data dialog box, select the well to be displayed under "Data view: Well arrangement" (Fig. 7A).

   Note: For instance, for A01 shown in Fig. 7A, choose all sites from the table cell to view all the acquired fields (each field = one image).

5. Select the wavelengths to be displayed. Once selected, an HCS-image array of thumbnails for each wavelength opens, showing all images acquired for each cover slip or well (Fig. 7B).
6. Click on a thumbnail for a site to analyze, and two separate full-resolution images representing the two wavelengths open. Each one displays the name of the wavelength at the top (Fig. 7B, DAPI or TRITC. Note that "TRITC" shows the image obtained with the TRITC/Cy3 filter.).
7. Correct the background for the full-resolution images, by subtracting from each image pixel the average intensity of a manually selected region of the image that does not contain cells. At this point, background-corrected images can be saved. This is desirable if the same images will be processed with a different module.

   Note: Because background intensities vary between different images, the background for each individual image must be determined and subtracted.

8. To begin configuring new settings, in the Review Plate Data dialog box choose "Multi Wavelength Cell Scoring" under the "Run Analysis" tab, then press the "Configure Settings" button (Fig. 7A).

   Note: Once the new settings are configured, the stored configuration settings can be retrieved by selecting the multiwavelength cell-scoring module from the application module list or from the Review Plate Data dialog box under the Run analysis tab, using "Analysis" and "Settings" lists to open the dialog box for the multiwavelength cell-scoring module (Fig. 7A).

9. In the multiwavelength cell-scoring dialog box, enter the total number of wavelengths in the experiment. Separate tabs for each wavelength will be displayed.

   Note: In the example in Fig. 5, the "All nuclei" tab corresponds to the nuclear marker DAPI and the "W2" tab represents the second marker, in this case TRITC/Cy3.

10. Open the wavelength tab for "All nuclei" and set the parameters for nuclear segmentation.

    Note: Fig. 5A (DAPI) shows the actual values used to segment the nuclei of HeLa cells.

11. Open the wavelength tab for W2 and set the parameters for cellular segmentation.

    Note: For our experiments, we generated two settings. The first setting had the same parameters as that for the DAPI wavelength to identify the intensity in the nuclei (Fig. 5A, Nucleus, TRITC). The second setting was based on segmentation of the entire cell to determine the intensity in the nucleus and cytoplasm (Fig. 5A, Nucleus and Cytoplasm, TRITC).

12. Press the "Preview" or "Test Run" button to display the original images with the segmentation overlaid (Fig. 5B). Cells that are not well segmented should be excluded from the analysis.

    Note: Two cells in Fig. 5B (marked with arrowheads) were not segmented well and are representative of the types of cells that would be excluded from the analysis by manual inspection of the data.

13. Proceed to Data Acquisition and Export.

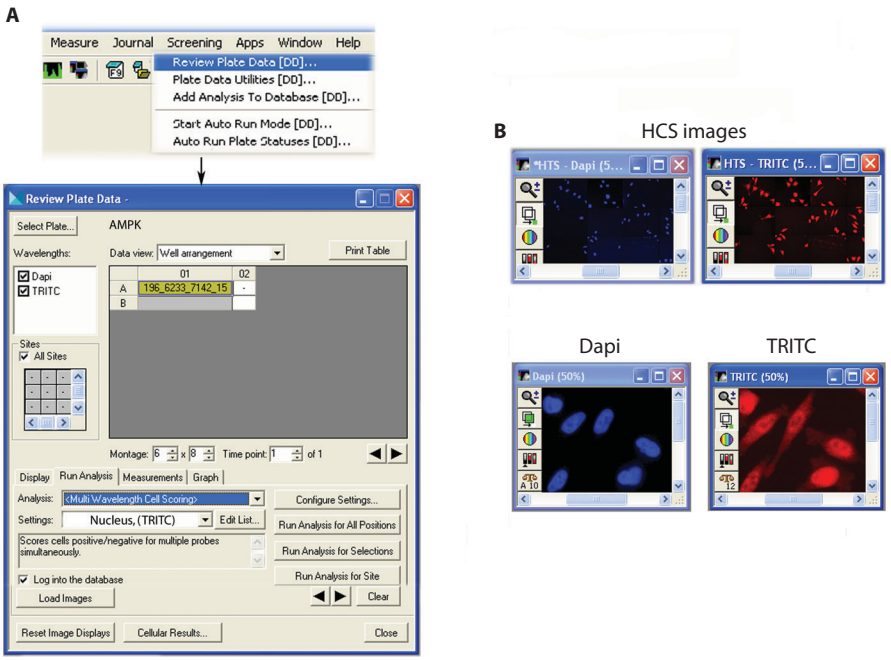

Fig. 7. Opening of images acquired with ImageXpress Micro and configuration of the analysis module. (**A**) The review plate data dialog box option is used to retrieve the acquired plate, open the image and select the analysis module. The analysis module settings can be configured with the Configure Settings button. (**B**) The HCS images show thumbnails of all the individual images that were acquired for the specified sites. After clicking on a single site, full-resolution DAPI and TRITC images are displayed simultaneously. On these images, analysis is carried out after a correction is made for the contribution of background fluorescence.

Configuring the Translocation-Enhanced Module to Quantify Nuclear and Cytoplasmic Distribution

The translocation-enhanced module determines the localization of a fluorescent probe with respect to a specific cellular compartment, such as the nucleus. It quantifies the fluorescence signal inside, as well as outside, of a defined compartment. The compartment of interest is identified with a fluorescent marker that is distinct from the fluorescent marker to be measured. In the example described, DAPI is used to stain nuclei and GFP with a nuclear localization sequence (NLS) (NLS-GFP) (*13*) is the protein of interest (Fig. 8). The software uses the DAPI image to define the margins of the compartment (Fig. 8A), on the basis of several criteria that are configured in the dialog box option settings (Fig. 8B). The criteria are similar to those for the multiwavelength cell-scoring module, with the addition of the approximate width of the compartment and the use of minimum and maximum area rather than diameter of the stained area. After identifying the compartment edge, the software creates two regions (segments) that are ring shaped either within or outside of the compartment. This segmentation is applied to the image of the protein of interest (in this case, NLS-GFP) (*13*) to measure the fluorescence intensity in both regions (Fig. 8C).

The translocation-enhanced module should be used when quantifying the relative distribution of a molecule between the nucleus and cytoplasm instead of the multiwavelength cell-scoring module when the cellular segmentation for the molecule of interest is problematic. Examples where segmentation may be problematic include the following: (i) situations in which the fluorescence intensity of the molecule of interest is not very high above background, which makes it difficult to identify the cell edges, that is the plasma membrane; (ii) cells in which the molecule of interest concentrates in nuclei or near the nuclear periphery; and (iii) samples in

which the density of the cells is high, which makes it difficult to adequately resolve individual cells.

However, there are conditions for which the translocation-enhanced module cannot be used. If the fluorescence intensity is not evenly distributed throughout the cytoplasmic compartment, then the selected outer area near the nuclear rim may not accurately represent the cytoplasmic distribution of the probe (see HuR as an example, below).

In the translocation-enhanced module, a background estimation method for background subtraction is available. However, this feature of the software is not well characterized and was, therefore, not applied in our studies.

Below are detailed instructions for configuring MetaXpress and analyzing images acquired with ImageXpress Micro using the translocation-enhanced module to quantify proteins localized in the nucleus and cytoplasm.

1. From the MetaXpress main screen, select "Screening."
2. From the drop-down menu, select "Review Plate Data."
3. In the Review Plate Data dialog box, press the "Select Plate" button in the upper left to retrieve acquired plate data (Fig. 7A).
4. In the Review Plate Data dialog box, select the well to be displayed under "Data view: Well arrangement" (Fig. 7A).
5. Select the wavelengths to be displayed. Once selected, an HCS-image array of thumbnails for each wavelength opens showing all images acquired for each cover slip or well (Fig. 7B).
6. Click on a thumbnail for a site to analyze and two separate full-resolution images representing the two wavelengths open. Each one displays the name of the wavelength at the top (Fig. 7B, DAPI or TRITC).
7. Correct the background for the full-resolution images by subtracting from each image pixel the average intensity of a manually selected region of the image that does not contain cells. At this point, background-corrected images can be saved.

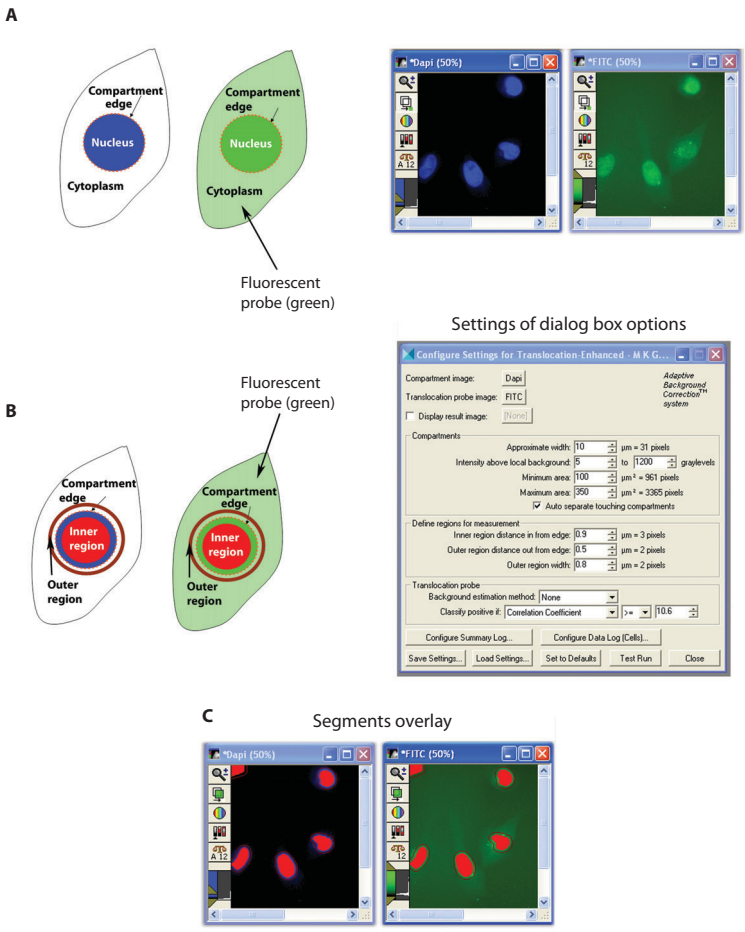

Fig. 8. The translocation-enhanced module is applied to analyze nuclear transport. (**A**) DAPI staining identifies the compartment of interest (nucleus); NLS-GFP is a nuclear reporter protein for which the nuclear and cytoplasmic fluorescence will be quantified (see also Fig. 13). (**B**) The dialog box for the translocation-enhanced module shows the settings that define the nuclear compartment, as well as the inner and outer regions that were selected for quantification. The cartoon depicts the position of the inner and outer regions with respect to the nucleus, as well as the edge of the nuclear compartment (orange dashed line). (**C**) Overlays were produced for the inner and outer regions either with the DAPI or the FITC (NLS-GFP) image to visualize the segmentation for acquired images.

8. To begin configuring new settings, in the Review Plate Data dialog box choose "Translocation enhanced" under the "Run Analysis" tab, then press the "Configure Settings" button (Fig. 7A).
9. In the translocation-enhanced dialog box (Fig. 8B), select the wavelengths of the compartment marker and the translocation probe, DAPI and FITC in the given example. Set the measurements to identify the compartment of interest (for instance, nucleus), and select to automatically separate touching compartments; this will ensure the accurate separation of adjacent compartments (in the example, nucleus and cytoplasm).
10. Define the inner and outer regions; this includes the region width and distance from the compartment edge (in our example, the boundary of the nucleus which is delineated by the NE; dashed orange line in Fig. 8A).
11. Press the "Test Run" button to display the original images with the segmentation overlaid (Fig. 8C). Cells that are not well segmented should be excluded from the analysis.
12. Proceed to "Data Acquisition and Export."

Configuring the Translocation-Enhanced Module to Quantify NE Fluorescence

By modifying the parameter settings that define the inner and outer regions, we adapted the translocation-enhanced module and used it to measure the intensity of a fluorescent probe at the NE (Fig. 9A). This new application of the module was generated by creating two different configurations for inner and outer regions (Fig. 9, B and C). The data from these two configurations are combined to quantify NE staining.

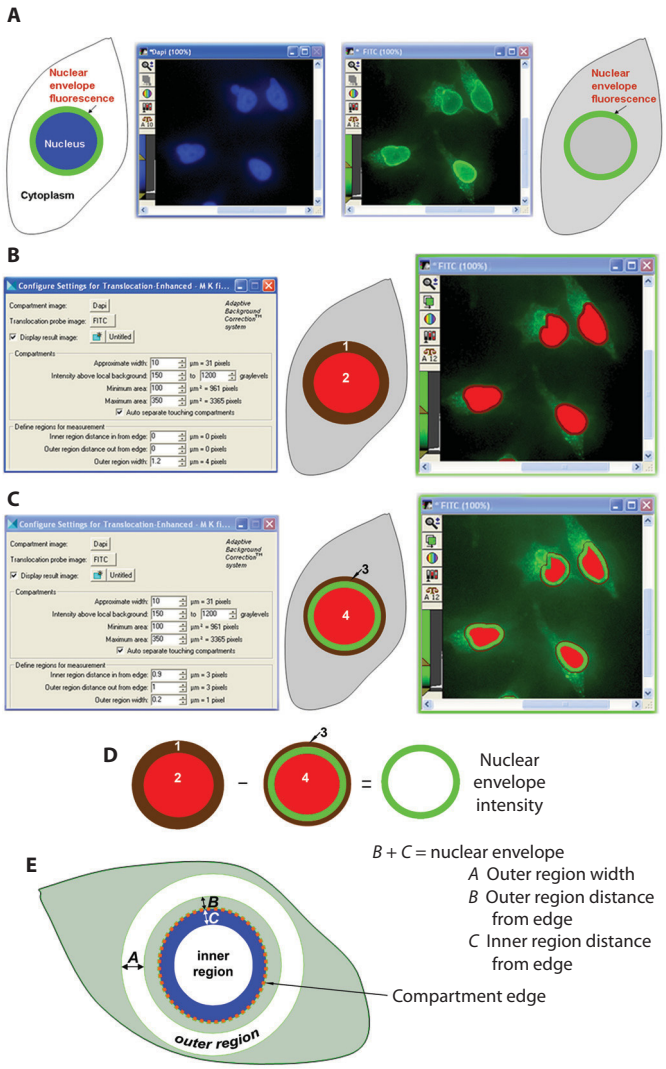

Fig. 9. The translocation-enhanced module was adapted to quantify fluorescence at the NE. (**A**) Nuclei are stained with DAPI (blue), and an NE protein is detected by green fluorescence. (**B**) Settings used to generate regions 1 and 2 and the overlay between the segments and the FITC image are shown. Note that there is no space between the inner and outer regions, i.e., regions 1 and 2. (**C**) Regions 3 and 4 are generated at the same position as regions 1 and 2. However, the settings introduce a gap between regions 3 and 4; this gap represents the NE. The overlay image for regions 3 and 4 should be compared with the overlay image in part B for regions 1 and 2. (**D**) The fluorescence intensity at the NE can be calculated by the simple formula: Intensities of regions (1 + 2) minus intensities of regions (3 + 4). (**E**) The positions of the outer region, inner region, and the compartment edge (orange dashed line) are illustrated.

In the first configuration, two regions (regions 1 and 2) are created that represent the fluorescence intensity in a small area around the nucleus and a portion of the NE facing the cytoplasm (region 1), as well as the nucleus and the rest of the NE (region 2). These two regions are adjoining at the edge of the compartment, with no space between the inner and outer regions. The settings used to produce these regions and the overlay on the image are shown in Fig. 9B.

In the second configuration, the inner and outer regions are produced in the same positions as above; however, a space is generated between the inner and the outer region by defining the distance from the edge. For the example in Fig. 9C, the inner region ends 0.9 μm from the edge and the outer region begins 1 μm from the edge of the compartment (the nucleus in our example). These settings produce regions 3 and 4; the gap between these regions coincides with the NE.

The measurements obtained for regions 1, 2, 3, and 4 can now be combined manually to determine the fluorescence intensity at the NE: Regions (1 + 2) minus regions (3 + 4) will provide a quantification of the fluorescence signals located at the NE (Fig. 9D). A schematic representation of the critical parameters used to define the size and position of different regions is depicted in Fig. 9E.

Below are detailed instructions for configuring MetaXpress and analyzing images acquired with ImageXpress Micro using the translocation-enhanced module to quantify NE localized proteins.

1. From the MetaXpress main screen, select “Screening.”
2. From the drop-down menu, select “Review Plate Data.”
3. In the Review Plate Data dialog box, press the “Select Plate” button in the upper left to retrieve acquired plate data (Fig. 7A).
4. In the Review Plate Data dialog box, select the well to be displayed under “Data view: Well arrangement” (Fig. 7A).
5. Select the wavelengths to be displayed. Once selected, an HCS-image array of thumbnails for each wavelength opens showing all images acquired for each cover slip or well (Fig. 7B).
6. Click on a thumbnail for a site to be analyzed, and two separate full-resolution images representing the two wavelengths open. Each one displays the name of the wavelength at the top (Fig. 7B, DAPI and TRITC).
7. Correct the background for the full-resolution images, by subtracting from each image pixel the average intensity of a manually selected region of the image that does not contain cells. At this point, background-corrected images can be saved.
8. To begin configuring new settings, in the Review Plate Data dialog box choose “Translocation enhanced” under the “Run Analysis” tab, then press the “Configure Settings” button (Fig. 7A).

9. In the translocation-enhanced dialog box (Fig. 8B), select the wavelengths of the compartment marker and the translocation probe, DAPI and FITC in the given example. Set the measurements to identify the compartment of interest (for instance, nucleus) and select to automatically separate touching compartments; this will ensure the accurate separation of adjacent compartments (i.e., nucleus and cytoplasm).
10. Define the inner and outer regions; this includes the region width and distance from the compartment edge (in our example, the boundary of the nucleus which is delineated by the NE; dashed orange line in Fig. 8A). For the NE quantification, you need to create two sets of inner and outer regions, use the configuration settings in Fig. 9, B and C to obtain appropriate segmentation.
11. Press the "Test Run" button to display the original images with the segmentation overlaid (Fig. 9, B and C). Cells that are not well segmented should be excluded from the analysis.
12. Proceed to "Data Acquisition and Export" and calculate the intensity for NE fluorescence (Fig. 9D).

Configuring the Multiwavelength Translocation Module

This module is a simplified version of the translocation-enhanced module; it uses the same principle as the translocation-enhanced module to identify the nuclei and regions, both inside and outside of the nuclear area. The module contains one key component for NE analysis; it allows the assignment of negative values for the distance of the outer region from the compartment. We took advantage of this feature and developed configuration settings that create an outer region that colocalizes with the NE. This enabled us to measure the fluorescence intensity at the NE in one step (Fig. 10, A to C). Nevertheless, measuring the NE intensity with the translocation-enhanced module can be used to verify the results obtained by the multiwavelength translocation module. The modules each give similar results for the NE fluorescence intensity (Fig. 11). Although the main application of the multiwavelength translocation module in our experiments is to quantify NE intensity, it can also be used to determine fluorescence intensities in the nucleus and other areas of the cell.

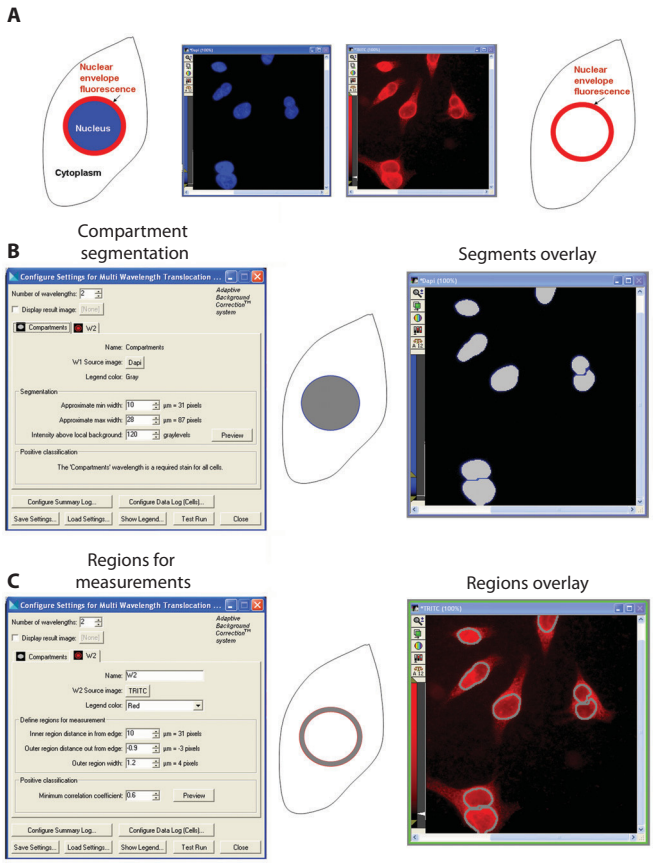

Fig. 10. The multiwavelength translocation module was adapted to quantify fluorescence at the NE. (**A**) The nuclear compartment is stained with DAPI and an NE protein is detected with a red fluorescent probe (TRITC) (*12*). (**B**) Settings to generate segments that define the nuclei and the overlay of segments and the DAPI image are illustrated. (**C**) Parameters are set to define the inner and outer regions. Note that the outer region coincides with the NE, whereas the inner region is set to be small to facilitate the visual inspection of overlay images (see text for details).

Below are detailed instructions for configuring MetaXpress and analyzing images acquired with ImageXpress Micro by using the multiwavelength translocation module.

1. From the MetaXpress main screen, select "Screening."
2. From the drop-down menu, select "Review Plate Data."
3. In the Review Plate Data dialog box, press the "Select Plate" button in the upper left to retrieve acquired plate data (Fig. 7A).
4. In the Review Plate Data dialog box, select the well to be displayed under "Data view: Well arrangement" (Fig. 7A).
5. Select the wavelengths to be displayed. Once selected, an HCS-image array of thumbnails for each wavelength opens, showing all images acquired for each cover slip or well (Fig. 7B).
6. Click on a thumbnail for a site to analyze, and two separate full-resolution images representing the two wavelengths open. Each one displays the name of the wavelength at the top (Fig. 7B; DAPI and TRITC).
7. Correct the background for the full-resolution images, by subtracting from each image pixel the average intensity of a manually selected region of the image that does not contain cells. At this point, background-corrected images can be saved.
8. To begin configuring new settings, in the Review Plate Data dialog box, choose "Multi Wavelength Translocation" under the "Run Analysis" tab, then press the "Configure Settings" button (Fig. 7A).

9. In the "multiwavelength translocation" dialog box, select compartments and configure the parameters to identify the compartment of interest, the nucleus in our example (Fig. 10B).
10. Select the W2 tab, then set the parameters to identify the inner and outer regions (Fig. 10C).

    Note that the outer region distance from edge has a negative value, and the segment generated colocalizes well with the NE. The inner region is set to be small; this simplifies the visual inspection to monitor an accurate match between the outer region and the NE.

11. Press the "Preview" or "Test Run" button to display the original images with the segmentation overlaid (Fig. 10, B and C). Cells that are not well segmented should be excluded from the analysis.
12. Proceed to "Data Acquisition and Export."

Analysis for Images Acquired by Confocal Microscopy

For each of the modules, images acquired by confocal microscopy may also be analyzed. The settings and parameters would be based on the same considerations as for those used for images acquired with ImageXpress Micro, and so, only the basic procedures are outlined here.

1. To analyze images acquired by confocal microscopy, open the image saved as an .lsm file in the MetaXpress main screen.
2. Correct the background by subtracting the average intensity from each image pixel of a manually selected region of the image that does not contain cells.
3. Select the "multiwavelength cell-scoring" module, the "translocation-enhanced module," or the "multiwavelength translocation" module from the "applications" button in the main screen; the corresponding dialog box will open.
4. Configure new settings.
5. Press the "Preview" or "Test Run" button to examine the segmentation accuracy and to modify the segmentation settings if necessary.
6. Proceed to "Data Acquisition and Export."

Data Acquisition and Export

1. Once the segmentation settings are accurate, open "log files" to save results in the format of Excel files: On the MetaXpress main screen, choose "Log," then select "Open Data Log," then "Open Data Log" window, then select "Dynamic Data Exchange (DDE)" and press "OK."
2. In the "Export Data Log" window, select "Microsoft Excel" and save the file, specifying the filename.
3. Select the measurements that should be saved in the file by opening the "Configure Summary Log" and "Configure Data Log" buttons in the "multiwavelength cell-scoring" dialog box, or the "translocation-enhanced" dialog box, or the "multiwavelength translocation" dialog box, choose the data to be logged into the file, and close the buttons.
4. Press the "Test Run" button and review the measurements for each cell in the image in the cellular data window that opens.

    Note: For each image analyzed, the cellular data will be logged automatically to the Excel file specified in the previous step.

5. Click on each individual cell in the image to highlight the data line corresponding to the selected cell. Each cell is identified by a number, which appears as "Label #" in the Excel file.
6. Visually verify the accuracy of the segmentation and exclude cells with incorrect segmentation from further analysis. This can be done by identifying the improperly segmented cells, by using their "Label #" and by highlighting the corresponding line on the Excel data sheet.

    Note: We routinely save results for correctly and incorrectly segmented cells, but delete data lines for cells that were not properly segmented before analyzing the numbers.

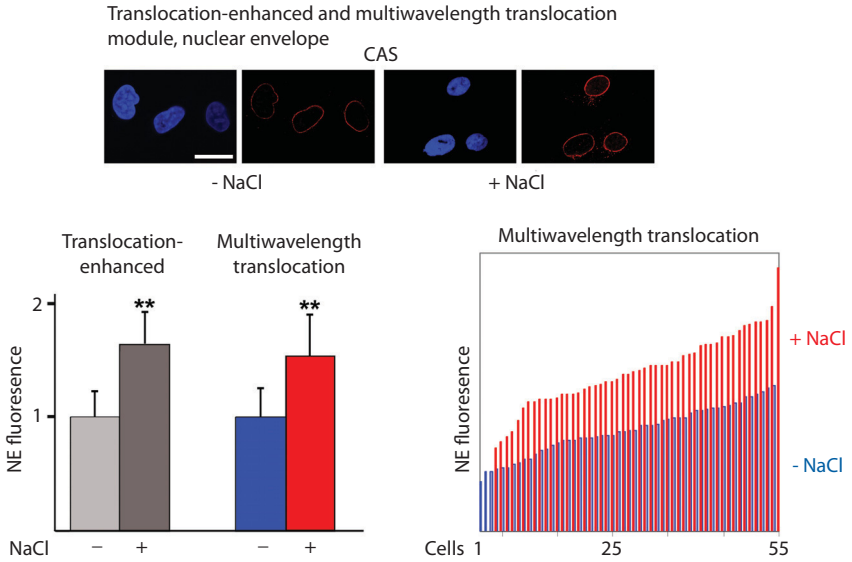

Fig. 11. Application of the translocation-enhanced and multiwavelength translocation modules to measure fluorescence located at the NE. NE binding of the fluorescently labeled nuclear carrier CAS (*12*) was analyzed in HeLa cells for controls (–NaCl) or salt-extracted specimen (+NaCl). Images were acquired by confocal microscopy and NE fluorescence intensity quantified with the translocation-enhanced or multiwavelength translocation module. Fluorescence intensities for samples –NaCl were defined as 1. Data obtained with the multiwavelength translocation module are also depicted on the right side for individual cells –NaCl (blue) and +NaCl (red). Size bar is 25 μm; $^{**}P < 0.01$ (see text for details). [Parts of Fig. 11 were reprinted from (*12*) with permission from Birkhäuser Verlag AG]

Notes and Remarks

The methods described here provide quantitative approaches for measuring the intensities of fluorescent probes in different cellular compartments, including, but not limited to, the nucleus, cytoplasm, and NE. We illustrate methods for image acquisition and analysis with three different software modules in MetaXpress (Table 1), which have been adapted to measure the fluorescence intensities in these compartments. Choosing the appropriate module will depend on the distribution of the fluorescent molecule to be quantified, the strength of the fluorescent signal in the cytoplasm, the experimental conditions (for example, transfected versus nontransfected cells), and the localization of the molecule of interest.

We have employed these strategies successfully to study the subcellular localization in mammalian cells of several proteins that are involved in different aspects of signaling (Figs. 11 to 13). The multiwavelength cell-scoring module was used to quantify the distribution of the protein HuR (Fig. 12), for which a larger portion is detected in the cytoplasm upon oxidative stress (*13*). The stress-induced relocation caused a decrease in the ratio of average nuclear to cytoplasmic (nuc/cyt) fluorescence (Fig. 12). The uneven distribution pattern of HuR in the cytoplasm of stressed cells requires that the fluorescence of the whole cytoplasmic compartment is measured to obtain an accurate quantification. This is achieved by applying the multiwavelength cell-scoring module. Because of the irregular distribution of HuR in stressed cells, neither the translocation-enhanced nor the multiwavelength translocation module will provide a correct measurement for HuR in the cytoplasm.

The multiwavelength cell-scoring module depends on the labeled protein to identify the cell boundaries. Depending on the protein studied other software modules may be more appropriate to quantify the nuclear and cytoplasmic fluorescence. For instance, cell boundaries can overlap for samples with densely plated cells, which results in inaccurate cellular segmentation. Furthermore, in experiments with transiently transfected cells, signals may be variable or too low to define cell edges. The same problem arises if the protein of interest is restricted to the nucleus under certain conditions. In these cases, the translocation-enhanced module provides the method of choice for quantification. For example, in HeLa cells that transiently synthesize NLS-GFP (Fig. 13, green), which is a reporter protein that localizes to

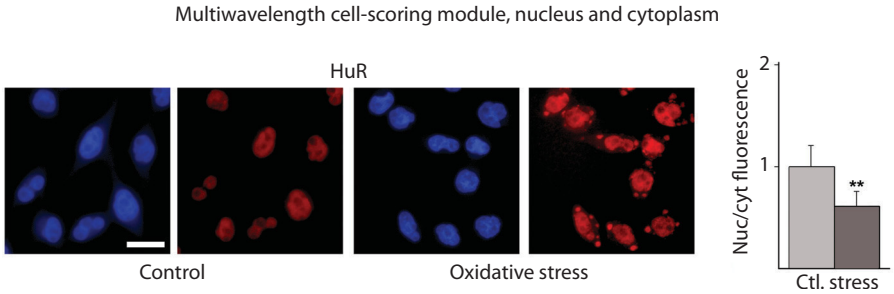

Fig. 12. Application of the multiwavelength cell-scoring module. The multiwavelength cell-scoring module is employed to measure the nuc/cyt fluorescence of HuR protein (red) under normal (control) and oxidative stress conditions (HuR) (*13*). Note that the irregular distribution of HuR in the cytoplasm of stressed cells requires the quantification of fluorescence in the whole cytoplasm. A γ-factor of 2 was applied to visualize the weak cytoplasmic signal, but the same image display settings are applied for all images in the same panel. Because the cytoplasmic fluorescence was weak, a low value of intensity above local background was selected to properly identify the cell edges. Changes in the ratio of average nuclear/cytoplasmic (nuc/cyt) fluorescence were determined for HCS images. The ratio of nuc/cyt fluorescence in unstressed control cells was defined as 1. [Parts of Fig. 12 were reprinted from (*13*) with permission from Elsevier]

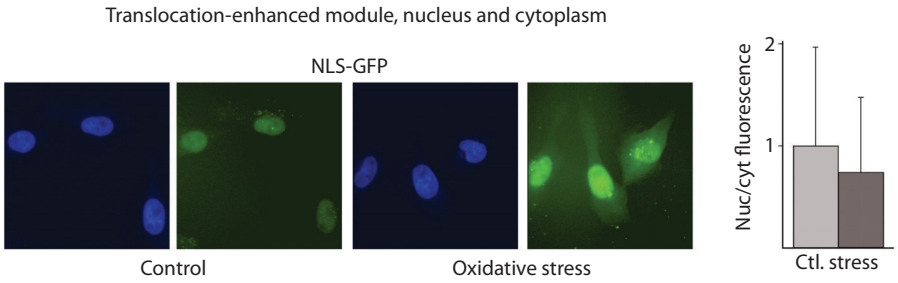

Fig. 13. Application of the translocation-enhanced module. The translocation-enhanced module is used to measure the nuc/cyt fluorescence of NLS-GFP (green) in transiently transfected HeLa cells under normal and oxidative stress conditions (*13*). Note that the weak cytoplasmic signal would prevent the accurate cellular segmentation with the multiwavelength cell-scoring module (see text). [Parts of Fig. 13 were reprinted from (*13*) with permission from Elsevier]

the nucleus under normal conditions (control), the abundance of NLS-GFP in the cytoplasm is low, which compromises cellular segmentation with the multiwavelength cell-scoring module. Therefore, the translocation-enhanced module is a better choice for measuring the nuclear and cytoplasmic fluorescence intensities of NLS-GFP, because the cell boundaries do not need to be identified. The appearance of green fluorescence in the cytoplasm of cells exposed to oxidative stress, quantified as a decrease in the nuc/cyt ratio (Fig. 13), indicates that nuclear import is less efficient under these conditions (*13*).

One of the major challenges in quantifying subcellular distribution of molecules is the quantification of fluorescence signals located at the NE. First, there are no modules provided by the MetaXpress software to quantify the signals located at the NE. Second, the NE area is very small compared with the nucleus and cytoplasm, which makes it difficult for the analysis software to define the NE compartment precisely. We adapted the translocation-enhanced and the multiwavelength translocation modules to measure fluorescence intensities at the NE (Fig. 11) (*12*). Using the translocation-enhanced module to quantify fluorescence signals at the NE requires the configuration of two settings and some post analysis data processing, whereas the multiwavelength translocation module is simpler because it makes the measurements in a single step. One advantage to the translocation-enhanced module is that it can be used to quantify fluorescence intensities for nuclear, NE, and cytoplasmic compartments in the same analysis, which may be required for more complex applications. For measurements of fluorescence located at the NE, results obtained with the translocation-enhanced module can be verified by the multiwavelength translocation module and vice versa (Fig. 11). Other modules of the MetaXpress software can be used to quantify the association of molecules with the plasma membrane or different cellular compartments. Some of these modules rely on a fluorescent marker that is used to identify the compartment of interest.

This protocol details the procedures for acquiring images for cells conventionally grown on cover slips and for quantifying the fluorescence intensities in defined cellular compartments. This is achieved by combining HCS for high-throughput image acquisition and adapting different software modules from MetaXpress for analyses. The methods described here provide resources to detect minor changes in the subcellular localization of proteins and other molecules that can be detected with fluorescent probes. The convenience, ease of use, and accuracy of these techniques make them powerful tools for the quantification of numerous biological processes. The procedures described here are ideal to explore, in a quantitative fashion, the various aspects of signal transduction cascades and their regulatory circuits, a major challenge given the complexity of these pathways. The ability to analyze single cells also provides the potential to determine subtle changes in subpopulations of cells rather than obtaining single measurements for whole-cell populations.

References and Notes

1. A. Zimber, Q. Nguyen, C. Gespach, Nuclear bodies and compartments: Functional roles and cellular signalling in health and disease. *Cell. Signal.* **16**, 1085–1104 (2004).
2. F. M. Boisvert, S. Van Koningsbruggen, J. Navascues, A. I. Lamond, The multifunctional nucleolus. *Nat. Rev. Mol. Cell Biol.* **8**, 574–585 (2007).
3. A. Akhtar, S. Gasser, The nuclear envelope and transcriptional control. *Nat. Rev. Genet.* **8**, 507–517 (2007).
4. C. R. Brown, C. J. Kennedy, V. A. Delmar, D. J. Forbes, P. A. Silver, Global histone acetylation induces functional genomic reorganization at mammalian nuclear pore complexes. *Genes Dev.* **22**, 627–639 (2008).
5. K. L. Reddy, J. M. Zullo, H. Singh, Transcriptional repression mediated by repositioning of genes to the nuclear lamina. *Nature* **452**, 243–247 (2008).
6. C. T. Chu, E. D. Plowey, Y. Wang, V. Patel, K. L. Jordan-Sciutto, Location, location, location: Altered transcription factor trafficking in neurodegeneration. *J. Neuropathol. Exp. Neurol.* **66**, 873–883 (2007).
7. M. Stewart, Molecular mechanism of the nuclear protein import cycle. *Nat. Rev. Mol. Cell Biol.* **8**, 195–208 (2007).
8. L. J. Terry, E. B. Shows, S. R. Wente, Crossing the nuclear envelope: Hierarchical regulation of nucleocytoplasmic transport. *Science* **318**, 1412–1416 (2007).
9. A. Köhler, E. Hurt, Exporting RNA from the nucleus to the cytoplasm. *Nat. Rev. Mol. Cell Biol.* **8**, 761–773 (2007).
10. I. K. Poon, D. A. Jans, Regulation of nuclear transport: Central role in development and transformation? *Traffic* **6**, 173–186 (2005).
11. P. Grote, K. Schaeuble, E. Ferrando-May, Commuting (to) suicide: An update on nucleocytoplasmic transport in apoptosis. *Arch. Biochem. Biophys.* **462**, 156–161 (2007).
12. M. Kodiha, P. Bański, D. Ho-Wo-Cheong, U. Stochaj, Dissection of the molecular mechanisms that control the nuclear accumulation of transport factors importin-α and CAS in stressed cells. *Cell. Mol. Life Sci.* **65**, 1756–1767 (2008).
13. M. Kodiha, D. Tran, C. Qian, A. Morogan, J. F. Presley, C. M. Brown, U. Stochaj, Oxidative stress mislocalizes and retains transport factor importin-α and nucleoporins Nup153 and Nup88 in nuclei where they generate high molecular mass complexes. *Biochim. Biophys. Acta* **1783**, 405–418 (2008).
14. Q. Li, R. R. Falsey, S. Gaitonde, V. Sotello, K. Kislin, J. D. Martinez, Genetic analysis of p53 nuclear importation. *Oncogene* **26**, 7885–7893 (2007).
15. L. P. Van Der Heide, M. F. Hoekman, M. P. Smidt, The ins and outs of FoxO shuttling: Mechanisms of FoxO translocation and transcriptional regulation. *Biochem. J.* **380**, 297–309 (2004).
16. H. Huang, D. J. Tindall, Dynamic FoxO transcription factors. *J. Cell Sci.* **120**, 2479–2487 (2007).
17. T. Tanaka, S. Ohkubo, I. Tatsuno, C. Prives, hCAS/CSE1L associates with chromatin and regulates expression of select p53 target genes. *Cell* **130**, 638–650 (2007).
18. A. G. Turjanski, J. P. Vaqué, J. S. Gutkind, MAP kinases and the control of nuclear events. *Oncogene* **26**, 3240–3253 (2007).
19. Y. D. Shaul, R. Seger, The MEK/ERK cascade: From signaling specificity to diverse functions. *Biochim. Biophys. Acta* **1773**, 1213–1226 (2007).
20. D. G. Hardie, AMP-activated/SNF1 protein kinases: Conserved guardians of cellular energy. *Nat. Rev. Mol. Cell Biol.* **8**, 774–785 (2007).
21. K. Hedbacker, M. Carlson, SNF1/AMPK pathways in yeast. *Front. Biosci.* **13**, 2408–2420 (2008).
22. M. Kodiha, J. G. Rassi, C. M. Brown, U. Stochaj, Localization of AMP kinase is regulated by stress, cell density, and signaling through the MEK→ERK1/2 pathway. *Am. J. Physiol. Cell Physiol.* **293**, C1427–C1436 (2007).

23. U. Ashery, O. Yizhar, B. Rotblat, Y. Kloog, Nonconventional trafficking of Ras associated with Ras signal organization. *Traffic* **7**, 1119–1126 (2006).
24. F. R. Bischoff, H. R. Ponstingl, Mitotic regulator protein RCC1 is complexed with a nuclear Ras-related polypeptide. *Proc. Natl. Acad. Sci. U.S.A.* **88**, 10830–10841 (1991).
25. J. M. Cronshaw, A. N. Krutchinsky, W. Zhang, B. T. Chait, M. J. Matunis, Proteomic analysis of the mammalian nuclear pore complex. *J. Cell Biol.* **158**, 915–927 (2002).
26. C. M. Brown, Fluorescence microscopy—avoiding the pitfalls. *J. Cell Sci.* **120**, 1703–1705 (2007).
27. This research was supported by grants from Canadian Institutes of Health Research and NSERC to U.S. Images were collected in the HTS/HCS (high-throughput/content-screening facility) and the Imaging Facility both part of the McGill Life Sciences Complex funded by the Canada Foundation for Innovation. M.K. was supported by fellowships from Fonds de la recherche en santé du Québec (FRSQ) and the Heart and Stroke Foundation of Canada. We are particularly grateful for the continuous support by J. Liu and the HTS/HCS group in the Department of Biochemistry at McGill University.

10.1126/scisignal.137pl2

Citation: M. Kodiha, C. M. Brown, U. Stochaj, Analysis of signaling events by combining high-throughput screening technology with computer-based image analysis. *Sci. Signal.* **1**, pl2 (2008).

FEBS Letters 583 (2009) 1987–1993

FEBS Letters

journal homepage: www.FEBSLetters.org

Interplay between MEK and PI3 kinase signaling regulates the subcellular localization of protein kinases ERK1/2 and Akt upon oxidative stress

Mohamed Kodiha, Piotr Bański, Ursula Stochaj *

Department of Physiology, McGill University, Montreal, PQ, Canada H3G 1Y6

ARTICLE INFO

Article history:
Received 8 April 2009
Revised 30 April 2009
Accepted 6 May 2009
Available online 14 May 2009

Edited by Gianni Cesareni

Keywords:
Stress
Oxidant
Signal transduction
ERK1/2
Akt
Imaging
Quantitative immunofluorescence

ABSTRACT

ERK and Akt kinases are key components that participate in numerous regulatory processes, including the response to stress. Using novel tools for quantitative immunofluorescence, we show that oxidant exposure controls the intracellular activation and localization of ERK1/2 and Akt. Oxidative stress alters the nuclear/cytoplasmic levels of the kinases, drastically changing phospho-ERK1/2 and phospho-Akt(Ser473) levels in the nucleus. Moreover, pharmacological inhibition of PI3 kinase modulates the intracellular distribution of phospho-ERK1/2, whereas MEK inhibition affects phospho-Akt(Thr308) and phospho-Akt(Ser473). Our studies identify a new signaling link in the nucleus of stressed cells, where changes in phospho-ERK1/2 levels correlate directly with changes in phospho-Akt(Ser473).

1. Introduction

Signaling through PI3 → Akt and MEK → ERK1/2 modules is essential for cell growth, proliferation and survival of different forms of stress. Various stimuli trigger the activation of Akt and ERK1/2, thereby inducing the phosphorylation of distinct target molecules located in the cytoplasm and in the nucleus. The specificity of signaling events not only depends on the activation of kinases, but also on their proper location. This is indicated by the fact that many kinases, phosphatases and their targets relocate within the cell upon changes in physiology [1–6]. Activation of the MAP kinases ERK1/2 by dual phosphorylation (here referred to as p-ERK1/2) is linked to the nuclear accumulation of the kinases [1]. Full activation of Akt requires the phosphorylation of both Thr308 and Ser473 (here referred to as p-Akt308 and p-Akt473) [7–9]. Thr308 is modified by PDK1; mTORC2 is the most prominent kinase that phosphorylates Ser473, but other kinases have been implicated in Ser473 modification as well [8–15]. Several publications suggest that the signaling events and cell type can determine which kinase phosphorylates Ser473, and some of the pathways leading to Ser473 phosphorylation are insensitive to PI3 kinase inhibitors [10–13,15]. Interestingly, recent data demonstrate that particular pools of activated Akt can be generated in the cytoplasm with regulators that are restricted to this compartment, whereas unique functions can be attributed to nuclear Akt [16,17].

Upon exposure to certain stimuli and for several types of cancer, signaling through both PI3 kinase and MEK → ERK modules is activated simultaneously (reviewed in [18–21]). As the activation of these two signaling cascades is likely to have different downstream effects, it is important to regulate the relative input from either pathway to achieve the appropriate response. This may occur by cross-talk between both signaling routes [22], adding more complexity to the spatio-temporal control of signaling. Of particular importance to the balancing of different signaling cascades and the ultimate downstream effects is the control of kinase levels in different cellular compartments, especially in the nucleus and cytoplasm.

Oxidative stress is crucial to human health as it is linked to a large number of diseases and pathologies, including diabetes, obesity and ischemia/reperfusion injury of the heart and brain [23–25]. In the studies presented here, we used diethyl maleate as an oxidant to analyze in a quantitative fashion the effects on ERK1/2 and Akt activation and localization. Furthermore, with pharmacological inhibitors of PI3 and MEK-mediated signaling we tested the hypothesis that interplay between these pathways affects kinase activation and localization. For the experiments described here, we took advantage of recent developments in imaging and image-analysis to monitor in a quantitative fashion changes in ERK1/2 and Akt kinase compartmentalization. The significance of Akt and MEK signaling were monitored by measuring the

* Corresponding author. Fax: +1 514 398 7452.
E-mail address: ursula.stochaj@mcgill.ca (U. Stochaj).

0014-5793/$36.00
doi:10.1016/j.febslet.2009.05.011

nucleocytoplasmic distribution of the transcription factor FoxO3a, a downstream target of both signaling pathways.

2. Materials and methods

2.1. Growth of cells, stress treatment and incubation with pharmacological inhibitors

HeLa cells were grown on poly-lysine coated cover slips and treated with diethyl maleate as described [3]. For treatment with pharmacological inhibitors, cells were pre-incubated for 1 h with the solvent DMSO (D), 50 μM LY294002 (LY), 25 μM PD98059 (PD) or a combination of both drugs (Calbiochem) followed by treatment with ethanol (controls) or 2 mM diethyl maleate (for 4 h at 37 °C). DMSO or inhibitors were present throughout the incubation with the solvent ethanol or DEM. Results were obtained for at least three independent experiments.

2.2. Antibodies

The following antibodies were used for immunofluorescence: dually phosphorylated ERK1/2 (p-ERK1/2; Cell Signaling, #9106), total ERK1/2 (t-ERK1/2; StressGen, KAP-MA001C), phosphorylated Akt-Thr308 (p-Akt308; Cell Signaling, #2965), phosphorylated Akt-Ser473 (p-Akt473; Santa Cruz Biotechnology, sc-7985), total Akt (t-Akt; Santa Cruz Biotechnology, sc-1619; Cell Signaling, #9272), FoxO3a (Cell Signaling; #2497); HuR (Santa Cruz Biotechnology, sc-5261); rp S6 (Santa Cruz Biotechnology, sc-13007); G3BP (BD Transduction Laboratories, # 611126). Antibodies were diluted as recommended by the suppliers. Antibodies against p-Akt308 and p-Akt473 are likely to recognize Akt independent of the phosphorylation state at residue Ser473 or Thr308, respectively. FITC- or Cy3-labeled secondary antibodies were generated in donkeys and affinity-purified to minimize cross-reactivity (Jackson ImmunoResearch).

2.3. Immunofluorescent staining and confocal microscopy

Established protocols were used for the fixation and permeabilization of cells and incubation with primary and secondary antibodies [5]. Confocal images were collected with a Zeiss LSM510 in the multi-track mode for an optical slice thickness of >0.7 μm. p-ERK1/2 and t-ERK1/2 were detected with FITC- and Cy3-labeled secondary antibodies, respectively. Settings for pinhole and detector gain were identical within each experiment and proper filters were used to minimize cross-talk between the channels.

2.4. Quantification of fluorescent signals

Quantification of pixel intensities in nuclear and cytoplasmic compartments was as described [5]. In brief, nuclear and cytoplasmic fluorescence was measured using the multiwavelength cell scoring module following recently developed protocols that have been described in detail [5]. For each condition the distribution of total and activated kinases was quantified for at least 50 cells. Bar graphs in Figs. 1–3 depict pixel intensities/area. Pixel intensities/area obtained for control conditions (DMSO, EtOH) were defined as 1. All changes in the pixel intensities/area are expressed relative to the control condition. For example, an increase to 1.6-fold indicates that the pixel intensity/area is 1.6 times the value observed in control cells.

2.5. Detection of polyA$^+$ RNA

PolyA$^+$ RNA was localized by hybridization with Cy3-labeled oligo dT(50) (Gene Link). Control and stressed cells were washed with PBS and fixed with 3.7% formaldehyde in PBS (15 min, room temperature), permeabilized in 0.3% Triton-X 100/PBS (10 min, room temperature) and washed in PBS. Following 15 min incuba-

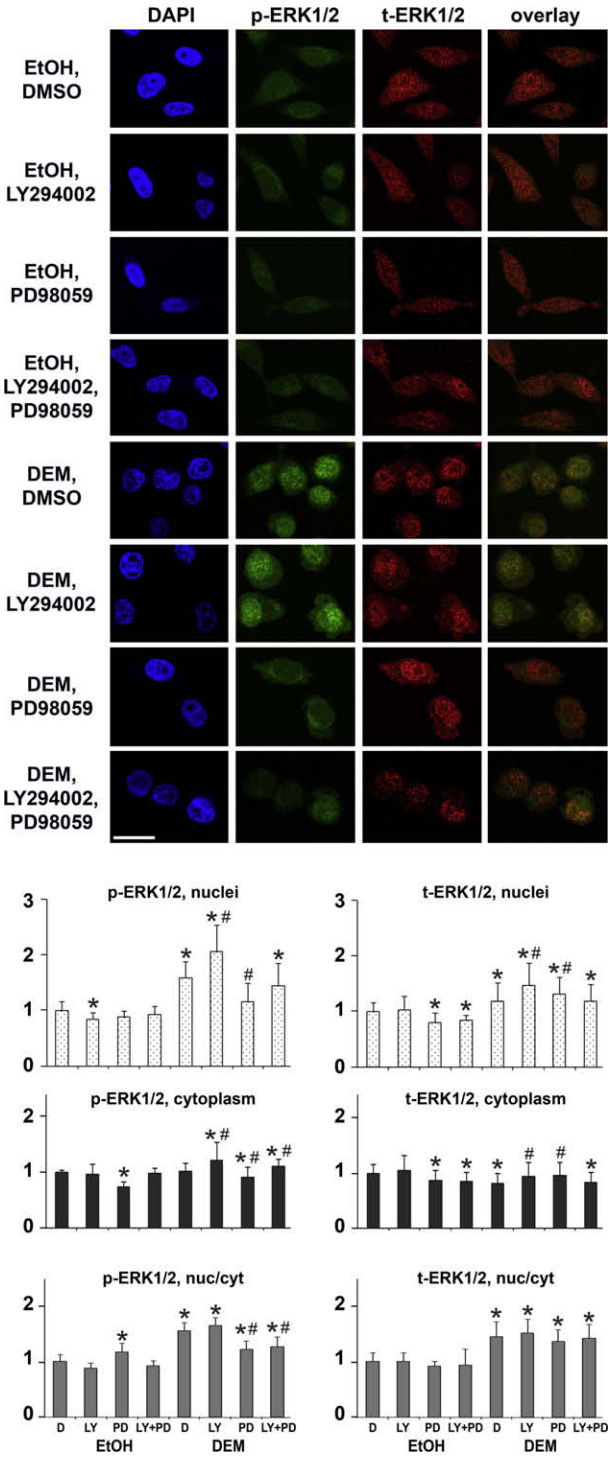

Fig. 1. Oxidative stress, PI3 kinase and MEK → ERK signaling alter the localization of activated ERK1/2. The localization of p-ERK1/2 and t-ERK1/2 was monitored by indirect immunofluorescence followed by confocal microscopy under the different conditions shown in the figure. Pixel intensities in nuclear and cytoplasmic compartments were quantified for dually phosphorylated and total ERK1/2. Nuclear and cytoplasmic fluorescence was quantified using the multiwavelength cell scoring module; for each condition the distribution of total and activated kinases was measured for at least 50 cells. The graphs depict pixel intensities/area. One-way ANOVA was used for multiple comparisons between all groups, with EtOH/DMSO treated cells as reference; * indicates $P < 0.05$. For comparisons of stressed cells, DEM/DMSO treatment served as reference and # denotes $P < 0.05$. Size bar is 20 μm.

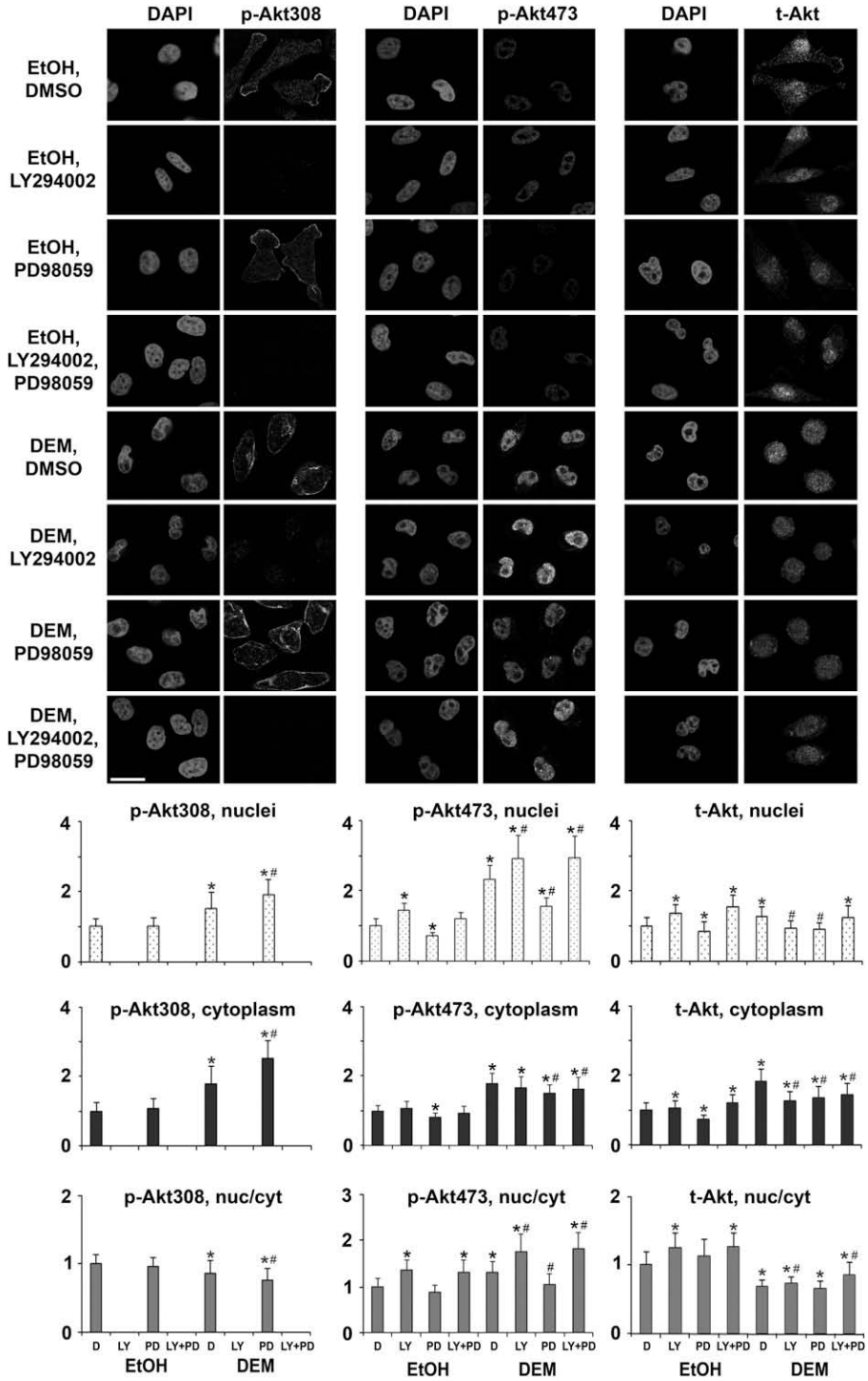

Fig. 2. The localization of Akt is regulated by oxidative stress as well as signaling through PI3 kinase and MEK → ERK. The levels of nuclear and cytoplasmic p-Akt308, p-Akt473 and t-Akt were quantified under different non-stress and stress conditions. The acquisition of confocal images, quantification of fluorescence intensities in the nuclear and cytoplasmic compartments was carried out as described for Fig. 1. Size bar is 20 μm.

tion in pre-hybridization buffer at 37 °C (2× SSC, 20% formamide, 2 mg/ml BSA, 1 mg/ml yeast tRNA), samples were hybridized overnight at 37 °C in pre-hybridization buffer containing 10% dextran sulfate and 1 nmol/ml Cy3-oligo-dT(50). Samples were washed in 2× SSC, 20% formamide (5 min, 42 °C), 2× SSC (5 min, 42 °C), 1× SSC (5 min, room temperature), PBS (5 min, room temperature), stained with DAPI and mounted in Vectashield.

2.6. Statistical analyses

Data were analyzed by one-way ANOVA to determine differences among groups. Multiple comparisons were carried out with control cells (EtOH, DMSO) as reference; * in Figs. 1–3 denotes $P < 0.05$. For multiple comparisons among stressed samples, cells incubated with DEM and DMSO served as reference; for these comparisons # indicates $P < 0.05$.

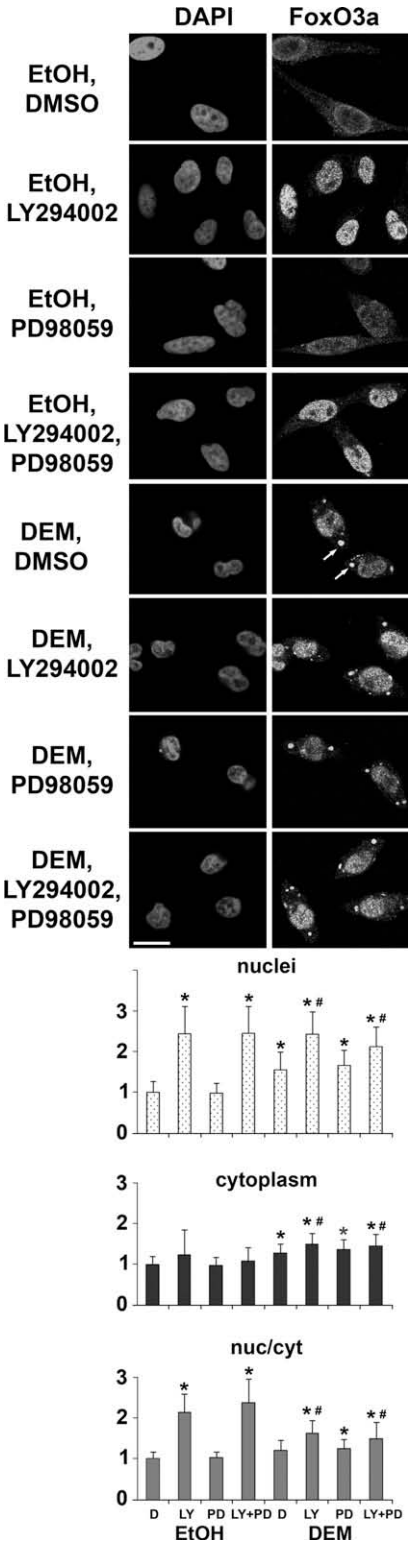

Fig. 3. The intracellular localization of transcription factor FoxO3a is controlled by stress and signaling through PI3 kinase and MEK → ERK1/2 pathways. HeLa cells were treated as in Fig. 1 and images were acquired by high-throughput screening technology [3,5]. Nuclear and cytoplasmic fluorescence was quantified using the MetaXpress multi wavelength cell scoring module; for each condition FoxO3a distribution was measured for at least 50 cells. Examples of SGs are marked with arrows; size bar is 20 μm. Note that in stressed cells nuclear FoxO3a levels are significantly different for treatment with LY294002 (DEM/LY) as compared to the incubation with both LY294002 and PD98059 (DEM/LY + PD).

3. Results

3.1. Oxidative stress alters the intracellular distribution of ERK1/2 and phosphorylated Akt

Cell fractionation is frequently used to determine the association of proteins with different organelles, a method that is tedious and prone to errors, in particular for proteins that bind to large cellular structures such as the filament systems. Moreover, procedures required to obtain pure fractions may lead to artificial phosphorylation or dephosphorylation of the protein of interest. Importantly, cell fractionation can not provide information on whether a component present in nuclear fractions is inside the nucleus, bound to the nuclear envelope or associated with the cytoplasmic side of the nuclear membranes. However, this knowledge is important to determine whether a kinase can access its substrates inside the nucleus. This is of particular interest to the analysis of ERK1/2 and Akt, since these kinases have numerous targets, in both the nuclear and cytoplasmic compartments.

To examine the spatial distribution of ERK1/2 and Akt kinases and detect subtle changes in their localization, we used recently developed protocols for the quantitative analysis of protein localization [5]. These procedures combine indirect immunofluorescence, confocal imaging and computer-based image-analysis to measure the *intra*nuclear and cytoplasmic levels of a particular protein [3–5].

With the immunofluorescence methods described above, the amounts of p-ERK1/2, t-ERK1/2, p-Akt308, p-Akt473 and t-Akt were quantified inside the nucleus and in the cytoplasm. Figs. 1 and 2 show the results for these experiments; the quantification is depicted as pixel intensities/area. Results were normalized to non-stress control conditions, which were defined as 1. All the numbers below depict the changes relative to the unstressed control. [For example, a 1.6-fold change in the nucleus denotes that the concentration in the nucleus was 1.6 times the amount detected in control nuclei; 1.0-fold means that there was no change relative to the control, and 0.8-fold indicates that the level decreased to 0.8 of the amount in control cells.]

In response to DEM treatment without kinase inhibitors (Figs. 1 and 2), the levels in nuclei increased significantly for p-ERK1/2 (to 1.6-fold, compare samples labeled D/EtOH with D/DEM), p-Akt308 (to 1.5-fold) and p-Akt473 (to 2.3-fold). In the cytoplasm, oxidative stress elevated the concentration of p-Akt308 (to 1.8-fold), p-Akt473 (to 1.8-fold) and t-Akt (to 1.8-fold), but not of p-ERK1/2 (1.0-fold) or t-ERK1/2 (to 0.8-fold).

We next tested whether the rise in nuclear p-ERK1/2 and p-Akt can be attributed to changes in the t-ERK1/2 and t-Akt distribution. Indeed, stress increased the levels of t-Erk1/2 (to 1.2-fold) and t-Akt (to 1.3-fold) in nuclei (Figs. 1 and 2). (Note that due to the different volumes of the nuclear and cytoplasmic compartments an increase in nuclear t-Akt will not lead to the same decrease in cytoplasmic levels of the kinase.) These results are consistent with the interpretation that a portion of ERK1/2 and Akt that was activated in the cytoplasm moves to the nucleus following oxidant exposure. Alternatively, ERK1/2 and Akt may first relocate to the nucleus to become subsequently phosphorylated.

Since the relative abundance of activated kinases in the nucleus and cytoplasm is likely to impact the endpoint of signaling, we determined whether their nuclear/cytoplasmic ratio changed in response to oxidant exposure (Figs. 1 and 2; bottom panels, nuc/cyt). This analysis revealed a significant rise in the nuclear/cytoplasmic ratio for p-ERK1/2 (to 1.6-fold), t-ERK1/2 (to 1.45-fold) and p-Akt473 (to 1.3-fold), whereas a reduction was observed for p-Akt308 (to 0.9-fold) and t-Akt (to 0.7-fold).

3.2. Inhibition of PI3 kinase and MEK activation regulates the distribution of kinases in stressed cells

Given that both PI3 kinase and MEK → ERK signaling cascades were activated by the oxidant DEM, we next tested whether pharmacological inhibition of PI3 kinase and MEK activation affected the intracellular distribution of ERK1/2 and Akt. The inhibitors LY294002 and PD98059, which target PI3 kinase or MEK1/2 and MEK5, respectively, were used as pharmacological tools to measure potential changes in the levels of kinases in the nuclear and cytoplasmic compartments.

Under non-stress conditions, p-Akt308 associates with the plasma membrane where it interacts with cortical F-actin [26, and references therein]. Likewise, in our studies p-Akt308 at the cell periphery partially co-localized with filamentous actin, as evident by staining with fluorescently labeled phalloidin (Supplementary Fig. 1). This partial co-localization was also observed when MEK signaling was inhibited with PD98059.

In stressed cells, LY294002 elevated the levels of p-ERK1/2 (to 2.1-fold), t-ERK1/2 (to 1.5-fold) and p-Akt473 (to 2.9-fold) in nuclei of stressed cells, but had a lesser effect on the cytoplasmic kinases (Figs. 1 and 2, LY/DEM).

A different scenario was observed for the MEK inhibitor PD98059, which increased p-Akt308 in nuclei (from 1.5-fold upon DEM treatment to 1.9-fold in DEM/ PD98059 incubated cells) and cytoplasm (from 1.8-fold to 2.6-fold). Interestingly, PD98059 had the opposite effect on p-Akt473, which decreased in the nuclear compartment of stressed cells (from 2.3-fold to 1.6-fold), whereas t-ERK1/2 changed from 1.2-fold to 1.3-fold and t-Akt from 1.3-fold to 0.9-fold. As expected, PD98059 reduced the levels of p-ERK1/2 in nuclei of stressed cells. When LY294002 was combined with PD98059, the effect of MEK inhibition on nuclear p-ERK1/2 and p-Akt473 was at least partially overcome by preventing PI3 kinase activation.

Taken together, our data suggest that PI3 kinase and MEK-dependent signaling control the distribution of p-ERK1/2, p-Akt308 and p-Akt473 under stress conditions (Table 1). Results obtained for the combination of PI3 kinase and MEK inhibitors further substantiate our hypothesis and support the model that these processes are controlled by the interplay between different signaling cascades. In particular, a direct correlation was observed for changes of p-ERK1/2 and p-Akt473 in the nucleus of stressed cells.

3.3. Effect of Akt and MEK-dependent signaling on the distribution of FoxO3a

To determine the consequences of stress as well as MEK and PI3 kinase signaling we have chosen FoxO3a, which is an authentic target of both signaling pathways. Members of the forkhead family of transcription factors (FoxO), such as FoxO3a, are key players in the regulation of gene expression under various physiological conditions [27,28]. Crucial to the control of FoxO-dependent transcription is the proper subcellular localization of FoxO proteins, which we analyzed here in a quantitative and systematic fashion. Fig. 3 shows FoxO3a distribution in control and stressed cells as well as the outcome of pharmacological kinase inhibition. In unstressed cells, the PI3 kinase inhibitor LY294002 increased the amount of FoxO3a in nuclei to 2.4-fold, whereas the MEK inhibitor PD98059 had no effect. Oxidative stress raised FoxO3a levels in nuclei to 1.5-fold; this was further augmented by PI3 kinase inhibition which increased nuclear levels to 2.4-fold. Collectively, our data suggest that activated Akt, known to promote FoxO3a nuclear export, is the limiting factor for nuclear accumulation of FoxO3a under stress conditions.

Data described above demonstrated cross-talk between MEK and PI3 kinase signaling which regulated the activation and localization of Akt and ERK1/2. Importantly, this interplay also affected the nuclear accumulation of FoxO3a, but was limited to oxidant-treated cells. The profile of DEM-induced changes in nuclear FoxO3a levels with or without kinase inhibitors was similar to those observed for p-Akt473 and p-ERK1/2. Moreover, simultaneous inhibition of PI3 and MEK kinases led to a statistically significant reduction of FoxO3a levels in nuclei when compared to PI3 kinase inhibition only ($P < 0.05$; multiple comparisons among DEM-treated cells with DEM/LY294002 as reference). Taken together, this suggests that PI3 kinase is the most important factor determining FoxO3a localization under normal and stress conditions, whereas signaling through MEK is not a limiting factor under non-stress conditions. However, in stressed cells and in the absence of PI3 kinase activation, MEK signaling contributes to FoxO3a distribution as well.

Surprisingly, DEM treatment not only changed the nuclear concentration of FoxO3a, but also altered its distribution in the cytoplasm, where FoxO3a became associated with granules (Fig. 3; arrows). Many forms of stress cause the formation of cytoplasmic stress granules (SGs), compartments that contain mRNA, RNA-binding and small ribosomal subunit proteins [29]. Indeed, following DEM incubation FoxO3a co-localized with HuR, G3BP1 and ribosomal protein S6 in cytoplasmic SGs, which were also enriched for polyA$^+$ RNA (Supplementary Fig. 2), suggesting a possible role for FoxO3a in the cytoplasm. In this scenario, the proper balance between nuclear and cytoplasmic levels would be important for FoxO3a functioning in both compartments, and we calculated the nuclear/cytoplasmic ratios for all experimental conditions (Fig. 3; bottom panels; nuc/cyt). The ratio was somewhat increased by stress (to 1.2-fold), but the most pronounced change was seen in unstressed cells following the inhibition of PI3 kinase (to 2.1-fold) or of both PI3 kinase and MEK (to 2.3-fold).

Collectively, our results demonstrate that PI3 kinase signaling is the most important component that determines FoxO3a localization. Nevertheless, upon oxidative stress, but not in unstressed cells, the nucleocytoplasmic FoxO3a distribution is also regulated by an interdependent network of PI3 kinase and MEK signaling. Moreover, our data show, for the first time, that oxidant treatment triggers the association of FoxO3a with cytoplasmic stress granules.

Table 1
Effect of oxidative stress on the nuclear and cytoplasmic levels of ERK1/2, Akt and FoxO3a. Results for the quantification of fluorescence intensities in nuclear (Nuc) and cytoplasmic (Cyt) compartments of stressed cells are summarized. The distribution of proteins in DEM-treated cells is compared to unstressed controls. The kinase concentrations in the nuclear and cytoplasmic compartments of untreated cells are defined as 1; all changes are expressed relative to the levels in unstressed controls. +++, increase to 2.1–2.9-fold; ++, increase to 1.5–2.0-fold; +, increase to 1.2–1.4-fold; +/−, 0.8–1.1-fold change in kinase levels. Note that the profile of changes in nuclei is similar for p-ERK1/2, pAkt-473 and FoxO3a.

Kinase	DMSO		LY294002		PD98059		LY294002 + PD98059	
	Nuc	Cyt	Nuc	Cyt	Nuc	Cyt	Nuc	Cyt
p-ERK1/2	++	+/−	+++	+	+	+/−	++	+/−
t-ERK1/2	+	+/−	++	+/−	+	+/−	+	+/−
p-Akt308	++	++	NA	NA	++	+++	NA	NA
p-Akt473	+++	++	+++	++	++	++	+++	++
t-Akt	+	++	+/−	+	+/−	+	+	++
FoxO3a	++	+	+++	++	++	+	+++	++

4. Discussion

With the experiments described here we advanced the understanding of the complex regulatory mechanisms that underlie the localized action of signaling events. To our knowledge, this is the first study that applies newly developed methods in confocal microscopy combined with computer-based image-analysis to provide a quantitative investigation of the activation and localiza-

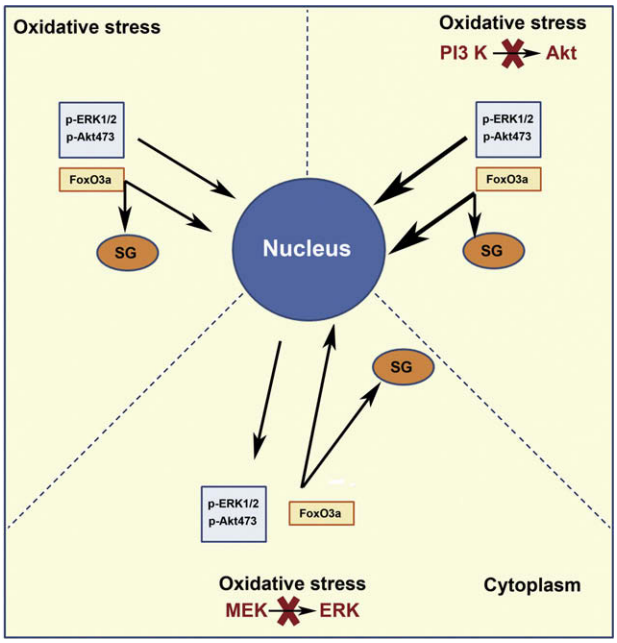

Fig. 4. Simplified model for stress-induced changes in the distribution of p-ERK1/2, p-Akt473 and FoxO3a. Arrows indicate changes in the nuclear levels of p-ERK1/2, p-Akt473 and FoxO3a. Protein kinase inhibition reveals that in stressed cells cross-talk between PI3 kinase and MEK pathways controls the nucleocytoplasmic distribution of p-ERK1/2 and p-Akt473. Moreover, FoxO3a association with different cellular compartments depends on oxidant exposure and kinase activation. Overall, the model proposes that compartmental changes in p-ERK1/2 and p-Akt473 kinase levels, together with cross-talk between both signaling modules, may modulate the nucleocytoplasmic distribution of numerous target molecules, including FoxO3a.

tion of Akt and ERK1/2 kinases under normal and oxidative stress conditions. Our research tested the hypothesis that oxidative stress alters the subcellular distribution of these kinases, possibly generating specific pools of signal transducers that may determine the end-point result of signaling events. Furthermore, we demonstrate that PI3 kinase activation affects MEK-dependent processes and vice versa, in line with the idea that interplay between both pathways participates in the control of signaling in response to oxidant exposure. At the molecular level, several mechanisms will contribute to the steady-state distribution of Akt, ERK1/2 and their target FoxO3a. This includes the modification by upstream kinases or phosphatases, trafficking in and out of the nucleus as well as retention in the nuclear or cytoplasmic compartment. The simplified model shown in Fig. 4 depicts the stress-induced changes for p-ERK1/2, p-Akt473 and the transcription factor FoxO3a, showing that these changes were distinct in the nuclear and cytoplasmic compartments. In particular, in stressed cells a striking correlation was detected between *nuclear* p-ERK1/2 and p-Akt473 levels, indicating that signaling in the nucleus through both pathways is linked. These results suggest that in oxidant-treated cells PI3 kinase and MEK → ERK1/2 signaling are interdependent events. Thus, inhibition of PI3 kinase signaling not only promotes ERK1/2 activation; it also leads to phosphorylation of Akt on Ser473.

It should be noted that in stressed cells treatment with LY294002 was able to override completely the effect of PD98059 for nuclear p-Akt473, but only partially for nuclear p-ERK1/2. The reasons for this difference are not understood, but as a consequence the nuc/cyt ratio was lower for p-ERK1/2 than for p-Akt473. Different not mutually exclusive scenarios may explain these results. For instance, MEK activity in cells treated with both inhibitors may be sufficient to generate p-Akt473 to an extent similar to LY294002-treated cells. Alternatively, other factors that determine the amount of p-Akt473 and p-ERK1/2 in nuclei may respond differently to the simultaneous addition of LY294002 and PD98059. Possible candidates are one or more of the phosphatases that regulate the levels of p-Akt473 or p-ERK1/2 [30–32].

Interestingly, in our studies PI3 kinase inhibition had distinct effects on Thr308 and Ser473 modification of Akt, which may be explained by the complex regulation of Akt phosphorylation. Whereas PDK1, a downstream target of PI3 kinase, phosphorylates Thr308, different pathways are implicated in the modification of Ser473, some of which are insensitive to inhibitors of PI3 kinase [8–15]. Based on the results described here we propose that PI3 kinase independent signaling plays a major role in modifying this Ser473 in our experimental settings, leading to an increase in Ser473 phosphorylation when Thr308 modification is abolished.

The cross-talk identified by us is likely to have intricate consequences for signal transduction. For instance, Ser473 phosphorylation of Akt is believed to stabilize the active conformation of the kinase [8], and p-Akt308 may differ in substrate specificity from Akt dually modified on Thr308 and Ser473 [8,9]. As such, Akt phosphorylated on both Thr308 and Ser473 seems to favor pro-survival signaling, in part by promoting FoxO phosphorylation in the nucleus [9]. In addition to the phosphorylation of Akt on Thr308 and Ser473, the appropriate nucleocytoplasmic distribution of the kinase will be crucial for downstream events. The proper localization will affect the phosphorylation not only of nuclear targets, but of cytoplasmic substrates as well. These cytoplasmic targets include, but are not limited to, components that modulate the organization and functions of the cytoplasmic compartment, such as actin and proteins involved in translational control.

The principles described for PI3 kinase inhibition also apply to signaling through MAPKs, and it is noteworthy that MEK inhibition altered the levels of p-Akt308 and p-Akt473 in stressed cells. Specifically, PD98059 increased the concentration of p-Akt308 in both nuclei and cytoplasm, whereas the amount of p-Akt473 in nuclei was reduced under stress and normal conditions. These observations indicate that MEK activities impinge differently on the phosphorylation of Akt residues 308 and 473, adding further complexity to the interplay between PI3 and MEK1/2 and MEK5 signaling pathways, consistent with reports that suggested cross-talk between Raf and Akt signaling [22]. However, data presented here go beyond previous studies as they provide a quantitative analysis of this interplay between Akt and ERK1/2 signaling events by measuring the compartment-specific changes in kinase distribution. This enabled us to identify a new link in the nucleus between p-ERK1/2 and p-Akt473. Recent studies by others demonstrate the importance of Akt signaling in the cytoplasm to achieve a specific physiological response [16]. Our data now provide evidence for specific signaling events and interplay between signaling cascades that are located in the nuclear compartment and are likely to impact numerous nuclear processes.

In conclusion, on the basis of the results described here, we propose that upon oxidative stress, signaling through PI3 kinase and MEK occurs in an interdependent fashion. The balance between both pathways will be critical to define the endpoint of the cellular response and ultimately the survival under oxidative stress conditions.

Acknowledgments

This research was supported by grants from CIHR, NSERC and HSFQ to US. MK is a recipient of a fellowship from the Heart and Stroke Foundation of Canada and PB is supported by a fellowship from FRSQ/Heart and Stroke Foundation of Canada.

Appendix A. Supplementary data

Supplementary data associated with this article can be found, in the online version, at doi:10.1016/j.febslet.2009.05.011.

References

[1] Chambard, J., Lefloch, R., Pouysségur, J. and Lenormand, P. (2007) ERK implication in cell cycle regulation. Biochim. Biophys. Acta 1773, 1299–1310.
[2] Lawrence, M.C., Jivan, A., Shao, C., Duan, L., Goad, S., Zaganjor, E., Osborne, J., McGlynn, K., Stippec, S., Earnest, S., Chen, W. and Cobb, M.D. (2008) The roles of MAPKs in disease. Cell Res. 18, 436–442.
[3] Kodiha, M., Rassi, J.G., Brown, C.M. and Stochaj, U. (2007) Localization of AMP kinase is regulated by stress, cell density, and signaling through the MEK → ERK1/2 pathway. Am. J. Physiol. Cell Physiol. 293, 1427–1436.
[4] Kodiha, M., Bański, P., Ho-Wo-Cheong, D. and Stochaj, U. (2008) Dissection of the molecular mechanisms that control the nuclear accumulation of transport factors importin-α and CAS in stressed cells. Cell Mol. Life Sci. 65, 1756–1767.
[5] Kodiha, M., Brown, C.M. and Stochaj, U. (2008) Analysis of signaling events by combining high throughput screening technology with computer based image analysis. Sci. Signal. 1, 12.
[6] Turjanski, A.G., Vaqué, J.P. and Gutkind, J.S. (2007) MAP kinases and the control of nuclear events. Oncogene 26, 3240–3253.
[7] Franke, T.F. (2007) Intracellular signaling by Akt: bound to be specific. Sci. Signal. 1, 29.
[8] Franke, T.F. (2008) PI3K/Akt: getting it right matters. Oncogene 27, 6473–6488.
[9] Sale, E.M. and Sale, G.J. (2008) Protein kinase B: signalling roles and therapeutic targeting. Cell Mol. Life Sci. 65, 113–127.
[10] Konishi, H., Matsuzaki, H., Tanaka, M., Ono, Y., Tokunaga, C., Kuroda, S. and Kikkawa, U. (1996) Activation of RAC-protein kinase by heat shock and hyperosmolarity stress through a pathway independent of phosphatidylinositol 3-kinase. Proc. Natl. Acad. Sci. USA 93, 7639–7643.
[11] Sable, C.L., Filippa, N., Hemmings, B. and Van Obbergen, O.E. (1997) cAMP stimulates protein kinase B in a wortmannin-insensitive manner. FEBS Lett. 409, 253–257.
[12] Mao, K., Kobayashi, S., Jaffer, Z.M., Huang, Y., Volden, P., Chernoff, J. and Liang, Q. (2008) Regulation of Akt/PKB activity by p21-activated kinase in cardiomyocytes. J. Mol. Cell Cardiol. 44, 429–434.
[13] Feng, J., Park, J., Cron, P., Hess, D. and Hemmings, B.A. (2004) Identification of a PKB/Akt hydrophobic motif Ser-473 kinase as DNA-dependent protein kinase. J. Biol. Chem. 279, 41189–41196.
[14] Dong, L.Q. and Liu, F. (2005) PDK2: the missing piece in the receptor tyrosine kinase signaling pathway puzzle. Am. J. Physiol. Endocrinol. Metab. 289, E187–E196.
[15] Kawakami, Y., Nishimoto, H., Kitaura, J., Maeda-Yamamoto, M., Kato, R.M., Littman, D.R., Leitges, M., Rawlings, D.J. and Kawakami, T. (2005) Protein kinase C βII regulates Akt phosphorylation on Ser-473 in a cell type- and stimulus-specific fashion. J. Biol. Chem. 279, 47720–47725.
[16] Vereshchagina, N., Ramel, M., Bitoun, E. and Wilson, C. (2008) The protein phosphatases PP2A-B' subunit Widerborst is a negative regulator of cytoplasmic activated Akt and lipid metabolism in Drosophila. J. Cell Sci. 121, 3383–3392.
[17] Miyamoto, S., Rubio, M. and Sussman, M.A. (2009) Nuclear and mitochondrial signalling Akts in cardiomyocytes. Cardiovasc. Res. doi:10.1093/cvr/cvp087.
[18] Meier, F., Schittek, B., Busch, S., Garbe, C., Smalley, K., Satyamoorthy, K., Li, G. and Herlyn, M. (2005) The Ras/Raf/MEK/ERK and PI3K signaling pathways present molecular targets for the effective treatment of advanced melanoma. Frontiers Biosci. 10, 2986–3001.
[19] Henson, E.S. and Gibson, S.B. (2006) Surviving cell death through epidermal growth factor (EGF) signal transduction pathways: implications for cancer therapy. Cell Signal. 18, 2089–2097.
[20] Rozengurt, E. (2007) Mitogenic signaling pathways induced by G protein-coupled receptors. Cell Physiol. 213, 589–602.
[21] Fischer, P. and Hilfiker-Kleiner, D. (2007) Survival pathways in hypertrophy and heart failure: the gp130-STAT3 axis. Basic Res. Cardiol. 102, 393–411.
[22] Zimmermann, S. and Moelling, K. (1999) Phosphorylation and regulation of Raf by Akt (protein kinase B). Science 286, 1741–1744.
[23] Lawlor, M.A. and Alessi, D.R. (2001) PKB/Akt: a key mediator of cell proliferation, survival and insulin responses? J. Cell Sci. 114, 2903–2910.
[24] Avogaro, A., Kreutzenberg, S. and Fadini, G. (2008) Oxidative stress and vascular disease in diabetes: Is the dichotomization of insulin signaling still valid? Free Rad. Biol. Med. 44, 1209–1215.
[25] Forbes, J.M., Coughlan, M.T. and Cooper, M.E. (2008) Oxidative stress as a major culprit in kidney disease in diabetes. Diabetes 57, 1446–1454.
[26] Vandermoere, F., Yazidi-Belkoura, I.E., Demont, Y., Slomianny, C., Antol, J., Lemoine, J. and Hondermarck, H. (2007) Proteomics exploration reveals that actin is a signaling target of the kinase Akt. Mol. Cell Proteom. 6, 114–124.
[27] Huang, H. and Tindall, D.J. (2007) Dynamic FoxO transcription factors. J. Cell Sci. 120, 2479–2487.
[28] Calnan, D.R. and Brunet, A. (2008) The FoxO code. Oncogene 27, 2276–2288.
[29] Anderson, P. and Kedersha, N. (2008) Stress granules: the Tao of RNA triage. Trends Biol. Sci. 33, 141–150.
[30] Brognard, J., Sierecki, E., Gao, T. and Newton, A.C. (2007) PHLPP and a second isoform, PHLPP2, differentially attenuate the amplitude of Akt signaling by regulating distinct Akt isoforms. Mol. Cell 25, 917–931.
[31] Yoon, S. and Seger, R. (2006) The extracellular signal-regulated kinase: multiple substrates regulate diverse cellular functions. Growth Factors 24, 21–44.
[32] Owens, D.M. and Keyse, S.M. (2007) Differential regulation of MAP kinase signaling by dual-specificity protein phosphatases. Oncogene 26, 3203–3213.

Cell. Mol. Life Sci. 65 (2008) 1756 – 1767
1420-682X/08/111756-12
DOI 10.1007/s00018-008-7588-2

Cellular and Molecular Life Sciences

Research Article

Dissection of the molecular mechanisms that control the nuclear accumulation of transport factors importin-α and CAS in stressed cells

M. Kodiha, P. Bański, D. Ho-Wo-Cheong and U. Stochaj*

Department of Physiology, McGill University, 3655 Promenade Sir William Osler, Montreal, PQ, H3G 1Y6 (Canada), Fax: +1 514 398 7452, e-mail: ursula.stochaj@mcgill.ca

Received 26 December 2007; received after revision 6 March 2008; accepted 31 March 2008
Online First 21 April 2008

Abstract. The physiological state of eukaryotic cells controls nuclear trafficking of numerous cargos. For example, stress results in the inhibition of classical protein import, which is characterized by the redistribution of several transport factors. As such, importin-α and cellular apoptosis susceptibility protein (CAS) accumulate in nuclei of heat-shocked cells; however, the mechanisms underlying this relocation are not fully understood. We now show that heat upregulates the initial docking of importin-α at the nuclear envelope and stimulates the translocation of CAS into the nuclear interior. Moreover, heat exposure compromises the exit of importin-α from nuclei and drastically increases its retention in the nucleoplasm, whereas CAS nuclear exit and retention are less affected. Taken together, our results support the idea that heat shock regulates importin-α and CAS nuclear accumulation at several levels. The combination of different stress-induced changes leads to the nuclear concentration of both transport factors in heat-stressed cells.

Keywords. Stress, heat shock, nucleus, transport.

In eukaryotic cells, transport of proteins and RNA in and out of the nucleus is mediated by nuclear pore complexes (NPCs), located at the junctions of inner and outer nuclear membranes. In addition to nucleoporins, many of these transport processes require soluble factors [1]. Nucleocytoplasmic trafficking of macromolecules is essential to maintain cellular homeostasis and is therefore subject to multifactorial regulation. This regulation may take place at the level of individual cargos or the transport apparatus by affecting either NPCs or soluble transport factors. For example, altered NPC function may modulate the passage of all macromolecules across the nuclear envelope (NE) [2, 3], and changing the activity or abundance of nuclear carriers can control transport of multiple cargos [4–6].

Classical nuclear import is mediated by a carrier system that moves numerous proteins into the nucleus, as the dimeric receptor importin-α/importin-β1 translocates proteins with classical nuclear localization signals (NLSs) across the NPC. Upon completion of the import reaction, both subunits of the classical import receptor return to the cytoplasm. Export of importin-α to the cytoplasm depends on cellular apoptosis susceptibility protein (CAS), a carrier of the importin-β family, and RanGTP [7, 8]. In addition to its crucial function as a nuclear exporter, CAS

* Corresponding author.

participates in mitotic spindle checkpoint control, contributes to proper development and was recently identified as a regulator of p53-dependent transcription [5, 9, 10]. Like CAS, importin-α has multiple functions that are not limited to nuclear transport [11, 12]. Importin-α traverses the NE while bound to importin-β1 or CAS; however, it also translocates into the nucleus in the absence of other factors, a pathway that is poorly defined [13].

Multiple physiological and pathophysiological states control the movement of macromolecules in and out of the nucleus [14, 15]. These include the age-dependent loss of nuclear transport efficiency in human fibroblasts which correlates with reduced levels of importin-α, CAS and RanBP1 [6]. Stress in particular regulates the movement of numerous classical and non-classical cargos. Different stressors exert a general control on nuclear trafficking by affecting several components of the transport machinery. As such, we and others have shown that the steady-state concentration of importin-α and CAS increases in nuclei of stressed cells [16, 17]. At present, the mechanisms that contribute to this relocation are not fully understood. A combination of several dynamic processes determines the steady-state distribution of macromolecules that shuttle between the nucleus and the cytoplasm. These include nuclear import, export and retention within the nuclear or cytoplasmic compartment. Each of these processes can make different contributions to the steady-state localization of a protein, and their input may adapt to changes in cell physiology. *In vitro* assays are particularly useful to dissect nuclear trafficking and evaluate the role of individual trafficking steps [18]. Here, we show that heat shock stimulates the nuclear accumulation of importin-α and CAS in a cell-free system, and we define several mechanisms that concentrate importin-α and CAS in nuclei *in vitro* and in growing cells. Our studies identify multiple heat-sensitive steps that contribute differently to the stress-induced nuclear accumulation of importin-α and CAS.

Materials and methods

Growth of HeLa cells and heat shock. HeLa cells were grown on multiwell chambers or cover slips following published procedures [19]. For heat treatment, cells at 50–70% confluence were incubated for 30 min at 45.5 °C. All of the results were obtained multiple times, with at least three independent experiments for each data point.

Immunofluorescent staining. All steps were carried out at room temperature, essentially as described elsewhere [20]. Antibodies against Ran (1:200), importin-α (1:200), CAS (1:100), all from Santa Cruz Biotechnology (Santa Cruz, CA), were diluted as indicated. Three different treatments were used for staining nuclear, cytoplasmic proteins or both (summarized in Fig. 1). For treatment 1, cells were fixed first and all membranes permeabilized with Triton X-100. This protocol monitors the protein distribution in all cellular compartments. Treatment 2 locates transport factors in the cytoplasm, including the cytoplasmic side of the nuclear envelope. To this end, cells were first fixed and then treated with digitonin to permeabilize the plasma membrane; all subsequent steps were carried out without detergent to prevent access of antibodies to the nuclear interior. The NE remains intact under these conditions (see Fig. 2A). Treatment 3 visualizes nuclear proteins and cytoplasmic proteins that were not solubilized by digitonin extraction. For this treatment, unfixed cells were incubated with digitonin. Following digitonin extraction, samples were fixed and nuclear membranes were permeabilized with Triton X-100. For treatment 1 and 3, after Triton X-100 permeabilization, samples were blocked in PBS/2 mg/ml BSA/0.05% Tween 20 (PBS/BSA/Tween) for 1 h, followed by overnight incubation with primary antibodies, diluted in PBS/BSA/Tween. Samples were washed three times in PBS/BSA/Tween and primary antibodies were detected with Cy3-conjugated secondary antibodies (1:500, 2 h; Jackson ImmunoResearch, West Grove, PA). After three washes with PBS/BSA/Tween, DNA was visualized with 4',6-diamidino-2-phenylindole (DAPI) and samples were mounted in Vectashield (Vector Laboratories, Burlingame, CA). For treatment 2, there was no permeabilization with Triton X-100, and Tween 20 was omitted from all steps of the procedure. Mounted samples were analyzed with a Nikon Optiphot at ×400 magnification and photographed with Kodak T-MAX 400 films or with a Zeiss LSM 510 (×63 objective, 1.4 NA). Images were processed with Photoshop 5.5 and 8.0.

Western blot analysis. Western blotting and ECL followed standard procedures [21]. In brief, HeLa cells were grown on dishes to 50–70% confluency. Control and heat-stressed cells were washed with PBS and stored at −70 °C until use. Crude extracts were prepared by solubilizing proteins in gel sample buffer, pH 8.0, containing protease inhibitors (aprotinin, leupeptin, pepstatin, each at 1 μg/ml, 1 mM PMSF), 20 mM β-glycerophosphate, 1 mM NaN_3, 2.5 mM NaF. Samples were incubated for 10 min at 95 °C and vortexed with glass beads to shear DNA. After centrifugation (5 min, 13 000 rpm, microfuge), aliquots were separated on the same gel. Protein was

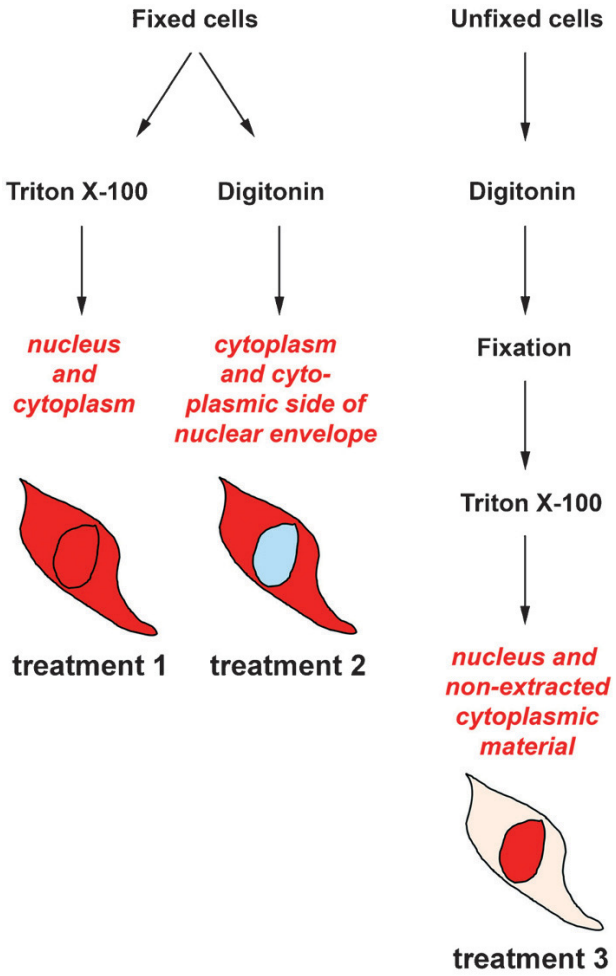

Figure 1. Processing of growing cells to detect proteins in nuclear and cytoplasmic compartments. The different treatments used to localize transport factors in the nucleus and cytoplasm are summarized. Material preferentially stained upon each treatment is shown in red. Treatment 1 localizes proteins in both nuclei and the cytoplasm. Treatment 2 stains material in the cytoplasm, including the cytoplasmic side of the nuclear envelope. Treatment 3 will detect antigens in the nucleus and cytoplasmic material that is resistant to digitonin extraction. See text for details.

stained with Coomassie and quantified by densitometry using Spot density tools software as recommended by Alpha Innotech Corporation (San Leandro, CA). For Western blotting, equal amounts of protein as determined by densitometry were separated by SDS-PAGE, transferred to nitrocellulose and incubated overnight with primary antibodies at 4 °C. Antibodies were used at the following dilutions: importin-α1 (1:500, sc-6917; Santa Cruz Biotechnology), importin-β1 (1:400, sc-11367), CAS (1:200, sc-1708), Ran (1:500, sc-1156), tubulin (1:2,000, sc-5286) and actin (1:1,000; Chemicon, Temecula, CA). Washed filters were incubated with HRP-conjugated secondary antibodies, washed and processed for ECL (GE Healthcare).

Classical nuclear import. Generation of the classical nuclear import substrate SV40-HSA, labeling and *in vitro* nuclear import have been described previously [22]. HeLa cells grown to 50–70% confluency were exposed to 45.5 °C for 30 min. Control and heat-shocked cells were permeabilized with 40 μg/ml digitonin in buffer B (20 mM Hepes, pH 7.3, 110 mM potassium acetate, 5 mM sodium acetate, 2 mM magnesium acetate, 1 mM EGTA, 2 mM DTT) and 1 μg/ml of protease inhibitors [aprotinin, leupeptin and pepstatin or protease inhibitor cocktail (Roche, Basel, Switzerland)] followed by incubation with 50 μg/ml fluorescent substrate in buffer B containing 10 mg protein/ml of cytosol, 1 mM ATP, 5 mM creatine phosphate, and 20 U/ml creatine kinase. After 30 min incubation at 30 °C, cells were washed with buffer B and fixed for 10 min with 3.7% formaldehyde in PBS at room temperature. Slides were rinsed with PBS, incubated with 1 μg/ml DAPI and mounted.

Purification of proteins synthesized in *Escherichia coli* and fluorescent labeling. Tagged proteins were synthesized in *E. coli* and purified under native conditions following standard procedures. Purified importin-α and CAS were labeled with Oregon Green 488 iodoacetamide or tetramethylrhodamine-maleimide (TMR; Molecular Probes) as recommended by the supplier. Covalent modification of sulfhydryl groups has been used successfully to study *in vitro* nuclear trafficking of importin-α, CAS and other nuclear transport factors [17, 23, 24]. In brief, purified proteins were dialyzed against 25 mM sodium phosphate pH 7.1 and centrifuged for 3 min at 13 000 rpm (microfuge). Oregon Green 488 iodoacetamide or TMR was dissolved in N,N-dimethyl formamide and a fivefold molar excess was added to the protein. Upon overnight incubation on ice, non-incorporated dye was removed by gel exclusion chromatography and aliquots of the labeled import substrates were stored at −70 °C.

***In vitro* nuclear import of importin-α and CAS.** Import of TMR-labeled importin-α or CAS was analyzed in semi-intact HeLa cells at a final concentration of 400 nM in buffer B [17, 25]. Import assays containing 1 mM ATP, 5 mM creatine phosphate, and 20 U/ml creatine kinase were supplemented with 3 mg/ml cytosol prepared from control or heat-shocked HeLa cells (30 min, 45.5 °C). After 5 min at 30 °C, samples were fixed and stained with DAPI. Fluorescently labeled transport factors were localized by confocal laser microscopy and intranuclear fluorescence was quantified as described below; for each condition 54–59 cells were scored.

Docking of importin-α and CAS at nuclear envelopes. Docking at the NE was tested with fluorescent proteins; all steps were carried out on ice. HeLa cells were washed in cold buffer B and incubated with 40 μg/ml digitonin in buffer B for 5 min. Cells were washed once with buffer C (buffer B without DTT and protease inhibitors) and extracted for 10 min with buffer B containing 1 M NaCl and 3 mg/ml BSA. Samples were rinsed twice with buffer B/BSA and incubated with fluorescently labeled importin-α (80 μg/ml) or CAS (160 μg/ml) for 10 min. After rinsing twice with buffer B/BSA and once with PBS, samples were fixed for 10 min in 3.7 % formaldehyde in PBS and nuclei were stained with DAPI. Binding of fluorescent substrates was quantified for 43–65 cells with the Multiwavelength Translocation Module (see below).

Nuclear exit of importin-α and CAS *in vitro*. Unstressed or heat-shocked HeLa cells were semi-permeabilized by a 5-min treatment with digitonin in buffer B, followed by incubation at 37 °C with transport buffer supplemented with an energy-regenerating system, 1 mM GTP and 50 μg/ml RanQ69L, a Ran mutant that mimics RanGTP. Samples were fixed after 5, 10 and 15 min. Controls (0 min) were fixed immediately after digitonin extraction. Importin-α and CAS were detected by immunofluorescent staining, followed by quantification of the fluorescence intensities. For each condition between 48 and 75 cells were quantified.

Measurement of intranuclear and nuclear envelope fluorescence. Intranuclear and nuclear envelope fluorescence were obtained by optical sectioning with a Zeiss LSM 510 laser scanning confocal microscope, using a NA 1.4 × 63 objective [17]. Image analysis was performed with Metamorph or MetaXpress software by adaptation of the Translocation Enhanced or Multiwavelength Translocation modules. Nuclei were identified as 100–350 μm^2 area with a width of ~ 10 μm and an intensity of DAPI staining over local background of > 5 intensity units. The segmentation region defined by DAPI staining was then used to measure pixel intensities of the Oregon Green or tetramethylrhodamine images. All images were corrected for the contributions of background intensity using regions of the images that did not contain cells. Average pixel intensities for nuclear or nuclear envelope areas were calculated for individual cells. All segmentation data sets were inspected manually to ensure accuracy of the data, and cells with inaccurate segmentation were excluded from the analysis. For each experimental condition, pixel intensities were measured for 43–75 cells that showed accurate segmentation.

Statistics. To measure fluorescence signals in nuclei and cytoplasm or docking at the nuclear envelope, data for 43–75 cells that showed accurate segmentation were acquired for each of the different conditions. Results are shown as means ± SD; statistical analyses were carried out essentially as described elsewhere [21].

Nuclear retention of transport factors. Nuclear retention in *unfixed* cells was monitored by extraction with KM buffer (10 mM N-morpholinoethanesulfonic acid, pH 6.2, 10 mM NaCl, 1.5 mM $MgCl_2$, 10 % glycerol, protease inhibitors), buffer containing detergent (Nonidet P-40; NP40), DNase, NaCl, DNase + RNase essentially as described previously [26]. Samples were fixed after each step and processed for immunofluorescent staining and confocal microscopy. This extraction protocol has been developed for the preparation of nuclear matrices [26]. The bulk of cellular protein (~ 60 %) is solubilized by treatment with NP40 at low ionic strength, whereas components of the cytoskeleton and several nuclear compartments are resistant to this treatment [26]. Subsequent incubation with DNase releases about 4 % of the protein, without drastically affecting nucleoli or the cytoskeleton. High salt removes about 29 % of the protein, including a portion of the cytoskeleton and histones. After the final DNase/RNase step, samples contain the nuclear matrix, remnants of nucleoli and the lamina. This material, resistant to all of the extraction steps, is equivalent to ~ 10 % of the cellular protein [26].

Results

Heat stress leaves nuclear envelopes intact and inhibits classical nuclear import *in vitro*. Various stresses, including heat shock, interfere with nuclear transport in growing cells, and we examined whether this can be recapitulated in a cell-free system. To this end, HeLa cells were pre-incubated for 30 min at 45.5 °C and subsequently treated with digitonin to permeabilize the plasma membrane. The NE remained intact under these conditions, and lamin B was not accessible to antibodies. However, antibodies bound when nuclear membranes were permeabilized with Triton X-100 (Fig. 2A). The effect of heat on classical nuclear import *in vitro* was monitored with digitonin-permeabilized cells, which were supplied with TRITC-labeled SV40-HSA as import substrate, energy and unstressed cytosol [22]. SV40-HSA efficiently translocated into nuclei of unstressed cells, where it concentrated in nucleoli. By contrast, heat-shocked semi-intact cells failed to accumulate the classical

import cargo in nuclei (Fig. 2B), supporting the idea that upon heat shock, semi-intact cells reiterate faithfully classical import inhibition. In the experiments described below, this *in vitro* system was used to analyze trafficking of nuclear transport factors.

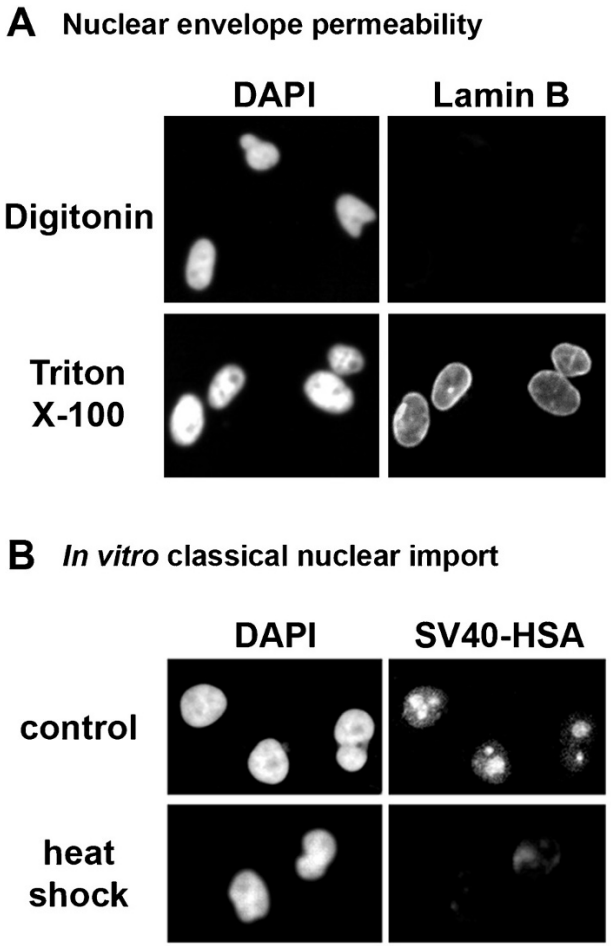

Figure 2. (*A*) NEs remain intact in heat-stressed cells. HeLa cells exposed to 30 min at 45.5 °C were treated with digitonin or Triton X-100 and incubated with antibodies against lamin B. After 1.5 h at 30 °C, cells were fixed, and binding of anti-lamin B antibodies was examined with FITC-conjugated secondary antibodies. Lamin B was not accessible to antibodies when cells were treated with digitonin only. However, antibodies bound to lamin B if nuclear membranes were permeabilized with Triton X-100. (*B*) Heat shock inhibits classical nuclear import *in vitro.* Classical nuclear import was analyzed with TRITC-SV40-HSA in semi-intact control and heat-shocked HeLa cells.

Heat stress relocates importin-α, CAS and Ran, but does not change transport factor abundance. The experiments in Figure 3A address several questions. First, we compared the distribution of import factors in whole cells (treatment 1) that were kept under normal growth conditions (Fig. 3A, control) or exposed to heat (heat shock). Furthermore, import factor levels in the nucleus (treatment 3) or cytoplasm (treatment 2) were monitored.

In intact cells (Fig. 3A, treatment 1) upon heat shock, significant changes were seen for Ran, importin-α and CAS. Ran partially relocated to the cytoplasm, whereas importin-α and CAS accumulated in nuclei. Treatment 3 was used next to determine the effect of heat stress on *nuclear* transport factors. Although digitonin extraction (Fig. 3A, treatment 3) of unfixed cells solubilized a portion of Ran in control and stressed samples, Ran was still detectable in nuclei. A more pronounced effect of heat shock was detected for the distribution of importin-α and CAS. After digitonin extraction, higher amounts of importin-α and CAS remained associated with heat-shocked nuclei compared to unstressed controls. These results were consistently observed in multiple experiments.

Interestingly, digitonin extraction affected the distribution of nuclear importin-α in control cells (compare treatment 1 with 3); it changed from predominantly nuclear rim localization to a distribution throughout the nucleus in digitonin-treated cells. One possible explanation for this relocation could be a labile association of importin-α with the nuclear envelope which is sensitive to digitonin treatment.

Treatment 2 monitors nuclear transport factors in the cytoplasm of control and stressed cells (Fig. 3A). Heat shock increased the levels of Ran in the cytoplasm, but diminished the cytoplasmic amounts for importin-α or CAS. These results are consistent with the staining pattern obtained for whole cells (Fig. 3A, treatment 1). Together, the data support the idea that stress increased the nuclear, but reduced the cytoplasmic concentration of importin-α and CAS. The opposite scenario applies to Ran.

To determine the effect of heat stress on the abundance of nuclear transport factors, crude extracts were prepared from control and heat-shocked cells. Equal amounts of protein were analyzed side-by-side by Western blotting, with tubulin and actin serving as controls. As shown in Figure 3B, no drastic changes for the levels of Ran, importin-α or CAS were detected in stressed cells.

Heat shock affects nuclear accumulation of importin-α and CAS *in vitro*. Importin-α can enter the nucleus by two pathways, either independent or dependent on cytosolic factors [13]. Figure 4 compares the nuclear accumulation of fluorescently labeled importin-α or CAS in the absence or presence of exogenously added cytosol. Cytosol was prepared from either unstressed or heat-shocked cells and combined with control or heat-treated semi-intact HeLa cells. In the absence of exogenous cytosol, importin-α and CAS entered the nucleus and heat shock stimulated this process significantly (Fig. 4A, C, cytosol –). These results are consistent with the idea that heat stress impinges on

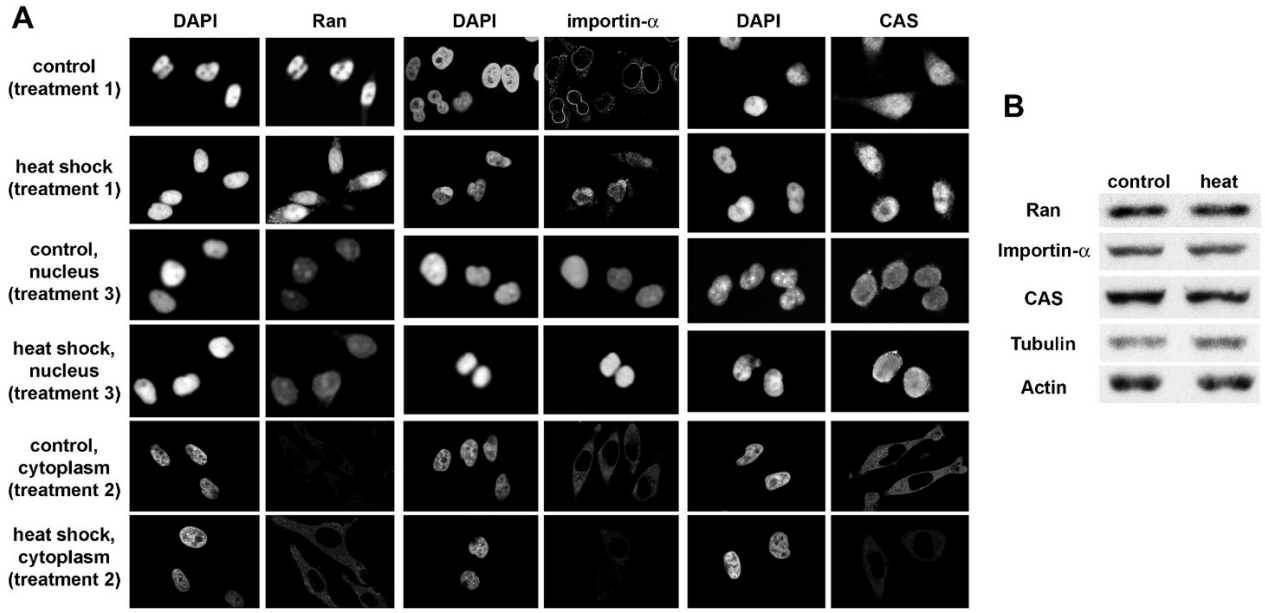

Figure 3. (*A*) Effect of heat stress on the distribution of nuclear transport factors. HeLa cells were grown at 37 °C (control) or stressed for 30 min at 45.5 °C (heat shock). Cells were either fixed immediately (treatment 1; see Fig. 1 for details) or treated with digitonin *before* fixation to stain preferentially nuclear protein (treatment 3). Alternatively, to visualize transport factors located in the cytoplasm (treatment 2), samples were fixed first, followed by permeabilization of the plasma membrane with digitonin. Note that importin-α and CAS concentrate in the nuclei of cells that have been exposed to heat, whereas little protein is detected in the cytoplasm. (*B*) Effect of heat stress on the abundance of Ran, importin-α and CAS. Crude extracts from control and heat-shocked (heat) cells containing equal amounts of protein were analyzed by Western blotting with antibodies against Ran, importin-α or CAS. Actin and tubulin were included as controls. All of the data are representative of at least three independent experiments with similar results.

semi-intact cells, possibly altering nucleoporins or other components of the NE.

A more complicated picture emerged for importin-α when cytosol was added to *in vitro* assays. The combination of heat-shocked cells (hs) with unstressed cytosol (un) led to a reduction of import when compared with import for unstressed cells/unstressed cytosol (Fig. 4C). However, in heat-shocked semi-intact cells, stressed cytosol significantly enhanced the nuclear accumulation of importin-α when compared with unstressed cytosol (Fig. 4C, xx). This suggests that heat treatment affected components of semi-intact cells as well as cytosolic factors, and both controlled nuclear transport of importin-α. For the carrier CAS, the highest nuclear accumulation was observed with heat-shocked cells/heat-shocked cytosol, and CAS nuclear import was significantly increased with respect to unstressed cells/unstressed cytosol (Fig. 4C, **) or stressed cells/unstressed cytosol (Fig. 4C, xx). Similar results were obtained for several independent experiments, as described in Materials and methods.

Binding of importin-α and CAS to nuclear envelopes *in vitro*. Results in the previous section demonstrated that the *in vitro* nuclear accumulation of importin-α and CAS was modulated by heat shock. Docking at the NE is the initial step required for nuclear import, and we tested whether this process was altered by heat (Fig. 5). Two different experiments addressed this question. First, semi-intact cells were incubated with fluorescently labeled importin-α or CAS, and their association with the NE was quantified (see Materials and methods). This assay measures the sites at the NE that are *free* to bind either transport factor. Second, semi-intact cells were extracted with salt to remove endogenous transport factors associated with nuclear membranes. Subsequent incubation with labeled importin-α or CAS measures the *total* binding sites at the NE that can be occupied.

Using these strategies, quantification of fluorescent signals at the nuclear periphery showed that docking of importin-α was increased upon heat stress. This applied both to free and total binding sites (Fig. 5B); more binding sites at the NE became available upon heat shock without (free binding sites) and with (total binding sites) salt extraction. A distinct scenario emerged for CAS, for which we did not detect a significant effect of heat on either free or total binding sites, suggesting that docking of importin-α and CAS may be regulated differently.

For both importin-α and CAS, extraction with salt increased the available binding sites in unstressed and heat-shocked cells (Fig. 5, compare – NaCl with

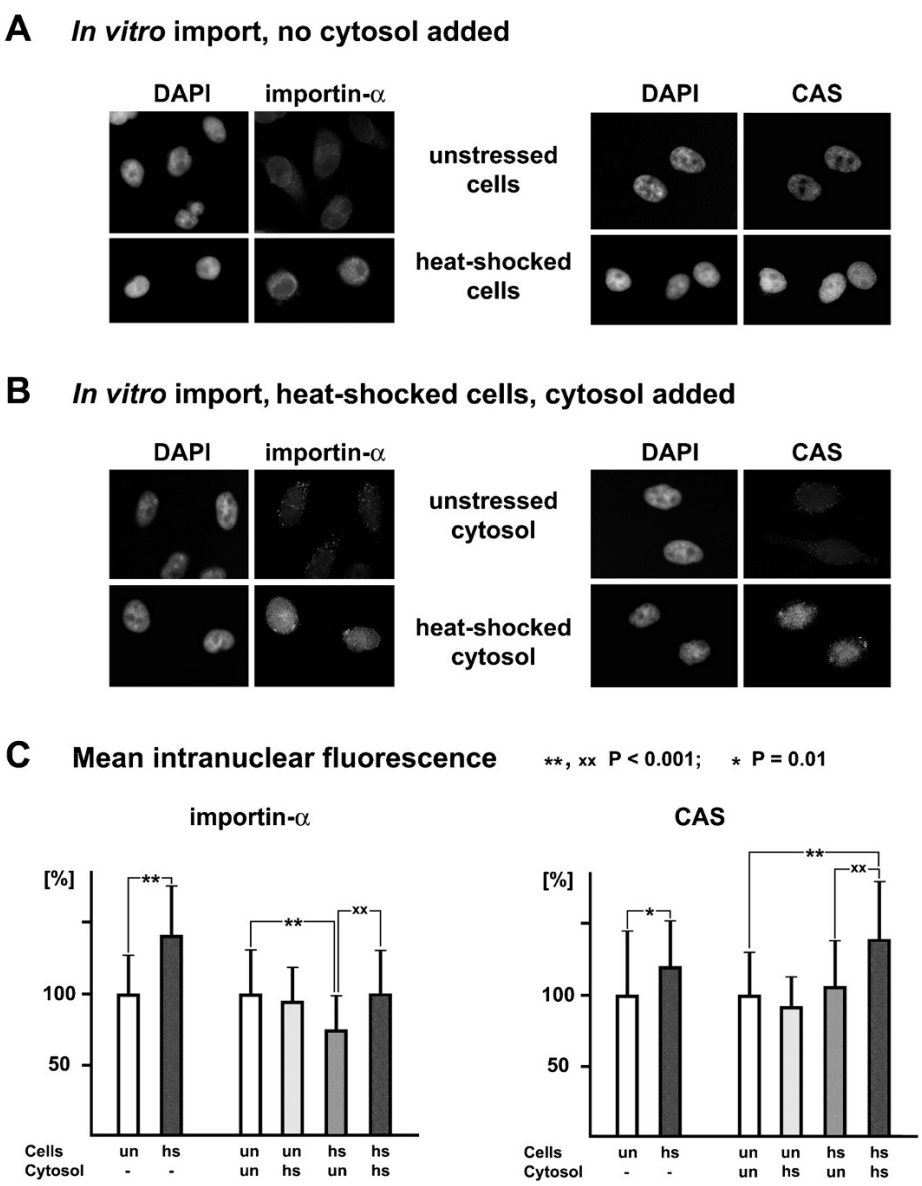

Figure 4. Heat stress alters the nuclear accumulation of importin-α and CAS *in vitro*. Nuclear import of fluorescently labeled importin-α or CAS was analyzed in unstressed and heat-shocked cells in the absence of exogenous cytosol (*A*) or upon addition of cytosol prepared from unstressed or heat-treated HeLa cells (*B*). (*C*) The mean intranuclear fluorescence was measured for each of the different conditions (see Materials and methods). In the absence of cytosol (cytosol –), average pixel intensities obtained for unstressed cells were defined as 100%. When cytosol was added to semi-intact cells, the combination unstressed cells/unstressed cytosol served as a 100% control. Means, SDs and statistical significance are shown with unstressed cells or unstressed cells/unstressed cytosol as reference (*, **). In addition, the nuclear accumulation of importin-α and CAS was significantly increased when heat-shocked cells/heat-shocked cytosol was compared with heat-shocked cells/unstressed cytosol (xx). All data points show results from at least three independent experiments; between 54 and 59 cells were quantified in each of these experiments (see Materials and methods for details).

+ NaCl). This is in line with the idea that salt treatment of semi-intact cells released endogenous transport factors from the nuclear envelope, thereby liberating binding sites for fluorescently labeled importin-α and CAS.

Taken together, results in this section are consistent with the idea that the first step of nuclear transport, i.e. docking at the nuclear envelope, is stress sensitive for importin-α and upregulated in response to heat.

Exit of importin-α and CAS from nuclei. The experiments described above indicated that heat shock stimulated significantly the docking of importin-α at the NE, while no drastic changes were observed for CAS. Since nuclear accumulation may result from changes of import, export and/or retention, we tested next whether heat stress affected importin-α or CAS movement from the nucleus to the cytoplasm. To this end, growing cells were heat-shocked and semi-permeabilized with digitonin. During this extraction, a portion of importin-α and CAS was removed from the nucleus (data not shown). Digitonin-treated cells were then incubated in transport buffer supplemented with energy and RanQ69L, conditions that stimulate the formation of export complexes which rely on members of the importin-β family. At different time points during the incubation, intranuclear importin-α and CAS were quantified (Fig. 6B; see Materials and methods for details). Under these conditions, the levels of importin-α decreased somewhat in unstressed cells over time; however, the changes were not statistically significant. In comparison, the levels

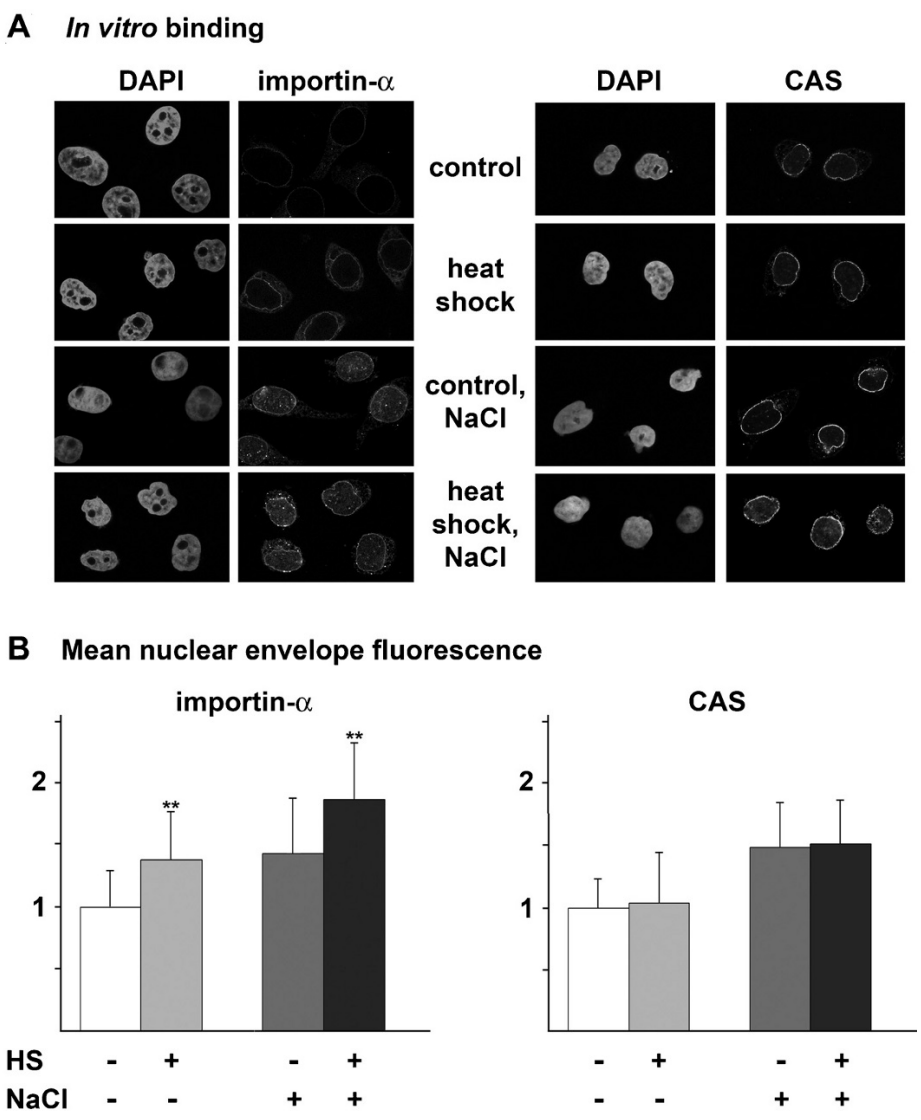

Figure 5. Effect of stress on NE docking of importin-α and CAS. *In vitro* binding of importin-α and CAS was analyzed with semi-intact cells grown at 37 °C or heat-stressed for 30 min at 45.5 °C. Semi-intact cells were pre-treated for 10 min with NaCl before incubation with purified transport factors as indicated. Importin-α or CAS associated with the cytoplasmic side of the NE was visualized by confocal microscopy (*A*), and fluorescence signals associated with NEs were quantified (*B*). Mean NE fluorescence for control cells without salt extraction was defined as 1. Means and SDs are shown; ** $p < 0.01$. Results are representative of at least three independent experiments; between 43–65 cells were quantified for individual data points.

of importin-α remained higher in nuclei of heat-shocked cells at all times; no drastic reduction of nuclear importin-α was observed for stressed cells during the incubation period. Similar results were observed for CAS; although a portion of the carrier moved out of the nucleus in control as well as heat-treated cells, CAS levels in stressed cells remained higher throughout the experiment.

Taken together, these results indicated that upon stress, a larger portion of importin-α did not exit to the cytoplasm; this portion remained concentrated in nuclei during the incubation period. Similarly, elevated levels of CAS remained associated with nuclei of stressed cells. This could be due either to reduced export efficiency, nuclear retention or a combination of these events. Experiments described in the following section analyzed the contribution of retention to the accumulation of importin-α and CAS in nuclei.

Nuclear retention of importin-α and CAS in heat stressed cells. Nuclear retention may interfere with the export of transport factors to the cytoplasm and lead to increased levels of transport factors in the nucleus. We addressed this question by extracting cells with buffer, detergent, DNase, salt, and a mixture of DNase plus RNase (see Materials and methods), using a protocol that was designed to prepare nuclear matrices [26]. For this procedure, all incubations were carried out with unfixed cells. The first step (KM buffer) uses a buffer with low ionic strength and pH 6.2; the shift from growth medium to KM buffer during the first extraction step likely causes the diffuse nuclear, rather than predominantly NE, staining of importin-α in control cells (compare controls in Fig. 7A with Fig. 3A). For unstressed cells, importin-α was efficiently solubilized following treatment with NP40 and DNase incubation. Following DNase and RNase treatment importin-α was almost completely

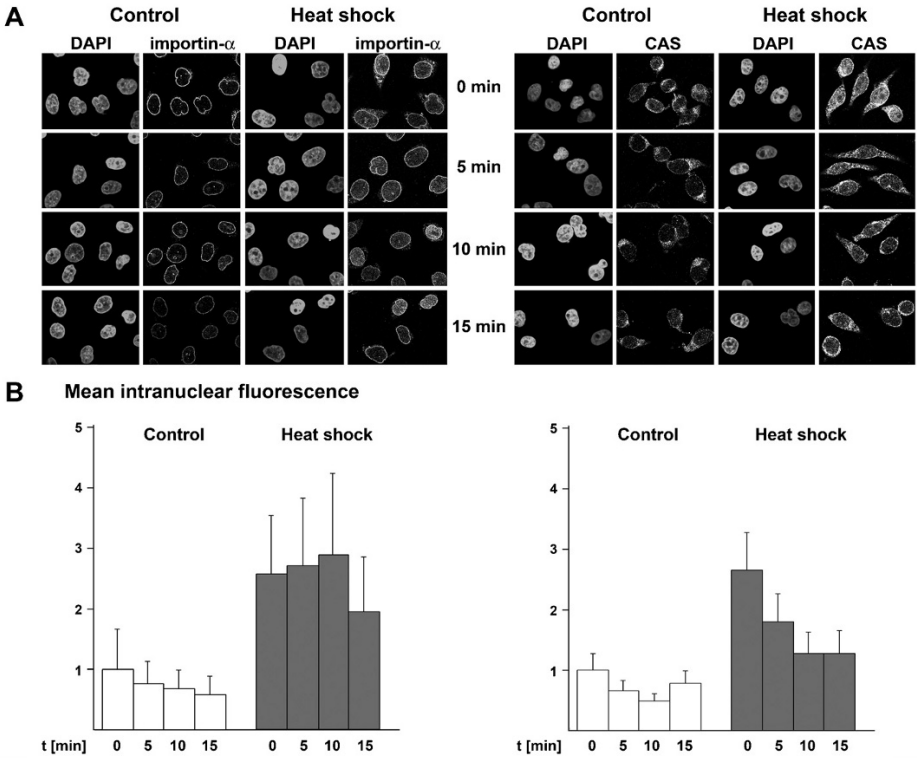

Figure 6. Exit of importin-α and CAS from nuclei of unstressed and heat-shocked cells. Control and heat-shocked HeLa cells were semi-permeabilized with digitonin, and incubated for 5, 10 and 15 min as described in Materials and methods. Cells were fixed and transport factors were detected by indirect immunofluorescence (*A*). Controls (0 min) were fixed immediately after incubation with digitonin. (*B*) The mean (± SD) intranuclear fluorescence was determined for different time points. The mean intranuclear fluorescence of unstressed cells measured at 0 min was defined as 1. Between 48 and 75 cells were quantified for each data point.

extracted from control cells. (Note that all images for Fig. 7A were taken at identical settings.) By contrast, in heat-shocked cells, only a portion of importin-α was solubilized by the different treatments, and high levels of the transport factor remained bound to nuclear structures even after the final extraction step. These results demonstrate that in response to heat shock, a portion of importin-α becomes resistant to extraction. Unlike importin-α, CAS was solubilized efficiently with NP40 in control and stressed cells (Fig. 7B). To detect changes during subsequent steps of the extraction, the detector gain of the confocal microscope was increased (Fig. 7B, part *b*), and all images in part (*b*) were acquired with identical settings. In heat-shocked cells, CAS was somewhat more resistant to the extraction with salt and DNase + RNase when compared to unstressed cells.

In summary, anchorage in nuclei increased in stressed cells for both importin-α and CAS, but the effect was much more prominent for importin-α.

Discussion

The results described here and in previous publications demonstrate that stress inhibits classical nuclear import [16, 17, 20]. This inhibition may be caused by different stress-induced changes of the transport apparatus, and we focused here on the heat-dependent relocation of nuclear transport factors. Importin-α and CAS are key components required for classical protein import; in response to heat shock, the steady-state concentration of both proteins increases in the nuclei of growing cells. We have used *in vitro* transport assays to analyze individual steps of importin-α and CAS nuclear trafficking and to identify the changes triggered by heat shock for each of these reactions. This approach was employed to determine the possible role of cytosolic factors in nuclear import, examine docking at the NE and exit from the nuclear interior. Taken together, our analyses support the conclusion that heat shock affects several of the processes that control the nucleocytoplasmic distribution of importin-α and CAS (summarized in Fig. 8 and Table 1).

In growing cells, heat shock concentrates importin-α and CAS in nuclei, a process determined by nuclear import, retention in the nucleus or cytoplasm and exit from the nucleus. At present, it is not known whether importin-α and CAS in heat-treated cells enter the nucleus by cytosol-independent and/or -dependent routes. Nevertheless, heat upregulates *in vitro* nuclear accumulation via either pathway for CAS and increases cytosol-independent nuclear import for importin-α. Moreover, the combination of cytosol and semi-intact cells indicates that soluble factors from stressed cells may stimulate the nuclear accumulation of importin-α and CAS upon heat shock. The effect of heat stress on cytosol-independent nuclear import

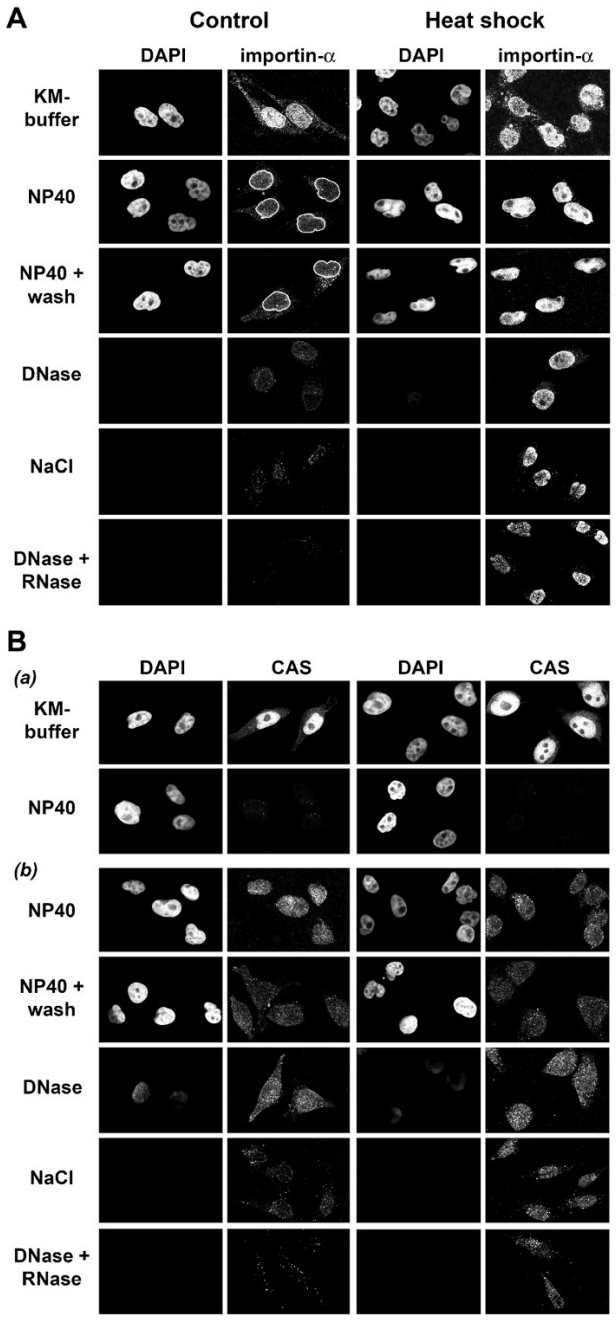

Figure 7. Solubilization of importin-α and CAS in control and heat-shocked cells. Unfixed control and stressed HeLa cells were treated sequentially with KM buffer, the detergent NP40, washed after detergent extraction (NP40 + wash), incubated with DNase, NaCl and a mixture of DNase + RNase. Samples were fixed immediately after each step and processed for indirect immunofluorescence. (*A*) Importin-α which was resistant to extraction by the different treatments, is shown. All images were collected with identical settings. (*B*) Most of CAS was readily extracted with NP40 (a). To monitor potential differences between control and stressed cells following the treatment with NP40, the detector gain was increased and kept constant for all subsequent extraction steps (b). Results shown are representative of at least three independent experiments.

Table 1. Heat alters the nucleocytoplasmic distribution of importin-α and CAS.

	Importin-α	CAS
Steady-state distribution in growing cells	↑ in nuclei	↑ in nuclei
In vitro nuclear accumulation without cytosol	↑	↑
In vitro nuclear accumulation with cytosol	↔	↑
NE docking	↑	↔
In vitro exit from nuclei	↓	↓
Nuclear retention	↑↑↑	(↑)

↑, heat-dependent increase; (↑), minor increase of the process; ↓, stress-induced reduction; ↔, no drastic change in response to stress.

suggests that stress modulates the function of semi-intact cells, possibly by altering components of the NE. As discussed below, for importin-α these stress-induced changes lead to the upregulation of docking. Nuclear import is initiated by docking at the NE, and we show for the first time that heat significantly upregulates the binding of importin-α to the NE, whereas docking of CAS is not drastically altered. Comparable results were obtained with salt-stripped nuclei, suggesting that the free and potential importin-α-binding sites increase upon stress. Based on these results, we propose that heat alters NE components that are involved in docking of importin-α, and nucleoporins are the most likely candidates for these heat-induced changes.

We and others demonstrated previously that stress may affect the retention of transport factors in nuclei [16, 17]. We have extended these studies and show now that heat shock increases nuclear retention of importin-α, which in part becomes resistant to the extraction with detergent, salt and nucleases, indicating drastic changes in solubility. In control cells, importin-α is released following treatment with both NP40 and DNase. Surprisingly, incubation with DNase efficiently liberated importin-α from nuclear envelopes, although only ~4% of the total cellular protein is released with DNase [26]. This may suggest a possible association of importin-α with chromatin at the nuclear periphery in control cells.

In contrast to unstressed cells, heat shock induced a portion of importin-α to become insoluble throughout the fractionation procedure. Although some CAS remains insoluble in stressed cells under these conditions, the effect is much less pronounced and CAS is solubilized to a large extent by detergent in control and heat-treated cells. Taken together, this heat-induced resistance to different extraction steps may suggest a stress-induced association of importin-α

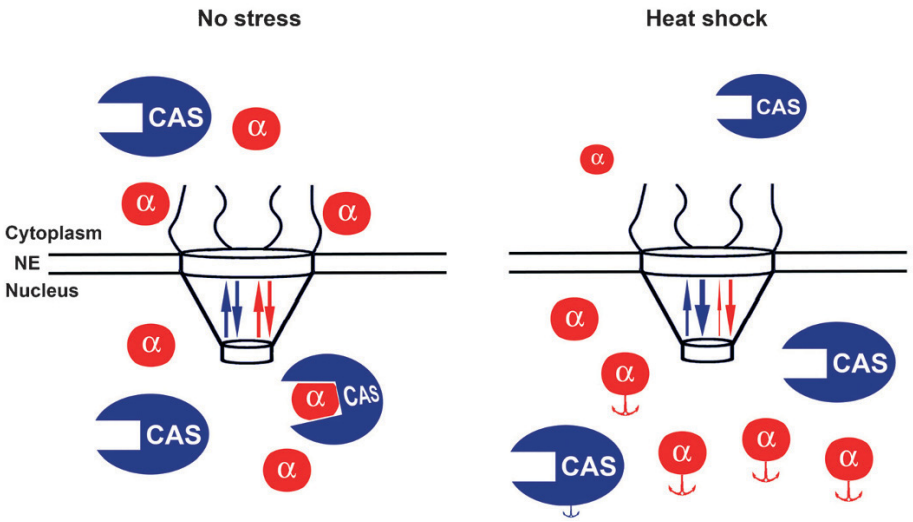

Figure 8. A combination of different mechanisms redistributes importin-α and CAS in heat-shocked cells. In response to heat stress, multiple steps contribute to the nuclear accumulation of importin-α and CAS. These include changes in nuclear import and exit and anchorage in the nucleoplasm. For simplicity, Ran has been omitted from the model. See text for details.

and, to a lesser extent, of CAS with components of the nuclear matrix.

In addition to the analyses of import, docking and retention, our studies address for the first time the exit of importin-α and CAS from nuclei. A cell-free system was used to quantify the levels of transport factors which remain in nuclei under conditions that promote export. These experiments reveal that a fraction of importin-α and CAS does not exit the nucleus in control or stressed cells. However, the levels of transport factors that remain in nuclei are increased by stress, and this effect was possibly somewhat more pronounced for importin-α. It is conceivable that the failure of importin-α to leave the nucleus is a consequence of its anchorage in the nucleoplasm. Similarly, nuclear retention of a small pool of CAS may explain why higher levels of the carrier persist in stressed nuclei, even under conditions that support exit to the cytoplasm. At present, we cannot rule out the possibility that following nuclear exit *in vitro*, a portion of importin-α or CAS is re-imported into nuclei of heat-shocked cells. This re-import could help sustain elevated intranuclear levels of the transport factors.

Based on our results for the exit of importin-α and CAS from nuclei, one might propose that importin-α becomes sequestered in the nucleoplasm by binding to immobilized CAS. However, this seems unlikely, since most of CAS was readily solubilized in stressed cells, whereas importin-α was resistant to extraction. We therefore favor the model that importin-α is anchored in nuclei by associating with nuclear factors other than CAS, and the factors could be components of the nuclear matrix.

Our results support an intricate model for the intracellular distribution of importin-α and CAS, with stress affecting multiple steps (Fig. 8, Table 1). These steps include changes in docking at the NE, nuclear import, the subsequent exit to the cytoplasm and retention in the nuclear interior. Importantly, the impact of heat is different for individual steps of importin-α and CAS nuclear trafficking. Stress-induced changes in NE docking, nuclear exit and retention are of particular importance to concentrate importin-α in nuclei, whereas upregulated nuclear import seems to play a more prominent role for CAS. On the basis of these data, a complex picture emerges for the effect of stress on the distribution of transport factors, nuclear function and organization. Besides changing classical import, it is tempting to speculate that the redistribution of CAS and importin-α will have additional consequences. For example, CAS was shown recently to control the expression of specific genes that are regulated by p53, and importin-α2 interacts with the promoter of the proapoptotic gene *PIG3* [10]. These results support the hypothesis that stress-induced changes in transport factor localization may lead to altered gene expression, thereby regulating the stress response and ultimately cell survival.

In addition to the mechanisms defined with our studies, other processes may play a role in regulating classical nuclear import during aging and for specific forms of neurodegenerative diseases. Thus, an age-dependent decline in import efficiency correlates with decreasing levels of transport factors in old human fibroblasts [6], changes we did not detect in heat-stressed cells. Interestingly, a mislocalization of importin-α1 was observed in hippocampal neurons from Alzheimer patients [27]. In these cells, the transport factor accumulates in Hirano bodies, inclusions located in the cytoplasm, which may affect nuclear trafficking [27]. Likewise, in a mouse model of amyotrophic lateral sclerosis, importin-α distribution was shifted toward the cytoplasm with reduced levels

in the nucleus [28]. Together with our results, these data suggest that several pathophysiological states, as exemplified by neurodegenerative diseases or stress, cause a relocation of transport factors. This unbalanced distribution of essential transport components is likely to impair nuclear trafficking, thereby interfering with correct nucleocytoplasmic communication and other cellular functions.

Acknowledgements. We are grateful to Dr. C. M. Brown and Dr. J. Liu (Life Science Imaging and HTS/HCS Facilities at McGill University) for help with image acquisition and data analyses. U.S. was supported by grants from CIHR and NSERC and is a chercheur national of FRSQ. M.K. was supported by doctoral fellowships from FRSQ and the Heart and Stroke Foundation of Canada.

1 Weis, K. (2005) Regulating access to the genome: nucleocytoplasmic transport throughout the cell cycle. Cell 112, 441–451.
2 Shulga, A., Mosammaparast, N., Wozniak, R. and Goldfarb, D. S. (2000) Yeast nucleoporins involved in passive nuclear envelope permeability. J. Cell Biol. 149, 1027–1038.
3 O'Brien, E. M., Gomes, D. A., Sehgal, S. and Nathanson, M. H. (2007) Hormonal regulation of nuclear permeability. J. Biol. Chem. 282, 4210–4217.
4 Callanan, M., Kudo, N., Gout, S., Brocard, M., Yoshida, M., Dimitrov, S. and Khochbin, S. (2000) Developmentally regulated activity of CRM1/XPO1 during early *Xenopus* embryogenesis. J. Cell Sci. 113, 451–459.
5 Tekotte, H., Berdnik, D., Török, T., Buszcak, M., Jones, L. M., Cooley, L., Knoblich, J. A. and Davis, I. (2002) Dcas is required for importin-α3 nuclear export and mechano-sensory organ cell fate specification in *Drosophila.* Dev. Biol. 244, 296–406.
6 Pujol, G., Söderqvist, H. and Radu, A. (2002) Age-associated reduction of nuclear protein import in human fibroblasts. Biochem. Biophys. Res. Commun. 274, 354–358.
7 Harel, A. and Forbes, D. J. (2004) Importin beta: conducting a much larger cellular symphony. Mol. Cell 16, 319–330.
8 Matsuura, Y. and Stewart, M. (2004) Structural basis for the assembly of a nuclear export complex. Nature 432, 872–877.
9 Behrens, P., Brinkmann, U. and Wellmann, A. (2003) CSE1L/CAS: its role in proliferation and apoptosis. Apoptosis 8, 39–44.
10 Tanaka, T., Ohkubo, S., Tatsuno, I. and Prives, C. (2007) hCAS/CSE1L associates with chromatin and regulates expression of select p53 target genes. Cell 130, 638–650.
11 Otis, K. O., Thompson, K. R. and Martin, K. C. (2006) Importin-mediated nuclear transport in neurons. Curr. Opin. Neurobiol. 16, 1–7.
12 Goldfarb, D. S., Corbett, A. H., Mason, D. A., Harreman, M. T. and Adam, S. A. (2004) Importin α: a multipurpose nuclear-transport receptor. Trends Cell Biol. 14, 505–514.
13 Miyamoto, Y., Hieda, M., Harreman, M. T., Fukumoto, M., Saiwaki, T., Hodel, A. E., Corbett, A. H. and Yoneda, Y. (2002) Importin α can migrate into the nucleus in an importin β- and Ran-independent manner. EMBO J. 21, 5833–5842.
14 Hood, J. K. and Silver, A. (1999) In or out? Regulating nuclear transport. Curr. Opin. Cell Biol. 11, 241–247.
15 Poon, I. K. and Jans, D. A. (2005) Regulation of nuclear transport: central role in development and transformation? Traffic 6, 173–186.
16 Miyamoto, Y., Saiwaki, Y., Yamashita, J., Yasuda, Y., Kotera, I., Shibata, S., Shigeta, M., Hiraoka, Y. Haraguchi, T. and Yoneda, Y. (2004) Cellular stresses induce the nuclear accumulation of importin α and cause a conventional nuclear import block. J. Cell Biol. 165, 617–623.
17 Kodiha, M., Tran, D., Qian, C., Morogan, A., Presley, J. F., Brown, C. M. and Stochaj, U. (2008) Oxidative stress mislocalizes and retains transport factor importin-α and nucleoporins Nup153 and Nup88 in nuclei where they generate high molecular mass complexes. Biochem. Biophys. Acta Mol. Cell Biol. 1783, 405–418.
18 Moore, M. S. and Blobel, G. (1992) The two steps of nuclear import, targeting to the nuclear envelope and translocation through the nuclear pore, require different cytosolic factors. Cell *69,* 939–950.
19 Chatterjee, S. and Stochaj, U. (1998) Diffusion of proteins across the NE of HeLa cells. BioTechniques 24, 668–674.
20 Kodiha, M., Chu, A., Lazrak, O. and Stochaj, U. (2005) Stress inhibits nucleocytoplasmic shuttling of heat shock protein hsc70. Am. J. Physiol. Cell Physiol. 289, C1034–C1041.
21 Kodiha, M., Rassi, J. G., Brown, C. M. and Stochaj, U. (2007) Localization of AMP kinase is regulated by stress, cell density, and signaling through the MEK → ERK1/2 pathway. Am. J. Physiol. Cell Physiol. 293, 1427–1436.
22 Stochaj, U. and Silver, P. (1992) A conserved phosphoprotein that specifically binds nuclear localization sequences is involved in nuclear import. J. Cell Biol. 117, 473–482.
23 Ribbeck, K., Lipowsky, G., Kent, H. M., Stewart, M. and Görlich, D. (1998) NTF2 mediates nuclear import of Ran. EMBO J. 17, 6587–6598.
24 Kodiha, M., Chu, A., Matusiewicz, N. and Stochaj, U. (2004) Multiple mechanisms promote the inhibition of classical nuclear import upon exposure to severe oxidative stress. Cell Death and Differ. 11, 862–874.
25 Truant, R., Fridell, R. A., Benson, E. R., Herold, A. and Cullen, B. R. (1998) Nucleocytoplasmic shuttling by protein nuclear import factors. Eur. J. Cell Biol. 77, 269–275.
26 Staufenbiel, I. M. and Deppert, W. (1984) Preparation of nuclear matrices from cultured cells: subfractionation of nuclei in situ. J. Cell Biol. 98, 1886–1894.
27 Lee, H., Ueda, M., Miyamoto, Y., Yoneda, Y., Perry, G., Smith, M. A. and Zhu, X. (2006) Aberrant localization of importin α1 in hippocampal neurons in Alzheimer disease. Brain Res. 1124, 1–4.
28 Zhang, J., Ito, H., Wate, R., Ohnishi, S., Nakano, S. and Kusaka, H. (2006) Altered distributions of nucleocytoplasmic transport-related proteins in the spinal cord of a mouse model of amyotrophic lateral sclerosis. Acta Neuropathol. 112, 673–680.

Cell Death and Differentiation (2004) 11, 862–874

www.nature.com/cdd

Multiple mechanisms promote the inhibition of classical nuclear import upon exposure to severe oxidative stress

M Kodiha[1], A Chu[1], N Matusiewicz[1] and U Stochaj*,[1]

[1] Department of Physiology, McGill University, 3655 Promenade Sir William Osler, Montreal, PQ, H3G 1Y6, Canada
* Corresponding author: U Stochaj. Tel.: +1 514 398 2949; Fax: +1 514 398 7452; E-mail: ursula.stochaj@mcgill.ca

Received 03.11.03; revised 07.2.04; accepted 17.2.04; published online 16.4.04
Edited by G Melino

Abstract

In growing HeLa cells, severe stress elicited by the oxidant hydrogen peroxide inhibits classical nuclear import. Oxidant treatment collapses the nucleocytoplasmic Ran concentration gradient, thereby elevating cytoplasmic GTPase levels. The Ran gradient dissipates in response to a stress-induced depletion of RanGTP and a decreased efficiency of Ran nuclear import. In addition, oxidative stress induces a relocation of the nucleoporin Nup153 as well as the nuclear carrier importin-β, and docking of the importin-α/β/cargo complex at the nuclear envelope is reduced. Moreover, Ran, importin-β and Nup153 undergo proteolysis upon oxidative stress. Caspases and the proteasome degrade Ran and importin-β; however, ubiquitination of these transport factors is not observed. Inhibition of caspases in stressed cells alleviates the mislocalization of importin-β, but does not restore the Ran concentration gradient or classical import. In summary, inhibition of classical nuclear import by hydrogen peroxide is caused by a combination of multiple mechanisms that target different components of the transport apparatus.
Cell Death and Differentiation (2004) **11,** 862–874.
doi:10.1038/sj.cdd.4401432
Published online 16 April 2004

Keywords: stress; oxidants; HeLa cells; nuclear transport; Ran

Abbreviations: BSA, bovine serum albumin; DAPI, 4′,6-diamidino-2-phenylindole; MAPK, mitogen-activated protein kinase; NE, nuclear envelope; NLS, nuclear localization signal; NPC, nuclear pore complex; RBD, Ran-binding domain; TMR, tetramethylrhodamine

Introduction

Stress is implicated in the pathophysiology of ischemia, heart failure, hypertension and cancer. Moreover, the appropriate response to oxidative stress determines aging and influences the life span of an organism (reviewed in Finkel and Holbrook[1]). On a subcellular level, stress changes the nucleocytoplasmic distribution of proteins (reviewed in Hood and Silver[2]). For instance, in cells that have been treated with reactive oxygen species, a variety of transcription factors relocalize within the cell to modulate gene expression (reviewed in Finkel and Holbrook[1] and Allen and Tresini[3]). Therefore, defining the response to stress on a subcellular level, in particular with respect to nucleocytoplasmic trafficking of macromolecules, will contribute significantly to our understanding of the stress response and stress-related pathophysiology.

Oxidative stress activates several signaling cascades, including the MAPK family members ERK1/2, JNK/SAPK and p38. Likewise, the PI(3)-kinase/Akt pathway becomes active (reviewed in Finkel and Holbrook,[1] Robinson and Cobb[4] and Rhee[5]). Importantly, cell-specific differences in the activation of signaling pathways have been observed (reviewed in Robinson and Cobb[4]). In HeLa cells, hydrogen peroxide induces phosphorylation of the MAPKs ERK, JNK/SAPK and p38.[6] Hydrogen peroxide not only activates several signal transduction pathways, it may also activate the nuclear proteasome, thereby increasing the degradation of proteins damaged by oxidants.[7]

Nucleocytoplasmic trafficking of macromolecules is sensitive to stress; heat shock, ethanol and oxidative stress inhibit classical nuclear protein import.[8,9,10] In growing yeast cells and in semi-permeabilized smooth muscle cells *in vitro*, oxidants have been shown to interfere with classical nuclear import. In these model systems, redistribution of the small GTPase Gsp1p/Ran from the nucleus to the cytoplasm is believed to contribute to nuclear import inhibition.[8,9] In digitonin-treated aortic smooth muscle cells, the MAPK ERK2 plays a role in classical transport inhibition triggered by hydrogen peroxide, and transport inhibition can be overcome if ERK2 activation is prevented.[9] So far, the effect of oxidative stress on classical nuclear import in growing mammalian cells has not been studied.

Like cytoplasmic transport factors, nucleoporins are involved in nucleocytoplasmic trafficking of proteins and RNA (reviewed in Stochaj and Rother,[11] Görlich and Kutay[12] and Kuersten *et al.*[13]). For instance, Nup153, a member of the FXFG family of nucleoporins, is located at the nuclear basket, where it participates in the termination of classical nuclear protein import.[14] Despite these previous studies, it is presently not clear how trafficking across the NPC changes in response to stress. To address these questions, we have now analyzed the effect of oxidative stress on classical nuclear import in growing HeLa cells and *in vitro*. Our results show that components of the nuclear transport apparatus are relocated in cells treated with hydrogen peroxide. Furthermore, exposure to severe oxidative stress decreases the availability of RanGTP and induces the degradation of Ran, importin-β and Nup153, components required for classical and several nonclassical nuclear trafficking pathways.

Results and Discussion

Oxidative stress inhibits classical nuclear import in growing HeLa cells

To determine how oxidative stress affects classical nuclear import in growing mammalian cells, we transiently transfected HeLa cells with plasmids encoding either NLS-GFP, a fluorescent reporter protein, which carries SV40-NLS fused to GFP, or the GFP-tag only.[10] The small size of NLS-GFP allows diffusion across the NPC, a process independent of active transport. In addition, the simple SV40-NLS is recognized by the classical transport apparatus, which imports NLS-GFP into the nucleus. The net distribution of the reporter protein is a combination of diffusion and transport, and nuclear accumulation requires classical import to be active. Concentrated in nuclei under normal conditions (Figure 1A, panel b), NLS-GFP also appears in the cytoplasm upon exposure to hydrogen peroxide (Figure 1A, d). By contrast, the localization of GFP, which can be found in the nucleus and cytoplasm, was not altered by this treatment (Figure 1A, f, h), supporting the idea that oxidative stress does not prevent diffusion across NPCs. Therefore, a redistribution of NLS-GFP in response to oxidative stress can be attributed to changes in classical import.

In initial experiments, we have tested the effect of different concentrations of hydrogen peroxide on NLS-GFP localization, and a 1 h treatment with 10 mM hydrogen peroxide was found to be optimal to mislocalize a portion of NLS-GFP to the cytoplasm. At lower concentrations, NLS-GFP remained accumulated in the nuclei. By contrast, upon addition of 20 mM of the oxidant, NLS-GFP completely equilibrated within the cells, and similar fluorescent signals were obtained for the nucleus and cytoplasm (not shown). On the basis of

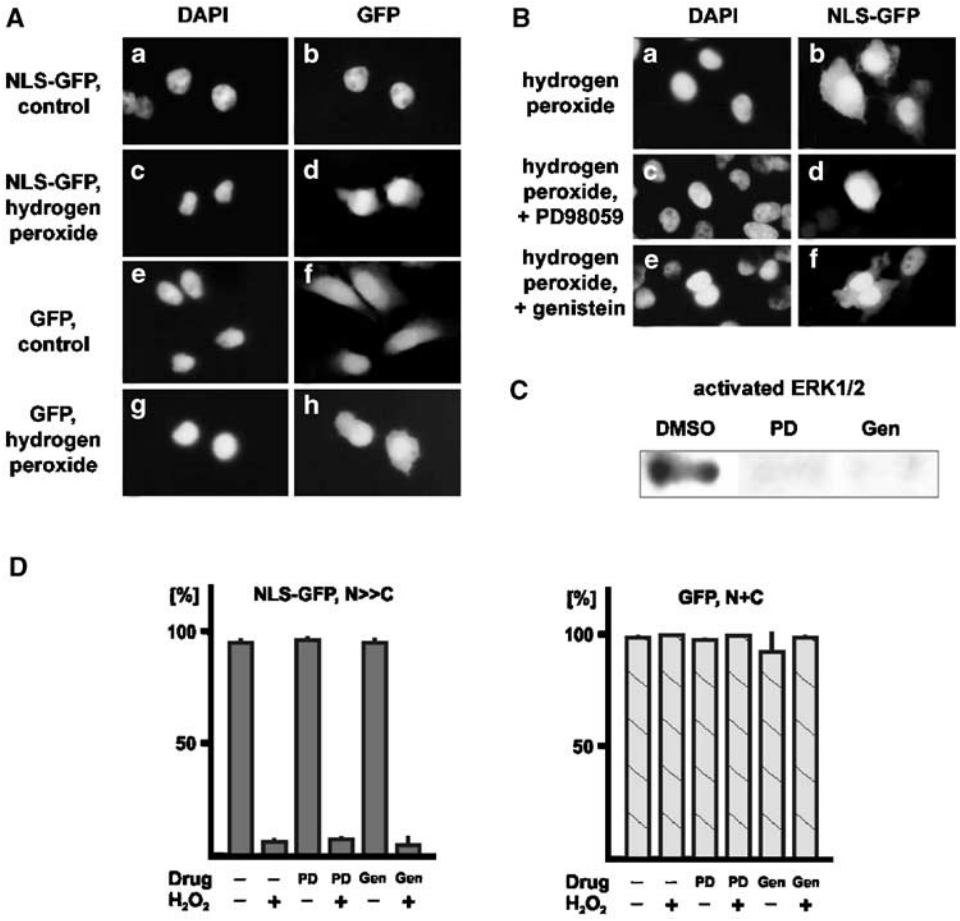

Figure 1 Oxidative stress inhibits classical nuclear import in growing HeLa cells; MAPK inhibitors do not abolish this import inhibition. Treatment with 10 mM hydrogen peroxide was carried out in growth medium for 1 h at 37°C. Control samples were incubated under identical conditions with the omission of oxidant. (**A**) Transiently transfected HeLa cells synthesizing NLS-GFP (a–d) or GFP (e–h) were incubated under nonstress conditions (control) or exposed to hydrogen peroxide. Cells were fixed and reporter proteins were localized by fluorescence microscopy. Nuclei were visualized with DAPI. (**B**) HeLa cells synthesizing NLS-GFP were incubated with hydrogen peroxide in the absence (a, b) or presence of PD98059 (c, d) or genistein (e, f). NLS-GFP and nuclei were detected as in part (**A**). (**C**) HeLa cells were exposed to hydrogen peroxide after preincubation with the solvent DMSO, PD98059 or genistein as indicated. DMSO or inhibitors were also present during exposure to oxidative stress. Equal amounts of protein were separated by SDS-PAGE, and ERK1/2 activation was detected by Western blotting with antibodies specific for dually phosphorylated ERK1/2. (**D**) Quantitation of the effect of hydrogen peroxide on NLS-GFP and GFP localization. Transiently transfected HeLa cells were monitored for the distribution of reporter proteins in nuclei ($N >> C$) or nuclei and cytoplasm ($N + C$). The inhibitors PD98059 (PD) or genistein (Gen) were present as indicated. Each bar represents the mean of results for three independent experiments and the standard deviation. At least 200 transfected cells were evaluated for each experiment

these results, we have chosen 10 mM hydrogen peroxide for our further experiments, as this treatment resulted only in partial mislocalization of the reporter protein to the cytoplasm. HeLa cells exposed to 10 mM hydrogen peroxide frequently changed their shape. This is caused by a reorganization of the F-actin cytoskeleton, which became obvious upon staining with FITC-phalloidin (data not shown). Ultimately, the treatment with hydrogen peroxide is toxic, as many of the cells detached from the surface. Furthermore, when stressed cells were incubated in fresh medium for 24 h, more than 70% of the cells exposed to hydrogen peroxide underwent apoptosis, as evident by TUNEL staining. By contrast, unstressed cells did not score positive in the TUNEL assay (data not shown).

As described above, upon hydrogen peroxide exposure NLS-GFP was detected in the cytoplasm (Figure 1A, d; 1B, b), whereas it was restricted to nuclei in unstressed cells (Figure 1A, b). To quantify the effect of hydrogen peroxide on the distribution of reporter proteins, their localization was assigned to the nuclei (Figure 1D, $N>>C$) or the nuclei and cytoplasm ($N+C$). Under the conditions used in our studies, NLS-GFP was restricted to the nuclei in more than 90% of the control cells. However, after treatment with hydrogen peroxide, in most of the cells NLS-GFP was also detected in the cytoplasm (Figure 1D).

It should be noted, however, that stressed cells did not necessarily equilibrate the reporter protein. Fluorescent signals for nuclei were brighter than for the cytoplasm, demonstrating that the transport substrate relocated only partially (Figure 1A, d; 1B, b, d, f).

Taken together, the data in Figure 1 show that transport of the classical nuclear import substrate NLS-GFP in growing HeLa cells is rapidly inhibited by severe oxidative stress induced by hydrogen peroxide.

Nuclear import inhibition by hydrogen peroxide cannot be abolished by MAPK inhibitors

Hydrogen peroxide has been reported to activate the MAPK ERK2, and changes in ERK2 activity can alter *in vitro* nuclear import in semi-permeabilized smooth muscle cells.[9] We therefore tested whether PD98059, a compound that abolishes the activation of ERK1/2 by inhibiting the upstream kinase MEK, and genistein, a more general inhibitor of MAPKs, interfere with classical import inhibition. To this end, HeLa cells were pretreated with either drug under conditions known to block the activation of ERK1/2.[10] As shown in Figure 1C and published previously,[10] the inhibitor concentrations used in our experiments prevented stress-induced phosphorylation and thereby activation of ERK1/2 in HeLa cells. However, neither PD98059 nor genistein were able to abolish the inhibitory effect of hydrogen peroxide on classical nuclear protein import (Figure 1B, d, f). Moreover, quantitative analysis of the NLS-GFP distribution in stressed cells showed that the effect of hydrogen peroxide was not changed by the treatment with MAPK inhibitors (Figure 1D). Likewise, PD98059 or genistein did not alter classical nuclear protein import in unstressed cells or the distribution of GFP under control and stress conditions (Figure 1D).

Oxidants redistribute nuclear transport factors

The soluble factors Ran and importin-β as well as the nucleoporin Nup153 are essential components of the classical nuclear import apparatus (reviewed in Stochaj and Rother,[11] Görlich and Kutay[12] and Künzler and Hurt[15]). Importantly, hydrogen peroxide treatment of HeLa cells interferes with the formation of the Ran concentration gradient (Figure 2A, d; 2B). This collapse of the Ran concentration gradient was not prevented by PD98059 or genistein (Figures 2B, 4). In unstressed cells importin-β is associated with nuclei, where it accumulates at the nuclear envelope (NE) (Figure 2A, f). In addition, a portion of importin-β can also be detected in the cytoplasm of control cells. However, after exposure to hydrogen peroxide, importin-β becomes confined to the nucleus and no longer accumulates at the nuclear periphery (Figure 2A, h). As observed for Ran, incubation of stressed cells with PD98059 or genistein does not prevent the redistribution of importin-β (Figure 2B). Like Ran and importin-β, Nup153 relocates within cells treated with hydrogen peroxide. Concentrated at the nuclear periphery in unstressed cells, Nup153 redistributes throughout the nucleus after exposure to hydrogen peroxide (Figure 2A, j, l). Since the antibody used for the detection of Nup153 also recognizes several proteolytic products of the nucleoporin, it is possible that intact Nup153, its degradation products or both were redistributed upon oxidant treatment. Relocation of proteins in hydrogen peroxide stressed cells is not a general effect; for instance, lamin B or hsc70 localization was not altered after incubation with this oxidant (Figure 3C and data not shown).

The relocation of nuclear transport factors cannot be ascribed to a simple permeabilization of the NE. We have tested the intactness of the NE by two independent assays. First, cells were transiently transfected with DNA encoding the cytoplasmic reporter protein GFP-β-galactosidase. When cells were treated with oxidant, GFP-β-galactosidase did not enter the nucleus at concentrations of 10 mM or lower (Figure 3A, b, d), demonstrating that the NE is still a barrier for macromolecules. Second, hydrogen peroxide-treated cells were semi-permeabilized with digitonin and incubated with antibodies against lamin B. If the NE is not intact, antibodies will have access to the nuclear lamina. However, this was not observed (Figure 3C, b, f). By contrast, permeabilization with the detergent Triton X-100 allowed antibodies to bind to lamin B (Figure 3C, d, h). Taken together, these results show that the redistribution of nuclear transport factors takes place when the NE and the NPCs do not permit free diffusion of macromolecules.

Hydrogen peroxide could inhibit classical protein import for several reasons. For instance, RanGTP is required in the nucleus to support classical and several nonclassical nuclear trafficking pathways, and dissipation of the Ran concentration gradient may affect these transport routes. In addition, oxidants could change the ratio of RanGTP/RanGDP, thereby interfering with nuclear transport. Like Ran, importin-β, a subunit of the classical NLS-receptor, and Nup153, the termination site for classical nuclear import, redistribute in cells treated with hydrogen peroxide. As such, the carrier importin-β was confined to the nucleus and its NE

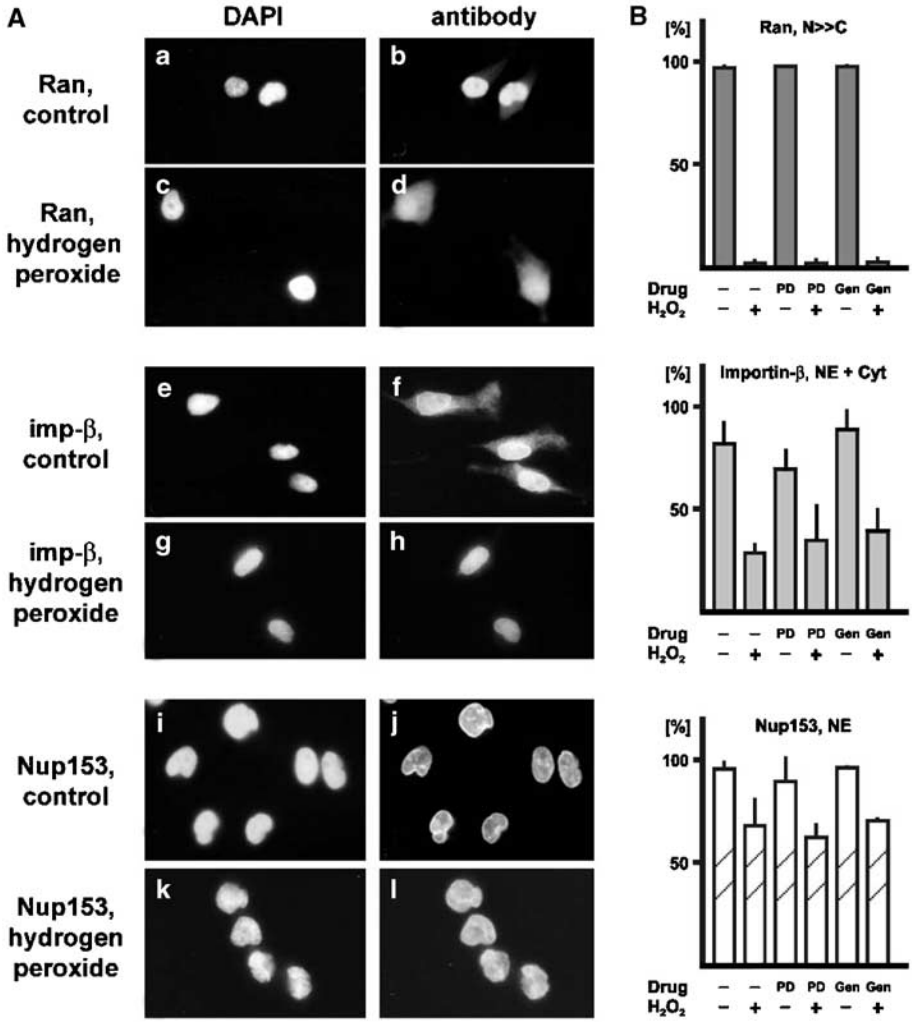

Figure 2 Effect of oxidative stress on the localization of Ran, importin-β, and Nup153. (**A**) Control HeLa cells or cells stressed with hydrogen peroxide as in Figure 1 were used to locate Ran (a–d), importin-β (e–h) and Nup153 (i–l) by immunofluorescent staining. Nuclei were stained with DAPI. (**B**) The distribution of Ran, importin-β and Nup153 was quantified for three independent experiments. For each result, the localization of transport factors was determined in at least 200 cells. The mean values and standard deviations are shown for each group. Changes in Ran nuclear accumulation ($N>>C$), importin-β location at the nuclear envelope and in the cytoplasm ($NE+Cyt$) and the continuous staining of the NE with anti-Nup153 antibodies were monitored

accumulation was reduced. Importin-β has been shown to remain close to the NPC upon completion of nuclear import.[16] It is believed that the carrier will be exported subsequently to the cytoplasm to participate in a new cycle of nuclear import. Hydrogen peroxide treatment could abolish or reduce importin-β exit from the nucleus for different reasons. First, as the Ran concentration gradient collapses, GTPase levels in the nucleus are decreased and may be insufficient to support importin-β export. Second, the association of importin-β with the NE is diminished, presumably because its association with NPCs has been altered. It is clear from our experiments that the NPC organization is modified in cells treated with hydrogen peroxide. In particular, Nup153, located at the nuclear basket in unstressed cells, redistributes in part to the nuclear interior. Furthermore, Nup153 is degraded in stressed cells (see below). Both the relocation and the proteolysis of Nup153 can be expected to affect the functional organization of the nuclear basket and thereby nuclear import and export reactions.

The localization of Ran is more sensitive to oxidative stress than classical nuclear import

Classical nuclear protein import was not efficiently inhibited by hydrogen peroxide concentrations lower than 10 mM (Figures 2, 4). Moreover, NLS-GFP only partially redistributed to the cytoplasm (see above), whereas the Ran concentration gradient was completely abolished under these conditions (Figures 2, 4). This suggests that the Ran concentration gradient is particularly sensitive to oxidative stress. When growing cells were exposed to lower levels of hydrogen peroxide, we detected elevated amounts of Ran in the cytoplasm at concentrations as low as 0.5 mM (Figure 4a).

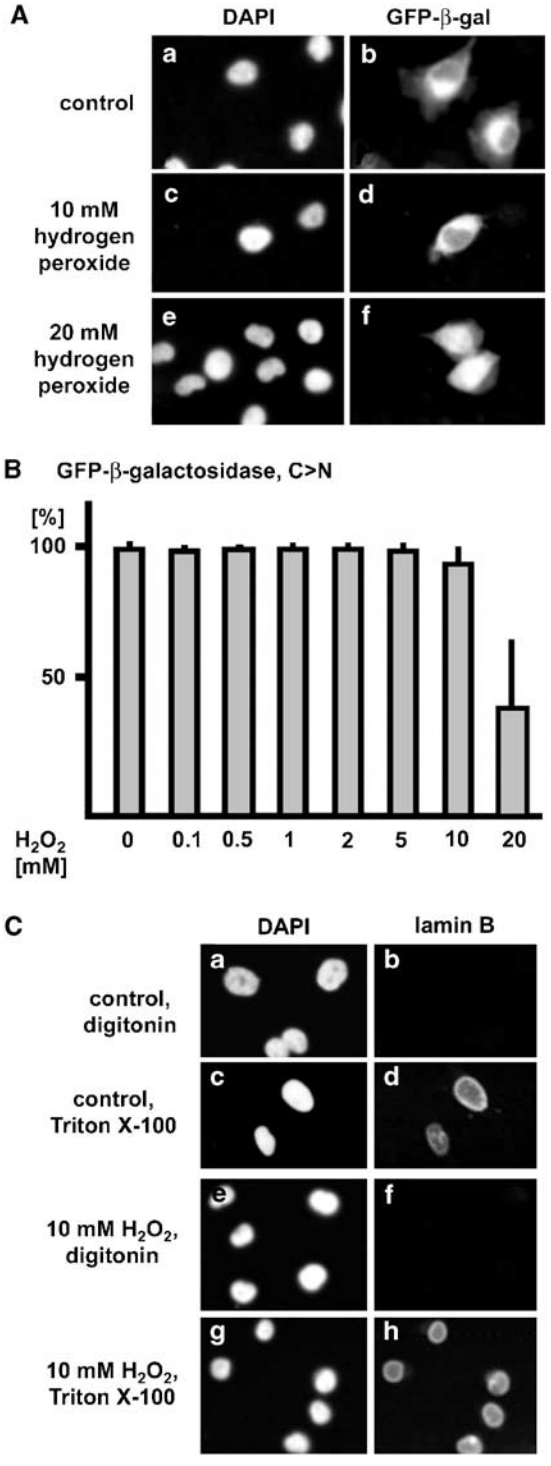

Figure 3 The NE remains intact in HeLa cells treated with hydrogen peroxide. (**A**) HeLa cells transiently synthesizing GFP-β-galactosidase were treated with different concentrations of hydrogen peroxide for 1 h at 37°C. After stress exposure, cells were immediately fixed, stained with DAPI and inspected by fluorescence microscopy. (**B**) At least 100 transfected cells were monitored for each concentration of the oxidant. The figure shows the results (means and S.D.) of three independent experiments. (**C**) Non-transfected HeLa cells were treated with hydrogen peroxide, fixed and permeabilized with digitonin or Triton X-100 as indicated. Cells were incubated with antibodies against lamin B, and primary antibodies were visualized with FITC-conjugated secondary antibodies (Materials and Methods)

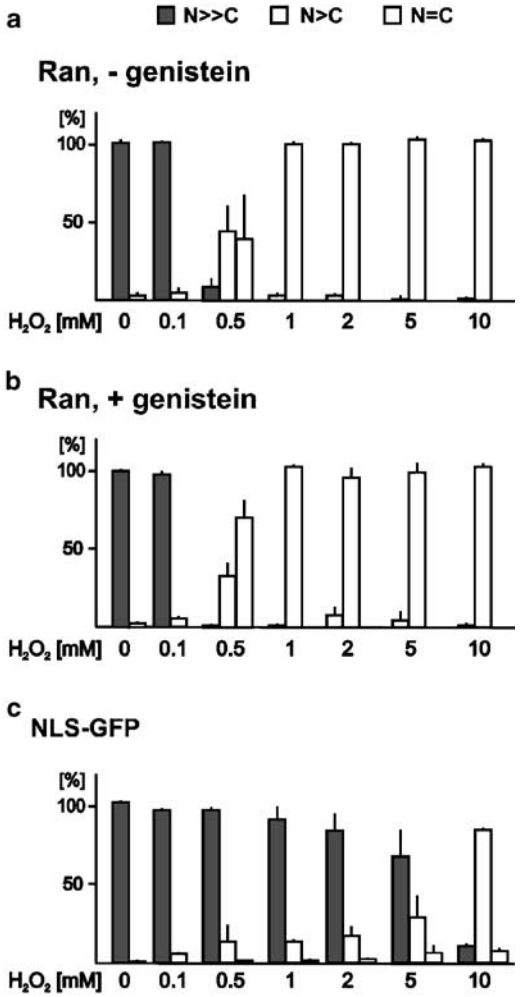

Figure 4 Sensitivity of the Ran concentration gradient and classical nuclear import to hydrogen peroxide. (**a**) Nontransfected HeLa cells were incubated for 1 h at 37°C with different concentrations of hydrogen peroxide. Cells were fixed and Ran was localized by indirect immunofluorescence. (**b**) The same experiment as in part (**a**) was carried out in the presence of genistein. (**c**) HeLa cells synthesizing NLS-GFP were treated with hydrogen peroxide and the reporter protein was located by fluorescence microscopy. The experiments were carried out three times; the distribution of Ran or NLS-GFP was determined for at least 100 cells in each experiment. Parts (**a**)–(**c**) of the figure show the means and the standard deviations for different concentrations of hydrogen peroxide

This redistribution could not be prevented by genistein, and the differences between controls and genistein-treated cells were not statistically significant. Surprisingly, elevated cytoplasmic levels of NLS-GFP were only detected for few cells at 0.5 mM hydrogen peroxide (Figure 4c). This suggests that even though the Ran concentration gradient had collapsed, classical nuclear transport was not drastically affected.

Hydrogen peroxide depletes cellular RanGTP pools

Like other stresses, hydrogen peroxide treatment may reduce the intracellular concentration of ATP, which could subse-

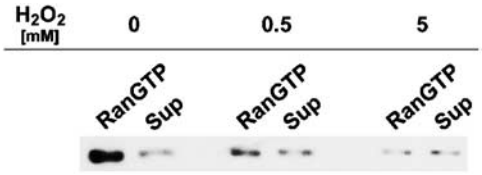

Figure 5 Hydrogen peroxide treatment reduces RanGTP levels. RanGTP was isolated with GST-RBD from controls and cells treated for 1 h at 37°C with different concentrations of hydrogen peroxide. Equal amounts of protein were used as starting material for control and stressed cells. Protein affinity purified with GST-RBD/glutathione-sepharose (RanGTP) and unbound material (Sup) were separated side-by-side, followed by Western blotting with Ran-specific antibodies. For control and stress conditions, the unbound material represents 3% of the affinity-purified protein

quently alter the GTP/GDP ratio. Changes in GTP/GDP may then decrease the levels of RanGTP and favor the formation of RanGDP, a process that will interfere with Ran-dependent trafficking across the NPC. To test this hypothesis, we isolated RanGTP from control and stressed cells with a GST fusion protein that contains the Ran-binding domain (RBD) of RanBP1, referred to as GST-RBD.[17] Crude cell extracts containing the same amount of protein were used as starting material for the purification of RanGTP as recently described,[18] and the isolation of RanGTP was monitored by Western blotting with Ran-specific antibodies. Since hydrogen peroxide treatment induces the degradation of Ran (Figures 7–9 below), we compared the amount of Ran that could be affinity-purified with GST-RBD (Figure 5, RanGTP) to the GTPase that failed to associate with GST-RBD (Figure 5, Sup). As shown in Figure 5, upon exposure to hydrogen peroxide, the relative levels of RanGTP that could be isolated from stressed cells were drastically reduced. A decrease of the ratio RanGTP/RanGDP was already obvious after 1 h exposure to 0.5 mM hydrogen peroxide and became even more pronounced at higher concentrations of the oxidant (Figure 5 and data not shown).

As a consequence of RanGTP depletion induced by oxidative stress, a variety of cellular processes that depend on RanGTP, such as nuclear import and export, will be affected. Furthermore, since RanGDP is unlikely to be retained in the nucleus, changes in the nucleocytoplasmic Ran concentration gradient can also be expected. Ultimately, this will increase cytoplasmic concentrations of the GTPase. Surprisingly, although RanGTP levels were reduced by hydrogen peroxide treatment, classical nuclear transport was not completely abolished under these conditions. One possible explanation for this result could be that even under stress conditions sufficient RanGTP persists in the nucleus to promote NLS-GFP import.

Oxidative stress reduces the import of Ran into the nuclei

In addition to changes in the RanGTP availability, failure to import Ran into the nuclei could also contribute to the relocation of the GTPase to the cytoplasm of hydrogen peroxide-treated cells. NTF2 is the carrier that translocates RanGDP across the NE, and *in vitro* systems have been developed to study this process.[19,20] To address the effect of oxidative stress on Ran nuclear import, we have tested the accumulation of tetramethylrhodamine-labeled RanGDP (TMR-Ran) in semi-intact cells. Under non-stress conditions, TMR-Ran accumulated rapidly in the nucleus and nucleolus if cells were provided with reticulocyte lysate, but treatment with oxidant reduced the capacity of semi-permeabilized cells to concentrate TMR-Ran in the nuclei (data not shown). These results suggested that components of semi-intact cells are sensitive to stress, and we further tested whether hydrogen peroxide also affects cytosolic factors that are required for Ran nuclear import. To this end, we prepared cytosol from control and oxidant-treated HeLa cells, which was combined with untreated or stressed semi-intact cells (Figure 6A). Control cells efficiently imported TMR-Ran when supplied with unstressed cytosol, whereas stressed semi-intact cells displayed increased levels of TMR-Ran in the cytosol. Furthermore, treatment of semi-intact cells with hydrogen peroxide abolished the concentration of TMR-Ran in nucleoli (Figure 6A, d). By contrast, addition of stressed cytosol to untreated semi-intact cells had no drastic effect on the distribution of Ran (Figure 6A, f). If stressed cytosol was combined with stressed semi-intact cells, results were similar to what we observed for the combination of stressed semi-intact cells and untreated cytosol (Figure 6A, compare d and h).

In summary, *in vitro* experiments indicate that Ran nuclear accumulation is reduced, but not abolished, in HeLa cells that have been exposed to severe oxidative stress. This deficiency can be attributed to stress-induced changes of semi-intact cells. As Ran import into nuclei was not prevented by oxidant treatment of cytosol, the source of NTF2 *in vitro*,[19] it is unlikely that the function of NTF2 as a nuclear carrier of the GTPase is abolished by hydrogen peroxide.

NTF2 associates with NEs in hydrogen peroxide-treated cells

Since Ran import was less efficient upon exposure to hydrogen peroxide and NTF2 is the nuclear transporter of Ran, it was important to determine whether NTF2 association with the NE is sensitive to oxidants. Although hydrogen peroxide treatment of cytosol did not prevent Ran nuclear import (Figure 6A), it was possible that stress-induced changes at the NPC prevent the carrier from binding to the NE. Therefore, the association of TMR-labeled GST-NTF2 with nuclei was measured under control and stress conditions using established procedures.[21] After treatment with 0.5, 5 or 10 mM hydrogen peroxide for 1 h, cells were semi-permeabilized and binding of TMR-GST-NTF2 to NEs was tested (Figure 6B and data not shown). TMR-GST-NTF2 accumulation at the nuclear periphery was detected both in the presence and absence of purified wild-type Ran as previously reported.[21] In control experiments, TMR-GST did not associate with semi-intact cells under any of the conditions tested (Figure 6B, j, l and data not shown). These experiments revealed that NTF2 associates with the nuclear membrane in control and stressed cells, suggesting that oxidants did not prevent the interaction between NTF2 and the NPC.

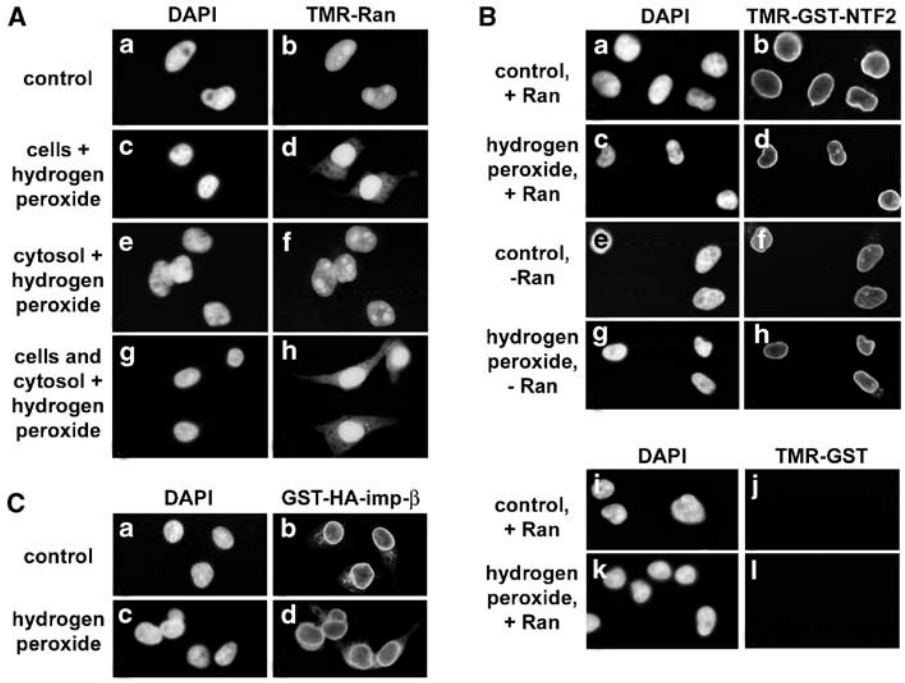

Figure 6 Effect of severe oxidative stress on Ran nuclear import, NTF2 binding to NEs and importin-β nuclear trafficking. For oxidant exposure, cells were incubated with 10 mM hydrogen peroxide for 1 h at 37°C. (**A**) Nuclear import of TMR-RanGDP was analyzed *in vitro* with HeLa cytosol and semi-intact cells. Cytosol and semi-permeabilized cells were prepared from controls or oxidant treated samples as indicated in the figure. (**B**) Binding of TMR-GST-NTF2 (a–h) or TMR-GST (i–l) was tested with semi-intact cells that were unstressed or pretreated with hydrogen peroxide. Unlabeled wild-type Ran was present for the experiments shown in panels (a–d) and (i–l). (**C**) Binding of the classical nuclear import complex importin-α/β/cargo was monitored in unstressed and oxidant treated semi-intact cells. GST-HA-importin-β was localized with antibodies against the HA tag

Nevertheless, Ran is at least in part mislocalized to the cytoplasm under these stress conditions and nuclear import of the GTPase is less efficient when compared to unstressed cells (Figures 2, 6A). There are several possible interpretations of these data: (a) the interaction between Ran and NTF2 is reduced in stressed cells. (b) Oxidants may chemically modify the complex RanGDP/NTF2, preventing it from docking at the NPC. (c) The translocation of RanGDP/NTF2 across the NPC is altered by oxidants. At present, we cannot rule out that hydrogen peroxide interferes with the RanGDP/NTF2 association or docking of the *stressed* RanGDP/NTF2 complex at the nuclear periphery. However, the observation that purified wild-type Ran combined with unstressed cytosol fails to be efficiently imported into the nuclei of stressed semi-intact cells (Figure 6A) indicates that translocation of the GTPase across the NPC is impeded by hydrogen peroxide.

Oxidative stress reduces docking of importin-β at the NE

We further tested whether binding of the import complex importin-α/β/cargo to the nuclear periphery was altered by hydrogen peroxide. To this end, semi-intact cells were incubated with GST-HA-tagged importin-β and the carrier was located with antibodies against the HA tag (Figure 6C). As expected, in semi-intact unstressed cells, importin-β accu-

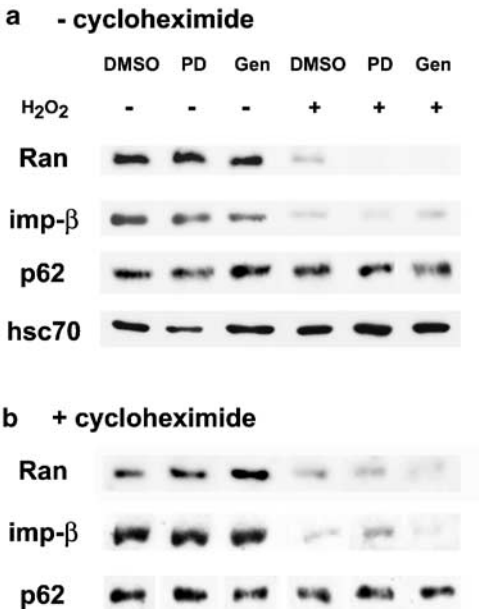

Figure 7 Degradation of Ran, importin-β, p62 or hsc70s in response to hydrogen peroxide treatment. (**a**) Equal amounts of protein from unstressed or stressed cells (1 h, 10 mM hydrogen peroxide, 37°C) were probed by Western blotting with antibodies against Ran, importin-β, p62 and hsc70s. Cells were incubated with the solvent DMSO, PD98059 (PD) or genistein (Gen) as indicated. (**b**) The same experiment was carried out with 100 μg/ml cycloheximide, which was present during stress exposure

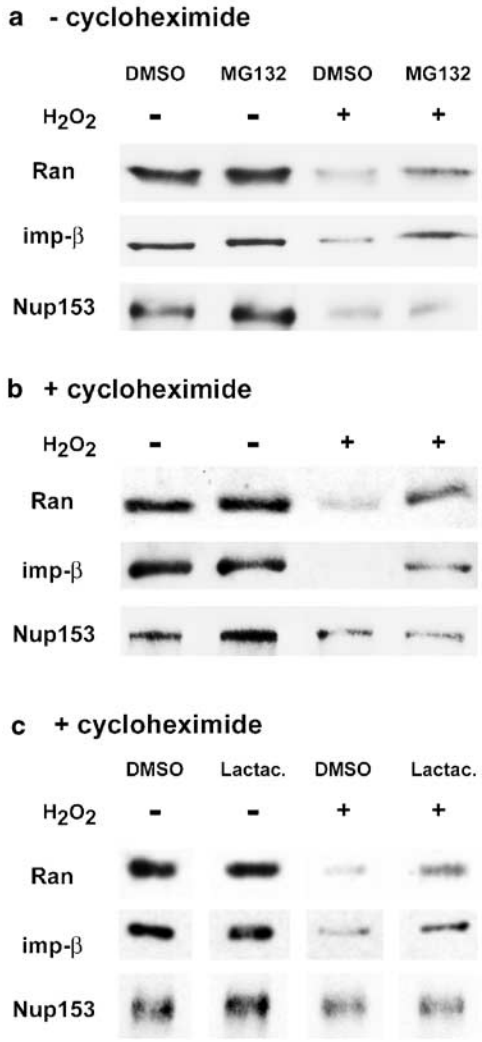

Figure 8 Role of the proteasome in stress-mediated degradation of Ran, importin-β and Nup153. For stress exposure, cells were treated with 10 mM hydrogen peroxide for 1 h at 37°C. Equal amounts of protein were separated side-by-side for each sample and analyzed by Western blotting with antibodies against Ran, importin-β and Nup153. (**a**) Cells were incubated with the solvent DMSO or the inhibitor MG132 as shown in the figure. (**b**) HeLa cells were stressed with hydrogen peroxide in the presence of cycloheximide and MG132. (**c**) HeLa cells preincubated with DMSO or lactacystin were exposed to hydrogen peroxide in the presence of cycloheximide (100 μg/ml)

mulated at the NE.[22] This docking reaction was diminished by oxidative stress, and elevated levels of importin-β remained in the cytoplasm (Figure 6C, d). Nevertheless, even upon hydrogen peroxide exposure, importin-β was able to concentrate at the nuclear periphery, albeit with reduced efficiency.

In summary, severe oxidative stress decreased, but did not prevent, docking of the complex importin-α/β/cargo at the NE. Since importin-β, importin-α or the cargo used in these experiments had not been exposed to stress, we conclude that components of the semi-intact cells are sensitive to hydrogen peroxide, and nucleoporins are possible candidates to be affected by stress.

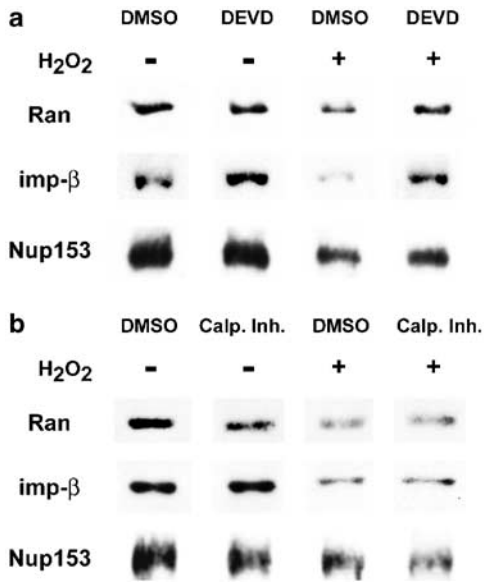

Figure 9 Caspase but not calpain inhibition reduces the degradation of Ran and importin-β upon hydrogen peroxide stress. (**a**) HeLa cells were pretreated with Ac-DEVD-CHO (DEVD) or (**b**) calpain inhibitor I (Calp. Inh.) for 2 h prior to the addition of 10 mM hydrogen peroxide and cycloheximide. Cells were exposed to stress for 1 h at 37°C and cell extracts were subsequently analyzed by Western blotting for the presence of nuclear transport factors, as described for Figure 8**c**

Hydrogen peroxide treatment induces the rapid degradation of Ran, importin-β and Nup153, but not of the nucleoporin p62

Exposure to stress may change the turnover of proteins, and we have analyzed the levels of Ran, importin-β and Nup153 in cells exposed to oxidant. Treatment with hydrogen peroxide reduced the concentration of Ran, importin-β and Nup153 (Figures 7–9). With the antibodies used in our experiments, we did not detect proteolytic products for Ran or importin-β by Western blotting, whereas monoclonal antibody SA1 recognized several degradation products. However, none of these Nup153-derived fragments accumulated upon severe oxidative stress (not shown).

The decrease in Ran, importin-β and Nup153 concentration was not abolished by PD98059 or genistein, and was consistently observed in the presence of MAPK inhibitors (Figure 7). In contrast, levels of hsc70, another soluble factor required for classical nuclear import, the nucleoporin p62 and lamin B were not altered drastically after exposure to hydrogen peroxide under identical conditions (Figure 7 and data not shown). To determine whether hydrogen peroxide diminished the concentration of transport factors by inhibition of their *de novo* synthesis, HeLa cells were incubated with cycloheximide during stress exposure. However, addition of cycloheximide gave similar results, indicating that hydrogen peroxide triggered the degradation of nuclear transport factors (Figure 7b).

Taken together, our data suggest that several nuclear transport factors are particularly prone to degradation when cells are exposed to hydrogen peroxide. Moreover, inhibition of ERK1/2 activation did not abolish their degradation.

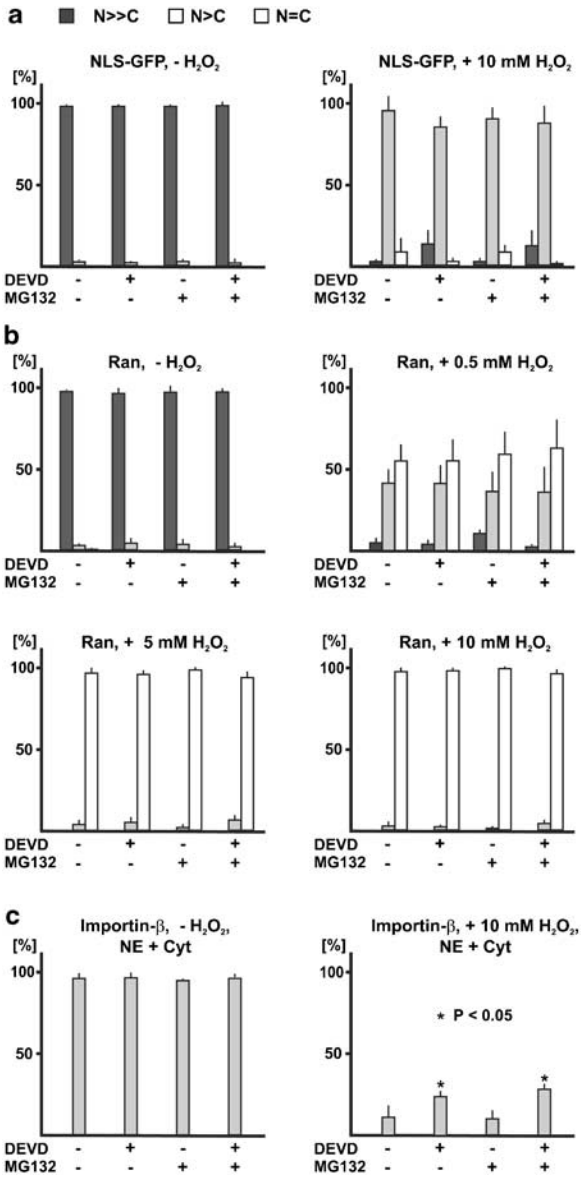

Figure 10 Caspase inhibitors do not abolish the inhibition of classical nuclear import or Ran relocalization, but partially restore the distribution of importin-β. HeLa cells were treated for 1 h at 37°C with different concentrations of hydrogen peroxide. DEVD or MG132 were present for 1 h prior to stress exposure and during the entire stress period. Control cells were incubated with the solvent DMSO only; all of the samples contained the same amount of solvent. Cells were fixed immediately upon oxidant treatment. At least 100 cells were monitored in each of three independent experiments for all of the different experimental conditions shown in the figure. (**a**) Classical nuclear import was monitored in transiently transfected cells synthesizing NLS-GFP, as described for Figure 1. (**b**) Ran was localized by indirect immunofluorescence as in Figure 4. (**c**) Importin-β was located in controls and cells exposed to 10 mM hydrogen peroxide. Incubation with DEVD or DEVD/MG132 significantly increased the number of cells that accumulated importin-β at the NE and also showed cytoplasmic localization of the carrier ($P<0.05$)

In cells treated with hydrogen peroxide, Ran and importin-β degradation is reduced by proteasome inhibitors

Both the 26S and 20S proteasome complexes contribute to the degradation of proteins. In particular, the nuclear 20S proteasome complex may play a role in the proteolysis of nuclear transport factors in stressed cells, as nuclear proteasome activity can be increased by oxidants.[23] Consistent with this hypothesis, MG132, a potent inhibitor of the mammalian proteasome, reduced Ran and importin-β proteolysis in stressed cells, but did not alter Ran or importin-β levels in control cells (Figure 8a, b). By contrast, under the same conditions, MG132 did not protect Nup153 against degradation, suggesting a mechanism independent of the 20S proteasome.

As MG132 may affect proteases other than the proteasome, we have further tested the effect of lactacystin, a distinct proteasome inhibitor, for which we obtained results similar to those described for MG132 (Figure 8c). Degradation of proteins via the proteasome may occur in an ATP/ubiquitin-dependent or -independent fashion. In general, ubiquitination seems to be repressed in cells stressed with oxidants, making ATP/ubiquitin-dependent protein degradation via the 26S proteasome unlikely.[24] Indeed, our data demonstrate that Ran or importin-β ubiquitination is not increased in oxidant-treated cells (see below), in line with ATP/ubiquitin-independent proteolysis. This is consistent with the observation that the 20S but not the 26S proteasome activity is upregulated in cells treated with hydrogen peroxide.[7] As stress-induced degradation of Ran and importin-β can be decreased by MG132 and lactacystin, we conclude that their proteolysis in cells treated with oxidants is partially mediated by the 20S proteasome complex.

Inhibition of caspases diminishes hydrogen peroxide-induced proteolysis of Ran and importin-β

Since HeLa cells underwent apoptosis 24 h after treatment with hydrogen peroxide, we tested whether caspases contribute to the degradation of nuclear transport factors. Proteins of the NPC and the NE have been shown previously to be targets of caspases in apoptotic cells.[25–28] The membrane-permeable compound Ac-DEVD-CHO efficiently inhibits caspase 3. In addition, caspases 6, 7, 8 and 10 can also be affected. The inhibitor reduced the degradation of Ran and importin-β, and the protection against proteolysis was more pronounced than for lactacystin (Figure 9a). For Nup153, the effect of Ac-DEVD-CHO was variable, but always less apparent than for Ran or importin-β.

In addition to the proteasome and caspases, proteases of the calpain family could be involved in the degradation of the transport factors analyzed by us. However, calpain inhibitor I did not alter the proteolysis of Ran, importin-β or Nup153 (Figure 9b). Thus, caspases, but not calpain, are important for the stress-induced proteolysis of Ran and importin-β.

Ran, importin-β and Nup153 are not modified by ubiquitin or SUMO-1 in hydrogen peroxide-treated cells

Ran is essential for classical and nonclassical nuclear transport pathways, the organization of mitotic spindles and reformation of the NE at the end of mitosis.[15,29–33] So far, the

Table 1 Effect of severe oxidative stress on classical nuclear import and nuclear transport factors

Factor or reaction analyzed	Unstressed conditions	Severe oxidative stress
Classical nuclear import of NLS-GFP	Nuclear accumulation	Reduced nuclear accumulation, a portion of NLS-GFP appears in the cytoplasm
Ran localization and stability	Concentrated in nuclei	Ran concentration gradient collapses; Ran degraded by caspases and proteasome
RanGTP		RanGTP/RanGDP ratio decreased
Ran transport *in vitro* into nuclei	Ran efficiently imported into nuclei, accumulation in nucleoli	Ran import with reduced efficiency, no accumulation in nucleoli
NTF2 binding to nuclear envelopes *in vitro*	Purified NTF2 accumulates at the nuclear envelope	No drastic changes, similar to unstressed cells
Importin-β localization and stability	NE, cytosol	NE, reduced amounts in cytosol; importin-β degraded by caspases and proteasome
Docking of import complex importin-α/β/cargo *in vitro*	Importin-α/β/cargo concentrates at the nuclear envelope	Importin-α/β/cargo concentrates at the nuclear envelope, but increased levels of importin-β in the cytoplasm
Nup153	Concentrated at the nuclear periphery	Partial relocation to nuclear interior; degradation

Nuclear accumulation of NLS-GFP, as well as the localization, stability and trafficking of classical nuclear transport factors, was monitored in unstressed controls and cells treated with hydrogen peroxide. See text for details; NE, nuclear envelope

degradation of transport factors under different physiological conditions has not been studied. Exposure to different types of stress can lead to covalent modification of proteins with ubiquitin or SUMO.[34] To determine whether Ran, importin-β and Nup153 are conjugated to ubiquitin or SUMO-1 upon exposure to hydrogen peroxide, we have immunoprecipitated equal amounts of protein from unstressed and stressed cells under denaturing conditions. Immunopurified proteins were then analyzed by Western blotting with antibodies recognizing ubiquitin or SUMO-1. Nuclear transport factors were efficiently purified under these conditions; however, we did not detect them to be ubiquitinated when probed with two different antibodies against ubiquitin. Similarly, two distinct antibodies against SUMO-1 did not reveal a sumoylation of the immunoprecipitated proteins (data not shown). Thus, exposure to hydrogen peroxide does not result in polyubiquitination or modification by SUMO-1 of Ran, importin-β or Nup153. These results are consistent with previous publications for Nup153. Although Nup153 has been shown recently to bind SENP2, a protease that cleaves SUMO-1 modifications, sumoylation of this nucleoporin has not been reported.[35,36] Furthermore, the consensus site for SUMO-1 modifications, ψKxE (with $\psi = $ L, I, V, F; Hay[34]) is not present in human Ran, importin-β or Nup153. In conclusion, severe oxidative stress did not trigger a modification of Ran, importin-β or Nup153 by ubiquitin or SUMO-1.

Effect of protease inhibitors on the oxidant-induced inhibition of classical nuclear import and the relocation of Ran and importin-β

As caspase and proteasome inhibitors reduced the degradation of Ran and importin-β in oxidant-treated cells, we tested whether these compounds also affected nuclear import of NLS-GFP or the redistribution of soluble transport factors in stressed cells. To this end, cells were preincubated with the solvent DMSO, the inhibitors DEVD, MG132 or a combination of DEVD and MG132 (Figure 10); these compounds were also present during the exposure to hydrogen peroxide. Treatment with DEVD or the combination DEVD/MG132 slightly increased the number of stressed cells that efficiently accumulated NLS-GFP in nuclei (Figure 10a, $N > > C$), but these changes were not statistically significant.

In addition to classical nuclear import, the distribution of Ran and importin-β was monitored in control and drug-treated cells (Figure 10b, c). Caspase and proteasome inhibitors did not prevent the relocalization of Ran in stressed cells, and similar results were obtained for different concentrations of hydrogen peroxide (Figure 10b). Unlike Ran, the redistribution of importin-β in stressed cells was partially reversed by DEVD. When DEVD or DEVD/MG132 was present, an increased number of cells concentrated importin-β at the NE and the carrier was also detected in the cytoplasm. By contrast, MG132 alone had no effect (Figure 10c). The changes seen for DEVD or DEVD/MG132 were statistically significant ($P < 0.05$).

Taken together, these results suggest that inhibiting the degradation of importin-β by caspases allows cells to retain importin-β in the cytosol, whereas no drastic changes could be observed for Ran or classical nuclear import. One possible interpretation of these data could be that upon severe oxidative stress cytoplasmic importin-β becomes rapidly degraded by caspases. With respect to classical import, however, the protection of importin-β against stress-induced proteolysis is not sufficient to restore the nuclear accumulation of NLS-GFP. This is consistent with the idea that importin-β degradation is not the limiting factor required to re-establish classical transport. Other processes, such as the depletion of RanGTP, might prevent the restoration of the Ran concentration gradient and nuclear trafficking.

Multiple mechanisms contribute to the inhibition of classical nuclear import in oxidant-treated cells

Cells have to cope with various types of insults to prevent or repair stress-induced damage. The effect of stress on protein kinase signaling cascades and the activation of gene transcription has been studied in some detail. However, it has yet to be defined how distinct forms of stress modulate other functions of the nucleus and its organization. To begin to

address this question, we have analyzed in growing HeLa cells and *in vitro* how classical nuclear import and several components of the import apparatus are affected by severe oxidative stress. We have now demonstrated that transport factor relocalization and degradation as well as a depletion of RanGTP are consequences of the exposure to hydrogen peroxide (summarized in Table 1). Each of these changes can be expected to contribute to the inhibition of classical nuclear import. For instance, environmental stress is known to deplete intracellular ATP levels (reviewed in Hardie *et al.*[37]), and we have proposed previously that ATP depletion decreases the concentration of RanGTP, thus favoring the formation of RanGDP.[8] This has recently been confirmed in HeLa cells, for which the reduction of ATP resulted in lower levels of RanGTP.[18] The increased consumption of ATP necessary to repair oxidant-induced damage may transiently alter the homeostasis of ATP production and consumption (reviewed in Dzeja and Terzic[38]). Under these conditions, RanGTP levels could become limiting for the support of nuclear trafficking. Furthermore, the lack of nuclear retention of RanGDP will promote a collapse of the nucleocytoplasmic Ran concentration gradient.

A prominent feature of Ran, importin-β and Nup153 is their increased sensitivity to proteolysis in response to severe oxidative stress. Hydrogen peroxide triggers the oxidation of SH groups and other amino-acid side chains (reviewed in Dean *et al.*[39]), which could target proteins for degradation via the proteasome. It was proposed that protein oxidation increases surface hydrophobicity, thereby enabling the 20S proteasome to recognize oxidized proteins even in the absence of ubiquitination,[24] a process that might take place for Ran and importin-β. By contrast, Nup153 degradation was independent of the proteasome, and inhibition of caspases had variable effects. Other studies have shown Nup153 to be a substrate for caspases in apoptotic cells.[25,27] However, Nup153 does not always undergo degradation during apoptosis[26] and differences are likely to exist for various cell types. These differences may also explain why importin-β and Ran are not degraded upon induction of apoptosis with cisplatin.[26]

Our experiments clearly show that ERK1/2 are not the limiting factors, that alter classical nuclear import in response to severe oxidative stress. As oxidants also activate signaling pathways other than the ERK1/2 cascade, classical nuclear transport inhibition is likely to be more complex in growing mammalian cells than previously reported for *in vitro* studies.[9] As well, cell type-specific differences may explain that in semi-permeabilized smooth muscle cells ERK2 is the critical component that controls classical import after exposure to hydrogen peroxide, whereas transport inhibition in HeLa cells involves multiple mechanisms.

In vitro experiments shown in this study suggest that NPCs are likely to be targets for damage induced by hydrogen peroxide. As such, Ran import into nuclei was reduced if semi-intact cells have been stressed. Furthermore, docking of the classical nuclear import complex at the NE was diminished. The simplest explanation of these results is a change in NPC function, and future studies will have to identify which nucleoporins, in addition to Nup153, are affected by oxidants.

Besides NPCs, several soluble factors required for classical nuclear import are shared with nonclassical trafficking pathways. As such, Ran and its interacting components are essential for transport that is mediated by members of the importin-β family. Changes in Ran localization, concentration and the RanGTP/RanGDP ratio after treatment with oxidants will therefore have a more general effect on nucleocytoplasmic transport of macromolecules. Not only classical transport but also nonclassical import as well as export from the nucleus will be affected. Taken together, our results underscore that severe oxidative stress can modulate nuclear functions on several levels, including the inhibition of nuclear trafficking reactions and the functional organization of NPCs.

Materials and Methods

Growth and stress exposure of HeLa cells

HeLa cells were grown in multiwell chambers as described.[40] At approximately 70% confluency, cells were subjected to 10 mM hydrogen peroxide (or the oxidant concentration given in the figure legends) in growth medium and incubated for 1 h at 37°C. Incubation with the kinase inhibitors PD98059 and genistein was carried out as in Chu *et al.*[10] To test the role of the proteasome, cells were preincubated for 30 min with 10 μM MG132 or for 2 h with 50 μM lactacystin (Calbiochem, San Diego, CA, USA) in growth medium. Cells were pretreated with 15 μM caspase inhibitor (Ac-DEVD-CHO, Calbiochem) or 50 μM calpain inhibitor I (MG101, Sigma, Oakville, ON, USA) 2 h before stress exposure. All inhibitors were present throughout the stress treatment.

Transfection of HeLa cells

HeLa cells were transfected with plasmids encoding the nuclear reporter protein NLS-GFP[10] or plasmid pHM830 coding for GFP-β-galactosidase[41] following standard procedures.[10,40]

Generation of GST-NTF2 and synthesis of fusion proteins in *E. coli*

GST-NTF2 was generated by fusing GST in frame to codon 4 of human NTF2. The correctness of the construct was verified by DNA sequencing. A plasmid encoding GST-HA-importin-β[22] was kindly provided by Dr. Y Yoneda, Osaka. Expression of genes encoding GST- or His6-fusion proteins was induced in bacteria with 0.5 mM IPTG for 2.5 h at 37°C.

Fluorescent labeling of His6-Ran and GST-NTF2

His6-tagged wild-type Ran, GST-NTF2 and GST were synthesized in *E. coli* and affinity purified under native conditions following standard procedures. Purified proteins were dialyzed against 50 mM potassium phosphate, pH 7.0, 2 mM magnesium acetate and concentrated with centrifugal filters (Millipore, Bedford, MA, USA). GDP-loaded Ran was labeled with tetramethylrhodamine-maleimide (TMR-maleimide; Molecular Probes, Eugene, OR, USA) for 3 h on ice essentially as described.[19] GST-NTF2 or GST were labeled overnight on ice. Non-incorporated label was removed by gel filtration using Sephadex G25 (Amersham Biosciences, Piscataway, NJ, USA) equilibrated with Ran import buffer (see below), which was supplemented with 200 μM GDP for the purification of labeled Ran.

Nuclear import of Ran

Nuclear import of fluorescent Ran was tested essentially as in Ribbeck *et al.*[19] In brief, HeLa cells were grown on poly-lysine-coated slides to 70% confluency and semi-permeabilized with 40 μg/ml digitonin in Ran import buffer. Cells were washed once in ice-cold import buffer and nuclear accumulation of Ran in import buffer containing 0.5 mM ATP, 0.5 mM GTP, 10 mM creatine phosphate, 2 mg/ml BSA and 4 mg/ml reticulocyte lysate, or 3 mg/ml HeLa cytosol was allowed for 3 min at room temperature. Cells were fixed immediately with 3.7% formaldehyde for 20 min at room temperature and nuclei were stained with 4′,6-diamidino-2-phenylindole (DAPI).

Binding of NTF2 to NEs

The association of fluorescent GST-NTF2 (TMR-GST-NTF2) or GST (TMR-GST) with nuclear membranes was tested essentially as described.[21] Binding of GST-NTF2 to NEs of semi-intact cells was tested with 0.45 μM TMR-GST-NTF2 (dimer) or TMR-GST combined with an energy-regenerating mix.[21] Wild-type RanGDP was present at 1.15 μM as indicated in Figure 6B. Upon incubation for 10 min at room temperature, cells were fixed for 20 min with 3.7% formaldehyde and nuclei were visualized with DAPI.

Docking of the classical nuclear import complex at nuclear membranes

Binding of purified GST-HA-importin-β was tested in semi-intact cells essentially as described.[22] Importin-α, GST-HA-importin-β and 50 μg/ml SV40-HSA were preincubated for 1 h on ice and centrifuged (5 min, microfuge, 13 000 rpm) before addition to semi-intact cells. After incubation for 20 min at room temperature, excess liquid was removed and cells were immediately fixed with 3.7% formaldehyde in PBS (20 min, room temperature). Importin-β was localized by indirect immunofluorescence with antibodies against the HA tag (see below).

Specificity of antibodies used for immunofluorescence and Western blotting

The following primary antibodies were used: mouse mab414 and monoclonal antibodies to the HA tag (BaBCo, Richmond, CA, USA), goat anti-lamin B (sc-6217, Santa Cruz Biotechnology, CA, USA), goat anti-Ran (sc-1155, sc-1156, Santa Cruz Biotechnology), monoclonal antibody 3E9 against importin-β (Affinity Bioreagents, Golden, CO, USA), monoclonal antibody SPA-815 against hsc70 (StressGen, Victoria, BC, Canada), cell culture supernatant SA1 (Bodoor *et al.*;[42] a generous gift of Dr. B Burke), specific for Nup153, and rabbit polyclonal and monoclonal antibodies to ubiquitin (sc-9133 and sc-8017, Santa Cruz Biotechnology), polyclonal and monoclonal antibodies recognizing SUMO-1 (sc-6375, sc-5308, Santa Cruz Biotechnology). Mab414 binds FXF repeat containing nucleoporins, including Nup153 and p62. Antibodies against lamin B, Ran, importin-β and hsc70 recognize a single band of the expected size on Western blots. Monoclonal antibody SA1 binds to the 180 kDa nucleoporin Nup153 and also to some of its degradation products. The different anti-ubiquitin antibodies bind to several bands for crude extracts upon Western blotting. Activated ERK1/2 was detected with monoclonal antibody E10 (Cell Signaling Tech., Beverly, MA, USA), which is specific for phospho-p44/42 MAPK, phosphorylated in positions thr202 and tyr204. Primary antibodies were diluted as suggested by the suppliers and supernatant SA1 was used undiluted.

Immunofluorescence

All steps were carried out at room temperature. Stressed cells and controls were fixed in 3.7% formaldehyde/PBS for 25 min. Cells were permeabilized in 0.1% Triton X-100 (5 min), blocked for 1 h in PBS/2 mg/ml BSA containing 0.05% Tween 20 and incubated overnight with primary antibodies. Bound primary antibodies were detected with FITC-conjugated anti-rabbit or anti-goat antibodies, or Cy3-conjugated antibodies to mouse IgG (Jackson ImmunoResearch, West Grove, PA, USA). Secondary antibodies were diluted between 1 : 200 and 1 : 250. DNA was visualized with DAPI and samples were mounted in Vectashield (Vector Laboratories, Burlingame, CA, USA). Cells were analyzed with a Nikon Optiphot at $\times$ 400 magnification and photographed with Kodak T-MAX 400 films. The negatives were scanned and processed with Photoshop 5.5.

Digitonin treatment of HeLa cells for immunofluorescence

Control and stressed HeLa cells were fixed and incubated with 40 μg/ml digitonin in PBS for 3 min on ice. In Figure 3C, cells were incubated with 0.1 μg/ml anti-lamin B antibodies overnight at room temperature. After three washes, samples were incubated with FITC-labeled secondary antibodies, washed and treated with DAPI. All incubations were carried out as described for immunofluorescent staining, except for the omission of Tween 20 in all buffers.

Western Blot analysis

HeLa cells were grown on dishes to about 70% confluency. Upon stress exposure, plates were washed with PBS and stored at -70°C until use. Proteins were solubilized in gel sample buffer and treated as described.[43] Equal amounts of protein were separated for controls and different stress conditions in SDS-PA gels and blotted to nitrocellulose filters. Blots were further processed as previously described.[10,43]

Purification of RanGTP

RanGTP was isolated with GST-RBD essentially as in Schwoebel *et al.*[18] Aliquots of affinity-purified RanGTP and material that did not bind to GST-RBD were separated side-by-side on 12% SDS-PA gels and Ran was detected by Western blotting.

Indirect immunoprecipitation

Protein G-sepharose (Amersham Biosciences) was preloaded with Ran-specific antibodies overnight at 4°C in RIPA-buffer (PBS/1% Triton X-100/0.1% SDS/0.5% sodium deoxycholate/1 mM NaN_3, pH 7.4). Control resin was incubated with RIPA buffer only. For immunopurification of denatured proteins, HeLa cell extracts were prepared in PBS containing 1 mM sodium orthovanadate, 1 mM PMSF and a cocktail of protease inhibitors (aprotinin, antipain, chymostatin, leupeptin and pepstatin, each at 0.1 μg/ml). DNA was sheared by vortexing samples in the presence of glass beads. Proteins precipitated with 5% TCA for 5 min on ice were collected by centrifugation. Sediments were resuspended in RIPA buffer containing inhibitors (see above) and preincubated with protein G-sepharose for 30 min at 4°C. Supernatants obtained after 5 min centrifugation (5000 rpm, microfuge, 4°C) were mixed with control resin or resin loaded with antibodies against Ran, importin-β, or Nup153. After overnight incubation at 4°C with gentle agitation, protein G-sepharose was collected

by centrifugation and washed four times in cold PBS/1 mM NaN_3. Proteins bound to the resin were eluted by boiling in gel sample buffer (10 min at 95°C), followed by Western blot analysis with antibodies against ubiquitin or SUMO-1.

Acknowledgements

We are grateful to B Burke for providing us with monoclonal antibody SA1. We thank T Stamminger and R Truant for plasmid pHM830, Y Yoneda and MS Moore for bacterial expression vectors encoding GST-HA-importin-β and GST-RBD, respectively. This work was supported by funds from CIHR, NSERC and The Heart and Stroke Foundation of Quebec. US is a chercheur boursier national of FRSQ, MK was supported by a Faculty of Medicine Internal Fellowship from McGill University and AC by a studentship from NSERC.

References

1. Finkel T and Holbrook NJ (2000) Oxidants, oxidative stress and the biology of ageing. Nature 408: 239–247
2. Hood JK and Silver PA (1999) In or out? Regulating nuclear import. Curr. Opin. Cell Biol. 11: 241–247
3. Allen RG and Tresini M. (2000) Oxidative stress and gene regulation. Free Radic. Biol. Med. 28: 463–499
4. Robinson M and Cobb MH (1997) Mitogen-activated protein kinase pathways. Curr. Opin. Cell Biol. 9: 180–186
5. Rhee SG (2000) Hydrogen peroxide: a key messenger that modulates protein phosphorylation through cysteine oxidation. Sci. STKE 1–23
6. Wang X, Martindale JL, Liu Y and Holbrook N (1998) The cellular response to oxidative stress: influences of mitogen-activated protein kinase signaling pathways on cell survival. Biochem. J. 333: 291–300
7. Ullrich O, Ciftci O and Hass R (2000) Proteasome activation by polyADP-ribose-polymerase in human myelomonocytic cells after oxidative stress. Free Radic. Biol. Med. 29: 995–1004
8. Stochaj U, Rassadi R and Chiu J (2000) Stress-mediated inhibition of the classical nuclear protein import pathway and nuclear accumulation of the small GTPase Gsp1p. FASEB J., 10.1096/fj.99-99-0751fje
9. Czubryt MP, Austria JA and Pierce GN (2000) Hydrogen peroxide inhibition of nuclear protein import is mediated by the mitogen-activated protein kinase ERK2. J. Cell Biol. 148: 7–15
10. Chu A, Matusiewicz N and Stochaj U (2001) Heat-induced nuclear accumulation of hsc70s is regulated by phosphorylation and inhibited in confluent cells. FASEB J., 10.1096/fj.00-0680fje
11. Stochaj U and Rother KL (1999) Nucleocytoplasmic trafficking of proteins: with or without Ran? BioEssays 21: 579–589
12. Görlich D and Kutay U (1999) Transport between the cell nucleus and the cytoplasm. Ann. Rev. Cell Dev. Biol. 15: 607–660
13. Kuersten S, Ohno M and Mattaj IW (2001) Nucleocytoplasmic transport: Ran, beta and beyond. Trends Cell Biol. 11: 497–503
14. Shah S, Tugendreich S and Forbes D (1998) Major binding sites for the nuclear import receptor are the internal nucleoporin Nup153 and the adjacent nuclear filament protein Tpr. J. Cell Biol. 141: 31–49
15. Künzler M and Hurt E (2001) Targeting of Ran: variation on a common theme? J. Cell Sci. 114: 3233–3241
16. Görlich D, Vogel F, Mills AD, Hartmann E and Laskey RA (1995) Distinct functions of the two importin subunits in nuclear protein import. Nature 377: 246–248
17. Beddow AL, Richards SA, Orem NR and Macara IG (1995) The Ran/TC4 GTPase-binding domain: identification by expression cloning and characterization of a conserved sequence motif. Proc. Natl. Acad. Sci. USA 92: 3328–3332
18. Schwoebel ED, Ho TH and Moore MS (2002) The mechanism of inhibition of Ran-dependent nuclear transport by cellular ATP depletion. J. Cell Biol. 157: 963–974
19. Ribbeck K, Lipowsky G, Kent HM, Stewart M and Görlich D (1998) NTF2 mediates nuclear import of Ran. EMBO J. 17: 6587–6598
20. Smith A, Brownawell A and Macara IG (1998) Nuclear import of Ran is mediated by the transport factor NTF2. Curr. Biol. 8: 1403–1406
21. Chaillan-Huntington C, Braslavsky CV, Kuhlmann J and Stewart M (2000) Dissecting the interactions between NTF2, RanGDP, and the nucleoporin XFXFG repeats. J. Biol. Chem. 275: 5874–5879
22. Kose S, Imamoto N, Tachibana T and Yoneda Y (1997) Ran-unassisted nuclear migration of a 97-kD component of nuclear pore-targeting complex. J. Cell Biol. 139: 841–849
23. Obin M, Shang F, Gong X, Handelman G, Blumberg J and Taylor A (1998) Redox regulation of ubiquitin-conjugating enzymes: mechanistic insights using the thiol-specific oxidant diamide. FASEB J. 12: 561–569
24. Davies KJA (2001) Degradation of oxidized proteins by the 20S proteasome. Biochimie 83: 301–310
25. Buendia B, Santa-Maria A and Courvalin JC (1999) Caspase-dependent proteolysis of integral and peripheral proteins of nuclear membranes and nuclear pore complex during apoptosis. J. Cell Sci. 112: 1743–1753
26. Faleiro L and Lazebnik Y (2000) Caspases disrupt the nuclear–cytoplasmic barrier. J. Cell Biol. 151: 951–959
27. Kihlmark M, Imreh G and Hallberg E (2001) Sequential degradation of proteins from the nuclear envelope during apoptosis. J. Cell Sci. 114: 3643–3653
28. Ferrando-May E, Cordes V, Biller-Ckovric I, Mirkovic J, Gorlich D and Nicotera P (2001) Caspases mediate nucleoporin cleavage, but not early redistribution of nuclear transport factors and modulation of nuclear permeability in apoptosis. Cell Death Differ. 8: 495–505
29. Clarke PR and Zhang C (2001) Ran GTPase: a master regulator of nuclear structure and function during eukaryotic cell division cycle. Trends Cell Biol. 11: 366–371
30. Moore JD (2001) The Ran GTPase and cell cycle control. BioEssays 23: 77–85
31. Sazer S and Dasso M (2000) The Ran decathlon: multiple roles of Ran. J. Cell. Sci. 113: 1111–1118
32. Hetzer M, Bilbao-Cortes D, Walther TC, Gruss OJ and Mattaj IW (2000) GTP hydrolysis by Ran is required for nuclear envelope assembly. Mol. Cell 5: 1013–1024
33. Zhang V and Clarke PR (2001) Roles of Ran-GTP and Ran-GDP in precursor vesicle recruitment and fusion during nuclear envelope assembly in a human cell-free system. Curr. Biol. 11: 208–212
34. Hay RT (2001) Protein modification by SUMO. Trends Biochem. Sci. 26: 332–333
35. Hang J and Dasso M (2002) Association of the human SUMO-1 protease SENP2 with the nuclear pore. J. Biol. Chem. 277: 25961–25966
36. Zhang H, Saitoh H and Matunis MJ (2002) Enzymes of the SUMO modification pathway localize to filaments of the nuclear pore complex. Mol. Cell. Biol. 22: 6498–6508
37. Hardie DG, Carling D and Halford N (1994) Roles of the Snf1/Rkin1/AMP-activated protein kinase family in the response to environmental and nutritional stress. Semin. Cell Biol. 5: 409–416
38. Dzeja PP and Terzic A (2003) Phosphotransfer networks and cellular energetics. J. Exp. Biol. 206: 2039–2047
39. Dean RT, Fu S, Stocker R and Davies MJ (1997) Biochemistry and pathology of radical-mediated protein oxidation. Biochem. J. 324: 1–18
40. Chatterjee S and Stochaj U (1998) Diffusion of proteins across the nuclear envelope of HeLa cells. BioTechniques 24: 668–674
41. Sorg G and Stamminger T (1999) Mapping of nuclear localization signals by simultaneous fusion to green fluorescent protein and to β-galactosidase. BioTechniques 26: 858–862
42. Bodoor K, Shaikh S, Salina D, Raharjo WH, Bastos R, Lohka M and Burke B (1999) Sequential recruitment of NPC proteins to the nuclear periphery at the end of mitosis. J. Cell Sci. 112: 2253–2264
43. Barth W, Chatterjee S and Stochaj U (1999) Targeting of the mammalian nucleoporin p62 to the nuclear envelope in the yeast *Saccharomyces cerevisiae* and HeLa cells. Biochem. Cell Biol. 77: 355–365